Flood Risk Assessment Due to Urbanisation and Climatic Factors using Geospatial Approach: A Case Study of Ghaggar River Basin

A Thesis

Submitted in Fulfillment of the Requirements for the award of the degree of

DOCTOR OF PHILOSOPHY

By:

SANJOY GORAI

(Regd. No. 901714004)

School of Energy and Environment

Thapar Institute of Engineering and Technology
Patiala-147004, India

November 2023

DECLARATION

I, at this moment, declare that the research work presented in this thesis entitled "**Flood Risk Assessment Due to Urbanisation and Climatic Factors using Geospatial Approach: A Case Study of Ghaggar River Basin**" for the requirement of the degree of Doctor of Philosophy in School of Energy and Environment, Thapar Institute of Engineering and Technology, Patiala, India is an authentic record of my research work carried out during the period from January 2018 to August 2023 under the supervision of Prof. Amit Dhir (Professor, School of Energy and Environment, Thapar Institute of Engineering and Technology, Patiala, India) and Prof. Dwarikanath Ratha (Professor, Department of Civil Engineering, Thapar Institute of Engineering and Technology, Patiala, India). Documents from other researchers' works embodied in this thesis are duly listed in the reference section.

The matter presented in this thesis has not been submitted, in part or full, for the award of any degree in any other University or Institute.

Sanjoy Gorai

Sanjoy Gorai
(Regd. No. 901714004)

i

CERTIFICATE

It is certified that the thesis entitled **"Flood Risk Assessment Due to Urbanisation and Climatic Factors using Geospatial Approach: A Case Study of Ghaggar River Basin"** which has been submitted by Mr. Sanjoy Gorai in the fulfillments of the requirements for the award of the degree of Doctor of Philosophy in School of Energy and Environment, Thapar Institute of Engineering and Technology, Patiala, India is a record of the candidate's own original research work carried out by him under our supervision and guidance. The matter embodied in this thesis has not been submitted, in part or full, for the award of any degree in any other University or Institute.

Dr. Amit Dhir
Professor
School of Energy and Environment
TIET, Patiala, India

Dr. Dwarikanath Ratha
Professor
Department of Civil Engineering
TIET, Patiala, India

ACKNOWLEDGEMENT

First and foremost, I wish to express my immense sense of gratitude to my supervisors, ***Prof. Amit Dhir****, Professor, School of Energy and Environment, Thapar Institute of Engineering and Technology (TIET), Patiala, India, and* ***Prof. Dwarikanath Ratha****, Professor, Department of Civil Engineering, TIET, Patiala, India for their continuous support in my Ph.D. study and related research. I appreciate all his time, ideas, motivation, knowledge, and funding contributions to make my Ph.D. experience productive and stimulating.*

I express my heartfelt gratitude to ***Prof. Padmakumar Nair****, Director, and* ***Prof. Prakash Gopalan****, Former-director, TIET, Patiala, for providing me the opportunity to work in this esteemed organization. Without their precious support, conducting this research would not be possible. I feel special gratitude towards* ***Prof. N Tejo Prakash****, Dean of Research and Development Cell, and* ***Prof. Rafat Siddique,*** *Former-Dean Research and Sponsored Projects, TIET, Patiala, India, for their valuable guidance and support during my research work.*

The cooperation and help extended by the ***Head, Faculty Members, Lab Technician,*** *and* ***Departmental staff*** *of the School of Energy and Environment and Department of Civil Engineering, TIET, Patiala, is gratefully acknowledged.*

I have had the pleasure of associating with the members of the Doctoral Committee, ***Prof. N. Tejo Prakash, Dr. Anoop Verma,*** *and* ***Dr. Tapas Karmaker,*** *with whom I have had many fruitful discussions, academic and otherwise. Their encouragement is greatly acknowledged.*

A modeling / experimental research program generally poses many hurdles at various stages. In my daily work, I have been blessed with friendly and cheerful lab mates who have made this adventure at Enviro-energy Research Lab at TIET, Patiala, truly a time I will never forget. It has been very helpful to have technical and general discussions with ***Dr. Himanshu Sharma, Bimalpreet Singh, Dr. Ina Thakur, Sheetal Sethi, Shelly Tiwari, Dr. Pali Rosha, and Prabhdeep Brar****.*

I wish to acknowledge the data provided by ***Indian Meteorological Department (IMD) Pune, Socioeconomic Data and Applications Center (SEDAC), United States Geological Survey (USGS), Oak Ridge National Laboratory Distributed Active Archive Center (ORNL DAAC) and Census India*** *for available the data used for the study,*

I want to thank my family for all their love and encouragement. For my parents, who have raised me with love and supported me in all my pursuits. I am also grateful to my other family members and friends who have supported me along the way. I have been blessed with my uncle, ***Mr. Bidya Sagar Gorain,*** *who has motivated me throughout my whole career. His guidance and motivation are highly acknowledged.*

I would like to give special thanks and love to my wife, ***Mrs. Sonali Kumari****, who has stood by me throughout my Ph.D. career with her love, care, and unfailing support.*

Finally, I thank one and all who have directly and indirectly helped me throughout this work and made this duration happy and memorable.

Above all, I owe it all to the Almighty God for granting me the wisdom, health, and strength to undertake this research task and enabling me to its completion.

Sanjoy Gorai
(901714004)

ABSTRACT

Flooding, among other natural disasters that can also be called anthropogenic, is the most frequent and devastating. Flooding over an area depends on rainfall and geomorphological, climatic, and social factors. From 1900 – 2021, approximately 5593 flood events occurred worldwide, out of which 66% occurred after 2000. In the Asian continent, 2324 flood events occurred during 1900-2021. In the Asian continent, 13.5% of the total Asian flood occurred in India, followed by China (13.3%), Indonesia (10.6%), Philippines (6.7%), Pakistan (4.6%), Afghanistan (4.2%), Bangladesh (4.1%) and other countries. The decadal economic losses in India found to be $0.1billion during 1960-1969, $1.6 billion during 1970-1979, $4.0 billion during 1980-1989, $9.5 billion during 1990-1999, $16.8 billion during 2000-2009, $41.2 billion during 2010-2019 and 13.6 billion during 2020-2021. Floods in India have majorly occurred in the well-known river basins of India such as Ganga, Brahmaputra, Yamuna, Mahanadi, Testa, Kosi, Cauveri, Narmada, Tapi, Krishna, etc. Studies of flood hazard and vulnerability has been conducted widely in large river basins or at the regional level. Less or no attention has been given to the small river basins. Ghaggar River Basin is one of the small basins located in northern India and sub-basins of the Indus River basin. Several flood events of different intensities have occurred in this river basin. However, the 1993 flood event was the most devasting flood in the basin. This study aims to determine the rainfall trend analysis and extreme rainfall events in the study area. This study focussed on analyzing flood zones in the Ghaggar River basin using rainfall trends and extreme rainfall as flood factors. The impact of change in land use land cover in urbanisation on flooding over an area has been analyzed, and future flood maps have been projected. The dataset used for this study was collected from different sources. Software such as ArcGIS, Terrset Idrisi, SPSS, R, and Climdex were used to analyze these datasets.

The descriptive statistics of monthly, seasonal, and annual rainfall were analyzed. The average rainfall ranges from 1.8 – 551.6 mm monthly, 7.6 – 1421mm seasonal, and 266.7 – 1703.2mm annually. The rainfall trend analysis was analyzed using the Mann-Kendall (MK) test and Innovative Trend Analysis (ITA) method and compared with the results. The serial correlation from the data was removed before the trend was analyzed using the MK test. 90% of the monthly, 85% of the seasonal, and 91% of the annual results were found to have similar trend direction on both MK test and ITA method. The trend slope, i.e., change in the amount of

rainfall, lies in the range of (-)9.4 – 5.65mm/year monthly, (-)17.02 – 7.21mm/year seasonal, and (-)23.09 – 4.93 mm/year annually. The annual rainfall trend is increasing at the highest rate at Lehal, whereas the decreasing rate at the highest rate at Banur region. The change point of rainfall trend was analyzed using Pettit's test, Standard Normality Homogeneity test, and Buishand's test. The change point was assumed where the two or more method shows a similar changepoint. The average rainfall lies in the 379.4 – 2223.2mm range before the change point, decreasing to 53.4 – 1470.9mm after the change point. After the change point, the average rainfall decreases at all stations except the Lehal. The trend magnitude of rainfall was (-)13.62 – 94.95mm/year before the change point, which decreased to (-) 43.9 – 23.35 mm/year after the change point. The rainfall trend has been observed to decrease after the change point.

Extreme rainfall was analyzed using Expert Team on Climate Change Detection Indices (ETCCDI), and ten indices were analyzed using Climdex software in R. The trend analysis of these indices was analyzed using the MK test and ITA method. The average CDD (Consecutive Dry Days) was found to be in the range of 69.5 – 223.2 days, whereas the average CWD (Consecutive Wet Days: wet days are when the rainfall for the day is 1mm or more) was found to be 3.4 – 9.6 days a year. The trend magnitude of CDD and CWD varies in the range of (-)2.97 – 24.97 days/year and (-)0.714 – 0.093 days/year, respectively. The total precipitation on wet days (PRCPTOT) varies in the range of 69.5 – 1828.6mm, and the trend magnitude changes in the range of (-)35.53 – 21.45 mm/year. The simple daily precipitation intensity index (SDII) lies in the range of 16.3 – 26.9 mm, and the trend magnitude of SDII lies in the range of (-)1.391 – 1.276 mm/year. R10mm, R20mm, and R30mm are the days received 10mm, 20mm, and 30mm of rainfall, respectively. The number of days for R10mm, R20mm, and R30mm lies in the range of 9.8 – 42.4, 5.9 – 27.5, and 3.6 – 19.2, respectively, and their trend magnitude lies in the range of (-)1.944 – 0.023 days/year, (-)0.805 – 0.116 days/year and (-)0.611 – 0.280 days/year respectively. The average rx1day, rx3day, and rx5day in the Ghaggar River basin lie in the range of 66.4 – 160.3 mm, 100.2 – 252.4 mm, and 114.2 – 311.3 mm, respectively, whereas the trend magnitude lies in the range of (-)2.803 – 6.011 mm/year, (-)4.73 – 9.25 mm/year and (-)3.898 – 9.688 mm/year respectively.

Flood risk was analyzed using Graph Theory and Analytical Hierarchy Process (AHP). The flood risk was analyzed by integrating flood hazard and flood vulnerability analysis. The factors used for flood hazard analysis are Elevation, Land Use Land Cover (LULC), Hydrologic Soil Groups (HSGs), Rx3day, and Distance from rivers and slopes. The factors used for flood vulnerability analysis are Population density, LULC, Household Density,

Distance from roads, literacy rate, Efficient drainage system, Distance from flood shelters, and Rainfall trend. The flood zones have been classified into five categories: very low, low, moderate, high, and very high, based on the score obtained from Graph Theory and the AHP method. It is observed from Graph theory results that around 29.8% of the basin area is prone to very high flood hazard, whereas 70.1% of the basin area is prone to high flood hazard. Similarly, around 17.4% of the basin area is prone to highly vulnerable to flood, whereas 82.5% of the basin area is prone to moderately vulnerable to flood. The flood hazard analysis using AHP methods shows that around 14.54% (2033.5 km^2) and 85.2% (11922.7 km^2) of the basin area lie under the high and very high categories of flood hazard, respectively. Around 0.15 % of the basin area (21.3 km^2) is observed under the moderate flood hazard category. 4.4% (620.7 km^2), 93.25% (13035.2 km^2), and 2.3% (322 km^2) of the basin area lying under the moderate, high and very high categories of flood vulnerability, respectively. The flood risk of the Ghaggar River basin varies from moderate to very high category. But, most of the basin, i.e., 94.1% (13165.2 km^2), is at high risk of flood, whereas only 5.52% (771.6 km^2) is at very high risk of flood. The basin areas under moderate risk of flooding were observed to be 0.2% (41.09 km^2). Both methods' results are compared, and high flood risk zone was obtained through graph theory and AHP.

Flood risk was also analyzed considering dynamic factors of urbanisation and population density changes and projection flood map based on the urbanisation and population density change map. Urbanization was analyzed using the LULC change analysis using the Land Change model. The LULC map of 2001 and 2010 was used to analyze LULC and predicted for 2019 to validate with the actual 2019 LULC map. The LULC map for 2030 is projected from the model. The urban built-up category of LULC has gained 8.59 sq. km of its area from Savannas (82.51%), grasslands (2.45%), and croplands (15.03%) during the 2001-2010 transition. The urban built-up of the study area was 450.72 sq. km in 2010 and increased by 8.68 sq. km in 2010, 14.97 sq. km in 2019, and 10.42 sq. km in both 2030 and 2040. The population density changes are analyzed directly using the rate of changes in density as per Macrotrends change rate. Ghaggar River basin's actual and predicted average population density is 457, 499, 549, and 582 per sq. km for 2011, 2019, 2030, and 2040, respectively. The flood hazard and vulnerability zone of the Ghaggar River basin, considering Urbanisation and population density changes, was analyzed using the AHP method and flood maps were projected for 2019, 2030, and 2040. The flood hazard analysis using urbanisation and population density changes shows that the high flood hazard zone increases with time from low and moderate hazard zone. The area under high and very high flood-vulnerable zones is

increasing with respect to time, and the area under moderate zones is decreasing. The moderate flood risk decreases, and the high flood risk zone increases with time. The area of flood hazard, vulnerability, and risk from the lower category to the upper category has been directly correlated with increased urbanization.

Keywords:

Rainfall Trend Analysis, Extreme Rainfall Analysis, Change Point analysis, ETCCDI, Analytical Hierarchy Process, Graph Theory, Floor risk analysis, Flood Hazard Analysis, Flood Vulnerability Analysis, Geospatial Analysis, Urbanisation, Land Change Model.

LIST OF FIGURES

Figure 1.1 Classification of floods (6) 3
Figure 1.2 Number of floods reported (a) worldwide (b) Asia and (c) India (7,8) 4
Figure 2.1 Vulnerability of flood on human, economic and material (15–23,35) 10
Figure 2.2 Keywords found articles in different journal for the period of 2010- 2020 (12) ... 11
Figure 2.3 No of studies reviewed for different countries 11
Figure 2.4 Mechanism of Urban Flooding 13
Figure 2.5 Flood modelling techniques 15
Figure 3.1 Flood inundated area of Ghaggar river basin during 2010 Punjab flood dated 14th July 2010 (Source: Bhuvan Disaster Services inundation map) 38
Figure 3.2 Study area of Ghaggar river basin in India 40
Figure 3.3 Methodology flow chart for watershed delineation and stream link 40
Figure 3.4 Individual digital elevation model used for watershed delineation (toposheet number wise) 42
Figure 3.5 Combined DEM of all DEM dataset 42
Figure 3.6 Fill map after removal of sinks or depressions from DEM 43
Figure 3.7 Flow direction map executed from fill map of DEM 44
Figure 3.8 Basin map executed from flow direction map 45
Figure 3.9 Polygon of basin executed from the basin raster 46
Figure 3.10 Study area basin, i.e., Ghaggar river basin clipped from the basin polygon 46
Figure 3.11 Flow accumulation map executed from flow direction raster 47
Figure 3.12 Reclassified flow accumulation raster of Ghaggar River basin 48
Figure 3.13 Stream link raster of Ghaggar river basin 49
Figure 3.14 Stream polyline of Ghaggar river basin 49
Figure 3.15 Stream order raster of Ghaggar river basin 50
Figure 3.16 Stream order polyline of Ghaggar river basin 50
Figure 3.17 Elevation profile of Ghaggar river basin. 52
Figure 3.18 Area under different elevation of Ghaggar river basin 52
Figure 3.19 Slope map of Ghaggar river basin 53
Figure 3.20 Land use land cover map of Ghaggar river basin for the year 2019 55
Figure 3.21 Hydrologic soil group of Ghaggar river basin 56
Figure 3.22 Population density of Ghaggar river basin 57

Figure 3.23 Tehsil wise household density of Ghaggar river basin.....58
Figure 3.24 Tehsil wise literacy rate of Ghaggar river basin.....58
Figure 3.25 Road connectivity map in the Ghaggar river basin 59
Figure 4.1 Innovative trend analysis methodology.....62
Figure 4.2 Spatial analysis of monthly (January - June) average rainfall in Ghaggar river basin 69
Figure 4.3 Spatial analysis of monthly (July - December) average rainfall in Ghaggar river basin 70
Figure 4.4 Spatial analysis of seasonal average rainfall in Ghaggar river basin 72
Figure 4.5 Spatial analysis of annual average rainfall in Ghaggar river basin 74
Figure 4.6 Spatial analysis of monthly (January - June) average rainfall trend slope using ITA method in Ghaggar river basin.....78
Figure 4.7 Spatial analysis of monthly (July - December) average rainfall trend slope using ITA method in Ghaggar river basin 79
Figure 4.8 Spatial analysis of seasonal average rainfall trend slope using ITA method in Ghaggar river basin.....81
Figure 4.9 Spatial analysis of annual average rainfall trend slope using ITA method in Ghaggar river basin.....81
Figure 4.10 Bar chart comparison of average annual rainfall of before and after change point 84
Figure 4.11 Spatial analysis of average annual rainfall before and after change point in the Ghaggar river basin.....84
Figure 4.12 Bar chart of comparison of average annual rainfall trend slope before and after change point in the Ghaggar river basin 85
Figure 4.13 Spatial analysis of average annual rainfall trend slope before and after change point in the Ghaggar river basin.....86
Figure 5.1 Bar chart comparison of average of CDD, CWD, PRCPTOT, r10mm, r20mm, and r30mm, rx1day, rx3day, rx5day and SDII 92
Figure 5.2 Spatial map of average extreme rainfall indices (CDD, CWD, PRCPTOT, R10mm, R20mm and R30mm).....93
Figure 5.3 Spatial map of average extreme rainfall indices (rx1day, rx3day, rx5day and SDII) 94
Figure 6.1 Methodologies applied for the study 99
Figure 6.2 Tree diagram of flood risk analysis 100
Figure 6.3 Digraph of flood hazard and flood vulnerability sub-system.....102

Figure 6.4 Flood Hazard, flood vulnerability and flood risk zoning of Ghaggar River basin using Graph Theory 114

Figure 6.5 Flood hazard, flood vulnerability, and flood risk zoning of Ghaggar river basin using AHP 117

Figure 6.6 Flood hazard, vulnerability and risk classification of Ghaggar river basin using graph theory. 119

Figure 7.1 Methodology for land change modeler.....122

Figure 7.2 Rank classified spatial map of the indicators 125

Figure 7.3 LULC of 2001, 2010, 2019, 2030, and 2040.....126

Figure 7.4 (a) Gain and losses of LULC in sq. km between 2001 and 2010; and (b) contribution to the net change in urban built up in sq. km 128

Figure 7.5 Bar chart of area for different LULC categories in the different periods.....129

Figure 7.6 Population density spatial map for the years 2011, 2019, 2030, and 2040 130

Figure 7.7 Percentage of area occupied different ranks population density in different periods 131

Figure 7.8 Spatial flood hazard map of the study basin in different periods 133

Figure 7.9 Spatial flood vulnerability map of the study basin in different periods 134

Figure 7.10 Spatial flood risk map of the study basin in different periods.....134

LIST OF TABLES

Table 1.1 Flood type classification based on the damages (6) 3

Table 1.2 Historical flood events in the Ghaggar river basin (10,11).....6

Table 2.1 List of Journals with number of articles reviewed.....12

Table 2.2 Model used for Flood or Urban flood risk analysis used in literature studies.....17

Table 2.3 Thematic layers or factor used in literature for flood risk analysis 21

Table 2.4 List flood vulnerability and flood hazard factors (93,123,212).....26

Table 2.5 List of dynamic and static factors.....27

Table 2.6 Trend analysis methodologies used in literatures.....29

Table 2.7 Details of rainfall indices by ETCCDI 32

Table 3.1 State, Districts, and Tehsils located in the Ghaggar river basin 39

Table 3.2 Dataset details of Digital Elevation Model (Source: Bhuvan) 41

Table 3.3 LULC dataset details 54

Table 3.4 Land use land covers (2019) category and its area.....55

Table 4.1 Monthly average of rainfall for different station of Ghaggar river basin 68

Table 4.2 Monthly standard deviation in rainfall for different station of the Ghaggar river basin 71

Table 4.3 Monthly coefficient of variance in rainfall for different station of the Ghaggar river basin 71

Table 4.4 Seasonal descriptive statistics of rainfall for different stations of the Ghaggar river basin (Unit: Mean – mm, SD- mm, CV - %).....73

Table 4.5 Annual descriptive statistics of rainfall for different stations of the Ghaggar river basin 74

Table 4.6 Presence of serial correlation in the monthly, seasonal and annual rainfall dataset of Ghaggar river basin.....75

Table 4.7 Magnitude of monthly rainfall trend analyzed using Sen Slope (SS) estimator and Innovative Trend Analysis (ITA) (* - significant at level of significance 0.05) 77

Table 4.8 Magnitude of seasonal and annual rainfall trend analyzed using Sen Slope (SS) estimator and Innovative Trend Analysis (ITA).....80

Table 4.9 Change point in number of years and represented years 82

Table 4.10 Descriptive statistics of average annual rainfall for different stations of the Ghaggar river basin before and after change point.....83

Table 4.11 Trend magnitude of average annual rainfall for different stations of the Ghaggar river basin before and after change point.....85

Table 5.1 ETCCDI extreme rainfall indices 87

Table 5.2 Mean, standard deviation (SD) and coefficient of variation (CV) of all extreme rainfall indices.....90

Table 5.3 Presence of serial correlation in extreme rainfall indices dataset of Ghaggar river basin 95

Table 5.4 Trend magnitude value of extreme rainfall events 96

Table 6.1 Qualitative measure of a system or sub-system used for flood risk analysis. 103

Table 6.2 Level of the interaction and their corresponding weightage for flood risk analysis. 104

Table 6.3 Importance scale of AHP model (193). 107

Table 6.4 RI values for the different order of the matrix (n) (193) 108

Table 6.5 Classification of various factors and their respective weights considered for flood hazard sub-system.....108

Table 6.6 Classification of various factors and their respective weights considered for flood vulnerability sub-system 109

Table 6.7 Flood zone classifications concerning its value.....110

Table 6.8 Level of interaction between the sub-subsystems of flood hazard sub-system 111

Table 6.9 Level of interaction between the sub-subsystems of flood vulnerability sub-system 111

Table 6.10 Comparison Matrix of each parameter of Flood hazard.....115

Table 6.11 Comparison Matrix of each parameter of flood vulnerability 116

Table 6.12 Normalized pair-wise comparison matrix of flood hazard 116

Table 6.13 Normalized pair-wise comparison matrix of flood vulnerability 116

Table 6.14 Comparison table of AHP and graph theory results 118

Table 7.1 Ranks relating to flood risk of different indicators.....123

Table 7.2 Classification of indicators and their respective ranks considered for flood risk analysis.....124

CONTENTS

DECLARATION i
CERTIFICATE ii
ACKNOWLEDGEMENT iii
ABSTRACT v
Keywords: viii
LIST OF FIGURES ix
LIST OF TABLES xii
CONTENTS xiv
NOMENCLATURE xviii
CHAPTER 1 1
1. Introduction 1
1.1. General 1
1.2. Classification of Floods 2
1.3. Problem statement 3
1.4. Objectives of the Study 6
1.5. Organization of Thesis 7
CHAPTER 2 9
2. Literature Review 9
2.1. General 9
2.2. Flooding over an area 9
2.3. Study on Flood Analysis 10
2.4. Mechanism and result of urban flooding 13
2.5. Flood model review 14
2.6. Flood modelling techniques used in literatures 16
2.7. Factors responsible for flood analysis 20
2.8. Rainfall trend analysis 27
2.8.1. Rainfall Trend Analysis throughout the World 28
2.8.2. Availability and type of Data 28
2.8.3. Methodology used for rainfall trend analysis 28
2.8.4. Rainfall trend analysis throughout the world 30
2.9. Extreme rainfall analysis 31

2.10. Urbanisation analysis 33
2.10.1. LULC changes analysis 33
2.10.2. Methodology used for LULC change analysis 34
2.11. Research Gaps 35
CHAPTER 3 37
3. Study Area 37
3.1. Flood history of the Ghaggar river basin 37
3.2. Overview of the Ghaggar river basin 38
3.3. Watershed delineation and stream link 40
3.3.1. DEM Acquisition 40
3.3.2. Combining all DEM 41
3.3.3. Fill sinks 43
3.3.4. Flow Direction 43
3.3.5. Basin formation 44
3.3.6. Basin Raster to Polygon 45
3.3.7. Clipping of basin 45
3.3.8. Flow accumulation 46
3.3.9. Reclassification of flow accumulation 47
3.3.10. Stream link 48
3.3.11. Stream Polyline 48
3.3.12. Stream order 49
3.3.13. Drainage Area 51
3.3.14. Watershed length 51
3.4. Elevation 51
3.5. Slope of the watershed 52
3.6. Climate 53
3.7. Land use land cover 54
3.8. Soil group 56
3.9. Population density 56
3.10. Household Density 57
3.11. Literacy rate 57
3.12. Road connectivity 58
3.13. Concluding Remarks 59

CHAPTER 4 60
4. Rainfall Analysis 60
4.1. Methodology 60
4.1.1. Segregation of Data 60
4.1.2. Descriptive Statistics 60
4.1.3. Rainfall Trend analysis 61
4.1.4. Change point analysis 65
4.1.5. Areal estimation of Rainfall 67
4.2. Descriptive Statistics 67
4.2.1. Monthly Analysis 67
4.2.2. Seasonal Analysis 71
4.2.3. Annual analysis 73
4.3. Trend Analysis 75
4.3.1. Monthly Trend Analysis 76
4.3.2. Seasonal Analysis 79
4.3.3. Annual analysis 81
4.4. Annual Change point analysis 82
4.4.1. Change point year 82
4.4.2. Descriptive statistics before and after change point 83
4.4.3. Trend analysis before and after change point 84
4.5. Concluding Remarks 86
CHAPTER 5 87
5. Extreme Rainfall Analysis 87
5.1. Methodology 87
5.2. Descriptive Statistics of Extreme rainfall indices 89
5.2.1. CDD and CWD 89
5.2.2. PRCPTOT 89
5.2.3. R10mm, R20mm and R30mm 93
5.2.4. rx1day, rx3day and rx5day 94
5.2.5. SDII 94
5.3. Trend analysis of Extreme rainfall indices 95
5.3.1. CDD and CWD 97
5.3.2. PRCPTOT 97

5.3.3. R10mm, R20mm and R30mm 97
5.3.4. rx1day, rx3day and rx5day 97
5.3.5. SDII 98
5.4. Concluding remarks 98
CHAPTER 6 99
6. Classification of Flood Zone 99
6.1. Methodology 99
6.1.1. Flood risk analysis using Graph theory 100
6.1.2. Analytical Hierarchy Process (AHP) for Flood risk mapping 106
6.2. Classification flood factors for flood analysis 108
6.3. Flood zone classification 109
6.4. Results and Discussion 110
6.4.1. Identification of flood risk zone of Ghaggar river basin using graph theory 110
6.4.2. Identification of flood risk zone of Ghaggar river basin using AHP 114
6.4.3. Comparison of the results obtained by these two methods 118
6.5. Concluding Remarks 120
CHAPTER 7 121
7. Urbanisation and Climatic Factor Impact on Flood 121
7.1. Methodology 121
7.1.1. Land Change Model 121
7.1.2. Ranks of the indicators 123
7.2. Results and Discussion 125
7.2.1. LULC change analysis 125
7.2.2. Population density change analysis 130
7.2.3. Flood risk analysis 131
7.2.4. Inferences 135
CHAPTER 8 137
Conclusion 137
Future Recommendation 142
Reference 143

NOMENCLATURE

1D	:	1 Dimensional
2D	:	2 Dimensional
3D	:	3 Dimensional
AHP	:	Analytical Hierachy Proces
ANN	:	Artificial Neural Network
C	:	HSG-C: moderately high runoff potential (<50% sand and 20-40% clay)
C/D	:	HSG-C/D: high runoff potential unless drained (<50% sand and 20-40% clay
CA Model	:	Celluar Automata Model
CDD	:	Consecutive Dry Days (rainfall<0.1mm)
CI	:	comprehensive meteorological drought index
CRED	:	Centre for Research on the Epidemiology of Disasters
CV	:	Coefficient of Variance
CWD	:	Consecutive Wet Days (rainfall>1mm)
D	:	HSG-D: high runoff potential (<50% sand and >40% clay)
D/D	:	HSG-D/D: high runoff potential unless drained (<50% sand and >40% clay)
DEM	:	Digital Elevation Model
EM-DAT	:	Emergency event database
ETCCDI	:	Expert Team on Climate Change Detection and Indices
GIS	:	Geological Information System
HEC - RAS	:	Hydrologic Engineering Center's River Analysis System
HEC-HMS	:	Hydrologic Engineering Center's Hydrologic Modeling System
HSG	:	Hydrologic Soil Group
IGBP	:	International Geosphere-Biosphere Programme
IMD	:	Indian Meteorological Department
ITA	:	Innovative Trend Analysis
KNN	:	K-Nearest Neighbors
LCM	:	Land Change Model
LRA	:	Linear Regression Analysis

LULC	:	Land Use Land Cover
MIKE SHE	:	MIKE Système Hydrologique Européen
MK	:	Mann-Kendall
MMK	:	Modified Mann-Kendall test
MODIS	:	Moderate Resolution Imaging Spectroradiometer
NDVI	:	Normalised Difference Vegetation Index
PDSI	:	Palmer drought Severity Index
Post Monsoon	:	October - December
PRCPTOT	:	Total Precipitation in Wet days
Pre-monsoon Season	:	March - May
R10mm	:	No of days having rainfall >10mm
R20mm	:	No of days having rainfall >20mm
R30mm	:	No of days having rainfall >30mm
RF	:	Random Forest
rx1day	:	1 Day maximum rainfall
rx3day	:	Consecutive 3 days maximum rainfall
rx5day	:	Consecutive 5 days maximum rainfall
SD	:	Standard Deviation
SDII	:	Simple Daily Precipitation Index
SEDAC	:	Socioeconomic Data and Applications Center
SNH	:	Standard Normal Homogeneity
Southwest Monsoon	:	June - September
SPI	:	Standardized Precipitation Index
SS Estimator	:	Sen Slope Estimator
SVM	:	Support Vector Machine
SWAT	:	Soil & Water Assessment Tool
SWE	:	Swallow Water Equation
SWMM	:	Storm Water Management Model
TFPW	:	Trend-Free Pre-Whitened
WCRP	:	World Climate Research Program
Winter Season	:	January - February
WMO	:	World Meteorological Organization

CHAPTER 1

1. Introduction

1.1. General

Water is a colourless and odourless substance vital for all the species living on the earth's surface. 70.9% of the total earth surface area is covered by water in different natural states such as gaseous, liquid, and solid or mixtures. Only 3% of available water is freshwater, as 97% of the earth's water is saline (ocean). Freshwater is further categorized as ice/glaciers (68.7%), groundwater (30.1%), surface water such as lakes, rivers, streams, etc. (0.3%), and other sources (0.9%) (1). Water serves as a vital element not just for sustaining life, but also for promoting immediate well-being and optimal health (2). Even, the Sustainable development is not possible without freshwater of adequate quantity and quality (3). The continuous balance of these water bodies is maintained by the water cycle. The water cycle is the prolonged water change within the earth's surface and atmosphere. The liquid forms of water from the earth's surface evaporate into water vapours as the temperature increases and accumulates in the atmosphere. Condensation of this water vapour again fell to the earth's surface as precipitation and balanced the water cycle. However, climate change interrupts the water cycle and misbalance the water cycle. The water cycle's interruption leads to hydro-meteorological natural disasters such as drought (due to less or no rainfall) and flood (due to extreme rainfall). The earth's surface temperature increases due to climate changes, leading to more water evaporation. According to the Paris Climate Agreement, global warming should be held below 2 °C, preferably under 1.5 °C (4).The warmer air can hold more water vapour and fall at higher intensity, as extreme rainfall events lead to floods. At the same time, some areas become dry, and the soil becomes dry out of water due to lack of precipitation over a long time. After a more extended period, the precipitation in those areas is drained to the stream or river due to the hard ground surface, and the soil remains dry. Therefore, floods and drought are natural disasters that significantly challenge the earth's surface.

Flooding, among other natural disasters that can also be called an anthropogenic disaster, is the most frequent and devastating. A natural disaster is a natural phenomenon such as flood, earthquake, drought, tsunami, cyclone, landslide, volcanic eruption, etc., whereas an anthropogenic disaster is a human-influenced disaster such as war, accidents, fires, terrorist attacks, nuclear explosions, etc. The increasing development worldwide is increasing the

possibilities of rapid climate change, unplanned rapid urbanization, increasing population, etc., which converts the number of natural disasters into anthropogenic disasters, and flooding is one of them. The flood frequency is often higher than other disasters such as earthquakes, forest fires, droughts, typhoons, and heavy snowfall (5).

Floods occur due to extreme rainfall, whereas droughts occur due to lack of rainfall for longer. So, the time scale for flood disasters is less, and drought is longer. The flood needed immediate action as the occurrence is sudden, and the impact of the flood is devastating on the lives and property. The drought occurs slowly, and the impact on lives and property is less. However, the agriculture of an area is highly affected due to droughts. The occurrence period and impact of water-related natural disaster floods are more devastating and frequent. The hydrological variability resulting floods stems primarily from climate change, population expansion, increased living standards, and disparities in water distribution (6). Therefore, risk analysis and management of flood disasters is imperative.

Flooding over an area depends not only on rainfall but also on geomorphological, other climatic factors, and social factors, etc. These factors can be static or dynamic. Static factors are constant over the period, whereas dynamic factors are changed with respect to time. Dynamic factors highly influencing the flood are rainfall trends, extreme rainfall, land use, land cover changes to impervious surfaces, population density, etc.

1.2. Classification of Floods

Flood over an area is classified into different categories based on location, duration, management, damages, etc. (Figure 1.1). Slow-onset flood last for longer periods and causes damage to crops, roads, etc. A rapid-onset flood is a rapidly generated flood that lasts for a shorter period. The impact of the rapid-onset flood is higher as the time for taking appropriate measures is less. Flash flood occurs within a few minutes to a few hours based on the frequency of extreme rainfall and has a broad impact. Coastal flood occurs in coastal areas due to natural phenomena such as tropical storms, earthquakes, giant tides, etc. River flood is the flood over the river beds due to an increase in the flow depth from the normal flow depth. Urban flood occurs due to stormwater accumulation due to impervious areas and an efficient drainage system in urban areas. Normal floods occur naturally, whereas abnormal floods occur due to extreme rainfall and poor watershed management. Damage-based classification of the flood has been classified into Class 1-5 floods, as defined in Table 1.1 (7).

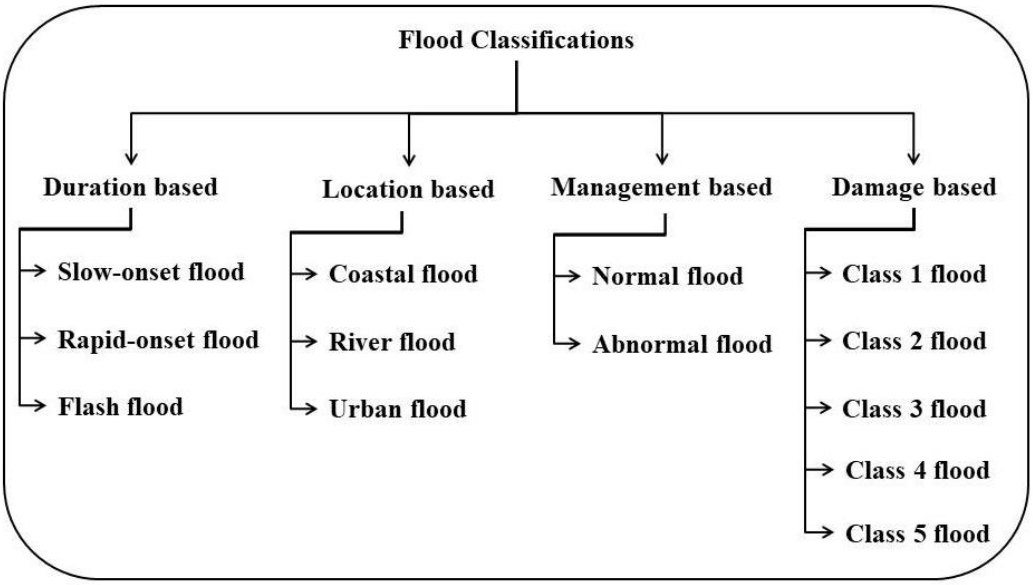

Figure 1.1 Classification of floods (7)

Table 1.1 Flood type classification based on the damages (7)

Flood Class	Type of Hazard	Impact of flood
Class 1	Moderate floods	Inconsiderable material loss
Class 2	High floods	Considerable material loss
Class 3	Extraordinary floods	Very large material loss
Class 4	Disastrous floods	Extreme damages
Class 5	Historical floods	Severe Damages

1.3. Problem statement

Emergency Events Database (EM-DAT) managed by the Centre for Research on the Epidemiology of Disasters (CRED), Belgian have reported 5593 flood events across the world during 1900-2021 out of which 66% of flood occurred from 2000 onwards whereas only 34% occurred during 1900-1999(8). In the last 22 years (2000-2021), 3661 floods occurred, of which 1725 occurred during 2000-2009, 1533 occurred during 2010-2019, and 403 occurred during 2020-2021. Worldwide, 7% of total floods have been reported in the last two years. Figure 1.2 shows the line chart of floods from 1901-2021. It indicates that the flood pattern has changed worldwide from 1990 onwards. Floods have caused estimated total losses of $923 billion during 1900-2021. However, the highest economic losses of $391 billion have been reported during 2010-2019, whereas it was $166 billion during 2000-2009 and $211 billion

during 1990-1999. However, $92 billion in losses have been reported in the last two years. Therefore, it will be easy to predict that the losses due to floods will increase rapidly as the number of flood events increases.

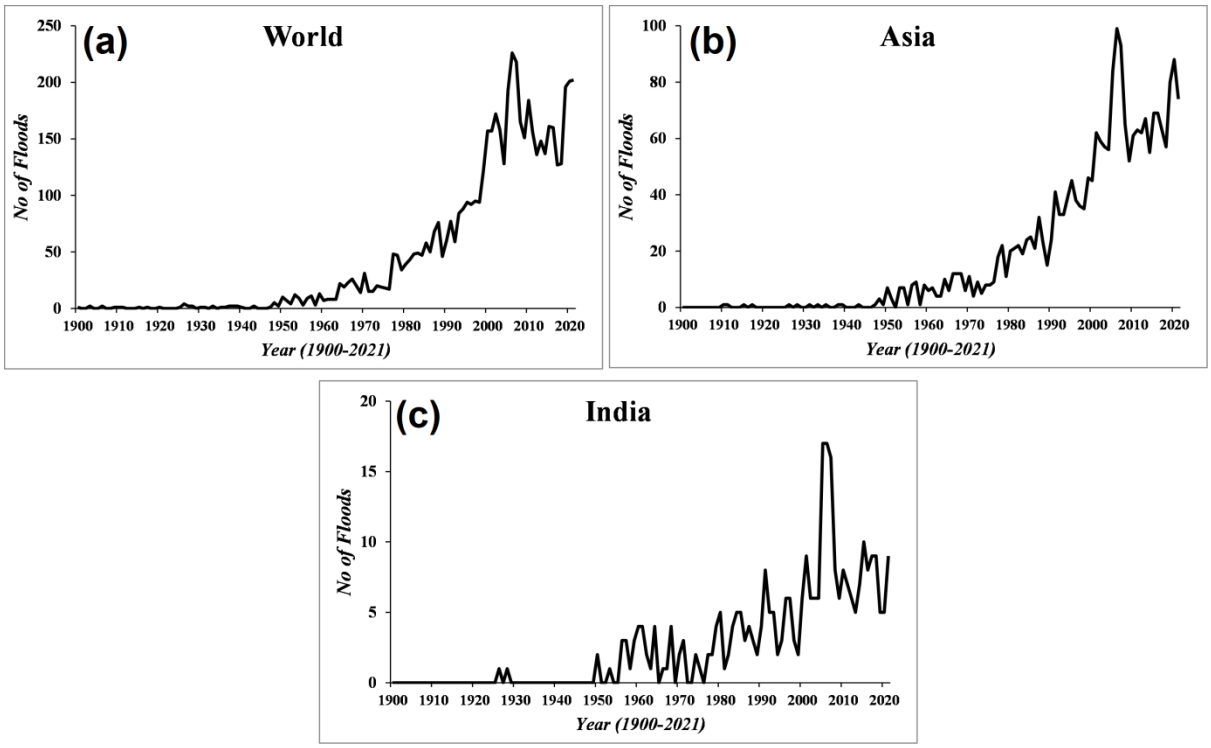

Figure 1.2 Number of floods reported (a) worldwide (b) Asia and (c) India (8,9)

The flood events in the continent have been recorded highest in Asia (41.6%), followed by America (23.0%), Africa (20.6%), Europe (12.1%) and Oceania (2.8%). In Asia, 2324 flood events have occurred during 1900-2021. Figure 1.2(b) shows the line chart of flood events from 1900-2021, indicating that the flood events are rapidly increasing from 1980 onwards. Jonkman (2005) has reported that the most severe river floods occur in Asia as more persons were died and affected (10). The economic loss in Asia is approximately 64% ($591 billion) of the total economic loss worldwide. The highest economic loss of $264 billion occurred from 2010-2019, followed by $143 billion from 1990-1999 and $77 billion from 2000-2009.

In the Asian continent, 13.5% of total Asian floods occurred in India, followed by China (13.3%), Indonesia (10.6), Philippines (6.7), Pakistan (4.6%), Afghanistan (4.2%), Bangladesh (4.1%) and other countries. The flood events in India and found that flood events have been increasing rapidly from 1990 onwards (Figure 1.2c). The National Flood Commission of India reported that about 40-million-hectare area, or 12% of India's geographical area, is vulnerable to flooding (National Flood Commission, 1980). Ministry of Water Resources, India, reported

that 3.19 million of the Indian population is affected by floods annually. No such year was found without any flood events in India after 1955. India has accounted for $86.8 billion, i.e., 14.6% of Asia's and 9.4% of the world's economic losses. The decadal analysis of economic losses found increasing in each decade. The decadal economic losses in India were $0.1billion during 1960-1969, $1.6 billion during 1970-1979, $4.0 billion during 1980-1989, $9.5 billion during 1990-1999, $16.8 billion during 2000-2009, $41.2 billion during 2010-2019 and 13.6 billion during 2020-2021. The economic losses become twice that of the previous decade in each decade. Monsoonal rain, heavy rain, torrential rain, early monsoonal rain, incessant rain, hailstorms, tropical cyclones, excessive rainfall, long-term rainfall, etc., are the origin of the flood. However, rainfall is the water source, whereas other factors such as elevation, slope, LULC, soil group, population density, etc., control water accumulation.

Floods in India have majorly occurred in the well-known river basins of India such as Ganga, Brahmaputra, Yamuna, Mahanadi, Testa, Kosi, Cauveri, Narmada, Tapi, Krishna, etc., and study of flood hazard and vulnerability has been conducted widely. Different Indian Government Agencies such as the Department of Science and Technology, Ministry of Environment, Forest and Climate Change, Ministry of Home Affairs, etc., are keenly interested in the well-known basin. Less or no attention has been given to the small river basins. Climate change and urbanisation throughout the country threaten the small river basin flooding. Therefore, the study of flood analysis is also important to conduct on small river basins to mitigate future flood risk and post-flood losses.

Ghaggar River Basin is one of the small basins located in northern India and sub-basins of the Indus River basin. Ghaggar river basin originated at Shivalik Himalaya of Himachal Pradesh and flows through Punjab and Haryana state to Rajasthan. This region belongs to a highly fertile agricultural zone, and most people in this basin depend on agriculture. The agriculture of this area continues throughout the year, and wheat, rice, maize, sugar cane, potato, and mustard seeds are the major crops of this basin. Ghaggar River basin is highly prone to flooding, and numerous high, moderate, and low-intensity flood events occurred (Table 1.2). Crop damages, live losses of humans and cattle, property damages, and economic losses are the effects of floods in the basin. The last high-intensity flood occurred in 2010. Approximately 7 lakh people of 1713 villages from Punjab and Haryana were severely affected, whereas 51 lives were lost in Haryana during the flood in the basin. Around 9 lakh acre croplands were damaged in the 2010 flood.

Table 1.2 Historical flood events in the Ghaggar river basin (11,12)

Type of flood	Year
Low Intensity	1976, 1981, 1996, 2008, 2015
Moderate Intensity	1989, 1994, 1997, 2000, 2001
High Intensity	1852, 1887, 1984, 1988, 1993, 1995, 2004, 2010

Numerous studies have been reported on surface water quality, groundwater quality, morphological structure, biophysical aspects, etc. Report and thesis on flood risk analysis have also been reported on the Ghaggar River basin. However, no study has been conducted considering the dynamics factors such as urbanisation, rainfall pattern, and population density. Around 5 million people live in the flood-prone area of the Ghaggar river basin, out of which 1.5 million are from the urban areas. So, the flood risk in urban areas is high as urbanisation, and population density increase with time. An analysis of the urban flooding must be analyzed as the urbanisation and population density is increasing with time. Climate is changing throughout the world, and it greatly impacts hydrometeorological disasters such as floods and droughts. Therefore, an analysis of climate change in terms of rainfall must be considered. The dynamic factors change with time; therefore, the flood risk is also changing based on these dynamic factors. Therefore, considering all the dynamic changes, a study is required in the Ghaggar River basin for flood risk assessment.

The remote-sensing and GIS approach, using satellite and airborne sensors, is rapidly entering the field of environmental sciences as a complementary tool for studying natural processes (13). The study conducted for the Ghaggar river basin is implementation of mathematical model in the GIS. We used ArcGIS for the GIS analysis.

1.4. Objectives of the Study

The problem statement against the flood analysis requirement in the Ghaggar River Basin. The objective of the study is to find out the rainfall trend analysis and extreme rainfall events in the study area. Rainfall is analysed as descriptive statistics, trend and magnitude of trend. The change point is also analysed. Descriptive statistics, trend and trend magnitude are also analysed before and after the change point. The descriptive statistics, trend and trend magnitude is analysed for extreme rainfall indices. Flood risk as integration of flood hazard and flood vulnerability is analysed using eleven flood factors. Graph theory is introduced as a method of flood risk whereas the results is validated with classical approach Analytical Hierarchy Process.

Land use land cover change and population density change is also analysed for considering these factors as dynamic flood factor. The impact of change in LULC in urbanisation on flooding over an area is also analysed, and the future flood maps are projected.

1.5. Organization of Thesis

Chapter 1 introduces the importance of water, floods, the classification of floods, the problem statement of flood analysis requirement, and the objective of the thesis.

Chapter 2 enlighten the state of art literature review on flooding, urban flooding, flood analysis, mechanism of urban flooding, different flood models, factors responsible for flooding over an area, rainfall trend analysis, and urbanisation analysis.

Chapter 3 discusses the watershed delineation of the study area Ghaggar river basin and the dataset used for the study of elevation, slope, climate, land use land cover, hydrologic soil group, population density, household density, literacy rate, and road connectivity.

Chapter 4 discusses the methodology and the result of rainfall descriptive analysis, trend analysis, the slope of rainfall trend, change point in rainfall trend, descriptive statistics of rainfall before and after change point, trend analysis of rainfall before and after change point, and slope of rainfall trend before and after change point.

Chapter 5 highlights the methodology and result of extreme rainfall events using extreme rainfall indices. This chapter includes descriptive analysis, trend analysis, and slope of rainfall trend of extreme rainfall indices.

Chapter 6 focused on the classification of flood zones using the Analytical Hierarchy Process (AHP) and Graph theory. The methodology of both the method were discussed. The comparison of the result from both the analysis is also discussed.

Chapter 7 discusses the impact of urbanisation on flooding. Therefore, the chapter includes the methodology of Land use land cover changes for urbanisation analysis. This chapter also included the population as a dynamic flood factor and projected future population density spatial maps. The flood maps have been prepared for now and projected for the future, considering urbanisation and population density as dynamic factors.

Chapter 8 concluded the results of rainfall analysis, extreme rainfall analysis, flood hazard zone, flood vulnerable zone, flood risk zone, urbanisation analysis, and projected future flood maps based on dynamic flood factors such as urbanisation and population density.

CHAPTER 2

2. Literature Review

2.1. General

This chapter highlights studies conducted for analysis and management of flood and urban flood. At the outset, studies conducted on flood and urban floods worldwide have been discussed to understand the mechanism for urban flooding and the methodology used for the modelling analysis. Flood over an area depends on various factors; therefore, factors used by different study for flood analysis have been discussed. Urban flooding is generally caused by three major parameters: extreme rainfall and urbanisation, which has been included in the state-of-the-art literature review.

2.2. Flooding over an area

Flooding is a natural event that impacts life losses, economic losses, building and infrastructure damages, etc. (14). Flood is defined as an upward condition of water levels from normal levels in flowing water bodies and inundation on the earth's surface. As a result of these floods, billions of populations are affected worldwide (15). In the last decade (2009 – 2019), approximately 50,000 people died due to flood events, whereas 10% of the world's population was affected (9). In the decade 2010 – 2020, around 0.82 million population were affected in both continents of America (16). The flood destruction level has been predicted to be double by 2050 (14). Figure 2.1 presented the impacts of the flood on humans, economics, and materials, as discussed in various studies (17–21). Major impacts of floods are human deaths, cattle losses, building damages, crop damages, and waterborne diseases (18–20,22–25). During a river flood, a bridge crossing the waterway may become submerged. In this case, the proper estimation of dynamic forces exerted by the flow on the structure is important for designing or evaluating the structure vulnerability (26). Anthropogenic activities worldwide, leading to climate change and increasing urbanisation, are causing urban flooding over cities (27–32). Urbanisation is increasing as people move towards urban areas to better search for lifestyle, housing, education, employment, energy, transport, health care center, etc. However, all these facilities are highly affected during an urban flood event. Studies reveal that the number of urban flood events will increase with respect to time (33–36). Urban flood impacts the human, economic, and material, as shown in Figure 2.1.

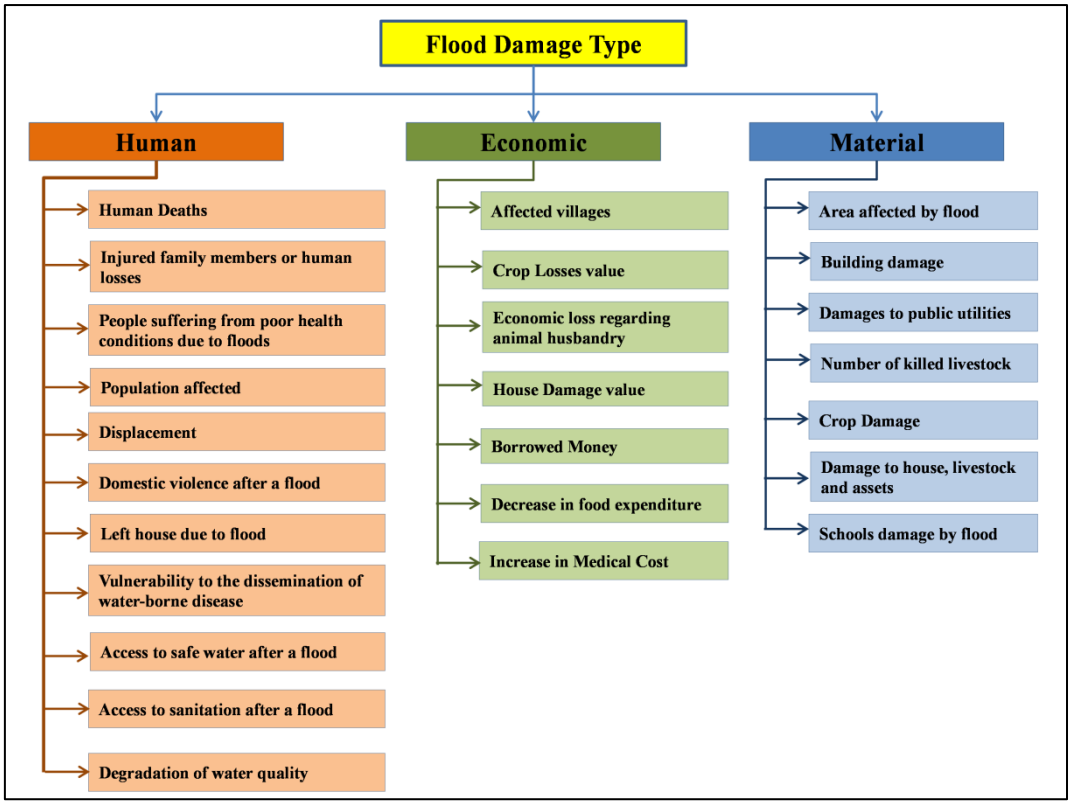

Figure 2.1 Vulnerability of flood on human, economic and material (17–25,37)

2.3. Study on Flood Analysis

Because of flood impacts on the earth's surface, various studies are conducted to determine the highly flood-prone zone over an area. The studies were conducted throughout the world at local and regional levels. Chan et al., (2022) conducted a review study on flood vulnerability analysis using GIS (14) different web links such as Springer, Science Direct, Taylor and Francis Journal, Sage journals, and JSTOR. The input keywords were *"flood," "flood vulnerability," "flood vulnerability assessment," and "flood vulnerability assessment and geographic information system."* Figure 2.2 shows the number of articles found for the keywords in different journal publishers. Large number of articles found for flood vulnerability and GIS. Intensive literature review indicates that huge studies have been conducted for flood risk assessment during 2018 – 2022 which include flood risk, flood hazard, flood vulnerability, urban flood, etc. The literature was classified on the basis of study area, methodology, the aim of the research, GIS techniques, flood factors used, name of the journal, etc. A total of 107 studies with different study are from the globe have been reviewed so far. The countries namely Alabama (38), Algeria (39,40), Australia (41), Bangladesh (42–48), Canada (49,50), Chile (51), China (52–79), Costa Rica (80), Egypt (81), Ethiopia (82), Europe (83), Germany (84), Ghana (85), Greece (86,87), Haiti (88), India (89–98), Indonesia (99), Iowa (100), Iran (101–

107), Italy (108,109), Japan (110), Korea (111,112), Malaysia (113,114), Myanmar (115), Pakistan (116,117), Philippines (118), Portugal (119–122), Romania (123), Saint Lucia (124), Saudi Arabia (125), Slovakia (126,127), Spain (128–132), Turkey (133–135), United States (136,137), Vietnam (138–141), Virginia (142), etc.

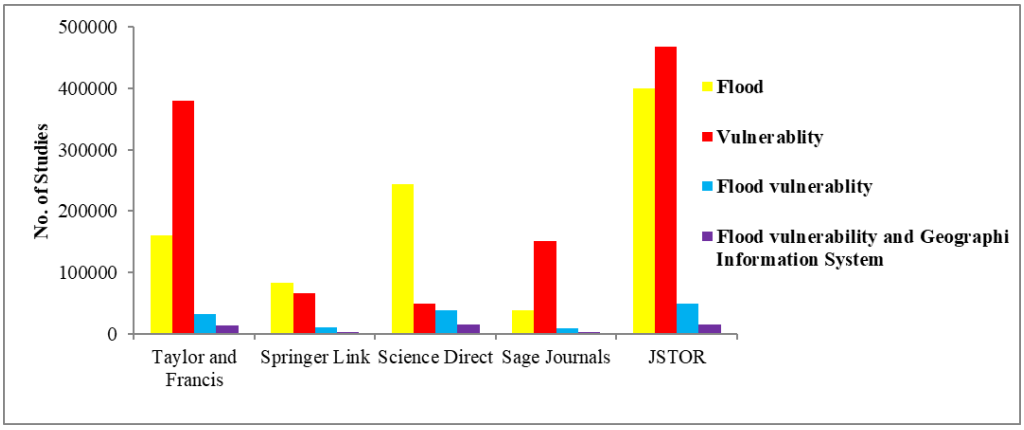

Figure 2.2 Keywords found articles in different journal for the period of 2010- 2020 (14)

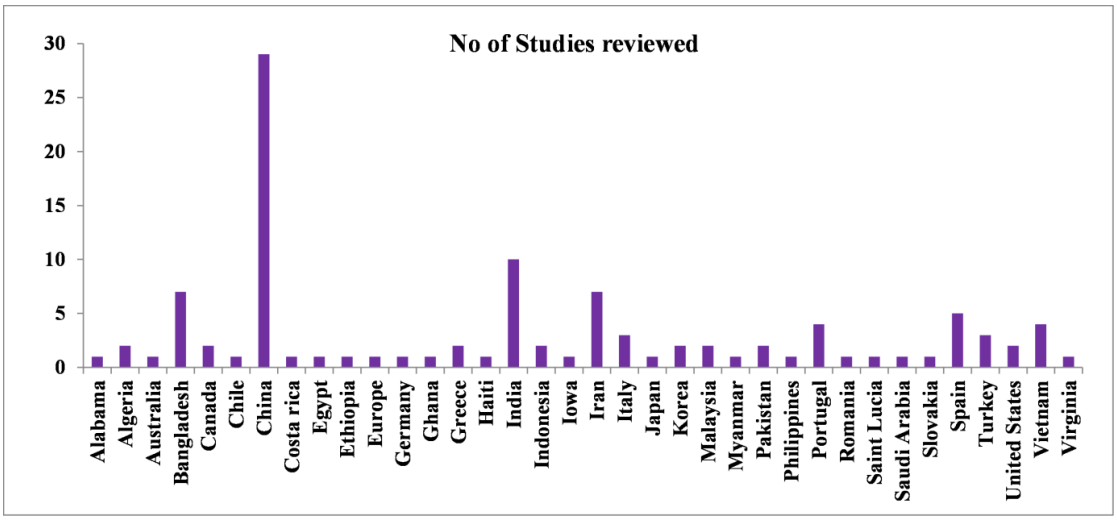

Figure 2.3 No of studies reviewed for different countries

Figure 2.3 shows the number of studies which have been conducted over the world. Table 2.1 shows the list of journals with the number of articles reviewed by that journal. The highest number of articles reviewed are published in the journal of "*Journal of Hydrology*" followed by the journals are "*International Journal of Disaster Risk Reduction*," "*Water*," "*Journal of Flood Risk Management*," "*Natural Hazards*," "*Science of Total Environment*," "*Sustainability*," "*Natural Hazards and Earth System Sciences*," etc.

Table 2.1 List of Journals with number of articles reviewed

Name of the Journal	No of Articles	Name	No of Articles
Acta Geophysica	2	Journal of Environmental Management	2
Applied Geomatics	1	Journal of Flood Risk Management	8
Arabian Journal of Geosciences	3	Journal of Hydrology	13
Atmosphere	2	Sustainable Cities and Society	3
Earth System and Environment	3	Land	2
Environment Systems and Decisions	1	Land Use Policy	1
Environmental Impact Assessment Review	1	International Journal of Geo-Information	1
Environmental Modelling & Software	1	Natural Hazards	7
Environmental Monitoring and Assessment	1	Modeling Earth Systems and Environment	1
Environmental Science and Policy	1	Neural Computing and Applications	1
Geocarto International	1	Progress in Disaster Science	1
Global Environmental Change	1	Remote Sensing	2
Hydrological Processes	2	Risk Analysis	1
Hydrology Research	1	Science of Total Environment	5
International Journal of Disaster Risk Reduction	12	Sustainability	5
International Journal of Environmental Research and Public Health	1	Journal of Water Resources Planning and Management	1
Natural Hazards and Earth System Sciences	4	Tunnelling and Underground Space Technology	1
International Journal of Disaster Risk Science	1	Water	11
Journal of Cleaner Production	2	Water and Environment Journal	1
Journal of Cultural Heritage	1	Water Resources Management	1

The articles reviewed are aimed to find out from their research are *"Dam-Break Hazard Risk Mapping", "Flash Flood Risk Analysis", "Flood and Drought risk", "Flood Control Operation", "Flood Damage and Risk Assessment", "Flood Disaster Risk Assessment", "Flood Hazard", "Flood risk", "Flood Hazard", "Exposure and Vulnerability", "Flood Susceptibility Assessment", "Urban Flood Analysis", "Urban Flood Hazard Mapping", "Urban Flood Prediction", "Urban Flood Risk Assessment", "Urban Flood Risk Propagation", "Urban Flood Susceptibility", "Urban Flood Vulnerability", "Ground water flood risk assessment", "Hurricane Flood Risk", "Multivariable Flood Risk", "Preliminary Flood Risk Assessment", "Ice-Jam Flood Risk Assessment and Hazard mapping", "Integrated Urban Flood Vulnerability Assessment", "Local-Scale Urban Flood Risk Assessment", "Flood and Water logging Susceptibility Mapping", "Risk Assessment and Sensitivity Analysis of Flash Floods", "Flood Hazard, Vulnerability and Risk Assessment", and "Flood Hazard Zonation and Flood Shelter Suitability Mapping".*

2.4. Mechanism and result of urban flooding

Natural and anthropogenic causes mainly mechanized urban flooding. Climate change-induced patterns of rainfall trend changes and extreme rainfall events are the natural causes of urban flooding (19). The impacts of warmer temperature are widely on the water system include rising in sea levels on the coast which leads to potential flooding in the low lying areas and heavily populated areas (143). The anthropogenic cause of urban flooding is human-induced urbanisation (144). Natural causes of the urban flood may need to be minimized effectively. However, control measures in the urbanisation causes can be taken, but due to several management barriers, it also acts as non-minimizable. Figure 2.4 shows the mechanism of increasing urban flooding over any area (145). Three major causes of urban flood are shown in Figure 2.4: Urbanisation, Climate change, and Urban flood management barriers.

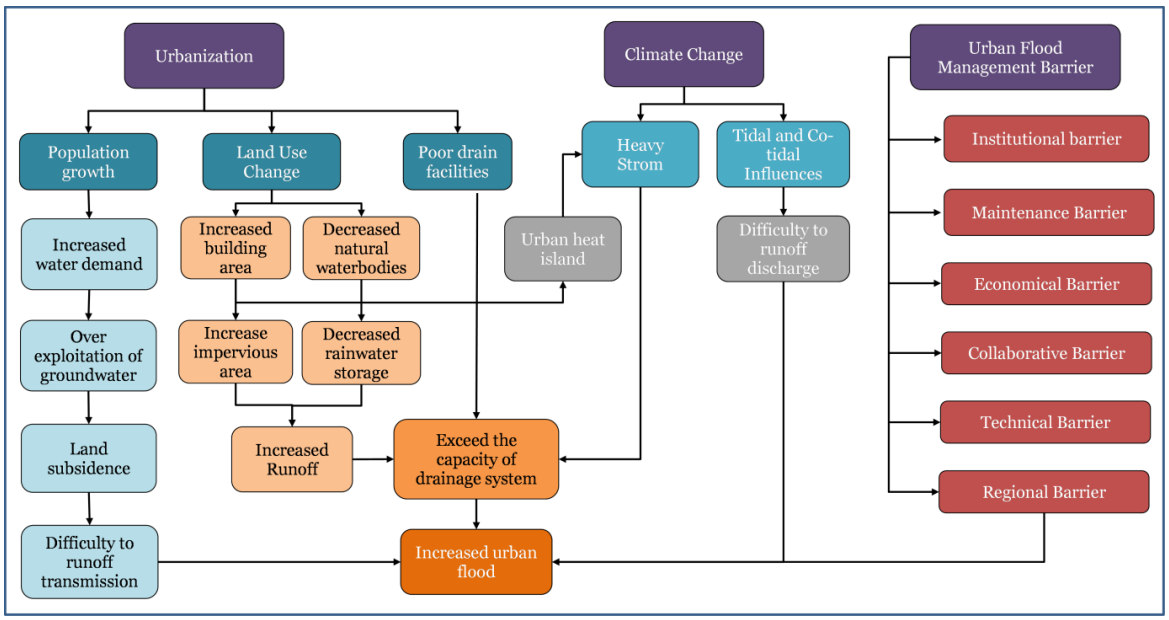

Figure 2.4 Mechanism of Urban Flooding

Urbanisation causes increased population growth, changes in land use, and poor drainage facilities. Population growth over an area increases the water demand, leading to over-exploitation of groundwater leads to land subsidence which is the gradual settling or sudden sinking of the Earth's surface. Land subsidence led to difficulty in the runoff process, increasing urban flooding. Land use changes are increased in building areas and decreased in natural water bodies. The result of increased building area is increased impervious areas and decreased natural water bodies in rainwater storage. Increased in impervious areas and decreased in rainwater storage is increased runoff. The increased building area has created the urban heat

island in that area. Urban heat islands and climate change resulted in heavy storms over an area. Increased runoff over an area, urbanisation caused poor drainage facilities and heavy storm leads to increase urban flood drainage system of an area exceeding its capacity. Climate change also resulted in tidal and co-tidal influences, which enhanced the difficulty in runoff discharges and increased urban flooding. Together with the probability of flooding, an accurate calculation of the loading applied by the flow on the structure is necessary for designing or evaluating its vulnerability (146).

Besides climate change and urbanisation, the lack of urban flood management influences the flood. The urban flood management barriers are Institutional, Maintenance, economic, Collaborative, technical, and regional barriers. These barriers directly increased urban flood.

2.5. Flood model review

A model is a clear image of the system used for analyzing and predicting or projecting different real-world scenarios such as flood, drought, climate change, energy balance, ecosystem, etc. Flood models are primarily used to identify, predict, or project flood risk and different hydrological processes over an area (147). Several researchers, scientists, consultants, governmental agencies, and academic institutions developed and implemented many flood models to simulate an area's water quality and quantity. A single simple categorization of an integrated urban flood model is hard to establish because of its challenges and extended scope. Figure 2.5 shows the classification of different flood models to identify and predict possible flood risk (145). The main mechanisms involved in flood models are modelling mechanisms, calculation algorithms, dimensionality, mathematical complexity, and spatial extent.

The modelling mechanism of urban flood models is database models and physically-based models. Data-based or data-driven models are numerical modelling work on the input numerical data and represent the data numerically (148). Examples of data-based models are Artificial Neural networks (ANNs), k – -nearest neighbor (KNN), Fuzzy Approach, Support Vector Machine (SVM), Neural Fuzzy Networks (NFS), multiple linear regression techniques, etc. Physically-based models are a detailed analysis of physical processes for flood modelling in an area where many physical parameters, such as elevation, land use, land cover, slope, soil group, etc., are involved (149).

The modelling mechanism of urban flood models is database models and physically-based models. Data-based or data-driven models are numerical modelling work on the input

numerical data and represent the data numerically (148). Examples of data-based models are Artificial Neural networks (ANNs), k – -nearest neighbor (KNN), Fuzzy Approach, Support Vector Machine (SVM), Neural Fuzzy Networks (NFS), multiple linear regression techniques, etc. Physically-based models are a detailed analysis of physical processes for flood modelling in an area where many physical parameters, such as elevation, land use, land cover, slope, soil group, etc., are involved (149).

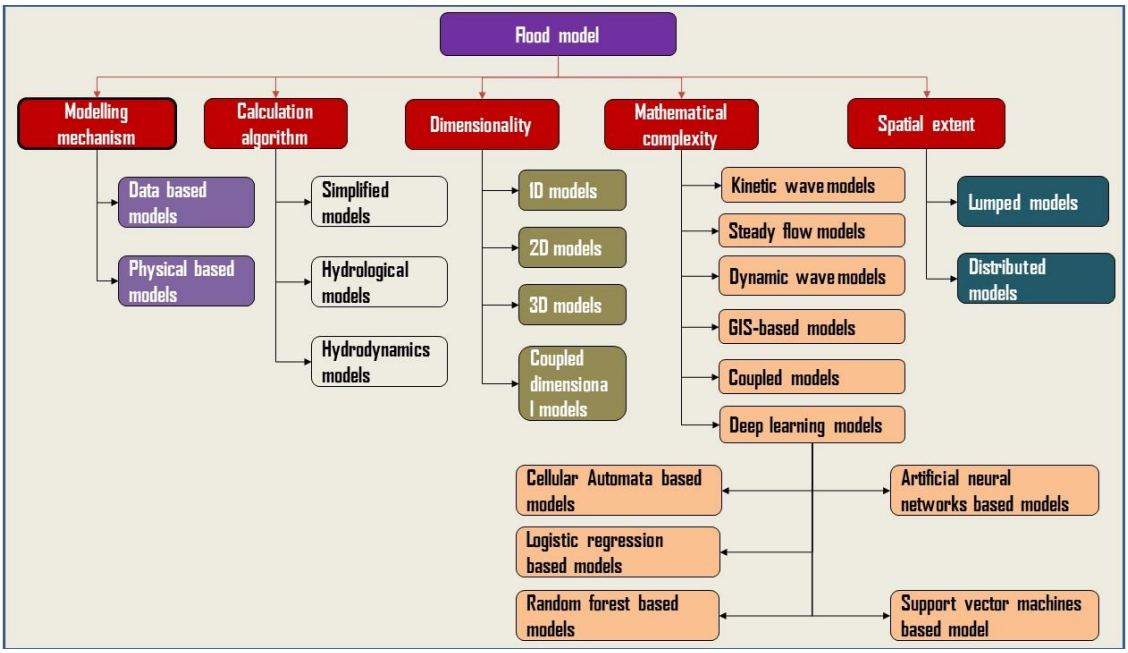

Figure 2.5 Flood modelling techniques

Calculation algorithm-based flood models are hydrological, hydrodynamic, and simplified models. Hydrological models are based on watershed hydrology, i.e., rainfall and runoff characteristics. Simulating rainfall with runoff characteristics, the flood risk analysis of an area can be analyzed using the hydrological model such as Soli and Water Assessment Tool (SWAT), Hydrologic Engineering Center - Hydrologic Modeling System (HEC-HMS), and MIKE System Hydrological European (MIKE-SHE), etc. (145,150). Hydrodynamic modeling of flood risk analysis is based on the Swallow Water Equation (SWE), which shows a definite physical meaning (151,152). SWE plays a significant role in the analysis of surface water flow for the hydrodynamic model (152,153). The analysis of SWE is conducted with techniques such as the cellular automata approach, adaptive mashes method, graphic processing unit, speeding up strategies, etc. (153–155). A simplified model is most beneficial for flood modeling tasks with low demand on flow dynamics accuracy and does not require velocity and flood process output (145).

Dimensionality techniques for flood modelling are the model development of different dimensions. There are several types of dimension models, such as 1D, 2D, 3D, and coupled dimensional models (145). 1D model or one-dimensional model is where water flows in a single dimension, such as within a channel, canal, river, or drain. In contrast, the 2D or two-dimensional models are where the water flows over an area such as a watershed, basin, parking lot, etc. HEC-RAS, MIKE 11, etc., are 1D models, whereas 2D models are MIKE21, Info Works 2D, JFLOW, and CCHE2D (156). 3D models or three-dimensional models analyze flood risk over the terrain along with flow over an area. The coupled dimensional model is the integrated model of two or more dimensions. For example, the coupled model 1D/2D is the most used commercial coupled model, which is complex to build and run (157). Storm Water Management Model (SWMM) and LISFLOOD-FP are widely used coupled dimensional models.

The best tools now for creating effective flood protection measures and great decision-supporters are mathematical models (158). The mathematical models widely used in different studies are kinetic wave models (159–161), steady flow models (89,94,113,144,162), dynamic wave models (161,163–165), GIS-based models (131,166–168), coupled models (86,151,157), and deep learning models (169). The examples of Deep learning models used in various flood modeling studies are cellular automata-based models (170–173), logistic regression-based models (70,174–177), random forest-based models (106,175,178), support vector machine models (178–180), artificial neural network-based models (70,174,181,182), etc.

Geographical Information System is a computer-based raster methodology for displaying the flood models spatially (54,116). The spatial model of flood risk can identify the type, extent, zone, risk level, etc. Two types of spatial flood models are lumped and distributed models. The lumped model is based on the unit hydrograph method (183), whereas the distributed model is based on the distributed hydrograph method (184).

2.6. Flood modelling techniques used in literatures

Table 2.2 shows different studies' flood modeling techniques used for flood hazard, risk, vulnerability, etc. analysis. More than a hundred models are used for risk analysis and river, urban, coastal, and ice flood management. However, Analytical Hierarchy Process (38,39,42,53,69,71,75,77,87,95,96,112,125,132,138,185), Hydrologic Engineering Center's - River Analysis System (HEC-RAS) (46,113,116,121,126,128,133,134), Multi Criteria

Decision Analysis (40,60,80,89,90,94,105,111,114,118,127,144), Machine Learning Models (70,102,103,122,123), Questionnaire Survey (44,48,135), Random Forest (RF) (106,175), MIKE-FLOOD (60,92,141), Entropy Weighting Method (101,112), and FLO-2D model (45,109) are the frequently used methodologies.

Table 2.2 Model used for Flood or Urban flood risk analysis used in literature studies

Sr. No	Methodology	Reference
1	Analytical Hierarchy process	(38,39,42,53,69,71,75,77,87, 95,96,112,125,132,138)
2	HEC-RAS	(46,113,116,121,126,128,13 3,134)
3	Multi Criteria Decision Analysis	(40,60,80,89,90,94,105,111, 114,118,127,144)
4	Machine Learning Models	(70,102,103,122,123)
5	Questionnaire Survey	(44,48,135)
6	Random Forest (RF)	(106,175)
7	MIKE-FLOOD	(60,92,141)
8	Entropy Weighting Method	(101,112)
9	FLO-2D model	(45,109)
10	Graph Theory	(186)
11	Game Theory	(71)
12	Constant Sum Scale (CSS)	(112)
13	3D visualization method coupling the PP-PSO algorithm	(56)
14	ABMDT (AdaBoost-DT) and BDT (Bagging-DT)	(140)
15	Annual Flood Extent Map	(97)
16	Approach for Extreme Rainfall Scaling and Storms Transposition	(108)
17	Areas Flooded During Recent Events Integrated with GIS	(130)
18	Bivariate Statistics	(123)
19	Copula Analysis	(65)
20	Joint Return Period Analysis	(65)
21	Creation of a risk Matrix	(131)
22	Delft3D model	(43)
23	Design rainfall-based flood and inundation risk	(110)
24	Equivalent drainage method upon combined rainfall-high tide-storm surge events	(64)
25	Extreme Climate characteristics	(55)
26	Demand over Capacity ratio map	(82)
27	Future Land-Use Simulation (FLUS) model	(72)
28	GARP Model	(187)
29	QUEST Model	(187)
30	Geomorphometric Approach	(41)
31	Geospatial Technology	(47)
32	GIS-based spatial multi-index model	(54)
33	GPU (Graphics Processing Unit)	(79)
34	Accelerated Surface Water Flow and Transport model	(79)
35	HEC-HMS	(113)
36	Fuzzy Comprehensive Evaluation	(78)
37	Integrated Maximum Likelihood Clustering Algorithm	(49)
38	Gray wolf optimizer-group method of data handling (GWO-GMDH)	(188)
39	Improved AHP	(61)
40	InfoWorks ICM (HR Wallingford)	(74)
41	Integrated Framework	(81)

42	Integrated k-means cluster algorithm	(68)
43	Improved entropy weight method	(68)
44	Interval FAHP-FCA approach	(76)
45	Jelesnianski method	(66)
46	Advanced Circulation (ADCIRC) model	(66)
47	Simulating Waves Nearshore (SWAN)	(66)
48	logistic regression	(175)
49	AdaBoost	(175)
50	Modified Susceptible Infected Recovered Model	(189)
51	Maximum Entropy Model	(118)
52	Multidimensional Vulnerability Index	(117)
53	Multiple Linear Regression-TOPSIS	(190)
54	Bayesian Network	(67)
55	Open LISEM, a spatial hydrological model	(88)
56	Optimised Additive Weighting Methodology	(129)
57	Paleo flood analysis	(51)
58	Particle Swarm Optimization (PSO)	(49)
59	Penn State Integrated Hydrologic Model (PIHM)	(86)
60	Artificial Neural Network (ANN),	(191)
61	Multi-Dimensional Integrated Flood Risk Assessment	(44)
62	Deep-Leaning Neural Network (DLNN)	(49)
63	Rainfall runoff SCS-CN method	(87)
64	Reservoir Flood Control Operation Coupled with Risk Assessment (RFCORA model)	(63)
65	River-Ice Model (RIVICE Model)	(50)
66	Safe Development Paradox: An agent-based model	(192)
67	Self-organizing Map Neural Network	(107)
68	Semi-supervised Machine Learning Model	(193)
69	Social Vulnerability Index (SVI)	(49)
70	Social-Ecological-Technological Systems	(137)
71	Rating Curves	(194)
72	Spontaneous-Triggered Risk Assessment Conceptual Model	(62)
73	Strongest Path Model (SPM)	(124)
74	TFN-AHP Method	(52)
75	Topography-based hydrological MODEL (TOPMODEL)	(60)
76	TOPSIS	(103)
77	TUFLOW model	(142)
78	UAV-borne	(85)
79	LiDAR-based elevation modelling	(85)
80	Web-based Flood Risk Assessment and Mitigation Environment (FRAME)	(100)
81	Weighted Overlay Analysis	(195)

Multi-criteria decision-making (MCDM), also known as Multi-Criteria Decision Analysis (MCDA), is the process of making judgments where numerous criteria (or objectives) must be examined simultaneously to rank or choose between options. MCDM, in combination with GIS, is used by numerous researchers to model and analyze flood risk (166,168,196). The AHP was proposed by Saaty in 1977, the most widely used MCDM model for flood analysis (76). AHP solves complex problems using hierarchical frameworks. The AHP is a statistical method for analyzing flood hazard, risk, and vulnerability. It is the most widely used multi-criteria decision-making method for flood risk analysis, which can integrate various assessment factors (95,167,168,190,197–199). The AHP analyzed the flood risk using the ranks and weightage of

various factors that influenced the flood. The factors selected for flood risk analysis in AHP methods are elevation, slope, distance from the river, rainfall, flow accumulation, land use, geology, topographic wetness index, population, drainage density, groundwater level, lithology, literacy rate, soil cover, hydrological soil group, etc. (104,125,168,174,190,200–202). The weightage of the factors is AHP is based on expert judgments. The entropy weighting method is used to overcome conflicting expert judgments. The entropy-weighting approach is one of the multi-criteria decision-making strategies that are used to maximize decision-making under a variety of qualitative, quantitative, and often competing considerations (101).

HEC-RAS is one of the hydrological modeling of used for flow analysis in the channel and flood plain delineation based on the flow data of the channel (116). A unique hydrodynamic professional toolbox for flood modeling, i.e., MIKE FLOOD, is widely used for 1D and 2D flood simulation models (60). MIKE FLOOD simulates the floodplain of rivers, streams, drainage networks, coastal areas, levees, etc. The FLO-2D is also used for flood hazard analysis, a hydrodynamic model (45).

Over the last two decades, machine learning (ML) technologies have been used to understand the complicated mathematical description of flood physical phenomena (203). The ML methods contributed highly to advancing prediction systems, providing better performance and cost-effective solutions. Random Forest (RF), Decision Tree, and Support Vector Machines are widely used machine learning techniques for flood risk analysis (70). The SVM algorithm is based on the concept of structural error minimization. The algorithm finds the best linear hyperplane to partition training data into classes and distinguishes between two groups (flood and no flood) (103). The Random Forest (RF) model is a supervised ML method developed for classification, regression, and other tasks. The advantages of the RF method are that the accuracy of prediction is very high, it efficiently handles larger datasets, it can analyze the relative importance of variables, etc. (103). Decision Tree (DT) is a non-parametric supervised ML method for regression and classification. The DT model explains the outcomes graphically. There are three nodes in the DT models: internal nodes (test on the features), branch nodes (the outcome), and leaf nodes (the final decision that is derived from computing the features) (204). ANN approach weighted sum of inputs arriving at each neuron is passed through an activation function (generally nonlinear) to generate an output signal (205).

The social method used for flood risk analysis is a questionnaire survey. The survey shows the social view of the reason behind the flood occurrence, post-flood damages, or the plans required to minimize future flood losses (44,48,135).

Among all the methodologies used for flood risk analysis, the AHP is the most widely used methodology for flood risk analysis due to its simplicity, flexibility, intuitive appeal, and ability to mix quantitative and qualitative criteria in the same decision framework (206). The AHP analyzed the flood risk using the ranks and weightage of various factors that influenced the flood. The factors used for the flood risk analysis are discussed in the next sub-chapter.

2.7. Factors responsible for flood analysis

Spatial maps of flood risk, hazard, and vulnerability were prepared by integrating mathematical equations using numerous thematic layers (174). These thematic layers have different impacts with the different importance levels of the thematic layers. For example, Elevation: Higher elevation has a lower probability of flood, whereas lower elevation has a higher probability of flood risk. Table 2.3 lists thematic layers or factors used for flood risk analysis in literature. However, Elevation, Slope, LULC, Distance from rivers, distance from roads, Rainfall trend, Extreme rainfall (3 days cumulative rainfall maximum), Soil group, distance from flood shelters, efficient drainage network, literacy rate, and household density, etc., are the most important and frequently used thematic layers for flood analysis. The discussion of these factors in flood risk analysis is discussed below.

i. ***Elevation:*** Elevation is the most crucial component in flood mapping (207–209). The flood risk of an area decreases with the elevation increases. The water flows rapidly from higher to lower elevations where the flow is less or near stagnant in lower elevations, which has a higher tendency for occurrence of flood (210).
ii. ***Slope:*** Slope over a region is dominant in flowing water, a crucial factor for flood risk analysis (208,211). The slope of a watershed directly relates to the flow velocity of water (210). The slope is the gradient line. The higher side of the gradient in the regions has a lower probability of flood occurrence, whereas the rapid decline in slope gradient has a higher probability of flood.

Table 2.3 Thematic layers or factor used in literature for flood risk analysis

Sr. No	Factors Name	Reference
1	Children Population density	(212)
2	Curvature	(200,213–215)
3	Curve Number	(104,125,166)
4	Density of drainage block sites	(212)
5	Distance from drainage block sites	(212)
6	Distance from flood shelters	(95,216)
7	Distance from rivers	(95,104,166,167,200,214–217)
8	Distance from road network	(95,216)
9	Distance from water bodies	(212)
10	Distance to Embankment Breach Locations	(95)
11	Distance to hospitals	(95)
12	Drainage area	(125,174)
13	Drainage density	(95,125,167,197,214,215)
14	Elevation	(95,104,166,167,174,197,200, 212,214–217)(2008,209,211,213,2
15	Employment Rate	(95,201)
16	Female Population	(95,212)
17	Flood depth	(174)
18	Flood Duration	(174)
19	Flow accumulation	(200,214)
20	Geology	(174,200,214)
21	Geomorphic Features	(95)
22	Ground water level	(104,167,217)
23	Household density	(201,216)
24	Land Use Land Cover	(95,125,167,174,197,200,201, 213–217)
25	Literacy Rate	(95,201,216)
26	Lithology	(167,197,215)
27	Maximum 3 days rainfall	(95,166)
28	Population density	(95,125,201,212,216)
29	Proximity to stream confluences	(95)
30	Rainfall	(104,125,167,174,197,200,214 ,216)
31	Runoff	(214)
32	Slope	(95,104,125,166,167,174,197, 200,201,213–217)
33	Soil	(174,213–215)
34	Topographic Wetness index	(166,200,215)

iii. ***Runoff:*** Runoff over an area is the amount of water that flows over the surface. The runoff is higher where the infiltration capacity of the soil is low. In the current trend of urbanization, surface runoff increases as the impermeable area increases with

urbanization (217,218). The accumulation of higher surface runoff over an area increases the probability of flood risk (214).

iv. ***Land Use Land Cover (LULC):*** LULC of an area is a type of land utilized or created by nature or artificial. Different categories of LULC have their impact on the environment. The surface runoff or stormwater generation is controlled or triggered by the LULC category. The generation of stormwater is higher where the LULC is bare rocks or urban built-up, whereas the generation of stormwater is less in the croplands, grasslands, forests, etc. The urban built-up of LULC has numerous benefits in association with the environment (219–221). The changes in the LULC pattern concerning time affect the natural influences and artificial activities (220,222,223). Activities such as deforestation and urbanization greatly impact natural hazards such as floods over an area (200). Urbanisation increases the impermeable area, leading to higher runoff over an area. Together with the probability of flooding, an accurate calculation of the loading applied by the flow on the structure is necessary for designing or evaluating its vulnerability.

v. ***Flow Accumulation:*** Flow accumulation is the flow concentration (200). High flow accumulation in any river, drain, stream, region, or watershed has a greater probability of flood (180). The volume of flow accumulation is ordinarily lower in the upper basin where tributaries of the basin are less. In the downstream part of the watershed or basin, as the number of tributaries is added to the mainstream, the flow accumulation is higher in the mainstream and watershed or basin. Therefore, higher flow accumulations generally increase the probability of flood.

vi. ***Hydrological Soil Group:*** Soil is classified into four hydrological soil groups (HSG) based on the runoff potential by the USDA-Natural Resource Conservation Service (224). These four categories are A, B, C, and D. The runoff potential of HSG are low, moderately low, moderately high, and high for A, B, C, and D soil group, respectively. The runoff potential of HSG is in direct relation to flood risk. The soil group D has a higher probability of flood occurrence as the runoff potential is high. For its runoff potential, literature considered HSG as a floor risk analysis factor (174,213–215).

vii. ***Curve Number:*** Curve number (CN) is the relation between hydrologic soil group (A, B, C, and D) and LULC of an area (125). The value of CN lies in the range 0 to 100, which defines high infiltration to no infiltration or high runoff, respectively (225). Therefore, the higher CN will directly impact flood risk due to higher runoff generation.

viii. ***Geology:*** The impact of geology on flood generation is less than other parameters. However, geology is considered as a flood risk factor due to the lithological characteristics of rock (174,200,214). The porosity and permeability of a rock influence flood intensity due to geology.

ix. ***Lithology:*** Lithology is one of the important factors for flood risk analysis (167). The lithology factor is related to the permeability of soil (167,226). Impermeable soil will increase the runoff, which increases the risk of flood. The lithology of the earth's surface, such as coarse sand, conglomerates, etc., increases the infiltration and decreases the flood risk as the runoff over the area will be less. On the other hand, lithology, such as marly, clay, gypsum, etc., is decreasing the infiltration and flood risk (226).

x. ***Drainage area:*** Precipitation falls into creeks, streams, rivers, lakes, and reservoirs throughout the drainage area. The drainage area is proportional to the risk of flooding (174). The higher drainage area will have a higher risk of flood.

xi. ***Drainage density:*** Drainage density measures the sum of the channel lengths per unit area. Drainage density increases with decreasing soil infiltration capacity, producing runoff (125). Therefore, drainage density also plays an important role in flood risk analysis. Drainage density directly relates to flood risk due to its hydrological response time (95,227,228).

xii. ***Curvature:*** The curvature map represents the topography as convergent and divergent runoff (213). The curvature map is delineated from the Digital Elevation Model. The value of curvature lies in the range of -0.1 to 0.1. The negative values define the concave shape of topography; the zero values define no curvature, and the positive values define postulated convex topography (200). The convex curvature has a higher probability of flood risk than the concave shape (214).

xiii. ***Topographic Wetness Index (TWI):*** The TWI is the impact of topography on runoff generation over an area and the amount of flow accumulation (208,229). The higher TWI regions have a higher probability of flood risk and vice-versa.

xiv. ***Groundwater Level:*** The soil infiltration capacity is highly affected by the level or depth of groundwater (230). The higher groundwater level rapidly saturates the soils and generates more runoff, which may lead to floods over the area.

xv. ***Geomorphic Features:*** Geomorphic features of the earth's surface impact flood risk as the inundation level depends on the geomorphic features (95).

xvi. ***Flood Depth:*** The flood depth is directly proportional to the flood risk over an area (174). The low flood risk is assigned where the flood depth is low, and high flood risk is assigned where the flood depth is high (231).

xvii. ***Flood Duration:*** Flood duration over an area exists from very long, long, medium, short, or no flood (174). Generally, the flood risk will be where the flood duration is very long and vice-versa. Therefore, the flood duration has a direct impact on flood risk analysis.

xviii. ***Population Density:*** Population density is directly proportional to the flood risk (95). The higher density of the population will be greatly affected during floods. Higher population density congested the locality, which may severely impact stormwater accumulation. Also, the increasing population density will expand soil impermeability by developing concrete structures (216). Therefore, population density is an important factor for flood risk analysis.

xix. ***Female Population:*** The female population is directly proportional to the flood risk (95,232). Women can face problems during flood activities due to pregnancy, their physical flexibility than men, and slower recovery due to family responsibilities 2(233). Therefore, the female population can be a risk factor for flood risk analysis.

xx. ***Literacy Rate:*** The literacy rate is inversely proportional to flood risk, i.e., a higher literacy rate will lower the flood risk. The literacy rate will impact socioeconomic attainment, creating awareness among people regarding the encroachment at flood plains, pre-post flood activities, safety and rescue during flood, and environmental management. Therefore, the research articles also considered the literacy rate an important factor for flood risk analysis (95,201,216).

xxi. ***Household density:*** Household density is directly related to an area's flood risk because it can increase the flood risk (216). Household density over an area is more connected with population density, resulting in soil impermeability due to construction. The impermeability of soil will increase the runoff, severely impacting flood generation.

xxii. ***Children Population density:*** Children and older people are the most vulnerable group during floods compared to young and mature age due to mobility during flood activities (232,233). Therefore, children's population density is directly proportional to the flood risk.

xxiii. ***Employment Rate:*** The employment rate of an area supports local economic health and loss recovery during or post-flood activities. Therefore, employment rate is also an

important factor for flood risk analysis. The flood risk is inversely proportional to the employment rate (95).

xxiv. ***Density of drainage block sites:*** Drainage block sites are where the drainage is clogged due to some natural or manmade activity, which produces overflow from the drain to the locality. Overflow of stormwater due to drainage block and drainage block site density will directly contribute to flood risk over an area(212).

xxv. ***Distance from drainage block sites:*** The flood risk is inversely proportional to the distance from drainage block sites. Therefore, the flood risk will decrease the distance from drainage block sites increasing (212).

xxvi. ***Distance from flood shelters:*** Flood shelters are important during flood events. The flood risk is directly proportional to the distance from flood shelters (95,216). The people near flood shelters will easily be accommodated safely at flood shelters where the higher distance people will face problems shifting them towards flood shelters.

xxvii. ***Distance from River:*** Flood detention areas serve the primary purpose of controlled water storage during large flood events in order to decrease the flood risk downstream along the river (233). Generally, the flood probability is higher alongside the river. Therefore, the distance from the river is an important factor for flood risk analysis (95,167,200,217). The risk probability decreases as the distance from rivers increases. The river has a lower elevation and lower slope compared to the surrounding of the basin. The water flows to the river from higher elevations and higher slopes. The river's accumulation or flow of water is higher than its surroundings.

xxviii. ***Proximity to stream confluences:*** Stream confluence is where two or more tributaries are joining together and become a single river. River confluences can create floods as storm discharge of two or more tributaries joined together, and it isn't easy to flow the volume in a single river or stream (234). The proximity to stream confluences is the distance from the confluences. The flood risk is decreasing with increasing the proximity of stream confluences (95,216,234).

xxix. ***Distance from road network:*** The availability of major roads near human settlements plays an important role during floods (216). The major road can transfer people to the safest location from the flood location. Therefore, the distances from the road network are directly proportional to the flood risk.

xxx. ***Distance from water bodies:*** Water bodies are lakes, rivers, streams, oceans, etc. These water bodies became high during flood events or extreme rainfall events, increasing inundation levels. Therefore, the flood risk is higher near water bodies, whereas the risk

is decreasing with respect to distance. Therefore, distance from water bodies is also considered a flood risk analysis factor (212).

xxxi. ***Distance to Embankment Breach Locations:*** An embankment breach is where a hole or wall break occurs in the drainage channel due to erosion during storm flow. The water flows to a nearby embankment breach locality, generating a flood there. The flood risk is inversely proportional to the distance from embankment break locations (95,234).

xxxii. ***Distance to hospitals:*** Distance to hospitals or health centers is inversely proportional to flood risk (95). Waterborne diseases, snack bites, hygiene, etc., are common problems that health centers or hospitals need to treat during or post-flood events. Therefore, the distance from the hospital is an important flood risk analysis factor.

These flood risk factors can be classified into two clusters, i.e., vulnerability and hazard, based on flood risk levels. Hazard factors are the causing factors of the flood, whereas the vulnerability factors are the flood-effecting factors. Researchers analyzed flood risk as integrating flood hazard and vulnerability (95,125,216). Table 2.4 shows the list of flood hazard and flood vulnerability factors used in the works of literature.

Table 2.4 List flood vulnerability and flood hazard factors (95,125,216)

Hazard	Vulnerability
Distance from rivers	Distance from flood shelters
Distance from water bodies	Distance from road network
Distance to Embankment Breach Locations	Distance to hospitals
Drainage area	Employment Rate
Drainage density	Female Population
Elevation	Household density
Geomorphic Features	Land Use Land Cover
Maximum 3 days rainfall	Literacy Rate
Proximity to stream confluences	Population density
Rainfall	Children Population density
Slope	

It has been observed from the literature that various dynamic and static factors have been used for flood risk mapping of a basin (95,104,197). Table 2.5 lists dynamic and static factors used for flood risk analysis. Each factor has its impact on floods over an area. LULC change, rainfall pattern, and population growth are the primary dynamic factors responsible for higher flood risk. The LULC changes have been accountable for flood risk in all cases when the pattern of

LULC changed to any impervious areas such as urban built-up. In contrast, increasing population density of an area directly affects the flood risk. Therefore, the change analysis of these primary dynamic factors (rainfall pattern, urbanization, and population growth) should be studied before preparing a flood risk map. The rainfall pattern analysis as rainfall trend and extreme rainfall events analysis, urbanization as LULC change analysis, and population increment analysis are discussed.

Table 2.5 List of dynamic and static factors

Dynamic Factor	Static Factor
Children Population density	Curvature
Density of drainage block sites	Curve Number
Distance from drainage block sites	Distance from rivers
Distance from flood shelters	Distance from water bodies
Distance from road network	Drainage area
Distance to Embankment Breach Locations	Drainage density
Distance to hospitals	Elevation
Employment Rate	Flood depth
Female Population	Flood Duration
Household density	Flow accumulation
Land Use Land Cover	Geology
Literacy Rate	Geomorphic Features
Maximum 3 days rainfall	Lithology
Population density	Proximity to stream confluences
Rainfall	Slope
Runoff	Soil
Ground water level	Topographic Wetness index

2.8. Rainfall trend analysis

Environmental factors such as light, wind, temperature and rainfall can vary greatly from one location to another (235). Rainfall is a component of the hydrological cycle that facilitates the water supply, agriculture, recharging of groundwater, and socio-economic development of a country. The changes in the rainfall pattern adversely impact the environment in terms of flooding, droughts, ecosystems, agriculture, fisheries, etc. The spatial and temporal variation of rainfall is the climate change indicator on a regional and local scale. The determinations of spatial and temporal rainfall variation on a local scale are dominant factors concerning agriculture production and disaster preparedness. Therefore, significant research on rainfall variability due to climate change is necessary for overall management. Considerable research has been conducted by several hydrologists on the monthly, seasonal, annual, or any specified

period on the pattern of rainfall trends worldwide and obtained different results from global to local scale (59,236–243).

2.8.1. Rainfall Trend Analysis throughout the World

Detailed literature review on rainfall trend analysis was conducted worldwide during 2017-2022. These studies were conducted in Algeria (244–252), Australia (253,254), Bangladesh (46,255–258), Brazil (259), China (239,260), Ethiopia (261–273), Ghana (274), Guinea (275), India (276–306), Iran (307,308), Italy (309–312), Kenya (313), Morocco (314), New Zealand (315), Pakistan (316,317), Saudi Arabia (318–320), Serbia(321), South Africa (322–324), Sri Lanka (325–329), Syria (330), Togo (331), Turkey (332), United Arab Emirates (333), and Vietnam (334–336). These studies were conducted at the local or regional level. For example, the study area can be any city, district, state, river basin, watershed, or country. However, some studies combine several countries, such as West Africa (337,338) and Continental Europe, Ireland, the United Kingdom, and the Mediterranean basin (339). In India, the studies were conducted in states such as Madhya Pradesh and Chhattisgarh (276,340), Uttarakhand (283,341,342), Jharkhand (290), Maharashtra (291), Haryana (300,305), etc. The rainfall trend analysis of Indian river basin such as Upper Godavari River Basin (279), Upper Kharun Catchment (280), Ghataprabha River Basin (286), Bhogavo River Basin Watershed (240), Kosi River Basin (293), Munneru River basin (295), Netravati basin (299), Tekeze-Atbara River basin (302), and Jhelum River Basin (304) has also been conducted.

2.8.2. Availability and type of Data

The analysis of rainfall trends required time series data. The time series data were collected in two forms: station-based or gridded. The station-based dataset was collected hourly, daily, weekly, or monthly at the rain gauge station. The gridded rainfall dataset are satellite data of different grid such as 0.25°, 0.50° or higher. These data are recorded from the local to regional level. There is numerous data collector and supplier available all over the world. Data availability is free or paid, depending on the data supplier. In India, the India Meteorological Department, Pune, is the largest data collector and supplier of rainfall data, providing station and gridded data.

2.8.3. Methodology used for rainfall trend analysis

Numerous methods have been developed and utilized for trend analysis of hydrometeorological parameters. These methodologies used in works of literature are shown in Table 2.6. The most

widely used methodologies are the Mann-Kendall test, Innovative Trend Analysis, Sen Slope Estimator or Theil-Sen Slope estimator, Modified Mann-Kendall test, and Linear Regression analysis. However other methodologies such as Seasonal Kendall test, Correlated Seasonal Mann-Kendal Test, Kendall Rank Correlation, Revised Mann-Kendall test, Pre-whitening Mann-Kendall (TFPW MK) test, Sequential Mann-Kendall Test, Innovative Partial Trend Methodology, Innovative Polygon Trend Analysis Method, Triangular trend Analysis methodology, Polynomial Regression Analysis, and Spearman Rho's test.

Table 2.6 Trend analysis methodologies used in literatures

Sr No	Method Name	Reference
1	Mann-Kendall test	(126,240,244–247,249,251,253,254,256–258,260,261,264–267,269–275,277–280,283–287,289–299,301–306,310,314,316–321,324–329,331,332,334,335,337,339,341,343–348)
2	Innovative Trend Analysis	(240,244,246,250,270,275,282,284,289,291,292,304,305,317,318,321,328,332,335,336,341,346–352),
13	Sen Slope Estimator or Theil-Sen Slope estimator	(126,240,244,245,249,251,254,256,258,260,261,264,265,267,269,270,272,274,275,277–280,284,285,290–292,294–299,301–304,310,312,314,316,317,319,320,322,324,326–329,331,333,339,341,343–346)
3	Seasonal Kendall test	(290,322)
4	Correlated Seasonal Mann-Kendal Test	(333)
5	Kendall Rank Correlation	(283)
6	Modified Mann-Kendall test	(258,263,271,282,289,291,292,318,319)
7	Revised Mann-Kendall test	(260,351)
8	Pre-whitening Mann-Kendall (TFPW MK) test	(318)
9	Sequential Mann-Kendall Test	(324,353)
10	Wavelets Analysis	(338,354)
11	Innovative Partial Trend Methodology	(355)
12	Innovative Polygon Trend Analysis Method	(249,335)
14	Triangular trend Analysis methodology	(250)
15	Linear Regression analysis	(240,268,269,282,291,292,301,323,344,353)
16	ANFIS Hybrid ANFIS	(307)
17	LSTM, WNN	(313,356)
18	Polynomial Regression Analysis	(308)
19	Spearman Rho's test	(256,260,280,291,296,344)
20	Entropy Analysis	(247)
21	Spatial Trend analysis	(252)
22	Fuzzy Cluster	(357)

The most common and classical trend detection method is the Mann-Kendall or MK test (318). The MK test is developed by Mann (1945) and Kendall (1955) (358,359). This non-parametric method is used for trend analysis of data collected over time and results as increasing or decreasing trends. Non-parametric methods work for all distributions, i.e., the collected dataset does not have to meet the normality assumption. The significance of the MK test result is analyzed using hypothesis testing. The null hypothesis of the MK test means a non-significant trend, whereas the alternate hypothesis means acceptance of trend significance. The trend can be increasing, decreasing, or non-null. However, the MK test has several disadvantages, such as the presence serial correlation of the collected time series data and higher dependence on the degree distribution and size of the samples, which determine the robustness and reliability of the trend analysis result (360). To overcome the disadvantages of the MK test, a Modified MK test or MMK test has been developed (361). The MMK test is also a non-parametric test suitable for auto-correlated data (362). Yue et al. (2002, 2003) proposed a method, namely the trend-free pre-whitened MK test or TFPW-MK Test, which analyses the trend after removal of serial correlation present in the time series data (318,363,364). The MK, MMK, or TFPW-MK tests have been used to analyze the trend direction.

However, the analysis of the rate of change is also important. Sen (1968) developed a slope method for measuring change per time (365). This method is known as the Sen Slope estimator or Theil-Sen Estimator. Sen Slope estimator is a nonparametric method widely used in literature to analyze the slope of the time series hydro-climatic data (270). A parametric method for trend analysis, namely Linear Regression Analysis (LRA), is also widely used (282,323,344). A regression line is drawn to explain the trend, and positive or negative values of the LRA slope define the increasing or decreasing trend. In 2012, Sen developed a new methodology, i.e., Innovative Trend Analysis (ITA), which is free from the assumption of serial autocorrelation, normality, and length of records (291). ITA can solve all the drawbacks found in the MK test (366). Therefore, studies conducted after 2012 has focused on ITA for trend detection. However, a flaw in the significance test of the trend was not developed earlier. Sen properly developed the statistical calculation with a significance test of ITA in 2017(367).

2.8.4. Rainfall trend analysis throughout the world

The result of rainfall trend analysis varies with the region, and worldwide rainfall trends have been discussed. In north Algeria, the rainfall trend is significantly decreasing over the central, and no trend is found in the north and south of the study area (247). Summer rainfall in Western

Australia should increase by 0.18 – 0.21 mm/year, whereas winter rainfall should decrease by 0.42-0.43 mm/year (253). The rainfall trend in Bangladesh has been increasing annually, as well as pre-monsoon, monsoon, and post-monsoon seasons, whereas the winter season (December – February) is decreasing (343). However, the significance of the trend was found at $p>0.10$. The rate of annual rainfall trend in Bangladesh was found to be 5.675 mm/year (343). The annual rainfall of the Yangtze River delta, China, is an increasing rainfall trend at a significance level of 0.01 in all stations included for trend analysis (239). In Ethiopia, the dry season (October – January) shows an increasing rainfall trend, while the long rainy season (June – September) shows a decreasing trend. In contrast, annual and other seasons found no significant trend (263). In the Buubu watershed of New Guinea, the annual rainfall trend was found to have a statistically significant decrease (275). In India, significant seasonal and annual rainfall trends were detected in almost all the sub-divisions (292). The northeastern part of the Calabria region in southern Italy has been experiencing a significantly decreasing annual rainfall trend. In contrast, the north-western part has been experiencing a significantly decreasing trend in winter and a significant increase in summer (310). The annual rainfall trend of the Er-Rbia River basin in Morocco is decreasing (314). In the Aseer Region of Saudi Arabia, the rainfall trend is decreasing, which is statistically significant (319). In the United Arab Emirates, the MK test showed an increasing trend in six rain gauge stations and a decreasing trend in two out of eighteen stations (333). The rainfall trend analysis of Sri Lanka shows an annual decreasing trend at 67% of rain gauge stations using ITA (328). Syria's rainfall trend analysis shows a decrease in most stations (330). The rainfall trend varies from annual to season and region to region.

2.9. Extreme rainfall analysis

Heat waves, cold waves, tropical cyclones, droughts, floods, or ecosystem shifts are examples of extreme climate events that have an unanticipated, uncommon, severe, or unseasonal impact on the world. Extreme weather and climate events encompass occurrences with a low likelihood during which a weather or climate parameter surpasses an upper (or lower) threshold within the observed range. These events typically have a probability of happening that is commonly below 10% (368). The extreme events of rainfall affect the environment in two main ways: drought and flood. Extreme rainfall events in terms of no rainfall lead to drought, where excess rainfall floods an area.

Numerous criteria are used to analyze extreme weather or climate events. These are depended on the specific geographical location or research perquisites. For example, the Palmer drought Severity Index (PDSI), standardized precipitation index (SPI), and comprehensive meteorological drought index (CI) are used for the analysis of extreme drought events in different areas of the world (369–372). The absence of comprehensive long-term global climate data and a consistent definition of indicators and thresholds for extreme events across different nations has somewhat impeded further research into global extreme weather and climate events. To overcome the situation, the World Meteorological Organization (WMO) and the World Climate Research Program (WCRP) collaboratively formed the Expert Team on Climate Change Detection and Indices (ETCCDI) during the early 21st century (373). They formulated a set of 27 representative climate indices to evaluate worldwide and regional variations in extreme climate change.

Expert Team on Climate Change Detection and Indices (ETCCDI) developed 27 indices for extreme events, 16 for temperature, and 11 for rainfall. These ETCCDI have been widely used in literature for extreme events analysis of rainfall and temperature (274,374–377). The eleven indices of ETCCDI for rainfall extremes are given in Table 2.7. The details of these indices can be found at http://etccdi.pacificclimate.org/list_27_indices.shtml .

Table 2.7 Details of rainfall indices by ETCCDI

Sr. No	Indices	Definition
1	Rx1day	Maximum 1-day precipitation
2	Rx5day	Maximum consecutive 5-day precipitation
3	SDII	Simple precipitation intensity index: (daily precipitation amount on wet days, wets days are >1mm of precipitation)
4	R10mm	Annual count of days when precipitation ≥ 10mm
5	R20mm	Annual count of days when precipitation ≥ 20mm
6	Rnnmm	Annual count of days when precipitation ≥ nmm
7	CDD	Maximum number of consecutive days with rainfall < 1mm:
8	CWD	Maximum number of consecutive days with rainfall ≥ 1mm:
9	R95pTOT	Annual total precipitation when rainfall > 95 percentile of precipitation on wet days
10	R99pTOT	Annual total precipitation when rainfall > 99 percentile of precipitation on wet days
11	PRCPTOT	Annual total precipitation in wet days (wets days are >1mm of precipitation)

2.10. Urbanisation analysis

Urbanization is a significant phenomenon in modern society, driven by industrialization, economic opportunities, and improved living standards. Urban areas can change land cover, demographics, social dynamics, and environmental conditions as they expand.

2.10.1. LULC changes analysis

Urbanization can be analyzed by analyzing the LULC changes. Land use/land cover (LULC) is a fundamental concept of the Earth's system intimately connected to many phases of the human and physical environment (378). LULC encompasses two standard terminologies: land use and land cover. LULC of an area is the information regarding the current landscape. Land use pertains to information regarding land utilization and characterizes elements based on human activities, such as transportation infrastructure, residential areas, commercial zones, and agricultural land (379) Conversely, land cover encompasses features that cover various areas like bodies of water, forests, or barren land (380). Detecting LULC features can be achieved through aerial or satellite imagery, although certain components necessitate supplementary socio-economic data for identification (381) With the rapid global growth for a better lifestyle, the LULC is changing with time. The changes in LULC become a global environmental concern as it's widely impacting environmental sustainability. The socio-economic changes, as well as natural changes, are triggering the LULC changes. However, the nature and extent of the area are also responsible for LULC changes (379). The main drivers of LULC changes are deforestation, industrialisation, agricultural expansion, infrastructure built-up, range land degradation, etc. (379). Rapid industrialisation also causing urbanisation polluting the groundwater which is the most precious source of drinking water all across the globe (382). Coupling LULC data from remote sensing with discharge/runoff information from urban catchments may help establish general relationships between LULC parameters and runoff (383). Analyzing LULC changes over a specific timeframe provides insights into evolving trends. Satellite remote sensing data can address information gaps, and freely available satellite images offer comprehensive and continuous data frequently used in LULC change investigations (384) Open-source satellite images constitute a crucial resource in LULC change research, underscoring the significance of remote sensing technology in contemporary planning and development (385,386). Consequently, globally, there is a burgeoning interest in LULC change analysis through remote sensing data (387–390).

2.10.2. Methodology used for LULC change analysis

Using different models, LULC changes can be analyzed based on two or more previous LULC maps. Geospatial techniques for image interpretation and classification serve natural resource management and planning objectives, aiding in predictive analyses for future scenarios. Time series Landsat data furnish valuable inputs for predictive studies (391). Monitoring the LULC pattern trend in a region is essential for anticipating future planning and developmental needs. Predictive applications of LULC play a consistent role in risk assessment, urban planning, and various other domains (392). The substantial progress in LULC modeling practices is attributed to advancements in data acquisition methods, including satellite imagery, citizen science-driven approaches, and big data platforms. In recent times, diverse static and dynamic models have emerged, integrated with Geographic Information Systems (GIS) and remote sensing to simulate future LULC conditions efficiently. The LULC change modeling may be of several types, such as Statistical Models, Cellular Automata Models, Economic Models, Agent-Based models, Hybrid Models, and time series models (393)Statistical models project the changes in LULC using mathematical relations between explanatory variables and LULC patterns (394). The transition probability maps are generated from the mathematical relations. The most used statistical models for LULC change analysis are based on the regression and stochastic models. Examples of these models are linear regression models, logistic regression models, generalized additive models, and Markov Chain models. Cellular Automata models employ designated transition rules, impacts from neighboring elements, and the expertise of professionals to analyze the spatial dynamics of transformation (394). The CA models generate suitability maps instead of transition probability matrices. These suitability maps can analyze the spatial change in the LULC (395). Economic models simulate the LULC change as a market process (396). The Agent-Based Models (ABMs) comprise multi-agent systems and their interconnections, functioning to replicate intricate processes of LULC change (397). The agents include farmers, laborers, landowners, policymakers, practitioners, professionals, and decision-makers (398). ABMs incorporate human choices regarding LULC change while considering social interactions, adaptation, and development across various stages (399). As each single model has advantages and disadvantages, Hybrid models are formed by combining two models to overcome the limitations of these models (400). For example, the CA-Markov model is a hybrid model of CA mode and Markov models (400,401). CA models analyze spatial change and have limitations with the analysis of temporal change, which can be analyzed using the Markov Model. The time series model is in the evolution phase (393) It utilizes multiple labeled

time-series images for training to predict the LULC class labels of unlabeled time-series remote sensing images (402).

The most used methodology for LULC change analysis includes logistic regression (403,404), Markov chain (405), artificial neural networks (ANN) (406), cellular automata (385,386), modified cellular automata-based SLEUTH (407–409) and Conversion of Land Use and its Effects (CLUE) (410). The Markov chain prediction model is a spatial model capable of predicting LULC changes based on historical transitions in LULC classes (411). These transition probabilities are derived from past changes, structured in a transition matrix, and utilized to predict forthcoming LULC distributions (412,413). Researchers have applied various static and dynamic prediction models to anticipate future LULC dynamics (411,414). The Markov chain model has been extensively utilized for LULC change detection and prediction endeavors (411,414,415).

Researchers have integrated diverse modeling techniques to overcome individual model limitations, catering to specific geographic conditions and applications. The evolving artificial neural network technique, inspired by the human nervous system, offers quantification and support for decision-making involving complex non-linear data patterns. The multilayer perceptron (MLP), a feed-forward ANN with input, output, and hidden layers, is trained through the supervised backpropagation algorithm, offering generalization capabilities for LULC transitions and simulations. It demands fewer inputs for training and generates numerous parameters in significantly less time for model calibration (416). Additionally, it can model multiple transitions simultaneously. Land Change Modeler (LCM), an integrated software within TerrSet, effectively merges remote sensing and GIS data. LCM allows for an integrated Multi-layer Perceptron–Markov Chain (MLP-MC) approach to model spatiotemporal changes in LULC (415,417). The software used to analyze LULC change is CLUE-S, DYNAMICA EGO, Land Change Model, SLEUTH, etc.

2.11. Research Gaps

The literature review has focused on the flood risk analysis, urbanisation analysis, rainfall trend analysis and extreme rainfall events. The research gaps found from the literature review are as follows.

- Flood risk analysis was analyzed at large rivers, well-known river basins, or regional. The small river basin is not the focus of the analysis. However, this small river basin has their importance in that area.
- Flood risk was analyzed using different methodologies. We found 78 methods used in the literature. Limited study is available in literature on application of graph theory for flood risk analysis. However, in watershed management Graph theory is widely used.
- Flood risk analysis is limited to static factors and dynamic factors also act as static factors. There is a limitation to the study of flood projection using dynamic flood factors.
- Ghaggar River Basin experienced numerous flood events of low to high intensity of flood and the major areas of the basin rely on agricultural activity. Flood risk analysis and vulnerability to flood zone analysis are important for the basin.
- The rainfall study focused on the larger area which can not signify the status of the local area. The rainfall study is required for the basin to fulfil the agricultural demand.
- The flood events in the basin are occurred during extreme events. Therefore, the analysis of extreme events of rainfall is required for the Ghaggar river basin.

CHAPTER 3

3. Study Area

This chapter discussed the study area and dataset used for this study. The chapter started with a discussion of flood history in the basin. The study area, i.e., the Ghaggar River Basin, has been extracted from the watershed delineation using multiple GIS tools such as DEM acquisition, Fill Sinks, Flow direction, and Basin formation. Later, this chapter also discusses other geological and social factors of the basin, such as elevation, slope, climate, Land use land cover (LULC), soil group, population density, Household density, literacy rate, and road connectivity. These factors are later used for flood zone analysis.

3.1. Flood history of the Ghaggar river basin

Flood events in the Ghaggar River basin occurred frequently. In the past few decades, the highest peak river discharge in Ghaggar River at Tatiana gauzing station was observed on 26th September 1988 (56353 cusecs), 12th July 1993 (100000 cusecs), 06th September 1995 (62070 cusecs), 06th August 2004 (61730 cusecs), and 08th July 2010 (63460 cusecs) (12). The most devastating flood occurred in 1993. However, the second-highest and endmost ruinous flood occurred in 2010 (11). Figure 3.1 shows the Ghaggar River basin's flood inundated and affected area during the 2010 Punjab flood. The middle part of the basin is inundated across the river channel. However, some portion of the upper middle part of the basin is also inundated. 2010 flood occurred during 06 – 12th July. Ambala, Patiala, Kurukshetra, Kaithal, Fatehabad, Sangrur, etc., districts of Punjab and Haryana were highly affected during the 2010 flood. Around 2 lakh hectares of agricultural area, scores of humans, and thousands of cattle losses, infrastructure such as roads, rail lines, bridges, buildings, etc., have been damaged due to the flood(11,418). On July 06^{th,} 2010, Ambala cantonment, Ambala city, and Shahbad of Ambala district of Haryana were flooded. On July 7^{th,} 2010, part of the Patiala district was inundated and overflowed. In the Patiala and Ambala districts, abnormal river flows were observed for 05-08 July 2010. The highest inundation and most affected areas are the Ambala district of Haryana and Patiala district of Punjab. Considering the high flood-prone areas of the Ghaggar river basin, this study covers the origin part of the Ghaggar river basin up to the covering of the Patiala and Ambala districts.

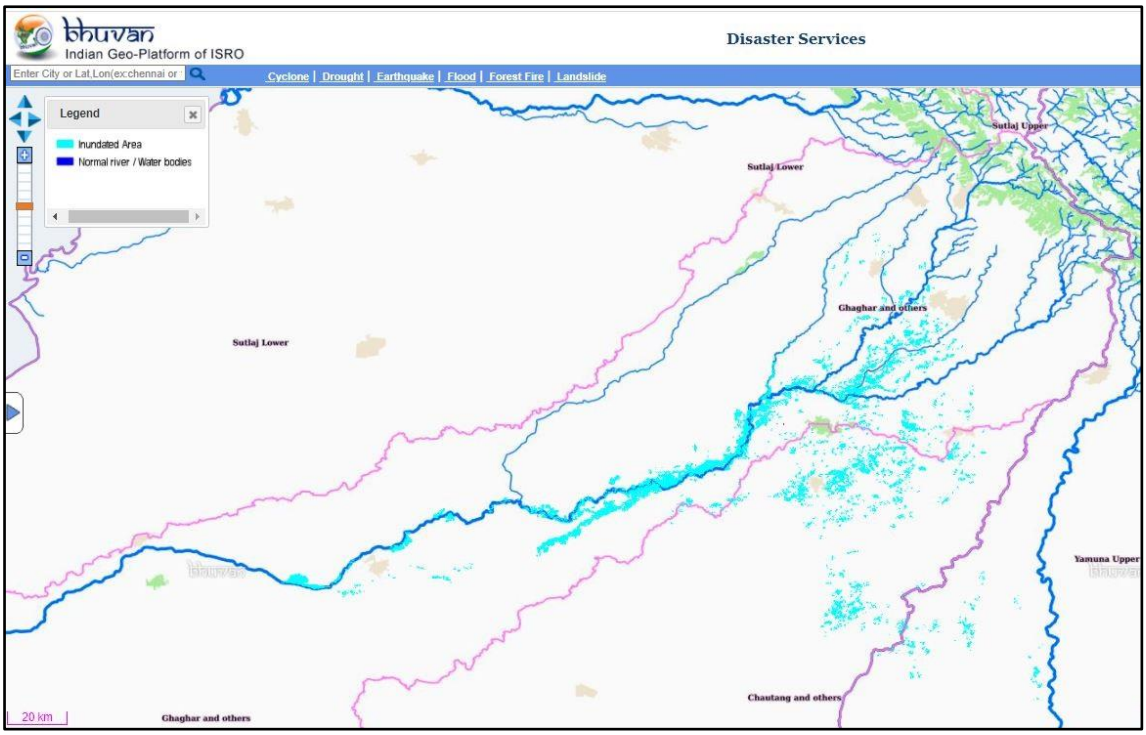

Figure 3.1 Flood inundated area of Ghaggar river basin during 2010 Punjab flood dated 14th July 2010 (**Source:** Bhuvan Disaster Services inundation map)

3.2. Overview of the Ghaggar river basin

Ghaggar river basin originated in the Shivalik hills of Himachal Pradesh and flows through Haryana, Punjab, and Rajasthan. The basin has disappeared in the Thar desert of Rajasthan. The total area of the Ghaggar river basin is 32132 sq. km. Under this Ghaggar river basin, the streams are Dungri Nadi (1138 sq. km), Saraswati (1511 sq. km), Saraswati (2272 sq. km), Phagna Nadi (2708 sq. km), Patiali Rao (1594 sq. km), Jainti Devki Rao (1862 sq. km), Choa Nadi (985 sq. km), and Ghaghar (20062 sq. km) (Source: http://cgwb.gov.in/watershed/cdghaghar.html).

The study area, the Ghaggar River basin, is extended in the northern latitude of 74°59'54.996"N to 77°23'34.1268"N and eastern longitude of 29°34'30.9792"E to 30°54'28.98"E. Figure 3.2 shows the location of Ghaggar river basin in India used for conducting this study. The total catchment area of the basin is 13978 sq. km and covers a part of the north Indian states of Himachal Pradesh, Punjab, and Haryana. Table 3.1 shows India's states, districts, and tehsil under the basin. Seven tehsils under two districts of Himachal Pradesh, fourteen tehsils under nine districts of Haryana, thirteen tehsils under seven districts, and the union territory of Chandigarh are located in the catchment of the Ghaggar river basin. Cities such as Chandigarh, Ambala, Patiala, and Rajpura are located in the catchment of the basin. Twelve hydro-

meteorological stations of the Indian Meteorological Department (IMD) are in the basin (Figure 3.2). Daily rainfall data of these twelve stations is collected and further used to analyze.

Table 3.1 State, Districts, and Tehsils located in the Ghaggar river basin

Country	State	District	Sr. No	Tehsil
India	Himachal Pradesh	Sirmaur	1	Nahan
			2	Pachhad
			3	Paonta
		Solan	4	Kasauli
			5	Solan
	Chandigarh (UT)	Chandigarh	6	Chandigarh
	Haryana	Ambala	7	Ambala
			8	Narayangarh
		Fatehabad	9	Fatehabad
			10	Ratia
			11	Tohana
		Jind	12	Narwana
		Kaithal	13	Gulha
			14	Kaithal
		Karnal	15	Karnal
		Kurukshetra	16	Pehowa
			17	Thanesar
		Panchkula	18	Kalka
		Sirsa	19	Sirsa
		Yamunanagar	20	Jagadhri
	Punjab	Fatehgarh Sahib	21	Sirhind
		Ludhiana	22	Khanna
		Mansa	23	Mansa
		Patiala	24	Nabha
			25	Patiala
			26	Rajpura
			27	Samana
		Rupnagar	28	Rupnagar
		Sahibzada Ajit Singh Nagar	29	Kharar
			30	Rajpura
		Sangrur	31	Maler Kotla
			32	Sangrur
			33	Sunam

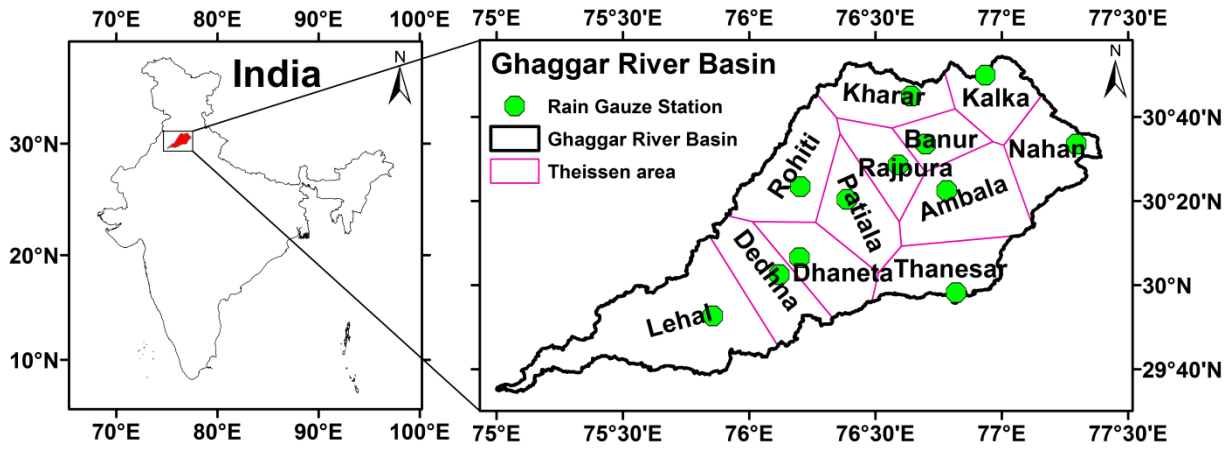

Figure 3.2 Study area of Ghaggar river basin in India

3.3. Watershed delineation and stream link

The perspective of watershed delineation describes the steps involved in delineating a watershed boundary from a Digital elevation model (DEM). The necessary step of the watershed delineation is processed using ArcGIS 10.5. The stream link is the channel through which water can be expected to flow. Several studies are available for watershed delineation and stream networks (419–422). The steps involved in watershed delineation and stream network for this study, as shown in Figure 3.3, are executed from the literature study.

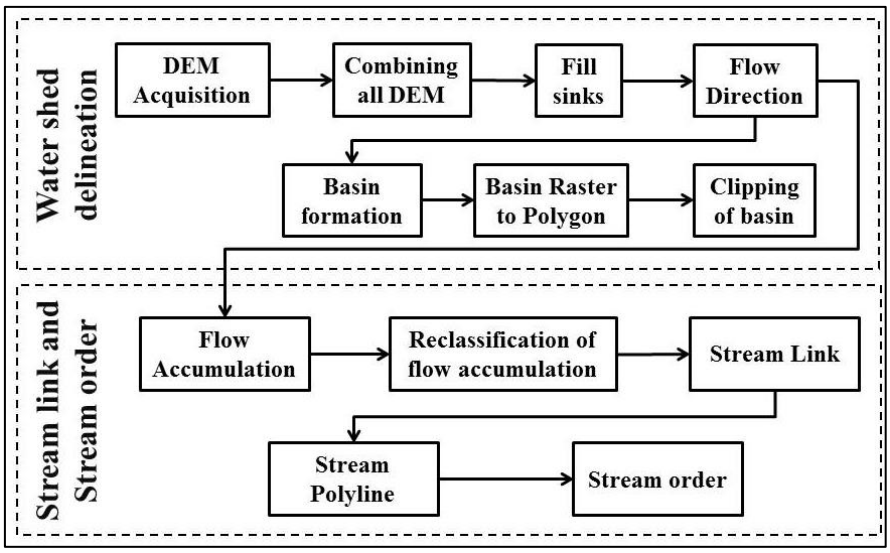

Figure 3.3 Methodology flow chart for watershed delineation and stream link

3.3.1. DEM Acquisition

Six digital elevation models covering the proposed study area were collected from Cartosat-1 (Version 1), Bhuvan (https://bhuvan-app3.nrsc.gov.in/data/download/). The selection process of the required DEM was based on the area of Patiala and Ambala districts and the origin of

the basin. Collected six DEMs entirely cover all the areas of the targeted areas. The size of each DEM file is 1° square dimension, and the resolution is 1arc second, i.e., 30m. Table 3.2 shows the collected DEM details such as the Name of the Dataset in Bhuvan, Toposheet no, Longitude, and Latitude extension. Figure 3.4 shows six DEMs used for watershed delineation. The latitude of the DEMs is extended from 75°E to 78°E and longitude from 29°N to 31°N. The elevation of DEMs lies in the range of 93m – 3483m. However, four out of six DEMs' elevation is less than 500m.

Table 3.2 Dataset details of Digital Elevation Model (Source: Bhuvan)

Sr. No	Name of the Dataset	Toposheet No	Coverage							
			Upper left		Upper Right		Lower left		Lower Right	
1	C1_DEM_16b_2006-2008_V1_75E29N_H43P	h43p	75E	30N	76E	30N	76E	29N	75E	29N
2	C1_DEM_16b_2006-2008_V1_75E30N_H43J	h43j	75E	31N	76E	31N	76N	30N	75E	30N
3	C1_DEM_16b_2006-2008_V1_76E29N_H43Q	h43q	76E	30N	77E	30N	77E	29N	76E	29N
4	C1_DEM_16b_2006-2008_V1_76E30N_H43K	h43k	76E	31N	77E	31N	77E	30N	76E	30N
5	C1_DEM_16b_2006-2008_V1_77E29N_H43R	h43r	77E	30N	78E	30N	78E	29N	77E	29N
6	C1_DEM_16b_2006-2008_V1_77E30N_H43L	h43l	77E	31N	78E	31N	78E	30N	77E	30N

3.3.2. Combining all DEM

After acquiring DEMs, combining all DEMs into a single raster file is the next step to forwarding the water delineation process. This step is necessary as the downloaded DEM are multiple numbers due to the larger basin area. The process flow of DEM combining process in ArcGIS is "*>>ArcGIS 10.5 → Arc Tool Box → Spatial Analyst Tools → Data Management Tools → Raster → Raster Dataset → Mosaic to new Raster → Select all DEM as input raster and give output name as combined DEM in Output Raster → OK".* Figure 3.5 shows the combined DEM of all DEMs. The combined DEM shows that a significant part of the basin is under 500m elevation, with higher elevation found in the northeastern part of the DEM.

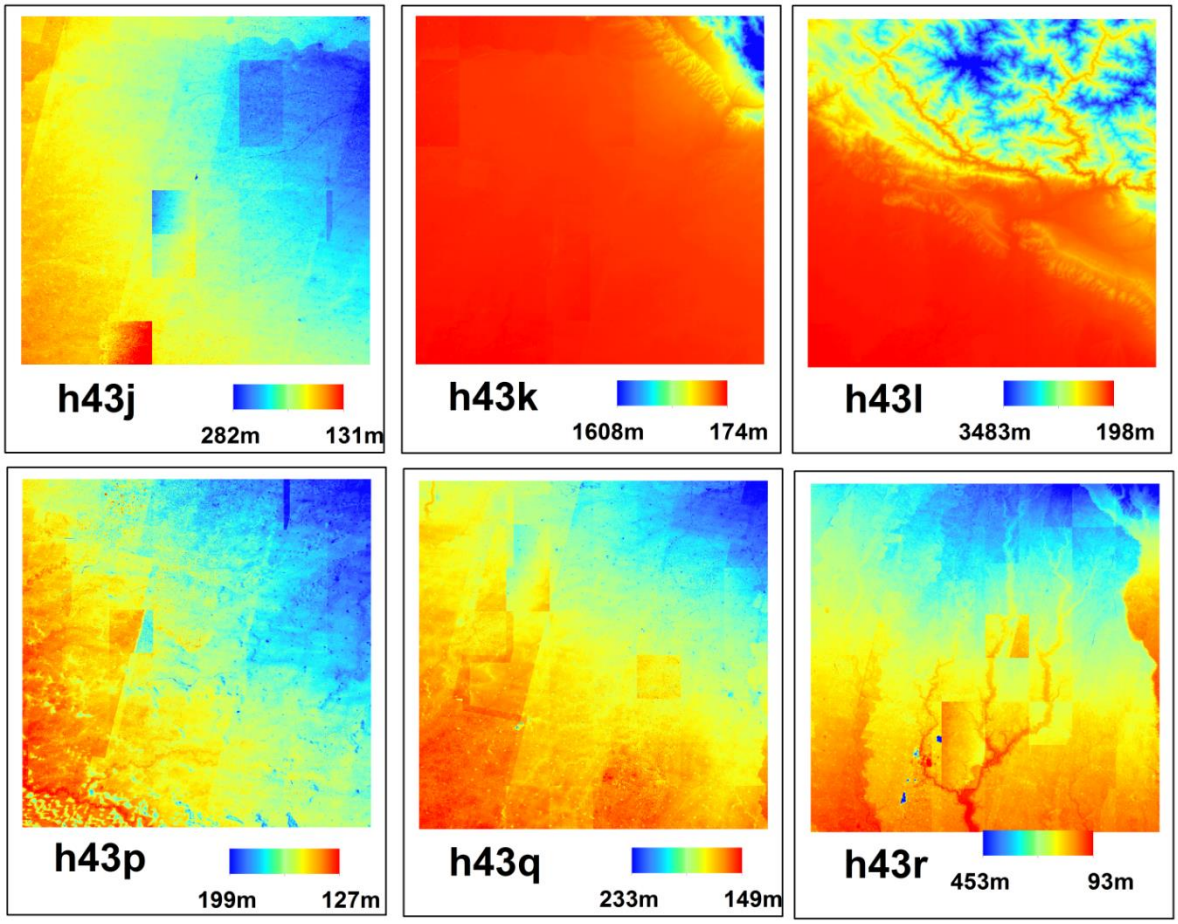

Figure 3.4 Individual digital elevation model used for watershed delineation (toposheet number wise)

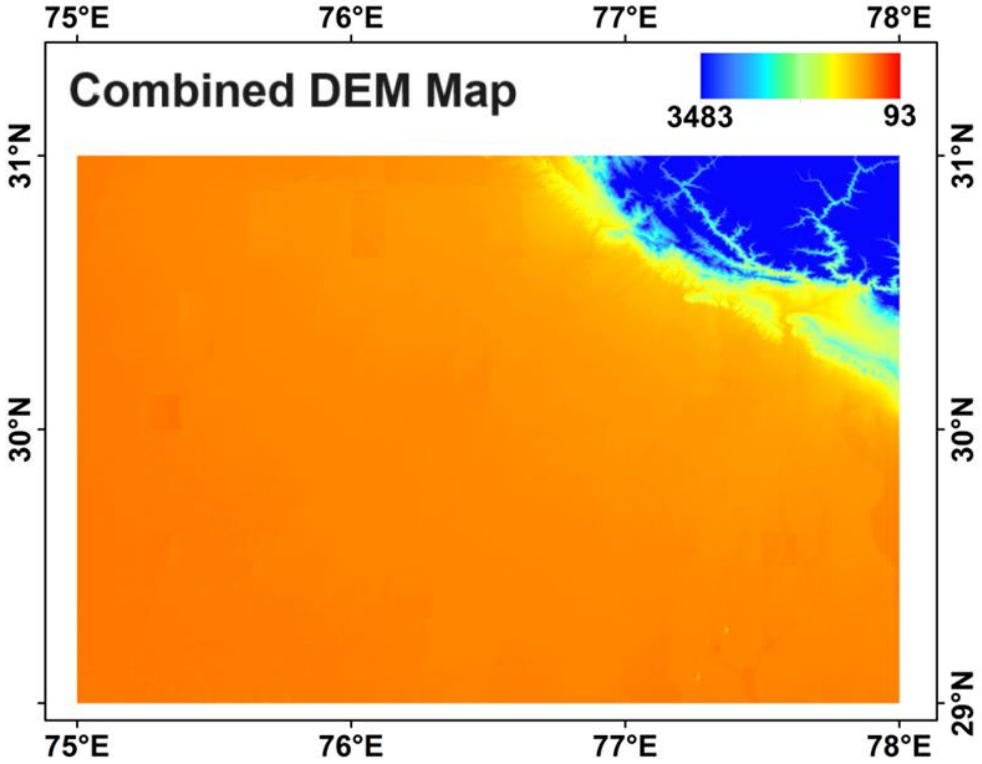

Figure 3.5 Combined DEM of all DEM dataset

3.3.3. Fill sinks

Fill sinks are the next step of watershed delineation to clean up the DEM as sink-free or depression-free. A sink or depression is an area of undefined DEM lateral flow or internal drainage (421). Fill sinks remove the depression of single or multiple pixels of DEM. Single-pixel depression is any pixel value lower than all other eight neighboring pixels, whereas multiple-pixel depression is a group of pixels value lower than its surrounding pixels. The process flow of fill sinks operation in ArcGIS is " *>>ArcGIS 10.5 → Arc Tool Box → Spatial Analyst Tools → Hydrology → Fill → Select combined DEM as Input Surface Raster and give output name as Fill map in Output Surface Raster → OK".* Figure 3.6 shows the filled map of the sink or depression-removed DEM.

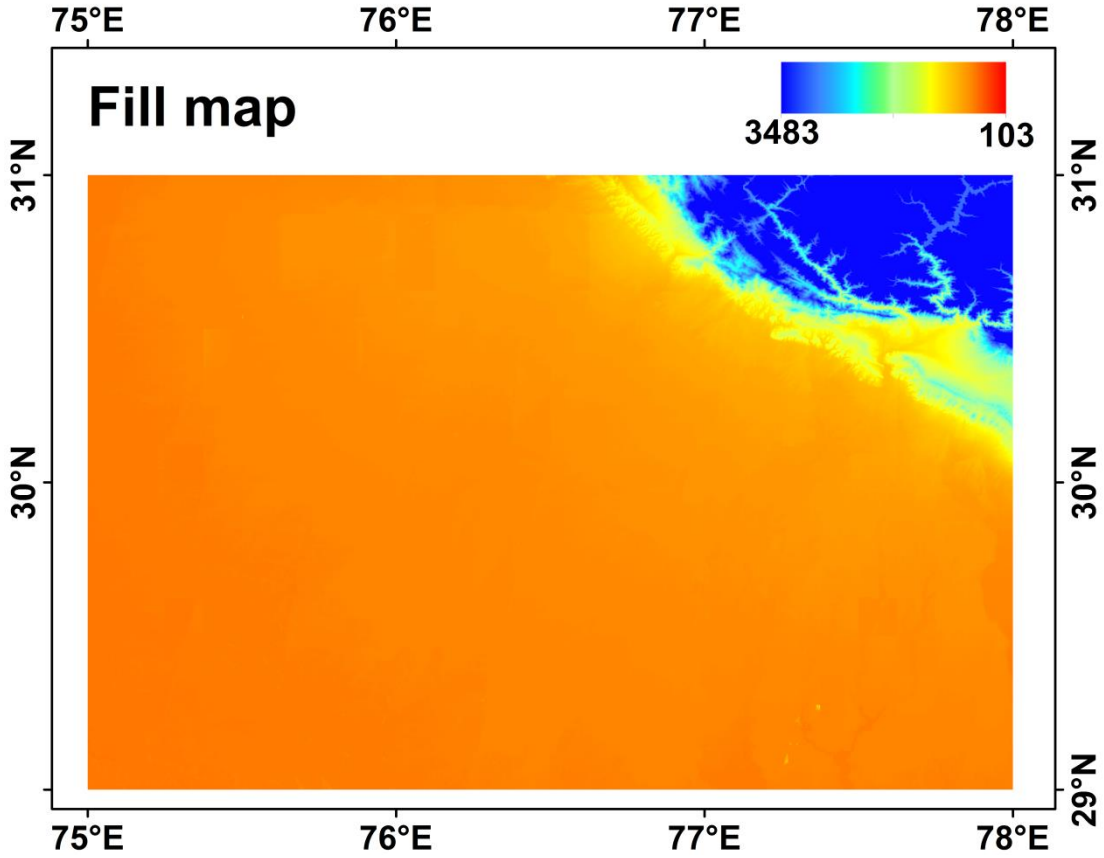

Figure 3.6 Fill map after removal of sinks or depressions from DEM

3.3.4. Flow Direction

Flow direction is the direction of flow in each pixel of the DEM. The flow direction is executed by comparing the elevation of one pixel with its neighboring pixels (421). There are eight flow directions, as one pixel is neighbored by eight pixels. The process flow of flow direction operation in ArcGIS is *">>ArcGIS 10.5 → Arc Tool Box → Spatial Analyst Tools → Hydrology → Flow Direction → Select Fill map as Input Surface Raster and give output name*

as flow direction in Output flow direction Raster → OK". Figure 3.7 shows the flow direction map executed from the fill map of DEM.

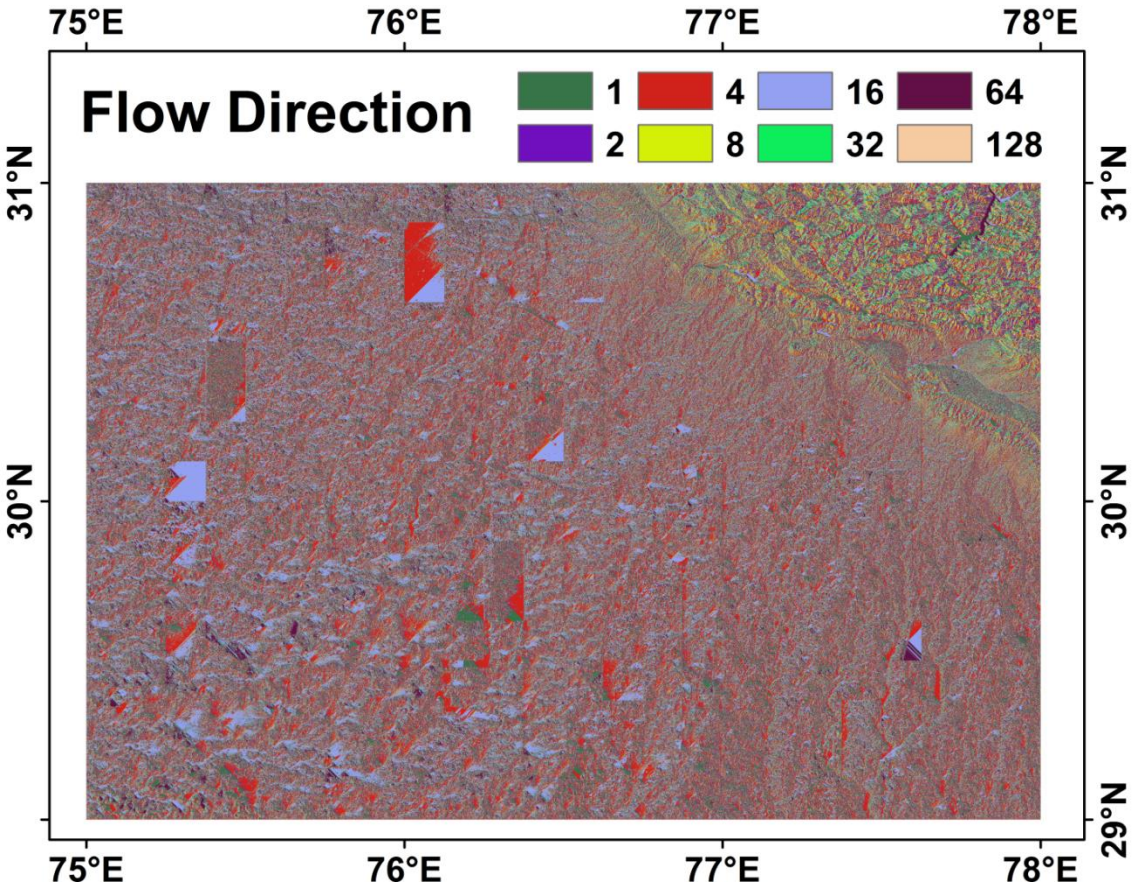

Figure 3.7 Flow direction map executed from fill map of DEM

3.3.5. Basin formation

The basin is analyzed using the flow direction raster connecting the cells that belong to the same drainage basin. The basin is created by locating the pour points at the edge of the analysis window, i.e., the flow pours out of the raster. The process flow for creating a basin map in ArcGIS is "*>>ArcGIS 10.5 → Arc Tool Box → Spatial Analyst Tools → Hydrology → Basin → Select Flow direction map as Input flow direction Raster and give output name as Basin map in Output Raster → OK*". Figure 3.8 shows the basin map executed from the flow direction map.

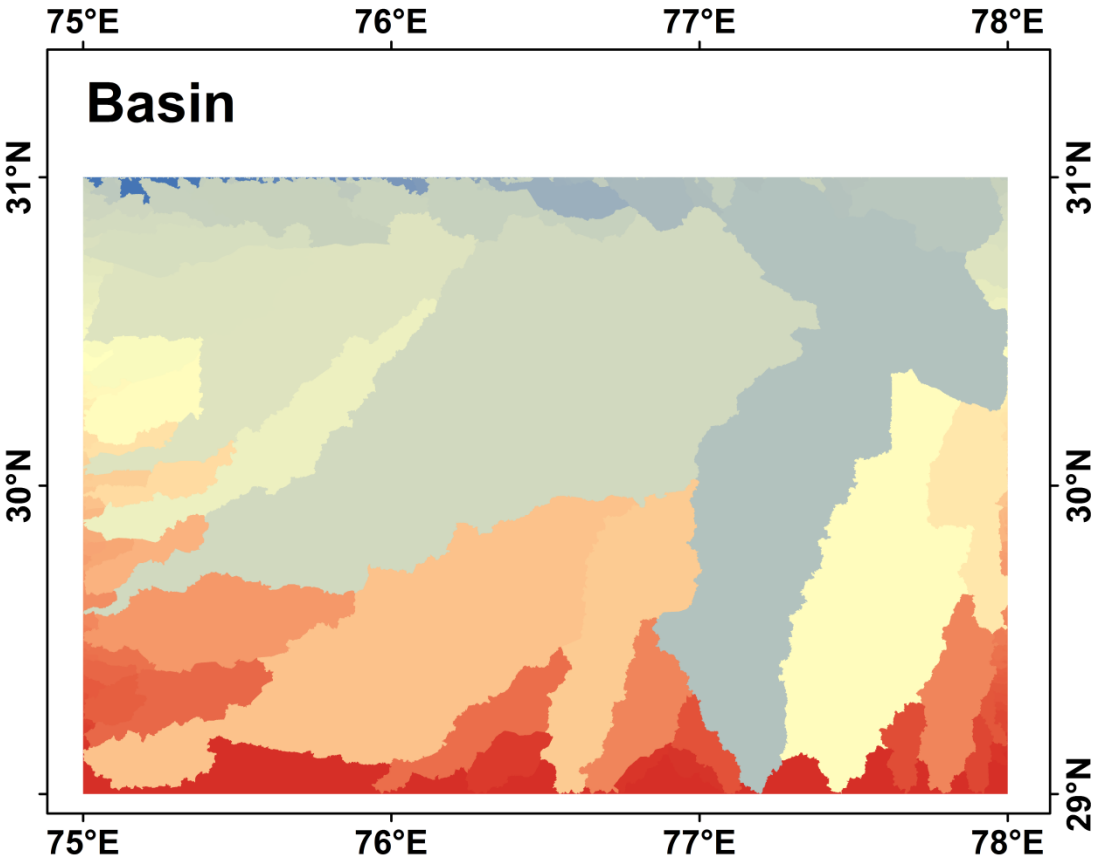

Figure 3.8 Basin map executed from flow direction map

3.3.6. Basin Raster to Polygon

The basin map is executed using a flow direction raster. This basin map is in raster form. Therefore, it must be converted to a polygon to identify the basin's boundary. The conversion of the raster of the basin to polygon in ArcGIS is "*>>ArcGIS 10.5 → Arc Tool Box → Conversion Tools → From Raster → Raster to Polygon → Select Basin map as Input Raster and give output name as Basin polygon in Output polygon features → OK*". Figure 3.9 shows the polygon of the basin executed from the basin raster.

3.3.7. Clipping of basin

The executed basin polygon map consists of numerous basins. Therefore, clipping the basin is the next necessary step to execute the watershed we need for further study. The process flow for clipping the basin in ArcGIS is "*>>ArcGIS 10.5 → Geoprocessing → Clip → Select Basin polygon as Input Features; Select Basin polygon as clip features and give output name as Basin shapefile Output feature class → OK*". Figure 3.10 shows the study area basin, i.e., the Ghaggar River basin clipped from the basin polygon. The latitude extension of the Ghaggar River basin is 29°34'30.9792"E to 30°54'28.98"E, and the longitude extension of the Ghaggar River basin is 74°59'54.996"N to 77°23'34.1268"N.

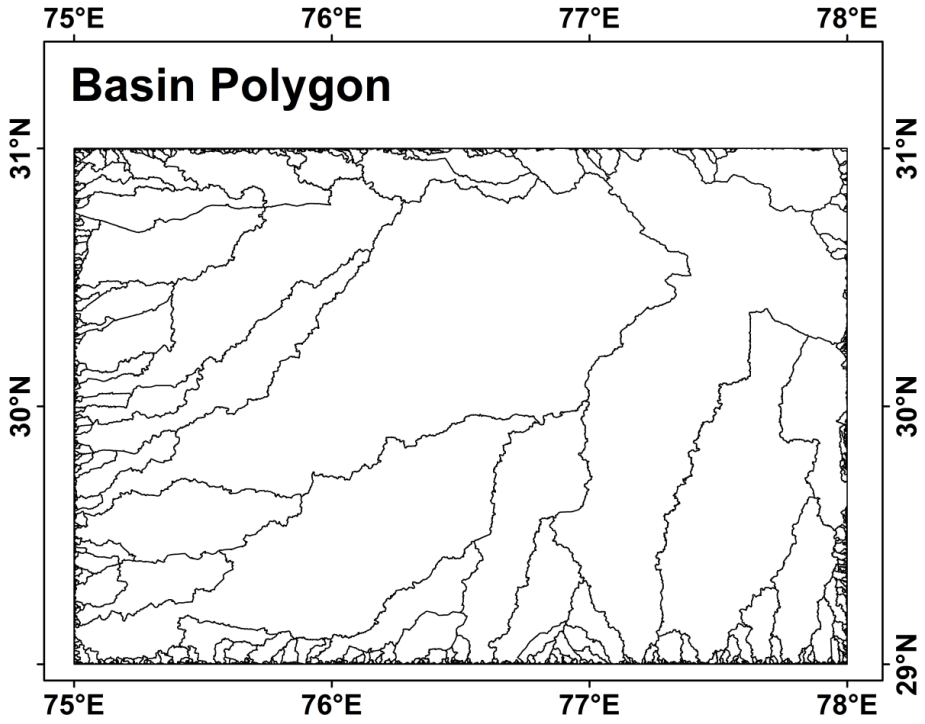

Figure 3.9 Polygon of basin executed from the basin raster

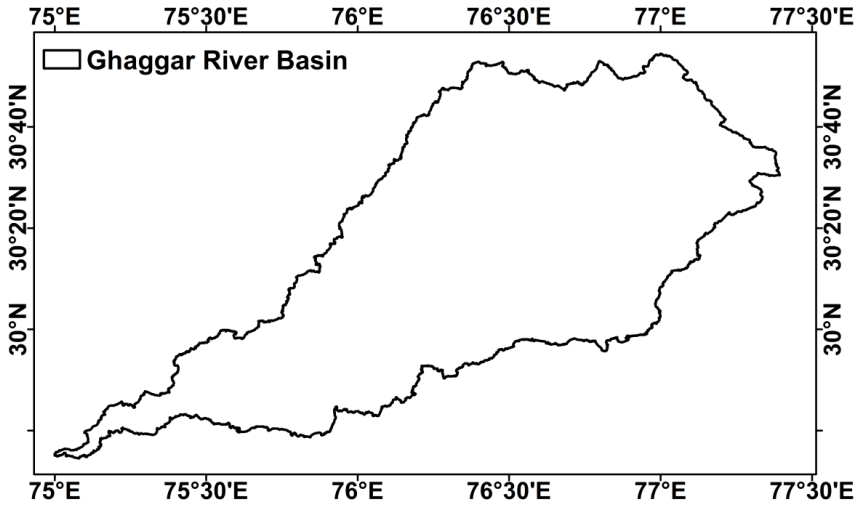

Figure 3.10 Study area basin, i.e., Ghaggar river basin clipped from the basin polygon

3.3.8. Flow accumulation

Flow accumulation is the calculation of accumulated flow in downslope cells of the output raster. The output flow accumulation raster value is calculated as the number of cells that flow into that cell. The flow accumulation can be derived for the DEM executed basin flow direction raster. The flow accumulation raster must be created only for the basin area. Therefore, setting up the environment in ArcGIS as the study basin should be taken so that further steps will only be worked in the study basin. The process of setting up the environment is "*>>ArcGIS 10.5 → Geoprocessing →Environments→ In processing extent, select the basin shapefile as Extent →*

In Raster Analysis, select the basin shapefile as Mask → OK". Now, the further steps will only apply to the basin area. The process flow for calculation of flow accumulation in ArcGIS is "*>>ArcGIS 10.5 → Arc Tool Box → Spatial Analyst Tools → Hydrology → Flow Accumulation → Select Flow direction map as Input flow direction Raster and give output name as Flow accumulation in Output accumulation Raster → OK*". Figure 3.11 shows the flow accumulation map created from the flow direction raster.

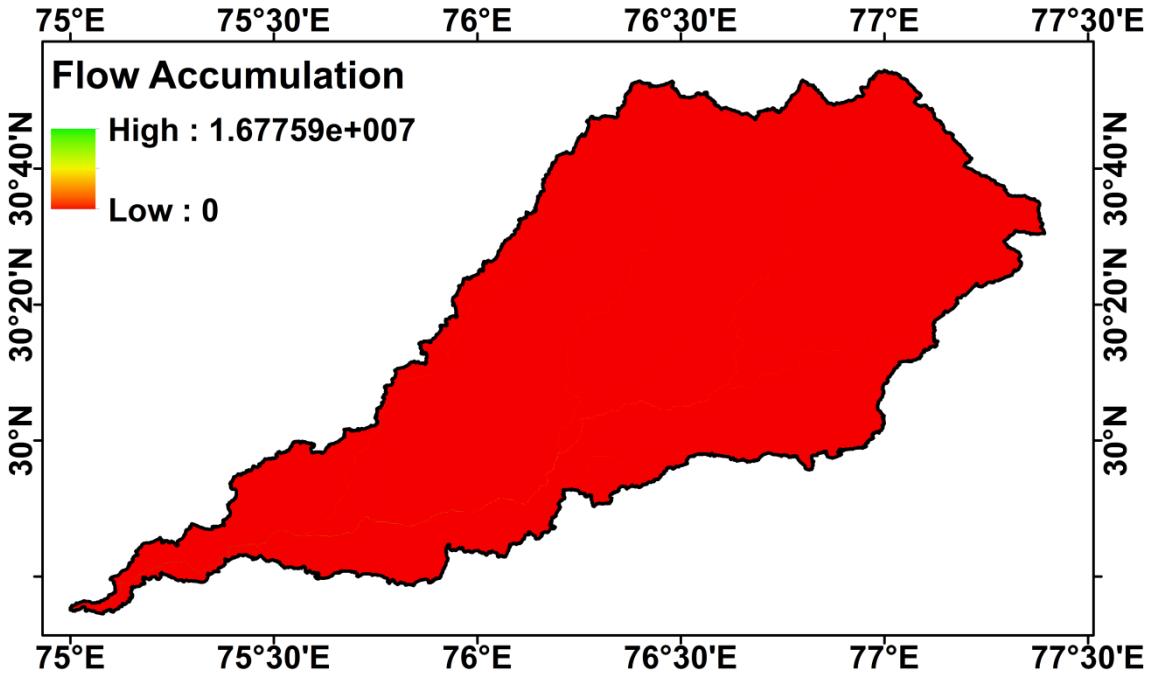

Figure 3.11 Flow accumulation map executed from flow direction raster

3.3.9. Reclassification of flow accumulation

The classification of the flow accumulation raster is necessary to find out the streamline. A threshold limit was taken where the accumulated flow starts to drain in a stream, and the lower threshold limit was considered no stream. In this study, a threshold limit of 10,000 cells was selected. Therefore, a streamline will be formed where the flow accumulation value is higher than 10000 and lower than 10000 will be counted as no stream. The steps involved in the reclassification of flow accumulation are "*>>ArcGIS 10.5 → Arc Tool Box → Spatial Analyst Tools → Map Algebra → Raster Calculator → Write by selecting flow accumulation map and put >10000 in math expression box → give output name as reclassified flow accumulation raster in Output raster → OK"*. Figure 3.12 shows the reclassified flow accumulation raster. The value 0 indicates no stream, whereas 1 indicates the raster of a stream.

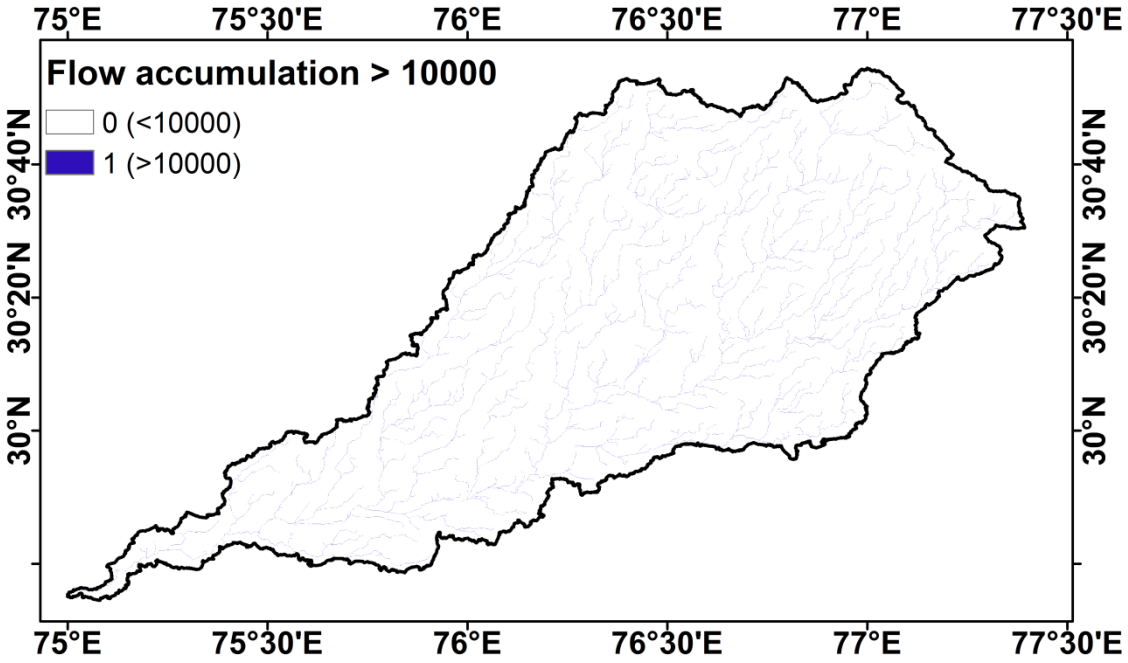

Figure 3.12 Reclassified flow accumulation raster of Ghaggar River basin

3.3.10. Stream link

Stream links are the steps of connecting two successive junctions of flow accumulation into one. Threshold-defined raster is used as an input stream to connect the joints. The steps for creating a stream link raster in ArcGIS are "*>>ArcGIS 10.5 → Arc Tool Box → Spatial Analyst Tools → Hydrology → Stream Link → Select reclassified flow accumulation raster as Input stream raster and select the flow direction raster as Input flow direction Raster and give output name as Stream link Raster in Output raster → OK*". Figure 3.13 shows the stream link raster of the Ghaggar river basin.

3.3.11. Stream Polyline

Stream link raster has generated the link of all junctions and created a stream link. However, the stream link is in the raster file. Therefore, a stream polyline should be created to show the line of the stream. The steps involved in creating stream polyline or streamline in ArcGIS are "*>>ArcGIS 10.5 → Arc Tool Box → Conversion Tools → From Raster → Raster to Polyline → Select reclassified stream link raster as Input Raster and give output name as Output polyline features → OK*". Figure 3.14 shows the stream polyline of the Ghaggar river basin. Stream polyline can also be abbreviated as streamline, drainage line, stream network, river, etc.

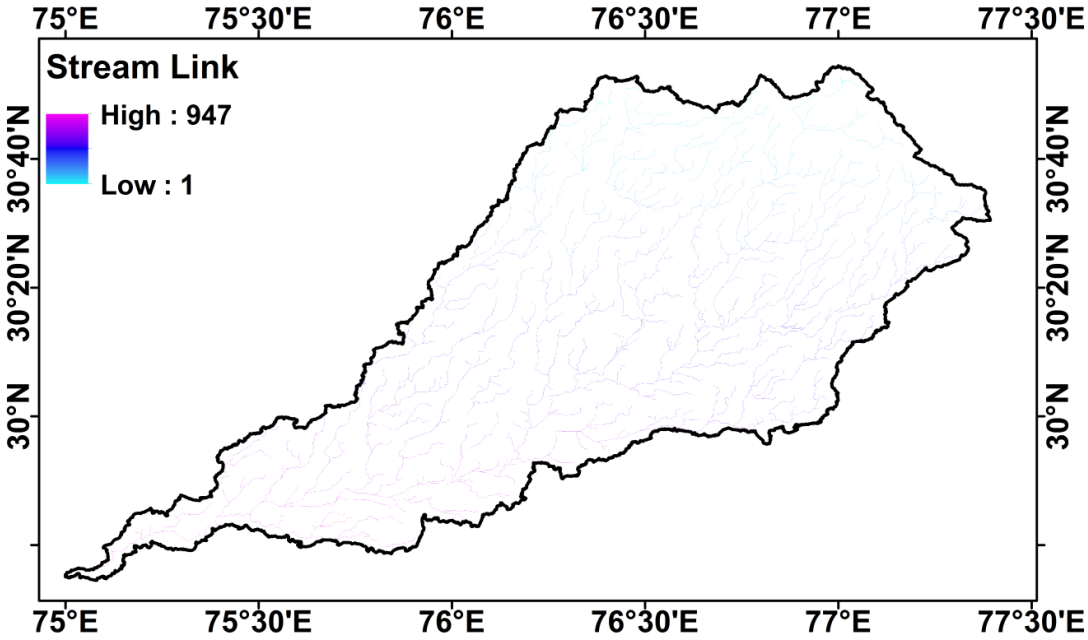

Figure 3.13 Stream link raster of Ghaggar river basin

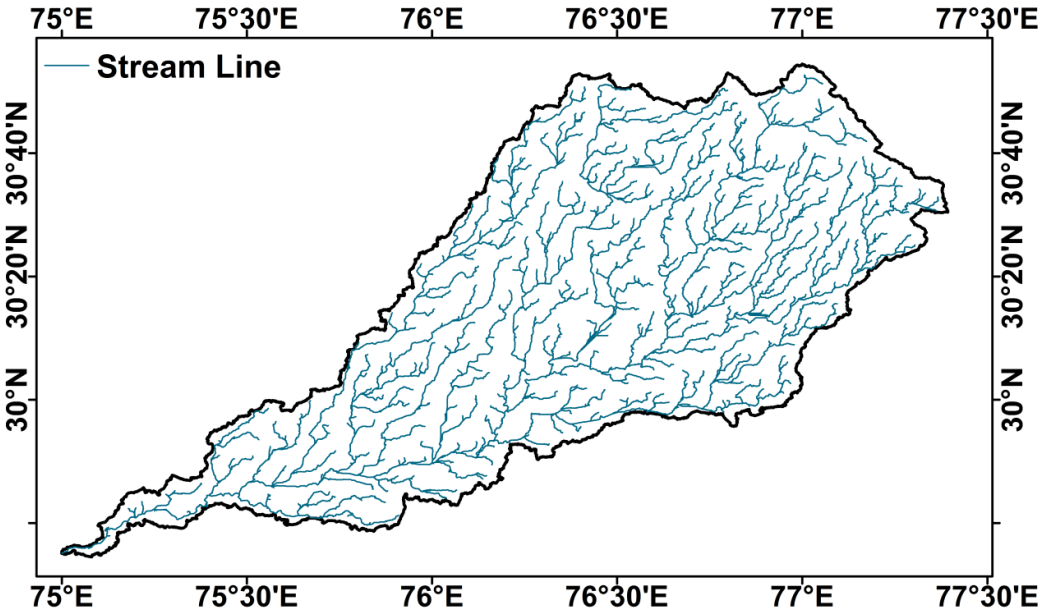

Figure 3.14 Stream polyline of Ghaggar river basin

3.3.12. Stream order

Stream order calculation is the first step of quantitative analysis of the watershed. Stream order is the channel of a different order, such as first, second, third, etc. The first-order stream is just the channel formed, the second-order stream where two or more first-order streams are joined, the third-order stream where two or more second-order streams are connected, etc. Two steps of stream order calculation are generating stream order in the raster file and converting the raster file to the polyline file. The stream order raster generation in ArcGIS was processed in

step as "*>>ArcGIS 10.5 → Arc Tool Box → Spatial Analyst Tools → Hydrology → Stream order → Select Stream link raster as Input stream raster and select the flow direction raster as Input flow direction Raster and give output name as Stream order Raster → OK*". Figure 3.15 shows the stream order raster of Ghaggar river basin. Five orders of the stream are shown in Figure 3.15. The polyline connection of stream order is generated using the steps "*>>ArcGIS 10.5 → Arc Tool Box → Spatial Analyst Tools → Hydrology → Stream to feature → Select Stream order raster as Input stream raster and select the flow direction raster as Input flow direction Raster and give output name as Stream order polyline → OK*". Figure 3.16 shows the stream order as a polyline of the Ghaggar river basin.

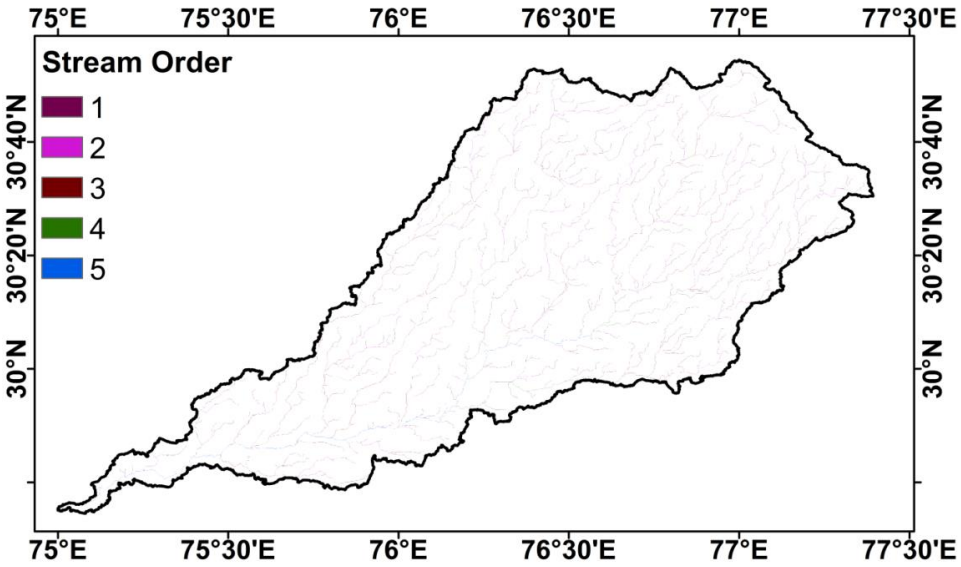

Figure 3.15 Stream order raster of Ghaggar river basin

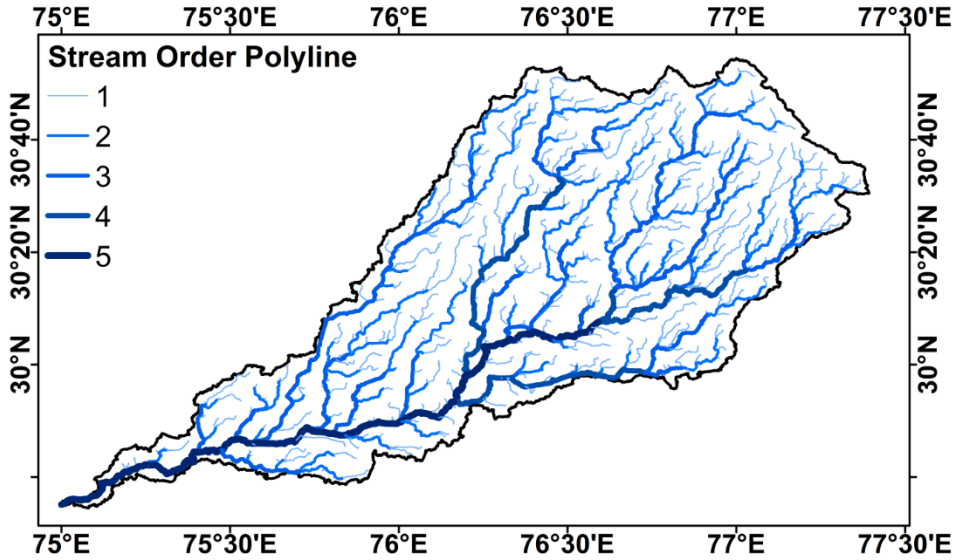

Figure 3.16 Stream order polyline of Ghaggar river basin

3.3.13. Drainage Area

The entire area drained by a stream or channel is the drainage area of the basin. The drainage area of the stream is increased with the order of the stream. The drainage area of the watershed is the total area of the watershed. Therefore, the total area of the watershed can be calculated directly using the cell number, resolution, etc. The total area of the watershed is found to be 13978 sq. km.

3.3.14. Watershed length

The watershed length is defined as the length of the main channel from its origin to the watershed outlet. Watershed length (W_L) is very dependent on the watershed area, and it can be mathematically expressed in equation 3.1.

$$W_L = 1.4 \times {D_a}^{0.568} \quad (3.1)$$

Where, D_a is the drainage area watershed in sq. km.

The length of the Ghaggar River basin watershed is found 316.76 km.

3.4. Elevation

Elevation data is the same DEM data collected for the Ghaggar River basin watershed delineation. The elevation for the Ghaggar River basin was clipped from the combined DEM shown in Figure 3.5. The elevation of the Ghaggar river basin lies in the range of 143m – 1790m. Figure 3.17 shows the spatial elevation map of the Ghaggar River basin. Figure 3.17 shows that a significant portion of the basin is less than 500m in elevation. Figure 3.18 was plotted to show the area under different elevations in the Ghaggar River basin. A significant portion (92%) of the basin is less than 350m, and around 8% of the total basin area is above 350m elevation. In contrast, only 1.5% of the basin area is above 1000m elevation. The upper part of the basin is at a higher elevation as this part of the basin is located at Shivalik Hill of Himachal Pradesh. A rapid decline in elevation is found at the end of the Shivalik hills and the start of the plain area. However, the average elevation of the basin is 247m±160m, calculated in the spatial map. The variation in elevation is found at 64.7%.

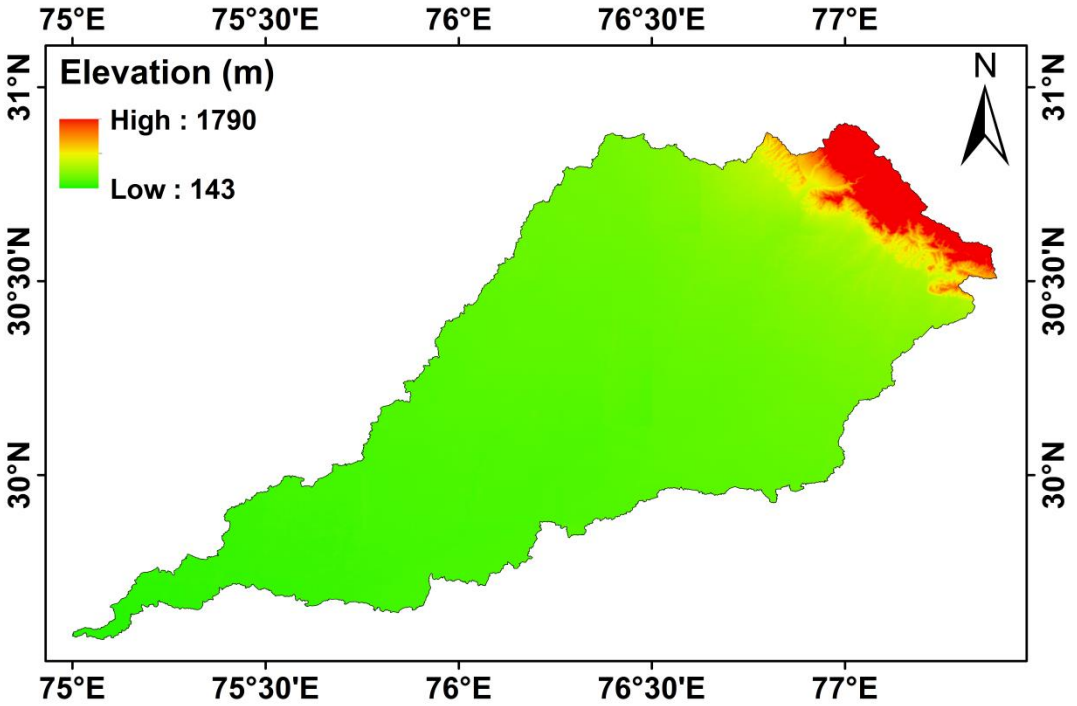

Figure 3.17 Elevation profile of Ghaggar river basin.

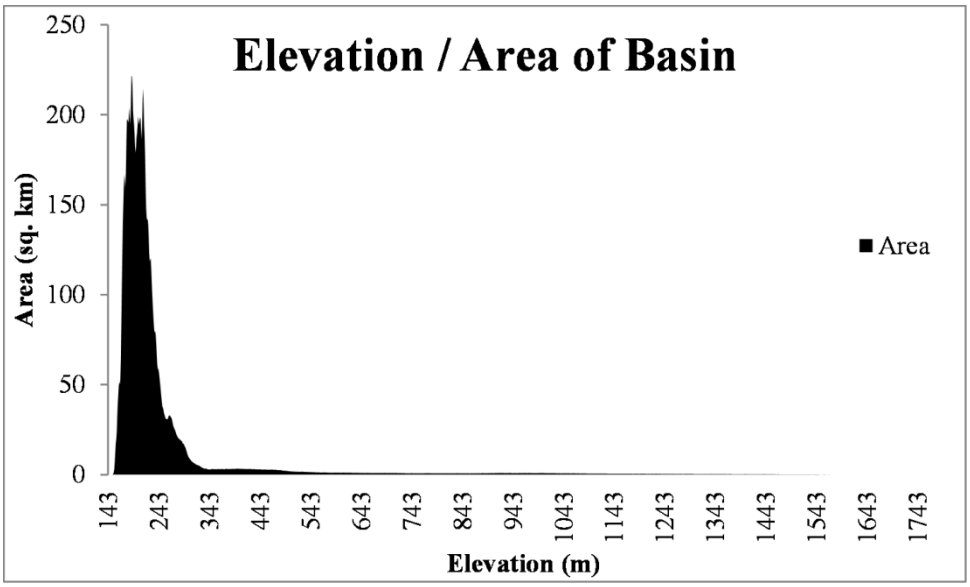

Figure 3.18 Area under different elevation of Ghaggar river basin

3.5. Slope of the watershed

The slope is the elevation change measurement, and the measurement unit can be ° (degree) or % (percentage) of rising. The basin slope is executed from the elevation map shown in Figure 3.17. The steps involved in executing the slope map in ArcGIS are "*>>ArcGIS 10.5 → Arc Tool Box → Spatial Analyst Tools → Surface → Slope → Select elevation model as Input*

Raster and give output name as Slope raster in Output raster; degree as output measurement and the z-factor is 9.26×10^{-6} → OK". Figure 3.19 shows the slope (°) map of the Ghaggar river basin. The slope of the basin lies in the range of 0-80.9°. The basin's average slope is 2.59°, and the standard deviation was found to be 3.99°. Therefore, the variation in the slope is 154%. A larger variation in slope is found. However, a significant portion of the basin is less than 6°.

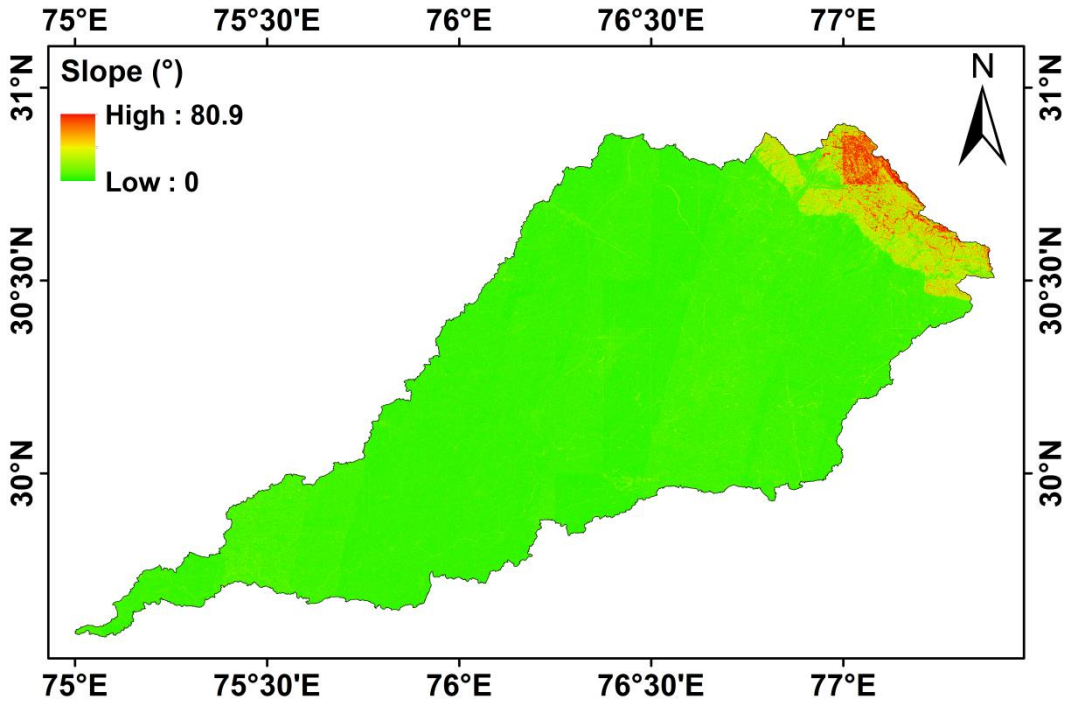

Figure 3.19 Slope map of Ghaggar river basin

3.6. Climate

The climatic condition of the Ghaggar River basin is arid, semi-arid, dry sub-humid, and moist sub-humid (423). The average temperature of the basin is 23.5°C, where summer temperature rises to 48.3°C, and winter temperature may decrease up to -2°C. The average rainfall over the basin was observed to be 698mm (424). The maximum rainfall occurred during the southwest monsoon season in the basin. Four climatic seasons as classified by the Indian Meteorological Department are applied to the basin. These seasons are pre-monsoon season (March-May), southwest monsoon season or monsoon season (June-September), post-monsoon season (October-December), and winter season (January-February). A detailed study on rainfall and extreme rainfall is carried out in this study itself.

3.7. Land use land cover

Land use land cover is the surface cover by grasslands, crops, urban built-up, water bodies, etc. The land use land cover (LULC) map is downloaded from Moderate Resolution Imaging Spectroradiometer (MODIS) Land Cover Type (MCD12Q1) Version 6. The 500m spatial resolution of the LULC is downloaded for 2019. Two spatial LULC map was downloaded, and the details of these maps are shown in Table 3.3. These downloaded maps were in HDF format. Therefore, these maps were converted to GeoTIFF format. After conversion, the maps are combined to create a single map. The LULC map of the Ghaggar River basin was clipped from the combined LULC map. Figure 3.20 shows the spatial distribution of the LULC of the Ghaggar River basin. MCD12Q1 International Geosphere-Biosphere Programme (IGBP) has classified LULC into 17 categories. However, only ten categories of LULC have been found in the Ghaggar River basin. Table 3.4 shows the different LULC categories found in the river basin with the area under that LULC category. A major portion of the basin is occupied by croplands (88.26%), savannas (6.16%), and urban built-up (3.39%). Other LULC categories also occupied the basin area; however, the occupied area is only 2.19%. Urban built-up includes buildings, roads, pavements, etc., with at least 30% impervious areas. Savannas, woody savannas, and mixed forests are mainly found at higher altitudes in the upper part of the basin. The LULC is dynamic as it changes over time. Therefore, the objective of this study also covers the analysis of urbanization. The analysis of urbanization needs two or more LULC maps. Therefore, 2001 and 2010 LULC maps are also collected from the MODIS. The resolution for 2001 and 2010 LULC map is 500m.

Table 3.3 LULC dataset details

Data Set Attribute	Attribute Value	Attribute Value
Local Granule ID	MCD12Q1.A2019001.h24v06.006.2020212132519.hdf	MCD12Q1.A2019001.h24v05.006.2020212132505.hdf
Entity ID	MCD12Q1.A2019001.h24v06.006	MCD12Q1.A2019001.h24v05.006
Acquisition Start Date	2019/01/01	2019/01/01
Acquisition End Date	2019/12/31	2019/12/31
Horizontal Tile Number	24	24
Vertical Tile Number	6	5
Day/Night Indicator	Day	Day
Version Number	6	6
Product Generation Algorithm	6.0.4	6.0.4
NW Corner Lat	30°01'59.16"N	40°03'14.40"N

NW Corner Long	69°01'31.08"E	78°06'42.84"E
NE Corner Lat	29°59'57.48"N	39°59'55.67"N
NE Corner Long	80°50'38.40"E	91°23'53.88"E
SE Corner Lat	19°54'00.72"N	29°50'42.36"N
SE Corner Long	74°29'34.44"E	80°46'52.32"E
SW Corner Lat	19°55'55.92"N	29°53'31.92"N
SW Corner Long	63°36'34.20"E	69°02'26.88"E

Table 3.4 Land use land covers (2019) category and its area

Sr. No	Abbreviation	LULC pattern	Area (%)
1	1	Evergreen Needle leaf forest	00.11
2	2	Evergreen broad leaf forest	00.00
3	5	Mixed Forest	00.90
4	8	Woody Savannas	00.50
5	9	Savannas	06.16
6	10	Grasslands	00.12
7	11	Permanent Wetlands	00.01
8	12	Croplands	88.26
9	13	Urban Built-up	03.39
10	14	Cropland/Natural Vegetation	00.54

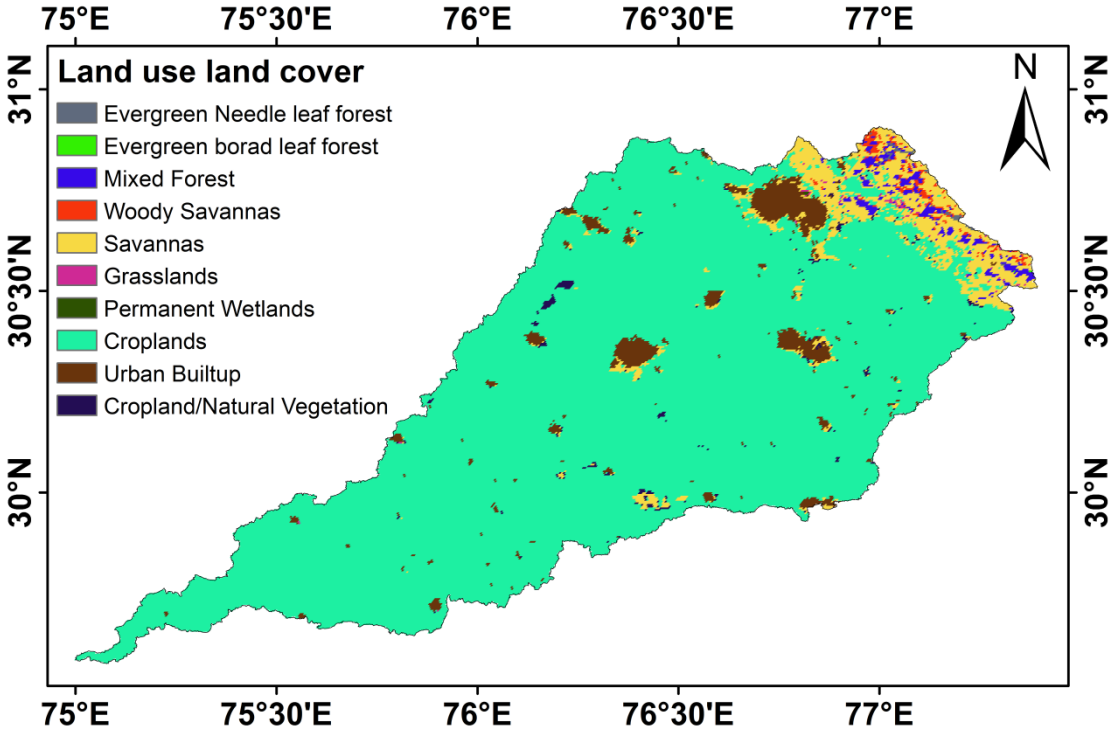

Figure 3.20 Land use land cover map of Ghaggar river basin for the year 2019

3.8. Soil group

The hydrologic soil groups (HSG) are classified as soil based on the runoff potential. Four primary classifications are A (low runoff potential), B (moderately low runoff potential), C (moderately high runoff potential), and D (high runoff potential) (178). 250 m resolution Hydrologic soil group data has been downloaded for India from Global Hydrologic Soil Groups (HYSOGs250m) for Curve Number-Based Runoff Modeling. The soil group map of the Ghaggar River basin is clipped from the original soil group map using ArcGIS. Figure 3.21 shows the soil group of the study area. The soil groups found in the study area are C (59.10%), D (0.24%), C/D (40.48%), and D/D (0.18%). So, the soil properties of the basin are moderately high to high runoff potential.

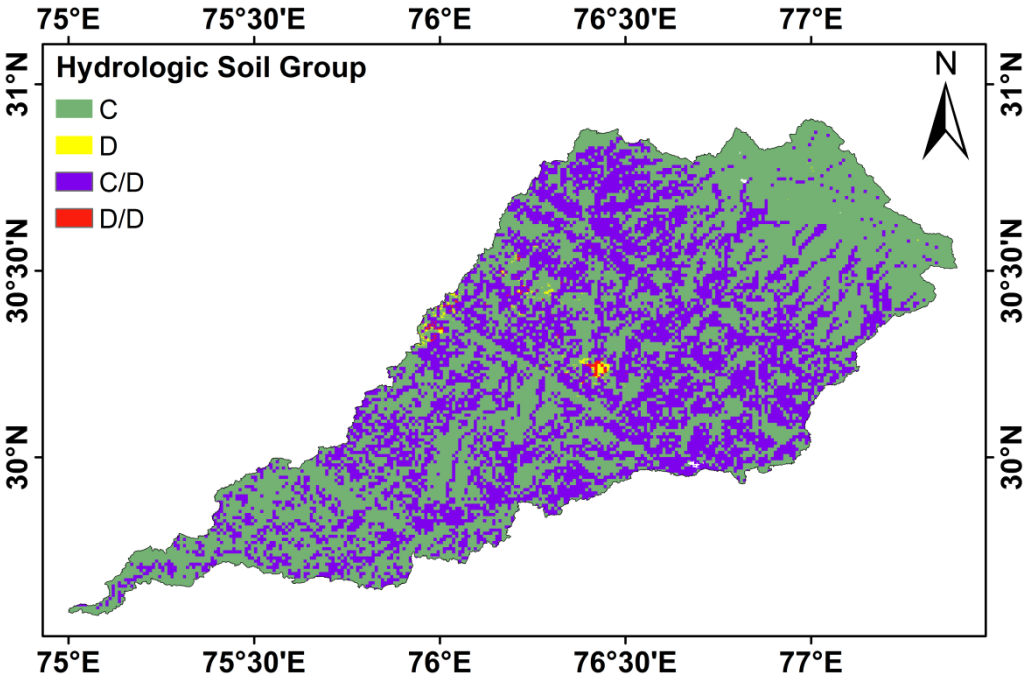

Figure 3.21 Hydrologic soil group of Ghaggar river basin

3.9. Population density

Population density is the number of people living in a square kilometre area. The spatial data of Census 2011 Indian population density (per sq. km) has been obtained from the Socioeconomic Data and Applications Center (SEDAC). The population density of the Ghaggar River basin is clipped from the spatial data in ArcGIS. Figure 3.22 shows the spatial population density map of the study area. The population density varies between 0 - 25177 people per sq. km. The major cities, such as Chandigarh, Patiala, Rajpura, and Ambala, have

the highest population density. The average population density of the basin is 457, and the standard deviation is 1007. The variation of the population from the mean is more than 200%.

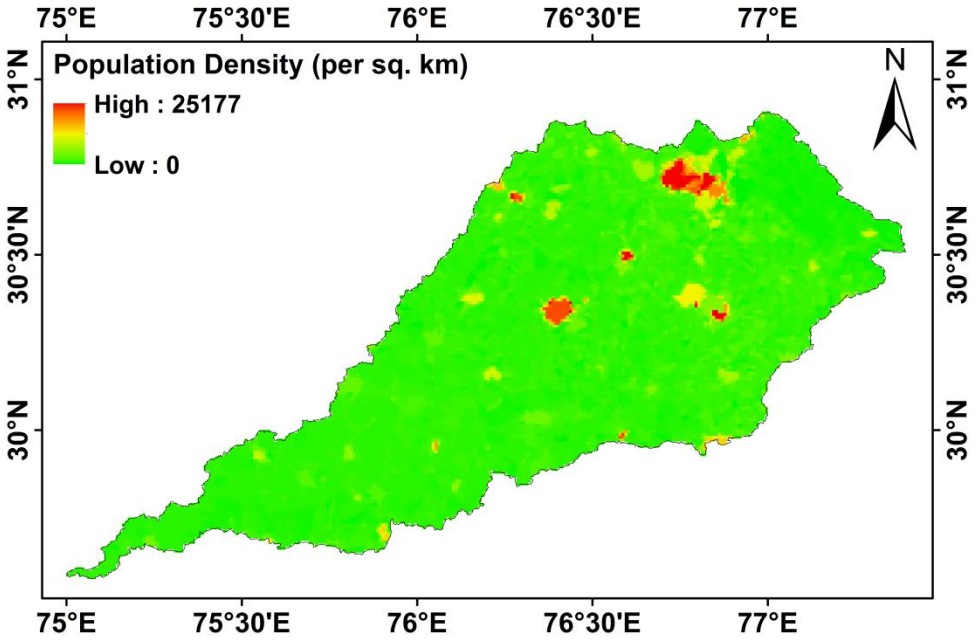

Figure 3.22 Population density of Ghaggar river basin

3.10. Household Density

Household density is the number of households present in a square kilometre. Tehsil-wise average household density data is extracted from Census 2011 data. The household density is spatially plotted using ArcGIS in the Ghaggar river basin map as its actual value over the tehsil. Figure 3.23 shows the tehsil-wise spatial plotting of household density over the Ghaggar River basin. The household density varies in the range of 9 -184 houses per sq. km in the study area. The Chandigarh union territory of India has the highest household density, 184 per sq. km.

3.11. Literacy rate

The literacy rate is the literate percentage of the population in an area. Tehsil-wise average literacy rate data was extracted from Census 2011 data. The literacy rate was spatially plotted using ArcGIS in the Ghaggar river basin map as its actual value over the tehsil. Figure 3.24 shows the spatial plotting of tehsil-wise literacy rate in percentage. The literacy rate in the study varied in the range of 52-76%. The highest literacy rate is found in Pachhad and Solan tehsil of Himachal Pradesh, whereas the lowest was observed in Mansa and Sunam of Punjab.

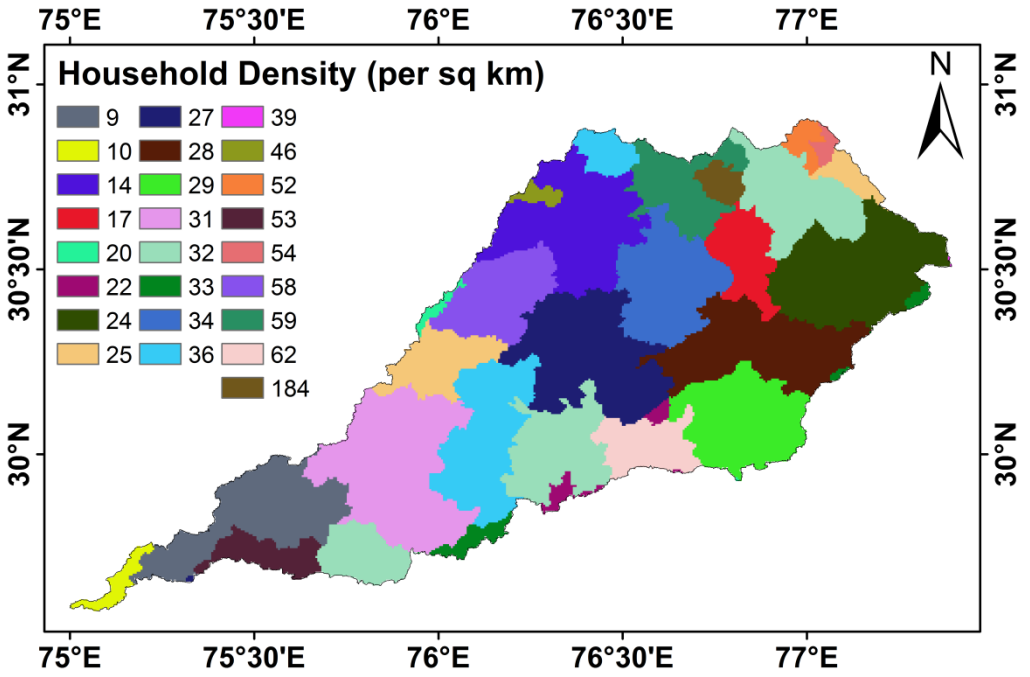

Figure 3.23 Tehsil wise household density of Ghaggar river basin

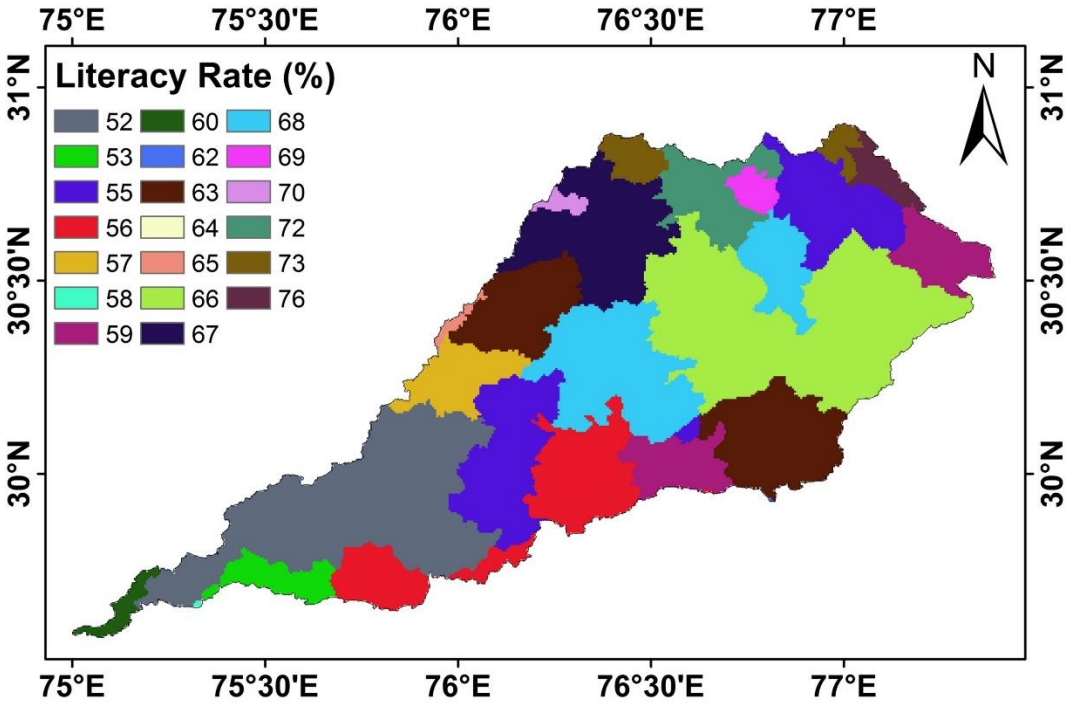

Figure 3.24 Tehsil wise literacy rate of Ghaggar river basin

3.12. Road connectivity

Ghaggar River basin is well connected with the national highway. Figure 3.25 shows the national highway distribution over the Ghaggar River basin. The National highway crosses over the basin are 5, 7, 42, 152, 205, 205A, and 344. The road connects megacities such as

Delhi, Chandigarh, Amritsar, Patiala, and Ambala. However, the maximum distance of a point in the basin from the national highway is 52km.

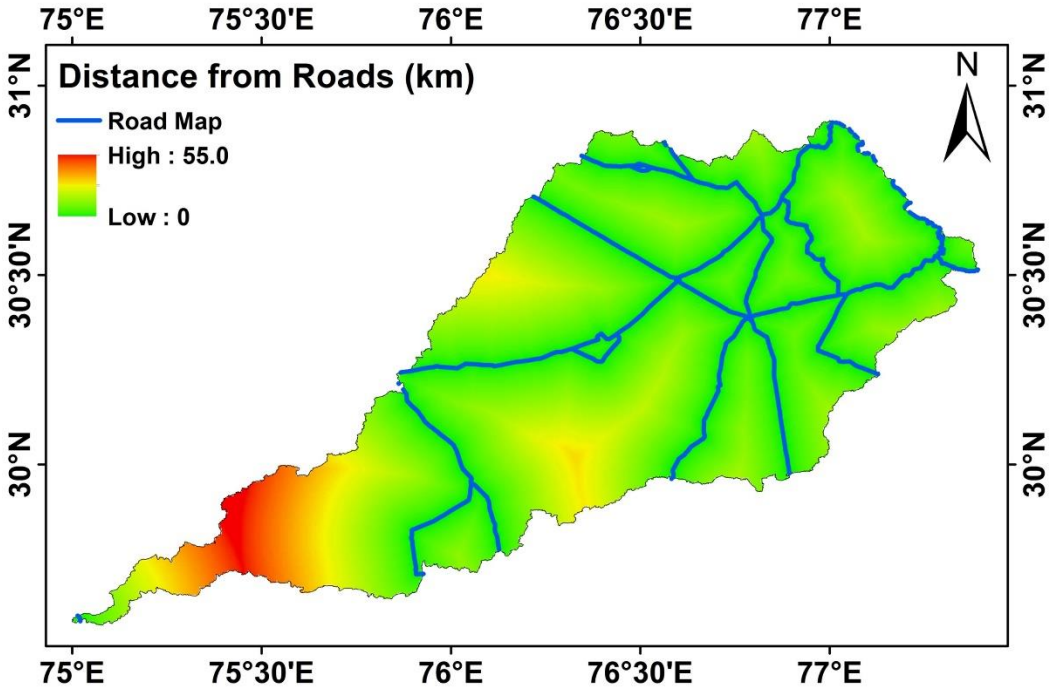

Figure 3.25 Road connectivity map in the Ghaggar river basin

3.13. Concluding Remarks

The total area of the Ghaggar river basin is 32132sq. km, out of which 13978 sq. km and the origin part of the basin is taken as the study area. The watershed for the study area is delineated and clipped using the function of ArcGIS and six DEM collected from Cartosat 1. The elevation of the basis were in the range of 143m – 1790m, whereas the slope of the basin was in the range of 0 – 80.9°. The climate of the river basin is semi-arid and the average temperature of the basin is 23.5°C. The land use land cover of the basin is mainly occupied by croplands (88.26%), savannas (6.16%), and urban built-up (3.39%). The basin's hydrologic soil group has moderately high runoff potential. The population density, household density, and literacy rate of the basin were in the range of 0 – 25177 persons per sq. km, 9 – 184 houses per sq. km, and 52 – 76%, respectively. The road network of the basin is well connected with National highway 5, 7, 42, 152, 205, 205A, and 344.

CHAPTER 4

4. Rainfall Analysis

This chapter started discussion with the rainfall data segregation and about the methodology adopted for descriptive statistics, trend analysis, slope analysis and change point analysis. Results have been briefed based on the methodology discussed. The descriptive statistics, trend and change point of the rainfall is analysed and discussed in this chapter. The trend and descriptive statistics of rainfall before and after change point is also analysed and discussed.

4.1. Methodology

The methodology used for rainfall analysis of descriptive statistics, trend analysis, change point analysis are discussed in this section.

4.1.1. Segregation of Data

Daily rainfall data of twelve stations was collected from Indian meteorological department as shown in Figure 3.2. The obtained data was segregated in three different time period are monthly, seasonal and annual. Total rainfall during the time period represents the rainfall for that period. For example: the total rainfall of March in the year 2004 is represented the data of rainfall for March 2004 and so on. Twelve each months, four season and annual data for the available period of data is segregated for further analysis.

4.1.2. Descriptive Statistics

Descriptive statistic is a statistic measurement that quantitatively sums up the highlights from an assortment of dataset. In descriptive statistics, the equation for calculation of mean, standard deviation, coefficient of variance, autocorrelation (serial correlation) analysis of data and removal of serial correlation from data using pre-whitening approach will be discussed. However, the descriptive statistics analysis is performed in IBM SPSS statistics 20.

4.1.2.1. Mean

The mean is the average of the dataset. Arithmetic mean is calculated for rainfall trend analysis. The arithmetic mean (μ) of given dataset is calculated using Equation 4.1.

$$\mu = \frac{\sum f_i}{N} \qquad \textbf{(4.1)}$$

Where, f_i is the function of the dataset and N is the total number of the dataset.

4.1.2.2.Standard Deviation

The standard deviation (SD) is the dispersion measurement of the dataset from its mean value. Standard deviation (σ) of the dataset is calculated using Equation 4.2.

$$\sigma = \sqrt{\frac{\sum(f_i - \mu)^2}{N}} \quad \textbf{(4.2)}$$

4.1.2.3.Coefficient of variation

Coefficient of variation (CV) is a sort of relative proportion of scattering. The mathematical expression of CV is ratio of the standard deviation to the arithmetic mean. The coefficient of variation is a dimensionless amount and is normally given as a percentage. The coefficient of variation (CV) is mathematical calculated using Equation 4.3.

$$\text{CV}\ (\%) = \frac{\sigma}{\mu} \times 100 \quad \textbf{(4.3)}$$

4.1.3. Rainfall Trend analysis

The analysis of rainfall trend was analyzed using Innovative trend analysis methodology and the results are compared with the most popular classical methodology of Mann-Kendall test and Sen Slope estimator.

4.1.3.1. Innovative trend analysis

Innovative trend analysis (ITA) is the latest methodology for trend analysis of time series hydrometeorological data, developed by Sen in 2012 (360). The basic theory of the ITA method is the statistical analysis of two halves of the time series data. The first half of the data is plotted on the *x*-axis and the second halves on the *y*-axis, and the plot is found a 45° angle straight line passing through the origin. Figure 4.1 describes the increasing trend, decreasing trend, and no trend. Equation 1 shows the basic calculation for the slope of the trend line.

$$S = \frac{2(\overline{y_2} - \overline{y_1})}{n} \quad \textbf{(4.4)}$$

Where, $\overline{y_1}$ is the arithmetic mean of the first halves of the dataset, $\overline{y_2}$ is the arithmetic mean of the second halves of the dataset and n is the length of Dataset. The arithmetic means of the first and second halves are stochastic variables. The mean of two halves plotted as (y_1, y2) is known as "centroid point," which is pointed on the data line. However, this methodology was not sufficient to analyze the significant of the trend.

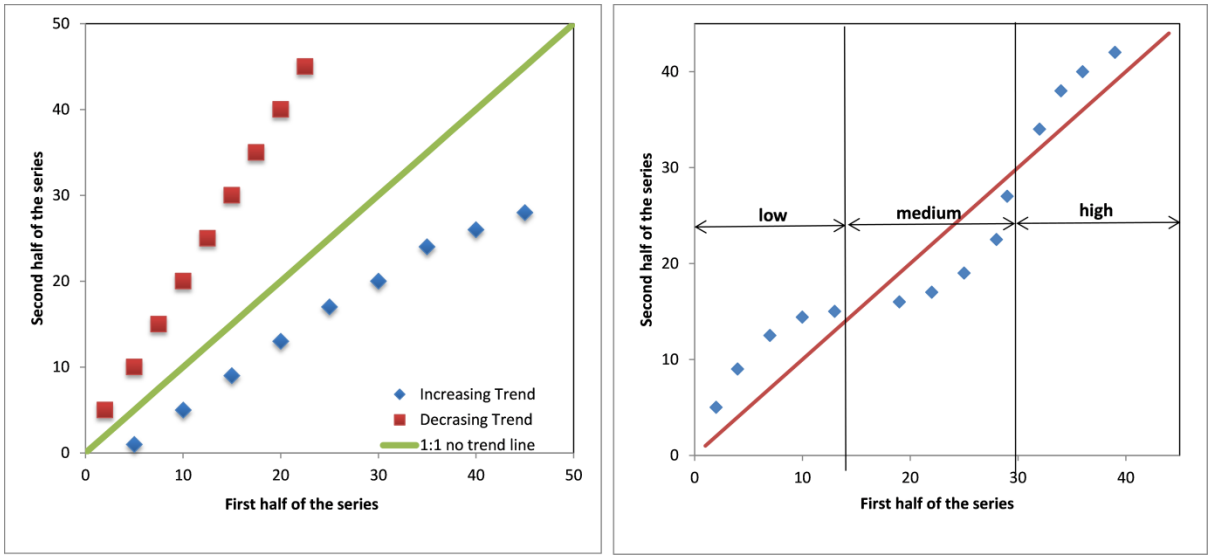

Figure 4.1 Innovative trend analysis methodology

Sen (2017) revised the ITA methodology and developed the significance test. The significance test of the slope value is calculated using hypothesis testing i.e., null hypothesis and alternative hypothesis. The null hypothesis is accepted where slope value S is below a critical value S_{cr} where the alternative is rejected i.e., $S < S_{cr}$. The first-order moment i.e., expectation of the slope E(S), can be calculated by taking expectation on both sides because the arithmetic means of the first and second halves are stochastic variables.

$$E(S) = \frac{2}{n}[E(\overline{y_2}) - E(\overline{y_1})] \quad \textbf{(4.5)}$$

The value of $E(\overline{y_2})$ will be the same as $E(\overline{y_1})$, if the centroid point falls on a 45° angle straight line i.e. $E(S) = 0$. The variance of the slope can be calculated as using Eq. (4.6).

$$\sigma_s^2 = E(S^2) - E^2(S) = \frac{4}{n^2}[E(\overline{y_2}^2) - 2E(\overline{y_1 y_2}) + E(\overline{y_1}^2)] \quad \textbf{(4.6)}$$

As, $E(\overline{y_2}^2) = E(\overline{y_1}^2)$, Eq. 4.6 can be transformed to the following form.

$$\sigma_s^2 = \frac{8}{n^2}[E(\overline{y_2}^2) - E(\overline{y_1 y_2})] \quad \textbf{(4.7)}$$

The correlation coefficient $(\rho_{\overline{y_1 y_2}})$ between $\overline{y_2}$and $-\overline{y_1}$is explained in Eq. 4.8.

$$\rho_{\overline{y_1 y_2}} = \frac{E(\overline{y_1 y_2}) - E(\overline{y_2})E(\overline{y_1})}{\sigma_{\overline{y_2}}\sigma_{\overline{y_1}}} \quad \textbf{(4.8)}$$

The final relation of slope variance is calculated by substitution of numerator correlation coefficient and considering $\sigma_{\overline{y_2}} = \sigma_{\overline{y_1}} = \sigma/\sqrt{n}$ in Eq. 4.7.

$$\sigma_s^2 = \frac{8}{n^2}\frac{\sigma^2}{n}(1 - \rho_{\overline{y_1 y_2}}) \quad \textbf{(4.9)}$$

So, the standard deviation of the slope (σ_s) can be calculated using Eq. 4.10.

$$\sigma_s = \frac{2\sqrt{2}}{n\sqrt{n}}\,\sigma\sqrt{(1 - \rho_{\overline{y_1 y_2}})} \quad \textbf{(4.10)}$$

The confidence limit (CL) of the trend slope is shown in Eq. 4.11 in which standard deviation is S_{cr}. The slope S of the time series is statistically significant if it falls outside the confidence limit.

$$CL_{(1-\alpha)} = 0 \pm S_{cr} \times \sigma_s \quad \textbf{(4.11)}$$

4.1.3.2. Mann-Kendall test

Mann-Kendall test is used in the present study for validation of the trend analysis results from ITA methodology. Mann-Kendall test is extensively used for the trend analysis of hydrometeorological data (425–427). The value of Z is defined the trends of data (428–430).The significant trend is defined on the acceptance of null hypothesis at 5% level of significance.

For a time series data of n years, calculate $(x_j - x_k)$ where j>k and (j=k+1). The value $(x_j - x_k)$ is denoted as -1, 0 and 1 for negative, neutral and positive value of $(x_j - x_k)$ and expressed as $sgn(x_j - x_k)$. Eq. 4.12 and 4.13 is used to determine the test of statistics *S* and variance of test statistics *Var(S)* (431,432).

$$S = \sum_{j=2}^{n}\sum_{k=1}^{j-1} sgn(x_j - x_k) \quad \textbf{(4.12)}$$

$$Var(S) = \frac{1}{18}\left[n(n-1)(2n+5) - \sum_{p-1}^{g} t_p(t_p - 1)(2t_p + 5)\right] \quad \textbf{(4.13)}$$

Where, g= number of tied groups and t_p = number of ties for p[th] value.

Now the Z statistics will be computed by using Eq. 4.14.

$$Z = \begin{cases} \frac{S-1}{\sqrt{Var(S)}} if S > 0 \\ 0\ if S = 0 \\ \frac{S+1}{\sqrt{Var(S)}} if S < 0 \end{cases} \quad \textbf{(4.14)}$$

The result of positive or negative of Z value will identify the positive or negative trend respectively. And the significant of trend will be identifying based on hypothesis testing. H_0 will be accepted or H_a will be rejected when Z value is greater than $Z_{\alpha/2}$ i.e., monotonic trend found and H_0will be rejected or H_a will be accepted if Z values is lesser than $Z_{\alpha/2}$ (433).

4.1.3.3. Sen Slope estimator

Sen Slope estimator is used for slope analysis of the trend i.e., the rate of changes per unit time period (237,426,430,434). The true slope i.e., change per unit time can be estimated as if there is a linear trend in time series. Eq. 4.15 represents the slope for n amount of data.

$$\text{Slope estimator } (Q_i) = \frac{x_j - x_k}{j-k} \text{ where } k < j \text{ for } j = 1, 2, 3, \dots\dots, n \qquad \textbf{(4.15)}$$

The sign of the estimated slope will be either Positive or negative which indicates either increasing or decreasing trend respectively and the magnitude of slope estimator indicates the rate of change per unit time.

4.1.3.4. Autocorrelation analysis

Absence of serial correlation in the time series data is the main assumption of Mann-Kendall test and Sen Slope estimator. But, the existence correlation in hydro-meteorological dataset is common. Therefore, an analysis of autocorrelation of the dataset before trend analysis is must be analyzed. If serial correlation in the dataset is absent, then the trend analysis will be directly employed. However, if serial correlation found in the dataset then the serial correlation of dataset must be removed. Von Storch (1995) has developed pre-whitening approach for removal of serial correlation from the dataset and prepares the data for trend analysis using Mann-Kendall test and Sen Slope estimator.

Auto correlation or serial correlation coefficient (C_k) of the time series dataset is analyzed using Equation 4.16 (435,436) .

$$C_k = \frac{\sum_{t=0}^{n-k}(x_t \cdot x_{t+k}) - \frac{1}{n-k}\sum_{t=0}^{n-k} x_t \cdot \sum_{t=0}^{n-k} x_{t-k}}{\left[\sum_{t=o}^{n-k} x_t^2 - \frac{1}{n-k}\left(\sum_{t=0}^{n-k} x_t\right)^2\right]^{\frac{1}{2}} \left[\sum_{t=o}^{n-k} x_{t+k}^2 - \frac{1}{n-k}\left(\sum_{t=0}^{n-k} x_{t+k}\right)^2\right]^{\frac{1}{2}}} \qquad \textbf{(4.16)}$$

Where, x_t = function of the data at t^{th} location; k = time lag; and n = length of the dataset(436,437).

The presence or absence of serial correlation is analyzed by using the confidence limit as shown in Eq. 4.17 and 4.18. The value of correlation coefficient beyond the confidence limit defines the presence of serial correlation.

$$C_k\ (upper) = \left\{\frac{1}{n-k}\right\}\left(-1 + z_{1-\alpha/2}\sqrt{n-k-1}\right) \quad \textbf{(4.17)}$$

$$C_k\ (lower) = \left\{\frac{1}{n-k}\right\}\left(-1 - z_{1-\alpha/2}\sqrt{n-k-1}\right) \quad \textbf{(4.18)}$$

Where, $z_{1-\alpha/2}$ = standard normal variate at α significance level.

4.1.3.5. Pre-whitening Approach

Pre-whitening approach is used for removal of serial correlation from the dataset is developed by von Storch in 1995 (438). The pre-whitened data (Y_t) of t^{th} time is analyzed using Eq. 4.19.

$$Y_t = X_t - C_k \cdot X_{t-1} \quad \textbf{(4.19)}$$

Where, X_t is the existing data of t^{th} time; X_{t-1} is the existing data of $(t\text{-}1)^{th}$ time; and C_k is the lag-1 correlation coefficient.

4.1.4. Change point analysis

The identification of the most probable change point years in the time series data has been analysed using Pettit's test, Buishand's test and Standard Normal Homogeneity test.

4.1.4.1. Pettit's test

The Pettit's test is a nonparametric test commonly used for change point detection developed by Pettit's in 1979 cited in numerous literature (242,425,439). The test detects the significant unusual changes in time series data which is a nonparametric test. Assuming t as change point of time series data of $x_1, x_2, x_3 \ldots x_n$ has a distribution function F(x) as $x_1, x_2, x_3 \ldots x_t$. The non-parametric test statistics U_t is described in Eq. 4.20.

$$U_t = \sum_{i=1}^{t}\sum_{j=t+1}^{n} \text{sign}(x_t - x_j) \quad \textbf{(4.20)}$$

Where,

$$\text{sign}(x_t - x_j) = \begin{cases} +1, & \text{if}(x_i - x_j) > 0 \\ 0, & \text{if}\,(x_i - x_j) = 0 \\ -1, & \text{if}\,(x_i - x_j) < 0 \end{cases} \quad \textbf{(4.21)}$$

The test statistics K computed as in Eq. 4.22.

$$K = \text{Max}|U_t| \quad \textbf{(4.22)}$$

The value of K defines the most probable change point. The associated confidence level (ρ) for n number of samples is described as Eq. 4.23.

$$\rho = \exp\left(\frac{-K}{n^2+n^3}\right) \quad \textbf{(4.23)}$$

The value of ρ is smaller than specified confidence level defines the rejection of null hypothesis.

4.1.4.2. Standard Normal Homogeneity (SNH) test

The change point is analysed using Pettit's test is validated using the SNH test. The test statistic of SNH test is used to compare the mean of first n observation with the mean of the remaining n-k observation n data points (425,439). The value of T_k is maximum when the change point is located at the year K. The test statics (T_k) is shown in Eq. 4.24.

$$T_k = kZ_1^2 + (n-k)Z_2^2 \quad \textbf{(4.24)}$$

Where,

$$Z_1 = \frac{1}{k}\sum_{i=1}^{k}\frac{(x_i - X)}{\sigma} \quad \textbf{(4.25)}$$

$$Z_2 = \frac{1}{n-k}\sum_{i=k+1}^{k}\frac{(x_i - X)}{\sigma} \quad \textbf{(4.26)}$$

X is mean and σ is standard deviation of data series x_1, x_2, x_3…… x_n. The year k is the change point year and consist a break where the value of T_k is maximum.

4.1.4.3. Buishand's test

Buishand's test is also used for the analysis of change point. The most probable change point is calculated as the adjusted partial sum (S_m) (439). The S_m is calculated using Equation 4.27.

$$S_m = \sum_{i=1}^{m}(x_i - \bar{x}) \quad \textbf{(4.27)}$$

Where, x_1, x_2, x_3…… x_m, x_n are the observed time series with mean $(\overline{x})$.

The significance test of Buishand's test is analysed comparing $\frac{R}{\sqrt{n}}$ with the critical value given by Buishand (1982) and Wijngaard et al., 2003 (440,441). The R can be calculated as given in Equation 4.28.

$$R = \frac{Max\,(S_m) - Min\,(S_m)}{\bar{x}} \quad \textbf{(4.28)}$$

4.1.5. Areal estimation of Rainfall

Rainfall over an area or basin recorded at different location. The average rainfall of that particular area is calculated using Thiessen polygon method. Thissen polygon method calculated the average rainfall from the area averaged calculation. Equation shows the calculation of areal average rainfall.

$$Areal\ Average\ Rainfall = \sum_{i=1}^{m} \frac{A_i}{A} R_i \quad \textbf{(4.29)}$$

Where,

m = the number of area;

A_i = area assigned to the station *i*; and

R_i = rainfall received at the station *i*.

4.2. Descriptive Statistics

Descriptive statistics of twelve meteorological stations over the Ghaggar river basin's rainfall data is analyzed using Eq. 4.1 to 4.3. The descriptive statistics analysis has been analyzed monthly, seasonally, and annually. The detailed analysis of rainfall data is described below as monthly analysis, seasonal analysis, and annual analysis.

4.2.1. Monthly Analysis

Tables 4.1, 4.2, and 4.3 show the average, standard deviation (SD), and coefficient of variation (CV) of monthly rainfall over the Ghaggar River basin. The spatial variation of average monthly rainfall over the Ghaggar River basin is shown in Figures 4.2 and 4.3. Average monthly rainfall is higher during July and lower during November. The monthly average

rainfall in the Ghaggar River basin lies in the range of 1.8-551.6mm. The variability, i.e., CV of the rainfall, is inverse to average rainfall. The variability is higher during November and lower during July.

Table 4.1 shows that the maximum average monthly rainfall is recorded at Nahan in all months except May and November. The maximum rainfall during May and November are recorded at Rohit and Kalka respectively. The minimum rainfall in the study region is recorded at Dedhna during December – March, June, and August – October, whereas Rajpura, Thanesar, Dhaneta, and Lehal reported minimum rainfall during April, May, July, and November, respectively.

Table 4.1 Monthly average of rainfall for different station of Ghaggar river basin

	JAN	FEB	MAR	APR	MAY	JUN	JUL	AUG	SEP	OCT	NOV	DEC
Banur	23	25.8	29.4	14.1	24.6	74.5	222.5	192.9	127	17.6	4.1	19.9
Dedhna	14.6	13.4	13.2	10.8	21	23.2	121.4	69	57.2	2.8	3.8	6.6
Dhaneta	17	23.8	15.2	17.6	25.8	46.1	119.4	151	84	10.1	6.8	9.3
Patiala	24.4	25.7	18.7	14.1	22.4	71.4	190.5	200.9	112.4	7.8	4.9	12.3
Rajpura	25.4	25.7	24.9	7.8	23.5	81	251.3	187.9	112.5	12.7	3.9	13.8
Rohiti	28.2	43.6	28.9	14.5	30.1	65.4	216.9	211.7	144.2	10.3	6.1	11.9
Ambala	25.2	31.3	22.7	12.3	27.8	82.4	228.8	213.5	124.9	13.5	3.6	19.6
Kharar	33.9	21.8	23.3	9.4	17.6	57.9	200.5	189.4	102.4	18.6	7.0	15.2
Kalka	39.5	37.8	28.9	11.0	26.9	105.7	319.4	335.0	168.0	18.6	9.9	16.3
Lehal	24.6	30.5	19.9	10.5	13.8	52.3	144.7	186.7	113.0	12.4	1.8	9.2
Thanesar	26.2	20.9	21.1	9.7	13.4	67.1	185.7	182.7	91.0	19.9	4.2	8.6
Nahan	51.5	56.3	51.1	19.4	29.2	186.4	551.6	549.7	225.0	45.5	9.6	31.3

The findings of Figure 4.2 and 4.3 showed that the average monthly rainfall was higher at the upper part or origin of the basin. The spatial maps were prepared in ArcGIS using Inverse distance weighted (IDW) interpolation method. Estimates of IDW interpolation are the weighted average values of surrounding points. The amount of rainfall is decreasing from upper part of the basin to the lower part. The maximum and minimum monthly amount rainfall received in the basin is shown in Figure 4.2 and 4.3 as high and low respectively. The highest monthly range of rainfall is received during July i.e., 119.4 – 551.4mm whereas the lowest recorded during November i.e., 1.8 – 9.8mm.

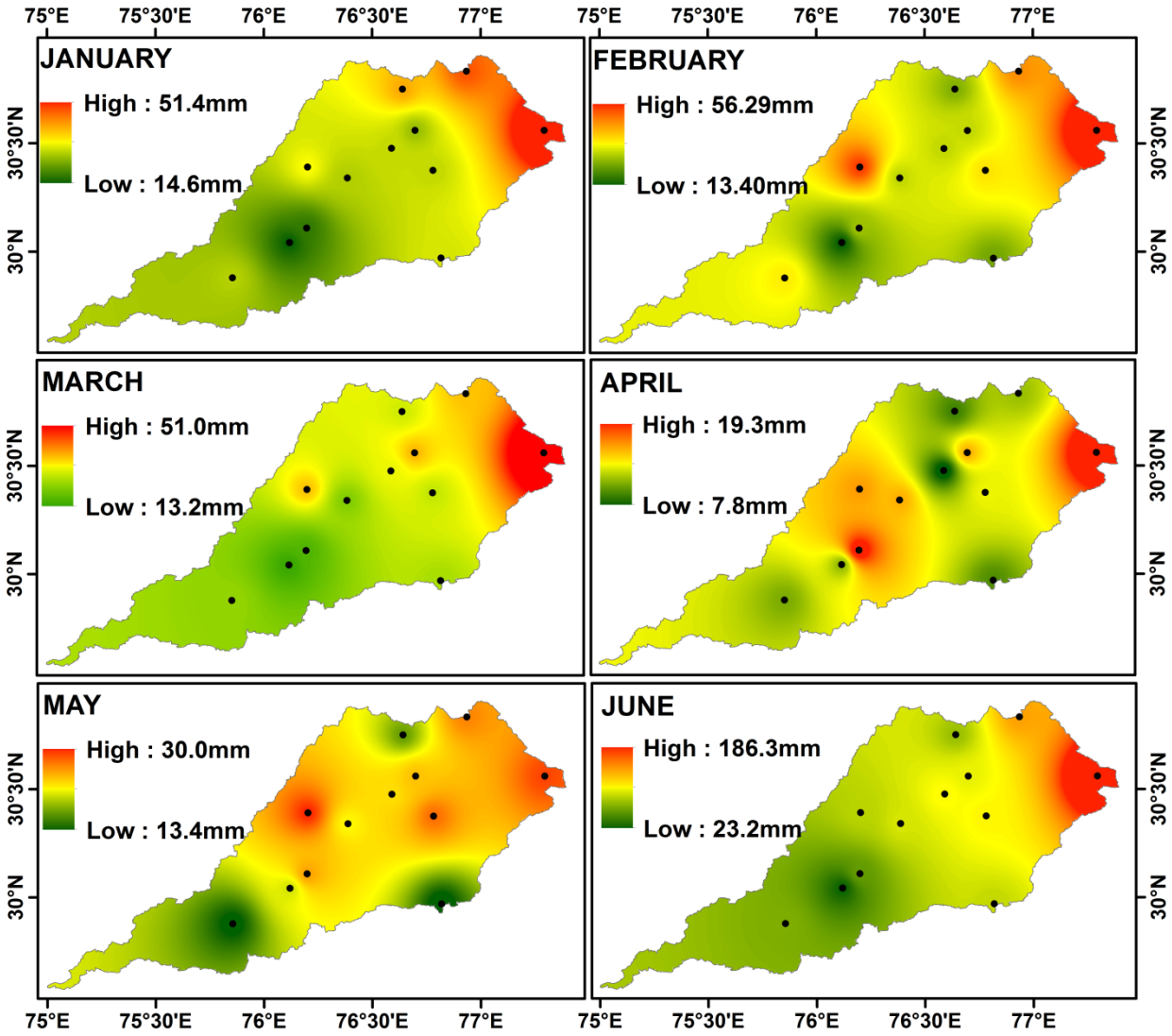

Figure 4.2 Spatial analysis of monthly (January - June) average rainfall in Ghaggar river basin

The average monthly weighted rainfall over the basin is 27.2, 30.1, 23.8, 12.4, 22.1, 72.3, 216.2, 216.3, 120.1, 15.0, 5.0, and 13.7 from January to December. The maximum average weight rainfall, i.e., 216mm, was received during July and August, whereas the lowest was received during November, i.e., 5mm.

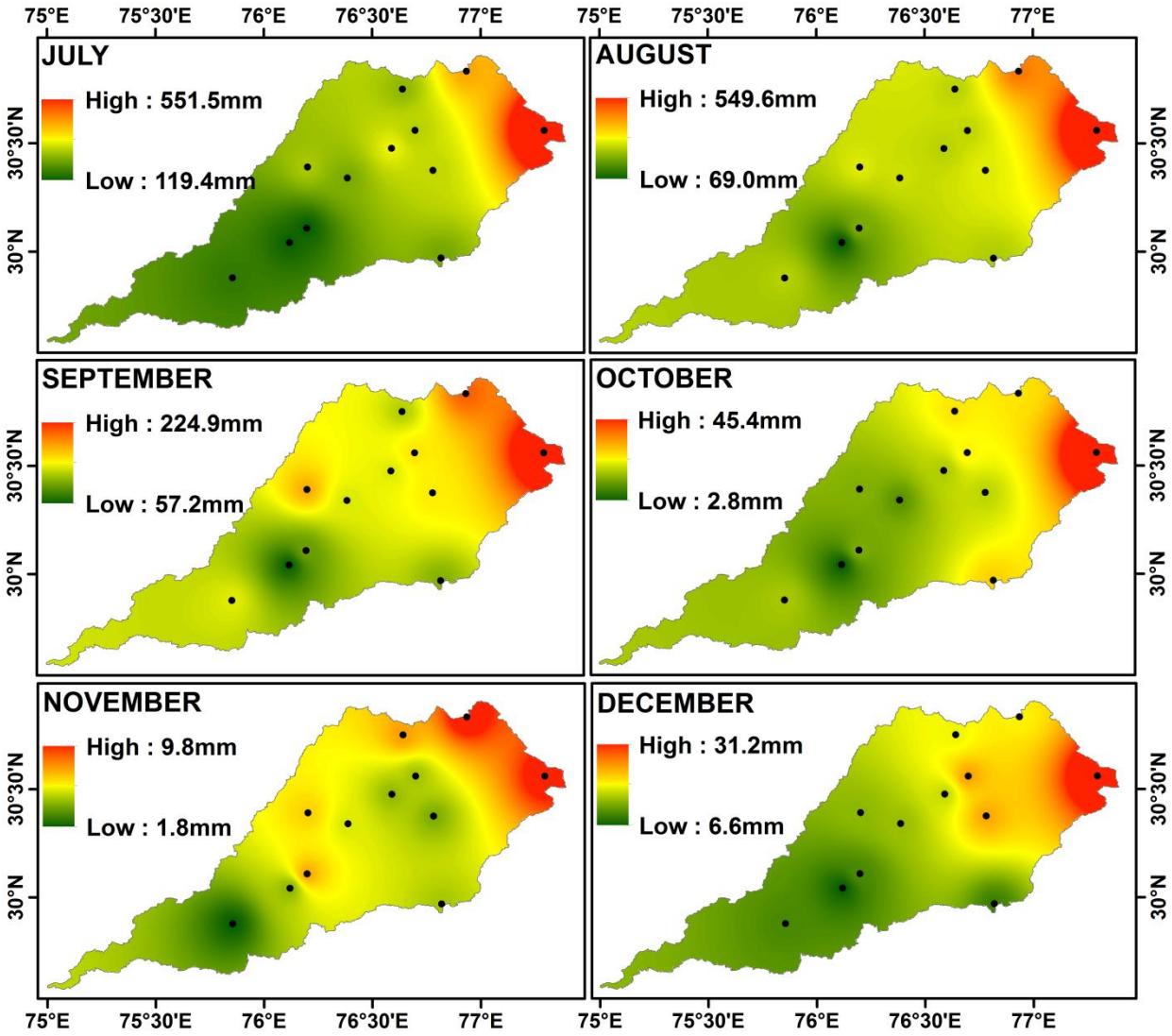

Figure 4.3 Spatial analysis of monthly (July - December) average rainfall in Ghaggar river basin

Table 4.2 shows the standard deviation, and Table 4.3 shows the coefficient variation (CV) of monthly rainfall of the Ghaggar River Basin. The standard deviation of the monthly rainfall varied in the range of 5.0 – 324.9 mm, whereas the CV varies in the 42.6 – 484.6% range. The lowest standard deviation is found in November at Lehal, whereas the highest is in July at Nahan. The higher rainfall variability is found during November at Rajpura, whereas the lower variability is found during August at Kalka. The higher variation in the rainfall pattern was observed during November, whereas the lower variation is found during August.

Table 4.2 Monthly standard deviation in rainfall for different station of the Ghaggar river basin

	JAN	FEB	MAR	APR	MAY	JUN	JUL	AUG	SEP	OCT	NOV	DEC
Banur	30.1	28.1	47.4	26.3	47.8	62.6	157.3	133	127.8	36.1	10.1	31.2
Dedhna	24.4	18.9	22.2	33.9	47.3	30.4	149.5	76.3	91.3	7.2	16.2	15.4
Dhaneta	27.4	26.3	20.3	33.3	45.1	45.5	107.6	176	109.7	29.3	18.8	16.6
Patiala	29.4	28.4	26.9	33.9	33.4	63.9	175.3	160.1	112.7	19.2	16.3	25.1
Rajpura	30.4	30.3	37.8	15.1	35.6	64.1	154.2	167	108.2	25.2	18.9	29.2
Rohiti	33.4	39.6	36.6	29.1	35.5	63.8	178	187	182.5	25.1	22.2	25
Ambala	26.8	33.0	23.5	15.0	31.0	49.3	132.8	148.2	92.5	25.2	8.1	27.3
Kharar	31.9	27.4	29.3	23.4	26.5	51.9	110.7	119.9	101.0	50.6	18.6	24.1
Kalka	40.5	47.4	33.8	20.1	35.1	101.4	194.6	142.5	127.7	38.9	24.6	25.7
Lehal	28.7	80.4	26.8	18.8	25.0	64.5	116.0	188.7	114.7	28.3	5.0	16.5
Thanesar	26.4	25.8	24.3	23.1	20.7	53.4	100.8	128.3	86.5	42.8	12.5	15.1
Nahan	42.6	57.1	54.5	23.7	28.9	149.7	324.9	275.9	181.0	84.1	19.1	44.8

Table 4.3 Monthly coefficient of variance in rainfall for different station of the Ghaggar river basin

	JAN	FEB	MAR	APR	MAY	JUN	JUL	AUG	SEP	OCT	NOV	DEC
Banur	130.9	108.9	161.2	186.5	194.3	84	70.7	68.9	100.6	205.1	246.3	156.8
Dedhna	167.1	141	168.2	313.9	225.2	131	123.1	110.6	159.6	257.1	426.3	233.3
Dhaneta	161.2	110.5	133.6	189.2	174.8	98.7	90.1	116.6	130.6	290.1	276.5	178.5
Patiala	120.5	110.5	143.9	240.4	149.1	89.5	92	79.7	100.3	246.2	332.7	204.1
Rajpura	119.7	117.9	151.8	193.6	151.5	79.1	61.4	88.9	96.2	198.4	484.6	211.6
Rohiti	118.4	90.8	126.6	200.7	117.9	97.6	82.1	88.3	126.6	243.7	363.9	210.1
Ambala	106.1	105.5	103.8	122.1	111.8	59.8	58.0	69.4	74.1	186.3	224.6	139.1
Kharar	94.1	125.9	125.7	248.8	150.7	89.5	55.2	63.3	98.6	271.7	265.5	158.5
Kalka	102.5	125.3	117.0	183.7	130.6	95.9	60.9	42.6	76.0	208.9	249.4	157.1
Lehal	116.5	263.7	134.4	178.9	180.6	123.4	80.2	101.1	101.5	228.0	274.6	179.5
Thanesar	100.9	123.6	115.0	239.2	154.2	79.5	54.3	70.2	95.0	214.8	300.1	176.2
Nahan	82.7	101.4	106.6	122.2	98.8	80.3	58.9	50.2	80.4	184.9	197.9	143.1

4.2.2. Seasonal Analysis

Figure 4.4 shows the spatial plotting of seasonal average rainfall. The seasonal average has been analyzed from the cumulative rainfall received during the seasons. Table 4.4 shows the descriptive statistics such as the average (mean), standard deviation (SD), and coefficient of variation (CV) of four seasons. The average seasonal rainfall ranges from 21 – 103.8 mm, 35.5 – 95.8mm, 202.6 – 1421mm, and 7.6 – 82.6 mm during winter, pre-monsoon, southwest, and

monsoon season. Dedhna received the lowest average seasonal rainfall during all the seasons, whereas Nahan received the highest average seasonal rainfall during all the seasons. The season's ascending order according to the seasonal average rainfall in the basin is post-monsoon> winter > pre-monsoon > southwest monsoon.

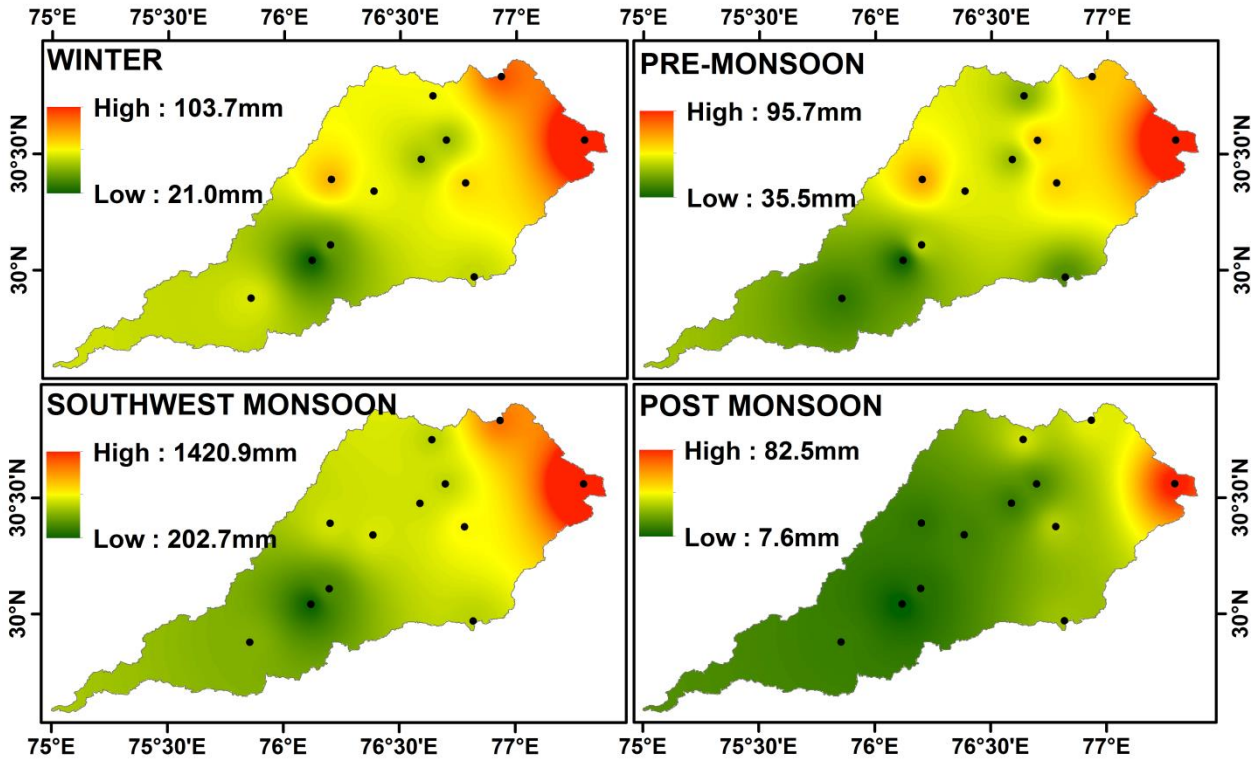

Figure 4.4 Spatial analysis of seasonal average rainfall in Ghaggar river basin

The highest seasonal SD of winter and pre-monsoon of the river basin was found at Lehal, whereas southwest monsoon and post-monsoon are found at Nahan. The lowest seasonal SD of winter, pre-monsoon, southwest monsoon, and post-monsoon is found at Dedhna, Banur, Kalka, and Banur, respectively. The range of seasonal SD varies in the range of 28.3 – 78.9, 39.4 – 81.9, 211.6 – 663.7, and 20.3 – 96.4 during winter, pre-monsoon, southwest monsoon, and monsoon seasons. The season's ascending order according to the SD of seasonal rainfall received in the basin was similar to average seasonal rainfall, i.e., post-monsoon> winter > pre-monsoon > southwest monsoon.

Table 4.4 Seasonal descriptive statistics of rainfall for different stations of the Ghaggar river basin (Unit: Mean – mm, SD- mm, CV - %)

	Winter			Premonsoon			Southwest Monsoon			Post Monsoon		
	Mean	SD	CV	Mean	SD	CV	Mean	SD	CV	Mean	SD	CV
Banur	41.2	36.4	88.3	62	81.9	132.1	533	326.6	61.3	19.3	30.5	158
Dedhna	21	28.3	134.8	35.5	60.3	169.9	202.6	266.2	131.4	7.6	20.3	267.1
Dhaneta	33.8	34.3	101.5	51.9	63.2	121.8	336.5	291.3	86.6	13.6	24.9	183.1
Patiala	50	39	78	55.2	65.7	119	575.2	281	48.9	17.6	33.8	192
Rajpura	41.6	37.8	90.9	49.2	56.7	115.2	553.3	322.4	58.3	16.3	33.5	205.5
Rohiti	61.9	48.7	78.7	66.2	65.3	98.6	563	384	68.2	14.9	33.3	223.5
Ambala	56.5	38.9	68.9	61.5	44.7	72.7	643.6	237.4	36.9	35.2	43.8	124.3
Kharar	50.6	46.9	92.8	47.3	55.5	117.2	527.6	211.6	40.1	38.6	57.8	149.6
Kalka	75.9	62.8	82.7	63.0	56.4	89.5	914.2	345.1	37.7	41.7	50.2	120.3
Lehal	47.6	78.9	165.7	39.7	39.4	99.1	429.8	300.3	69.9	16.7	40.7	244.5
Thanesar	44.8	35.4	78.9	42.4	44.0	103.7	522.0	217.6	41.7	32.1	47.4	147.7
Nahan	103.8	72.0	69.4	95.8	71.1	74.2	1421.0	663.7	46.7	82.6	96.4	116.7

Seasonal rainfall variability is higher during the post-monsoon season and lower during the southwest monsoon season. The season's ascending order according to the seasonal rainfall variability received in the basin was similar to average seasonal rainfall, i.e., southwest monsoon > winter > pre-monsoon > post-monsoon. The variability of the seasonal rainfall in the river basin varies in the range of 68.9 – 165.7%, 72.7 – 169.9%, 36.9 – 131.4%, and 116.7 – 267.1% during winter, pre-monsoon, southwest monsoon, and monsoon season. The higher seasonal rainfall variability is found at Dedhna during all seasons except the winter, whereas the higher variability during winter is found at Lehal. The lower seasonal rainfall variability is found at Ambala during all seasons except post-monsoon season, whereas the lower variability during post-monsoon season is found at Nahan.

4.2.3. Annual analysis

Figure 4.5 shows the spatial plotting of average annual rainfall. The average annual rainfall was analyzed from the cumulative annual rainfall for each year. Table 4.5 shows the descriptive statistics such as average (mean), standard deviation (SD), and coefficient of variation (CV) of average annual rainfall.

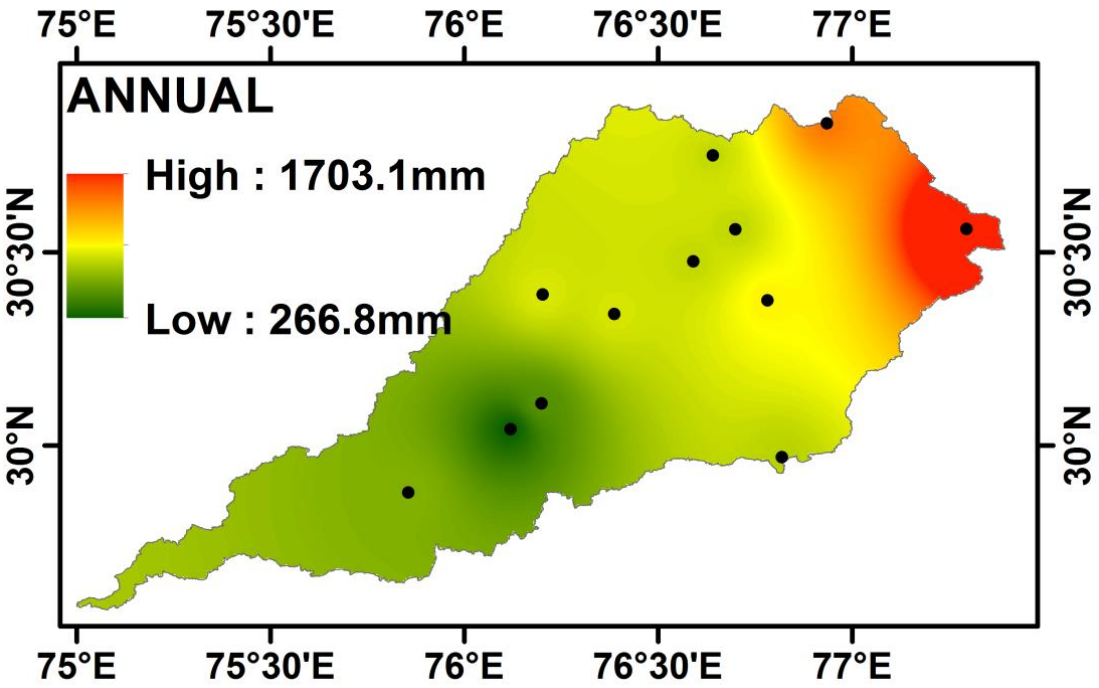

Figure 4.5 Spatial analysis of annual average rainfall in Ghaggar river basin

Table 4.5 Annual descriptive statistics of rainfall for different stations of the Ghaggar river basin

	Mean (mm)	SD (mm)	CV (%)
Banur	655.5	402.1	61.3
Dedhna	266.7	316.2	118.6
Dhaneta	435.7	342.4	78.6
Patiala	698	297.3	42.6
Rajpura	660.4	343.6	52
Rohiti	705.9	391.6	55.5
Ambala	796.8	245.5	30.8
Kharar	664.2	260.4	39.2
Kalka	1094.8	351.2	32.1
Lehal	533.8	338.7	63.5
Thanesar	641.3	244.1	38.1
Nahan	1703.2	718.3	42.2

The average annual rainfall in the Ghaggar River basin varies in the range of 266.7 – 1703.2mm, whereas the highest average annual rainfall is found at Nahan and lowest at Dedhna. The ascending order of station based on the average annual rainfall received was Dedhna > Dhaneta > Lehal > Thanesar > Banur > Rajpura > Kharar > Patiala > Rohiti > Ambala > Kalka > Nahan. The SD and CV of average annual rainfall in the Ghaggar river lied between 244.1 – 718.3mm and 30.8 – 118.6%, respectively. The higher and lower variability of annual

average rainfall is found at Dedhna and Ambala, respectively, whereas the highest and lowest SD was found at Nahan and Thanesar. The ascending of station based on the SD of average annual rainfall received was Thanesar > Ambala > Kharar > Patiala > Dedhna > Lehal > Dhaneta > Rajpura > Kalka > Rohiti > Banur > Nahan. In contrast, the variability of average annual rainfall received was Ambala > Kalka > Thanesar > Kharar > Nahan > Patiala > Rajpura > Rohiti > Banur > Lehal > Dhaneta > Dedhna.

4.3. Trend Analysis

Rainfall trend analysis of the Ghaggar River basin was analyzed using Innovative trend analysis and validated using the Mann-Kendall test and the Sen Slope estimator. The trend analysis using ITA is analyzed using Equation 4.12 – 4.15. However, autocorrelation analysis is necessary before analyzing trends using the MK test and SS estimator. The main consequence of the MK test and SS estimator is serial correlation in the dataset. Autocorrelation analysis of the dataset was analyzed to check the presence of serial correlation. The analysis of autocorrelation is analyzed using Equation 4.16 – 4.18. Table 4.6 shows the serial correlation in the dataset for different periods of different meteorological stations. No serial correlation was found during January, May, August – September, and November, whereas no serial correlation was found in the Banur station dataset. The presence of serial correlation of the dataset was removed using the pre-whitened approach, as discussed in Equation 4.19, followed by Equation 4.16 – 4.18. The dataset used for trend analysis using the MK test and SS estimator is replaced with the pre-whitened data where the serial correlation is present. The trend direction and slope are analyzed using the MK test and SS estimator. Equation 4.12 – 4.15 is used to analyze trends using the MK test and SS estimator.

Table 4.6 Presence of serial correlation in the monthly, seasonal and annual rainfall dataset of Ghaggar river basin

	FEB	MAR	APR	JUN	JUL	OCT	DEC	WIN	PRM	SWM	POM	ANN
Ambala				Yes		Yes	Yes				Yes	
Dedhna		Yes						Yes			Yes	
Dhaneta					Yes						Yes	
Kalka	Yes		Yes						Yes			
Kharar			Yes			Yes			Yes		Yes	Yes
Lehal										Yes		Yes
Nahan					Yes	Yes				Yes	Yes	Yes
Patiala											Yes	
Rajpura									Yes			
Rohiti										Yes		Yes
Thanesar	Yes					Yes			Yes		True	

4.3.1. Monthly Trend Analysis

Table 4.7 shows the monthly trend magnitude value with the trend direction of the Ghaggar River basin. Innovative trend analysis analyses trend direction, trend magnitude, and significance of trend. The MK test analyzed the trend direction and significance of the trend, whereas the slope of the trend was analyzed using the SS estimator. The negative value in the trend magnitude is defined as a negative or decreasing or downward or declining trend. In contrast, the positive value in the trend magnitude is defined as a positive or increasing or upward or incline trend. The magnitude value zero defined no trend. The trend significance was analyzed at a 5% level of significance. The ***** with bold font marked values in Table 4.7 has a significant trend at a significance level 0.05. The trend magnitude result of both the ITA and MK tests is compared in Table 4.7, and it found that more than 90% of results are in a similar trend direction. The result of the ITA method validates more than 90% of trend direction similarity, and the discussion of trend magnitude is discussed with the result of the ITA method. Figure 4.6 – 4.7 shows the spatial plotting of the trend magnitude of January – June and July – December. The monthly rainfall trend magnitude values lied in the range of (-)1.77 – 0.06, (-)0.98 – 0.41, (-)1.79 – 0.54, (-)1.33 – 0.41, (-)2.81 – 0.67, (-)2.46 – 1.9, (-)9.4 – 5.65, (-)7.61 – 3.43, (-)3.82 – 2.41, (-)1.22 – 0.84, (-)0.53 – (-)0.05, (-)1.83 – 0.22 during January – December, respectively. Both trend directions are found during all months except November, whereas the trend is only decreasing during November. The highest magnitude of rainfall trend was found at Banur, Rohiti, Ambala, Nahan, Rohiti, Rohiti, Rohiti, Lehal, Lehal, Lehal, Nahan, and Kalka from January to December, respectively, and lowest at Lehal, Lehal, Dedhna, Dedhna, Dedhna, Dhaneta, Dedhna, Dedhna, Dedhna, Nahan, Dedhna and Banur during January – December, respectively. 36.1% of the trend was increasing, whereas 63.2% was decreasing, and the rest cases with no definite trend.

Table 4.7 Magnitude of monthly rainfall trend analyzed using Sen Slope (SS) estimator and Innovative Trend Analysis (ITA) (* - significant at level of significance 0.05)

	Month	JAN	FEB	MAR	APR	MAY	JUN	JUL	AUG	SEP	OCT	NOV	DEC
Ambala	**SS**	0.08	-0.32	0.01	0.16	0.13	0.54	-2.69	**-4.59***	-2.11	0	0	0
	ITA	**0.02***	-0.45	0.54	**-0.01***	0.17	0.75	-5.77	-5.04	-2.33	-0.51	-0.3	-0.95
Banur	**SS**	-0.43	0	-0.3	0	-0.75	-1.92	-8.51	-4.39	-3.18	0	0	0
	ITA	-1.77	**-0.08***	-1.53	-0.94	-2.69	-1.42	-8.9	-5.37	-3.38	**0.00***	-0.39	-1.83
Dedhna	**SS**	-0.5	-0.56	-0.77	0	0	-0.53	-5.41	-4.33	-1.91	0	0	0
	ITA	-1.72	-0.48	-1.79	-1.33	-2.81	-1.1	-9.4	-7.61	-3.82	-0.37	-0.53	-1.15
Dhaneta	**SS**	-0.43	-0.19	-0.75	-0.19	0	-2.14	-8.48	-4.51	-1.31	0	0	0
	ITA	-1.27	0.36	-1.25	-0.6	-1.61	-2.46	-7.92	**1.29***	**0.71***	0.58	-0.27	-0.76
Kalka	**SS**	0.15	0.47	0.52	0.16	0.71	0.42	0.74	0.81	0.49	0.52	0.29	1
	ITA	-0.35	**0.04***	**0.06***	0.24	0.21	**0.05***	1.34	**0.28***	0.5	**-0.12***	-0.14	0.22
Kharar	**SS**	**-0.48***	0.04	-0.15	0	0	0.25	**-2.15***	**-2.89***	-0.33	0	0	0
	ITA	-0.63	**-0.04***	-0.49	0.12	**-0.06***	-0.14	-1.84	-2.29	-1.52	-0.58	-0.28	0.09
Lehal	**SS**	0	0	0	0	0	**1***	0.14	3.01	2.03	0	0	0
	ITA	**0.06***	**-0.98***	-0.37	-0.49	0.19	1.89	3.2	3.43	2.41	**0.84***	-0.09	-0.52
Nahan	**SS**	-0.48	0.31	-0.02	**-0.1***	0.37	1.52	-1.2	**-3.65***	0.17	-0.02	0	0
	ITA	-0.39	-0.23	-0.42	0.41	0.47	0.75	-5.24	-7.31	-0.88	-1.22	**-0.05***	0.15
Patiala	**SS**	0	0	0	0	0.09	0.63	-3.28	-2.44	0.46	0	0	0
	ITA	**-0.06***	**0.12***	-0.18	**-0.27***	0.4	1.33	-6.22	-4.36	1.54	0.44	-0.29	-0.37
Rajpura	**SS**	-0.34	0	-0.04	0	-0.14	0.16	-3.63	-4.1	0.43	0	0	0
	ITA	-1.1	**0.05***	-0.93	**0.03***	-0.55	1.56	-4.09	-1.13	**0.87***	0.21	-0.28	-0.4
Rohiti	**SS**	0	0	-0.47	0	0	0.55	-0.93	-1.64	0.44	0	0	0
	ITA	-0.96	0.41	-1.3	**-0.10***	0.67	1.9	5.65	**0.52***	1.42	0.79	-0.47	-0.53
Thanesar	**SS**	**-0.34***	0.06	-0.01	0	0	0.36	**-1.58***	**-2.07***	-0.26	0	0	0
	ITA	-0.24	0.21	0.06	0.24	0.24	0.13	-1.67	-1.71	-0.74	-0.36	-0.07	-0.09

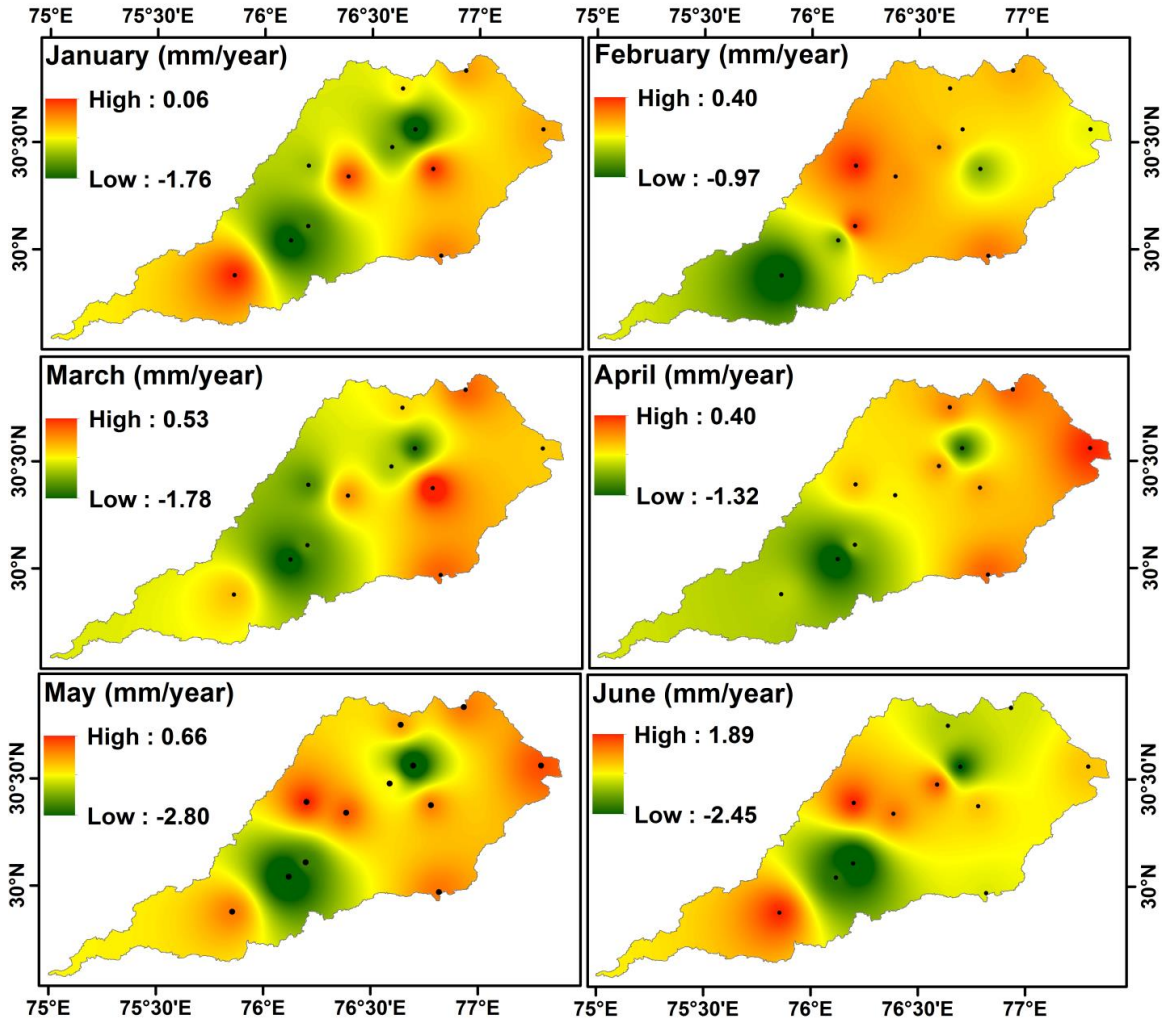

Figure 4.6 Spatial analysis of monthly (January - June) average rainfall trend slope using ITA method in Ghaggar river basin

The significant trend was found at Ambala, Lehal, and Patiala during January; Banur, Kalka, Kharar, Lehal, Patiala, and Rajpura during February; Kalka during March; Ambala, Patiala, Rajpura, and Rohiti during April; Kharar during May, Kalka during June, Dhaneta, Kalka and Rohiti during August; Dhaneta and Rajpura during September; Kalka and Lehal during October; and Nahan during November. There was no significant trend found during July and December.

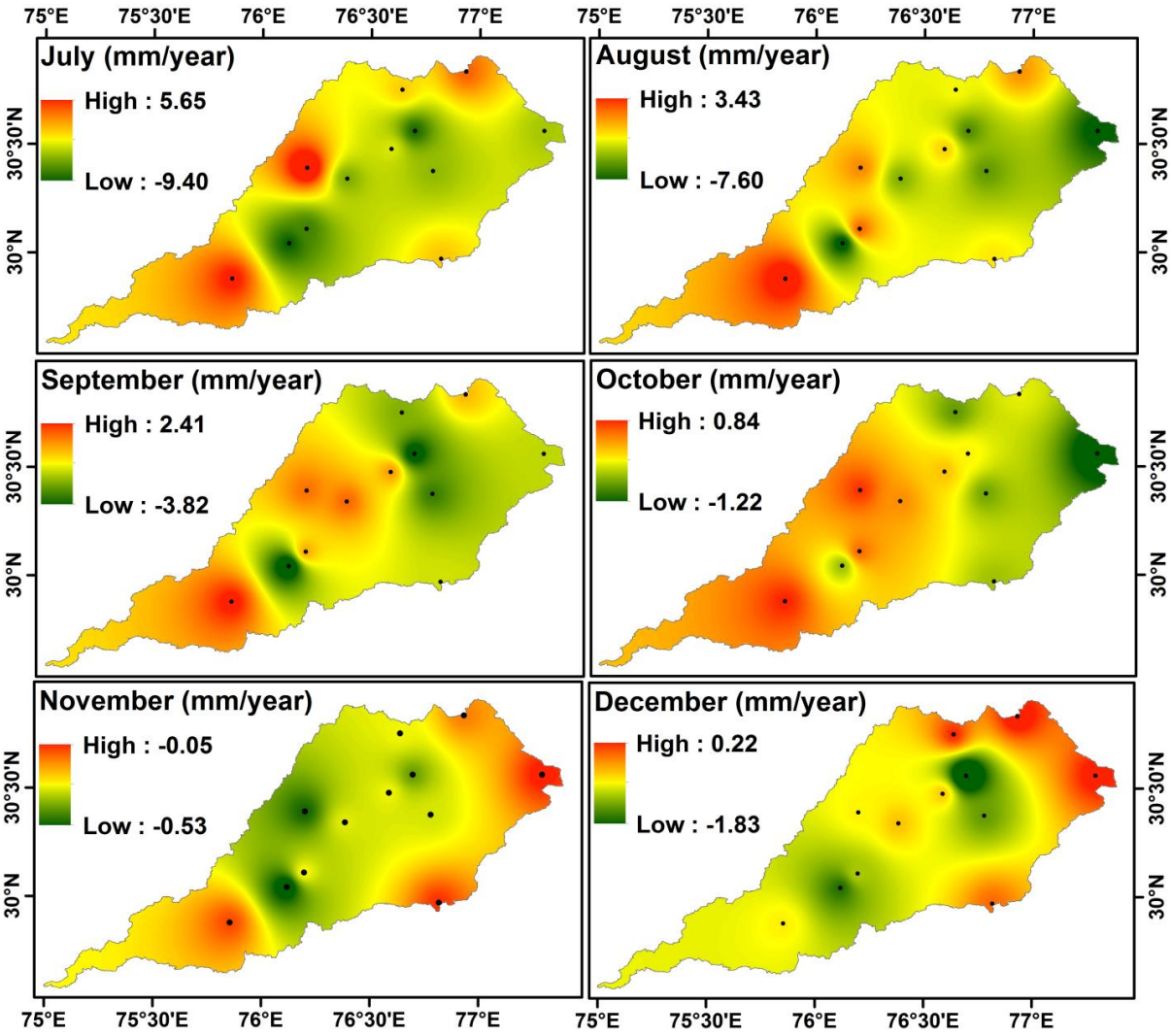

Figure 4.7 Spatial analysis of monthly (July - December) average rainfall trend slope using ITA method in Ghaggar river basin

4.3.2. Seasonal Analysis

Table 4.8 shows the seasonal trend magnitude value with the Ghaggar River basin trend direction analyzed using the SS estimator and ITA methods. More than 85% of the ITA method and the MK test results are found in a similar direction trend. The discussion of seasonal rainfall trends is based on the result of the ITA method. Figure 4.8 shows the spatial plotting of seasonal trend magnitude using the ITA method. The range trend magnitude varies in the range of (-)1.6 – 0.06, (-)4.38 – 0.74, (-17.02) – 7.21, and (-)1.8 – 0.07 during winter, pre-monsoon, southwest monsoon and post-monsoon season. The increasing and highest rate of trend magnitude was found at Patiala, Kalka, Lehal, and Kalka during winter – post-monsoon season, respectively, whereas the decreasing and lowest rate trend magnitude found at Banur, Dedhna, Nahan, and Ambala during winter – post-monsoon season respectively. Significant trends at a level of

significance 0.05 are found at Patiala during winter and premonsoon season, Nahan during the pre-monsoon season, Kalka during the post-monsoon season, and Thanesar during the post-monsoon season.

Table 4.8 Magnitude of seasonal and annual rainfall trend analyzed using Sen Slope (SS) estimator and Innovative Trend Analysis (ITA)

	Month	Winter	Premonsoon	Southwest Monsoon	Post Monsoon	Annual
Ambala	**SS**	-0.307	-0.22	**-11.02***	-0.9	-12.5
	ITA	-0.44	0.56	-13.75	-1.8	-2.83
Banur	**SS**	-1.48	-2.48	-16.86	0	-24.07
	ITA	-1.6	-4.19	-15.69	-1.6	-23.09
Dedhna	**SS**	-0.83	-0.63	-9.13	0	-14.32
	ITA	-1.32	-4.38	-14.77	-1.03	-21.5
Dhaneta	**SS**	-0.73	-1.5	-12.85	-0.15	-18.38
	ITA	-1.08	-2.79	-6.06	-1.04	-10.98
Kalka	**SS**	0.7	0.44	0.93	0.8	0.92
	ITA	-0.4	0.74	2.85	**0.07***	3.26
Kharar	**SS**	**-0.71***	**-0.45***	**-7.1***	**-0.25***	**-9.43***
	ITA	-0.76	-0.54	-6.13	-0.77	-8.22
Lehal	**SS**	0.008	-0.4	2.28	0	1.03
	ITA	-0.96	-0.62	7.21	-0.67	4.93
Nahan	**SS**	0.18	0.76	**-5.07***	**-1.08***	-6.2
	ITA	-0.42	**0.12***	-17.02	-1.37	-18.69
Patiala	**SS**	-0.08	0.46	-5.89	0	-6.97
	ITA	**0.06***	**-0.05***	-7.7	-0.71	-8.41
Rajpura	**SS**	-1.05	-1.15	-10.97	0	-14.43
	ITA	-0.91	-1.17	-10.91	-0.67	-13.67
Rohiti	**SS**	-0.94	0	-5.52	0	-8.98
	ITA	-1.12	-0.56	4.67	-0.7	2.28
Thanesar	**SS**	-0.19	0	**-4.62***	-0.23	**-5.24***
	ITA	-0.06	0.56	-3.74	**-0.47***	-3.72

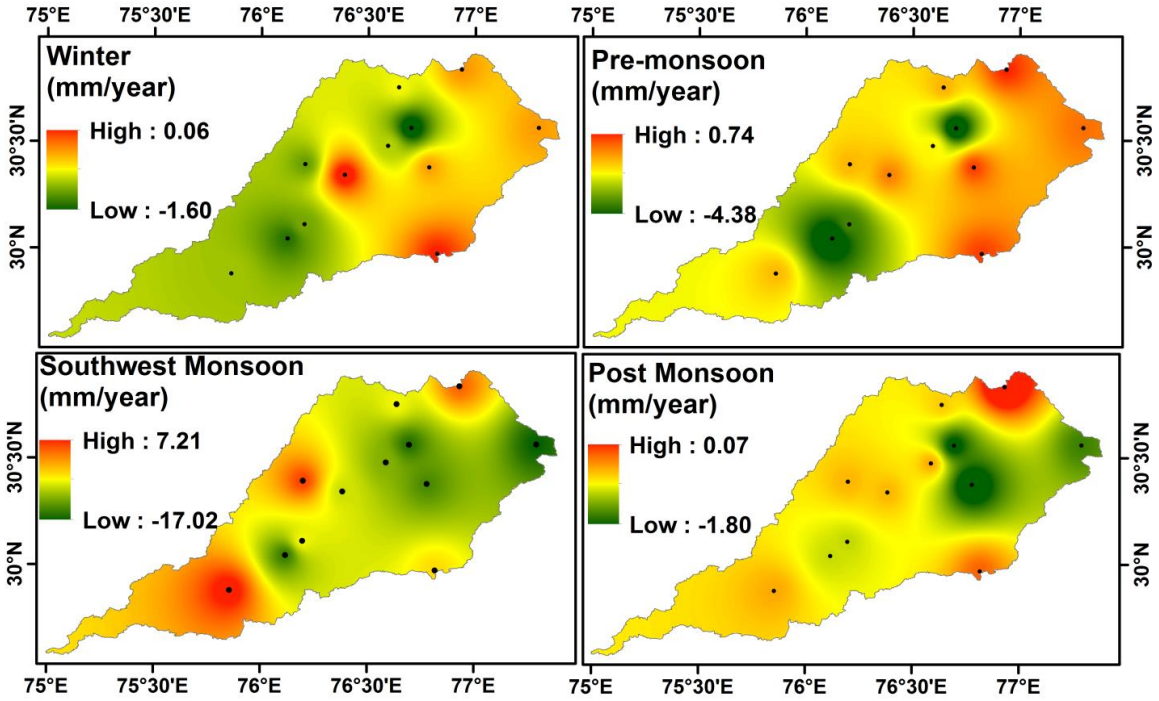

Figure 4.8 Spatial analysis of seasonal average rainfall trend slope using ITA method in Ghaggar river basin

4.3.3. Annual analysis

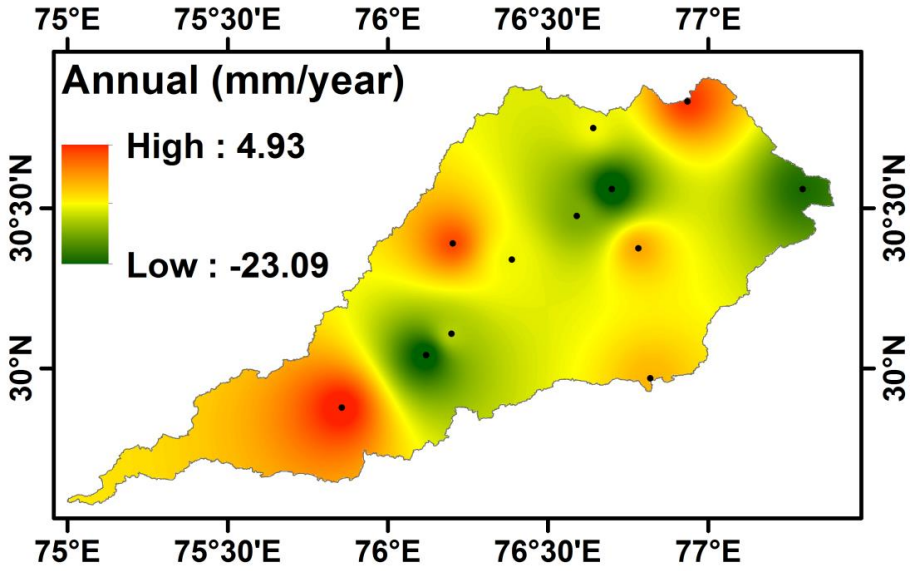

Figure 4.9 Spatial analysis of annual average rainfall trend slope using ITA method in Ghaggar river basin

Figure 4.9 shows the spatial map of the annual rainfall trend magnitude using the ITA method. The last column of Table 4.8 shows the annual trend magnitude value using the ITA method and MK test. The result of trend analysed using ITA analysis is 100% validated with MK test results. The discussion of the annual rainfall trend is based on the result of the ITA method. The highest magnitude of rainfall trend is found to increase at the rate of 4.93mm/year at Lehal,

whereas the lowest magnitude of rainfall trend is found to decrease at 23.09mm/year at Banur. No significant trend at a significance level of 0.05 is found using the ITA method. However, MK test analysis found a significant trend at Kharar and Thanesar. 75 % of total meteorological stations are experiencing declining rainfall, whereas 25% is inclining.

4.4. Annual Change point analysis

The homogeneity analysis in the rainfall pattern defines the change point in the rainfall pattern. The change point is where the rainfall pattern is suddenly changed. The analysis of change point is analyzed using Pettit's test (Equation 4.20 – 4.23), SNH test (Equation 4.24 – 4.26), and Buishand's test (Equation 4.27 – 4.28).

4.4.1. Change point year

Table 4.9 shows the change point in the number of years and particular years using three different methods for the analyzed data period. The significance analysis of the change point is analyzed for a level of significance of 0.05 and marked as * in Table 4.9.

Table 4.9 Change point in number of years and represented years

		Pettit's test		**SNH test**		**Buishand's test**	
Station Name	**Data Duration**	**No of Year**	**Year**	**No of Year**	**Year**	**No of Year**	**Year**
Patiala	**(1975-2017)**	**24***	**1999***	24	1999	**24***	**1999***
Banur	**(1976-2010)**	**25***	**2001***	**25***	**2001***	**23***	**1999***
Dedhna	**(1975-2010)**	**19***	**1994***	**21***	**1996***	**19***	**1994***
Dhaneta	**(1976-2010)**	**23***	**1999***	27	2003	**23***	**1999***
Rajpura	**(1975-2017)**	**31***	**2006***	**31***	**2006***	**31***	**2006***
Rohiti	**(1975-2010)**	26	2001	**27***	**2002***	**26***	**2001***
Kharar	**(1950-2018)**	**33***	**1983***	**33***	**1983***	**33***	**1983***
Ambala	**(1985-2018)**	**21***	**2006***	**21***	**2006***	**21***	**2006***
Kalka	**(1951-2010)**	53	2004	53	2004	53	2004
Lehal	**(1975-2010)**	13	1988	13	1988	**13***	**1988***
Thanesar	**(1950-2011)**	**27***	**1977***	49	1999	49	1999
Nahan	**(1951-2007)**	**18***	**1969***	**17***	**1968***	**18***	**1969***

(*) Significant at 5% level of significance

The change year is selected based on the two or more similar values of the change point or the significance of the change point. For example, at Banur, the change point was taken as 25 years as two out of three methods are showing similar results; at Patiala, the change point is taken as

24 years as all method results are similar; and at Thanesar the change point is taken as 27 years as all method results are different but significant at 27 years.

4.4.2. Descriptive statistics before and after change point

The dataset of annual rainfall was divided into before and after change points at the year of change point. Table 4.10 shows the descriptive statistics of average annual rainfall for different stations of the Ghaggar river basin before and after the change point using Equation 4.1 – 4.3. Figure 4.10 shows the bar chart comparison of average annual rainfall before and after the change point. Figure 4.11 shows the spatial plotting of average annual rainfall before and after the change point.

Table 4.10 Descriptive statistics of average annual rainfall for different stations of the Ghaggar river basin before and after change point

Station Name	Before Change Point			After Change Point		
	Mean (mm)	SD	CV (%)	Mean (mm)	SD	CV (%)
Ambala	913.7	210.5	23.0	607.9	171.0	28.1
Banur	839.2	352.9	42.1	239.9	172.1	71.7
Dedhna	461.8	318.0	68.9	53.4	119.5	223.8
Dhaneta	601.1	316.0	52.6	144.7	168.7	116.6
Kalka	1133.5	353.5	31.2	824.1	109.3	13.3
Kharar	785.4	211.4	26.9	549.9	256.7	46.7
Lehal	379.4	147.9	39.0	632.6	390.5	61.7
Nahan	2223.2	960.8	43.2	1470.9	529.3	36.0
Patiala	820.0	300.8	36.7	556.2	237.2	42.6
Rajpura	795.2	298.3	37.5	346.7	259.2	74.8
Rohiti	831.6	389.5	46.8	405.0	200.4	49.5
Thanesar	728.0	185.9	25.5	570.3	248.1	43.5

It is inferred from Figure 4.10 that the average annual rainfall decreases after the change point at all stations except Lehal. Annual rainfall in the Ghaggar River basin varies in the range of 379.4 – 2223.2 mm before the change point, which decreases to 53.4 – 1470.9mm after the change point. The highest change, i.e., 752.3mm in average annual rainfall after the change point, is found at Nahan. The SD of annual rainfall decreases after the change point at all stations except Lehal. The SD range changes from 147.9 – 960.8mm to 109.3 – 529.3mm after the change point. The highest decreasing SD change is reported at Nahan, i.e., 431.5mm.

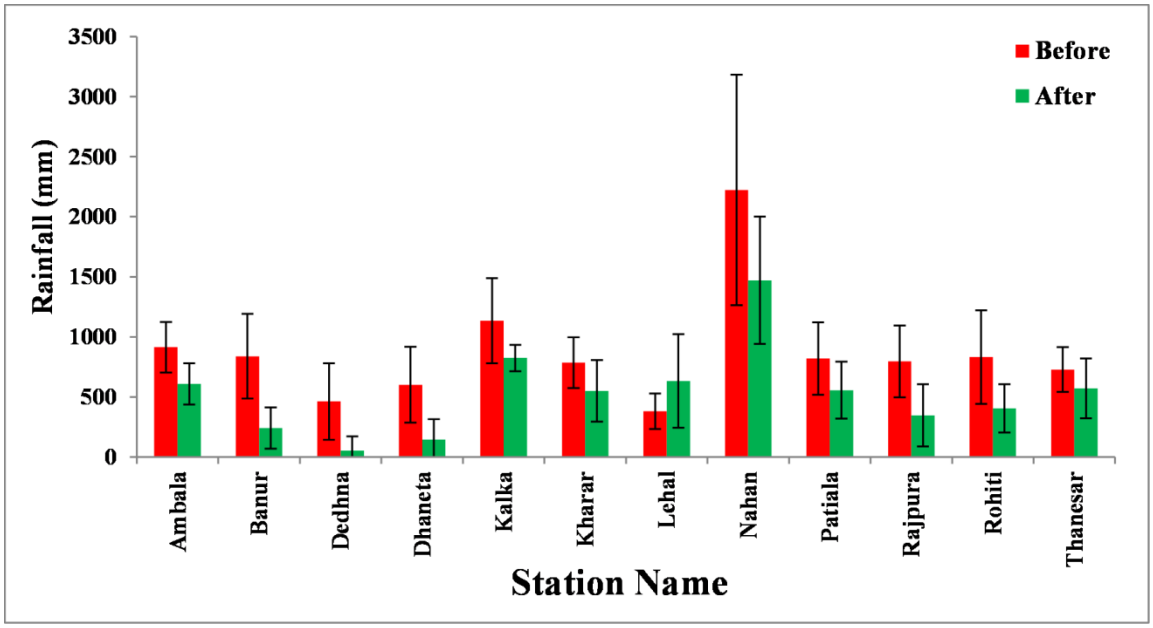

Figure 4.10 Bar chart comparison of average annual rainfall of before and after change point

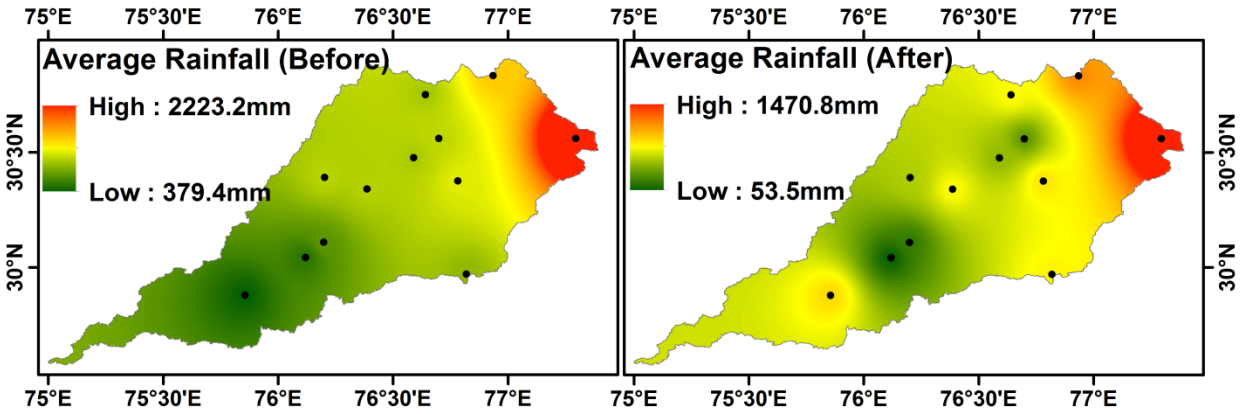

Figure 4.11 Spatial analysis of average annual rainfall before and after change point in the Ghaggar river basin

4.4.3. Trend analysis before and after change point

Trend analysis of annual rainfall before and after the change point was analyzed using the ITA method and validated using the MK test and SS estimator. Equations 4.11 – 4.14 are used for the trend analysis. Table 4.11 shows the trend magnitude with the trend direction sign for the different stations of the Ghaggar river basin using the ITA method and SS estimator. The trend direction result of the ITA method is more than 90% similar to the result of the MK test. The result of trend analysis before and after the change point has been discussed based on the ITA method result. Figure 4.12 and 4.13 shows the bar chart comparison and spatial plotting of trend magnitude value before and after the change point.

Table 4.11 Trend magnitude of average annual rainfall for different stations of the Ghaggar river basin before and after change point

Station Name	Before		After	
	Sen Slope	ITA slope	Sen Slope	ITA slope
Ambala	-2.83	-0.83	**28.73***	**11.48***
Banur	-6.39	**-3.57***	-13.33	**-38.50***
Dedhna	7.00	6.02	**-1.41***	**-5.22***
Dhaneta	5.17	6.18	**-31.98***	**-32.91***
Kalka	**6.47***	**6.69***	-0.15	**-10.44***
Kharar	**-6.47***	**-11.83***	**-16.60***	**-16.42***
Lehal	-3.64	**12.33***	**-32.26***	**-37.98***
Nahan	**65.22***	**94.95***	**9.52***	**21.44***
Patiala	**10.20***	**8.35***	**16.31***	**23.35***
Rajpura	**-6.77***	**-11.39***	-0.32	**-20.92***
Rohiti	23.47	**34.63***	-33.56	**-43.90***
Thanesar	**-6.84***	**-13.62***	**-3.84***	**4.20***

(*) Significant at level of significance 0.05

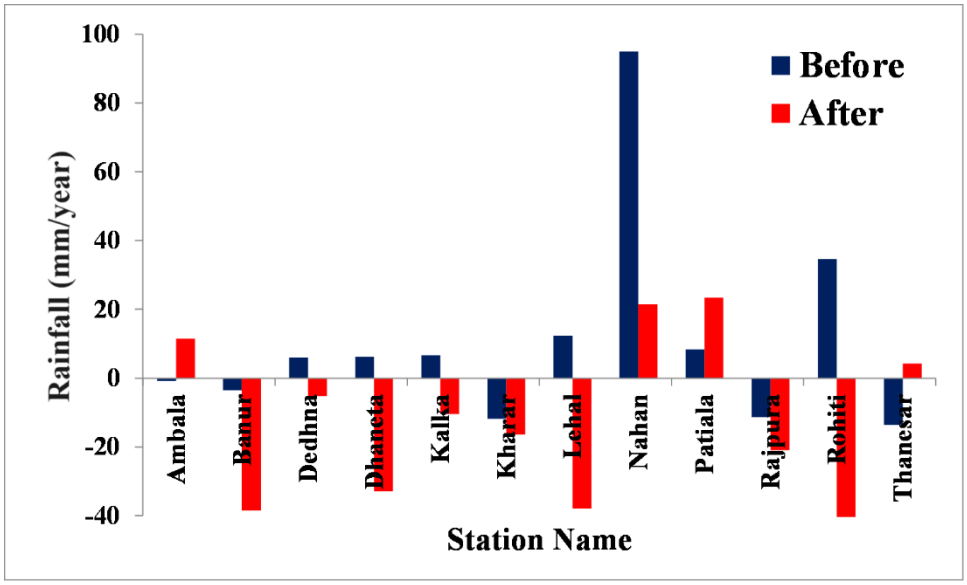

Figure 4.12 Bar chart of comparison of average annual rainfall trend slope before and after change point in the Ghaggar river basin

The trend magnitude of the annual rainfall varied in the range of (-)13.62 – 94.95mm/year before the change point and (-43.9) – 23.35mm/year after the change point. The trend magnitude decreases after the change point. The number of decreasing trend stations is increased from 5 to 8 after the change point. The biggest changes in the trend magnitude were

found at Rohiti station, from an increasing trend magnitude of 34.63mm/year to a decreasing trend magnitude of 43.9mm/year. The trend magnitude is found significant at the significance level of 0.05 at all stations after the change point, whereas before the change point, the trend magnitude was also found significant at all stations except Ambala, Dedhna, and Dhaneta.

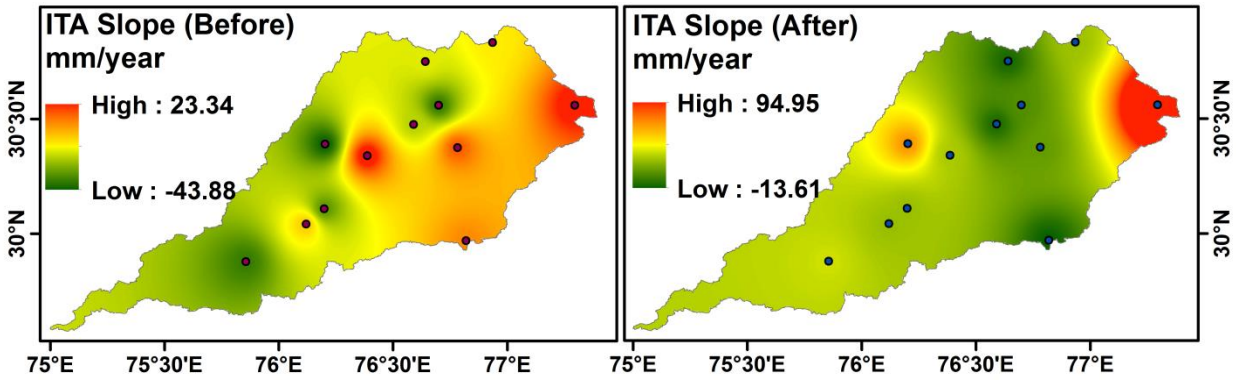

Figure 4.13 Spatial analysis of average annual rainfall trend slope before and after change point in the Ghaggar river basin

4.5. Concluding Remarks

The mean and standard deviation of rainfall over the various stations varies in the range of 266-1703mm and 244-718.3mm respectively. The coefficient of variation varies in the range of 30-118 indicating wider variation of rainfall at some of the stations. The maximum annual rainfall fluctuation is recorded at Dedhna region (118.6mm) whereas the minimum rainfall fluctuation is recorded at Ambala region (30.8mm) indicating the unstable incidence of rainfall at Dedhna. It is observed from the seasonal analysis that the annual rainfall trend of the basin is completely reflecting in southwest monsoon season of the rainfall. The trend analysis of the basin shows the decreasing trend in all stations except Lehal for southwest monsoon analysis whereas the decreasing trend is found in all stations for annual analysis except Lehal and Rohiti region. It is found that most of the regions of the basins have change point after the year 1990. The mean annual rainfall after the change point is found to have decreased for all the stations except Lehal station. The negative trend is found in most of the regions after change point except Patiala, Ambala, Kharar and Nahan stations. Similarly, the variability of rainfall is found to have increased in most of the regions after the change point indicates the climate change.

CHAPTER 5

5. Extreme Rainfall Analysis

This chapter discusses the analysis of extreme rainfall using ETCCDI indices. The chapter starts with the methodology for analyzing ETCCDI indices and discusses the descriptive statistics of these indices. The trend analysis of these indices is also analysed using the trend analysis method, as discussed in the previous Chapter 4.

5.1. Methodology

Extreme events are described from the given list of indices by the Expert Team on Climate Change Detection indices team. The indices used in the study are given in Table 5.1. Rainfall indices are CDD, CWD, PRCPTOT, R10mm, R20mm, R30mm, rx1day, rx3day, rx5day, and SDII used for the extreme events of annual basis. These rainfall indices are calculated using Climdex, an additional R software. The daily rainfall dataset is formatted in text format of "year month date rainfall" and applied for the analysis. The statistical and trend analysis of extreme rainfall indices is analysed using Equation 4.1 – 4.19. However, the frequency analysis of the extreme rainfall events is discussed below.

Table 5.1 ETCCDI extreme rainfall indices

Sr. No	Abbreviation	Index	Unit of measurements	Type of Analysis
1	CDD	Consecutive Dry Days (rainfall<0.1mm)	Days	Annual-Monthly
2	CWD	Consecutive Wet Days (rainfall>1mm)	Days	Annual-Monthly
3	PRCPTOT	Total Precipitation in Wet days	mm	Annual-Monthly
4	R10mm	No of days having rainfall >10mm	Days	Annual-Monthly
5	R20mm	No of days having rainfall >20mm	Days	Annual-Monthly
6	R30mm	No of days having rainfall >30mm	Days	Annual-Monthly
7	rx1day	1 Day maximum rainfall	mm	Annual-Monthly
8	rx3day	Consecutive 3 days maximum rainfall	mm	Annual-Monthly
9	rx5day	Consecutive 5 days maximum rainfall	mm	Annual-Monthly
10	SDII	Simple Daily Precipitation Index	mm	Annual

The mathematical expression of the indices are given below.

Rx1day: Let RR_{ij} be the daily precipitation amount on day i in period j. The maximum 1-day value for period j are

$$\boldsymbol{Rx1day_j = max\,(RR_{ij})} \qquad \textbf{(5.1)}$$

Rx3day: Let RR_{lj} be the precipitation amount for the 3-day interval ending l, period j. Then maximum 3-day values for period j are

$$\boldsymbol{Rx3day_j = max\,(RR_{lj})} \qquad \textbf{(5.2)}$$

Rx5day: Let RR_{kj} be the precipitation amount for the 5-day interval ending k, period j. Then maximum 5-day values for period j are

$$\boldsymbol{Rx5day_j = max\,(RR_{kj})} \qquad \textbf{(5.3)}$$

SDII: Let $\boldsymbol{RR_{wj}}$ be the daily precipitation amount in wet days, $\boldsymbol{w}$ ($\boldsymbol{RR \geq 1mm}$) in period $\boldsymbol{j}$. If $\boldsymbol{W}$ represents number of wet days in $\boldsymbol{j}$, then:

$$\boldsymbol{SDII_j = \frac{\sum_{w=1}^{W} RR_{wj}}{W}} \qquad \textbf{(5.4)}$$

R10mm: Let RR_{ij} be the daily precipitation amount on day i in period j. Count the number of days where $RR_{ij} \geq 10mm$.

R20mm: Let RR_{ij} be the daily precipitation amount on day i in period j. Count the number of days where $RR_{ij} \geq 20mm$.

R30mm: Let RR_{ij} be the daily precipitation amount on day i in period j. Count the number of days where $RR_{ij} \geq 30mm$.

CDD: Maximum length of dry spell: maximum number of consecutive days with $RR < 1mm$
Let RR_{ij} be the daily precipitation amount on day i in period j. Count the largest number of consecutive days where $RR_{ij} < 1mm$.

CWD: Maximum length of wet spell: maximum number of consecutive days with $RR \geq 1mm$
Let RR_{ij} be the daily precipitation amount on day i in period j. Count the largest number of consecutive days where $RR_{ij} \geq 1mm$.

PRCPTOT: Annual total precipitation on wet days: Let RR_{ij} be the daily precipitation amount on day i in period j, then:

$$PRCPTOT_j = \sum_{i=1}^{I} RR_{ij} \quad (5.5)$$

5.2. Descriptive Statistics of Extreme rainfall indices

The analysis of all eleven rainfall indices is shown in Table 5.1. The input file Climdex software was formatted in two columns: date and the amount of rainfall for the respective date. The daily data for the whole period of analysis is required for the analysis. The output file from the software shows the year-wise extreme events for all rainfall indices. These rainfall indices were further analysed for descriptive analysis. Table 5.2 shows the extreme rainfall indices' mean, standard deviation (SD), and coefficient of variance (CV). Figure 5.1 shows the bar chart of the average for each rainfall index.

5.2.1. CDD and CWD

Consecutive dry days (CDD) and consecutive wet days (CWD) are the number of consecutive days that did not receive or received rainfall over an area. The average number of CDD lies in the range of 69.5 – 223.2, whereas the average number of CWD lies in the 3.4 – 9.6 days range. The highest number of CWD and lowest number of CDD was found at Nahan, whereas the lowest number of CWD and highest number of CDD was observed at Dedhna. The standard deviation (SD) of CDD and CWD lies in the range of 25.5 – 293.1 and 1.3 – 3.5, respectively, whereas the coefficient of variation (CV) of CDD and CWD lies in the range of 28.3 – 131.3 and 28.4 – 63.9. The highest SD and CV of CDD are found at Dedhna, whereas the lowest SD of CDD was found at Nahan, and the lowest CV of CDD was found at Kalka. The highest and lowest SD of CWD was found at Nahan and Dhaneta, respectively, whereas the highest and lowest CV of CWD was found at Dedhna and Ambala, respectively.

5.2.2. PRCPTOT

The total precipitation on wet days (PRCPTOT) is the consecutive rainfall received throughout a year during wet days (wet days are the days that received 1mm or higher). The average PRCPTOT in the Ghaggar River basin lies in the 69.5 – 1828.6 mm range, whereas the SD and CV lied in the 229 – 686.4 and 27.9 – 86.4 range, respectively. The highest average and SD of PRCPTOT were found at Nahan, whereas the highest CV is at Dedhna. The lowest average, CV and SD, was found at Ambala.

Table 5.2 Mean, standard deviation (SD) and coefficient of variation (CV) of all extreme rainfall indices

Parameters	Statistics	Patiala	Banur	Dedhna	Dhaneta	Rohiti	Rajpura	Ambala	Kalka	Kharar	Lehal	Nahan	Thanesar
CDD	Mean	98.6	116.7	223.2	97.1	111.0	108.3	75.8	93.1	82.6	119.7	69.5	88.4
	SD	52.5	62.5	293.1	44.3	57.7	57.5	27.1	26.3	31.3	69.3	25.5	30.5
	CV	53.2	53.6	131.3	45.6	52.0	53.1	35.7	28.3	37.9	57.9	36.7	34.5
CWD	Mean	3.9	4.5	3.4	3.9	4.1	4.1	4.9	7.2	5.2	3.8	9.6	4.9
	SD	1.6	1.9	2.2	1.3	1.4	1.6	1.4	2.8	1.6	1.6	3.5	1.7
	CV	40.6	41.8	63.9	33.8	35.3	39.9	28.4	39.3	30.2	42.7	36.6	34.1
PRCPTOT	Mean	688.5	913.4	337.4	614.1	863.6	779.8	821.8	1065.2	734.7	633.5	1828.6	639.7
	SD	282.1	429.7	291.7	347.5	360.0	276.4	229.0	377.4	242.5	379.3	686.4	256.2
	CV	41.0	47.0	86.4	56.6	41.7	35.4	27.9	35.4	33.0	59.9	37.5	40.1
r10mm	Mean	18.0	25.5	9.8	16.4	25.7	18.2	22.5	31.6	20.8	18.1	42.4	18.6
	SD	6.2	12.9	7.6	6.5	6.8	6.1	5.2	9.7	5.5	6.8	7.9	6.3
	CV	34.3	50.4	78.0	39.5	26.7	33.4	22.9	30.9	26.4	37.4	18.6	33.8
r20mm	Mean	10.6	16.4	5.9	9.3	16.3	11.5	13.2	20.1	12.0	9.7	27.5	10.6
	SD	4.8	9.3	5.4	3.8	5.6	4.8	4.0	7.4	4.8	4.8	7.9	4.7
	CV	45.6	56.8	92.1	41.1	34.3	42.1	30.7	36.8	40.2	49.3	28.8	44.5
r30mm	Mean	6.9	11.2	3.6	5.3	10.2	8.0	8.2	12.5	7.8	6.4	19.2	6.4
	SD	3.3	5.6	3.3	2.9	4.3	3.6	2.9	5.6	3.8	3.8	7.0	4.0
	CV	47.2	49.9	90.9	55.9	42.0	44.3	35.1	45.1	49.3	59.0	36.2	62.6
rx1day	Mean	124.0	102.8	66.4	109.2	121.9	127.1	105.5	96.0	91.3	120.3	160.3	87.1
	SD	80.9	44.5	51.8	85.2	70.0	54.8	49.7	42.9	35.0	84.0	58.1	33.6
	CV	65.3	43.3	77.9	78.0	57.4	43.1	47.1	44.7	38.3	69.8	36.2	38.6
rx3day	Mean	158.4	179.6	100.2	153.2	197.4	187.7	166.1	155.6	142.5	171.8	252.4	128.3
	SD	93.5	85.3	87.4	141.7	123.3	93.9	79.9	58.2	51.7	103.7	94.7	49.0
	CV	59.0	47.5	87.3	92.5	62.5	50.0	48.1	37.4	36.3	60.4	37.5	38.2

Parameters	Statistics	Patiala	Banur	Dedhna	Dhaneta	Rohiti	Rajpura	Ambala	Kalka	Kharar	Lehal	Nahan	Thanesar
rx5day	Mean	172.9	217.4	114.2	163.5	223.1	198.9	188.4	185.9	157.2	185.2	311.3	143.6
	SD	103.5	98.4	99.1	139.9	141.9	94.0	83.9	69.3	58.4	105.8	119.7	54.9
	CV	59.9	45.3	86.8	85.6	63.6	47.3	44.5	37.3	37.2	57.1	38.5	38.2
SDII	Mean	21.1	26.4	16.5	19.9	26.2	26.9	17.4	20.8	18.3	24.8	24.7	16.3
	SD	6.7	7.5	9.4	10.2	7.0	11.0	4.6	7.2	5.0	6.8	9.8	4.8
	CV	31.6	28.6	56.7	51.2	26.9	41.0	26.2	34.8	27.2	27.2	39.7	29.3

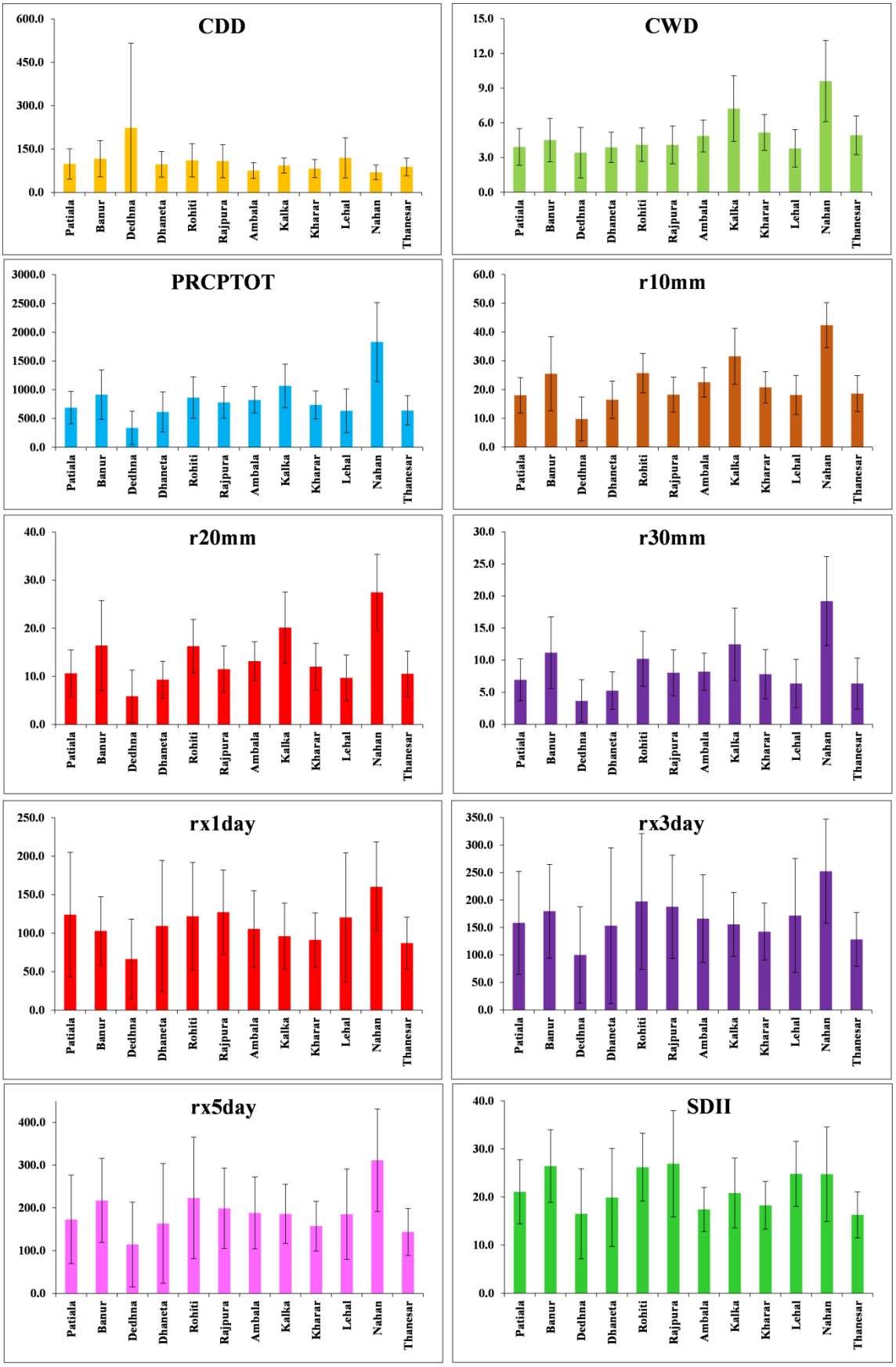

Figure 5.1 Bar chart comparison of average of CDD, CWD, PRCPTOT, r10mm, r20mm, and r30mm, rx1day, rx3day, rx5day and SDII

5.2.3. R10mm, R20mm and R30mm

R10mm, R20mm, and R30mm are the days that received 10mm, 20mm, and 30mm of rainfall, respectively. The average of R10mm, R20mm, and R30mm lies in the range of 9.8 – 42.4, 5.9 – 27.5, and 3.6 – 19.2, respectively. The average R10mm, R20mm, and R30mm days were highest at Nahan and lowest at Dedhna. The SD of R10mm, R20mm, and R30mm lie in the range of 5.2 – 12.9, 3.8 – 9.3, and 2.9 – 7 respectively. The highest SD of R10mm, R20mm, and R30mm were found at Banur, Banur, and Nahan, respectively, whereas the lowest is found at Ambala, Dhaneta, and Dhaneta, respectively. The CV of R10mm, R20mm, and R30mm lied in the range of 18.6 – 78%, 28.8 – 92.1%, and 35.1 – 90.9%, respectively. The highest CV of R10mm, R20mm, and R30mm were found at Dedhna, whereas the lowest CV of R10mm, R20mm, and R30mm are found at Nahan, Nahan, and Ambala, respectively.

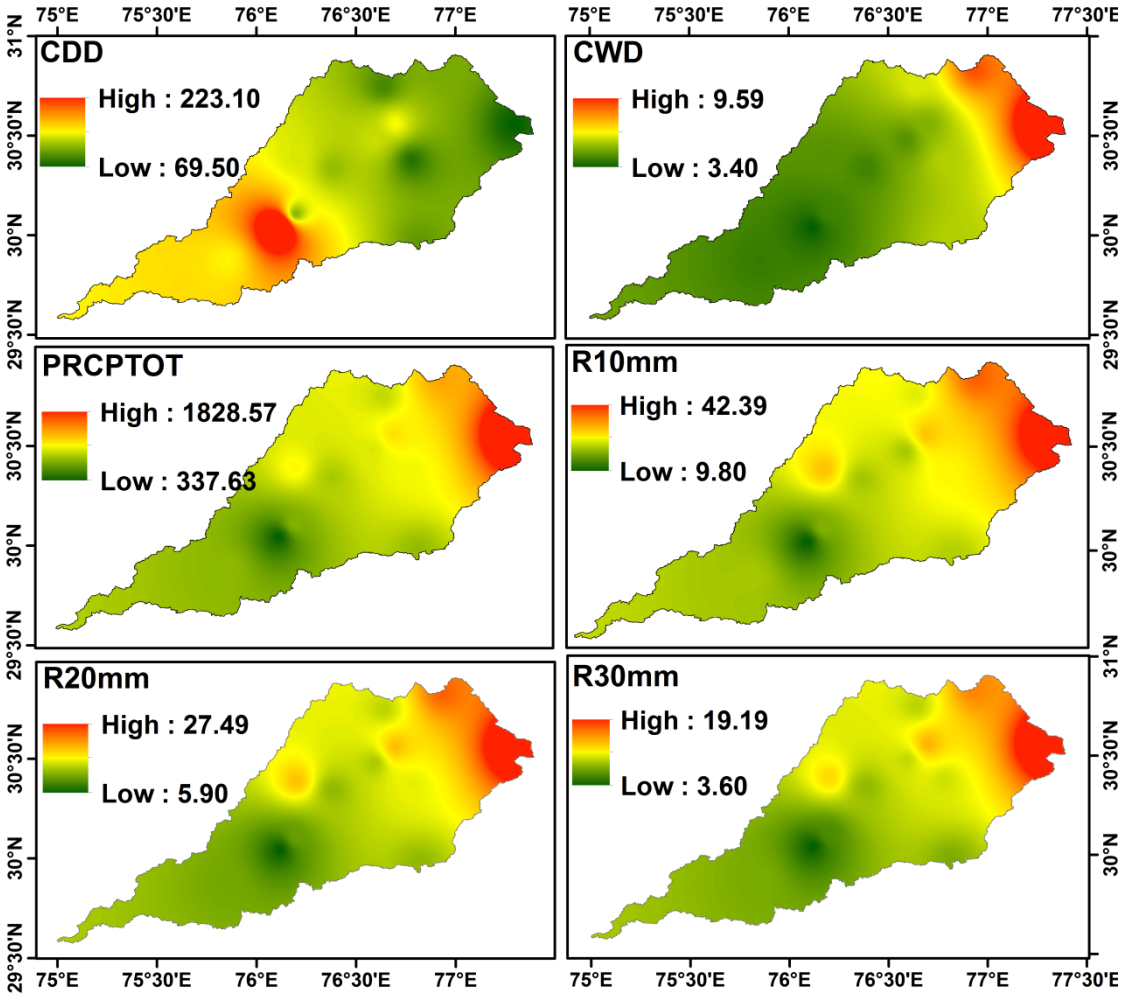

Figure 5.2 Spatial map of average extreme rainfall indices (CDD, CWD, PRCPTOT, R10mm, R20mm and R30mm)

5.2.4. rx1day, rx3day and rx5day

The rx1day is the highest rainfall received in one day over a year. The rx3day and rx5day are the rainfall received in three and five consecutive days over a year, respectively. The average rx1day, rx3day, and rx5day in the Ghaggar River basin lied in the range of 66.4 – 160.3 mm, 100.2 – 252.4 mm, and 114.2 – 311.3 mm, respectively. The highest and lowest average amount of rx1day, rx3day, and rx5day was found at Nahan and Dedhna, respectively. The SD of rx1day, rx3day, and rx5day lie in the range of 33.6 – 85.2, 49.0 – 141.7, and 54.9 – 141.9, respectively. The SD of rx1day and rx3day was highest at Dhaneta and lowest at Thanesar, whereas the SD of rx5day is highest at Rohiti and lowest at Thanesar. The CV of rx1day, rx3day, and rx5day lied in the range of 36.2 – 78%, 36.3 – 92.5%, and 37.2 – 86.5%, respectively. The highest and lowest CVs of rx1day were found at Dhaneta and Nahan, respectively. The lowest CV of rx3day and rx5day was found at Kharar. The highest CV of rx3day is found at Dhaneta, whereas the highest CV of rx5day was observed at Dedhna.

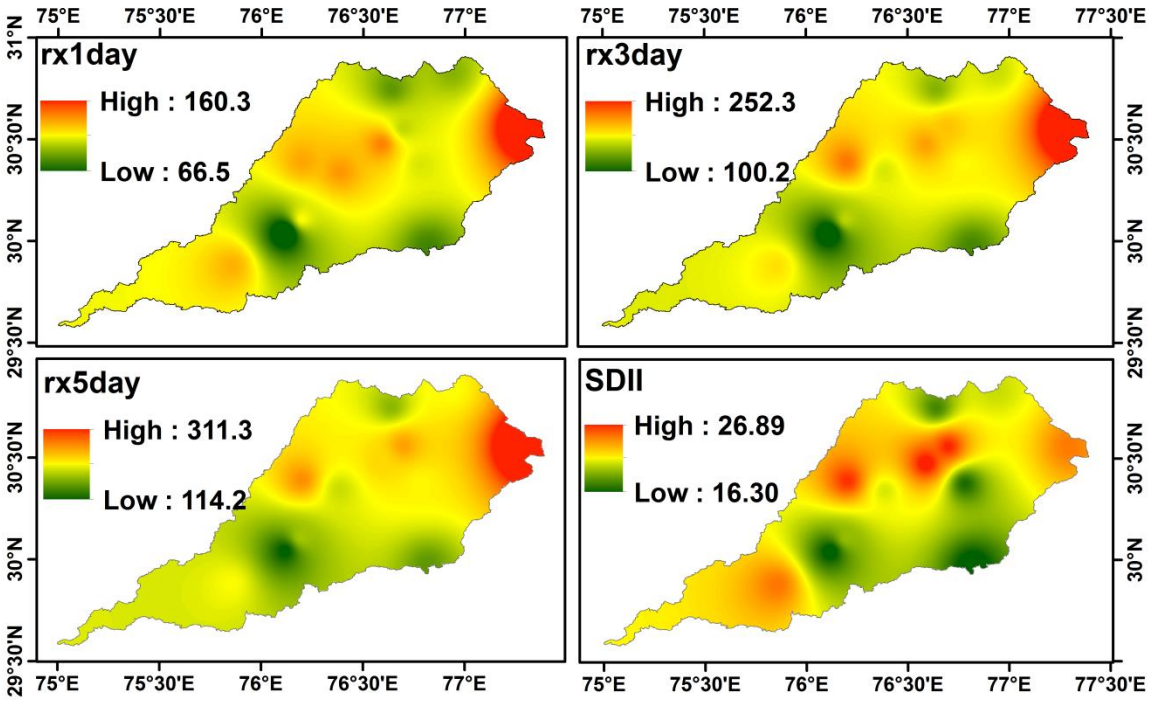

Figure 5.3 Spatial map of average extreme rainfall indices (rx1day, rx3day, rx5day and SDII)

5.2.5. SDII

The simple precipitation intensity index (SDII) is the total rainfall received during wet days divided by the number of wet days in that year. The SDII of the Ghaggar river basin lies in the range of 16.3 – 26.9 mm, whereas the highest amount of SDII is found at Rajpura and lowest at Thanesar. The SD and CV of SDII lied in the range of 4.6 – 11 and 26.2 – 56.7%,

respectively. The CV and SD of SDII are highest at Rajpura and Dedhna, respectively, whereas the CV and SD of SDII are lowest at Ambala.

5.3. Trend analysis of Extreme rainfall indices

Trend analysis of extreme rainfall indices was analyzed using the ITA method and validated using the MK test and SS estimator. Equation 4.4 – 4.19 analyzes trend, autocorrelation, and pre-whitening approach to remove serial correlation. Table 5.3 shows serial correlation in the extreme rainfall indices dataset. Serial correlation from these datasets is removed using a pre-whitening approach. The pre-whitened data for trend analysis is used only for the MK test and SS estimator.

Table 5.3 Presence of serial correlation in extreme rainfall indices dataset of Ghaggar river basin

Station Name	CDD	CWD	PRCPTOT	r10mm	r20mm	r30mm	rx1day	rx3day	rx5day	SDII
Ambala			Yes			Yes				Yes
Banur										
Dedhna	Yes	Yes		Yes						
Dhaneta										
Kalka			Yes	Yes	Yes	Yes	Yes	Yes		Yes
Kharar										
Lehal										
Nahan			Yes		Yes	Yes	Yes	Yes	Yes	Yes
Patiala		Yes								
Rajpura		Yes	Yes							Yes
Rohiti			Yes			Yes				
Thanesar			Yes	Yes		Yes				

Innovative trend analysis analyses trend direction, trend magnitude, and significance of trend. The MK test analysed the trend direction and significance of the trend, whereas the slope of the trend was analysed using the SS estimator. Table 5.4 shows the trend magnitude, direction, and significance of the trend analysed using the ITA method and SS estimator with the MK test. The positive and negative sign in the value shows increasing and decreasing trend, respectively; the bold and star mark values showed a significant trend at a significance level of 0.05; and the value itself shows the magnitude of the trend. 91.7% of extreme event trends show similar trend direction using both methods. Therefore, the result of the ITA method can be used to analyze the trend for this extreme event trend study. Further, the extreme rainfall trend is discussed on the result of the ITA method. The trend significance of extreme events shows that 18% of trends are significant at the level of significance 0.05. The trend analysis of extreme rainfall has been discussed in details.

Table 5.4 Trend magnitude value of extreme rainfall events

		CDD	CWD	PRCPTOT	r10mm	r20mm	r30mm	rx1day	rx3day	rx5day	SDII
Ambala	**ITA**	-1.132	-0.714	-17.47	-0.443	-0.352	-0.224	-1.262	-2.46	-3.898	-0.42
	MK Test	-0.666	**-0.064***	**-17.32***	**-0.428***	**-0.3***	**-0.176***	**-1.884***	**-3.32***	**-5.236***	**-0.431***
Banur	**ITA**	**2.111***	**-0.055***	-35.53	-1.944	-0.805	-0.611	4.694	9.25	2.138	**0.056***
	MK Test	6.833	-0.25	-60.125	**-2.761***	-1.266	-0.807	2.25	1.472	-5.583	-0.041
Dedhna	**ITA**	24.97	-0.22	-31.429	-1.044	-0.735	-0.441	-2.803	**-1.882***	**-0.6***	**-0.318***
	MK Test	**12.611***	-0.218	**-31.429***	**-1***	**-0.666***	**-0.292***	**-4.934***	-5.277	-5.083	-0.174
Dhaneta	**ITA**	6.218	0	**9.07***	-0.484	-0.109	**0.031***	5.835	8.926	7.176	1.276
	MK Test	**5.05***	0	-7.775	-0.4	-0.085	0	0.571	1.861	0.896	0.809
Kalka	**ITA**	-0.184	**0.005***	-5.373	-0.075	-0.128	-0.113	-0.382	**0.053***	-0.548	-0.243
	MK Test	-0.362	0	**-9.58***	-0.184	**-0.181***	**-0.162***	**-0.895***	-0.812	-0.927	**-0.319***
Kharar	**ITA**	0.148	-0.028	-7.131	-0.07	-0.053	-0.066	-0.762	-1.595	-1.71	-0.129
	MK Test	0.476	-0.277	**-9.927***	**-0.147***	**-0.166***	**-0.142***	-0.728	**-1.786***	**-1.921***	**-0.129***
Lehal	**ITA**	-2.97	**0.035***	17.5	**-0.023***	0.105	**0.058***	6.011	7.719	8.152	0.393
	MK Test	0	0	8.8	-0.055	-0.111	0	3.7	3.153	5.857	0.209
Nahan	**ITA**	-0.285	-0.024	-9.201	-0.095	-0.086	-0.063	-0.595	-1.405	-2.222	-0.257
	MK Test	0.243	0	-3.158	-0.102	-0.074	-0.054	-0.202	-0.8	-1	**-0.12***
Patiala	**ITA**	**-0.09***	**-0.007***	-9.473	-0.17	-0.102	-0.071	-2.639	-3.129	-3.637	-0.24
	MK Test	-0.066	0	-10.595	-0.2	-0.187	-0.125	-1.028	-1.978	-1.926	**-0.651***
Rajpura	**ITA**	2.479	0.033	-16.468	-0.157	-0.223	-0.223	-2.033	-4.73	**-0.500***	-1.391
	MK Test	0.333	0	**-24***	**-0.04***	**-0.375***	**0.312***	-1.69	-5.375	-4.644	**-1.447***
Rohiti	**ITA**	3.274	0.093	21.453	**0.023***	**0.116***	0.28	4.419	6.589	9.688	0.595
	MK Test	5.142	0	-4.681	-0.333	-0.166	0.09	3.636	1	3.75	0.396
Thanesar	**ITA**	0.313	-0.009	-6.464	-0.126	-0.105	-0.076	-1.141	-1.466	-1.447	-0.117
	MK Test	0	0	**-7.893***	**-0.166***	**-0.15***	**-0.111***	**-1***	**-1.416***	**-1.681***	**-0.183***

5.3.1. CDD and CWD

The trend magnitude of CDD and CWD varied in the range of (-)2.97 – 24.97 days/year and (-)0.714 – 0.093 days/year, respectively. The highest trend magnitude, increasing trend, was found at Dedhna, whereas the lowest trend magnitude, decreasing trend, was found at Lehal. 41% of total stations trend of CDD and 59% of total stations of CWD is decreasing trend whereas the rest of trends of both CDD and CWD is increasing. A significant trend of CDD was found at Banur, which was increasing, and Patiala, which was decreasing. A significant trend of CWD is found at Banur and Patiala, which are decreasing. The significant increasing trend of CWD is found at Kalka and Lehal.

5.3.2. PRCPTOT

The trend of PRCPTOT is decreasing in 83% of the station, where only 17% of the station is increasing. A significant trend was found at Dhaneta, increasing at 9.07 mm/year. The trend magnitude of PRCPTOT lied in the range of (-)35.53 – 21.45 mm/year. The highest trend magnitude, i.e., increasing, was found at Rohiti, and the lowest, i.e., decreasing, wa found at Banur.

5.3.3. R10mm, R20mm and R30mm

The trend magnitude of R10mm, R20mm, and R30mm varies in the range of (-)1.944 – 0.023 days/year, (-)0.805 – 0.116 days/year, and (-)0.611 – 0.280 days/year respectively. The significant trend of R10mm and R20mm was found at Rohiti, increasing at 0.023 days/year and 0.116 days/year, respectively. A significant decreasing trend of R10mm was found at Lehal (0.023 days/year). The significant trend of R30mm increased at Dhaneta (0.031 days/year) and Lehal (0.058 days/year). 92% of R10mm, 83% of R20mm, and 75% of R30mm of trend was decreasing.

5.3.4. rx1day, rx3day and rx5day

The trend magnitude of rx1day lied in the range of (-)2.803 – 6.011 mm/year, where the highest, i.e., increasing, was found at Lehal and lowest, i.e., decreasing, found at Dedhna. No significant trend was found in the rx1day trend. 33.3% of the rx1day trend was increased, while the rest were decreasing. The trend magnitude of rx3day and rx5day lies in the range of (-)4.73 – 9.25 mm/year and (-)3.898 – 9.688 mm/year, respectively. A significant trend of rx3day is found at Dedhna (-1.882 mm/year) and Kalka (0.053 mm/year). The trend of rx5day significantly

decreases at Dedhna (-0.600 mm/year) and Rajpura (-0.500 mm/year). 41.6% of rx3day and 33.3% of rx5day were found increasing trend, and the rest were decreasing trend.

5.3.5. SDII

The trend of SDII was increasing at 33.3% of stations and decreasing at 66.6% of stations. The increasing significant trend is found at Banur (0.056mm/year) and a decreasing significant trend at Dedhna (0.318mm/year). The trend magnitude of SDII lied in the range of (-)1.391 – 1.276 mm/year. The highest trend magnitude, i.e., increasing, was found at Dhaneta, and the lowest, i.e., decreasing, was found at Rajpura.

5.4. Concluding remarks

The CWD, PRCPTOT, r10mm, r20mm, r30mm, rx1day, rx3day, and rx5day were found highest at Nahan and lowest at Dedhna, whereas the CDD was found highest at Dedhna and lowest at Nahan. The SDII was observed highest at Rajpura and lowest at Thanesar. The trend magnitude result of the MK test and the ITA method is compared, and 91.7% of the trends are in a similar direction. 18% of all rainfall indices trend at the different meteorological stations were significant at 0.05 level of significance The extreme rainfall events are analyzed as rainfall indices show that the trend of CWD, R10mm, R20mm, R30mm, rx1day, rx3day, rx5day, SDII, and PRCPTOT are decreasing at more than 66% of the station, whereas the only CDD is increasing at 59% of the stations.

CHAPTER 6

6. Classification of Flood Zone

This chapter discussed the flood risk zone analysis and classification of flood zones based on the score using the Analytical Hierarchy Process and Graph Theory. The chapter started with the formulation of the methodology for both methods. The classification of the factors used for flood risk analysis is also discussed. The result and discussion of the flood risk analysis are also discussed separately as analyzed from both methods.

6.1. Methodology

The present study used two different methodologies for flood risk analysis. They are Graph theory application and Analytical Hierarchy Process (AHP). Graph theory was applied to determine the flood risk of the Ghaggar basin, and AHP was used to validate the results obtained through graph theory application. AHP is the most widely used classical approach for flood risk mapping, whereas graph theory is a system-integrated approach introduced in the present study for flood risk mapping. The detailed algorithm of methodology is shown in Figure 6.1.

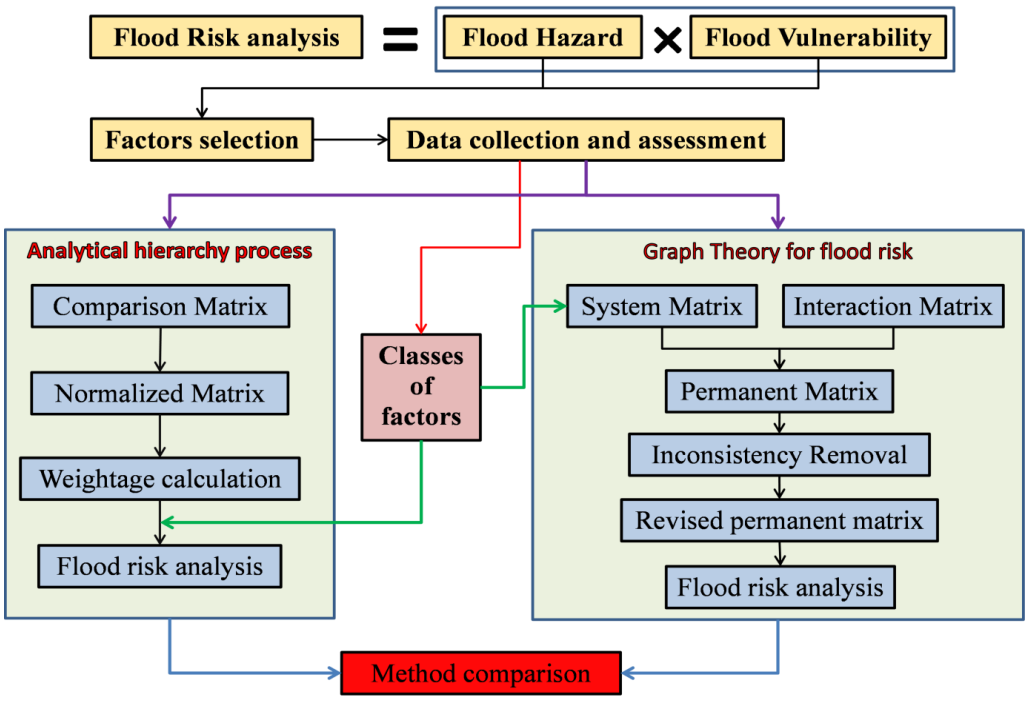

Figure 6.1 Methodologies applied for the study

6.1.1. Flood risk analysis using Graph theory

The graph theory approach is an integrated system approach that considers the influence and interactions between the various sub-systems, an advantage over the other system approaches. However, AHP evaluates the sub-systems affecting the main system through a hierarchy process but does not consider the interaction between the sub-systems, which may impact the performance of a system. The permanent matrix determined using graph theory integrates all the sub-systems and their interactions, which can be used to evaluate and analyze complex problems with all possible alternative solutions.

Identifying structural constituents of flood risk systems for any river basin and understanding their impact on the system is the first step to developing a mathematical model using graph theory. Two major sub-systems are identified for flood risk systems, whereas several sub-systems are identified which can affect the sub-systems. The effective management of flood hazard and flood vulnerability, which are the two sub-systems of a flood risk system, can reduce the flood risk of a basin.

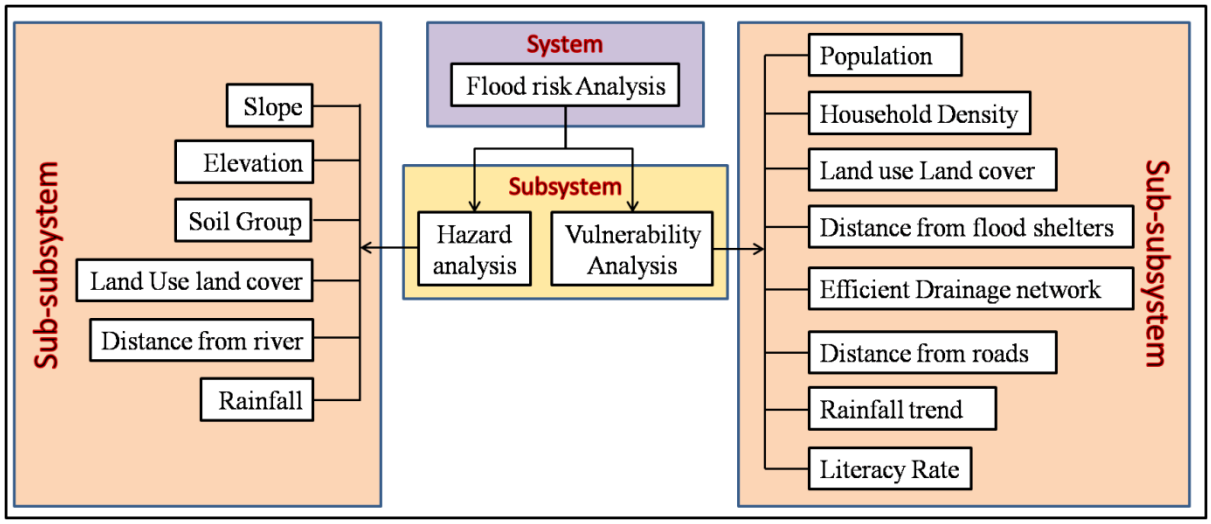

Figure 6.2 Tree diagram of flood risk analysis

Figure 6.2 shows the tree diagram of the flood risk system, which represents two lower levels of sub-systems. The first lower-level sub-systems are flood hazard and flood vulnerability. The conditioning factors for the two sub-systems, flood hazard, and flood vulnerability, have been identified and represented in Figure 3 as sub-subsystems. The factors of flood hazard are the internal driving factors that induce the flood risk, whereas the factors of flood vulnerability are the resistance of the flood risk.

A system or a sub-system can be evaluated using graph theory by identifying the parameters affecting the system/sub-system and preparing a system/sub-system permanent matrix. The

magnitude of the diagonal elements of this matrix will be the weightage of each parameter based on its actual performance in the sub-system, and the magnitude of the off-diagonal elements of this matrix is based on the interaction between one sub-system with the other, which may be described as strong, moderate, mild or no interaction. These interactions between two sub-systems are either one-directional or both directions. The present study will follow the bottom-up approach in which sub-subsystems will be considered to evaluate the sub-systems of the flood risk system. Figure 6.2 shows that six sub-subsystems are affecting the flood hazard sub-system. The runoff generated due to rainfall sub-subsystem will be affected by slope, elevation, LULC, soil group, and distance from a river. The higher runoff volume and the quick peak occur for a steep slope terrain, leading to an increase in the flood hazard.

The change in slope may also occur during runoff due to soil erosion. Similarly, the higher runoff volume along with quick peak occurs due to urbanisation, whereas the presence of forest and vegetation decreases the magnitude of runoff peak, which indicates the effect of LULC and Normalised Difference Vegetation Index (NDVI) on runoff. Vegetation plays an important role in influencing the mean and turbulent flow field in a river body (442). Urbanisation occurs in the area where water is available, revealing the interdependency of urbanisation and distance from the river. If the place where rainfall occurs is close to the river course, then the quick runoff to the river will cause an immediate increase in river discharge, leading to flood hazards. The soil group is also a factor that affects the volume of runoff. The rainfall usually occurs at a higher elevation of a basin. It quickly collects the water to the river's main course and may create flood hazards in the basin at lower elevations. The runoff generated due to rainfall will be affected by higher NDVI, which leads to a decrease in the possibility of flood hazards. This phenomenon shows that the slope strongly interacts with rainfall, whereas rainfall has a mild interaction with the slope. Similarly, a strong interaction exists between LULC and rainfall and rainfall. The soil group has moderate interaction with rainfall, whereas the rainfall has mild or no interaction with the soil group.

Similarly, Figure 6.2 shows that eight sub-subsystems affect the flood vulnerability sub-system. Population sub-subsystem directly impacts household density, LULC, distance from flood shelters, distance from roads, and literacy rate. Urbanisation and agricultural land cause an increase in population as well as household density. The flood shelters are usually constructed in floodplain areas with good communication facilities. The drainage network should be efficient in urbanized floodplain areas. It is observed that there is a strong interaction existing between population and LULC, population and household density, population and literacy, population and distance from flood shelter, population and efficient drainage network,

population and distance from roads, and population and rainfall trend. There is mild or no interaction between rainfall trend and literacy rate, literacy rate and distance from roads, literacy rate, efficient drainage network, literacy rate, and distance from flood shelter.

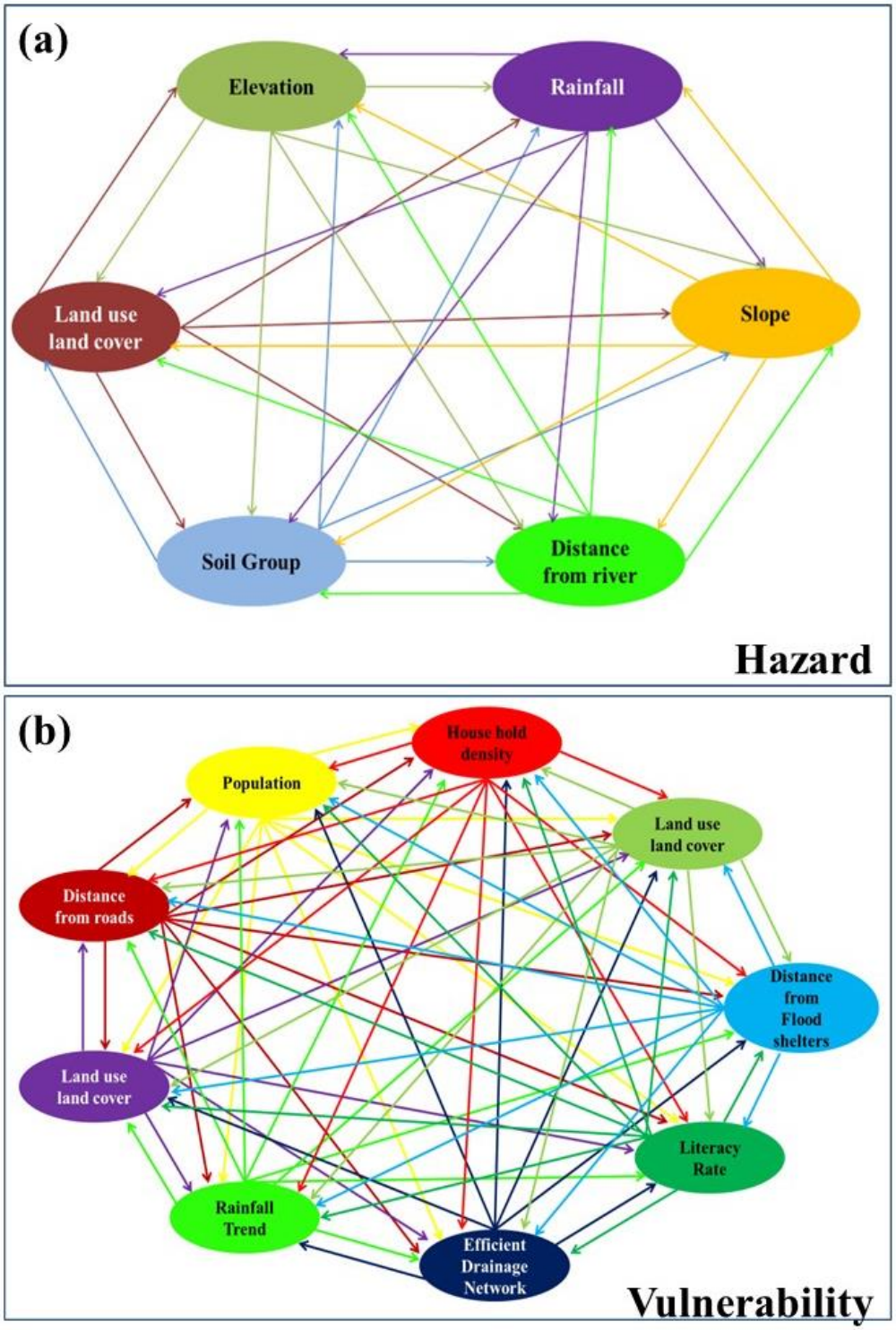

Figure 6.3 Digraph of flood hazard and flood vulnerability sub-system

The performance of a system/sub-system depends on the performance of sub-systems/sub-subsystems. The system and its sub-systems are represented as nodes, whereas edges represent their interdependencies. The interactions between these sub-subsystems are represented in Figure 6.3(a & b) through nodes and edges with direction, known as a digraph. Figure 6.2 shows the tree diagram, a non-mathematical model, whereas Figure 6.3 (a & b) shows the digraph, a mathematical model. The digraph can be processed through a matrix model. The interrelationship values of sub-systems ($P_{i,j}$) are represented in the adjacency matrix. In the system matrix, the diagonal values are taken using the importance level of that element with respect to flood hazard/flood vulnerability, and weightage is assigned based on its importance. Table 6.1 shows the qualitative measure of a system/sub-system representing diagonal values of system/sub-system permanent matrix, on a scale of 1-8 in which weightage of 1 indicates exceptionally low, whereas weightage of 8 indicates exceptionally high to cause flood hazard/flood vulnerability. In the interaction matrix, the off-diagonal elements are taken using the level of interaction/interdependency between two sub-subsystems of the flood hazard/flood vulnerability sub-system, and weightage is assigned based on their level of interaction. Table 6.2 shows the weightage of off-diagonal values on a scale of 0-3, in which a weightage of 0 indicates there is no interaction between two sub-subsystems, whereas a weightage of 3 indicates there is a strong interaction between two sub-subsystems. Although many divisions can be created for the qualitative measure of the interdependencies between the sub-systems / sub-subs systems, authors feel that experts will need clarification/bias while assigning the type of interaction between sub-systems and assigning that interaction into a qualitative measure. Therefore, the present study adopted the weightage ranging from 0-3 for the off-diagonal elements.

Table 6.1 Qualitative measure of a system or sub-system used for flood risk analysis.

Weightage	**Diagonal or system**
1	Exceptionally low
2	Extremely low
3	Very low
4	Normal
5	High
6	Very High
7	Extremely High
8	Exceptionally high

Table 6.2 Level of the interaction and their corresponding weightage for flood risk analysis.

Weightage	Level of interaction between one sub-system with
0	No interaction
1	Weak
2	Moderate
3	Strong

The system matrix and interaction matrix summation represent a system permanent matrix. Eq. 6.1 shows the system matrix, interaction matrix, and system permanent matrix for the flood hazard sub-system, whereas Eq. 6.2 shows the system matrix, interaction matrix, and system permanent matrix for the flood vulnerability sub-system. Since there are six constituents for the flood hazard sub-system, the sub-system permanent matrix is shown in Eq. 6.1 consists of a 6x6 matrix, whereas Equations shows the flood vulnerability sub-system permanent matrix. 6.2 consists of an 8 x 8 matrix, as eight constituents are considered for the flood vulnerability sub-system.

$$\begin{bmatrix} H_1 & 0 & 0 & 0 & 0 & 0 \\ 0 & H_2 & 0 & 0 & 0 & 0 \\ 0 & 0 & H_3 & 0 & 0 & 0 \\ 0 & 0 & 0 & H_4 & 0 & 0 \\ 0 & 0 & 0 & 0 & H_5 & 0 \\ 0 & 0 & 0 & 0 & 0 & H_6 \end{bmatrix} + \begin{bmatrix} 0 & H_{12} & H_{13} & H_{14} & H_{15} & H_{16} \\ H_{21} & 0 & H_{23} & H_{24} & H_{25} & H_{26} \\ H_{31} & H_{32} & 0 & H_{34} & H_{35} & H_{36} \\ H_{41} & H_{42} & H_{43} & 0 & H_{45} & H_{46} \\ H_{51} & H_{52} & H_{53} & H_{54} & 0 & H_{56} \\ H_{61} & H_{62} & H_{63} & H_{64} & H_{65} & 0 \end{bmatrix}$$

$$= \begin{bmatrix} \mathbf{H_1} & \boldsymbol{H_{12}} & \boldsymbol{H_{13}} & \boldsymbol{H_{14}} & \boldsymbol{H_{15}} & \boldsymbol{H_{16}} \\ \boldsymbol{H_{21}} & \mathbf{H_2} & \boldsymbol{H_{23}} & \boldsymbol{H_{24}} & \boldsymbol{H_{25}} & \boldsymbol{H_{26}} \\ \boldsymbol{H_{31}} & \boldsymbol{H_{32}} & \mathbf{H_3} & \boldsymbol{H_{34}} & \boldsymbol{H_{35}} & \boldsymbol{H_{36}} \\ \boldsymbol{H_{41}} & \boldsymbol{H_{42}} & \boldsymbol{H_{43}} & \mathbf{H_4} & \boldsymbol{H_{45}} & \boldsymbol{H_{46}} \\ \boldsymbol{H_{51}} & \boldsymbol{H_{52}} & \boldsymbol{H_{53}} & \boldsymbol{H_{54}} & \mathbf{H_5} & \boldsymbol{H_{56}} \\ \boldsymbol{H_{61}} & \boldsymbol{H_{62}} & \boldsymbol{H_{63}} & \boldsymbol{H_{64}} & \boldsymbol{H_{65}} & \mathbf{H_6} \end{bmatrix} \quad \textbf{(6.1)}$$

$$\begin{bmatrix} V_1 & 0 & 0 & 0 & 0 & 0 & 0 & 0 \\ 0 & V_2 & 0 & 0 & 0 & 0 & 0 & 0 \\ 0 & 0 & V_3 & 0 & 0 & 0 & 0 & 0 \\ 0 & 0 & 0 & V_4 & 0 & 0 & 0 & 0 \\ 0 & 0 & 0 & 0 & V_5 & 0 & 0 & 0 \\ 0 & 0 & 0 & 0 & 0 & V_6 & 0 & 0 \\ 0 & 0 & 0 & 0 & 0 & 0 & V_7 & 0 \\ 0 & 0 & 0 & 0 & 0 & 0 & 0 & V_8 \end{bmatrix} + \begin{bmatrix} 0 & V_{12} & V_{13} & V_{14} & V_{15} & V_{16} & V_{17} & V_{18} \\ V_{21} & 0 & V_{23} & V_{24} & V_{25} & V_{26} & V_{27} & V_{28} \\ V_{31} & V_{32} & 0 & V_{34} & V_{35} & V_{36} & V_{37} & V_{38} \\ V_{41} & V_{42} & V_{43} & 0 & V_{45} & V_{46} & V_{47} & V_{48} \\ V_{51} & V_{52} & V_{53} & V_{54} & 0 & V_{56} & V_{57} & V_{58} \\ V_{61} & V_{62} & V_{63} & V_{64} & V_{65} & 0 & V_{67} & V_{68} \\ V_{71} & V_{72} & V_{73} & V_{74} & V_{75} & V_{76} & 0 & V_{78} \\ V_{81} & V_{82} & V_{83} & V_{84} & V_{85} & V_{86} & V_{87} & 0 \end{bmatrix}$$

$$= \begin{bmatrix} \mathbf{V_1} & \mathbf{V_{12}} & \mathbf{V_{13}} & \mathbf{V_{14}} & \mathbf{V_{15}} & \mathbf{V_{16}} & \mathbf{V_{17}} & \mathbf{V_{18}} \\ \mathbf{V_{21}} & \mathbf{V_2} & \mathbf{V_{23}} & \mathbf{V_{24}} & \mathbf{V_{25}} & \mathbf{V_{26}} & \mathbf{V_{27}} & \mathbf{V_{28}} \\ \mathbf{V_{31}} & \mathbf{V_{32}} & \mathbf{V_3} & \mathbf{V_{34}} & \mathbf{V_{35}} & \mathbf{V_{36}} & \mathbf{V_{37}} & \mathbf{V_{38}} \\ \mathbf{V_{41}} & \mathbf{V_{42}} & \mathbf{V_{43}} & \mathbf{V_4} & \mathbf{V_{45}} & \mathbf{V_{46}} & \mathbf{V_{47}} & \mathbf{V_{48}} \\ \mathbf{V_{51}} & \mathbf{V_{52}} & \mathbf{V_{53}} & \mathbf{V_{54}} & \mathbf{V_5} & \mathbf{V_{56}} & \mathbf{V_{57}} & \mathbf{V_{58}} \\ \mathbf{V_{61}} & \mathbf{V_{62}} & \mathbf{V_{63}} & \mathbf{V_{64}} & \mathbf{V_{65}} & \mathbf{V_6} & \mathbf{V_{67}} & \mathbf{V_{68}} \\ \mathbf{V_{71}} & \mathbf{V_{72}} & \mathbf{V_{73}} & \mathbf{V_{74}} & \mathbf{V_{75}} & \mathbf{V_{76}} & \mathbf{V_7} & \mathbf{V_{78}} \\ \mathbf{V_{81}} & \mathbf{V_{82}} & \mathbf{V_{83}} & \mathbf{V_{84}} & \mathbf{V_{85}} & \mathbf{V_{86}} & \mathbf{V_{87}} & \mathbf{V_8} \end{bmatrix} \quad \textbf{(6.2)}$$

Eq. 6.1 shows the permanent matrix formed using sub-system matrix and interaction matrix for flood hazard analysis. Six variables have been used for flood hazard. H*i* (*i* =1, 2, 3---6) represents the contribution of six sub-subsystems of flood hazard sub-system and are represented as diagonal members. H_{ij} (*i* =1, 2, 3---6; *j* =1, 2, 3, ---6) represents the interaction of i^{th} sub-subsystem with j^{th} sub-subsystem and are represented as off-diagonal elements. Similarly, Eq. 6.2 shows the permanent matrix formed using sub-system matrix and interaction matrix for flood vulnerability analysis. Eight variables have been used for flood vulnerability analysis. V_i (*i* =1, 2, 3, …. 8) represents the contribution of eight sub-subsystems of flood vulnerability sub-system and are represented as diagonal members. V*ij* (*i* =1, 2, 3, … 8 ; *j* =1, 2, 3, … 8) represents the interaction of i^{th} sub-subsystem with j^{th} sub-subsystem and are represented as off-diagonal elements.

$$\begin{aligned} \boldsymbol{per}\,(\boldsymbol{H}) = {} & \textstyle\prod_{z=1}^{M} \boldsymbol{H_z} + \sum_i \sum_j \sum_k \dots\dots\dots \sum_M (\boldsymbol{H_{ij}H_{ji}})\,\boldsymbol{H_k H_l} \dots\dots \boldsymbol{H_M} + \\ & \sum_i \sum_j \sum_k \dots\dots\dots \sum_M (\boldsymbol{H_{ij}H_{jk}H_{ki}} + \boldsymbol{H_{ik}H_{kj}H_{ji}})\boldsymbol{H_l H_m} \dots\dots \boldsymbol{H_M} + \\ & \left[\left(\sum_i \sum_j \sum_k \dots\dots\dots \sum_M (\boldsymbol{H_{ij}H_{ji}} + \boldsymbol{H_{kl}H_{lk}})\boldsymbol{H_m} \dots\dots\dots \boldsymbol{H_M}\right) + \right. \\ & \left. \left(\sum_i \sum_j \sum_k \dots\dots\dots \sum_M (\boldsymbol{H_{ij}H_{jk}H_{kl}H_{li}} + \boldsymbol{H_{il}H_{lk}H_{kj}H_{ji}})\boldsymbol{H_m} \dots\dots \boldsymbol{H_M}\right)\right] + \\ & \left[\left(\sum_i \sum_j \sum_k \dots\dots\dots \sum_M \left(\boldsymbol{H_{ij}H_{ji}}\right)\left(\boldsymbol{H_{kl}H_{lm}H_{mk}} + \boldsymbol{H_{km}H_{ml}H_{lk}}\right)\right) + \right. \\ & \left. \left(\sum_i \sum_j \sum_k \dots\dots\dots \sum_M \left(\boldsymbol{H_{ij}H_{ji}}\right)\left(\boldsymbol{H_{ij}H_{jk}H_{kl}H_{lm}H_{mi}} + \boldsymbol{H_{im}H_{ml}H_{lk}H_{kj}H_{ji}}\right) + \right. \right. \\ & \left. \left. \boldsymbol{H_n} \dots\dots\dots \boldsymbol{H_M}\right)\right] + \cdots \end{aligned} \quad \textbf{(6.3)}$$

The permanent matrix is developed and represented in Eq. 6.3 in a general form. There are M+1 numbers of terms in Eq. 6.3, and a quantitative value will be obtained after solving Eq. 6.3. Since there is no negative sign in any of the terms of Eq. 6.3, the numerical index obtained contains each term's information. The analysis of Permanent matrix value is calculated using an online tool, D-Code (https://www.dcode.fr/matrix-permanent).

6.1.1.1. Inconsistency removal of the matrix

The weights in Eq. 6.1, several experts usually formulate, and 6.2. Therefore, the weights assigned by different experts will differ. Removing such inconsistency is necessary to evaluate the flood risk system accurately. When multiple experts provide the weights, the decision-

maker has to combine the weights of all experts and convert them into a single coherent weightage. Behavioural aggregation and mathematical aggregation are the two major ways to combine the decisions of multiple experts (443). The experts are in a single place, and weights are decided at a consensus called behavioral aggregation. The Delphi technique can also be used when the experts are under the control of analysts. In mathematical aggregation, opinion pool and Bayesian aggregation are usually used (443). The present study used behavioural aggregation, where the weights were decided in a consensus of all three experts.

Further, Eq. 6.4 is used to remove the presence of any inconsistencies.

$$(\boldsymbol{P} - \boldsymbol{\lambda I})\boldsymbol{x^T} = \mathbf{0} \qquad \textbf{(6.4)}$$

Where,

I = Identity matrix

x^T = Transpose of the weight vector $(x_1, x_2, x_3 \dots \dots x_n)$

$(P - \lambda I) = 0$ Yields Eigen spectrum

$\lambda_{max}$is identified from the Eigen spectrum and is used to calculate weight vector such that$\sum P_i = 1$. Eq. 6.5 shows the revised hazard sub-system permanent matrix.

$$\textbf{Permanent matrix} = \begin{bmatrix} \mathbf{H_1.P_1} & \mathbf{H_{12}.P_2} & \mathbf{H_{13}.P_3} & \mathbf{H_{14}.P_4} & \mathbf{H_{15}.P_5} & \mathbf{H_{16}.P_6} \\ \mathbf{H_{21}.P_1} & \mathbf{H_2.P_2} & \mathbf{H_{23}.P_3} & \mathbf{H_{24}.P_4} & \mathbf{H_{25}.P_5} & \mathbf{H_{26}.P_6} \\ \mathbf{H_{31}.P_1} & \mathbf{H_{32}.P_2} & \mathbf{H_3.P_3} & \mathbf{H_{34}.P_4} & \mathbf{H_{35}.P_5} & \mathbf{H_{36}.P_6} \\ \mathbf{H_{41}.P_1} & \mathbf{H_{42}.P_2} & \mathbf{H_{43}.P_3} & \mathbf{H_4.P_4} & \mathbf{H_{45}.P_5} & \mathbf{H_{46}.P_6} \\ \mathbf{H_{51}.P_1} & \mathbf{H_{52}.P_2} & \mathbf{H_{53}.P_3} & \mathbf{H_{54}.P_4} & \mathbf{H_5.P_5} & \mathbf{H_{56}.P_6} \\ \mathbf{H_{61}.P_1} & \mathbf{H_{62}.P_2} & \mathbf{H_{63}.P_3} & \mathbf{H_{64}.P_4} & \mathbf{H_{65}.P_5} & \mathbf{H_6.P_6} \end{bmatrix} \qquad \textbf{(6.5)}$$

$P_1 \dots \dots P_6$ are the weight vector calculated from $\sum P_i = 1$. The system permanent matrix formed in Eq. 6.5 is free from any bias and the composite score evaluated using Eq. 6.3 will inform the level of flood hazard in the basin.

6.1.2. Analytical Hierarchy Process (AHP) for Flood risk mapping

AHP is a multi-criteria decision-making approach that decomposes the complex problem into a hierarchy structure. The decision-makers can evaluate each element independently and compare it with others to their impact on an element above them in a hierarchy. Saaty in 1977 proposed this robust and flexible methodology for decision-making where multi-factors are involved in a complex problem(444). This method prepares a pair-wise comparison between factors using an importance level of 1 to 9 (Lowest to highest importance) as shown in Table 6.3. For example, if the relative importance of factor A is stronger than factor B for system

analysis, then the importance level of factor A to B will reflect as 7, whereas the importance level of factor B to A will reflect as 1/7 in the pair-wise comparison matrix.

Table 6.3 Importance scale of AHP model (197).

Importance	**Definition**
1	Equal Importance
3	Moderate importance
5	Strong importance
7	Very strong or demonstrated
9	Extreme importance
2, 4, 6, 8	Intermediate Values

The AHP model was performed using the following steps:

- A list of factors (n) is selected which are responsible for flood hazard and flood vulnerability in the basin.
- Pair-wise comparison matrix (M) is developed using importance value based on the literature review and expert advice in which diagonal elements are equal to 1 (95,125,167,197). Weights in the range of 1-9 are assigned in each row of the upper triangular matrix based on the relative importance between two factors, and the inverse of the weights are assigned in each row of the lower triangular matrix. Eq. 6.6 shows the pair-wise comparison matrix of n factors.

$$\boldsymbol{M} = \begin{bmatrix} \boldsymbol{1} & \boldsymbol{a12} & . & . & . & \boldsymbol{a1n} \\ \boldsymbol{1/a12} & \boldsymbol{1} & . & . & . & \boldsymbol{a2n} \\ . & . & . & . & . & . \\ . & . & . & . & . & . \\ . & . & . & . & . & . \\ \boldsymbol{1/a1n} & \boldsymbol{1/a2n} & . & . & . & \boldsymbol{1} \end{bmatrix} \quad \textbf{(6.6)}$$

- Calculate the normalized matrix of the pair-wise comparison matrix shown in Eq. 6.6.
- Calculate the mean of each row in the normalized matrix, and the resulting values represent the weight of those factors (W_i).
- The AHP based flood model will be analyzed using the summation of weightage of each factor (W_i) multiplied by the class of the respective factor(R_i).

$$\boldsymbol{AHP} = \sum_{\boldsymbol{i=1}}^{\boldsymbol{n}} \boldsymbol{W_i} \times \boldsymbol{R_i} \quad \textbf{(6.7)}$$

- The consistency of the AHP model is checked through consistency ratio (CR). Eq. 8can be used to calculate CR (216).

$$\boldsymbol{CR} = \frac{\boldsymbol{CI}}{\boldsymbol{RI}} \quad \textbf{(6.8)}$$

Where CI is the consistency index, and RI is the random index. The random index for different n values is shown in Table 6.4. The CI can be calculated as

$$CI = \frac{\lambda_{max} - n}{n-1} \quad \textbf{(6.9)}$$

Where, λ_{max} is the principal Eigenvalue of the normalized matrix (Radwan et al. 2019), and n is the order of the matrix.

Table 6.4 RI values for the different order of the matrix (n) (197)

n	3	4	5	6	7	8	9	10	11	12	13	14
RI	0.58	0.9	1.12	1.24	1.32	1.41	1.45	1.49	1.51	1.54	1.56	1.57

6.2. Classification flood factors for flood analysis

Table 6.5 Classification of various factors and their respective weights considered for flood hazard sub-system

Sub-subsystems	**Classification**	**Weights(R_i)**	**Weighted area**	**Sub-subsystems**	**Classification**	**Weights(R_i)**	**Weighted area**
Elevation (m)	0-300	8	0.9065	**Slope (°)**	0-10	8	0.9541
	300-500	7	0.0458		10-20	7	0.0322
	500-700	6	0.0159		20-30	6	0.0103
	700-900	5	0.0105		30-40	5	0.0028
	900-1100	4	0.0109		40-50	4	0.0004
	1100-1300	3	0.0061		50-60	3	0.0001
	1300-1500	2	0.0034		60-70	2	0.0000
	>1500	1	0.0009		70-80	1	0.0000
Land use Land cover (LULC)	Evergreen Needle leaf Forest	3	0.0102	**Rx3day (mm)**	<100	4	0.0000
	Evergreen Broad leaf Forest				100-140	5	0.0667
	Mixed Forest				140-170	6	0.6355
	Woody Savannas	4	0.0678		170-200	7	0.2514
	Savannas				>200	8	0.0465
	Grasslands			**Distance from rivers (m)**	<200	8	0.2981
	Permanent Wetlands	7	0.0001		200-500	7	0.3205
	Croplands	8	0.9219		500-800	6	0.1028
	Urban Built-up				800-1100	5	0.1777
	Cropland/ Natural Vegetation				1100-1400	4	0.0296
Soil Group	C	6	0.5911		1400-1700	3	0.0397
	D C/D D/D	8	0.4089		1700-2000	2	0.0195
					>2000	1	0.0121

It is observed that both graph theory and AHP calculate the system's performance through the hierarchy process. The weights are usually assigned to all the factors affecting the system and calculate an overall performance in the form of a numeric value in both methods. But the graph theory also considers the interaction between the sub-systems during the evaluation process

and therefore acts as an integrated system of performance management. Tables 6.5 and 6.6 show the classification, weightage, and area under the respective classification of various sub-subsystems of flood hazard and vulnerability sub-system, respectively. These classifications and their respective weights are used in the present study to prepare flood risk zone using both graph theory and AHP.

The importance level for both flood hazard and flood vulnerability is taken between 1 and 8 for graph theory and AHP methods. Since the weights are converted into percentage form, the numeric value for flood hazard and flood vulnerability in AHP will lie between 100 and 800, and the numeric value for flood risk will lie in the range between 10000-640000 as per Eq. 6.10.

Table 6.6 Classification of various factors and their respective weights considered for flood vulnerability sub-system

Sub-subsystems	Classification	Weights (R_i)	Weighted area	Sub-subsystems	Classification	Weights (R_i)	Weighted area
Population density (person/sq.km)	<100	1	0.0956	**Land use Land cover (LULC)**	Evergreen Needle leaf Forest	3	0.0102
	100-150	2	0.0867		Evergreen Broad leaf Forest		
	150-250	3	0.3224		Mixed Forest		
	250-500	4	0.3610		Woody Savannas	4	0.0678
	500-1000	5	0.0721		Savannas		
	1000-3000	6	0.0381		Grasslands		
	3000-5000	7	0.0114		Permanent Wetlands	7	0.0001
	>5000	8	0.0128		Croplands	8	0.9219
Household Density (number/sq.km)	0-20	1	0.1745		Urban Built-up		
	20-40	2	0.6802		Cropland/ Natural Vegetation		
	40-60	3	0.1103	**Distance from roads (m)**	<200	8	0.0303
	60-80	4	0.0264		200-500	7	0.0390
	80-100	5	0.0000		500-800	6	0.0468
	100-120	6	0.0000		800-1100	5	0.0189
	120-150	7	0.0000		1100-1400	4	0.0448
	>150	8	0.0085		1400-1700	3	0.0171
Literacy rate (%)	>70	4	0.0662		1700-2000	2	0.0255
	60-70	6	0.4791		>2000	1	0.7775
	50-60	7	0.2963	**Distance From Flood shelters**	No flood shelter in the basin. Therefore the weightage is the same for the whole basin	8	1.0000
	<50	8	0.1584	**Rainfall trend**	Positive trend	8	0.0496
Efficient Drainage System	No efficient drainage system in the basin. Therefore the weightage is the same for the whole basin	8	1.0000		Negative trend	4	0.9504

6.3. Flood zone classification

The permanent value of a system permanent matrix will provide the performance of a system in terms of numeric value. The minimum numeric value will be when the diagonal element of

the system permanent matrix is 1, whereas the maximum numeric value will be when the diagonal element of the system permanent matrix is 8. The off-diagonal element of flood hazard and flood vulnerability sub-system permanent matrix is shown in Table 6.8 – 6.9. The minimum numeric value of flood hazard sub-system permanent matrix is 1.52, whereas the maximum value is 31.57. Similarly, the minimum numeric value of flood vulnerability sub-system permanent matrix is 0.,036, whereas the maximum value is 4.57. The minimum numeric value of the flood risk system permanent matrix is 0.06, whereas the maximum value is 144.26. The present study made five classifications: very low, low, moderate, high, and very high flood risk/flood hazard/flood vulnerability zone. These classifications have been done in a similar proportion for both graph theory and AHP methods. Table 6.7 shows the flood zone classification in the form of numeric value for both AHP and Graph theory methods used in the present study.

Table 6.7 Flood zone classifications concerning its value

	AHP			**Graph Theory**		
Zone	**Hazard**	**Vulnerability**	**Risk**	**Hazard**	**Vulnerability**	**Risk**
Very Low	<200	<200	<40000	<2.41	<0.12	<0.28
Low	200-400	200-400	40000-160000	2.41-5.85	0.12-0.33	0.28-1.93
Moderate	400-500	400-500	160000-250000	5.86-9.01	0.34-0.66	1.93-5.94
High	500-700	500-700	250000-490000	9.01-20.93	0.66-2.44	5.94-51.19
Very High	>700	>700	>490000	>20.93	>2.44	>51.19

6.4. Results and Discussion

Flood risk analysis is the composite of flood hazard and flood vulnerability analysis which can be expressed as,

$$\textbf{Flood Risk} = \textbf{Flood Hazard} \times \textbf{Flood Vulnerability} \quad (6.10)$$

The present study applied graph theory and AHP to identify the flood risk zone of the Ghaggar river basin, and the following points were discussed.

- Identification of flood risk zone of Ghaggar river basin using graph theory
- Identification of flood risk zone of Ghaggar river basin using AHP
- Comparison of the results obtained by these two methods.

6.4.1. Identification of flood risk zone of Ghaggar river basin using graph theory

The combined effects of all sub-systems on the sub-systems and subsequent flood risk systems were assessed using graph theory. The flood risk analysis was analyzed by calculating the

permanent matrix of the flood hazard and vulnerability sub-system. Table 6.8 shows the level of interaction between the sub-subsystems of the flood hazard sub-system, whereas Table 6.9 shows the level of interaction between the sub-subsystems of the flood vulnerability sub-system. Sr.no of sub-subsystems are mentioned in each column of the level of interaction with which it is interacting. For example, the slope has strong interaction with elevation (sr. no 2), land use land cover (sr. no 4), and rainfall (sr. no 6), whereas it has moderate interaction with the soil group (sr. no 3) and weak interaction with distance from the river (sr. no 5) for causing the flood hazard. These levels of interactions between the various components of flood hazard or flood vulnerability sub-system were identified through expert advice. Table 6.8 and Table 6.9 were prepared with the consent of three hydrology experts (445,446).

Table 6.8 Level of interaction between the sub-subsystems of flood hazard sub-system

Sr. No	Sub-subsystems	Level of the interaction of one sub-subsystem with other sub-subsystems for causing flood hazard			
		Strong (3)	Moderate (2)	Weak (1)	No (0)
1	Slope	2, 4, 6	3	5	
2	Elevation	1, 4, 6	3, 5		
3	Soil group	2, 4	1, 6		5
4	Land use land cover	1, 2, 6	3, 5		
5	Distance from river	4	1, 2, 6	3	
6	Rainfall	1, 2, 4	3, 5		

Table 6.9 Level of interaction between the sub-subsystems of flood vulnerability sub-system

Sr. No	Sub-subsystem	Level of the interaction of one sub-subsystem with other sub-subsystem for causing flood vulnerability sub-system			
		Strong (3)	Moderate (2)	Weak (1)	Nil (0)
1	Population	2, 3, 5	4,6, 7, 8		
2	Household Density	1	4,6, 7, 8	3, 5	
3	Land use land cover	1,2,7	5, 6	4, 8	
4	Distance from flood shelters		1,2,7	3, 5, 6	8
5	Efficient Drainage Network		1, 2, 3	4, 6, 7	8
6	Distance from roads		3, 4	1, 2, 5	7,8
7	Rainfall trends	4	1,2,3, 5	6	8
8	Literacy rate		1,2	3, 4, 5	6,7

The weights assigned to the diagonal element of a permanent matrix represent the actual performance of that system. The present study assigned the weights to the diagonal elements in Eq. 6.1 as per the performance of sub-subsystems in the Ghaggar River basin. Since twelve (12) rain gauge stations exist in this basin, the whole basin has been divided into twelve different areas using the Thiessen polygon method. The weights of various flood hazard and flood vulnerability sub-subsystems for all these areas have been assigned according to Tables

6.5 and 6.6. These values represent the actual performance of the respective parameters in that area of the basin. It is assumed that there is no spatial variation in the characteristics of conditioning factors within their respective area. Therefore, the weights assigned in that area will remain constant. These weights become the diagonal member of the sub-system matrix. Eq. 6.11 – 6.16 shows the complete sub-system matrix of the effective area covered for the Rohiti rain gauge station. Similarly, sub-system matrices for all other areas for different rain gauge stations were prepared by changing the diagonal element's weightage according to that parameter's performance in the respective area.

$$\boldsymbol{Permanent\ matrix\ of\ flood\ hazard} = \begin{matrix} \mathbf{7.99} & \mathbf{3} & \mathbf{2} & \mathbf{3} & \mathbf{1} & \mathbf{3} \\ \mathbf{3} & \mathbf{8} & \mathbf{2} & \mathbf{3} & \mathbf{2} & \mathbf{3} \\ \mathbf{1} & \mathbf{3} & \mathbf{7} & \mathbf{3} & \mathbf{0} & \mathbf{2} \\ \mathbf{3} & \mathbf{3} & \mathbf{2} & \mathbf{7.97} & \mathbf{2} & \mathbf{3} \\ \mathbf{2} & \mathbf{2} & \mathbf{1} & \mathbf{3} & \mathbf{5.77} & \mathbf{2} \\ \mathbf{3} & \mathbf{3} & \mathbf{2} & \mathbf{3} & \mathbf{2} & \mathbf{6.73} \end{matrix} \quad (6.11)$$

$$\boldsymbol{Permanent\ matrix\ of\ flood\ vulnerability} = \begin{matrix} \mathbf{3.48} & \mathbf{3} & \mathbf{3} & \mathbf{2} & \mathbf{3} & \mathbf{2} & \mathbf{2} & \mathbf{2} \\ \mathbf{3} & \mathbf{2.23} & \mathbf{1} & \mathbf{2} & \mathbf{1} & \mathbf{2} & \mathbf{2} & \mathbf{2} \\ \mathbf{3} & \mathbf{3} & \mathbf{7.97} & \mathbf{1} & \mathbf{2} & \mathbf{2} & \mathbf{3} & \mathbf{1} \\ \mathbf{2} & \mathbf{2} & \mathbf{1} & \mathbf{8} & \mathbf{1} & \mathbf{1} & \mathbf{2} & \mathbf{0} \\ \mathbf{2} & \mathbf{2} & \mathbf{2} & \mathbf{1} & \mathbf{8} & \mathbf{1} & \mathbf{1} & \mathbf{0} \\ \mathbf{1} & \mathbf{1} & \mathbf{2} & \mathbf{2} & \mathbf{1} & \mathbf{1.54} & \mathbf{0} & \mathbf{0} \\ \mathbf{2} & \mathbf{2} & \mathbf{2} & \mathbf{3} & \mathbf{2} & \mathbf{1} & \mathbf{4.33} & \mathbf{1} \\ \mathbf{2} & \mathbf{2} & \mathbf{1} & \mathbf{1} & \mathbf{1} & \mathbf{1} & \mathbf{0} & \mathbf{6.15} \end{matrix} \quad (6.12)$$

The inconsistency of the matrix was removed by finding the weight vector using Eq. 6.4. Eq.6.13 – 6.14 shows the weight vector used for the removal of inconsistency and the updated subsystem matrix for flood hazard and flood vulnerability are shown in Eq. 6.15 – 6.16.

$$\boldsymbol{Hazard\ weight\ factor} = (\mathbf{1}: \mathbf{0.1726}; \mathbf{2}: \mathbf{0.1810}; \mathbf{3}: \mathbf{0.1748}; \mathbf{4}: \mathbf{0.1806}; \mathbf{5}: \mathbf{0.1242}; \mathbf{6}: \mathbf{0.1674}) \quad (6.13)$$

$$\boldsymbol{Vulnerability\ weight\ factor} = (\mathbf{1}: \mathbf{0.1535}; \mathbf{2}: \mathbf{0.0.1071}; \mathbf{3}: \mathbf{0.0.1917}; \mathbf{4}: \mathbf{0.0.1260}; \mathbf{5}: \mathbf{0.0.1319}; \mathbf{6}: \mathbf{0.0.0652}; \mathbf{7}: \mathbf{0.0.1314}; \mathbf{8}: \mathbf{0.0929}) \quad (6.14)$$

The updated flood hazard and flood vulnerability subsystem permanent matrix are represented in Eq. 6.15 – 6.16.

$$Updated\ permanent\ matrix\ of\ hazard =$$

$$\begin{matrix} 1.3788 & 0.5430 & 0.3495 & 0.5419 & 0.1241 & 0.5004 \\ 0.5177 & 1.4481 & 0.3495 & 0.5419 & 0.2484 & 0.5004 \\ 0.1726 & 0.5430 & 1.2234 & 0.8450 & 0 & 1.0009 \\ 0.5177 & 0.5430 & 0.3495 & 1.4397 & 0.2484 & 0.5004 \\ 0.3451 & 0.3620 & 0.1748 & 0.5419 & 0.7166 & 0.3336 \\ 0.5177 & 0.5430 & 0.3495 & 0.5419 & 0.2484 & 1.1227 \end{matrix} \quad (6.15)$$

$$Updated\ permanent\ matrix\ of\ vulnerability =$$

$$\begin{matrix} 0.5345 & 0.3215 & 0.5751 & 0.2521 & 0.3958 & 0.2638 & 0.2628 & 0.1858 \\ 0.4608 & 0.2390 & 0.1917 & 0.2521 & 0.1319 & 0.2638 & 0.2628 & 0.1858 \\ 0.4608 & 0.3215 & 1.5280 & 0.1261 & 0.2638 & 0.2638 & 0.3942 & 0.0929 \\ 0.3072 & 0.2143 & 0.1917 & 1.0086 & 0.1319 & 0.1319 & 0.2628 & 0 \\ 0.3072 & 0.2143 & 0.3834 & 0.1261 & 1.0553 & 0.1319 & 0.1314 & 0 \\ 0.1536 & 0.1072 & 0.3834 & 0.2521 & 0.1319 & 0.2032 & 0 & 0 \\ 0.3072 & 0.2143 & 0.3834 & 0.3782 & 0.2638 & 0.1319 & 0.5690 & 0.0929 \\ 0.3072 & 0.2143 & 0.1917 & 0.1261 & 0.1319 & 0.1319 & 0 & 0.5714 \end{matrix} \quad (6.16)$$

The permanent matrix for flood hazard and flood vulnerability as shown in Eq. 6.15 – 6.16 are for the Rohiti rain-gauze station. Similarly, the permanent matrix for other meteorological station were prepared. Solving the permanent equation analyses the flood hazard and flood vulnerability score. The quantitative value using the permanent matrix of flood hazard and flood vulnerability sub-system for the effective area covered under each rain gauge station was calculated as shown in the map (Figure 6.4 a and 6.4b). Subsequently, the performances of the flood risk system in the form of a numeric value for the effective area covered under each rain gauge station were calculated. It has been observed from Figures 6.4a and 6.4b that the flood hazard characterization of the Ghaggar River basin is found to vary from high to very high hazard, whereas flood vulnerability characterization is found to vary from moderate to highly vulnerable. Figure 6.4c shows the spatial variation of performance of the flood risk system of the Ghaggar basin in the form of a numeric value. It is observed that the area covered under Rohiti, Ambala, Banur, and Rajpura shows a higher numeric value, which indicates the high flood risk zone in comparison to the area covered by other rain gauge stations. It is observed that around 29.8% of the basin area is prone to very high flood hazards, whereas 70.1% of the basin area is prone to high flood hazards. Similarly, around 17.4% of the basin area is prone to highly vulnerable to flood, whereas 82.5% of the basin area is prone to moderately vulnerable to flood.

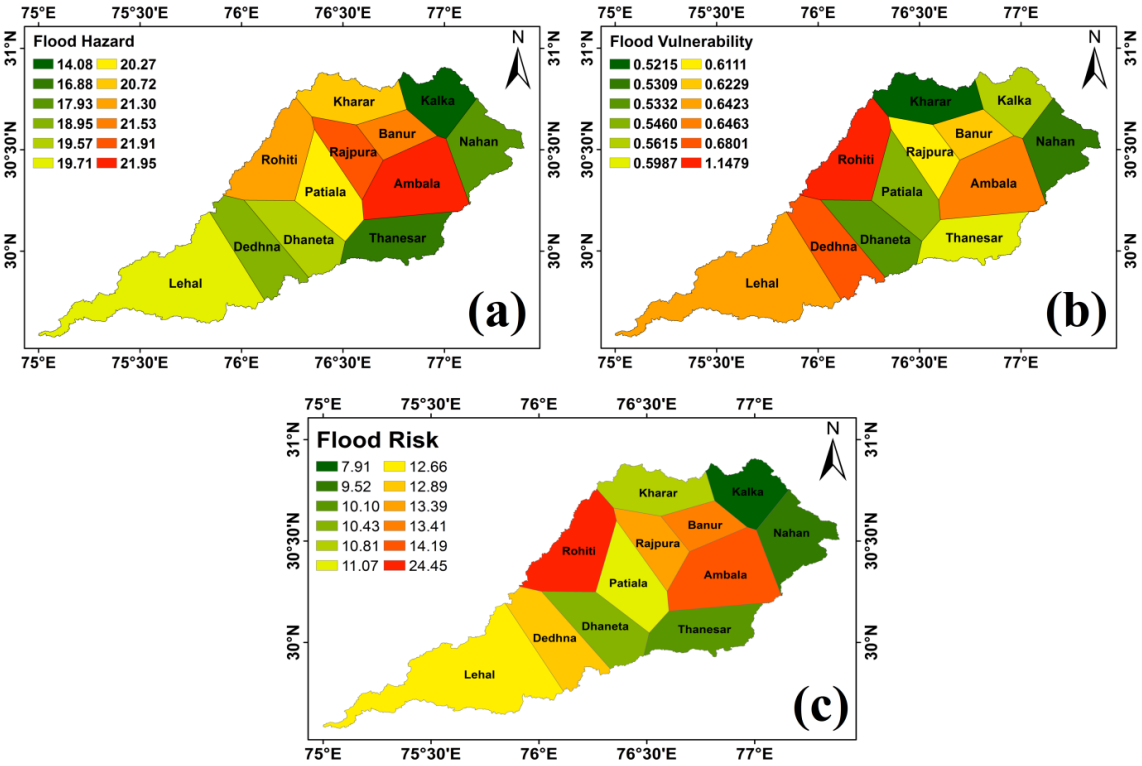

Figure 6.4 Flood Hazard, flood vulnerability and flood risk zoning of Ghaggar River basin using Graph Theory

6.4.2. Identification of flood risk zone of Ghaggar river basin using AHP

The combined effect of all factors affecting flood hazard and flood vulnerability of the Ghaggar River basin was determined using AHP. Subsequently, the basin was divided into various zones based on its flood risk. Initially, the pair-wise comparison matrix was prepared based on the importance level of one factor over others (95,125,197). Tables 6.10 and 6.11 show the pair-wise comparison matrix for flood hazard and flood vulnerability, respectively. Each row of these tables describes the relative importance of parameters positioned in a row with all six parameters placed in the column. For example, the first row of Table 6.10 represents the importance level of elevation with elevation, slope, LULC, soil group, rainfall, and distance from rivers. The diagonal elements of Table 6.10 – 6.11 are equal to 1 as the factor in row and column is the same. Table 6.3 was used to assign the relative importance of each factor over other factors. The pair-wise hazard and vulnerability comparison matrix was transformed into a normalized matrix. The normalized matrix of flood hazard variables was calculated by dividing each column value of Table 6.10 by the summation of all values positioned in that column, shown in Table 6.12.

Similarly, Table 6.13 shows the normalized matrix of flood vulnerability factors normalized similarly using Table 6.11. The last column of Tables 6.12 and 6.13 shows the weights of each parameter in percentage. The weights of each flood hazard and flood vulnerability factor were calculated by the average of each row corresponding to that factor and converted into percentage form. Flood hazard and flood vulnerability were calculated using Eq. 6.17 and 6.18, in which the weights calculated in Tables 6.12 and 6.13 were used.

$$Flood\ Hazard = (Elevation\ \times 3.38) + (Slope\ \times 28.28) + (LULC \times 26.49) + (Soil\ Group\ \times 8.54) + (rx3day\ \times 29.11) + (Distance\ from\ rivers\ \times 4.20) \quad (6.17)$$

$$\boldsymbol{Flood\ Vulnerability} = (\boldsymbol{Population\ Density}\ \times \mathbf{7.48}) + (\boldsymbol{Household\ Density}\ \times \mathbf{5.68}) + (\boldsymbol{LULC}\ \times \mathbf{24.37}) + (\boldsymbol{Distance\ from\ roads}\ \times \mathbf{4.26}) + (\boldsymbol{Distance\ from\ flood\ shelters}\ \times \mathbf{8.59}) + (\boldsymbol{Literacy\ rate}\ \times \mathbf{2.91}) + (\boldsymbol{Rainfall\ trend}\ \times \mathbf{22.93}) + (\boldsymbol{Efficient\ Drainage\ System}\ \times \mathbf{24.19}) \quad (6.18)$$

The principal Eigenvalue (λ_{max}) of pair-wise matrixes for flood hazard and vulnerability were 6.298 and 8.893, respectively. The consistency index (CI) was calculated using Eq. 6.9 and found 0.059 and 0.127 for flood hazard and vulnerability, respectively. The Random Index (RI) values from Table 6.4 are 1.24 and 1.41 for flood hazard and flood vulnerability, respectively. The consistency ratio (CR) was calculated using Eq. 6.8 and found as 0.048 and 0.091 for flood hazard and flood vulnerability, respectively. If the CR value of the comparison matrix is greater than 0.10, then the comparison matrix is inconsistent and should be revised (174). In the present study, since the CR is less than 0.1, so the comparison matrixes for flood hazard and flood vulnerability are consistent.

Table 6.10 Comparison Matrix of each parameter of Flood hazard

	Elevation	**Slope**	**LULC**	**Soil Group**	**Rainfall**	**Distance from Rivers**
Elevation	1	0.14	0.14	0.2	0.11	1
Slope	7	1	1	7	1	5
LULC	7	1	1	5	1	5
Soil Group	5	0.14	0.20	1	0.20	3
Rx3day	9	1	1	5	1	7
Distance from Rivers	1	0.20	0.20	0.33	0.14	1

Table 6.11 Comparison Matrix of each parameter of flood vulnerability

	Population Density	Household density	LULC	Distance from roads	Distance flood shelter	Literacy rate	Rainfall trend	Drainage network
Population Density	1	1	1	1	1	3	0.2	0.14
Household density	1	1	0.2	3	0.33	3	0.2	0.14
LULC	1	5	1	5	7	7	1	1
Distance from roads	1	0.33	0.2	1	0.2	3	0.2	0.2
Distance flood shelter	1	3	0.14	5	1	3	0.2	0.2
Literacy rate	0.33	0.33	0.14	0.33	0.33	1	0.14	0.14
Rainfall trend	5	5	1	5	5	7	1	1
Drainage network	7	7	1	5	5	7	1	1

Table 6.12 Normalized pair-wise comparison matrix of flood hazard

	Elevation	Slope	LULC	Soil Group	Rainfall	Distance from Rivers	Weighatge (%)
Elevation	0.0333	0.0410	0.0403	0.0108	0.0322	0.0455	3.38
Slope	0.2333	0.2869	0.2823	0.3778	0.2895	0.2273	28.28
LULC	0.2333	0.2869	0.2823	0.2698	0.2895	0.2273	26.49
Soil Group	0.1667	0.0410	0.0565	0.0540	0.0579	0.1364	8.54
Rx3day	0.3000	0.2869	0.2823	0.2698	0.2895	0.3182	29.11
Distance from Rivers	0.0333	0.0574	0.0565	0.0178	0.0414	0.0455	4.20

Table 6.13 Normalized pair-wise comparison matrix of flood vulnerability

	Population Density	Household density	LULC	Distance from roads	Distance flood	Literacy rate	Rainfall trend	Drainage network	Weightage (%)
Population Density	0.0577	0.0441	0.2137	0.0395	0.0504	0.0882	0.0508	0.0366	7.48
Household density	0.0577	0.0441	0.0427	0.1184	0.0166	0.0882	0.0508	0.0366	5.68
LULC	0.0577	0.2207	0.2137	0.1974	0.3525	0.2059	0.2538	0.2618	24.37
Distance from roads	0.0577	0.0146	0.0427	0.0395	0.0101	0.0882	0.0508	0.0524	4.26
Distance flood shelter	0.0577	0.1324	0.0299	0.1974	0.0504	0.0882	0.0508	0.0524	8.59
Literacy rate	0.0190	0.0146	0.0299	0.0130	0.0166	0.0294	0.0355	0.0366	2.51
Rainfall trend	0.2885	0.2207	0.2137	0.1974	0.2518	0.2059	0.2538	0.2618	22.93
Drainage network	0.4039	0.3089	0.2137	0.1974	0.2518	0.2059	0.2538	0.2618	24.19

6.4.2.1. Spatial variation of flood hazard analysis

The flood hazard map of the Ghaggar River basin was prepared in ArcMap 10.5 (Raster Analysis) using Eq. 6.17, and the classified flood zone is shown in Table 6.7. The spatial map of flood hazard is shown in Figure 6.5a, and found that the flood hazard level of the basin varies from high to very high category. It is observed from Figure 6.5a that around 14.54% (2033.5 km^2) and 85.2% (11922.7 km^2) of the basin area are lying under the high and very high categories of flood hazard, respectively. Around 0.15 % of the basin area (21.3 km^2) is observed

under the moderate flood hazard category. A moderate level of flood hazard is observed in the upper portion of the basin, where the elevation is greater than 500m.

6.4.2.2. Spatial variation in flood vulnerability analysis

The flood vulnerability map of the Ghaggar River basin was prepared in ArcMap (Raster Analysis) using Eq. 6.18, and the classified flood zone is shown in Table 6.7. The spatial map of flood vulnerability is shown in Figure 6.5b. It has been observed from Figure 6.5b that around 93.25% (13035.2 km^2) and 2.3% (322 km^2) of the basin area are lying under the high and very high categories of flood vulnerability, respectively. Around 4.44 % of the basin area (620.7 km^2) is observed under the moderate flood vulnerable category.

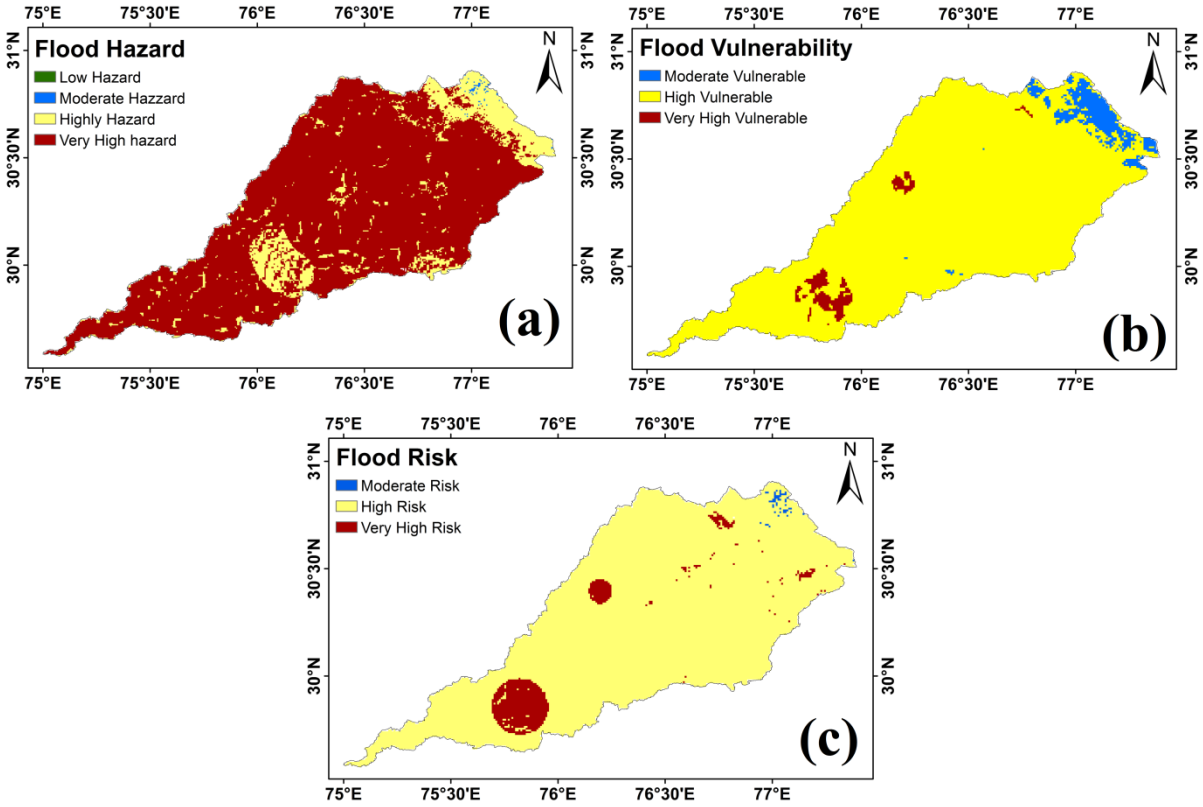

Figure 6.5 Flood hazard, flood vulnerability, and flood risk zoning of Ghaggar river basin using AHP

6.4.2.3. Spatial variation of flood risk analysis

The spatial variation of the flood risk map was processed in ArcGIS 10.5 using raster analysis. Figure 6.5c shows the flood risk mapping of the Ghaggar River basin, and it is observed from Figure 6.5c that the flood risk of the Ghaggar River basin varies from moderate to very high category. But, most of the basin, i.e., 94.1% (13165.2 km^2), is at high risk of flood, whereas only 5.52% (771.6 km^2) is at very high risk of flood. The basin areas under moderate risk of flooding are observed to be 0.2% (41.09 km^2). The upper part of the basin, which is at a higher

elevation, rapidly declined slope, forest cover, and lowest population density, has been observed as a moderate flood risk area. Although the magnitude of the rx3day is very high at the upper part of the basin, other hazard or vulnerability factors are such that the overall flood risk is moderate. The major part of the basin is at high risk of flood due to lying in a plane area, urbanization, high population density, lack of efficient drainage network, and absence of flood shelters.

6.4.3. Comparison of the results obtained by these two methods

Flood hazard, vulnerability, and risk zone obtained through graph theory were compared with results obtained through AHP and shown in Table 6.14.

Table 6.14 Comparison table of AHP and graph theory results

Stations	Hazard		Vulnerability		Risk	
	AHP	Graph Theory	AHP	Graph Theory	AHP	Graph Theory
Ambala	Very High	Very High	High	Moderate	High	High
Banur	Very High	Very High	High	Moderate	High	High
Dedhna	Very High	High	High	High	High	High
Dhaneta	Very High	High	High	Moderate	High	High
Kalka	High	High	High	Moderate	High	High
Kharar	Very High	High	High	Moderate	High	High
Lehal	Very High	High	High	Moderate	High	High
Nahan	Very High	High	High	Moderate	High	High
Patiala	Very High	High	High	Moderate	High	High
Rajpura	Very High	Very High	High	Moderate	High	High
Rohiti	Very High	Very High	High	High	High	High
Thanesar	Very High	High	High	Moderate	High	High

It is observed from Table 6.14 that a high flood risk zone was obtained through both graph theory and AHP, whereas there is a small difference in results obtained in flood hazard and vulnerability characterization. Both methods obtained Similar flood hazard characterization for Ambala, Banur, Rajpura, Rohiti, and Kalka rain gauge stations. Other basin areas were observed as very high flood hazard zones in AHP, whereas high hazard zones were obtained through graph theory. Similarly, most of the basin area was observed as highly vulnerable to flood through AHP, whereas moderate vulnerability to the flood was observed for those areas through graph theory. Since graph theory considers the interaction between sub-systems/sub-subsystems, the results obtained integrate all the interactions/effects between all system

components. They are believed to be more accurate in managing a complex problem. It is concluded from Table 6.14 that the characterization of flood hazard and flood vulnerability using graph theory predicts than AHP.

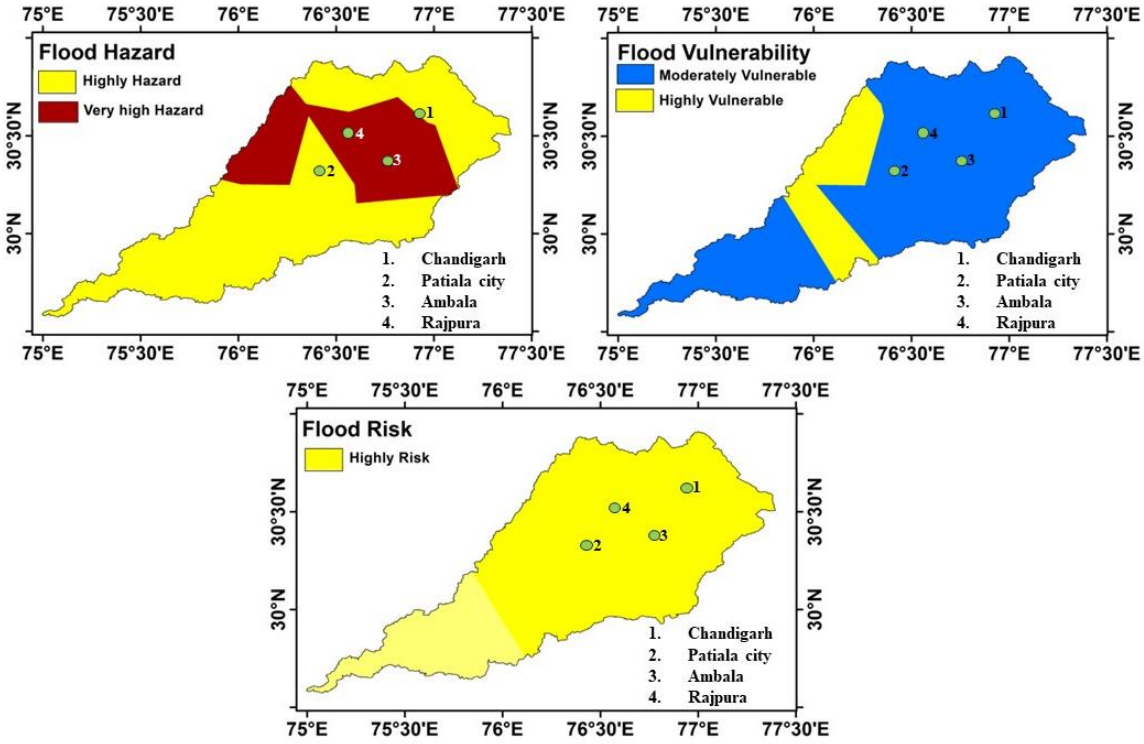

Figure 6.6 Flood hazard, vulnerability and risk classification of Ghaggar river basin using graph theory.

The graph theory is a multi-criteria decision-making approach and provides possible alternate solutions for decision-makers. Table 6.14 and Figure 6.6 show the flood hazard, vulnerability, and risk of the Ghaggar River basin. It is observed that the basin is at high flood risk, which AHP also confirms. The graph theory analysis will help decision-makers to provide possible solutions for effective flood management of the basin. The minimum numeric value of the flood risk system permanent matrix is 0.06, whereas the maximum value is 144.26. According to the classification of flood risk mentioned in Table 6.7, if the numeric value of the flood risk system permanent matrix lies between 0.06-5.94, the basin will be under very low to moderate flood risk. The numeric value of permanent depends on the diagonal value of the system matrix. When the inheritance of system/sub-systems efficiently reduces the flood risk of a basin, the matrix will contain diagonal elements equal to 1, and the numeric value of the permanent matrix will be minimal. The sub-subsystems, which directly affect the flood risk of a basin, require improvement. Once the performance of the sub-subsystems improves, the weights of the diagonal element of the permanent matrix will lie in the range of 1-4, i.e., exceptionally low –

normal flood risk. It is observed from Eq. 6.11 that the weights of all the diagonal elements of the flood hazard permanent matrix equation are on the higher side.

Similarly, it is observed from Eq. 6.12 that the weights of LULC, distance from flood shelters, efficient drainage network, and literacy rate sub-subsystems represented in the diagonal elements of the flood vulnerability permanent matrix equation are on the higher side. These weights will be reduced when their effect on the flood vulnerability is minimal, and decision-makers should provide the solutions to subdue the impact of LULC, distance from flood shelters, efficient drainage network, and literacy rate sub-subsystems by providing efficient drainage in the basin, constructing flood shelters and restricting the construction in the flood plain. Subsequently, sub-subsystems' performance will improve, and the qualitative characteristics of respective diagonal elements will change from extreme risk to normal or low risk. The numeric value of the system's permanent matrix will also shift from extreme flood vulnerability to moderate or low vulnerability. Similarly, decision-makers should provide solutions to reduce the worst impact of conditioning factors on the flood hazard of the Ghaggar River basin. When the flood hazard and flood vulnerability impact is reduced, the river basin will be at low flood risk.

6.5. Concluding Remarks

The flood hazard, vulnerability, and risk are characterised into five zones: very low, low, moderate, high, and very high. It is observed from the AHP method that around 85.2%, 14.54%, and 0.15% area of the basin are under very high, high, and moderate flood hazard zone respectively, whereas graph theory suggests that around 29.8 and 70.2% area of the basin shows very high and high flood hard zone respectively. The area under flood vulnerability using AHP shows that 2.3%, 93.25%, and 4.44% are very high, high, and moderately vulnerable to flood zone respectively, whereas graph theory suggests that around 17.47 and 82.53% of areas are high and moderately vulnerable to flood respectively. The flood risk analysis using the AHP method shows most part of the basin i.e., 94.1% (13165.2 km2), is at high risk to flood, whereas only 5.52% (771.6 km2) under very high risk. The basin areas under moderate risk to flood are observed to be 0.2% (41.09 km2). Graph theory suggests that all the considered study areas of the basin are under high flood risk zone. It is concluded that both AHP and graph theory methods are suggesting similar results for the Ghaggar river basin, and it is concluded that the Ghaggar river basin is prone to a high risk of flood.

CHAPTER 7

7. Urbanisation and Climatic Factor Impact on Flood

This chapter discusses the methodology of LULC change analysis for urbanization analysis. This chapter also discusses the population dynamics changes. The flood zone is analysed using two dynamic factors LULC change and population density changes with time. The flood maps have also been projected for 2030 and 2040.

7.1. Methodology

The study aims to determine the impact of LULC changes, rainfall trends, extreme rainfall events, and population density on flood risk analysis. However, extreme rainfall events and rainfall trends of the basin are executed from the rainfall and extreme rainfall analysis. The change rate of population density is directly used to execute the projected population density map in ArcGIS. Therefore, analysis of LULC changes and flood risk analysis methodology is necessary to complete this study. LULC change is analyzed utilizing a land change modeler in TerrSet. Flood risk analysis is analyzed using the Analytical hierarchy process. This methodology section also discusses the rank or importance level of the indicators for flood risk analysis.

7.1.1. Land Change Model

The dynamic variable of LULC change was analyzed using a Land change modeler (LCM). LCM is one of the TerrSet applications. Terrset, formerly IDRISI, was developed by Clark's Labs. LCM can also project future LULC under various drivers or variables. The first step of the LCM was to prepare the model's sub-transition, which is analyzed using a multi-layer perception (MLP) neural network. The MLP Neural Network is an inbuilt calculation method used to analyze the transition from one land use category to another or vice versa. The variables or drivers may be static or dynamic, such as DEM, distance from roads, distance from an urban area, distance from a river, population density, etc. The transition model gives a result of accuracy for the projection and creates a potential map, which is further used for prediction. The change prediction is used for the future forecast of LULC using the Markov chain model, an inbuilt application setup. Markov chain model predicts the change using transition potential from year to year. Two output models, namely hard prediction and soft prediction, is the finding

from change prediction. Hard prediction is the projected LULC, and soft prediction is the changes during the projection. The hard prediction is validated using the actual map.

The validation of the model is examined using the Kappa Index, which indicates the accuracy between actual and predicted maps (379). The statistical Equation of the Kappa index (K_p) is shown in Equation 1.

$$K_p = \frac{O_a - P_a}{1 - P_a} \quad (7.1)$$

O_a is the relative observed agreement between actual and predicted maps; P_a is the probability of agreement. The value of K_p lies between 0 and 1, indicating that 0 has no validation and 1 has complete validation. The Kappa index value for our analysis was higher than 0.8, which is acceptable as validation (447).

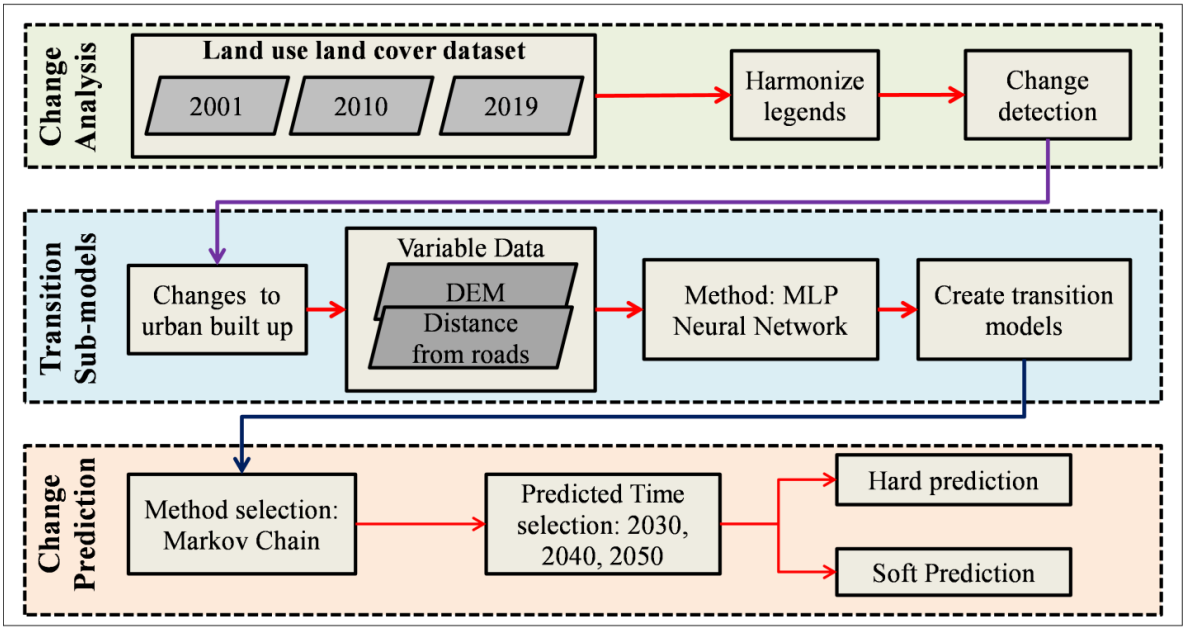

Figure 7.1 Methodology for land change modeler.

Figure 7.1 shows the flow chart of LCM used for this study. Two LULC observed data from 2001 and 2010 were used for the change analysis. The legends of the LULC category are harmonized for both maps to get better accuracy and identification of the results. The change analysis from one land use category to another is analyzed in sq. km. After change analysis, the transition potential of the changes is explored using an MLP neural network and two drivers (DEM and distance from roads). The transition potential map is created based on the changes as gain or loss from each category to urban built-up. The prediction of the 2019 LULC was projected using the transition potential map and Markov chain model. The projected 2019

LULC is compared with the actual LULC for validation of LCM. After confirmation of the LCM, projections of 2030 and 2040 spatial maps are executed.

7.1.2. Ranks of the indicators

The rank of indicator calculation is essential to analyze flood risk analysis using Equation 1. All indicators used for flood risk analysis have been classified into different categories, providing a rank value relating to flood risk. The rank value lies in 1 to 8, which indicates exceptionally low to exceptionally high (Table 7.1). Table 7.2 shows the indicators' classification and assigned rank with the respective area. Figure 7.2 shows the spatial map rank-wise indicators used for the study. The rank of indicators are either taken from literature or by the expert advice (39,95,96).

Table 7.1 Ranks relating to flood risk of different indicators.

Rank	Definition
1	Exceptionally low
2	Extremely low
3	Very low
4	Normal
5	High
6	Very High
7	Extremely High
8	Exceptionally high

Table 7.2 Classification of indicators and their respective ranks considered for flood risk analysis

Indicators	Classification	Ranks	Weighted area
Elevation (m)	0-300	8	0.9065
	300-500	7	0.0458
	500-700	6	0.0159
	700-900	5	0.0105
	900-1100	4	0.0109
	1100-1300	3	0.0061
	1300-1500	2	0.0034
	>1500	1	0.0009
Land use Land cover (LULC)	Evergreen Needle leaf Forest Evergreen Broadleaf Forest Mixed Forest	3	0.0102
	Woody Savannas Savannas Grasslands	4	0.0678
	Permanent Wetlands Croplands	7	0.8881
	Cropland/ Natural Vegetation Urban Built-up	8	0.0339
Soil Group	C	6	0.5911
	D C/D D/D	8	0.4089
Population density (person/sq.km)	<100	1	0.0956
	100-150	2	0.0867
	150-250	3	0.3224
	250-500	4	0.361
	500-1000	5	0.0721
	1000-3000	6	0.0381
	3000-5000	7	0.0114
	>5000	8	0.0128
Household Density (number/sq.km)	0-20	1	0.1745
	20-40	2	0.6802
	40-60	3	0.1103
	60-80	4	0.0264
	80-100	5	0
	100-120	6	0
	120-150	7	0
	>150	8	0.0085

Indicators	Classification	Ranks	Weighted area
Slope (°)	0-10	8	0.9541
	10-20	7	0.0322
	20-30	6	0.0103
	30-40	5	0.0028
	40-50	4	0.0004
	50-60	3	0.0001
	60-70	2	0
	70-80	1	0
Rx3day (mm)	<100	4	0
	100-140	5	0.0667
	140-170	6	0.6355
	170-200	7	0.2514
	>200	8	0.0465
Distance from rivers (m)	<200	8	0.2981
	200-500	7	0.3205
	500-800	6	0.1028
	800-1100	5	0.1777
	1100-1400	4	0.0296
	1400-1700	3	0.0397
	1700-2000	2	0.0195
	>2000	1	0.0121
Distance from roads (m)	<200	8	0.0303
	200-500	7	0.039
	500-800	6	0.0468
	800-1100	5	0.0189
	1100-1400	4	0.0448
	1400-1700	3	0.0171
	1700-2000	2	0.0255
	>2000	1	0.7775
Distance From Flood shelters	No flood shelter in the basin; therefore, the weightage is the same for the whole basin	8	1
Rainfall trend	Positive trend	8	0.0496
	Negative trend	4	0.9504
Literacy rate (%)	>70	4	0.0662
	60-70	6	0.4791
	50-60	7	0.2963
	<50	8	0.1584
Efficient Drainage System	No efficient drainage system in the basin. Therefore, the weightage is the same for the whole basin	8	1

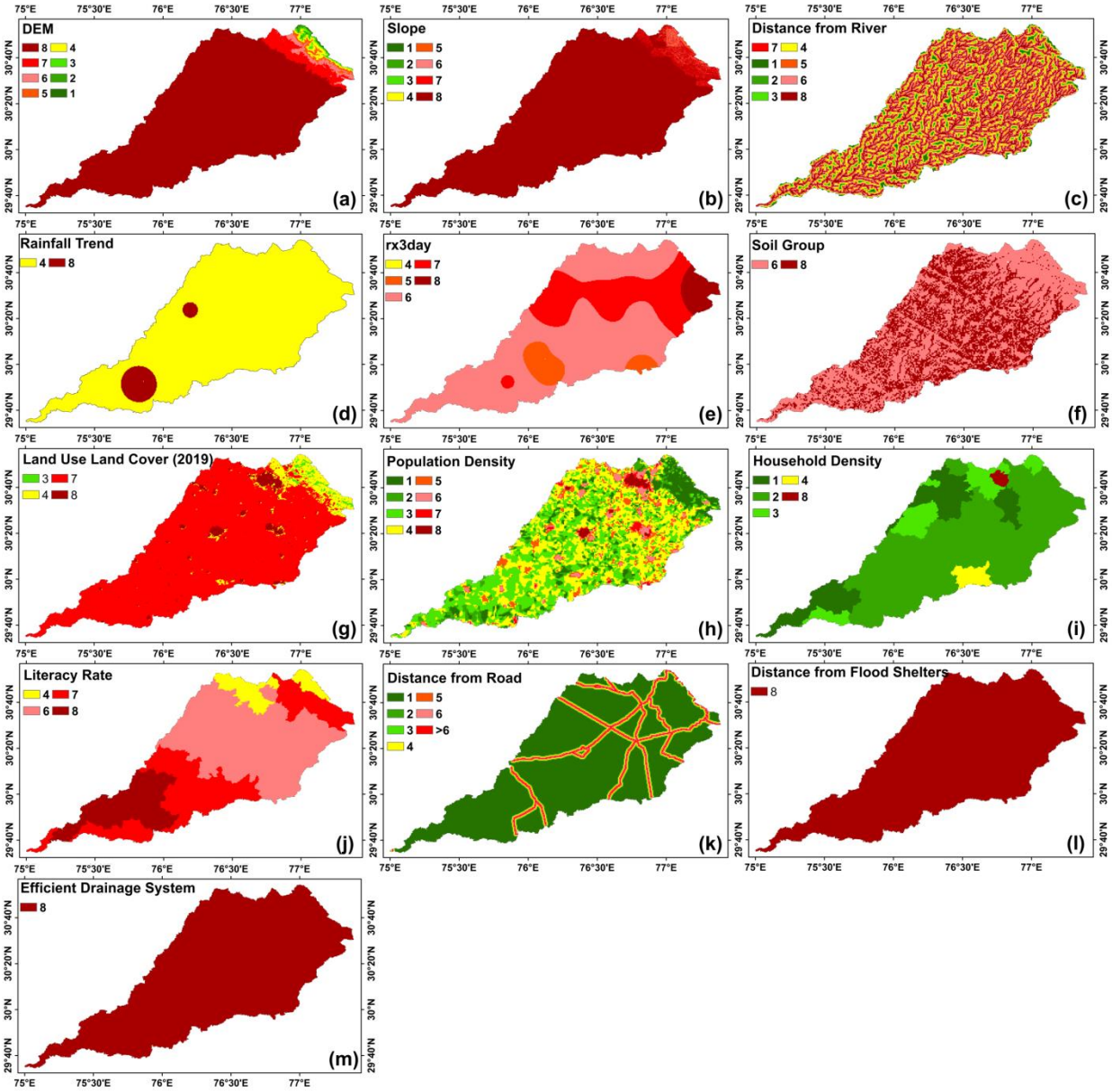

Figure 7.2 Rank classified spatial map of the indicators

7.2. Results and Discussion

The results of this section are discussed as LULC change analysis, Population density changes, and flood risk analysis integrating the flood hazard and flood vulnerability analysis.

7.2.1. LULC change analysis

Figure 7.3(a-c) shows the spatial distribution of LULC for 2001, 2010, and 2019 of the Ghaggar River basin used for LULC change analysis. The LULC map of 2001 and 2010 is used for the land change analysis and predicted map for 2019. The predicted 2019 LULC map is validated with the actual 2019 map. The validation of the model is examined using the Kappa Index, which indicates the accuracy between actual and predicted maps (379). The kappa statics

values of the map were above 80%, and the standard Kappa index, quantity Kappa index, and location Kappa index were 82%, 84%, and 86%. The Kappa statics value above 80% is considered a good land change prediction (447–450). The accuracy of the predicted maps is 82%.

This model is further used for executing spatial LULC maps of 2030 and 2040. The predicted spatial map of LULC for 2030 and 2040 is shown in Figure 7.3(d-e). The changes have been analyzed for eleven predefined LULC categories shown in Figure 7.3 as legends. The spatial maps of 2001, 2010, 2019, 2030, and 2040 are used for the flood risk analysis of different periods and compared the risk with time.

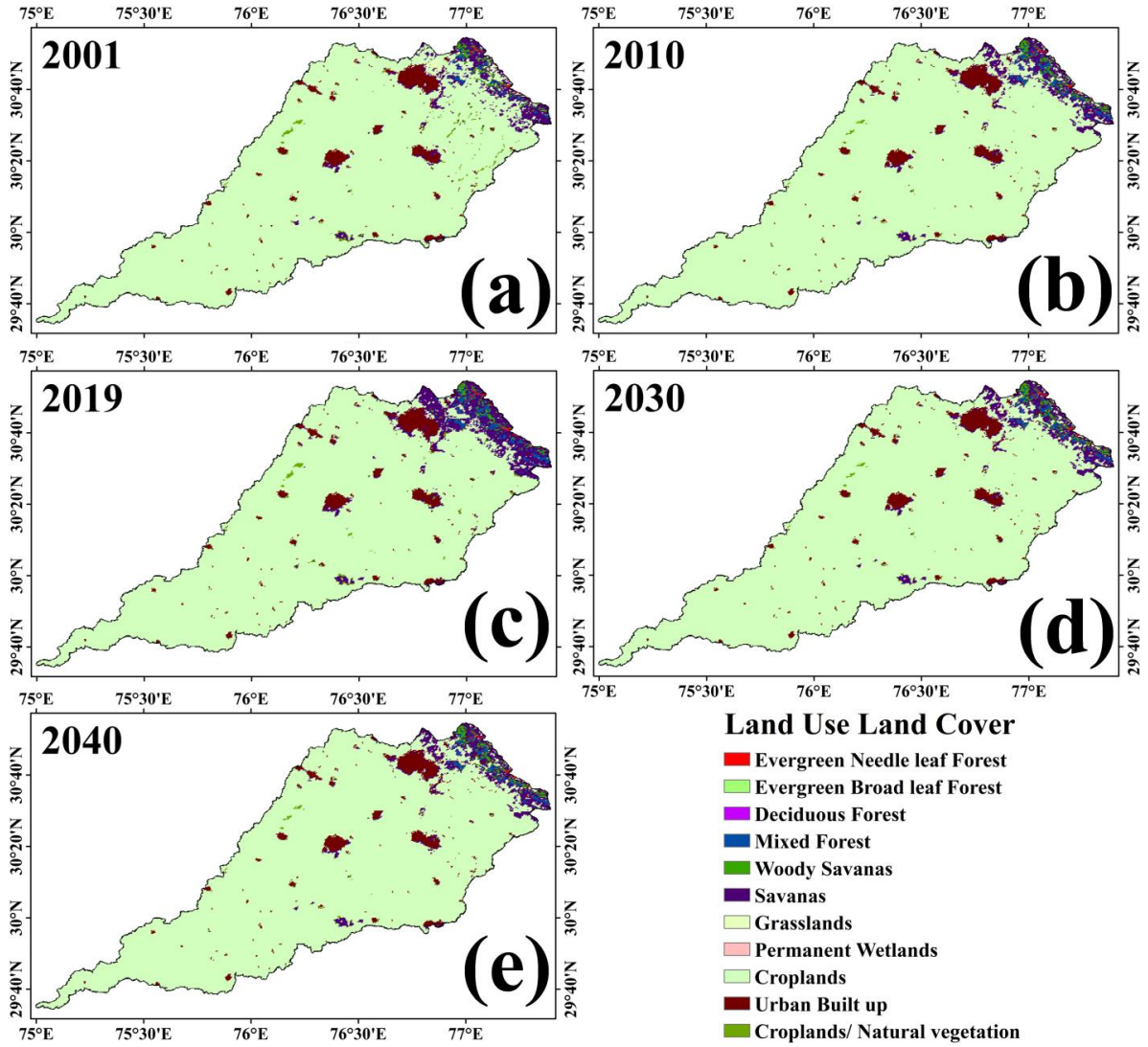

Figure 7.3 LULC of 2001, 2010, 2019, 2030, and 2040.

Figure 7.4a shows the gain and losses of LULC in sq. km between 2001 and 2010, and Figure 7.4b shows the contribution to the net change in urban built-up in sq. km. Similar figures as

Figure 7.4b were also formed for other LULC categories; these figures are not given. However, these figures are incorporated into discussions. It is found from Figure 7.4b that the urban built-up category of LULC has gained 8.59 sq. km of its area from Savannas (82.51%), grasslands (2.45%), and croplands (15.03%). The barren/sparsely vegetated (0.21 sq. km) has been transformed into grasslands. The croplands/natural vegetation area has been transformed into (81.36%) or savannas (18.63%). Croplands gained 119.35 sq. km and lost an area of 125.79 sq. km in 2010 LULC. Croplands gained area from croplands/natural vegetation (95.54%) and open shrublands (0.46%) and lost areas to savannas (48.16%), grasslands (49.38%), and urban built-up (2.45%). Overall, cropland lost its area of 6.44 sq. km. Permanent wetlands gained an area of 0.21 sq. km from grasslands (100%). Grasslands gained 40.14 sq. km and lost 69.98 sq. km from and to other LULC categories, and overall, the grasslands lost approximately 30 sq. km of area. Grasslands gained area from croplands (99.19%) and barren/sparsely vegetated (0.81%). Grasslands lost area to savannas (89.28%), woody savannas (9.96%), permanent wetlands (0.37%), and urban built-up (0.37%). Savannas gained an area of 175.38 sq. km and lost 147.47 sq. km. The area lost to evergreen needle leaf forests (3.33%), evergreen broadleaf forests (0.36%), deciduous forests (1.10%), mixed forests (42.23%), woody savannas (40.74%), and urban built-up (12.21%); and gained from grasslands (58.25%), croplands (29.79%) and cropland/natural vegetation (12.25%). Overall, savannas gained 27.91 sq. km of area. Woody savannas gained 42.93 sq. km and lost 30.48 sq. km area from and to different LULCs. Woody savannas were lost to evergreen needle leaf forests (6.39%) and mixed forest (93.60%) and gained from savannas (80.88%) and grasslands (19.11%). Overall, woody savannas gained 12.45 sq. km area during 2001 and 2010. The total area of open shrublands (0.21 sq. km) was lost to croplands (100%). Mixed forest gained 42.07 sq. km and lost 0.86 sq. km from and to different LULC categories. Mixed forests gained area from evergreen needle leaf Forests (1.55%), evergreen broadleaf forests (0.50%), Deciduous Forest (0.50%), Woody Savannas (38.03%), and Savannas (59.39%). Deciduous forest gained 0.64 sq. km from savannas and lost 0.21 sq. km to the mixed forest. Evergreen broadleaf forest lost 0.21 sq. km to savannas and gained 0.43 sq. km from the mixed forest (50%) and evergreen needle leaf forest (50%). Evergreen needle leaf forest gained 3.22 sq. km and lost 0.64 sq. km from and to different LULC categories. Evergreen needle leaf forest gained area from the evergreen broadleaf forest (6.54%), woody savannas (33.33%), and savannas (60.12%) and lost to the mixed forest (100%).

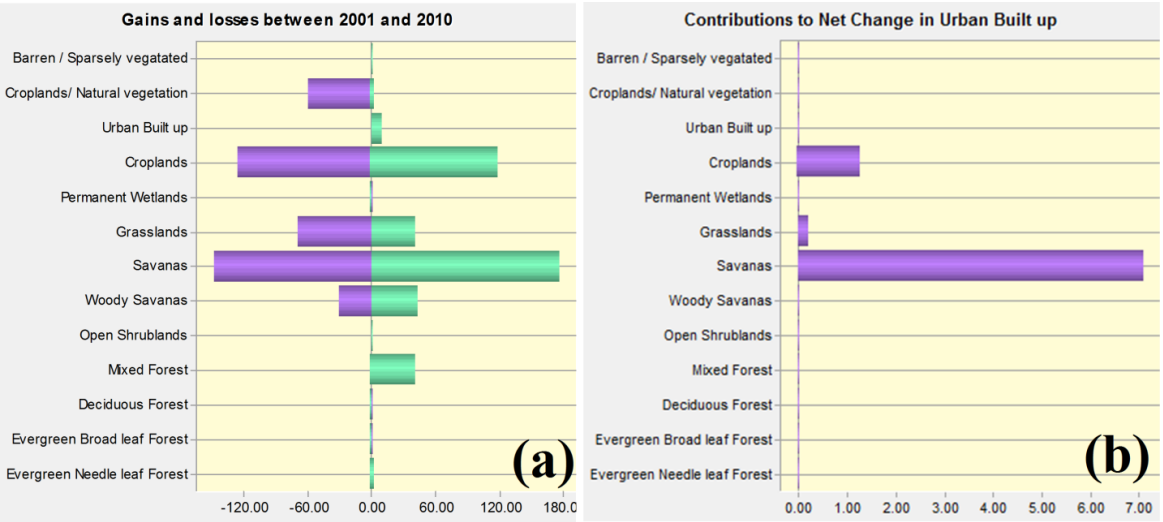

Figure 7.4 (a) Gain and losses of LULC in sq. km between 2001 and 2010; and (b) contribution to the net change in urban built up in sq. km

Figure 7.5 compares different LULC patterns for 2001, 2010, 2019, 2030, and 2040. The area of the LULC is extracted from the spatial map of Figure 7.3 (a-e). The LULC category of open shrublands, deciduous forest, and barren, sparsely vegetated lost its total area and has yet to be gained again. The permanent wetlands, evergreen needle leaf forest, mixed forest, urban built-up, woody savannas, cropland/natural vegetation, and savannas were acquired area with time. However, with time, croplands, grasslands, and evergreen broadleaf forests lost area. The urban built-up of the study area was 450.72 sq. km and increased by 8.68 sq. km in 2010, 14.97 sq. km in 2019, and 10.42 sq. km in both 2030 and 2040.

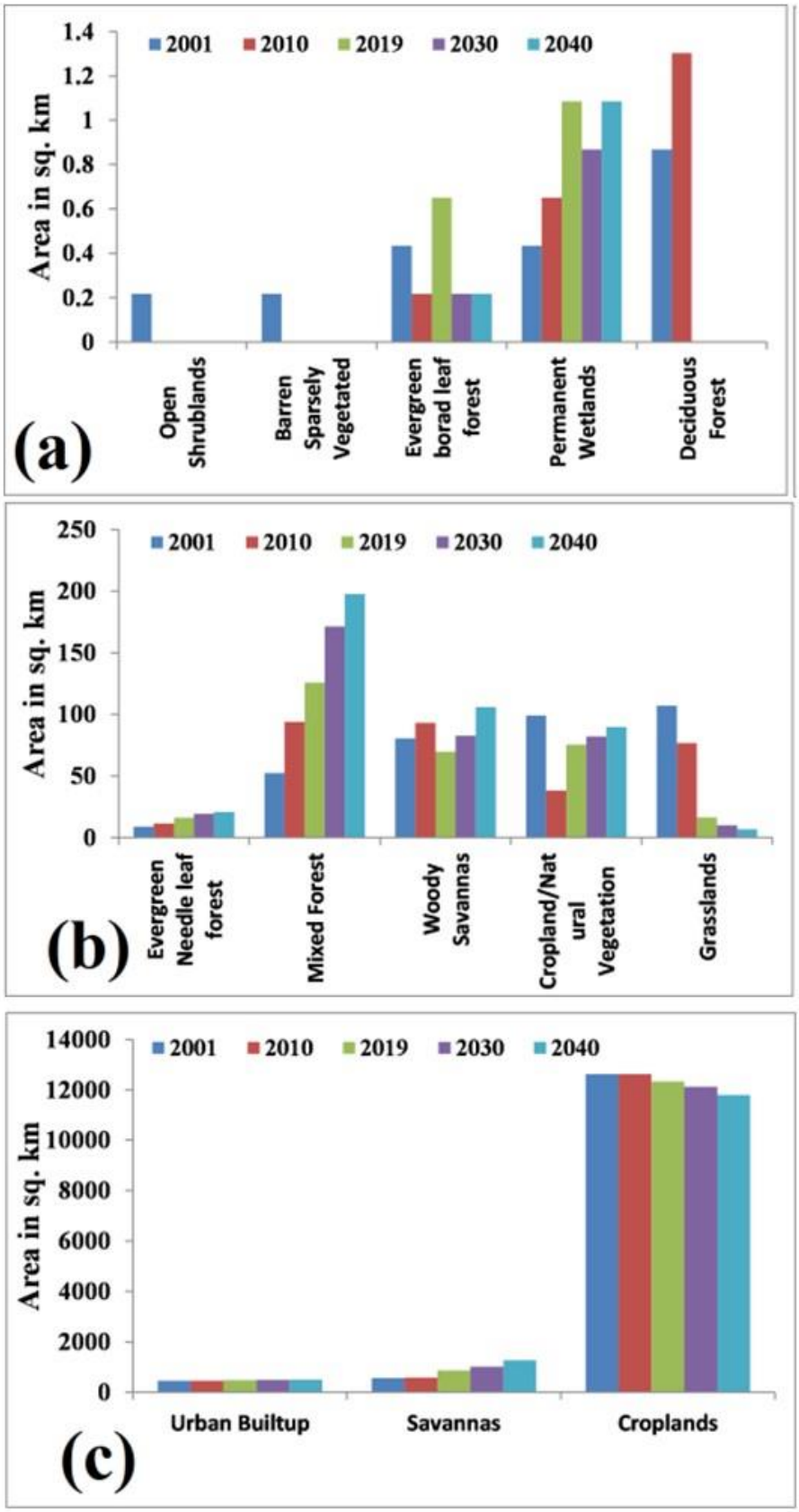

Figure 7.5 Bar chart of area for different LULC categories in the different periods.

7.2.2. Population density change analysis

The population density changes were analyzed using the percentage of density increasing yearly. The rate of population density changes has been extracted from the United Nations, Department of Economic and Social Affairs, Population Division (2019), and Macrotrends (2021). The average rate of population density changes per year in India is directly processed in the Census 2011 population density map. Year-wise maps after 2011 are executed according to population density increases. However, three projected spatial maps of 2019, 2030, and 2040 were considered for this study. The selection of these years concerns the LULC map year. Figure 7.6 shows spatial maps of 2011, 2019, 2030, and 2040 population density per sq. km. These maps' legend classification is based on the rank-wise distribution, as shown in Table 7.2.

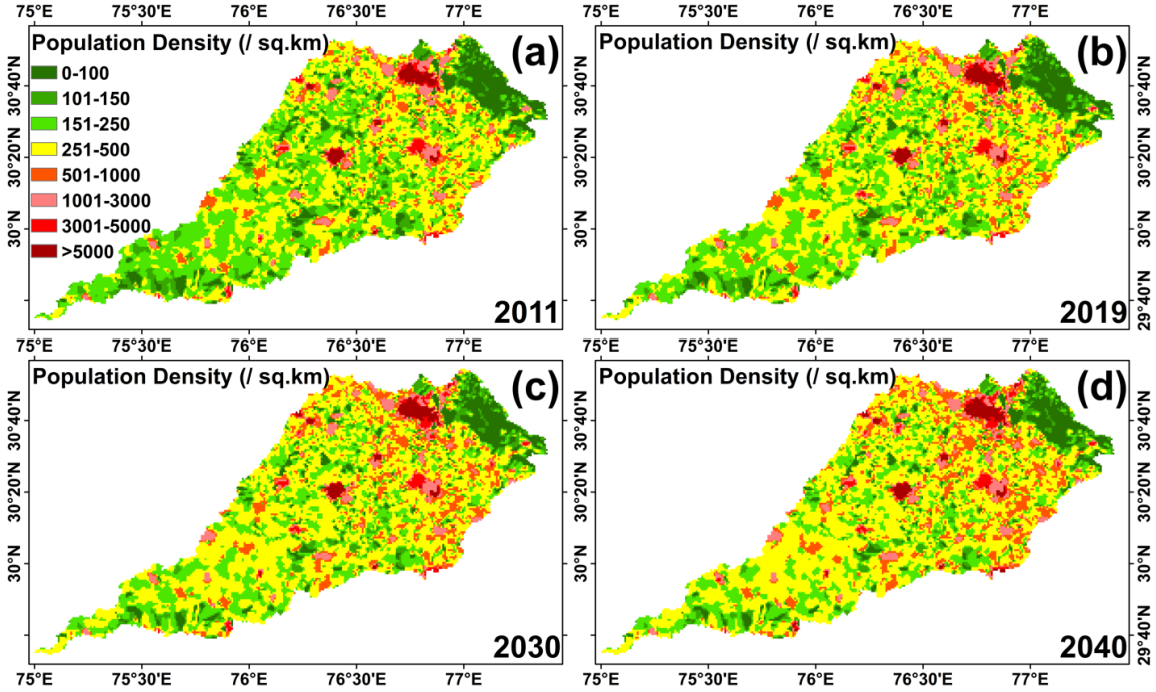

Figure 7.6 Population density spatial map for the years 2011, 2019, 2030, and 2040

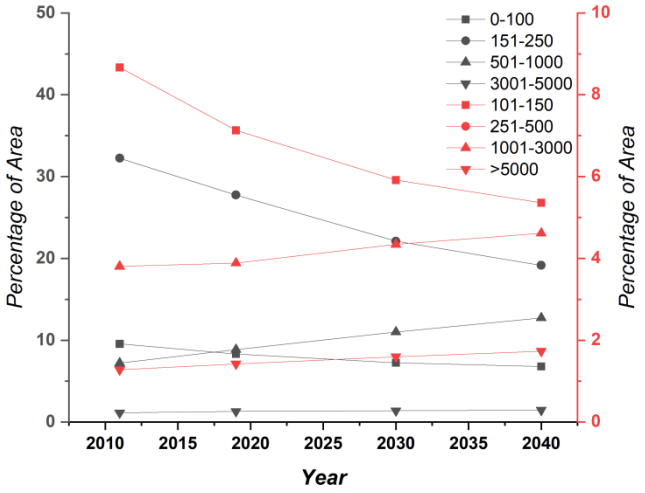

Figure 7.7 Percentage of area occupied different ranks population density in different periods

Figure 7.7 shows the percentage of area occupied by different population density ranks. The area under Rank 1-3 is decreasing, whereas Rank 4-8 is increasing. The study area's actual and predicted average population density is 457, 499, 549, and 582 per sq. km for 2011, 2019, 2030, and 2040, respectively. The average population density of the basin is higher than the average population density of India. The highest population density of the study area was 25177 persons per sq. km in 2011, projected to be 27515 people per sq. km in 2019, 30278 people per sq. km in 2030, and 32071 persons per sq. km in 2040.

7.2.3. Flood risk analysis

Flood risk analysis is an integrated function of flood hazard and vulnerability analysis (95,104,125,167,201,216). Flood hazard is the occurrence of floods due to natural phenomena over an area, whereas flood vulnerability is the loss due to natural phenomena (216). The flood risk map is executed by multiplying the flood hazard and flood risk maps (Equation 7.2).

$$\boldsymbol{Flood\ risk = Flood\ hazard \times Flood\ vulnerability} \qquad (7.2)$$

Thirteen indicators have been considered based on the literature review and best data availability for this study. The indicators considered for flood hazard analysis are elevation, slope, LULC, soil group, rx3day, and distance from rivers. In contrast, indicators considered for flood vulnerability are population density, household density, literacy rate, rainfall trend, distance from flood shelters, efficient drainage system, LULC, and distance from roads (95,125,216).

The weights of the indicators for flood hazard and flood vulnerability were calculated using the comparison matrix in our work. After calculating the weight of the indicators, the Equation

can be revised as Equation 7.3 for flood hazard analysis and Equation 7.4 for flood vulnerability analysis.

$$\boldsymbol{Flood\ Hazard} = (\boldsymbol{Elevation} \times \mathbf{3.38}) + (\boldsymbol{Slope} \times \mathbf{28.28}) + (\boldsymbol{LULC} \times \mathbf{26.49}) + (\boldsymbol{Soil\ Group} \times \mathbf{8.54}) + (\boldsymbol{rx3day} \times \mathbf{29.11}) + (\boldsymbol{Distance\ from\ rivers} \times \mathbf{4.20}) \quad (7.3)$$

$$\boldsymbol{Flood\ Vulnerability} = (\boldsymbol{Population\ Density} \times \mathbf{7.48}) + (\boldsymbol{Household\ Density} \times \mathbf{5.68}) + (\boldsymbol{LULC} \times \mathbf{24.37}) + (\boldsymbol{Distance\ from\ roads} \times \mathbf{4.26}) + (\boldsymbol{Distance\ from\ flood\ shelters} \times \mathbf{8.59}) + (\boldsymbol{Literacy\ rate} \times \mathbf{2.91}) + (\boldsymbol{Rainfall\ trend} \times \mathbf{22.93}) + (\boldsymbol{Efficient\ Drainage\ System} \times \mathbf{24.19}) \quad (7.4)$$

The consistency ratio value of the flood hazard matrix is 0.048, and the flood vulnerability matrix is 0.091. These two matrices are consistent as the value below 0.1 is considered a consistent matrix (174). The detailed methodology of AHP can be found in chapter 6.

The flood hazard, flood vulnerability, and flood risk map are classified into different zones according to hazard, risk, and vulnerability levels. The flood zone is organized into five: very low, low, moderate, high, and very high (166,167,197,213). The numerical range of flood hazard and flood vulnerability for different flood zones is less than 200 for very low, 200-400 for low, 400-500 for moderate, 500-700 for high, and more than 700 for very high. The numerical ranges of flood risk are directly square of the flood hazard or flood vulnerability as the flood risk numerical value is the multiplication of flood hazard and flood vulnerability numerical value. The flood hazard, vulnerability, and risk map are executed for 2011, 2019, 2030, and 2040. The LULC of 2010 is considered the 2011 LULC for this study.

7.2.3.1. Flood Hazard Map

Equation 7.3 is utilized for the execution of a flood hazard map using the Map Algebra tool (Raster Calculator) in ArcGIS 10.5. Four flood hazard maps of four different periods, i.e., 2011, 2019, 2030, and 2040, are executed using the flood hazard indicators. All the flood hazard indicators were considered static except LULC. LULC is considered dynamic, and LULC of different periods executes that period's flood hazard map. Figure 7.8 (a-d) shows the 2011, 2019, 2030, and 2040 spatial flood hazard maps. Low, Moderate, and High-hazard zone is found in the study area during different periods. The flood hazard of the basin was highly hazardous as the major part of the basin is under a highly hazardous zone. The highly hazard zone of the basin is also increasing with time, and the area under the highly hazard zone in 2011, 2019, 2030, and 2040 is found to be 13527.5, 13602.9, 13609.4, 13635.8 sq. km,

respectively. The area under moderate and low hazard zones is decreasing with time. The area under the moderate hazard zone in 2011, 2019, 2030, and 2040 is found to be 443.4, 369.2, 363.0, and 336.7 sq. km, respectively. The area under the low hazard zone in 2011, 2019, 2030, and 2040 is 7.1, 5.9, 5.6, and 5.6 sq. km, respectively. Overall, the flood hazard of the study area is high, and the area under the high flood hazard zone is increasing with time.

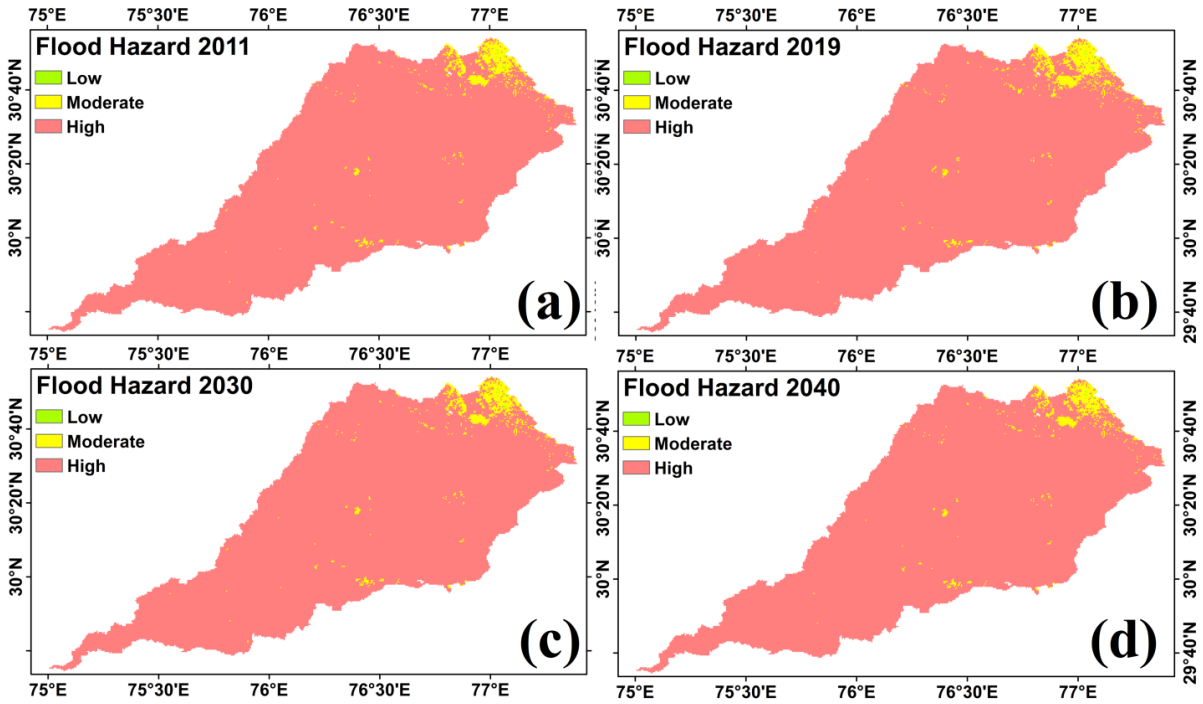

Figure 7.8 Spatial flood hazard map of the study basin in different periods

7.2.3.2. Flood vulnerability map

Equation 7.4 was utilized to execute the flood vulnerability map of the study area using the Map Algebra tool (Raster Calculator) in ArcGIS 10.5. The flood vulnerability map of four different periods is executed using eight indicators. LULC and population density are used as dynamic indicators, and different period flood vulnerability maps are executed using that period LULC and population density map. Figure 7.9 (a-d) shows the 2011, 2019, 2030, and 2040 spatial flood vulnerability maps. Moderate, high, and very highly vulnerable flood zone is found in the basin. However, the major portion of the basin is under a highly vulnerable zone. The area under the moderately vulnerable zone decreases, whereas the area under the high and very highly vulnerable zone increases with time. The area under the moderately vulnerable zone is found 538.3, 455.9, 396.0, and 366.7 sq. km during 2011, 2019, 2030, and 2030, respectively. The area under the highly vulnerable zone is found at 13382.2, 13466.9, 13522.2, and 13548.5 sq. km during 2011, 2019, 2030, and 2040, respectively. The area under the very highly vulnerable zone is 57.5, 55.2, 59.8, and 62.8 sq. km during 2011, 2019, 2030, and 2030,

respectively. Overall, the flood vulnerability of the study area is high, and the area under the high and very high flood vulnerability zone is increasing with time.

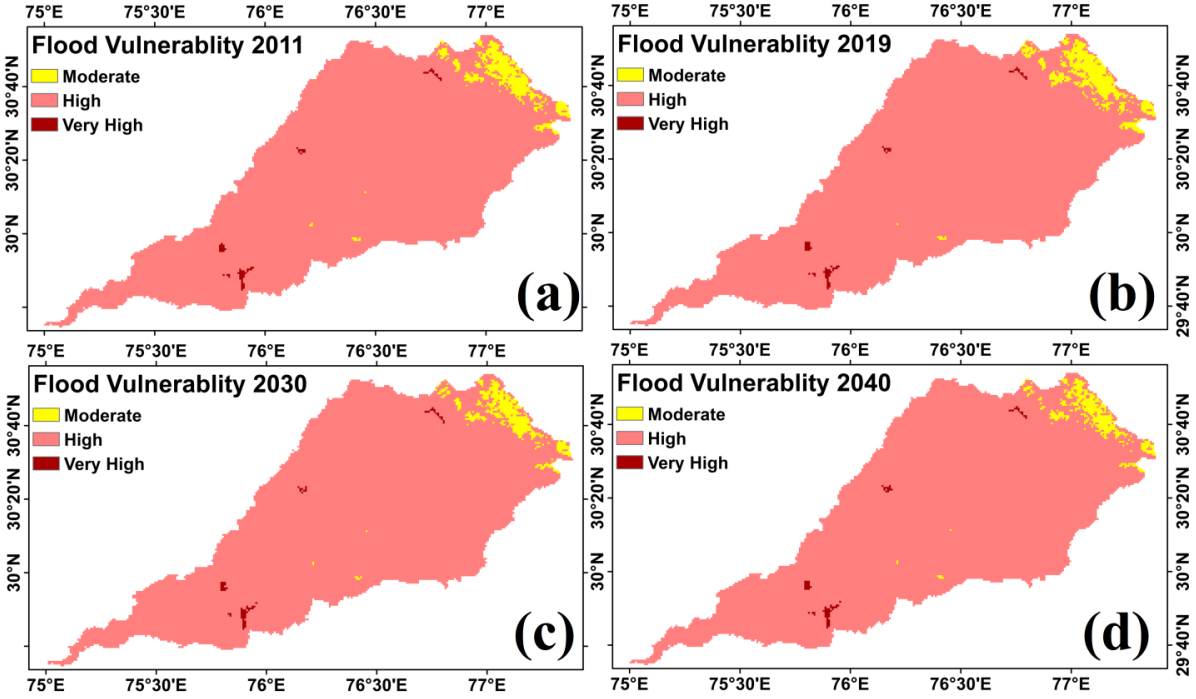

Figure 7.9 Spatial flood vulnerability map of the study basin in different periods

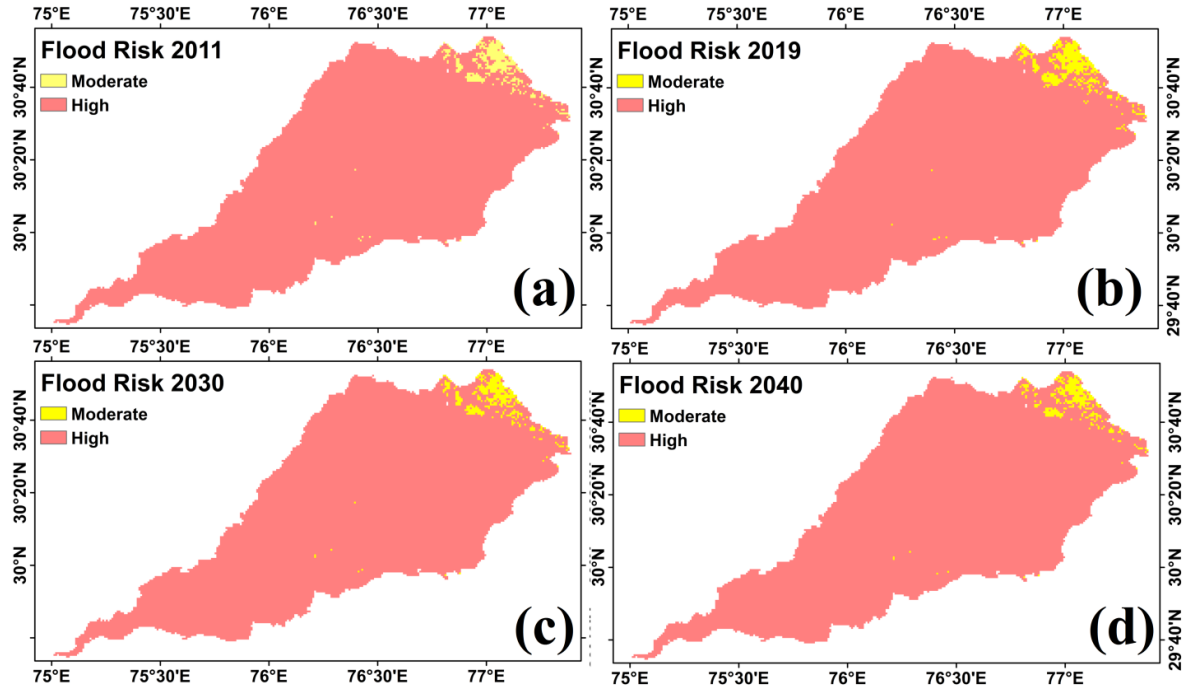

Figure 7.10 Spatial flood risk map of the study basin in different periods

7.2.3.3. Flood risk map

Equation 7.2 is utilized for the execution of a flood risk map, i.e., direct multiplication of flood hazard and flood vulnerability map using the Map Algebra tool (Raster Analysis) in ArcGIS

10.5. The flood hazard map and flood vulnerability map of similar years are used to execute the flood risk map of the different periods. Figure 7.10 (a-d) shows the spatial flood risk of 2011, 2019, 2030, and 2040. The study area's risk is moderate and high; however, the major portion of the basin is under the high flood risk zone. The area under moderate flood risk decreases with time, whereas the area under a high-risk zone increases with time. The area under the moderate risk zone is 371.4, 309.0, 291.5, and 267.2 sq. km during 2011, 2019, 2030, and 2030, respectively. The high-risk zone area is 13606.6, 13669.0, 13686.5, and 13710.8 sq. km during 2011, 2019, 2030, and 2040.

7.2.4. Inferences

The flood risk map of the different periods is executed using that period flood hazard and flood vulnerability map, where the flood hazard and flood vulnerability map is executed using Equation 7.3 and 7.4, respectively. Two dynamic factors used for the risk analysis are LULC and population density. LULC change analysis and population density increase with time. The area flood zone of hazard, vulnerability, and risk increases, and the order of zone also increases as the area increases in urban built-up and population density. Therefore, a direct relation is found between the increment of dynamic factors and flood risk.

The flood hazard, vulnerability, and risk also depend on other flood indicators. Figure 7.8 – 7.10 shows that the upper part of the basin is under a low or moderate zone, possibly due to the stiff slope and elevation. The population density is also under low and very low rank in the upper part of the basin. The higher rainfall in the upper part of the basin is the reason for the low and moderate zone. The literacy rate and rx3day are the reasons behind the upper category of the flood zone, as it is expected to be under a very low zone. In case of lower rainfall and an upper literacy rate in the upper part of the basin, the upper part will lie under a very low zone. A very highly vulnerable flood zone is found in the urban area of the basin, and it is expected due to the expansion of urban built-up and increasing population density. Increasing rainfall trends may be responsible for the very highly vulnerable zone in the lower and middle parts of the basin.

The major part of the basin is under a high-risk, highly vulnerable flood zone. The indicators are mainly responsible for this elevation, slope, distance from flood shelters, efficient drainage system, literacy rate, LULC, rx3day, and soil group. However, household density, distance from the road, and rainfall trends are lowering flood risk, hazard, and vulnerability. The major portion of the basin is under high rank for slope and elevation due to lower elevation and plain

slope, whereas the whole basin is at the high rank for the indicators of the efficient drainage system and distance from flood shelters. Increasing the literacy rate of the basin, placement of proper drainage density, built-up flood shelters, etc., will be adapting policy to prevent losses from future floods.

CHAPTER 8

Conclusion

The present study emphasized rainfall analysis, extreme rainfall analysis, flood zone analysis, and flood risk projection using urbanization for the Ghaggar river basin. Rainfall analysis was analyzed by descriptive statistics, trend analysis, change point analysis, descriptive statistics before and after change point, and trend analysis before and after change point. Extreme rainfall analysis is the analysis of rainfall indices described by ETCCDI. The descriptive statistics and trends were analyzed for ten rainfall indices for extreme rainfall analysis. The flood risk zone was analyzed using the analysis of flood hazard and flood vulnerability zone. Graph theory and the AHP method was used to analyze flood risk zone. The result of both methods for flood risk analysis were compared. The flood map was also projected for 2030 and 2040 using two dynamic factors: land use land cover changes as urbanisation, and population density changes. Results have been summed up below.

- The elevation of the basin lies in the range of 143 – 1790m, out of which 92% of the basin area is under 350m, and around 8% of the total basin area is above 350m elevations, whereas only 1.5% of the basin area is located above 1000m elevation. Therefore, the average slope of the basin is 2.59°. However, the slopes lie in the range of 0 – 80.9°.
- The LULC of the Ghaggar River basin is majorly occupied by croplands (88.26%), savannas (6.16%), and urban built-up (3.39%). The hydrological soil group of the basin has moderately high to high runoff potential.
- The population density of the basin lies in the range of 0 – 25177 / sq. km, whereas the average population density of the basin is 457 / sq. km. The highly populated areas in the Ghaggar river basin are Chandigarh, Rajpura, Patiala, and Ambala. The household density of the area is lies in the range of 9 – 184 per sq. km, and the highest household density found in Chandigarh. The literacy rate for the basin lies in the range of 52 – 76%, and the highest literacy rate is found in Pachhad and Solan tehsils of Himachal Pradesh. The river basin is well connected with the National Highway of India.
- The monthly average rainfall in the Ghaggar River basin lies in the range of 1.8 - 551.6mm during the study. The standard deviation of the monthly rainfall varies in the 5.0 – 324.9 mm range, whereas the CV varies in the 42.6 – 484.6% range. The

maximum average weighted rainfall, i.e., 216mm, was received during July and August, whereas the lowest was received during November, i.e., 5mm.

- The range of average seasonal rainfall is varying in the range of 21 – 103.8 mm, 35.5 – 95.8mm, 202.6 – 1421mm, and 7.6 – 82.6 mm, and their standard deviation varies in the range of 28.3 – 78.9, 39.4 – 81.9, 211.6 – 663.7, and 20.3 – 96.4 during winter, pre-monsoon, southwest monsoon and monsoon season, respectively. Dedhna received the lowest average seasonal rainfall during all the seasons, whereas Nahan received the highest average seasonal rainfall during all the seasons.
- The average annual rainfall in the Ghaggar river basin varied in the range of 266.7 – 1703.2mm, whereas the highest average annual rainfall was found at Nahan and lowest at Dedhna. The SD and CV of average annual rainfall in the Ghaggar river basis lied in the range of 244.1 – 718.3mm and 30.8 – 118.6%, respectively. The higher and lower variability of annual average rainfall were observed at Dedhna and Ambala, respectively, whereas the highest and lowest SD was found at Nahan and Thanesar.
- The trend results from the ITA and MK methods are compared, and more than 90% are similar. 36.1% of the monthly trend is increasing, whereas 63.2% is decreasing, and rest is no trend. The monthly trend magnitude lies in the ranges of (-) 9.4 – 5.65 mm/year, i.e., for the highest variation in the monthly analysis and found in July.
- More than 85% of results of both the ITA method and MK test were found in similar direction seasonal trends. The trend magnitude values lie in the range of (-)17.02 – 7.21 mm/year and were found in the southwest monsoon season. The highest rainfall trend was found to increase at the rate of 4.93mm/year at Lehal, whereas the lowest rainfall trend was found to decrease at 23.09mm/year at Banur. 75 % of total meteorological stations are experiencing a declining annual rainfall trend, whereas 25% is inclining.
- Annual rainfall in the Ghaggar River basin varied in the range of 379.4 – 2223.2 mm before the change point, which decreases to 53.4 – 1470.9mm after the change point. The highest change, i.e., 752.3mm in average annual rainfall after the change point, was found at Nahan. The trend magnitude of the annual rainfall varies in the range of (-)13.62 – 94.95mm/year before the change point and (-43.9) – 23.35mm/year after the change point. The trend magnitude decreases after the change point. The number of decreasing trend stations increased from 5 to 8 after the change point.
- Consecutive dry days (CDD) lie in the range of 69.5 – 223.2, whereas the average number of consecutive wet days (CWD) lies in the 3.4 – 9.6 days range. The highest

number of CWD and lowest number of CDD was found at Nahan, whereas the lowest number of CWD and highest number of CDD was found at Dedhna. The average precipitation on wet days (PRCPTOT) in the Ghaggar River basin lies in the 69.5 – 1828.6 mm range. The highest average of PRCPTOT was found at Nahan, whereas the lowest average is found at Ambala.

- The average of R10mm, R20mm, and R30mm lies in the range of 9.8 – 42.4, 5.9 – 27.5, and 3.6 – 19.2, respectively. The average R10mm, R20mm, and R30mm days were highest at Nahan and lowest at Dedhna.
- The average rx1day, rx3day, and rx5day in the Ghaggar River basin lie in the range of 66.4 – 160.3 mm, 100.2 – 252.4 mm, and 114.2 – 311.3 mm, respectively. The highest and lowest average amount of rx1day, rx3day, and rx5day was found at Nahan and Dedhna, respectively. The SDII of the Ghaggar river basin lied in the range of 16.3 – 26.9 mm, whereas the highest amount of SDII is found at Rajpura and lowest at Thanesar.
- The trend magnitude of CDD and CWD varies in the range of (-)2.97 – 24.97 days/year and (-)0.714 – 0.093 days/year, respectively. The highest trend magnitude, increasing trend, was found at Dedhna, whereas the lowest trend magnitude, decreasing trend, was observed at Lehal. 41% of total stations trend of CDD and 59% of total stations of CWD is decreasing trend whereas the rest of trends of both CDD and CWD is increasing.
- The trend of PRCPTOT was decreasing in 83% of the station, where only 17% of the station was increasing. The trend magnitude of PRCPTOT lies in the range of (-)35.53 – 21.45 mm/year. The highest trend magnitude, i.e., increasing, was found at Rohiti, and the lowest, i.e., decreasing, was found at Banur.
- The trend magnitude of R10mm, R20mm, and R30mm varies in the range of (-)1.944 – 0.023 days/year, (-)0.805 – 0.116 days/year, and (-)0.611 – 0.280 days/year respectively. The significant trend of R10mm and R20mm was found at Rohiti, increasing at 0.023 days/year and 0.116 days/year, respectively.
- The trend magnitude of rx1day lies in the range of (-)2.803 – 6.011 mm/year where the highest, i.e., increasing, was found at Lehal and lowest, i.e., decreasing, at Dedhna. The trend magnitude of rx3day and rx5day lies in the range of (-)4.73 – 9.25 mm/year and (-)3.898 – 9.688 mm/year, respectively.
- The trend of SDII is increasing at 33.3% of stations and decreasing at 66.6% of stations. The trend magnitude of SDII lies in the range of (-)1.391 – 1.276 mm/year. The highest

trend magnitude, i.e., increasing, was found at Dhaneta, and the lowest, i.e., decreasing, was found at Rajpura.

- The flood risk was analyzed using Graph theory and Analytical Hierarchy process. The graph theory results reveal that around 29.8% of the basin area has been prone to very high flood hazards, whereas 70.1% is prone to high flood hazards. Similarly, around 17.4% of the basin area is prone to highly vulnerable to flood, whereas 82.5% of the basin area is prone to moderately vulnerable to flood. The flood risk has been observed to be high in the whole basin using Graph theory.
- AHP method reveals that around 14.54% (2033.5 km^2) and 85.2% (11922.7 km^2) of the basin area lie under the high and very high categories of flood hazard, respectively. Around 0.15 % of the basin area (21.3 km^2) is observed under the moderate flood hazard category. 93.25% (13035.2 km^2) and 2.3% (322 km^2) of the Ghaggar River basin area lie under the high and very high categories of flood vulnerability, respectively. Most of the basin, i.e., 94.1% (13165.2 km^2), is at high risk of flood, whereas only 5.52% (771.6 km^2) is at very high risk of flood. The basin areas under moderate risk of flooding are observed to be 0.2% (41.09 km^2).
- The comparison of the flood analysis method of AHP and Graph theory found that a high flood risk zone was obtained through both graph theory and AHP. In contrast, there is a small difference in results obtained in flood hazard and vulnerability characterization. Both methods obtained Similar flood hazard characterization for Ambala, Banur, Rajpura, Rohiti, and Kalka rain gauge stations. Other basin areas were observed as very high flood hazard zones in AHP, whereas high hazard zones were obtained through graph theory. Similarly, most of the basin area was observed as highly vulnerable to flood through AHP, whereas moderate vulnerability to the flood was observed for those areas through graph theory.
- The LULC map of 2001 and 2010 was used for the land change analysis/urbanisation and predicted map for 2019. The predicted 2019 LULC map was validated with the actual 2019 map. This model is further used for executing spatial LULC maps of 2030 and 2040. The urban built-up category of LULC has gained 8.59 sq. km of its area from Savannas (82.51%), grasslands (2.45%), and croplands (15.03%).
- The study area's actual and predicted average population density is 457, 499, 549, and 582 per sq. km for 2011, 2019, 2030, and 2040, respectively.

- The flood hazard analysis using urbanisation and population density changes shows that the high flood hazard zone in the study increases with time from low and moderate hazard zone. The highly hazard zone of the basin is also increasing with time, and the area under the highly hazard zone in 2011, 2019, 2030, and 2040 is found to be 13527.5, 13602.9, 13609.4, 13635.8 sq. km, respectively.
- The area under high and very high flood-vulnerable zones is increasing with respect to time, and the area under moderately zones is decreasing. The area under the highly vulnerable zone is found at 13382.2, 13466.9, 13522.2, and 13548.5 sq. km during 2011, 2019, 2030, and 2040, respectively. The area under the very highly vulnerable zone is 57.5, 55.2, 59.8, and 62.8 sq. km during 2011, 2019, 2030, and 2030, respectively.
- The moderate flood risk is decreasing, and the high flood risk zone increases with time. The high-risk flood zone area is 13606.6, 13669.0, 13686.5, and 13710.8 sq. km during 2011, 2019, 2030, and 2040.
- The area flood zone of hazard, vulnerability, and risk increases, and the order of zone increases as the area increases in urban built-up and population density. Therefore, a direct relation was found between the increment of dynamic factors and flood risk.

Future Recommendation

The study focussed on Flood Risk Assessment Due to Urbanisation and Climatic Factors using Geospatial Approach in the Ghaggar River Basin and it was completed per the availability of data and the feasibility of analysis. However, some studies are recommended for future work based on this study.

- The area taken for this study was13978 sq. km, whereas the whole area of the Ghaggar river basin is 32132 sq. km. Therefore, the analysis of the lower part of the basin or whole part of the basin can be the extended work for this work.
- The rainfall analysis for the basin was analyzed. However, the trend of temperature analysis and extreme temperature events is a suggestion for future study.
- There are multiple factors used for flood risk analysis. In this study, eleven factors are used. The number of factors can be increased for the analysis of flood risk.
- This study is limited to two dynamic factors; however, more dynamic factors consideration will give the model with a better output. Therefore, a recommendation for considering other dynamic factors in flood risk analysis will be an opportunity to step up this study.
- The present study doesnot consider the social vulnerability factors. Integrating social vulnerability factors, such as community preparedness, access to healthcare, and social support networks into flood vulnerability assessments could enhance the socio-economic perspective of this study. This could be especially relevant for understanding impacts on marginalized communities and can be considered in future study.
- Engaging local communities in flood risk reduction strategies is crucial. Conducting surveys or workshops to understand community perceptions of flood risks and involving them in the decision-making process can lead to more effective and culturally sensitive interventions. This can also be considered in future study for comprehensive flood risk analysis.

Reference

1. Ahmadvand S, Abbasi B, Azarfar B, Elhashimi M, Zhang X, Abbasi B. Looking Beyond Energy Efficiency: An Applied Review of Water Desalination Technologies and an Introduction to Capillary-Driven Desalination. Water (Basel). 2019 Apr;11(4):696.
2. Forde M, Izurieta R, Ôrmeci B. Water and health. Water Quality in the Americas. 2019;27:27–46.
3. Singh KR, Goswami AP, Kalamdhad AS, Kumar B. Development of irrigation water quality index incorporating information entropy. Environ Dev Sustain. 2020 Apr 11;22(4):3119–32.
4. Liu J, Yuan C, Hafeez M, Yuan Q. The relationship between environment and logistics performance: Evidence from Asian countries. J Clean Prod. 2018 Dec;204:282–91.
5. Lyu HM, Zhou WH, Shen SL, Zhou AN. Inundation risk assessment of metro system using AHP and TFN-AHP in Shenzhen. Sustain Cities Soc [Internet]. 2020 May;56:102103. Available from: https://linkinghub.elsevier.com/retrieve/pii/S2210670720300901
6. Ganesamoorthy R, Vadivel VK, Kumar R, Kushwaha OS, Mamane H. Aerogels for water treatment: A review. J Clean Prod. 2021 Dec;329:129713.
7. Istomina MN, Kocharyan AG, Lebedeva IP. Floods: Genesis, Socioeconomic and Environmental Impacts. Water Resources. 2005 Jul;32(4):349–58.
8. CRED. Disasters in numbers. Brussels; 2021.
9. CRED: EM-DAT. The International Disaster Databes [Internet]. 2019. Available from: https://www.emdat.be/database
10. Jonkman SN. Global Perspectives on Loss of Human Life Caused by Floods. Natural Hazards. 2005 Feb;34(2):151–75.
11. Bhattacharya S, Kumar V. Unprecedented floods in Ghaggar Basin. Dams Rivers and People [Internet]. 2010;(July):1–9. Available from: https://sandrp.files.wordpress.com/2018/03/an_analysis_of_the_flood_disaster_in_ghaggar_basin_in_july_2010.pdf
12. Saini SS, Kaushik SP. Risk and vulnerability assessment of flood hazard in part of Ghaggar Basin : A case study of Guhla block , Kaithal , Haryana , India. International Journal of Geomatics and Geosciences. 2012;3(1):42–54.
13. Ben-Dor E. Quantitative remote sensing of soil properties. In 2002. p. 173–243.
14. Chan SW, Abid SK, Sulaiman N, Nazir U, Azam K. A systematic review of the flood vulnerability using geographic information system. Heliyon [Internet]. 2022 Mar;8(3):e09075. Available from: https://linkinghub.elsevier.com/retrieve/pii/S2405844022003632
15. Zarekarizi M, Srikrishnan V, Keller K. Neglecting uncertainties biases house-elevation decisions to manage riverine flood risks. Nat Commun [Internet]. 2020 Dec 26;11(1):5361. Available from: https://www.nature.com/articles/s41467-020-19188-9
16. Rehman S, Sahana M, Hong H, Sajjad H, Ahmed B Bin. A systematic review on approaches and methods used for flood vulnerability assessment: framework for future research. Natural Hazards [Internet]. 2019 Mar 6;96(2):975–98. Available from: http://link.springer.com/10.1007/s11069-018-03567-z
17. Moreira LL, de Brito MM, Kobiyama M. Review article: A systematic review and future prospects of flood vulnerability indices. Natural Hazards and Earth System Sciences [Internet]. 2021 May 17;21(5):1513–30. Available from: https://nhess.copernicus.org/articles/21/1513/2021/
18. Chaliha S, Sengupta A, Sharma N, Ravindranath NH. Climate variability and farmer's vulnerability in a flood-prone district of Assam. Int J Clim Chang Strateg Manag [Internet]. 2012 May 11;4(2):179–200. Available from: https://www.emerald.com/insight/content/doi/10.1108/17568691211223150/full/html
19. Jamshed A, Birkmann J, Feldmeyer D, Rana IA. A Conceptual Framework to Understand the Dynamics of Rural–Urban Linkages for Rural Flood Vulnerability. Sustainability [Internet]. 2020 Apr 5;12(7):2894. Available from: https://www.mdpi.com/2071-1050/12/7/2894
20. Abbas A, Amjath-Babu TS, Kächele H, Usman M, Amjed Iqbal M, Arshad M, et al. Sustainable survival under climatic extremes: linking flood risk mitigation and coping with flood damages in rural

Pakistan. Environmental Science and Pollution Research [Internet]. 2018 Nov 20;25(32):32491–505. Available from: http://link.springer.com/10.1007/s11356-018-3203-8
21. Okazawa Y, Yeh PJF, Kanae S, Oki T. Development of a global flood risk index based on natural and socio-economic factors. Hydrological Sciences Journal [Internet]. 2011 Jul 12;56(5):789–804. Available from: http://www.tandfonline.com/doi/abs/10.1080/02626667.2011.583249
22. Baeck SH, Choi SJ, Choi GW, Lee DR. A study of evaluating and forecasting watersheds using the flood vulnerability assessment index in Korea. Geomatics, Natural Hazards and Risk [Internet]. 2014 Jul 3;5(3):208–31. Available from: http://www.tandfonline.com/doi/abs/10.1080/19475705.2013.803268
23. Carlier B, Puissant A, Dujarric C, Arnaud-Fassetta G. Upgrading of an index-oriented methodology for consequence analysis of natural hazards: application to the Upper Guil catchment (southern French Alps). Natural Hazards and Earth System Sciences [Internet]. 2018 Aug 23;18(8):2221–39. Available from: https://nhess.copernicus.org/articles/18/2221/2018/
24. Bertilsson L, Wiklund K, de Moura Tebaldi I, Rezende OM, Veról AP, Miguez MG. Urban flood resilience – A multi-criteria index to integrate flood resilience into urban planning. J Hydrol (Amst) [Internet]. 2019 Jun;573:970–82. Available from: https://linkinghub.elsevier.com/retrieve/pii/S0022169418304748
25. Miguez MG, Veról AP. A catchment scale Integrated Flood Resilience Index to support decision making in urban flood control design. Environ Plan B Urban Anal City Sci [Internet]. 2017 Sep 27;44(5):925–46. Available from: http://journals.sagepub.com/doi/10.1177/0265813516655799
26. Malavasi S, Riva M, Vanali M, Larcan E. Hydrodynamic forces on a submerged bridge. WIT Transactions on The Built Environment. 2001;56.
27. Yin J, Ye M, Yin Z, Xu S. A review of advances in urban flood risk analysis over China. Stochastic Environmental Research and Risk Assessment [Internet]. 2015 Mar 10;29(3):1063–70. Available from: http://link.springer.com/10.1007/s00477-014-0939-7
28. Dash P, Punia M. Governance and disaster: Analysis of land use policy with reference to Uttarakhand flood 2013, India. International Journal of Disaster Risk Reduction [Internet]. 2019 May;36:101090. Available from: https://linkinghub.elsevier.com/retrieve/pii/S2212420918309476
29. Diakakis M, Andreadakis E, Nikolopoulos EI, Spyrou NI, Gogou ME, Deligiannakis G, et al. An integrated approach of ground and aerial observations in flash flood disaster investigations. The case of the 2017 Mandra flash flood in Greece. International Journal of Disaster Risk Reduction [Internet]. 2019 Feb;33:290–309. Available from: https://linkinghub.elsevier.com/retrieve/pii/S2212420918303935
30. Li Z, Zhang X, Ma Y, Feng C, Hajiyev A. A multi-criteria decision making method for urban flood resilience evaluation with hybrid uncertainties. International Journal of Disaster Risk Reduction [Internet]. 2019 May;36:101140. Available from: https://linkinghub.elsevier.com/retrieve/pii/S2212420919300056
31. Xu H, Xu K, Lian J, Ma C. Compound effects of rainfall and storm tides on coastal flooding risk. Stochastic Environmental Research and Risk Assessment [Internet]. 2019 Jul 20;33(7):1249–61. Available from: http://link.springer.com/10.1007/s00477-019-01695-x
32. Xu T, Li K, Engel BA, Jia H, Leng L, Sun Z, et al. Optimal adaptation pathway for sustainable low impact development planning under deep uncertainty of climate change: A greedy strategy. J Environ Manage [Internet]. 2019 Oct;248:109280. Available from: https://linkinghub.elsevier.com/retrieve/pii/S030147971930982X
33. Hammond MJ, Chen AS, Djordjević S, Butler D, Mark O. Urban flood impact assessment: A state-of-the-art review. Urban Water J [Internet]. 2015 Jan 2;12(1):14–29. Available from: http://www.tandfonline.com/doi/abs/10.1080/1573062X.2013.857421
34. Pradhan-Salike I, Raj Pokharel J. Impact of Urbanization and Climate Change on Urban Flooding: A case of the Kathmandu Valley. Journal of Natural Resources and Development. 2017;56–66.
35. Huong HTL, Pathirana A. Urbanization and climate change impacts on future urban flooding in Can Tho city, Vietnam. Hydrol Earth Syst Sci. 2013;17(1):379–94.
36. Miller JD, Hutchins M. The impacts of urbanisation and climate change on urban flooding and urban water quality: A review of the evidence concerning the United Kingdom. J Hydrol Reg Stud [Internet]. 2017 Aug;12:345–62. Available from: https://linkinghub.elsevier.com/retrieve/pii/S2214581817300435

37. Ahmad D, Afzal M. Household vulnerability and resilience in flood hazards from disaster-prone areas of Punjab, Pakistan. Natural Hazards [Internet]. 2019 Oct 21;99(1):337–54. Available from: http://link.springer.com/10.1007/s11069-019-03743-9
38. Hossain MK, Meng Q. A fine-scale spatial analytics of the assessment and mapping of buildings and population at different risk levels of urban flood. Land use policy [Internet]. 2020 Dec;99:104829. Available from: https://linkinghub.elsevier.com/retrieve/pii/S0264837720305640
39. Goumrasa A, Guendouz M, Guettouche MS, Belaroui A. Flood hazard susceptibility assessment in Chiffa wadi watershed and along the first section of Algeria North–South highway using GIS and AHP method. Applied Geomatics [Internet]. 2021 Dec 2;13(4):565–85. Available from: https://link.springer.com/10.1007/s12518-021-00381-4
40. Faregh W, Benkhaled A. GIS-based multicriteria approach for flood risk assessment in Sigus city, east Algeria. Arabian Journal of Geosciences [Internet]. 2021 Jun 11;14(12):1152. Available from: https://link.springer.com/10.1007/s12517-021-07314-w
41. Ahmed A, Hewa G, Alrajhi A. Flood susceptibility mapping using a geomorphometric approach in South Australian basins. Natural Hazards [Internet]. 2021 Mar 4;106(1):629–53. Available from: http://link.springer.com/10.1007/s11069-020-04481-z
42. Haque MdN, Siddika S, Sresto MA, Saroar MdM, Shabab KR. Geo-spatial Analysis for Flash Flood Susceptibility Mapping in the North-East Haor (Wetland) Region in Bangladesh. Earth Systems and Environment [Internet]. 2021 Jun 11;5(2):365–84. Available from: https://link.springer.com/10.1007/s41748-021-00221-w
43. Baky MA Al, Islam M, Paul S. Flood Hazard, Vulnerability and Risk Assessment for Different Land Use Classes Using a Flow Model. Earth Systems and Environment [Internet]. 2020 Mar 5;4(1):225–44. Available from: http://link.springer.com/10.1007/s41748-019-00141-w
44. Mondal MdSH, Murayama T, Nishikizawa S. Assessing the flood risk of riverine households: A case study from the right bank of the Teesta River, Bangladesh. International Journal of Disaster Risk Reduction [Internet]. 2020 Dec;51:101758. Available from: https://linkinghub.elsevier.com/retrieve/pii/S2212420920312607
45. Rahman M, Chen N, Islam MM, Mahmud GI, Pourghasemi HR, Alam M, et al. Development of flood hazard map and emergency relief operation system using hydrodynamic modeling and machine learning algorithm. J Clean Prod [Internet]. 2021 Aug;311:127594. Available from: https://linkinghub.elsevier.com/retrieve/pii/S0959652621018126
46. Islam MF, Bhattacharya B, Popescu I. Flood risk assessment due to cyclone-induced dike breaching in coastal areas of Bangladesh. Natural Hazards and Earth System Sciences [Internet]. 2019 Feb 14;19(2):353–68. Available from: https://nhess.copernicus.org/articles/19/353/2019/
47. Uddin K, Matin MA. Potential flood hazard zonation and flood shelter suitability mapping for disaster risk mitigation in Bangladesh using geospatial technology. Progress in Disaster Science [Internet]. 2021 Oct;11:100185. Available from: https://linkinghub.elsevier.com/retrieve/pii/S2590061721000454
48. Khairul IM, Rasmy M, Ohara M, Takeuchi K. Developing Flood Vulnerability Functions through Questionnaire Survey for Flood Risk Assessments in the Meghna Basin, Bangladesh. Water (Basel) [Internet]. 2022 Jan 26;14(3):369. Available from: https://www.mdpi.com/2073-4441/14/3/369
49. Chakraborty L, Thistlethwaite J, Minano A, Henstra D, Scott D. Leveraging Hazard, Exposure, and Social Vulnerability Data to Assess Flood Risk to Indigenous Communities in Canada. International Journal of Disaster Risk Science [Internet]. 2021 Dec 10;12(6):821–38. Available from: https://link.springer.com/10.1007/s13753-021-00383-1
50. Das A, Rokaya P, Lindenschmidt KE. Ice-Jam Flood Risk Assessment and Hazard Mapping under Future Climate. J Water Resour Plan Manag [Internet]. 2020 Jun;146(6):04020029. Available from: http://ascelibrary.org/doi/10.1061/%28ASCE%29WR.1943-5452.0001178
51. Link O, Brox-Escudero LM, González J, Aguayo M, Torrejón F, Montalva G, et al. A paleo-hydro-geomorphological perspective on urban flood risk assessment. Hydrol Process [Internet]. 2019 Dec 15;33(25):3169–83. Available from: https://onlinelibrary.wiley.com/doi/10.1002/hyp.13590

52. Cai S, Fan J, Yang W. Flooding Risk Assessment and Analysis Based on GIS and the TFN-AHP Method: A Case Study of Chongqing, China. Atmosphere (Basel) [Internet]. 2021 May 12;12(5):623. Available from: https://www.mdpi.com/2073-4433/12/5/623
53. Liu Q, Yang H, Liu M, Sun R, Zhang J. An Integrated Flood Risk Assessment Model for Cities Located in the Transitional Zone between Taihang Mountains and North China Plain: A Case Study in Shijiazhuang, Hebei, China. Atmosphere (Basel) [Internet]. 2019 Feb 26;10(3):104. Available from: http://www.mdpi.com/2073-4433/10/3/104
54. Zhang D, Shi X, Xu H, Jing Q, Pan X, Liu T, et al. A GIS-based spatial multi-index model for flood risk assessment in the Yangtze River Basin, China. Environ Impact Assess Rev [Internet]. 2020 Jul;83:106397. Available from: https://linkinghub.elsevier.com/retrieve/pii/S0195925520300287
55. Liang C, Li D, Yuan Z, Liao Y, Nie X, Huang B, et al. Assessing urban flood and drought risks under climate change, China. Hydrol Process [Internet]. 2019 Apr 30;33(9):1349–61. Available from: https://onlinelibrary.wiley.com/doi/10.1002/hyp.13405
56. Zhi G, Liao Z, Tian W, Wu J. Urban flood risk assessment and analysis with a 3D visualization method coupling the PP-PSO algorithm and building data. J Environ Manage [Internet]. 2020 Aug;268:110521. Available from: https://linkinghub.elsevier.com/retrieve/pii/S0301479720304552
57. Delalay M, Ziegler AD, Shrestha MS, Gopal V. Methodology for future flood assessment in terms of economic damage: Development and application for a case study in Nepal. J Flood Risk Manag [Internet]. 2020 Sep 26;13(3). Available from: https://onlinelibrary.wiley.com/doi/10.1111/jfr3.12623
58. Chen W, Wang X, Deng S, Liu C, Xie H, Zhu Y. Integrated urban flood vulnerability assessment using local spatial dependence-based probabilistic approach. J Hydrol (Amst) [Internet]. 2019 Aug;575:454–69. Available from: https://linkinghub.elsevier.com/retrieve/pii/S0022169419304883
59. Wu H, Li X, Qian H, Chen J. Improved partial trend method to detect rainfall trends in Hainan Island. Theor Appl Climatol [Internet]. 2019;137(3):2539–47. Available from: https://doi.org/10.1007/s00704-018-02762-z
60. Li W, Lin K, Zhao T, Lan T, Chen X, Du H, et al. Risk assessment and sensitivity analysis of flash floods in ungauged basins using coupled hydrologic and hydrodynamic models. J Hydrol (Amst) [Internet]. 2019 May;572:108–20. Available from: https://linkinghub.elsevier.com/retrieve/pii/S0022169419302197
61. Lin K, Chen H, Xu CY, Yan P, Lan T, Liu Z, et al. Assessment of flash flood risk based on improved analytic hierarchy process method and integrated maximum likelihood clustering algorithm. J Hydrol (Amst) [Internet]. 2020 May;584:124696. Available from: https://linkinghub.elsevier.com/retrieve/pii/S0022169420301566
62. Ma C, Chen Z, Zhao K, Xu H, Qi W. Improved urban flood risk assessment based on spontaneous-triggered risk assessment conceptual model considering road environment. J Hydrol (Amst) [Internet]. 2022 May;608:127693. Available from: https://linkinghub.elsevier.com/retrieve/pii/S0022169422002682
63. Meng X, Chang J, Wang X, Wang Y, Wang Z. Flood control operation coupled with risk assessment for cascade reservoirs. J Hydrol (Amst) [Internet]. 2019 May;572:543–55. Available from: https://linkinghub.elsevier.com/retrieve/pii/S0022169419302847
64. Qiang Y, Zhang L, He J, Xiao T, Huang H, Wang H. Urban flood analysis for Pearl River Delta cities using an equivalent drainage method upon combined rainfall-high tide-storm surge events. J Hydrol (Amst) [Internet]. 2021 Jun;597:126293. Available from: https://linkinghub.elsevier.com/retrieve/pii/S0022169421003401
65. Wang H, Huang S, Fang W, Hou B, Leng G, Huang Q, et al. Multivariable flood risk and its dynamics considering project reasonable service life in a changing environment. J Hydrol (Amst) [Internet]. 2020 Nov;590:125524. Available from: https://linkinghub.elsevier.com/retrieve/pii/S0022169420309847
66. Wang S, Mu L, Yao Z, Gao J, Zhao E, Wang L. Assessing and zoning of typhoon storm surge risk with a geographic information system (GIS) technique: a case study of the coastal area of Huizhou. Natural Hazards and Earth System Sciences [Internet]. 2021 Jan 29;21(1):439–62. Available from: https://nhess.copernicus.org/articles/21/439/2021/

67. Wu Z, Shen Y, Wang H, Wu M. Urban flood disaster risk evaluation based on ontology and Bayesian Network. J Hydrol (Amst) [Internet]. 2020 Apr;583:124596. Available from: https://linkinghub.elsevier.com/retrieve/pii/S0022169420300561
68. Xu H, Ma C, Lian J, Xu K, Chaima E. Urban flooding risk assessment based on an integrated k-means cluster algorithm and improved entropy weight method in the region of Haikou, China. J Hydrol (Amst) [Internet]. 2018 Aug;563:975–86. Available from: https://linkinghub.elsevier.com/retrieve/pii/S0022169418304827
69. Li Z, Song K, Peng L. Flood Risk Assessment under Land Use and Climate Change in Wuhan City of the Yangtze River Basin, China. Land (Basel) [Internet]. 2021 Aug 21;10(8):878. Available from: https://www.mdpi.com/2073-445X/10/8/878
70. Ma M, Liu C, Zhao G, Xie H, Jia P, Wang D, et al. Flash Flood Risk Analysis Based on Machine Learning Techniques in the Yunnan Province, China. Remote Sens (Basel) [Internet]. 2019 Jan 17;11(2):170. Available from: http://www.mdpi.com/2072-4292/11/2/170
71. Lai C, Chen X, Wang Z, Yu H, Bai X. Flood Risk Assessment and Regionalization from Past and Future Perspectives at Basin Scale. Risk Analysis [Internet]. 2020 Jul 2;40(7):1399–417. Available from: https://onlinelibrary.wiley.com/doi/10.1111/risa.13493
72. Lin W, Sun Y, Nijhuis S, Wang Z. Scenario-based flood risk assessment for urbanizing deltas using future land-use simulation (FLUS): Guangzhou Metropolitan Area as a case study. Science of The Total Environment [Internet]. 2020 Oct;739:139899. Available from: https://linkinghub.elsevier.com/retrieve/pii/S0048969720334197
73. Zhao G, Pang B, Xu Z, Yue J, Tu T. Mapping flood susceptibility in mountainous areas on a national scale in China. Science of The Total Environment [Internet]. 2018 Feb;615:1133–42. Available from: https://linkinghub.elsevier.com/retrieve/pii/S0048969717327419
74. Zhou Y, Shen D, Huang N, Guo Y, Zhang T, Zhang Y. Urban flood risk assessment using storm characteristic parameters sensitive to catchment-specific drainage system. Science of The Total Environment [Internet]. 2019 Apr;659:1362–9. Available from: https://linkinghub.elsevier.com/retrieve/pii/S004896971930004X
75. Zhang J, Chen Y. Risk Assessment of Flood Disaster Induced by Typhoon Rainstorms in Guangdong Province, China. Sustainability [Internet]. 2019 May 14;11(10):2738. Available from: https://www.mdpi.com/2071-1050/11/10/2738
76. Lyu HM, Shen SL, Zhou AN, Zhou WH. Flood risk assessment of metro systems in a subsiding environment using the interval FAHP-FCA approach. Sustain Cities Soc [Internet]. 2019 Oct;50:101682. Available from: https://linkinghub.elsevier.com/retrieve/pii/S2210670719305293
77. Lyu HM, Shen SL, Zhou A, Yang J. Perspectives for flood risk assessment and management for mega-city metro system. Tunnelling and Underground Space Technology [Internet]. 2019 Feb;84:31–44. Available from: https://linkinghub.elsevier.com/retrieve/pii/S0886779818305716
78. Cai T, Li X, Ding X, Wang J, Zhan J. Flood risk assessment based on hydrodynamic model and fuzzy comprehensive evaluation with GIS technique. International Journal of Disaster Risk Reduction [Internet]. 2019 Apr;35:101077. Available from: https://linkinghub.elsevier.com/retrieve/pii/S2212420918313505
79. Wang N, Hou J, Du Y, Jing H, Wang T, Xia J, et al. A dynamic, convenient and accurate method for assessing the flood risk of people and vehicle. Science of The Total Environment [Internet]. 2021 Nov;797:149036. Available from: https://linkinghub.elsevier.com/retrieve/pii/S0048969721041085
80. Quesada-Román A. Flood risk index development at the municipal level in Costa Rica: A methodological framework. Environ Sci Policy [Internet]. 2022 Jul;133:98–106. Available from: https://linkinghub.elsevier.com/retrieve/pii/S1462901122000995
81. Elboshy B, Kanae S, Gamaleldin M, Ayad H, Osaragi T, Elbarki W. A framework for pluvial flood risk assessment in Alexandria considering the coping capacity. Environ Syst Decis [Internet]. 2019 Mar 4;39(1):77–94. Available from: http://link.springer.com/10.1007/s10669-018-9684-7
82. De Risi R, Jalayer F, De Paola F, Carozza S, Yonas N, Giugni M, et al. From flood risk mapping toward reducing vulnerability: the case of Addis Ababa. Natural Hazards [Internet]. 2020 Jan 2;100(1):387–415. Available from: http://link.springer.com/10.1007/s11069-019-03817-8

83. Haer T, Husby TG, Botzen WJW, Aerts JCJH. The safe development paradox: An agent-based model for flood risk under climate change in the European Union. Global Environmental Change [Internet]. 2020 Jan;60:102009. Available from: https://linkinghub.elsevier.com/retrieve/pii/S0959378018314079
84. Schwiersch N, Heyer T, Stamm J. Enriching flood risk analyses with distributions of soil mechanical parameters through the statistical analysis of classification experiments. J Flood Risk Manag [Internet]. 2022 Jun 8;15(2). Available from: https://onlinelibrary.wiley.com/doi/10.1111/jfr3.12791
85. Trepekli K, Balstrøm T, Friborg T, Fog B, Allotey AN, Kofie RY, et al. UAV-borne, LiDAR-based elevation modelling: a method for improving local-scale urban flood risk assessment. Natural Hazards [Internet]. 2022 Mar 22; Available from: https://link.springer.com/10.1007/s11069-022-05308-9
86. Yu X, Moraetis D, Nikolaidis NP, Li B, Duffy C, Liu B. A coupled surface-subsurface hydrologic model to assess groundwater flood risk spatially and temporally. Environmental Modelling & Software [Internet]. 2019 Apr;114:129–39. Available from: https://linkinghub.elsevier.com/retrieve/pii/S1364815218309204
87. Skilodimou HD, Bathrellos GD, Alexakis DE. Flood Hazard Assessment Mapping in Burned and Urban Areas. Sustainability [Internet]. 2021 Apr 16;13(8):4455. Available from: https://www.mdpi.com/2071-1050/13/8/4455
88. Glas H, De Maeyer P, Merisier S, Deruyter G. Development of a low-cost methodology for data acquisition and flood risk assessment in the floodplain of the river Moustiques in Haiti. J Flood Risk Manag [Internet]. 2020 Jun 19;13(2). Available from: https://onlinelibrary.wiley.com/doi/10.1111/jfr3.12608
89. Arya AK, Singh AP. Multi criteria analysis for flood hazard mapping using GIS techniques: a case study of Ghaghara River basin in Uttar Pradesh, India. Arabian Journal of Geosciences [Internet]. 2021 Apr 2;14(8):656. Available from: https://link.springer.com/10.1007/s12517-021-06971-1
90. Roy S, Bose A, Chowdhury IR. Flood risk assessment using geospatial data and multi-criteria decision approach: a study from historically active flood-prone region of Himalayan foothill, India. Arabian Journal of Geosciences [Internet]. 2021 Jun 27;14(11):999. Available from: https://link.springer.com/10.1007/s12517-021-07324-8
91. Chakrabortty R, Chandra Pal S, Rezaie F, Arabameri A, Lee S, Roy P, et al. Flash-flood hazard susceptibility mapping in Kangsabati River Basin, India. Geocarto Int [Internet]. 2021 Jul 26;1–23. Available from: https://www.tandfonline.com/doi/full/10.1080/10106049.2021.1953618
92. Singh P, Sinha VSP, Vijhani A, Pahuja N. Vulnerability assessment of urban road network from urban flood. International Journal of Disaster Risk Reduction [Internet]. 2018 Jun;28:237–50. Available from: https://linkinghub.elsevier.com/retrieve/pii/S2212420918303261
93. Waghwala RK, Agnihotri PG. Flood risk assessment and resilience strategies for flood risk management: A case study of Surat City. International Journal of Disaster Risk Reduction [Internet]. 2019 Nov;40:101155. Available from: https://linkinghub.elsevier.com/retrieve/pii/S2212420918314493
94. Karmokar S, De M. Flash flood risk assessment for drainage basins in the Himalayan foreland of Jalpaiguri and Darjeeling Districts, West Bengal. Model Earth Syst Environ [Internet]. 2020 Dec 13;6(4):2263–89. Available from: https://link.springer.com/10.1007/s40808-020-00807-9
95. Chakraborty S, Mukhopadhyay S. Assessing flood risk using analytical hierarchy process (AHP) and geographical information system (GIS): application in Coochbehar district of West Bengal, India. Natural Hazards [Internet]. 2019;99(1):247–74. Available from: https://doi.org/10.1007/s11069-019-03737-7
96. Chattaraj D, Paul B, Sarkar S. Integrated Multi-parametric Analytic Hierarchy Process (AHP) and Geographic Information System (GIS) based Spatial modelling for Flood and Water logging Susceptibility Mapping: A case study of English Bazar Municipality of Malda, West Bengal, India. Natural Hazards and Earth System Sciences Discussions. 2021;(January):1–20.
97. Tripathi G, Pandey AC, Parida BR. Flood Hazard and Risk Zonation in North Bihar Using Satellite-Derived Historical Flood Events and Socio-Economic Data. Sustainability [Internet]. 2022 Jan 27;14(3):1472. Available from: https://www.mdpi.com/2071-1050/14/3/1472

98. Gayen S, Villalta IV, Haque SM. Flood Risk Assessment and Its Mapping in Purba Medinipur District, West Bengal, India. Water (Basel) [Internet]. 2022 Mar 26;14(7):1049. Available from: https://www.mdpi.com/2073-4441/14/7/1049
99. Yudianto D, Ginting BM, Sanjaya S, Rusli SR, Wicaksono A. A Framework of Dam-Break Hazard Risk Mapping for a Data-Sparse Region in Indonesia. ISPRS Int J Geoinf [Internet]. 2021 Feb 26;10(3):110. Available from: https://www.mdpi.com/2220-9964/10/3/110
100. Yildirim E, Demir I. An Integrated Flood Risk Assessment and Mitigation Framework: A Case Study for Middle Cedar River Basin, Iowa, US. International Journal of Disaster Risk Reduction [Internet]. 2021 Apr;56:102113. Available from: https://linkinghub.elsevier.com/retrieve/pii/S2212420921000790
101. Malekinezhad H, Sepehri M, Pham QB, Hosseini SZ, Meshram SG, Vojtek M, et al. Application of entropy weighting method for urban flood hazard mapping. Acta Geophysica [Internet]. 2021 Jun 3;69(3):841–54. Available from: https://link.springer.com/10.1007/s11600-021-00586-6
102. Eini M, Kaboli HS, Rashidian M, Hedayat H. Hazard and vulnerability in urban flood risk mapping: Machine learning techniques and considering the role of urban districts. International Journal of Disaster Risk Reduction [Internet]. 2020 Nov;50:101687. Available from: https://linkinghub.elsevier.com/retrieve/pii/S2212420920303484
103. Rafiei-Sardooi E, Azareh A, Choubin B, Mosavi AH, Clague JJ. Evaluating urban flood risk using hybrid method of TOPSIS and machine learning. International Journal of Disaster Risk Reduction [Internet]. 2021 Dec;66:102614. Available from: https://linkinghub.elsevier.com/retrieve/pii/S2212420921005756
104. Darabi H, Choubin B, Rahmati O, Torabi Haghighi A, Pradhan B, Kløve B. Urban flood risk mapping using the GARP and QUEST models: A comparative study of machine learning techniques. J Hydrol (Amst) [Internet]. 2019;569:142–54. Available from: https://www.sciencedirect.com/science/article/pii/S0022169418309302
105. Mohammadi M, Darabi H, Mirchooli F, Bakhshaee A, Torabi Haghighi A. Flood risk mapping and crop-water loss modeling using water footprint analysis in agricultural watershed, northern Iran. Natural Hazards [Internet]. 2021 Jan 30;105(2):2007–25. Available from: http://link.springer.com/10.1007/s11069-020-04387-w
106. Farhadi H, Najafzadeh M. Flood Risk Mapping by Remote Sensing Data and Random Forest Technique. Water (Basel) [Internet]. 2021 Nov 4;13(21):3115. Available from: https://www.mdpi.com/2073-4441/13/21/3115
107. Rahmati, Darabi, Haghighi, Stefanidis, Kornejady, Nalivan, et al. Urban Flood Hazard Modeling Using Self-Organizing Map Neural Network. Water (Basel) [Internet]. 2019 Nov 12;11(11):2370. Available from: https://www.mdpi.com/2073-4441/11/11/2370
108. Lompi M, Caporali E, Mediero L, Mazzanti B. Improving flash flood risk assessment using a simple approach for extreme rainfall scaling and storms transposition. J Flood Risk Manag [Internet]. 2022 Mar 24; Available from: https://onlinelibrary.wiley.com/doi/10.1111/jfr3.12796
109. Apollonio C, Bruno MF, Iemmolo G, Molfetta MG, Pellicani R. Flood Risk Evaluation in Ungauged Coastal Areas: The Case Study of Ippocampo (Southern Italy). Water (Basel) [Internet]. 2020 May 21;12(5):1466. Available from: https://www.mdpi.com/2073-4441/12/5/1466
110. Jiang X, Yang L, Tatano H. Assessing Spatial Flood Risk from Multiple Flood Sources in a Small River Basin: A Method Based on Multivariate Design Rainfall. Water (Basel) [Internet]. 2019 May 17;11(5):1031. Available from: https://www.mdpi.com/2073-4441/11/5/1031
111. Park K, Won J hun. Analysis on distribution characteristics of building use with risk zone classification based on urban flood risk assessment. International Journal of Disaster Risk Reduction [Internet]. 2019 Aug;38:101192. Available from: https://linkinghub.elsevier.com/retrieve/pii/S2212420919301542
112. Joo H, Choi C, Kim J, Kim D, Kim S, Kim HS. A Bayesian Network-Based Integrated for Flood Risk Assessment (InFRA). Sustainability [Internet]. 2019 Jul 9;11(13):3733. Available from: https://www.mdpi.com/2071-1050/11/13/3733
113. Romali NS, Yusop Z. Flood damage and risk assessment for urban area in Malaysia. Hydrology Research [Internet]. 2021 Feb 1;52(1):142–59. Available from: https://iwaponline.com/hr/article/52/1/142/75723/Flood-damage-and-risk-assessment-for-urban-area-in

114. Ziarh GF, Asaduzzaman M, Dewan A, Nashwan MS, Shahid S. Integration of catastrophe and entropy theories for flood risk mapping in peninsular Malaysia. J Flood Risk Manag [Internet]. 2021 Mar 25;14(1). Available from: https://onlinelibrary.wiley.com/doi/10.1111/jfr3.12686
115. Shrestha BB, Kawasaki A. Quantitative assessment of flood risk with evaluation of the effectiveness of dam operation for flood control: A case of the Bago River Basin of Myanmar. International Journal of Disaster Risk Reduction [Internet]. 2020 Nov;50:101707. Available from: https://linkinghub.elsevier.com/retrieve/pii/S221242092030412X
116. Mahmood S, Rahman A ur, Shaw R. Spatial appraisal of flood risk assessment and evaluation using integrated hydro-probabilistic approach in Panjkora River Basin, Pakistan. Environ Monit Assess [Internet]. 2019 Sep 17;191(9):573. Available from: http://link.springer.com/10.1007/s10661-019-7746-z
117. Rana IA, Routray JK. Multidimensional Model for Vulnerability Assessment of Urban Flooding: An Empirical Study in Pakistan. International Journal of Disaster Risk Science [Internet]. 2018 Sep 27;9(3):359–75. Available from: http://link.springer.com/10.1007/s13753-018-0179-4
118. Cabrera JS, Lee HS. Flood risk assessment for Davao Oriental in the Philippines using geographic information system-based multi-criteria analysis and the maximum entropy model. J Flood Risk Manag [Internet]. 2020 Jun 18;13(2). Available from: https://onlinelibrary.wiley.com/doi/10.1111/jfr3.12607
119. Figueiredo R, Romão X, Paupério E. Flood risk assessment of cultural heritage at large spatial scales: Framework and application to mainland Portugal. J Cult Herit [Internet]. 2020 May;43:163–74. Available from: https://linkinghub.elsevier.com/retrieve/pii/S1296207419306521
120. Santos PP, Pereira S, Zêzere JL, Tavares AO, Reis E, Garcia RAC, et al. A comprehensive approach to understanding flood risk drivers at the municipal level. J Environ Manage [Internet]. 2020 Apr;260:110127. Available from: https://linkinghub.elsevier.com/retrieve/pii/S0301479720300657
121. Ferreira TM, Santos PP. An Integrated Approach for Assessing Flood Risk in Historic City Centres. Water (Basel) [Internet]. 2020 Jun 9;12(6):1648. Available from: https://www.mdpi.com/2073-4441/12/6/1648
122. Motta M, de Castro Neto M, Sarmento P. A mixed approach for urban flood prediction using Machine Learning and GIS. International Journal of Disaster Risk Reduction [Internet]. 2021 Apr;56:102154. Available from: https://linkinghub.elsevier.com/retrieve/pii/S2212420921001205
123. Costache R. Flood Susceptibility Assessment by Using Bivariate Statistics and Machine Learning Models - A Useful Tool for Flood Risk Management. Water Resources Management [Internet]. 2019 Jul 6;33(9):3239–56. Available from: http://link.springer.com/10.1007/s11269-019-02301-z
124. Najafi MR, Zhang Y, Martyn N. A flood risk assessment framework for interdependent infrastructure systems in coastal environments. Sustain Cities Soc [Internet]. 2021 Jan;64:102516. Available from: https://linkinghub.elsevier.com/retrieve/pii/S2210670720307332
125. Radwan F, Alazba AA, Mossad A. Flood risk assessment and mapping using AHP in arid and semiarid regions. Acta Geophysica [Internet]. 2019;67(1):215–29. Available from: https://doi.org/10.1007/s11600-018-0233-z
126. Zeleňáková M, Fijko R, Labant S, Weiss E, Markovič G, Weiss R. Flood risk modelling of the Slatvinec stream in Kružlov village, Slovakia. J Clean Prod [Internet]. 2019 Mar;212:109–18. Available from: https://linkinghub.elsevier.com/retrieve/pii/S0959652618337107
127. Solín Ľ, Rusnák M. Preliminary flood risk assessment: Case study of systematic processing of available or readily derivable information. Water and Environment Journal [Internet]. 2020 Dec 8;34(S1):683–98. Available from: https://onlinelibrary.wiley.com/doi/10.1111/wej.12570
128. Criado M, Martínez-Graña A, San Román J, Santos-Francés F. Flood Risk Evaluation in Urban Spaces: The Study Case of Tormes River (Salamanca, Spain). Int J Environ Res Public Health [Internet]. 2018 Dec 20;16(1):5. Available from: http://www.mdpi.com/1660-4601/16/1/5
129. Jato-Espino D, Lobo A, Ascorbe-Salcedo A. Urban flood risk mapping using an optimised additive weighting methodology based on open data. J Flood Risk Manag [Internet]. 2019 Oct 17;12(S1). Available from: https://onlinelibrary.wiley.com/doi/10.1111/jfr3.12533

130. Betancourt-Suárez V, García-Botella E, Ramon-Morte A. Flood Mapping Proposal in Small Watersheds: A Case Study of the Rebollos and Miranda Ephemeral Streams (Cartagena, Spain). Water (Basel) [Internet]. 2021 Jan 4;13(1):102. Available from: https://www.mdpi.com/2073-4441/13/1/102
131. Garrote J, Díez-Herrero A, Escudero C, García I. A Framework Proposal for Regional-Scale Flood-Risk Assessment of Cultural Heritage Sites and Application to the Castile and León Region (Central Spain). Water (Basel) [Internet]. 2020 Jan 23;12(2):329. Available from: https://www.mdpi.com/2073-4441/12/2/329
132. Tascón-González L, Ferrer-Julià M, Ruiz M, García-Meléndez E. Social Vulnerability Assessment for Flood Risk Analysis. Water (Basel) [Internet]. 2020 Feb 17;12(2):558. Available from: https://www.mdpi.com/2073-4441/12/2/558
133. Ertan S, Çelik RN. The Assessment of Urbanization Effect and Sustainable Drainage Solutions on Flood Hazard by GIS. Sustainability [Internet]. 2021 Feb 20;13(4):2293. Available from: https://www.mdpi.com/2071-1050/13/4/2293
134. Yalcin E. Two-dimensional hydrodynamic modelling for urban flood risk assessment using unmanned aerial vehicle imagery: A case study of Kirsehir, Turkey. J Flood Risk Manag [Internet]. 2019 Oct 21;12(S1). Available from: https://onlinelibrary.wiley.com/doi/10.1111/jfr3.12499
135. Eryılmaz Türkkan G, Hırca T. The investigation of flood risk perception as a quantitative analysis from socio-demographic perspective. Natural Hazards [Internet]. 2021 Mar 2;106(1):715–33. Available from: http://link.springer.com/10.1007/s11069-020-04488-6
136. Sajjad M, Lin N, Chan JCL. Spatial heterogeneities of current and future hurricane flood risk along the U.S. Atlantic and Gulf coasts. Science of The Total Environment [Internet]. 2020 Apr;713:136704. Available from: https://linkinghub.elsevier.com/retrieve/pii/S004896972030214X
137. Chang H, Pallathadka A, Sauer J, Grimm NB, Zimmerman R, Cheng C, et al. Assessment of urban flood vulnerability using the social-ecological-technological systems framework in six US cities. Sustain Cities Soc [Internet]. 2021 May;68:102786. Available from: https://linkinghub.elsevier.com/retrieve/pii/S2210670721000780
138. Dung NB, Long NQ, An DT, Minh DT. Multi-geospatial flood hazard modelling for a large and complex river basin with data sparsity: a case study of the Lam River Basin, Vietnam. Earth Systems and Environment [Internet]. 2021 Mar 29; Available from: http://link.springer.com/10.1007/s41748-021-00215-8
139. Luu C, von Meding J, Mojtahedi M. Analyzing Vietnam's national disaster loss database for flood risk assessment using multiple linear regression-TOPSIS. International Journal of Disaster Risk Reduction [Internet]. 2019 Nov;40:101153. Available from: https://linkinghub.elsevier.com/retrieve/pii/S221242091830949X
140. Pham BT, Luu C, Phong T Van, Nguyen HD, Le H Van, Tran TQ, et al. Flood risk assessment using hybrid artificial intelligence models integrated with multi-criteria decision analysis in Quang Nam Province, Vietnam. J Hydrol (Amst) [Internet]. 2021 Jan;592:125815. Available from: https://linkinghub.elsevier.com/retrieve/pii/S0022169420312762
141. Nguyen HD, Fox D, Dang DK, Pham LT, Viet Du QV, Nguyen THT, et al. Predicting Future Urban Flood Risk Using Land Change and Hydraulic Modeling in a River Watershed in the Central Province of Vietnam. Remote Sens (Basel) [Internet]. 2021 Jan 13;13(2):262. Available from: https://www.mdpi.com/2072-4292/13/2/262
142. Shen Y, Morsy MM, Huxley C, Tahvildari N, Goodall JL. Flood risk assessment and increased resilience for coastal urban watersheds under the combined impact of storm tide and heavy rainfall. J Hydrol (Amst) [Internet]. 2019 Dec;579:124159. Available from: https://linkinghub.elsevier.com/retrieve/pii/S0022169419308947
143. Örmeci B. An Overview of Water Supply, Use and Treatment in Canada. In 2015. p. 114–27.
144. Waghwala RK, Agnihotri PG. Flood risk assessment and resilience strategies for flood risk management: A case study of Surat City. International Journal of Disaster Risk Reduction [Internet]. 2019 Nov;40:101155. Available from: https://linkinghub.elsevier.com/retrieve/pii/S2212420918314493

145. Qi W, Ma C, Xu H, Chen Z, Zhao K, Han H. A review on applications of urban flood models in flood mitigation strategies. Natural Hazards [Internet]. 2021 Aug 30;108(1):31–62. Available from: https://link.springer.com/10.1007/s11069-021-04715-8
146. Malavasi S, Guadagnini A. Hydrodynamic Loading on River Bridges. Journal of Hydraulic Engineering. 2003 Nov;129(11):854–61.
147. Devia GK, Ganasri BP, Dwarakish GS. A Review on Hydrological Models. Aquat Procedia [Internet]. 2015;4:1001–7. Available from: https://linkinghub.elsevier.com/retrieve/pii/S2214241X15001273
148. Hadid B, Duviella E, Lecoeuche S. Data-driven modeling for river flood forecasting based on a piecewise linear ARX system identification. J Process Control [Internet]. 2020 Feb;86:44–56. Available from: https://linkinghub.elsevier.com/retrieve/pii/S0959152419304688
149. Perera EDP, Lahat L. Fuzzy logic based flood forecasting model for the Kelantan River basin, Malaysia. Journal of Hydro-environment Research [Internet]. 2015 Dec;9(4):542–53. Available from: https://linkinghub.elsevier.com/retrieve/pii/S1570644314000835
150. Sahoo GB, Ray C, De Carlo EH. Calibration and validation of a physically distributed hydrological model, MIKE SHE, to predict streamflow at high frequency in a flashy mountainous Hawaii stream. J Hydrol (Amst). 2006 Jul;327(1–2):94–109.
151. Leandro J, Djordjević S, Chen AS, Savić DA, Stanić M. Calibration of a 1D/1D urban flood model using 1D/2D model results in the absence of field data. Water Science and Technology [Internet]. 2011 Sep 1;64(5):1016–24. Available from: https://iwaponline.com/wst/article/64/5/1016/16965/Calibration-of-a-1D1D-urban-flood-model-using-1D2D
152. Su B, Huang H, Zhu W. An urban pluvial flood simulation model based on diffusive wave approximation of shallow water equations. Hydrology Research [Internet]. 2019 Feb 1;50(1):138–54. Available from: https://iwaponline.com/hr/article/50/1/138/38826/An-urban-pluvial-flood-simulation-model-based-on
153. Hou J, Simons F, Mahgoub M, Hinkelmann R. A robust well-balanced model on unstructured grids for shallow water flows with wetting and drying over complex topography. Comput Methods Appl Mech Eng [Internet]. 2013 Apr;257:126–49. Available from: https://linkinghub.elsevier.com/retrieve/pii/S0045782513000339
154. Hu X, Song L. Hydrodynamic modeling of flash flood in mountain watersheds based on high-performance GPU computing. Natural Hazards [Internet]. 2018 Mar 8;91(2):567–86. Available from: http://link.springer.com/10.1007/s11069-017-3141-7
155. Datta P, Das S. Analysis of long-term seasonal and annual temperature trends in North Bengal, India. Spatial Information Research [Internet]. 2019;27(4):475–96. Available from: https://doi.org/10.1007/s41324-019-00250-8
156. ShahiriParsa A, Noori M, Heydari M, Rashidi M. Floodplain Zoning Simulation by Using HEC-RAS and CCHE2D Models in the Sungai Maka River. Air, Soil and Water Research [Internet]. 2016 Jan 19;9:ASWR.S36089. Available from: http://journals.sagepub.com/doi/10.4137/ASWR.S36089
157. Wu X, Wang Z, Guo S, Lai C, Chen X. A simplified approach for flood modeling in urban environments. Hydrology Research [Internet]. 2018 Dec 1;49(6):1804–16. Available from: https://iwaponline.com/hr/article/49/6/1804/40890/A-simplified-approach-for-flood-modeling-in-urban
158. De Wrachien D, Mambretti S, Sole A. Mathematical models in flood management: overview and challenges. In 2010. p. 61–72. Available from: http://library.witpress.com/viewpaper.asp?pcode=FRIAR10-006-1
159. Jacovkis PM, Tabak EG. A kinematic wave model for rivers with flood plains and other irregular geometries. Math Comput Model [Internet]. 1996 Dec;24(11):1–21. Available from: https://linkinghub.elsevier.com/retrieve/pii/S0895717796001690
160. Vergara H, Kirstetter PE, Gourley JJ, Flamig ZL, Hong Y, Arthur A, et al. Estimating a-priori kinematic wave model parameters based on regionalization for flash flood forecasting in the Conterminous United States. J Hydrol (Amst) [Internet]. 2016 Oct;541:421–33. Available from: https://linkinghub.elsevier.com/retrieve/pii/S0022169416303626
161. Tsai CW. Applicability of Kinematic, Noninertia, and Quasi-Steady Dynamic Wave Models to Unsteady Flow Routing. Journal of Hydraulic Engineering [Internet]. 2003 Aug;129(8):613–27.

Available from: https://ascelibrary.org/doi/10.1061/%28ASCE%290733-9429%282003%29129%3A8%28613%29
162. Masood M, Takeuchi K. Assessment of flood hazard, vulnerability and risk of mid-eastern Dhaka using DEM and 1D hydrodynamic model. Natural Hazards [Internet]. 2012;61(2):757–70. Available from: https://doi.org/10.1007/s11069-011-0060-x
163. Barati R, Rahimi S, Akbari GH. Analysis of dynamic wave model for flood routing in natural rivers. Water Science and Engineering [Internet]. 2012;5(3):243–58. Available from: https://www.sciencedirect.com/science/article/pii/S1674237015302003
164. Perdikaris J, Gharabaghi B, Rudra R. Evaluation of the Simplified Dynamic Wave, Diffusion Wave and the Full Dynamic Wave Flood Routing Models. Earth Science Research [Internet]. 2018 May 4;7(2):14. Available from: http://www.ccsenet.org/journal/index.php/esr/article/view/75183
165. Bharali B, Misra UK. An approach for prediction of flood hydrograph at outlet of an ungauged basin using modified dynamic wave model. ISH Journal of Hydraulic Engineering [Internet]. 2021 Mar 23;1–11. Available from: https://www.tandfonline.com/doi/full/10.1080/09715010.2021.1901250
166. Tang Z, Zhang H, Yi S, Xiao Y. Assessment of flood susceptible areas using spatially explicit, probabilistic multi-criteria decision analysis. J Hydrol (Amst) [Internet]. 2018;558:144–58. Available from: https://www.sciencedirect.com/science/article/pii/S0022169418300349
167. Souissi D, Zouhri L, Hammami S, Msaddek MH, Zghibi A, Dlala M. GIS-based MCDM – AHP modeling for flood susceptibility mapping of arid areas, southeastern Tunisia. Geocarto Int [Internet]. 2020 Jul 3;35(9):991–1017. Available from: https://doi.org/10.1080/10106049.2019.1566405
168. Hammami S, Zouhri L, Souissi D, Souei A, Zghibi A, Marzougui A, et al. Application of the GIS based multi-criteria decision analysis and analytical hierarchy process (AHP) in the flood susceptibility mapping (Tunisia). Arabian Journal of Geosciences [Internet]. 2019;12(21):653. Available from: https://doi.org/10.1007/s12517-019-4754-9
169. Fu M, Fan T, Ding Z, Salih SQ, Al-Ansari N, Yaseen ZM. Deep Learning Data-Intelligence Model Based on Adjusted Forecasting Window Scale: Application in Daily Streamflow Simulation. IEEE Access [Internet]. 2020;8:32632–51. Available from: https://ieeexplore.ieee.org/document/9007531/
170. Gibson MJ, Savic DA, Djordjevic S, Chen AS, Fraser S, Watson T. Accuracy and Computational Efficiency of 2D Urban Surface Flood Modelling Based on Cellular Automata. Procedia Eng [Internet]. 2016;154:801–10. Available from: https://linkinghub.elsevier.com/retrieve/pii/S1877705816317970
171. Ghimire B, Chen AS, Guidolin M, Keedwell EC, Djordjević S, Savić DA. Formulation of a fast 2D urban pluvial flood model using a cellular automata approach. Journal of Hydroinformatics [Internet]. 2013 Jul 1;15(3):676–86. Available from: https://iwaponline.com/jh/article/15/3/676/3279/Formulation-of-a-fast-2D-urban-pluvial-flood-model
172. Jamali B, Bach PM, Cunningham L, Deletic A. A Cellular Automata Fast Flood Evaluation (CA-ffé) Model. Water Resour Res [Internet]. 2019 Jun 21;55(6):4936–53. Available from: https://onlinelibrary.wiley.com/doi/10.1029/2018WR023679
173. Guidolin M, Chen AS, Ghimire B, Keedwell EC, Djordjević S, Savić DA. A weighted cellular automata 2D inundation model for rapid flood analysis. Environmental Modelling & Software [Internet]. 2016 Oct;84:378–94. Available from: https://linkinghub.elsevier.com/retrieve/pii/S1364815216303243
174. Rahman M, Ningsheng C, Islam MM, Dewan A, Iqbal J, Washakh RMA, et al. Flood Susceptibility Assessment in Bangladesh Using Machine Learning and Multi-criteria Decision Analysis. Earth Systems and Environment [Internet]. 2019;3(3):585–601. Available from: https://doi.org/10.1007/s41748-019-00123-y
175. Li X, Yan D, Wang K, Weng B, Qin T, Liu S. Flood Risk Assessment of Global Watersheds Based on Multiple Machine Learning Models. Water (Basel) [Internet]. 2019 Aug 10;11(8):1654. Available from: https://www.mdpi.com/2073-4441/11/8/1654
176. Pradhan B. Flood susceptible mapping and risk area delineation using logistic regression, GIS and remote sensing. Journal of Spatial Hydrology. 2010;9(2):1–18.
177. Pourghasemi HR, Moradi HR, Fatemi Aghda SM. Landslide susceptibility mapping by binary logistic regression, analytical hierarchy process, and statistical index models and assessment of their

performances. Natural Hazards [Internet]. 2013 Oct 25;69(1):749–79. Available from: http://link.springer.com/10.1007/s11069-013-0728-5
178. Abraham S, Huynh C, Vu H. Classification of Soils into Hydrologic Groups Using Machine Learning. Data (Basel) [Internet]. 2019 Dec 19;5(1):2. Available from: https://www.mdpi.com/2306-5729/5/1/2
179. Tehrany MS, Jones S, Shabani F. Identifying the essential flood conditioning factors for flood prone area mapping using machine learning techniques. Catena (Amst) [Internet]. 2019;175:174–92. Available from: https://www.sciencedirect.com/science/article/pii/S0341816218305472
180. Tehrany MS, Pradhan B, Mansor S, Ahmad N. Flood susceptibility assessment using GIS-based support vector machine model with different kernel types. Catena (Amst) [Internet]. 2015 Feb;125:91–101. Available from: https://linkinghub.elsevier.com/retrieve/pii/S034181621400294X
181. Elsafi SH. Artificial neural networks (ANNs) for flood forecasting at Dongola Station in the River Nile, Sudan. Alexandria Engineering Journal. 2014;53(3):655–62.
182. Chu PS, Zhao X, Ruan Y, Grubbs M. Extreme rainfall events in the Hawaiian Islands. J Appl Meteorol Climatol. 2009;48(3):502–16.
183. Muzik I. Lumped Modeling and GIS in Flood Prediction. In 1996. p. 269–301. Available from: http://link.springer.com/10.1007/978-94-015-8745-7_10
184. MUZIK I. FLOOD MODELLING WITH GIS-DERIVED DISTRIBUTED UNIT HYDROGRAPHS. Hydrol Process [Internet]. 1996 Jan 1;10(10):1401–9. Available from: https://doi.org/10.1002/(SICI)1099-1085(199610)10:10%3C1401::AID-HYP469%3E3.0.CO
185. Nsangou D, Kpoumié A, Mfonka Z, Bateni SM, Ngouh AN, Ndam Ngoupayou JR. The Mfoundi Watershed at Yaoundé in the Humid Tropical Zone of Cameroon: A Case Study of Urban Flood Susceptibility Mapping. Earth Systems and Environment. 2022 Jan 23;6(1):99–120.
186. Online R, Ogie RI, Holderness T, Dunn S, Turpin E. Vulnerability analysis of hydrological infrastructure to flooding in coastal cities - a graph theory approach. In: Transforming the Future of Infrastructure Through Smarter Information: Proceedings of the International Conference on Smart Infrastructure and Construction [Internet]. 2016. p. 633–44. Available from: http://ro.uow.edu.au/eispapers/6441
187. Darabi H, Choubin B, Rahmati O, Torabi Haghighi A, Pradhan B, Kløve B. Urban flood risk mapping using the GARP and QUEST models: A comparative study of machine learning techniques. J Hydrol (Amst) [Internet]. 2019 Feb;569:142–54. Available from: https://linkinghub.elsevier.com/retrieve/pii/S0022169418309302
188. Rezaie F, Bateni SM, Heggy E, Lee S. Utilizing the SAR, GIS, and Novel Hybrid Metaheuristic-GMDH Algorithm for Flood Susceptibility Mapping. In: 2021 IEEE International Geoscience and Remote Sensing Symposium IGARSS. IEEE; 2021. p. 8612–5.
189. Wang P, Li Y, Yu P, Zhang Y. The analysis of urban flood risk propagation based on the modified susceptible infected recovered model. J Hydrol (Amst) [Internet]. 2021 Dec;603:127121. Available from: https://linkinghub.elsevier.com/retrieve/pii/S0022169421011719
190. Luu C, Von Meding J, Kanjanabootra S. Assessing flood hazard using flood marks and analytic hierarchy process approach: a case study for the 2013 flood event in Quang Nam, Vietnam. Natural Hazards [Internet]. 2018;90(3):1031–50. Available from: https://doi.org/10.1007/s11069-017-3083-0
191. Sahoo GB, Ray C, De Carlo EH. Use of neural network to predict flash flood and attendant water qualities of a mountainous stream on Oahu, Hawaii. J Hydrol (Amst). 2006 Aug;327(3–4):525–38.
192. Haer T, Husby TG, Botzen WJW, Aerts JCJH. The safe development paradox: An agent-based model for flood risk under climate change in the European Union. Global Environmental Change [Internet]. 2020 Jan;60:102009. Available from: https://linkinghub.elsevier.com/retrieve/pii/S0959378018314079
193. Zhao G, Pang B, Xu Z, Peng D, Xu L. Assessment of urban flood susceptibility using semi-supervised machine learning model. Science of The Total Environment [Internet]. 2019 Apr;659:940–9. Available from: https://linkinghub.elsevier.com/retrieve/pii/S0048969718350800
194. Sahoo GB, Ray C. Flow forecasting for a Hawaii stream using rating curves and neural networks. J Hydrol (Amst). 2006 Feb;317(1–2):63–80.
195. Handayani W, Chigbu UE, Rudiarto I, Putri IHS. Urbanization and Increasing Flood Risk in the Northern Coast of Central Java—Indonesia: An Assessment towards Better Land Use Policy and Flood

Management. Land (Basel) [Internet]. 2020 Sep 23;9(10):343. Available from: https://www.mdpi.com/2073-445X/9/10/343
196. Rana VK, Suryanarayana TMV. GIS-based multi criteria decision making method to identify potential runoff storage zones within watershed. Ann GIS [Internet]. 2020 Apr 2;26(2):149–68. Available from: https://www.tandfonline.com/doi/full/10.1080/19475683.2020.1733083
197. Dahri N, Abida H. Monte Carlo simulation-aided analytical hierarchy process (AHP) for flood susceptibility mapping in Gabes Basin (southeastern Tunisia). Environ Earth Sci [Internet]. 2017;76(7):302. Available from: https://doi.org/10.1007/s12665-017-6619-4
198. De Brito MM, Evers M. Multi-criteria decision-making for flood risk management: A survey of the current state of the art. Natural Hazards and Earth System Sciences. 2016;16(4):1019–33.
199. Shahiri Tabarestani E, Afzalimehr H. A comparative assessment of multi-criteria decision analysis for flood susceptibility modelling. Geocarto Int [Internet]. 2021 Apr 30;1–24. Available from: https://doi.org/10.1080/10106049.2021.1923834
200. Das S. Geographic information system and AHP-based flood hazard zonation of Vaitarna basin, Maharashtra, India. Arabian Journal of Geosciences [Internet]. 2018;11(19):576. Available from: https://doi.org/10.1007/s12517-018-3933-4
201. Ekmekcioğlu Ö, Koc K, Özger M. District based flood risk assessment in Istanbul using fuzzy analytical hierarchy process. Stochastic Environmental Research and Risk Assessment [Internet]. 2020; Available from: https://doi.org/10.1007/s00477-020-01924-8
202. Thanh Son N, Thi Thu Trang N, Bui XT, Thi Da C. Remote sensing and GIS for urbanization and flood risk assessment in Phnom Penh, Cambodia. Geocarto Int [Internet]. 2021 Jun 10;1–18. Available from: https://doi.org/10.1080/10106049.2021.1941307
203. Mosavi A, Ozturk P, Chau K wing. Flood Prediction Using Machine Learning Models: Literature Review. Water (Basel) [Internet]. 2018 Oct 27;10(11):1536. Available from: https://www.mdpi.com/2073-4441/10/11/1536
204. Tehrany MS, Jones S, Shabani F. Identifying the essential flood conditioning factors for flood prone area mapping using machine learning techniques. Catena (Amst). 2019;175:174–92.
205. Bhatti MS, Kapoor D, Kalia RK, Reddy AS, Thukral AK. RSM and ANN modeling for electrocoagulation of copper from simulated wastewater: Multi objective optimization using genetic algorithm approach. Desalination. 2011 Jul;274(1–3):74–80.
206. Ramanathan R. Multicriteria Analysis of Energy. In: Encyclopedia of Energy. Elsevier; 2004. p. 77–88.
207. Pradhan B. Groundwater potential zonation for basaltic watersheds using satellite remote sensing data and GIS techniques. Open Geosciences [Internet]. 2009 Jan 1;1(1). Available from: https://www.degruyter.com/document/doi/10.2478/v10085-009-0008-5/html
208. Mojaddadi H, Pradhan B, Nampak H, Ahmad N, Ghazali AH bin. Ensemble machine-learning-based geospatial approach for flood risk assessment using multi-sensor remote-sensing data and GIS. Geomatics, Natural Hazards and Risk [Internet]. 2017 Dec 15;8(2):1080–102. Available from: https://www.tandfonline.com/doi/full/10.1080/19475705.2017.1294113
209. Botzen WJW, Aerts JCJH, van den Bergh JCJM. Individual preferences for reducing flood risk to near zero through elevation. Mitig Adapt Strateg Glob Chang [Internet]. 2013 Feb 27;18(2):229–44. Available from: http://link.springer.com/10.1007/s11027-012-9359-5
210. Das S, Pardeshi SD. Morphometric analysis of Vaitarna and Ulhas river basins, Maharashtra, India: using geospatial techniques. Appl Water Sci [Internet]. 2018 Oct 18;8(6):158. Available from: http://link.springer.com/10.1007/s13201-018-0801-z
211. Tehrany MS, Pradhan B, Jebur MN. Spatial prediction of flood susceptible areas using rule based decision tree (DT) and a novel ensemble bivariate and multivariate statistical models in GIS. J Hydrol (Amst) [Internet]. 2013 Nov;504:69–79. Available from: https://linkinghub.elsevier.com/retrieve/pii/S0022169413006872
212. Sowmya K, John CM, Shrivasthava NK. Urban flood vulnerability zoning of Cochin City, southwest coast of India, using remote sensing and GIS. Natural Hazards. 2015;75(2):1271–86.
213. Costache R, Tien Bui D. Identification of areas prone to flash-flood phenomena using multiple-criteria decision-making, bivariate statistics, machine learning and their ensembles. Science of The Total

Environment [Internet]. 2020;712:136492. Available from: https://www.sciencedirect.com/science/article/pii/S0048969719364885
214. Mahmoud SH, Gan TY. Urbanization and climate change implications in flood risk management: Developing an efficient decision support system for flood susceptibility mapping. Science of the Total Environment [Internet]. 2018 Sep 15 [cited 2019 Apr 28];636:152–67. Available from: https://www.sciencedirect.com/science/article/pii/S0048969718314591?via%3Dihub
215. Arabameri A, Rezaei K, Cerdà A, Conoscenti C, Kalantari Z. A comparison of statistical methods and multi-criteria decision making to map flood hazard susceptibility in Northern Iran. Science of The Total Environment [Internet]. 2019;660:443–58. Available from: https://www.sciencedirect.com/science/article/pii/S004896971930021X
216. Ghosh A, Kar SK. Application of analytical hierarchy process (AHP) for flood risk assessment: a case study in Malda district of West Bengal, India. Natural Hazards [Internet]. 2018;94(1):349–68. Available from: https://doi.org/10.1007/s11069-018-3392-y
217. Fernández DS, Lutz MA. Urban flood hazard zoning in Tucumán Province, Argentina, using GIS and multicriteria decision analysis. Eng Geol [Internet]. 2010;111(1–4):90–8. Available from: http://dx.doi.org/10.1016/j.enggeo.2009.12.006
218. Zhang H, Ma W chun, Wang X rong. Rapid Urbanization and Implications for Flood Risk Management in Hinterland of the Pearl River Delta, China: The Foshan Study. Sensors [Internet]. 2008 Mar 28;8(4):2223–39. Available from: http://www.mdpi.com/1424-8220/8/4/2223
219. Cetin M, Adiguzel F, Kaya O, Sahap A. Mapping of bioclimatic comfort for potential planning using GIS in Aydin. Environ Dev Sustain [Internet]. 2018 Feb 16;20(1):361–75. Available from: http://link.springer.com/10.1007/s10668-016-9885-5
220. Das S, Pardeshi SD, Kulkarni PP, Doke A. Extraction of lineaments from different azimuth angles using geospatial techniques: a case study of Pravara basin, Maharashtra, India. Arabian Journal of Geosciences [Internet]. 2018 Apr 11;11(8):160. Available from: http://link.springer.com/10.1007/s12517-018-3522-6
221. Kaya E, Agca M, Adiguzel F, Cetin M. Spatial data analysis with R programming for environment. Human and Ecological Risk Assessment: An International Journal [Internet]. 2019 Aug 18;25(6):1521–30. Available from: https://www.tandfonline.com/doi/full/10.1080/10807039.2018.1470896
222. Cetin M. Using GIS analysis to assess urban green space in terms of accessibility: case study in Kutahya. International Journal of Sustainable Development & World Ecology [Internet]. 2015 Jun 22;1–5. Available from: http://www.tandfonline.com/doi/full/10.1080/13504509.2015.1061066
223. Cetin M, Sevik H. Assessing Potential Areas of Ecotourism through a Case Study in Ilgaz Mountain National Park. In: Tourism - From Empirical Research Towards Practical Application [Internet]. InTech; 2016. Available from: http://www.intechopen.com/books/tourism-from-empirical-research-towards-practical-application/assessing-potential-areas-of-ecotourism-through-a-case-study-in-ilgaz-mountain-national-park
224. Ross CW, Prihodko L, Anchang J, Kumar S, Ji W, Hanan NP. HYSOGs250m, global gridded hydrologic soil groups for curve-number-based runoff modeling. Sci Data [Internet]. 2018 Dec 15;5(1):180091. Available from: http://www.nature.com/articles/sdata201891
225. Li R, Rui X, Zhu AX, Liu J, Band LE, Song X. Increasing detail of distributed runoff modeling using fuzzy logic in curve number. Environ Earth Sci [Internet]. 2015 Apr 9;73(7):3197–205. Available from: http://link.springer.com/10.1007/s12665-014-3620-z
226. Çelik HE, Coskun G, Cigizoglu HK, Ağıralioğlu N, Aydın A, Esin Aİ. The analysis of 2004 flood on Kozdere Stream in Istanbul. Natural Hazards [Internet]. 2012 Sep 6;63(2):461–77. Available from: http://link.springer.com/10.1007/s11069-012-0165-x
227. Hu S, Cheng X, Zhou D, Zhang H. GIS-based flood risk assessment in suburban areas: a case study of the Fangshan District, Beijing. Natural Hazards [Internet]. 2017 Jul 17;87(3):1525–43. Available from: http://link.springer.com/10.1007/s11069-017-2828-0
228. Meraj G, Romshoo SA, Yousuf AR, Altaf S, Altaf F. Assessing the influence of watershed characteristics on the flood vulnerability of Jhelum basin in Kashmir Himalaya. Natural Hazards

[Internet]. 2015 May 13;77(1):153–75. Available from: http://link.springer.com/10.1007/s11069-015-1605-1
229. Gokceoglu C, Sonmez H, Nefeslioglu HA, Duman TY, Can T. The 17 March 2005 Kuzulu landslide (Sivas, Turkey) and landslide-susceptibility map of its near vicinity. Eng Geol [Internet]. 2005 Sep;81(1):65–83. Available from: https://linkinghub.elsevier.com/retrieve/pii/S0013795205001596
230. Fernández DS, Lutz MA. Urban flood hazard zoning in Tucumán Province, Argentina, using GIS and multicriteria decision analysis. Eng Geol [Internet]. 2010 Feb;111(1–4):90–8. Available from: https://linkinghub.elsevier.com/retrieve/pii/S001379520900310X
231. Tingsanchali T, Karim MF. Flood hazard and risk analysis in the southwest region of Bangladesh. Hydrol Process [Internet]. 2005 Jun 30;19(10):2055–69. Available from: https://onlinelibrary.wiley.com/doi/10.1002/hyp.5666
232. Cutter SL, Boruff BJ, Shirley WL. Social Vulnerability to Environmental Hazards *. Soc Sci Q [Internet]. 2003 Jun;84(2):242–61. Available from: https://onlinelibrary.wiley.com/doi/10.1111/1540-6237.8402002
233. Alam A, Bhat MS, Farooq H, Ahmad B, Ahmad S, Sheikh AH. Flood risk assessment of Srinagar city in Jammu and Kashmir, India. Int J Disaster Resil Built Environ [Internet]. 2018 Apr 9;9(2):114–29. Available from: https://www.emerald.com/insight/content/doi/10.1108/IJDRBE-02-2017-0012/full/html
234. Hazarika N, Barman D, Das AK, Sarma AK, Borah SB. Assessing and mapping flood hazard, vulnerability and risk in the Upper Brahmaputra River valley using stakeholders' knowledge and multicriteria evaluation (MCE). J Flood Risk Manag [Internet]. 2018 Feb;11:S700–16. Available from: https://onlinelibrary.wiley.com/doi/10.1111/jfr3.12237
235. Smyth K, Vendramelli R, Dankewich D, Yuan Q. Seasonal variations in cold climate nutrient removal: A comparison of facultative and aerated lagoons. J Environ Manage. 2018 May;214:224–31.
236. Salman SA, Shahid S, Ismail T, Ahmed K, Chung ES, Wang XJ. Characteristics of Annual and Seasonal Trends of Rainfall and Temperature in Iraq. Asia Pac J Atmos Sci [Internet]. 2019;55(3):429–38. Available from: https://doi.org/10.1007/s13143-018-0073-4
237. Alemu MM, Bawoke GT. Analysis of spatial variability and temporal trends of rainfall in Amhara region, Ethiopia. Journal of Water and Climate Change [Internet]. 2020 Dec 1;11(4):1505–20. Available from: https://iwaponline.com/jwcc/article/11/4/1505/70022/Analysis-of-spatial-variability-and-temporal
238. Praveen B, Talukdar S, Shahfahad, Mahato S, Mondal J, Sharma P, et al. Analyzing trend and forecasting of rainfall changes in India using non-parametrical and machine learning approaches. Sci Rep [Internet]. 2020;10(1):10342. Available from: https://doi.org/10.1038/s41598-020-67228-7
239. Wang Y, Xu Y, Tabari H, Wang J, Wang Q, Song S, et al. Innovative trend analysis of annual and seasonal rainfall in the Yangtze River Delta, eastern China. Atmos Res [Internet]. 2020;231:104673. Available from: http://www.sciencedirect.com/science/article/pii/S0169809519303230
240. Patel PS, Rana SC, Joshi GS. Temporal and spatial trend analysis of rainfall on Bhogavo River watersheds in Sabarmati lower basin of Gujarat, India. Acta Geophysica [Internet]. 2021 Feb 3;69(1):353–64. Available from: http://link.springer.com/10.1007/s11600-020-00520-2
241. Sa'adi Z, Shahid S, Ismail T, Chung ES, Wang XJ. Trends analysis of rainfall and rainfall extremes in Sarawak, Malaysia using modified Mann–Kendall test. Meteorology and Atmospheric Physics. 2019;131(3):263–77.
242. Waghaye AM, Rajwade YA, Randhe RD, Kumari N. Trend analysis and change point detection of rainfall of Andhra Pradesh and Telangana, India. Journal of Agrometeorology. 2018;20(2):160–3.
243. Degefu MA, Bewket W. Variability and trends in rainfall amount and extreme event indices in the Omo-Ghibe River Basin, Ethiopia. Reg Environ Change. 2014;14(2):799–810.
244. Achite M, Caloiero T. Analysis of temporal and spatial rainfall variability over the Wadi Sly basin, Algeria. Arabian Journal of Geosciences [Internet]. 2021 Sep 24;14(18):1867. Available from: https://link.springer.com/10.1007/s12517-021-08221-w
245. Benzater B, Elouissi A, Dabanli I, Benaricha B, Hamimed A. Extreme rain trend analysis in Macta watershed North West Algeria. Arabian Journal of Geosciences [Internet]. 2021 Feb 12;14(4):302. Available from: http://link.springer.com/10.1007/s12517-021-06636-z

246. Boudiaf B, Şen Z, Boutaghane H. Climate change impact on rainfall in north-eastern Algeria using innovative trend analyses (ITA). Arabian Journal of Geosciences [Internet]. 2021 Mar 14;14(6):511. Available from: http://link.springer.com/10.1007/s12517-021-06644-z
247. Ghorbani MA, Kahya E, Roshni T, Kashani MH, Malik A, Heddam S. Entropy analysis and pattern recognition in rainfall data, north Algeria. Theor Appl Climatol [Internet]. 2021 Apr 6;144(1–2):317–26. Available from: http://link.springer.com/10.1007/s00704-021-03542-y
248. Harkat S, Kisi O. Trend analysis of precipitation records using an innovative trend methodology in a semi-arid Mediterranean environment: Cheliff Watershed Case (Northern Algeria). Theor Appl Climatol [Internet]. 2021 May 13;144(3–4):1001–15. Available from: https://link.springer.com/10.1007/s00704-021-03520-4
249. Achite M, Ceribasi G, Ceyhunlu AI, Wałęga A, Caloiero T. The Innovative Polygon Trend Analysis (IPTA) as a Simple Qualitative Method to Detect Changes in Environment—Example Detecting Trends of the Total Monthly Precipitation in Semiarid Area. Sustainability [Internet]. 2021 Nov 16;13(22):12674. Available from: https://www.mdpi.com/2071-1050/13/22/12674
250. Zerouali B, Al-Ansari N, Chettih M, Mohamed M, Abda Z, Santos CAG, et al. An Enhanced Innovative Triangular Trend Analysis of Rainfall Based on a Spectral Approach. Water (Basel) [Internet]. 2021 Mar 7;13(5):727. Available from: https://www.mdpi.com/2073-4441/13/5/727
251. Achite M, Caloiero T, Wałęga A, Krakauer N, Hartani T. Analysis of the Spatiotemporal Annual Rainfall Variability in the Wadi Cheliff Basin (Algeria) over the Period 1970 to 2018. Water (Basel) [Internet]. 2021 May 25;13(11):1477. Available from: https://www.mdpi.com/2073-4441/13/11/1477
252. Aieb A, Kadri I, Lefsih K, Madani K. Spatiotemporal trend analysis of runoff and actual evapotranspiration in Northern Algeria between 1901 and 2020. Model Earth Syst Environ [Internet]. 2022 Jul 9; Available from: https://link.springer.com/10.1007/s40808-022-01453-z
253. Waha K, Clarke J, Dayal K, Freund M, Heady C, Parisi I, et al. Past and future rainfall changes in the Australian midlatitudes and implications for agriculture. Clim Change [Internet]. 2022 Feb 14;170(3–4):29. Available from: https://link.springer.com/10.1007/s10584-021-03301-y
254. Yildirim G, Rahman A. Homogeneity and trend analysis of rainfall and droughts over Southeast Australia. Natural Hazards [Internet]. 2022 Jun 28;112(2):1657–83. Available from: https://link.springer.com/10.1007/s11069-022-05243-9
255. Mullick MdRA, Nur RM, Alam MdJ, Islam KMA. Observed trends in temperature and rainfall in Bangladesh using pre-whitening approach. Glob Planet Change [Internet]. 2019 Jan;172:104–13. Available from: https://linkinghub.elsevier.com/retrieve/pii/S0921818117302552
256. Khan MHR, Rahman A, Luo C, Kumar S, Islam GMA, Hossain MA. Detection of changes and trends in climatic variables in Bangladesh during 1988–2017. Heliyon [Internet]. 2019 Mar;5(3):e01268. Available from: https://linkinghub.elsevier.com/retrieve/pii/S2405844018348928
257. Chowdhury AK, Kar KK, Shahid S, Chowdhury R, Rashid MdM. Evaluation of spatio-temporal rainfall variability and performance of a stochastic rainfall model in Bangladesh. International Journal of Climatology [Internet]. 2019 Sep;39(11):4256–73. Available from: https://onlinelibrary.wiley.com/doi/10.1002/joc.6071
258. Nashwan MS, Shahid S, Wang X. Uncertainty in Estimated Trends Using Gridded Rainfall Data: A Case Study of Bangladesh. Water (Basel) [Internet]. 2019 Feb 19;11(2):349. Available from: https://www.mdpi.com/2073-4441/11/2/349
259. Sobral BS, de Oliveira-Júnior JF, Alecrim F, Gois G, Muniz-Júnior JG, de Bodas Terassi PM, et al. PERSIANN-CDR based characterization and trend analysis of annual rainfall in Rio De Janeiro State, Brazil. Atmos Res [Internet]. 2020 Jul;238:104873. Available from: https://linkinghub.elsevier.com/retrieve/pii/S0169809519314085
260. Gao F, Wang Y, Chen X, Yang W. Trend Analysis of Rainfall Time Series in Shanxi Province, Northern China (1957–2019). Water (Basel) [Internet]. 2020 Aug 20;12(9):2335. Available from: https://www.mdpi.com/2073-4441/12/9/2335
261. Asfaw A, Simane B, Hassen A, Bantider A. Variability and time series trend analysis of rainfall and temperature in northcentral Ethiopia: A case study in Woleka sub-basin. Weather Clim Extrem

[Internet]. 2018 Mar;19:29–41. Available from: https://linkinghub.elsevier.com/retrieve/pii/S2212094717300932
262. Gedefaw M, Yan D, Wang H, Qin T, Girma A, Abiyu A, et al. Innovative trend analysis of annual and seasonal rainfall variability in Amhara Regional State, Ethiopia. Atmosphere (Basel). 2018;9(9).
263. Elzopy KA, Chaturvedi AK, Chandran KM, Gopinath G, K N, Surendran U. Trend analysis of long-term rainfall and temperature data for Ethiopia. South African Geographical Journal [Internet]. 2021 Jul 6;103(3):381–94. Available from: https://www.tandfonline.com/doi/full/10.1080/03736245.2020.1835699
264. Worku T, Khare D, Tripathi SK. Spatiotemporal trend analysis of rainfall and temperature, and its implications for crop production. Journal of Water and Climate Change [Internet]. 2019 Dec 1;10(4):799–817. Available from: https://iwaponline.com/jwcc/article/10/4/799/38985/Spatiotemporal-trend-analysis-of-rainfall-and
265. Miheretu BA. Temporal variability and trend analysis of temperature and rainfall in the Northern highlands of Ethiopia. Phys Geogr [Internet]. 2021 Sep 3;42(5):434–51. Available from: https://www.tandfonline.com/doi/full/10.1080/02723646.2020.1806674
266. Adane GB, Hirpa BA, Song C, Lee WK. Rainfall Characterization and Trend Analysis of Wet Spell Length across Varied Landscapes of the Upper Awash River Basin, Ethiopia. Sustainability [Internet]. 2020 Nov 5;12(21):9221. Available from: https://www.mdpi.com/2071-1050/12/21/9221
267. Gemeda DO, Feyssa DH, Garedew W. Meteorological data trend analysis and local community perception towards climate change: a case study of Jimma City, Southwestern Ethiopia. Environ Dev Sustain [Internet]. 2021 Apr 25;23(4):5885–903. Available from: https://link.springer.com/10.1007/s10668-020-00851-6
268. Marie M, Yirga F, Haile M, Ehteshammajd S, Azadi H, Scheffran J. Time-series trend analysis and farmer perceptions of rainfall and temperature in northwestern Ethiopia. Environ Dev Sustain [Internet]. 2021 Sep 29;23(9):12904–24. Available from: https://link.springer.com/10.1007/s10668-020-01192-0
269. Duguma FA, Feyessa FF, Demissie TA, Januszkiewicz K. Hydroclimate Trend Analysis of Upper Awash Basin, Ethiopia. Water (Basel) [Internet]. 2021 Jun 17;13(12):1680. Available from: https://www.mdpi.com/2073-4441/13/12/1680
270. Harka AE, Jilo NB, Behulu F. Spatial-temporal rainfall trend and variability assessment in the Upper Wabe Shebelle River Basin, Ethiopia: Application of innovative trend analysis method. J Hydrol Reg Stud [Internet]. 2021 Oct;37:100915. Available from: https://linkinghub.elsevier.com/retrieve/pii/S2214581821001440
271. Hordofa AT, Leta OT, Alamirew T, Chukalla AD. Spatiotemporal Trend Analysis of Temperature and Rainfall over Ziway Lake Basin, Ethiopia. Hydrology [Internet]. 2021 Dec 22;9(1):2. Available from: https://www.mdpi.com/2306-5338/9/1/2
272. Worku MA, Feyisa GL, Beketie KT. Climate trend analysis for a semi-arid Borana zone in southern Ethiopia during 1981–2018. Environmental Systems Research [Internet]. 2022 Dec 4;11(1):2. Available from: https://environmentalsystemsresearch.springeropen.com/articles/10.1186/s40068-022-00247-7
273. Malede DA, Agumassie TA, Kosgei JR, Linh NTT, Andualem TG. Analysis of rainfall and streamflow trend and variability over Birr River watershed, Abbay basin, Ethiopia. Environmental Challenges [Internet]. 2022 Apr;7:100528. Available from: https://linkinghub.elsevier.com/retrieve/pii/S2667010022000877
274. Larbi I, Hountondji F, Annor T, Agyare W, Mwangi Gathenya J, Amuzu J. Spatio-Temporal Trend Analysis of Rainfall and Temperature Extremes in the Vea Catchment, Ghana. Climate [Internet]. 2018 Oct 31;6(4):87. Available from: http://www.mdpi.com/2225-1154/6/4/87
275. Doaemo W, Wuest L, Athikalam PT, Moraes AS, Molerio-Leon LF. Rainfall characterization of the Bumbu watershed, Papua New Guinea. Theor Appl Climatol [Internet]. 2022 Jan 19;147(1–2):127–41. Available from: https://link.springer.com/10.1007/s00704-021-03808-5
276. Sanikhani H, Kisi O, Mirabbasi R, Meshram SG. Trend analysis of rainfall pattern over the Central India during 1901–2010. Arabian Journal of Geosciences [Internet]. 2018;11(15):437. Available from: https://doi.org/10.1007/s12517-018-3800-3

277. Ramkar P, Yadav SM. Rainfall Trend Analysis Using Nonparametric Test: A Case Study of Malegaon City. In: Water Resources and Environmental Engineering II [Internet]. Singapore: Springer Singapore; 2019. p. 25–33. Available from: http://link.springer.com/10.1007/978-981-13-2038-5_3
278. Panda A, Sahu N. Trend analysis of seasonal rainfall and temperature pattern in Kalahandi, Bolangir and Koraput districts of Odisha, India. Atmospheric Science Letters [Internet]. 2019 Oct 17;20(10). Available from: https://onlinelibrary.wiley.com/doi/10.1002/asl.932
279. Biswas B, Jadhav RS, Tikone N. Rainfall Distribution and Trend Analysis for Upper Godavari Basin, India, from 100 Years Record (1911–2010). Journal of the Indian Society of Remote Sensing [Internet]. 2019 Oct 19;47(10):1781–92. Available from: http://link.springer.com/10.1007/s12524-019-01011-8
280. Kumar N, Tischbein B, Beg MK. Multiple trend analysis of rainfall and temperature for a monsoon-dominated catchment in India. Meteorology and Atmospheric Physics [Internet]. 2019 Aug 3;131(4):1019–33. Available from: http://link.springer.com/10.1007/s00703-018-0617-2
281. Malik A, Kumar A, Guhathakurta P, Kisi O. Spatial-temporal trend analysis of seasonal and annual rainfall (1966–2015) using innovative trend analysis method with significance test. Arabian Journal of Geosciences [Internet]. 2019 May 17;12(10):328. Available from: http://link.springer.com/10.1007/s12517-019-4454-5
282. Saini

A, Sahu N, Kumar P, Nayak S, Duan W, Avtar R, et al. Advanced Rainfall Trend Analysis of 117 Years over West Coast Plain and Hill Agro-Climatic Region of India. Atmosphere (Basel) [Internet]. 2020 Nov 13;11(11):1225. Available from: https://www.mdpi.com/2073-4433/11/11/1225
283. Malik A, Kumar A. Spatio-temporal trend analysis of rainfall using parametric and non-parametric tests: case study in Uttarakhand, India. Theor Appl Climatol [Internet]. 2020 Apr 4;140(1–2):183–207. Available from: http://link.springer.com/10.1007/s00704-019-03080-8
284. Marak JDK, Sarma AK, Bhattacharjya RK. Innovative trend analysis of spatial and temporal rainfall variations in Umiam and Umtru watersheds in Meghalaya, India. Theor Appl Climatol [Internet]. 2020 Nov 21;142(3–4):1397–412. Available from: https://link.springer.com/10.1007/s00704-020-03383-1
285. Nair SC, Mirajkar AB. Spatio–temporal rainfall trend anomalies in Vidarbha region using historic and predicted data: a case study. Model Earth Syst Environ [Internet]. 2021 Mar 18;7(1):503–10. Available from: https://link.springer.com/10.1007/s40808-020-00928-1
286. Pathak AA, Dodamani BM. Trend analysis of rainfall, rainy days and drought: a case study of Ghataprabha River Basin, India. Model Earth Syst Environ [Internet]. 2020 Sep 6;6(3):1357–72. Available from: https://link.springer.com/10.1007/s40808-020-00798-7
287. Deshpande NR, Kulkarni JR. Spatio-temporal variability in the stratiform/convective rainfall contribution to the summer monsoon rainfall in India. International Journal of Climatology [Internet]. 2022 Jan 21;42(1):481–92. Available from: https://onlinelibrary.wiley.com/doi/10.1002/joc.7255
288. Patel PS, Rana SC, Joshi GS. Temporal and spatial trend analysis of rainfall on Bhogavo River watersheds in Sabarmati lower basin of Gujarat, India. Acta Geophysica [Internet]. 2021 Feb 3;69(1):353–64. Available from: http://link.springer.com/10.1007/s11600-020-00520-2
289. P Z S, K V J. Comparative study of innovative trend analysis technique with Mann-Kendall tests for extreme rainfall. Arabian Journal of Geosciences [Internet]. 2021 Apr 17;14(7):536. Available from: https://link.springer.com/10.1007/s12517-021-06906-w
290. Gupta N, Banerjee A, Gupta SK. Spatio-temporal Trend Analysis of Climatic Variables over Jharkhand, India. Earth Systems and Environment [Internet]. 2021 Jan 2;5(1):71–86. Available from: http://link.springer.com/10.1007/s41748-021-00204-x
291. Singh R, Sah S, Das B, Vishnoi L, Pathak H. Spatio-temporal trends and variability of rainfall in Maharashtra, India: Analysis of 118 years. Theor Appl Climatol [Internet]. 2021 Feb 15;143(3–4):883–900. Available from: http://link.springer.com/10.1007/s00704-020-03452-5
292. Singh R, Sah S, Das B, Potekar S, Chaudhary A, Pathak H. Innovative trend analysis of spatio-temporal variations of rainfall in India during 1901–2019. Theor Appl Climatol [Internet]. 2021 Jul 28;145(1–2):821–38. Available from: https://link.springer.com/10.1007/s00704-021-03657-2

293. Srivastava PK, Pradhan RK, Petropoulos GP, Pandey V, Gupta M, Yaduvanshi A, et al. Long-Term Trend Analysis of Precipitation and Extreme Events over Kosi River Basin in India. Water (Basel) [Internet]. 2021 Jun 18;13(12):1695. Available from: https://www.mdpi.com/2073-4441/13/12/1695
294. Mehta D, Yadav SM. An analysis of rainfall variability and drought over Barmer District of Rajasthan, Northwest India. Water Supply [Internet]. 2021 Aug 1;21(5):2505–17. Available from: https://iwaponline.com/ws/article/21/5/2505/80559/An-analysis-of-rainfall-variability-and-drought
295. Buri ES, Keesara VR, Loukika KN. Long-term trend analysis of observed gridded precipitation and temperature data over Munneru River basin, India. Journal of Earth System Science [Internet]. 2022 Jun 9;131(2):115. Available from: https://link.springer.com/10.1007/s12040-022-01864-7
296. Gupta N, Gond S, Gupta SK. Spatiotemporal trend characteristics of rainfall and drought jeopardy over Bundelkhand Region, India. Arabian Journal of Geosciences [Internet]. 2022 Jun 11;15(12):1155. Available from: https://link.springer.com/10.1007/s12517-022-10389-8
297. Ahmed M, Hoque A, Islam MK. A Trend Analysis of Climatic Variables in the Karimganj District of Assam, India. Indian J Sci Technol [Internet]. 2022 Mar 15;15(10):442–50. Available from: https://indjst.org/articles/a-trend-analysis-of-climatic-variables-in-the-karimganj-district-of-assam-india
298. Thotli LR, Gugamsetty B, Kalluri ROR, Tandule CR, Kotalo RG, Akkiraju B, et al. Long–term (2001-2020) trend analysis of temperature and rainfall and drought characteristics by in-situ measurements at a tropical semi-arid station from southern peninsular India. International Journal of Climatology [Internet]. 2022 Jul 3; Available from: https://onlinelibrary.wiley.com/doi/10.1002/joc.7783
299. Jose DM, Dwarakish GS. Frequency-intensity-distribution bias correction and trend analysis of high-resolution CMIP6 precipitation data over a tropical river basin. Theor Appl Climatol [Internet]. 2022 Jul 6;149(1–2):683–94. Available from: https://link.springer.com/10.1007/s00704-022-04078-5
300. Chauhan AS, Singh S, Maurya RKS, Rani A, Danodia A. Spatio-temporal and trend analysis of rain days having different intensity from 1901 – 2020 at regional scale in Haryana, India. Results in Geophysical Sciences [Internet]. 2022 Jun;10:100041. Available from: https://linkinghub.elsevier.com/retrieve/pii/S2666828922000025
301. Mehta P, Jangra MS, Bhardwaj SK, Paul S. Variability and time series trend analysis of rainfall in the mid-hill sub humid zone: a case study of Nauni. Environmental Science and Pollution Research [Internet]. 2022 Jun 18; Available from: https://link.springer.com/10.1007/s11356-022-21507-0
302. Abebe BA, Grum B, Degu AM, Goitom H. Spatio-temporal rainfall variability and trend analysis in the <scp>Tekeze-Atbara</scp> river basin, northwestern Ethiopia. Meteorological Applications [Internet]. 2022 Mar 19;29(2). Available from: https://onlinelibrary.wiley.com/doi/10.1002/met.2059
303. Singh MC, Satpute S, Prasad V, Sharma KK. Trend analysis of temperature, rainfall, and reference evapotranspiration for Ludhiana district of Indian Punjab using non-parametric statistical methods. Arabian Journal of Geosciences [Internet]. 2022 Feb 28;15(3):275. Available from: https://link.springer.com/10.1007/s12517-022-09517-1
304. Umar S, Lone MA, Goel NK, Zakwan M. Trend analysis of hydro-meteorological parameters in the Jhelum River basin, North Western Himalayas. Theor Appl Climatol [Internet]. 2022 May 15;148(3–4):1417–28. Available from: https://link.springer.com/10.1007/s00704-022-04014-7
305. Chauhan AS, Singh S, Maurya RKS, Rani A, Danodia A. Spatio-temporal trend analysis and future projections of precipitation at regional scale: a case study of Haryana, India. Journal of Water and Climate Change [Internet]. 2022 May 1;13(5):2143–70. Available from: https://iwaponline.com/jwcc/article/13/5/2143/88181/Spatio-temporal-trend-analysis-and-future
306. Goyal M. Statistical Analysis of Long Term Trends of Rainfall During 1901–2002 at Assam, India. Water Resources Management. 2014 Apr 1;28.
307. Farrokhi A, Farzin S, Mousavi SF. A New Framework for Evaluation of Rainfall Temporal Variability through Principal Component Analysis, Hybrid Adaptive Neuro-Fuzzy Inference System, and Innovative Trend Analysis Methodology. Water Resources Management [Internet]. 2020 Aug 14;34(10):3363–85. Available from: https://link.springer.com/10.1007/s11269-020-02618-0
308. Bahrami M, Mahmoudi MR. Long-term temporal trend analysis of climatic parameters using polynomial regression analysis over the Fasa Plain, southern Iran. Meteorology and Atmospheric

Physics [Internet]. 2022 Apr 27;134(2):42. Available from: https://link.springer.com/10.1007/s00703-022-00875-9
309. Caloiero T, Coscarelli R, Ferrari E. Application of the Innovative Trend Analysis Method for the Trend Analysis of Rainfall Anomalies in Southern Italy. Water Resources Management [Internet]. 2018 Dec 25;32(15):4971–83. Available from: http://link.springer.com/10.1007/s11269-018-2117-z
310. Caloiero T, Filice E, Coscarelli R, Pellicone G. A Homogeneous Dataset for Rainfall Trend Analysis in the Calabria Region (Southern Italy). Water (Basel) [Internet]. 2020 Sep 11;12(9):2541. Available from: https://www.mdpi.com/2073-4441/12/9/2541
311. Caloiero T, Coscarelli R, Pellicone G. Trend Analysis of Rainfall Using Gridded Data over a Region of Southern Italy. Water (Basel) [Internet]. 2021 Aug 19;13(16):2271. Available from: https://www.mdpi.com/2073-4441/13/16/2271
312. Chiaravalloti F, Caloiero T, Coscarelli R. The Long-Term ERA5 Data Series for Trend Analysis of Rainfall in Italy. Hydrology [Internet]. 2022 Jan 28;9(2):18. Available from: https://www.mdpi.com/2306-5338/9/2/18
313. Ouma YO, Cheruyot R, Wachera AN. Rainfall and runoff time-series trend analysis using LSTM recurrent neural network and wavelet neural network with satellite-based meteorological data: case study of Nzoia hydrologic basin. Complex & Intelligent Systems [Internet]. 2022 Feb 15;8(1):213–36. Available from: https://link.springer.com/10.1007/s40747-021-00365-2
314. Ouatiki H, Boudhar A, Ouhinou A, Arioua A, Hssaisoune M, Bouamri H, et al. Trend analysis of rainfall and drought over the Oum Er-Rbia River Basin in Morocco during 1970–2010. Arabian Journal of Geosciences [Internet]. 2019 Feb 12;12(4):128. Available from: http://link.springer.com/10.1007/s12517-019-4300-9
315. Caloiero T. Evaluation of rainfall trends in the South Island of New Zealand through the innovative trend analysis (ITA). Theor Appl Climatol [Internet]. 2020 Jan 2;139(1–2):493–504. Available from: http://link.springer.com/10.1007/s00704-019-02988-5
316. Alam F, Salam M, Khalil NA, Khan O, Khan M. Rainfall trend analysis and weather forecast accuracy in selected parts of Khyber Pakhtunkhwa, Pakistan. SN Appl Sci [Internet]. 2021 May 21;3(5):575. Available from: https://link.springer.com/10.1007/s42452-021-04457-z
317. Gul S, Ren J. Application of non-parametric innovative trend analysis of different time scale precipitation during (1951–2016) in Khyber Pakhtunkhwa, Pakistan. Acta Geophysica [Internet]. 2022 Feb 18;70(1):485–503. Available from: https://link.springer.com/10.1007/s11600-021-00703-5
318. Mallick J, Talukdar S, Alsubih M, Salam R, Ahmed M, Kahla N Ben, et al. Analysing the trend of rainfall in Asir region of Saudi Arabia using the family of Mann-Kendall tests, innovative trend analysis, and detrended fluctuation analysis. Theor Appl Climatol [Internet]. 2021 Jan 13;143(1–2):823–41. Available from: http://link.springer.com/10.1007/s00704-020-03448-1
319. AlSubih M, Kumari M, Mallick J, Ramakrishnan R, Islam S, Singh CK. Time series trend analysis of rainfall in last five decades and its quantification in Aseer Region of Saudi Arabia. Arabian Journal of Geosciences [Internet]. 2021 Mar 15;14(6):519. Available from: http://link.springer.com/10.1007/s12517-021-06935-5
320. Ateeq-ur-Rauf, Ahmad N, Ajmal M, Malik A, Rahman Z ur. Meteorological trend analysis for Najd and Hejaz regions, Saudi Arabia. Meteorology and Atmospheric Physics [Internet]. 2022 Apr 4;134(2):35. Available from: https://link.springer.com/10.1007/s00703-022-00873-x
321. Arab Amiri M, Gocić M. Innovative trend analysis of annual precipitation in Serbia during 1946–2019. Environ Earth Sci [Internet]. 2021 Dec 17;80(23):777. Available from: https://link.springer.com/10.1007/s12665-021-10095-w
322. Nyikadzino B, Chitakira M, Muchuru S. Rainfall and runoff trend analysis in the Limpopo river basin using the Mann Kendall statistic. Physics and Chemistry of the Earth, Parts A/B/C [Internet]. 2020 Jun;117:102870. Available from: https://linkinghub.elsevier.com/retrieve/pii/S147470651930107X
323. Harmse CJ, Du Toit JCO, Swanepoel A, Gerber HJ. Trend analysis of long-term rainfall data in the Upper Karoo of South Africa. Transactions of the Royal Society of South Africa [Internet]. 2021 Jan 2;76(1):1–12. Available from: https://www.tandfonline.com/doi/full/10.1080/0035919X.2020.1834467

324. Banda VD, Dzwairo RB, Singh SK, Kanyerere T. Trend analysis of selected hydro-meteorological variables for the Rietspruit sub-basin, South Africa. Journal of Water and Climate Change [Internet]. 2021 Nov 1;12(7):3099–123. Available from: https://iwaponline.com/jwcc/article/12/7/3099/82671/Trend-analysis-of-selected-hydro-meteorological
325. Alahacoon N, Matheswaran K, Pani P, Amarnath G. A Decadal Historical Satellite Data and Rainfall Trend Analysis (2001–2016) for Flood Hazard Mapping in Sri Lanka. Remote Sens (Basel) [Internet]. 2018 Mar 13;10(3):448. Available from: https://www.mdpi.com/2072-4292/10/3/448
326. Khaniya B, Jayanayaka I, Jayasanka P, Rathnayake U. Rainfall Trend Analysis in Uma Oya Basin, Sri Lanka, and Future Water Scarcity Problems in Perspective of Climate Variability. Advances in Meteorology [Internet]. 2019 May 8;2019:1–10. Available from: https://www.hindawi.com/journals/amete/2019/3636158/
327. Rathnayake U. Comparison of Statistical Methods to Graphical Methods in Rainfall Trend Analysis: Case Studies from Tropical Catchments. Advances in Meteorology [Internet]. 2019 Sep 2;2019:1–10. Available from: https://www.hindawi.com/journals/amete/2019/8603586/
328. Nisansala WDS, Abeysingha NS, Islam A, Bandara AMKR. Recent rainfall trend over Sri Lanka (1987–2017). International Journal of Climatology [Internet]. 2020 Jun 15;40(7):3417–35. Available from: https://onlinelibrary.wiley.com/doi/10.1002/joc.6405
329. Pawar U, Rathnayake U. Spatiotemporal rainfall variability and trend analysis over Mahaweli Basin, Sri Lanka. Arabian Journal of Geosciences [Internet]. 2022 Feb 15;15(4):370. Available from: https://link.springer.com/10.1007/s12517-022-09646-7
330. Zeleňáková M, Abd-Elhamid HF, Krajníková K, Smetanková J, Purcz P, Alkhalaf I. Spatial and Temporal Variability of Rainfall Trends in Response to Climate Change—A Case Study: Syria. Water (Basel) [Internet]. 2022 May 23;14(10):1670. Available from: https://www.mdpi.com/2073-4441/14/10/1670
331. Gadedjisso-Tossou A, Adjegan KI, Kablan AKM. Rainfall and Temperature Trend Analysis by Mann–Kendall Test and Significance for Rainfed Cereal Yields in Northern Togo. Sci [Internet]. 2021 Mar 6;3(1):17. Available from: https://www.mdpi.com/2413-4155/3/1/17
332. Serencam U. Innovative trend analysis of total annual rainfall and temperature variability case study: Yesilirmak region, Turkey. Arabian Journal of Geosciences [Internet]. 2019 Dec 19;12(23):704. Available from: http://link.springer.com/10.1007/s12517-019-4903-1
333. Hussein KA, Alsumaiti TS, Ghebreyesus DT, Sharif HO, Abdalati W. High-Resolution Spatiotemporal Trend Analysis of Precipitation Using Satellite-Based Products over the United Arab Emirates. Water (Basel) [Internet]. 2021 Aug 29;13(17):2376. Available from: https://www.mdpi.com/2073-4441/13/17/2376
334. Quan NT, Khoi DN, Hoan NX, Phung NK, Dang TD. Spatiotemporal Trend Analysis of Precipitation Extremes in Ho Chi Minh City, Vietnam During 1980–2017. International Journal of Disaster Risk Science [Internet]. 2021 Feb;12(1):131–46. Available from: http://link.springer.com/10.1007/s13753-020-00311-9
335. Şan M, Akçay F, Linh NTT, Kankal M, Pham QB. Innovative and polygonal trend analyses applications for rainfall data in Vietnam. Theor Appl Climatol [Internet]. 2021 May 1;144(3–4):809–22. Available from: https://link.springer.com/10.1007/s00704-021-03574-4
336. Phuong DND, Hai LM, Dung HM, Loi NK. Temporal Trend Possibilities of Annual Rainfall and Standardized Precipitation Index in the Central Highlands, Vietnam. Earth Systems and Environment [Internet]. 2022 Jan 20;6(1):69–85. Available from: https://link.springer.com/10.1007/s41748-021-00211-y
337. Ilori OW, Ajayi VO. Change Detection and Trend Analysis of Future Temperature and Rainfall over West Africa. Earth Systems and Environment [Internet]. 2020 Sep 30;4(3):493–512. Available from: https://link.springer.com/10.1007/s41748-020-00174-6
338. Nouaceur Z, Murarescu O. Rainfall Variability and Trend Analysis of Rainfall in West Africa (Senegal, Mauritania, Burkina Faso). Water (Basel) [Internet]. 2020 Jun 19;12(6):1754. Available from: https://www.mdpi.com/2073-4441/12/6/1754

339. Caloiero T, Caloiero P, Frustaci F. Long-term precipitation trend analysis in Europe and in the Mediterranean basin. Water and Environment Journal [Internet]. 2018 Aug;32(3):433–45. Available from: https://onlinelibrary.wiley.com/doi/10.1111/wej.12346
340. Pal L, Ojha CSP, Chandniha SK, Kumar A. Regional scale analysis of trends in rainfall using nonparametric methods and wavelet transforms over a semi-arid region in India. International Journal of Climatology [Internet]. 2019 Apr 1;39(5):2737–64. Available from: https://doi.org/10.1002/joc.5985
341. Malik A, Kumar A, Guhathakurta P, Kisi O. Spatial-temporal trend analysis of seasonal and annual rainfall (1966–2015) using innovative trend analysis method with significance test. Arabian Journal of Geosciences [Internet]. 2019 May 17;12(10):328. Available from: http://link.springer.com/10.1007/s12517-019-4454-5
342. Sharma C, Arora H, Ojha CSP. Assessment of the effect of climate change on historical and future rainfall in Uttarakhand. In.
343. Mullick MRA, Nur MRM, Alam MJ, Islam KMA. Observed trends in temperature and rainfall in Bangladesh using pre-whitening approach. Glob Planet Change [Internet]. 2019;172(May 2017):104–13. Available from: https://doi.org/10.1016/j.gloplacha.2018.10.001
344. Towfiqul Islam ARMd, Rahman MdS, Khatun R, Hu Z. Spatiotemporal trends in the frequency of daily rainfall in Bangladesh during 1975–2017. Theor Appl Climatol [Internet]. 2020 Aug 16;141(3–4):869–87. Available from: https://link.springer.com/10.1007/s00704-020-03244-x
345. Sobral BS, de Oliveira-Júnior JF, Alecrim F, Gois G, Muniz-Júnior JG, de Bodas Terassi PM, et al. PERSIANN-CDR based characterization and trend analysis of annual rainfall in Rio De Janeiro State, Brazil. Atmos Res [Internet]. 2020 Jul;238:104873. Available from: https://linkinghub.elsevier.com/retrieve/pii/S0169809519314085
346. Gedefaw M, Yan D, Wang H, Qin T, Girma A, Abiyu A, et al. Innovative Trend Analysis of Annual and Seasonal Rainfall Variability in Amhara Regional State, Ethiopia. Atmosphere (Basel) [Internet]. 2018 Aug 21;9(9):326. Available from: http://www.mdpi.com/2073-4433/9/9/326
347. Caloiero T, Coscarelli R, Ferrari E. Application of the Innovative Trend Analysis Method for the Trend Analysis of Rainfall Anomalies in Southern Italy. Water Resources Management [Internet]. 2018;32(15):4971–83. Available from: https://doi.org/10.1007/s11269-018-2117-z
348. Caloiero T. Evaluation of rainfall trends in the South Island of New Zealand through the innovative trend analysis (ITA). Theor Appl Climatol [Internet]. 2020 Jan 2;139(1–2):493–504. Available from: http://link.springer.com/10.1007/s00704-019-02988-5
349. Bouklikha A, Habi M, Elouissi A, Hamoudi S. Annual, seasonal and monthly rainfall trend analysis in the Tafna watershed, Algeria. Appl Water Sci [Internet]. 2021 Apr 15;11(4):77. Available from: https://link.springer.com/10.1007/s13201-021-01404-6
350. Wang Y, Xu Y, Tabari H, Wang J, Wang Q, Song S, et al. Innovative trend analysis of annual and seasonal rainfall in the Yangtze River Delta, eastern China. Atmos Res [Internet]. 2020 Jan;231:104673. Available from: https://linkinghub.elsevier.com/retrieve/pii/S0169809519303230
351. Sanikhani H, Kisi O, Mirabbasi R, Meshram SG. Trend analysis of rainfall pattern over the Central India during 1901–2010. Arabian Journal of Geosciences [Internet]. 2018 Aug 9;11(15):437. Available from: http://link.springer.com/10.1007/s12517-018-3800-3
352. Phuong DND, Huyen NT, Liem ND, Hong NT, Cuong DK, Loi NK. On the use of an innovative trend analysis methodology for temporal trend identification in extreme rainfall indices over the Central Highlands, Vietnam. Theor Appl Climatol [Internet]. 2022 Jan 20;147(1–2):835–52. Available from: https://link.springer.com/10.1007/s00704-021-03842-3
353. Islam ARMdT, Karim MdR, Mondol MAH. Appraising trends and forecasting of hydroclimatic variables in the north and northeast regions of Bangladesh. Theor Appl Climatol [Internet]. 2021 Jan 3;143(1–2):33–50. Available from: https://link.springer.com/10.1007/s00704-020-03411-0
354. Goyal MK. Monthly rainfall prediction using wavelet regression and neural network: an analysis of 1901–2002 data, Assam, India. Theor Appl Climatol [Internet]. 2014 Oct 21;118(1–2):25–34. Available from: http://link.springer.com/10.1007/s00704-013-1029-3
355. Harkat S, Kisi O. Trend analysis of precipitation records using an innovative trend methodology in a semi-arid Mediterranean environment: Cheliff Watershed Case (Northern Algeria). Theor Appl Climatol

[Internet]. 2021 May 13;144(3–4):1001–15. Available from: https://link.springer.com/10.1007/s00704-021-03520-4
356. Kohen E, Farhi N, Shavitt Y, Mamane H. Prediction of a full scale WWTP activated sludge SVI test using an LSTM neural network. Environ Sci (Camb). 2022;8(11):2786–95.
357. Goyal MK, Gupta V. Identification of Homogeneous Rainfall Regimes in Northeast Region of India using Fuzzy Cluster Analysis. Water Resources Management. 2014 Oct 8;28(13):4491–511.
358. Kendall MG. Rank Correlation Methods. Griffin, London; 1955.
359. Mann HB. Nonparametric Tests Against Trend. Econometrica [Internet]. 1945 Nov 4;13(3):245–59. Available from: http://www.jstor.org/stable/1907187
360. Şen Z. Innovative Trend Analysis Methodology. J Hydrol Eng [Internet]. 2012 Sep;17(9):1042–6. Available from: http://ascelibrary.org/doi/10.1061/%28ASCE%29HE.1943-5584.0000556
361. Yue S, Wang C. The Mann-Kendall Test Modified by Effective Sample Size to Detect Trend in Serially Correlated Hydrological Series. Water Resources Management [Internet]. 2004 Jun;18(3):201–18. Available from: http://link.springer.com/10.1023/B:WARM.0000043140.61082.60
362. Hamed KH, Ramachandra Rao A. A modified Mann-Kendall trend test for autocorrelated data. J Hydrol (Amst) [Internet]. 1998 Jan 30 [cited 2020 May 4];204(1–4):182–96. Available from: https://www.sciencedirect.com/science/article/pii/S002216949700125X
363. Yue S, Pilon P, Phinney B, Cavadias G. The influence of autocorrelation on the ability to detect trend in hydrological series. Hydrol Process [Internet]. 2002 Jun 30;16(9):1807–29. Available from: https://onlinelibrary.wiley.com/doi/10.1002/hyp.1095
364. YUE S, PILON P, PHINNEY B. Canadian streamflow trend detection: impacts of serial and cross-correlation. Hydrological Sciences Journal [Internet]. 2003 Feb;48(1):51–63. Available from: http://www.tandfonline.com/doi/abs/10.1623/hysj.48.1.51.43478
365. Sen PK. Estimates of the Regression Coefficient Based on Kendall's Tau. J Am Stat Assoc [Internet]. 1968 Dec 1;63(324):1379–89. Available from: https://www.tandfonline.com/doi/abs/10.1080/01621459.1968.10480934
366. Machiwal D, Gupta A, Jha MK, Kamble T. Analysis of trend in temperature and rainfall time series of an Indian arid region: comparative evaluation of salient techniques. Theor Appl Climatol. 2019;136(1–2):301–20.
367. Şen Z. Innovative trend significance test and applications. Theor Appl Climatol [Internet]. 2017 Feb 23;127(3–4):939–47. Available from: http://link.springer.com/10.1007/s00704-015-1681-x
368. Qin D, Zhang J, Shan C, Song L. China national assessment report on risk management and adaptation of climate extremes and disasters. Science Report: Beijing, China. 2015;
369. Dai A, Trenberth KE, Karl TR. Global variations in droughts and wet spells: 1900–1995. Geophys Res Lett. 1998;25(17):3367–70.
370. Wang ZW. Climate change in drought over northern China during 1950–2000. Acta Geographica Sinica. 2003;58:61.
371. Li XZ, Ma ZG, Liu XD. Inter-decadal characteristics of aridification over northern China in association with variations of the atmospheric circulation during the last fifty years. 2006;
372. Zhang Q, Zou X, Xiao F, Lu H, Liu H, Zhu C, et al. Classification of meteorological drought. China Standardization Association GB/T20481-2006 Tech Doc. 2006;
373. YIN H, SUN Y. Characteristics of extreme temperature and precipitation in China in 2017 based on ETCCDI indices. Advances in Climate Change Research. 2018 Dec;9(4):218–26.
374. Soldini L, Darvini G. Extreme rainfall statistics in the Marche region, Italy. Hydrology Research. 2017;48(3):686–700.
375. Kumar S, Chanda K, Pasupuleti S. Spatiotemporal analysis of extreme indices derived from daily precipitation and temperature for climate change detection over India. Theor Appl Climatol. 2020;140(1–2):343–57.
376. Panda DK, Panigrahi P, Mohanty S, Mohanty RK, Sethi RR. The 20th century transitions in basic and extreme monsoon rainfall indices in India: Comparison of the ETCCDI indices. Atmos Res [Internet]. 2016;181:220–35. Available from: http://dx.doi.org/10.1016/j.atmosres.2016.07.002

377. Zhou B, Xu Y, Wu J, Dong S, Shi Y. Changes in temperature and precipitation extreme indices over China: Analysis of a high-resolution grid dataset. International Journal of Climatology. 2016;36(3):1051–66.
378. Pandey PC, Koutsias N, Petropoulos GP, Srivastava PK, Ben Dor E. Land use/land cover in view of earth observation: data sources, input dimensions, and classifiers—a review of the state of the art. Geocarto Int. 2021 May 28;36(9):957–88.
379. Khoshnood Motlagh S, Sadoddin A, Haghnegahdar A, Razavi S, Salmanmahiny A, Ghorbani K. Analysis and prediction of land cover changes using the land change modeler (<scp>LCM</scp>) in a semiarid river basin, Iran. Land Degrad Dev [Internet]. 2021 Jun 11;32(10):3092–105. Available from: https://onlinelibrary.wiley.com/doi/10.1002/ldr.3969
380. Rujoiu-Mare MR, Mihai BA. Mapping Land Cover Using Remote Sensing Data and GIS Techniques: A Case Study of Prahova Subcarpathians. Procedia Environ Sci. 2016;32:244–55.
381. Shalaby A, Tateishi R. Remote sensing and GIS for mapping and monitoring land cover and land-use changes in the Northwestern coastal zone of Egypt. Applied Geography. 2007 Jan;27(1):28–41.
382. Das L, Bhatti MS, Gilhotra V, Sarkar S, Ahmad Kazmi A. Remediation of arsenic contaminated groundwater by electrocoagulation: Process optimization using response surface methodology. Miner Eng. 2022 Nov;189:107881.
383. Saaroni H, Ben-Dor E, Bitan A, Potchter O. Spatial distribution and microscale characteristics of the urban heat island in Tel-Aviv, Israel. Landsc Urban Plan. 2000 Apr;48(1–2):1–18.
384. Roy A, Inamdar AB. Multi-temporal Land Use Land Cover (LULC) change analysis of a dry semi-arid river basin in western India following a robust multi-sensor satellite image calibration strategy. Heliyon. 2019 Apr;5(4):e01478.
385. Khwarahm NR, Najmaddin PM, Ararat K, Qader S. Past and future prediction of land cover land use change based on earth observation data by the CA–Markov model: a case study from Duhok governorate, Iraq. Arabian Journal of Geosciences. 2021 Aug 28;14(15):1544.
386. Khwarahm NR, Qader S, Ararat K, Fadhil Al-Quraishi AM. Predicting and mapping land cover/land use changes in Erbil /Iraq using CA-Markov synergy model. Earth Sci Inform. 2021 Mar 27;14(1):393–406.
387. Kar R, Obi Reddy GP, Kumar N, Singh SK. Monitoring spatio-temporal dynamics of urban and peri-urban landscape using remote sensing and GIS – A case study from Central India. The Egyptian Journal of Remote Sensing and Space Science. 2018 Dec;21(3):401–11.
388. Kassawmar T, Eckert S, Hurni K, Zeleke G, Hurni H. Reducing landscape heterogeneity for improved land use and land cover (LULC) classification across the large and complex Ethiopian highlands. Geocarto Int. 2018 Jan 2;33(1):53–69.
389. Morshed N, Yorke C, Zhang Q. Urban Expansion Pattern and Land Use Dynamics in Dhaka, 1989–2014. The Professional Geographer. 2017 Jul 3;69(3):396–411.
390. Roy DP, Yan L. Robust Landsat-based crop time series modelling. Remote Sens Environ. 2020 Mar;238:110810.
391. Lu Y, Wu P, Ma X, Li X. Detection and prediction of land use/land cover change using spatiotemporal data fusion and the Cellular Automata–Markov model. Environ Monit Assess. 2019 Feb 14;191(2):68.
392. Nath B, Wang Z, Ge Y, Islam K, P. Singh R, Niu Z. Land Use and Land Cover Change Modeling and Future Potential Landscape Risk Assessment Using Markov-CA Model and Analytical Hierarchy Process. ISPRS Int J Geoinf. 2020 Feb 24;9(2):134.
393. Gaur S, Singh R. A Comprehensive Review on Land Use/Land Cover (LULC) Change Modeling for Urban Development: Current Status and Future Prospects. Sustainability. 2023 Jan 4;15(2):903.
394. Serneels S, Said MY, Lambin EF. Land cover changes around a major east African wildlife reserve: The Mara Ecosystem (Kenya). Int J Remote Sens. 2001 Jan 25;22(17):3397–420.
395. Lin YP, Chu HJ, Wu CF, Verburg PH. Predictive ability of logistic regression, auto-logistic regression and neural network models in empirical land-use change modeling – a case study. International Journal of Geographical Information Science. 2011 Feb 23;25(1):65–87.
396. Islam K, Rahman MdF, Jashimuddin M. Modeling land use change using Cellular Automata and Artificial Neural Network: The case of Chunati Wildlife Sanctuary, Bangladesh. Ecol Indic. 2018 May;88:439–53.

397. Calvin K V., Snyder A, Zhao X, Wise M. Modeling land use and land cover change: using a hindcast to estimate economic parameters in gcamland v2.0. Geosci Model Dev. 2022 Jan 19;15(2):429–47.
398. Lambin EF, Geist H. Land-Use and Land-Cover Change. Lambin EF, Geist H, editors. Berlin, Heidelberg: Springer Berlin Heidelberg; 2006.
399. Evans TP, Phanvilay K, Fox J, Vogler J. An agent-based model of agricultural innovation, land-cover change and household inequality: the transition from swidden cultivation to rubber plantations in Laos PDR. J Land Use Sci. 2011 Jun;6(2–3):151–73.
400. Poelmans L, Van Rompaey A. Complexity and performance of urban expansion models. Comput Environ Urban Syst. 2010 Jan;34(1):17–27.
401. Jokar Arsanjani J, Helbich M, Kainz W, Darvishi Boloorani A. Integration of logistic regression, Markov chain and cellular automata models to simulate urban expansion. International Journal of Applied Earth Observation and Geoinformation. 2013 Apr;21:265–75.
402. Yan J, Wang L, Song W, Chen Y, Chen X, Deng Z. A time-series classification approach based on change detection for rapid land cover mapping. ISPRS Journal of Photogrammetry and Remote Sensing. 2019 Dec;158:249–62.
403. Kumar R, Nandy S, Agarwal R, Kushwaha SPS. Forest cover dynamics analysis and prediction modeling using logistic regression model. Ecol Indic. 2014 Oct;45:444–55.
404. Siddiqui A, Siddiqui A, Maithani S, Jha AK, Kumar P, Srivastav SK. Urban growth dynamics of an Indian metropolitan using CA Markov and Logistic Regression. The Egyptian Journal of Remote Sensing and Space Science. 2018 Dec;21(3):229–36.
405. Mishra VN, Rai PK. A remote sensing aided multi-layer perceptron-Markov chain analysis for land use and land cover change prediction in Patna district (Bihar), India. Arabian Journal of Geosciences. 2016 Apr 24;9(4):249.
406. Rahman MTU, Tabassum F, Rasheduzzaman Md, Saba H, Sarkar L, Ferdous J, et al. Temporal dynamics of land use/land cover change and its prediction using CA-ANN model for southwestern coastal Bangladesh. Environ Monit Assess. 2017 Nov 17;189(11):565.
407. Berberoğlu S, Akın A, Clarke KC. Cellular automata modeling approaches to forecast urban growth for adana, Turkey: A comparative approach. Landsc Urban Plan. 2016 Sep;153:11–27.
408. Dietzel C, Clarke KC. Toward Optimal Calibration of the SLEUTH Land Use Change Model. Transactions in GIS. 2007 Feb;11(1).
409. Saxena A, Jat MK. Land suitability and urban growth modeling: Development of SLEUTH-Suitability. Comput Environ Urban Syst. 2020 May;81:101475.
410. Veldkamp A, Fresco LO. CLUE: a conceptual model to study the Conversion of Land Use and its Effects. Ecol Modell. 1996 Mar;85(2–3):253–70.
411. Mirkatouli J, Hosseini A, Neshat A. Analysis of land use and land cover spatial pattern based on Markov chains modelling. City, Territory and Architecture. 2015 Dec 24;2(1):4.
412. Aaviksoo K. Simulating vegetation dynamics and land use in a mire landscape using a Markov model. Landsc Urban Plan. 1995 Feb;31(1–3):129–42.
413. Anand V, Oinam B. Future land use land cover prediction with special emphasis on urbanization and wetlands. Remote Sensing Letters. 2020 Mar 3;11(3):225–34.
414. Iacono MA, Levinson DB, El-geneidy AC, Wasfi RD. A Markov chain model of land use change in the Twin A MARKOV CHAIN MODEL OF LAND USE CHANGE. TeMA Journal of Land Use, Mobility and Environment TeMA [Internet]. 2015;1(3):49–62. Available from: http://dx.doi.org/10.6092/1970-9870/2431
415. Ahmed B, Ahmed R. Modeling Urban Land Cover Growth Dynamics Using Multi-Temporal Satellite Images: A Case Study of Dhaka, Bangladesh. ISPRS Int J Geoinf. 2012 Feb 23;1(1):3–31.
416. Hornik K, Stinchcombe M, White H. Multilayer feedforward networks are universal approximators. Neural Networks. 1989 Jan;2(5):359–66.
417. Megahed Y, Cabral P, Silva J, Caetano M. Land Cover Mapping Analysis and Urban Growth Modelling Using Remote Sensing Techniques in Greater Cairo Region—Egypt. ISPRS Int J Geoinf. 2015 Sep 14;4(3):1750–69.
418. Talwar AR. State Disaster Management Plan Punjab. Punjab, India; 2011.

419. Jenson SK, Domingue JO. Extracting topographic structure from digital elevation data for geographic information-system analysis. Photogramm Eng Remote Sensing [Internet]. 1988;54(11):1593–600. Available from: http://pubs.er.usgs.gov/publication/70142175
420. Carrara A. Drainage and Divide Networks Derived from High-Fidelity Digital Terrain Models. In: Quantitative Analysis of Mineral and Energy Resources [Internet]. Dordrecht: Springer Netherlands; 1988. p. 581–97. Available from: http://link.springer.com/10.1007/978-94-009-4029-1_34
421. Tarboton DG, Bras RL, Rodriguez-Iturbe I. On the extraction of channel networks from digital elevation data. Hydrol Process [Internet]. 1991 Jan;5(1):81–100. Available from: https://onlinelibrary.wiley.com/doi/10.1002/hyp.3360050107
422. O'Callaghan JF, Mark DM. The extraction of drainage networks from digital elevation data. Comput Vis Graph Image Process [Internet]. 1984 Dec;28(3):323–44. Available from: https://linkinghub.elsevier.com/retrieve/pii/S0734189X84800110
423. Raju BMK, Rao K V, Venkateswarlu B, Rao AVMS, Rao CAR, Rao VUM, et al. Revisiting climatic classification in India: a district-level analysis. Curr Sci [Internet]. 2013 Dec 25;105(4):492–5. Available from: http://www.jstor.org/stable/24098002
424. Gorai S, Ratha D, Dhir A. Adapting Rainfall Variability to Flood Risk: A Case Study of the Ghaggar River Basin. Journal of the Geological Society of India [Internet]. 2021 Nov 21;97(11):1347–54. Available from: https://link.springer.com/10.1007/s12594-021-1873-1
425. Kundu S, Mondal D. Analysis of long-term rainfall trends and change point in West Bengal, India. Theor Appl Climatol. 2019 Jun 25;138.
426. Sharma CS, Panda SN, Pradhan RP, Singh A, Kawamura A. Precipitation and temperature changes in eastern India by multiple trend detection methods. Atmos Res [Internet]. 2016;180:211–25. Available from: http://dx.doi.org/10.1016/j.atmosres.2016.04.019
427. Wu H, Qian H. Innovative trend analysis of annual and seasonal rainfall and extreme values in Shaanxi, China, since the 1950s. International Journal of Climatology [Internet]. 2017 Apr 1;37(5):2582–92. Available from: https://doi.org/10.1002/joc.4866
428. Croitoru AE, Piticar A, Burada DC. Changes in precipitation extremes in Romania. Quaternary International [Internet]. 2016;415:325–35. Available from: http://dx.doi.org/10.1016/j.quaint.2015.07.028
429. Westra S, Fowler HJ, Evans JP, Alexander L V., Berg P, Johnson F, et al. Future changes to the intensity and frequency of short-duration extreme rainfall. Reviews of Geophysics. 2014;52(3):522–55.
430. Jain SK, Kumar V, Saharia M. Analysis of rainfall and temperature trends in northeast India. International Journal of Climatology. 2013;33(4):968–78.
431. Jaiswal RK, Lohani AK, Tiwari HL. Statistical Analysis for Change Detection and Trend Assessment in Climatological Parameters. Environmental Processes. 2015;2(4):729–49.
432. Rai RK, Upadhyay A, Ojha CSP. Temporal Variability of Climatic Parameters of Yamuna River Basin: Spatial Analysis of Persistence, Trend and Periodicity. The Open Hydrology Journal. 2010 Mar 20;4(1):184–210.
433. Asfaw A, Simane B, Hassen A, Bantider A. Variability and time series trend analysis of rainfall and temperature in northcentral Ethiopia: A case study in Woleka sub-basin. Weather Clim Extrem [Internet]. 2018;19(June 2017):29–41. Available from: https://doi.org/10.1016/j.wace.2017.12.002
434. Panwar M, Agarwal A, Devadas V. Analyzing land surface temperature trends using non-parametric approach: A case of Delhi, India. Urban Clim [Internet]. 2018;24(January):19–25. Available from: https://doi.org/10.1016/j.uclim.2018.01.003
435. Haan , CT. Statistical methods in hydrology. Ames, Iowa: Iowa State Press; 2002.
436. Machiwal D, Jha MK. Hydrologic Time Series Analysis: Theory and Practice [Internet]. Dordrecht: Springer Netherlands; 2012. Available from: http://link.springer.com/10.1007/978-94-007-1861-6
437. Anderson RL. Distribution of the Serial Correlation Coefficient. The Annals of Mathematical Statistics [Internet]. 1942 Mar;13(1):1–13. Available from: http://projecteuclid.org/euclid.aoms/1177731638
438. von Storch H. Misuses of Statistical Analysis in Climate Research. In: Analysis of Climate Variability [Internet]. Berlin, Heidelberg: Springer Berlin Heidelberg; 1995. p. 11–26. Available from: http://link.springer.com/10.1007/978-3-662-03167-4_2

439. Salehi S, Dehghani M, Mortazavi SM, Singh VP. Trend analysis and change point detection of seasonal and annual precipitation in Iran. International Journal of Climatology [Internet]. 2020;40(1):308–23. Available from: https://doi.org/10.1002/joc.6211
440. Buishand TA. Some methods for testing the homogeneity of rainfall records. J Hydrol (Amst) [Internet]. 1982 Aug;58(1–2):11–27. Available from: https://linkinghub.elsevier.com/retrieve/pii/002216948290066X
441. Wijngaard JB, Klein Tank AMG, Können GP. Homogeneity of 20th century European daily temperature and precipitation series. International Journal of Climatology [Internet]. 2003 May;23(6):679–92. Available from: https://onlinelibrary.wiley.com/doi/10.1002/joc.906
442. Devi TB, Kumar B. Flow characteristics in an alluvial channel covered partially with submerged vegetation. Ecol Eng. 2016 Sep;94:478–92.
443. Wilson KJ. An investigation of dependence in expert judgement studies with multiple experts. Int J Forecast. 2017 Jan;33(1):325–36.
444. Saaty TL. A scaling method for priorities in hierarchical structures. J Math Psychol [Internet]. 1977;15(3):234–81. Available from: https://www.sciencedirect.com/science/article/pii/0022249677900335
445. Ratha D, Agrawal VP. Structural Modeling and Analysis of Water Resources Development and Management System: A Graph Theoretic Approach. Water Resources Management [Internet]. 2014;28(10):2981–97. Available from: https://doi.org/10.1007/s11269-014-0650-y
446. Ratha D, Agrawal VP. A digraph permanent approach to evaluation and analysis of integrated watershed management system. J Hydrol (Amst) [Internet]. 2015;525:188–96. Available from: https://www.sciencedirect.com/science/article/pii/S0022169415002176
447. Anand J, Gosain AK, Khosa R. Prediction of land use changes based on Land Change Modeler and attribution of changes in the water balance of Ganga basin to land use change using the SWAT model. Science of The Total Environment [Internet]. 2018;644:503–19. Available from: https://www.sciencedirect.com/science/article/pii/S0048969718324926
448. Gumindoga W, Rientjes T, Shekede M, Rwasoka D, Nhapi I, Haile A. Hydrological Impacts of Urbanization of Two Catchments in Harare, Zimbabwe. Remote Sens (Basel) [Internet]. 2014 Dec 12;6(12):12544–74. Available from: http://www.mdpi.com/2072-4292/6/12/12544
449. Mango LM, Melesse AM, McClain ME, Gann D, Setegn SG. Land use and climate change impacts on the hydrology of the upper Mara River Basin, Kenya: results of a modeling study to support better resource management. Hydrol Earth Syst Sci [Internet]. 2011 Jul 18;15(7):2245–58. Available from: https://hess.copernicus.org/articles/15/2245/2011/
450. Pontius RG, Huffaker D, Denman K. Useful techniques of validation for spatially explicit land-change models. Ecol Modell [Internet]. 2004;179(4):445–61. Available from: https://www.sciencedirect.com/science/article/pii/S0304380004002716

JOURNAL GEOLOGICAL SOCIETY OF INDIA
Vol.97, November 2021, pp.1347-1354

Adapting Rainfall Variability to Flood Risk: A Case Study of the Ghaggar River Basin

Sanjoy Gorai[1], Dwarikanath Ratha[2,*] and Amit Dhir[1]

[1]School of Energy & Environment. [2]Department of Civil Engineering,
Thapar Institute of Engineering & Technology, Patiala – 147 001, India
E-mail: *kumarsanjoy7@gmail.com; dnath.ratha@thapar.edu*; amit.dhir@thapar.edu*

ABSTRACT

Floods are the most common natural disasters influenced by climatic variables and anthropogenic activities. Ghaggar is a seasonal river of north-western region of India and this basin has been experiencing moderate to high intensity of floods frequently. The present study aims to find out the impact of the rainfall variability on the flooding scenario of this basin using hydro-meteorological data. The rainfall data was collected for 12 stations of the basin. The rainfall and extreme rainfall of the Ghaggar basin was determined using innovative trend analysis which was further validated by Mann-Kendall test. The runoff generated from the average annual rainfall and extreme rainfall in terms of rx1day was determined using SCS-CN method. It is found from the analysis that the southwest monsoon is dominant all over the basin and is the main reason for causing the flood. The rx1day rainfall trend is positive at the stations situated in the middle of the basin which is another factor for causing the flood. It is also found that the runoff generated at the uppermost part of the basin due to heavy rainfall at Kalka and Nahan meteorological divisions when combined with runoff generated from middle of basin is creating the flood situation at middle of the basin. Flood hazard mapping was also carried out for vulnerability analysis and found that the basin area is moderate to highly vulnerable to floods.

INTRODUCTION

The impact of climatic variability, anthropogenic activities and terrain characteristics influences the annual runoff of a river basin which leads to natural hazards such as flood or drought. A small fluctuation of rainfall due to altered hydrological cycle affects a catchment in large proportion and incurs huge economic loss. Urbanisation is also another factor which forces the engineers and scientists to assess periodically the demand, availability and extremity of future water resources of a city. The poor urban planning along with its high population existing at lower elevation of river basin leads to flood. India is experiencing erratic rainfall in last 20 years due to which the disaster like flood is frequently occurring and much more attention is required to study the hydro-meteorological behaviour inorder to predict such disasters. Since the rainfall trend is periodically changing due to climate change, the time series analysis is necessary to detect the trend of hydro-meteorological behaviour which triggers the natural hazards. Numerous studies are conducted for finding out the changes in trend of rainfall, temperature, number of rainy days etc. (Wang et al. 2020; Saádi et al. 2019; Kulkarni and Pardesi 2019; Pal et al. 2019; Caloiero et al. 2018; Mishra and Shah 2018). These studies are conducted at global, regional and local scale for monthly, seasonally, annually or any specified period of the year and found the different result either significantly or non-significantly for the increasing or decreasing trend and their magnitude. The climate change impact on flood generation is mainly dependent on the pattern of rainfall. Mishra and Shah (2018) raised questions on unprecedented extreme precipitation and runoff which caused the Kerala flood in 2018 despite of the significant decreasing trend of monsoon precipitation, 1 day and 2 day annual maximum precipitation and subsequent total runoff. The frequency of flood in urban or rural areas is continuously increasing which is influenced by both urbanisation and climate change.

Most of the hydrological and meteorological studies in India are conducted for larger basin but very few similar studies are found for smaller and medium river basins. Smaller towns and villages in India are situated in the medium river basin and their growth usually occurs in an unplanned manner. The climate change in these basins leads to floods and cause huge economic loss. Ghaggar river basin in India is a medium range basin along which most of the small towns are situated. Instantaneous heavy discharge along with human interferences and non-maintenance of canal embankment in this basin are the reasons for occurrence of floods of different extent (CWC, 2014). The origin of the basin lies in moist sub-humid region, middle of the basin lies in semi-arid region and downstream of the basin lies in arid region. It is expected that the heavy rainfall at the watershed of Himachal (origin of the basin) along with moderate to heavy rainfall in middle of the basin (semi-arid region) causes flood at the middle of the basin. Several flood history during 1960-2010 has been reported in the report of Revenue Department of Punjab (Talwar, 2011). Therefore, authors undertook this basin to study the flood related hazards.

The objective of the present study is to observe the average rainfall and extreme rainfall trend of Ghaggar basin using innovative trend analysis (ITA) method which was subsequently validated by Mann-Kendall (MK) test. Flood causing factors on Ghaggar basin are identified through the study of climatic variability of this region. Also the present study identifies an area in this basin which is vulnerable to flood through flood hazard mapping.

METHODOLOGY

The prediction of runoff and the probability of occurrence of flood due to rainfall in a catchment depend largely on both the climate and basin characteristics. The present study used a methodology in which the rainfall and extreme rainfall variability were studied using hydro-meteorological data and further run off was predicted. Initially the missing rainfall data for each station was identified and 5% lesser missing data stations were used for the study. The Thiessen polygon method was used to determine the effective area for a rain gauge station. The present study used ITA test to analyse the trend and magnitude of trend.The results obtained from ITA test have been compared with MK test and Sen slope estimator. The results obtained from trend analysis were used to check the variability of rainfall with respect to space and time over the catchment. Homogeneity analysis of the time series data was done using Pettit's test for finding out the most probable

0016-7622/2021-97-11-1347/$ 1.00 © GEOL. SOC. INDIA | DOI: 10.1007/s12594-021-1873-1

Table 1. Source and Resolution of different dataset used for this study

Sr. No.	Data used	Source
1	Hydrometeorological data	Indian Meteorological Department (IMD) (http://dsp.imdpune.gov.in/)
2	30m resolution DEM data	Shuttle Radar Topography Mission (SRTM) (https://earthexplorer.usgs.gov/)
3	500m resolution (LULC)	MODIS Land cover V6 (https://earthexplorer.usgs.gov/)
4	250m resolution (HSG) data	Global Hydrologic Soil Groups (HYSOGs250m) (https://daac.ornl.gov/SOILS/guides/Global_Hydrologic_Soil_Group.html)

change point of the rainfall trend. Inorder to predict the occurrence of flood in a catchment, the rx1day (annual maximum 1 day rainfall) parameter was selected to determine the magnitude of extreme events and runoff. Soil Conservation Service Curve Number (SCS-CN) method was used for the analysis of total runoff over the basins. Further, the flood vulnerability of the study area was identified from the calculated runoff from the basin (Lin et al. 2017).The spatial analysis for rainfall, rx1day and their trend variability was made using inverse distance weighted (IDW) interpolation techniques in ArcGIS 10.5. Table 1 shows the type and source of various data used in the present study.

Innovative Trend Analysis (ITA)

This methodology was developed by Sen (2017) and usually performed by dividing the time series data into two halves. The first half of the data is plotted on the x-axis and the second half on the y-axis. The trend analysis result depends on the position of the data around a 45° angle straight line. For calculation of the slope of the trend line Equation 1 is used

$$S = \frac{2(\bar{y}_2 - \bar{y}_1)}{n} \quad (1)$$

Where, $\bar{y}_1$is the arithmetic mean of the first half of the dataset, $\bar{y}_2$ is the arithmetic mean of the second half of the dataset and *n* is the length of dataset.

SCS-CN method for run-off calculation

Soil Conservation Service Curve Number (SCS-CN) method (Al-Juaidi, 2018; Uwizeyimana et al. 2019) was used in the present study for the analysis of total runoff from the extreme and average annual rainfall. The amount of runoff was calculated using Eq. (2) assuming the initial abstraction is 0.2S where S is the potential maximum retention after runoff starts.

$$Q = \frac{(p - 0.2S)^2}{(p - 0.8S)} \quad (2)$$

The potential maximum retention after runoff starts (S) was calculated using Eq. 3.

$$S = \frac{25400}{CN} - 254 \quad (3)$$

Where, P and Q are the rainfall and runoff in mm respectively. The volume of runoff generation over an area was calculated by multiplying the area with the runoff. Curve Number (CN) is a dimensionless parameter whose value ranges from 0-100 based on HSG and LULC. LULC and HSG have been superimposed on the DEM of a catchment to determine the CN. Geo-HMS tool of ArcGIS 10.2 was used to generate the CN map. The slope adjustment for CN number (CN_s) was calculated using Huang method (Huang et al., 2006) as in Eq. 4.

$$CN_s = CN \times \frac{322.79 + 15.63s}{s + 323.52} \quad (4)$$

where *s* is the slope and CN is the curve number for AMC II. The spatial map runoff is generated by using Eqs. (2-4) in raster analysis of ArcGIS 10.5.

STUDY AREA

Ghaggar river is a seasonal flow river which is originated from Shivalik hills of Himachal Pradesh and flows through the northern part of India, i.e., Haryana, Punjab, Chandigarh and Rajasthan. The total area of the basin is 32132 sq.km. Figure 1(a) shows the study area and the location of the rain gauge stations. The basin area where generally flood occurs was identified and delineated using the Digital Elevation Model (DEM) as shown in Figure 1(b). The present study area lies within latitude of 29.30ºN to 30.50ºN and longitude 75.0ºE to 77.20ºE. The elevation of the basin lies in the range of 143-1790m above the mean sea level. The land use land cover (LULC) of the basin comprises croplands (88.1%), savannas (6.22%) and urban built up (3.3%). The major towns of northern India such as Ambala, Chandigarh, Patiala, Rajpura and Mohali are located in the watershed of Ghaggar basin. The geographical location and available rainfall data period for each rain gauge station are represented in Table 2. These stations were considered for the study based on the complete availability of the rainfall data in the basin.

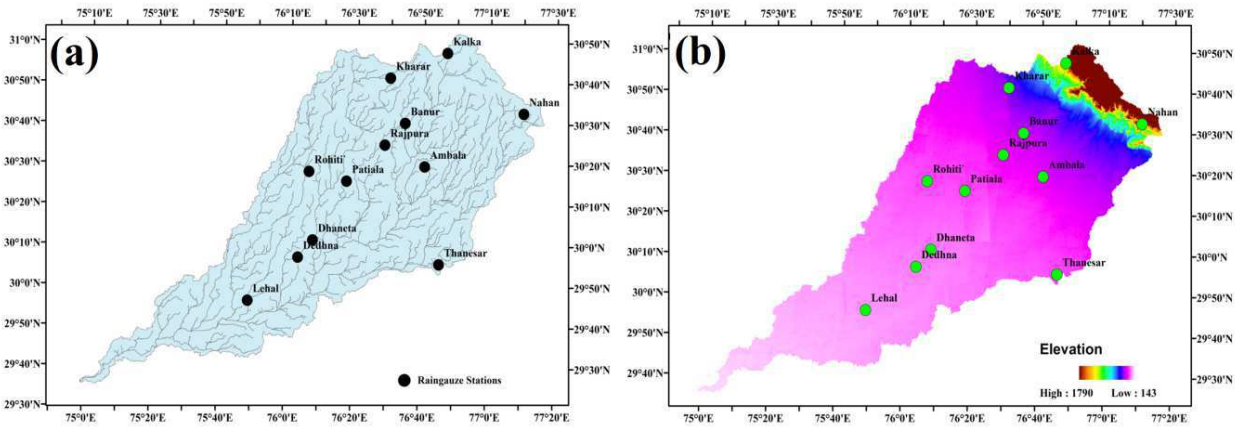

Fig.1. (a) Ghaggar river basin and location of the rain gauge stations and **(b)** Digital Elevation Model of Ghaggar river basin.

Table 2. Details of rain gauge station, data period and descriptive statistics of average rainfall

Sr. No.	Station Name	Latitude (N)	Longitude (E)	Elevation (m)	Data Period	Duration (years)	Area (km^2)	Average Rainfall					
								Southwest Monsoon			Annual		
								Mean (mm)	Std. Dev.	Coefficient of Variation	Mean (mm)	Std. Dev.	Coefficient of Variation
1	Ambala	30.375200	76.782100	264	1985-2018	34	1578	643.6	237.4	36.9	796.8	245.5	30.8
2	Banur	30.559356	76.699154	278	1976-2010	35	574	533.0	326.6	61.3	655.5	402.1	61.3
3	Dedhna	30.041859	76.119674	227	1975-2010	36	1140	202.6	266.2	131.4	266.7	316.2	118.6
4	Dhaneta	30.108413	76.199384	244	1976-2010	35	1038	336.5	291.3	86.6	435.7	342.4	78.6
5	Kalka	30.833300	76.935700	656	1951-2010	60	840	862.3	360.1	41.8	1033.6	373.6	36.1
6	Kharar	30.749800	76.641100	309	1950-2018	59	965	527.6	211.6	40.1	664.2	260.4	39.2
7	Lehal	29.878190	75.856301	240	1975-2010	35	2721	429.8	300.3	69.9	533.8	338.7	63.5
8	Nahan	30.559900	77.295500	932	1951-2007	51	1015	1421.0	663.7	46.7	1703.2	718.3	42.2
9	Patiala	30.339910	76.387072	255	1975-2017	43	1044	575.2	281.0	48.9	698.0	297.3	42.6
10	Rajpura	30.476545	76.590489	273	1975-2017	43	723	553.3	322.4	58.3	660.4	343.6	52.0
11	Rohiti	30.390482	76.202644	255	1975-2010	35	1302	563.0	384.0	68.2	705.9	391.6	55.5
12	Thanesar	29.969900	76.819300	232	1950-2011	62	1036	522.0	217.6	41.7	641.3	244.1	38.1

RESULT AND DISCUSSION

The average and extreme rainfall trend and corresponding runoff of the study area were analysed. The results obtained in the present study are discussed below.

Descriptive Analysis of Seasonal and Annual Rainfall

Table 2 shows the statistical analysis such as average, standard deviation and coefficient of variance for all the stations. The mean and standard deviation of rainfall over the various stations varies in the range of 266-1703mm and 244-718.3mm respectively. The coefficient of variation varies in the range of 30-118 indicating wider variation of rainfall at some of the stations. Figure 2(a&b) shows the variation of annual and southwest monsoon rainfall during 1950-2015. It is seen from Figure 2(a&b) that Kalka and Nahan are the stations which receive more than 1000mm average annual rainfall whereas all other stations are receive rainfall between 600mm to 800mm annually except Dedhna, Dhaneta and Lehal. Figure 2(c&d) shows the spatial distribution of average annual and monsoon rainfall. It is seen from Figure 2(c&d) that the maximum annual rainfall fluctuation is recorded at Dedhna region (118.6mm) whereas the minimum rainfall fluctuation is recorded at Ambala region (30.8mm) indicating the unstable incidence of rainfall at Dedhna. It is observed from the seasonal analysis that the annual rainfall trend of the basin is completely reflecting in southwest monsoon season of the rainfall. The runoff of the basin is totally dependent on the rainfall received during the southwest monsoon season. Since this river flows mostly during the southwest monsoon season, the probability of occurring of flood in non-monsoon season will be very less.

Seasonal and Annual Rainfall Trend Analysis

The trend analysis of the basin shows the decreasing trend in all stations except Lehal for southwest monsoon analysis whereas the decreasing trend is found in all stations for annual analysis except Lehal and Rohiti region. This indicates that the annual and southwest

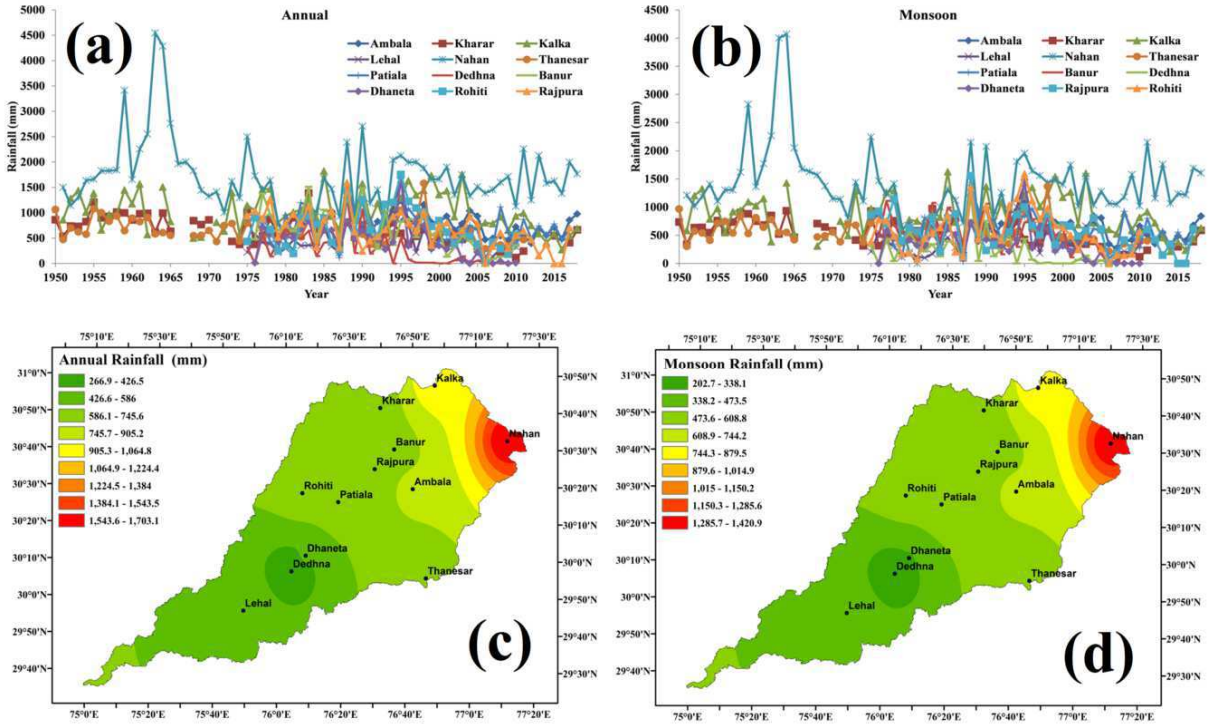

Fig.2. Variation of **(a)** annual and **(b)** south west monsoon rainfall with time; and spatial distribution of average **(c)** annual and **(d)** southwest monsoon rainfall.

monsoon season analysis is more or less consistent in all over the basin. The decreasing trend during southwest monsoon rainfall for Punjab state is also reported by Praveen et al., 2020. The trend and their change in magnitude obtained from ITA method was validated with MK and Sen Slope estimator and similar results are found for most of the regions. The spatial analysis of annual and southwest monsoon season of trend magnitude is shown in Fig. 3(a&b). It is seen from Fig.3(a&b) that Kharar and Thanesar region are showing significant negative trend from southwest monsoon whereas Kalka region is showing significant negative trend from annual analysis by both ITA and MK test. The higher annual magnitude change is obtained at Banur, Dhaneta and Rajpura regions which is greater than 10mm/year whereas the lower magnitude change is obtained at Kalka which is less than 1mm/year. The magnitude change in percentage is spatially plotted in Fig.3(c&d) for both seasonal and annual analysis respectively. It is found from Fig.3(c&d) that the seasonal magnitude changes in percentage for all regions are varying in the range of 8.4% to -254.5% and 19.1% to -162.2% whereas 32.3% to -290.2% and6.9% to -193.2% for annual analysis for the methods of ITA and Sen Slope respectively.

The most probable change point analysis for annual average rainfall trend is executed using Pettit's test and supported by SNH test and Buishand's range test. Figure 4(a-d) shows the spatial distribution of average annual rainfall and magnitude of trend before and after change point respectively. It is found that most of the regions of the basins have change point after the year 1990 and the similar results for Punjab meteorological sub-division is reported by Praveen et al., (2020). Atri and Tyagi (2010) reported that the annual mean temperature of India is generally above the normal since 1990. It is found from the literature that there exists a relationship between temperature and extreme rainfall. Gautam et al. (2009) reported that aerosol absorption with respect to tropospheric temperature likely to induce changes in earth's hydrological cycle and hence increasing rainfall variability and concluded that the steady increase in early summer monsoon rainfall could be led by enhanced pre-monsoon tropospheric warming overserved over Himalayas and subsequent strengthening of the land-sea thermal gradient. Also, Hoegh-Guldberg et al. (2018) reported that an average warming of 1.5°C across the whole globe raises the risk of heat waves and heavy rainfall events. Therefore, it is expected that the unprecedented linear increase in surface temperature after 1990 changed the rainfall trend of Ghaggar basin.

The mean annual rainfall after the change point is found to have decreased for all the stations except Lehal station. The negative trend is found in most of the regions after change point except Patiala, Ambala, Kharar and Nahan stations. Similarly, the variability of rainfall is found to have increased in most of the regions after the change point indicates climate change. It is anticipating that the variability of rainfall leads to increase the frequency of higher intensity rainfall in the basin and resulting higher magnitude floods.

Runoff Determination

SCS-CN method was used for the analysis of total runoff generated from the study area in mm over the year. Figure 5a shows the LULC map which is superimposed on HSG map and DEM to generate the CN map which is shown in Figure 5b. It is observed that the CN value of this river basin lies in the range of 70-99 describing moderate to higher runoff potential. Figure 6(a&b) shows the spatial analysis of annual and southwest monsoon runoff generated from various regions which is lying in the range of 219-1668mm and it is found that the maximum runoff is generated from Nahan and Kalka hill region. The higher runoff generated from upstream hill region is contributing to the middle of the basin and the other regions cause sudden increase in runoff as well as gauge level at the middle of the basin. Infact, the increase in urbanisation should increase the runoff trend due to increase in the impervious areas. In order to establish the same, the runoff generated from the basin for the years 2018 as shown in Fig.6(a) and

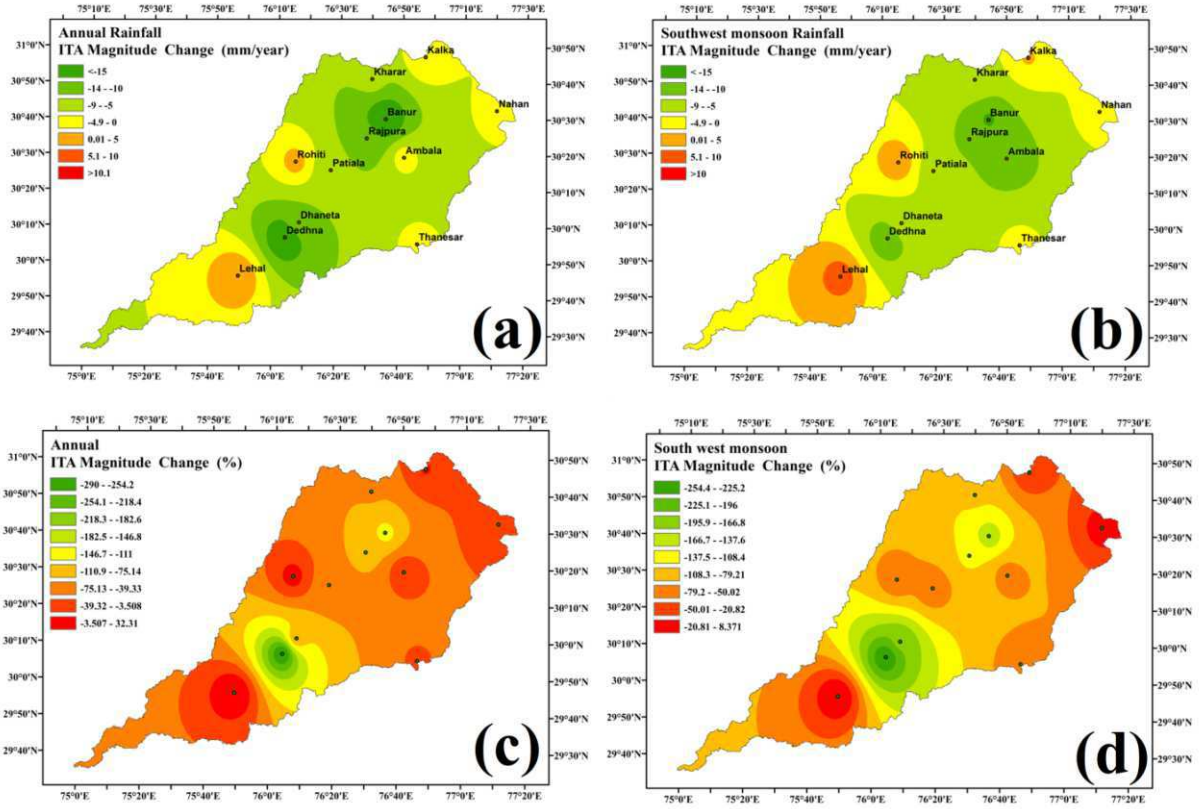

Fig.3. Spatial distribution of trend magnitude of average **(a)** annual **(b)** southwest monsoon rainfall; and spatial distribution of trend magnitude change in percentage for **(c)** annual and **(d)** southwest monsoon rainfall.

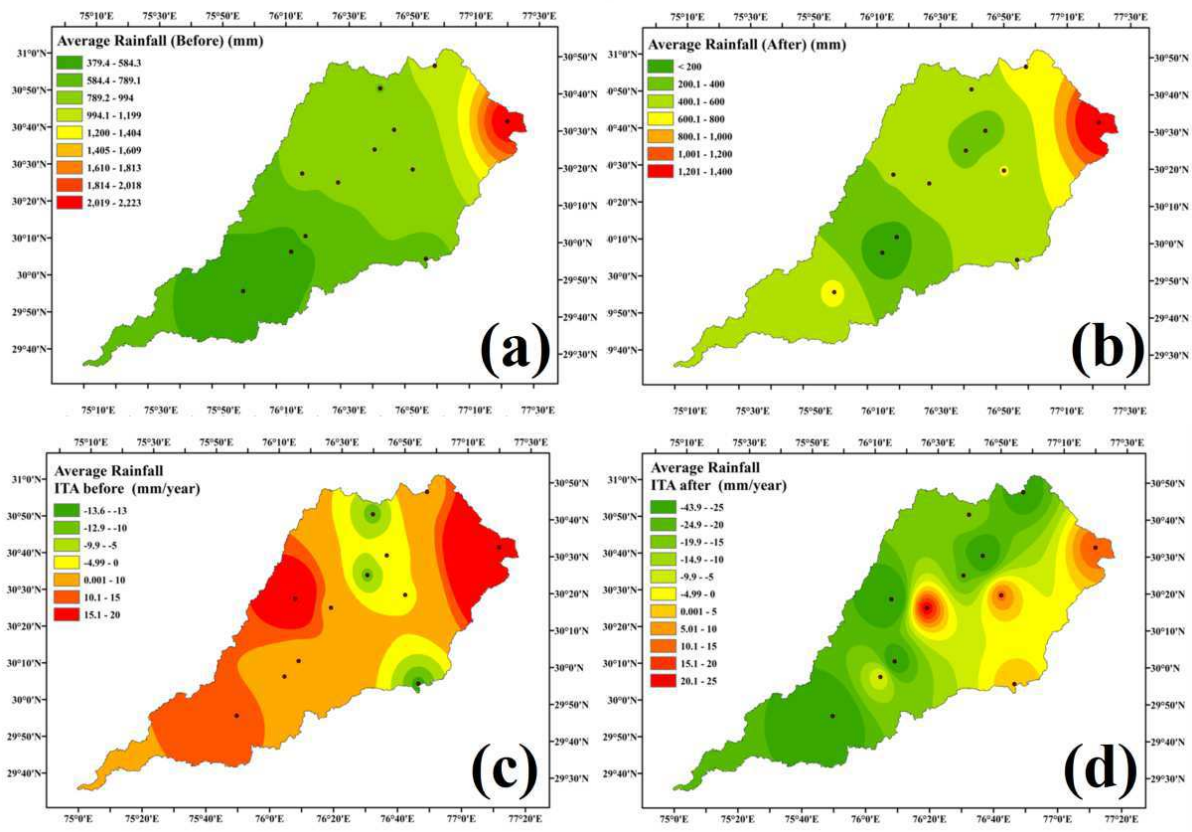

Fig. 4. Spatial distribution of mean annual rainfall **(a)** before and **(b)** after change point and their magnitude of trend using ITA methods **(c)** before and **(d)** after change point.

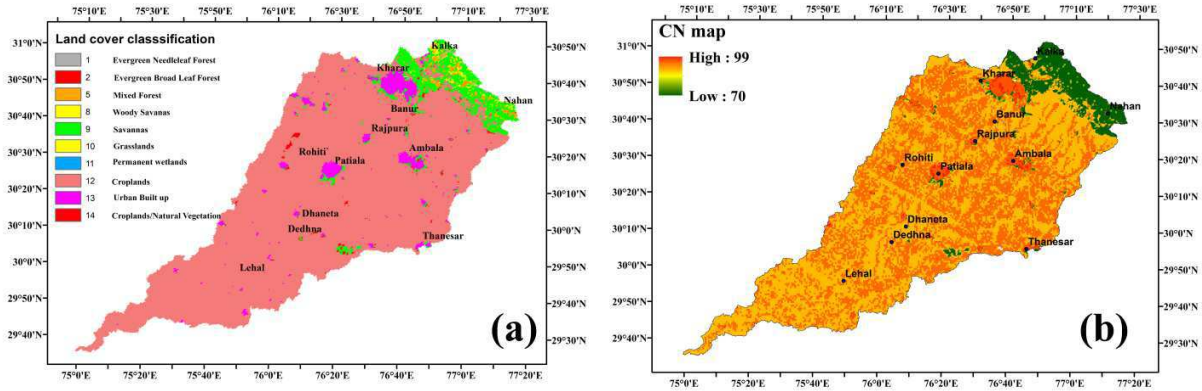

Fig.5. (a) Land cover land use data extracted from MODI's (USGS) and **(b)** CN map for runoff analysis

2001 as shown in Fig.7(a) were prepared considering the weighted average annual rainfall and LULC of 2001 and 2018. Figure 7(b) shows the difference in runoff generated from changed LULC pattern and it is observed that most of the upper part and a few locations of middle part of the basin shows increasing trend of runoff as the LULC pattern of these areas changed. The middle part of the basin where urbanisations occurred during 2001-2018 witnessed increase in runoff whereas the upper part of the basin where both urbanisation and deforestation are the reasons for increase in runoff. The increase in runoff at upper part of the basin, which is a mountainous area, is found despite negative rainfall trend. Although the annual and southwest monsoon seasonal runoff trend at most of the region of the basin is negative, Ghaggar basin has still experienced high intensity flood in the year 1988, 1993, 1995, 2004 and 2010 apart from several moderate and low level flood as per the report of state disaster management plan, Punjab (Talwar, 2011) due to increase in runoff. It is anticipated that the anthropogenic activities such as urbanisation, industrialisation and deforestation cause rise in ambient temperature which alters the rainfall trend, increase the extreme event and subsequent runoff. Therefore, the present study examines the effect of extreme rainfall (rx1day) on the occurrence of flooding in this basin.

The present study also made an effort to validate the runoff generated using ArcGIS despite of non-availability of hourly rainfall and daily runoff data. Very few peak discharge data of Tatiana gauge point of Ghaggar river was found in literature (Bhattacharya and Kumar, 2010; Saini and Kaushik, 2012). Tatiana watershed was delineated using DEM and SCS method synthetic unit hydrograph (NRCS 2010) was used to calculate the peak runoff using catchment characteristics and daily average rainfall which are shown in Table 3 and 4. It is observed that the peak discharge rate using SCS unit hydrograph under predicts the observed peak runoff. Similarly the peak discharge obtained by SCS unit hydrograph method was compared

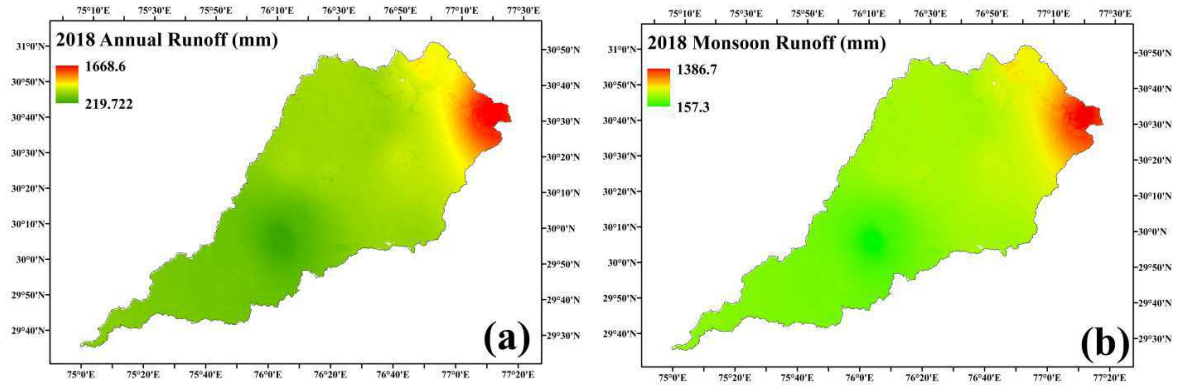

Fig.6. Spatial distribution of (a) annual and (b) southwest monsoon total run off using 2018 LULC and average annual rainfall using SCS-CN method

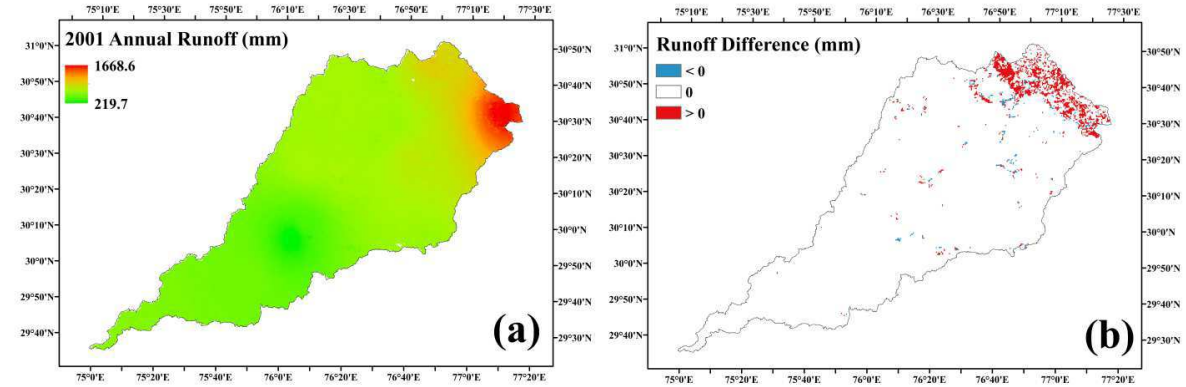

Fig.7. (a) Spatial distribution of annual total runoff using 2001 LULC and average annual rainfall in SCS-CN method and **(b)** change in runoff in the basin due to change in LULC during 2001-2018

with average runoff obtained by ArcGIS for various randomly considered daily average rainfalls and the similar percentage of under prediction is observed. Therefore, it is concluded that the runoff obtained through ArcGIS is in similar line with actual runoff but difference in magnitude might be due to following reasons. (1) the daily average rainfall was considered instead of actual intensity of rainfall (2) the rainfall of some stations on the flooding days are showing zero which might be erroneous (3) the time of discharge measurement was unknown (4) merging of various tributaries with main channel.

Effect of extreme rainfall in terms of rx1day on flooding

The trend of rx1day was also determined by ITA test and validated by MK test. The mean, change in magnitude and percentage of change in magnitude of rx1day was spatially plotted which is shown in Fig.8 and Figs. 9(a & b). It is found from Fig.8 that the mean rx1day rainfall of the basin lies in the range of 66-160mm which is higher than the daily average rainfall.The mean runoff generated from rx1day rainfall for the basin lies in the range of 36-120mm which is very higher side in comparison to mean runoff generated from average annual rainfall and this extreme runoff generated from extreme rainfall might sufficient to cause flood in Ghaggar basin. It is observed from Fig.9a that there is positive trends of rx1day rainfall at lower middle and lower part of the basin whereas most of the upper part of the basin has negative rx1day rainfall trend except Banur.Although the decreasing rx1day trend is observed at certain stations existing at middle of the basin, the rate is very low which is observed from Fig. 9b.

Table 3. Peak discharge of unit hydrograph for Tatiana watershed

L (km)	CN (Weighted average)	S	t_l (hr.)	T_r (hr.)	A (km^2)	t_p (hr.)	t_c (hr.)	Q_p (m^3/s)
87.9	86.3	1.58	57.81	24	1027	69.81	96.35	30.59

Table 4. Calculation of peak discharge using SCS unit hydrograph for known observed discharge

Date of runoff measurement	Observed peak discharge (m^3/s)	Weighted average Rainfall (cm)	Peak discharge for average daily rainfall (SCS UH method) (m^3/s)	Variation
12/07/1993	2831	47	1437.73	49.24%

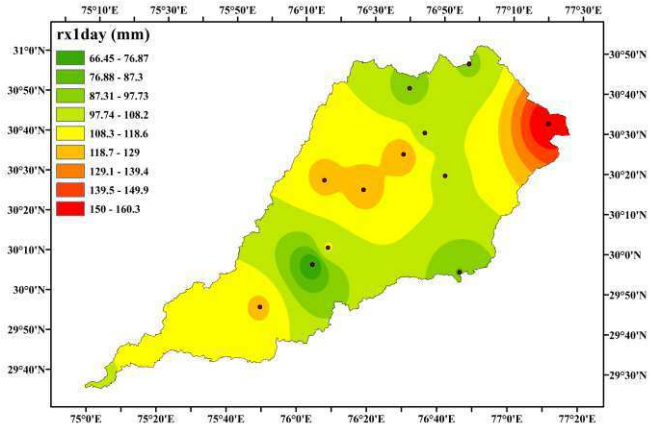

Fig.8. Spatial distribution of annual mean rx1day

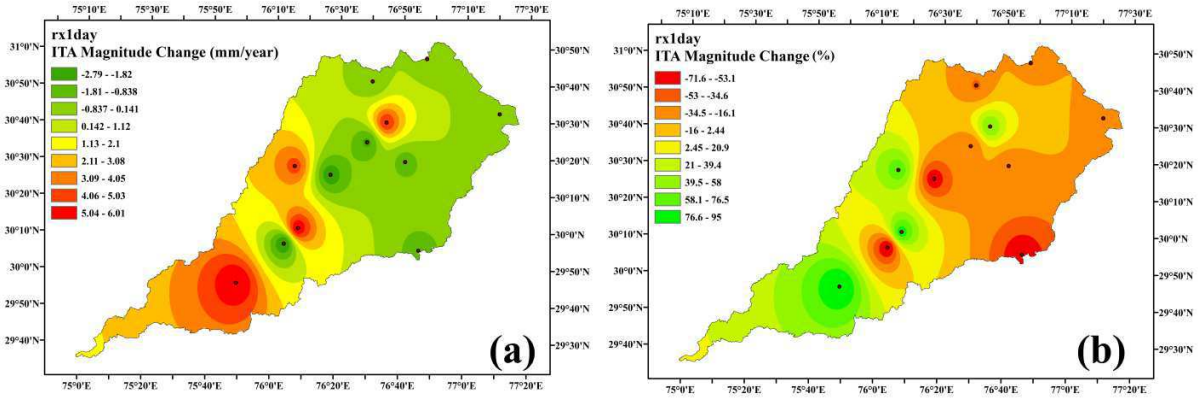

Fig.9. Spatial distribution of (a) trend and (b) % of change in trend magnitude of mean rx1day using ITA method.

Flood in Ghaggar basin during July 6-15, 2010 occurred due to breaching of series of embankments and cause heavy losses in certain parts of Punjab and Haryana. The rx1day rainfall during the first week of July 2010 was extreme case for Ambala, Rajpura, Lehal and Thanesar and also at Nahan region which is at initial portion of basin received 105mm in one day on 5th July 2010. The extreme rx1day rainfall at Nahan was 177.6mm on 17th July 2010. The high intensity rainfall during these days at different locations of the upstream of the basin generated a huge runoff and breached a series of embankments existing in the middle of the basin caused flood during July 6-15, 2010. Similar major flood event had also occurred in the Ghaggar basin during the year September 1988. The peak flood discharge of Tatiana watershed provided by Saini and Kaushik 2012 shows that the maximum runoff obtained at Tatiana watershed was 2831 m^3/s which has a return period of 23 years. It is observed that the frequency of various intensities of flood at Ghaggar basin is increasing despite of negative rainfall trend. Mishra and Shah (2018) also found and discussed the similar results for 2018 Kerala flood. The lower magnitude of decreasing trend of rx1day along with the increase in intensity of rainfallat upstream of the basin located at hilly area, the increasing trend of rx1day at middle of the basin and their combined effects are the reasons for frequently occurring of flood at certain regions of the Ghaggar basin. The effect of anthropogenic activities, such as the increasing urbanisation, its pattern, encroachment towards the basin etc., on the occurrence of flood at this basin requires more research as these parameters affect the geomorphic processes of river such as river profiling, bathymetric profiling, lateral entrenchment ratio, sinuosity index etc.

Vulnerability Analysis of Study Area

The vulnerability to flood analysis has been made by developing a flood hazard map of the study area. The flood hazard map of the study area has been divided into four classes. They are very highly vulnerable, highly vulnerable, moderately vulnerable and least vulnerable. The flood hazard mapping is generated using weighted overlay method (González-Arqueros et al., 2018). The basic inputs used for the analysis are DEM, slope of the basin, land use land cover, soil, CN map, drainage density and rx1day rainfall. The drainage density of the basin is found 0.27km/km^2. Figure 10 shows the flood hazard map of the rx1day rainfall. It is seen from Fig.10 that the flood vulnerability in the present study area has been divided into moderate and highly vulnerable area. Most of the locations in Fig.10 are found moderately vulnerable whereas the locations such as Ambala, Patiala, Rajpura, Chandigarh and lower portion of Nahan are highly vulnerable to flood which is very similar to the places where flood occurred during July 2010 and September 1988. This concludes that the climate change along with the urbanisation and their encroachment towards the basin is causing the area vulnerable to high floods.

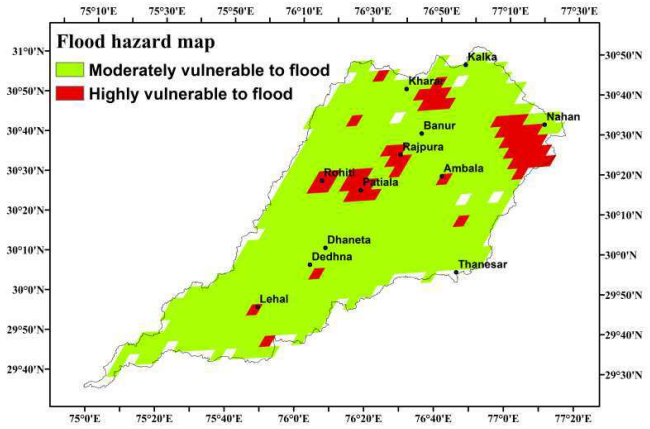

Fig.10. Flood hazard map of the Ghaggar basin

CONCLUSION

The present study investigates the impact of climate variability on extreme rainfall and it's flooding Scenario in Ghaggar basin. The basin area which is vulnerable to flood from its past history was delineated and rainfall trend and extreme rainfall in terms of rx1day trend was analysed for the study area. The runoff generated from average annual rainfall and extreme rainfall in terms of rx1day was determined using SCS-CN method. It is found from the analysis that the southwest monsoon season is completely reflecting in annual trend of the rainfall over the basin. The runoff generated from various regions lies in the range of 219-1668mm. Although the rainfall is decreasing at most of the regions in the basin, it is found that the rx1day rainfall trend is positive at four stations and the rate of decreasing of magnitude of rx1day rainfall at other stations are very less. It is also found that the runoff generated at the uppermost part of the basin due to heavy rainfall at Kalka and Nahan meteorological divisions when combined with runoff generated from middle of basin is creating the flood situation at certain locations of the basin. Area vulnerable to flood in this basin are identified through flood hazard mapping and found that the urbanised areas such as Patiala and Ambala situated in the basin are highly vulnerable which also confirms from actual occurrence of flood during the year 2010. Since palaeo competence and palaeo stage methods illustrates the sensitiveness of flood occurrence to climate change and therefore can be a future scope for acquiring more information on this basin.

Acknowledgement: We gratefully acknowledge the Indian Meteorological Department (IMD), Pune for providing rainfall data used in this study.

References

Al-Juaidi, A. E. M. (2018) A simplified GIS-based SCS-CN method for the assessment of land-use change on runoff. Arabian Jour. Geosci., v.11(11), pp.269.

Attri, S.D. and Tyagi, A. (2010) Climate profile of India. Contribution to the Indian Network of Climate Change Assessment (National Communication-II)., v.1, pp.1-129.

Bhattacharya, S. and Kumar, V. (2010) Unprecedented floods in Ghaggar Basin, Dams, Rivers & People. Available: https://sandrp.files.wordpress.com/2018/03/an_analysis_of_the_flood_disaster_in_ghaggar_basin_in_july_2010.pdf

Caloiero, T., Coscarelli, R. and Ferrari, E. (2018) Application of the Innovative Trend Analysis Method for the Trend Analysis of Rainfall Anomalies in Southern Italy. Water Resour. Managmt., v.32(15), pp.4971–4983.

CWC (2014) Annual Report 2013- 14, Government of India Ministry of Water Resources, River Development & Ganga Rejuvenation. Online available at: http://mowr.gov.in/annual-report

Gautam, R., Hsu, N.C., Lau, K.-M., and Kafatos, M. (2009) Aerosol and rainfall variability over the Indian monsoon region: distributions, trends and coupling, Annales Geophysicae, v.27, pp.3691–3703

González-Arqueros, M.L., Mendoza, M.E., Bocco, G. and Castillo, B.S. (2018) Flood susceptibility in rural settlements in remote zones: The case of a mountainous basin in the Sierra-Costa region of Michoacán, Mexico. Jour. Environ. Managmt., v.223, pp.685-693.

Hoegh-Guldberg, O. et al., (2018) Impacts of 1.5ºC Global Warming on Natural and Human Systems. *In:* Global Warming of 1.5°C. An IPCC Special Report.

Huang, M., Gallichand, J., Wang, Z. and Goulet, M. (2006) A modification to the Soil Conservation Service curve number method for steep slopes in the Loess Plateau of China. Hydrological Processes, v.20, pp.579-589.

Kulkarni, P.P. and Pardeshi, S.D. (2019) Evaluation and interpolation of rainfall trends over the semi-arid upper Godavari basin. Meteorology and Atmospheric Physics, v.131(5), pp.1565–1576.

Lin, W. et al. (2017) Using modified Soil Conservation Service curve number method to simulate the role of forest in flood control in the upper reach of the Tingjiang River in China. Jour. Mountain Sci., v.14(1), pp.1–14.

Mishra, V. and Shah, H.L. (2018) Hydro-climatological Perspective of the Kerala Flood of 2018. Jour. Geol. Soc. India., v.92, pp.645–650.

NRCS (2010) Time of concentration. National Engineering Handbook., Chapter 15.

Pal, L. et al. (2019) Regional scale analysis of trends in rainfall using nonparametric methods and wavelet transforms over a semi-arid region in India. Internat. Jour. Climatol., v.39(5), pp.2737–2764.

Praveen, B., Talukdar, S., Shahfahad et al. (2020) Analyzing trend and forecasting of rainfall changes in India using non-parametrical and machine learning approaches. Scientific Reports., v.10, pp.10342.

Sa'adi, Z. et al. (2019) Trends analysis of rainfall and rainfall extremes in Sarawak, Malaysia using modified Mann–Kendall test. Meteorology and Atmospheric Physics., v.131(3), pp.263–277.

Saini, S.S. and Kaushik, S.P. (2012) Risk and vulnerability assessment of flood hazard in part of Ghaggar Basin: A case study of Guhla block, Kaithal, Haryana, India. Internat. Jour. Geomatics and Geosci., v.3, pp.42-54

Sen, Z. (2017) Innovative trend significance test and applications. Theoretical and Applied Climatol., v.127(3-4), pp.939–947

Talwar, A.R. (2011) State Disaster Management Plan Punjab, Department of Revenue. Rehabilitation and Disaster Management, Government of Punjab, India

Uwizeyimana, D. et al. (2019) Modelling surface runoff using the soil conservation service-curve number method in a drought prone agro-ecological zone in Rwanda. Internat. Soil and Water Conserv. Res., v.7(1), pp.9–17.

Wang,Y., Xu, Y., Tabari H., et al. (2020) Innovative trend analysis of annual and seasonal rainfall in the Yangtze River Delta, eastern China. Atmospheric Res., v. 231, pp.104673.

(Received: 21 November 2020; Revised form accepted: 29 April 2021)

Geocarto International

ISSN: (Print) (Online) Journal homepage: https://www.tandfonline.com/loi/tgei20

Prediction of flood risk zone of Ghaggar river basin, India using graph theory technique

Sanjoy Gorai, Dwarikanath Ratha & Amit Dhir

To cite this article: Sanjoy Gorai, Dwarikanath Ratha & Amit Dhir (2021): Prediction of flood risk zone of Ghaggar river basin, India using graph theory technique, Geocarto International, DOI: 10.1080/10106049.2021.2019836

To link to this article: https://doi.org/10.1080/10106049.2021.2019836

Published online: 27 Dec 2021.

Submit your article to this journal

Article views: 66

View related articles

View Crossmark data

Full Terms & Conditions of access and use can be found at
https://www.tandfonline.com/action/journalInformation?journalCode=tgei20

GEOCARTO INTERNATIONAL
https://doi.org/10.1080/10106049.2021.2019836

Taylor & Francis
Taylor & Francis Group

Check for updates

Prediction of flood risk zone of Ghaggar river basin, India using graph theory technique

Sanjoy Gorai[a], Dwarikanath Ratha[b] and Amit Dhir[a]

[a]School of Energy and Environment, Thapar Institute of Engineering and Technology, Patiala, Punjab, India; [b]Department of Civil Engineering, Thapar Institute of Engineering and Technology, Patiala, Punjab, India

ABSTRACT

Ghaggar river basin of northern India has been experiencing flash floods many times during the last three decades despite locating in semi-arid/arid regions. Identification of the flood risk zone of a basin is essential where the availability of flood-related data is limited. The present study proposed the graph theory to identify the flood risk zone using spatial database of the digital elevation model, land use and land cover, soil cover, population, rainfall, drainage density, distance from roads, rivers, and flood shelters. Further, the results obtained from graph theory were compared with the results obtained by Analytical Hierarchy Process. It is observed that graph theory can also identify the flood risk zone of a basin precisely with acceptable accuracy. Around 94.1% of the study area is observed to have a high flood risk using Analytical Hierarchy Process, whereas 100% area is observed to have a high flood risk using graph theory.

ARTICLE HISTORY
Received 14 August 2021
Accepted 13 December 2021

KEYWORDS
Flood risk assessment; graph theory; analytical hierarchy processes; flood hazard; flood vulnerability

1. Introduction

Flood is one of the most frequently occurring natural disasters that damage infrastructure and property and cause loss of life. The frequency of higher magnitude floods over the world is increasing during the last two decades due to climate change. It is observed that the flood risk is continuously rising in Asia, America, and Europe (Kittipongvises et al. 2020). Anthropogenic activities such as urbanisation in flood plains and deforestation are likely to cause climate change, extreme events such as floods, and frequent changes in the river course. The increase in such anthropogenic activities along most of the river basins of the Indian subcontinent is one reason that makes it highly vulnerable to flooding and subsequent damages. It is observed from the various extreme events that floods are impossible to prevent, but the negative consequences can be minimised with proper planning and management. India is one of the most flood-prone countries in the world. Literature shows that flood risk mapping is a primary step in reducing flood hazards and flood vulnerability by adequately managing the flood-prone areas (Tang et al. 2018). Also, early flood event can be detected by applying conventional artificial intelligence and computational intelligence methods (Fotovatikhah et al. 2018; Kaya et al. 2019). Flood hazard

CONTACT Dwarikanath Ratha dnath.ratha@thapar.edu
© 2021 Informa UK Limited, trading as Taylor & Francis Group

is the probability of occurrence of the flood event at a location due to certain hydrological and geological factors. On the other hand, flood vulnerability is the amount of loss likely to occur from the occurrence of a flood at a location (Ghosh and Kar 2018). The extent of a flood of an area links to the topographic factors such as elevation, land use land cover (LULC), hydrologic soil group, soil cover, distance from the river, etc.; social factors such as population density, building types, specified areas such as airports, institutes, etc.; and climatic factors such as rainfall or extreme rainfall. These factors are static as well as dynamic in nature. Dynamic factors such as land use land cover, rainfall, and population are considered changes with time. The changes of these dynamic factors are required to be frequently analysed using various techniques.

The latest statistical and machine learning techniques are beneficial for finding the flood-prone area, but no single method is sufficient for flood susceptibility mapping over a basin (Costache and Tien Bui 2020). The integration of Multi-Criteria Decision Making (MCDM) with Geographical Information system (GIS) can be applied to identify the areas of high flood risk by considering several independent criteria (Tang et al. 2018). Since the spatial analysis of multi-criteria decision support systems is possible through GIS, the integration of MCDM with GIS is widely used by managers or policymakers. Multi-criteria decision-making is a technique for the decision-making process based on formulating and quantifying different responsible factors (Levy 2005). Analytical Hierarchy Process (AHP) is the most widely used multi-criteria decision-making method for flood risk analysis (De Brito and Evers 2016; Dahri and Abida 2017; Luu et al. 2018; Chakraborty and Mukhopadhyay 2019; Hammami et al. 2019; Souissi et al. 2020; Shahiri Tabarestani and Afzalimehr 2021).

Several researchers have proposed different methods to assess the flood risk of a catchment. Broadly those methods can be categorised into a) hydrological methods, b) statistical methods, and c) data mining/machine learning algorithms (Arabameri et al. 2019). Figure 1 shows the various feasible alternative methods that can be adapted to identify the flood risk zone in a catchment scale.

Using the hydrological and hydrodynamic models, identifying flood risk zones is time-consuming and requires careful calibration for accurate identification (Asare-Kyei et al. 2015). The conventional rainfall-runoff model is always unsuitable and inappropriate for flood risk analysis as it requires the kind of data that is mostly not available in a catchment scale. Therefore, researchers have inclined to use GIS and machine learning methods to analyze the risk in a catchment (Taormina and Chau 2015; Kalantari et al. 2017; Mosavi et al. 2018; Fu et al. 2020; Shamshirband et al. 2020). AHP is the most widely accepted approach in multi-criteria decision making (MCDM), which can integrate various assessment factors. Since the AHP method identifies the flood risk zone based on expert opinion, it may be subjected to a cognitive limitation with uncertainty and subjectivity (Dahri and Abida 2017). The uncertainty of the AHP during flood risk assessment cannot be eliminated, but it can be mitigated (Lyu et al. 2020).

The flood risk of an area is defined as the multiplication of flood vulnerability and flood hazard (Wisner et al. 2004; Masood and Takeuchi 2012). The factors selected for flood risk analysis in AHP methods are elevation, slope, distance from the river, rainfall, flow accumulation, land use, geology, topographic wetness index, population, drainage density, groundwater level, lithology, literacy rate, soil cover, hydrological soil group, etc. (Das 2018; Luu et al. 2018; Darabi et al. 2019; Hammami et al. 2019; Radwan et al. 2019; Rahman et al. 2019; Ekmekcioğlu et al. 2021; Thanh Son et al. 2021). The minor changes in these factors may lead to an increase or decrease in the flood risk area. For example, the increase in urban built-up and land use land cover will increase the flooding area,

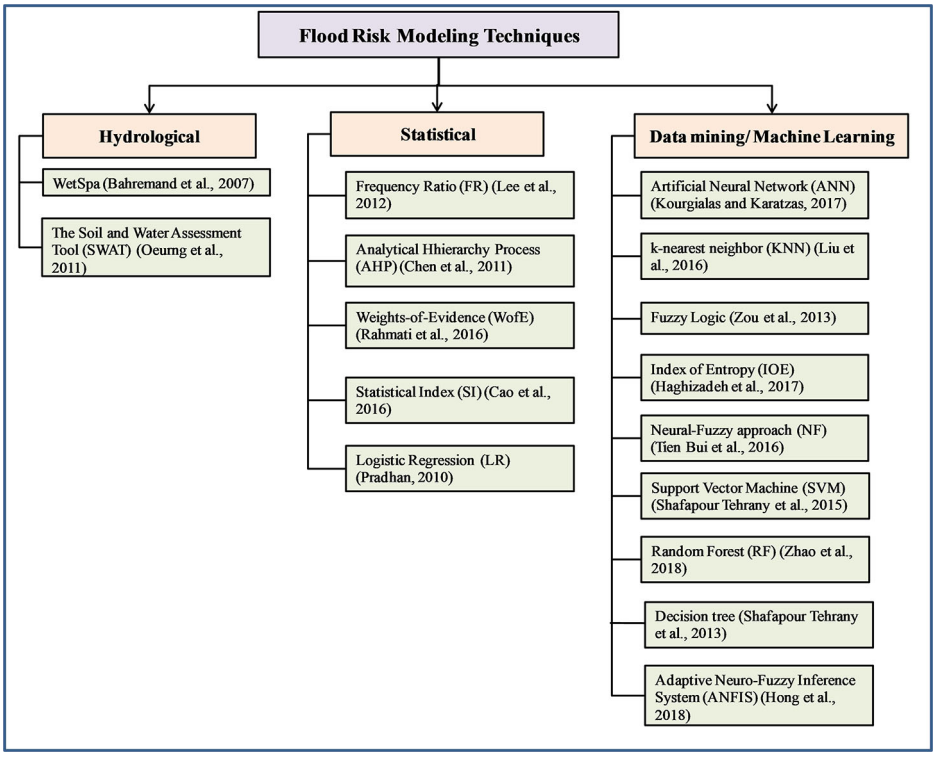

Figure 1. Methods used for identification of flood risk zone.

whereas the decline in rainfall trend will decrease flood risk. Therefore, the future prediction of the flood risk map requires predicting the dynamic factors affecting it.

Numerous studies have been conducted to analyze and predict rainfall trends using gridded and station data set of long-term daily rainfall (Mondal et al. 2015; Caloiero et al. 2018; Heidinger et al. 2018; Praveen et al. 2020; Wang et al. 2020). Innovative trend analysis and the Mann Kendall test, along with the Sen Slope estimator, are the most widely classical approaches used for rainfall trend analysis. Climate change is one of the factors of urban flooding analysis. On the other hand, the changes in LULC, population density, drainage network, etc., become essential factors for urban flooding leading to global environmental change(Anand et al. 2018).

Limited studies are available in the literature on the application of graph theory in various fields of water resource management (Mohan et al. 2008; Ratha and Agrawal 2014; Ratha and Agrawal 2015). However, it is observed from the literature that the graph theory concept has been widely applied in the water distribution network(Fortini et al. 2014; Hajebi et al. 2016; Pagano et al. 2019). Food risk management is also a complex phenomenon, and applying the system approach is expected to provide a better solution. The graph theory approach is an integrated system approach that considers the influence and interactions between the various sub-systems, an advantage over the other system approaches. However, AHP evaluates the sub-systems affecting the main system through a hierarchy process but does not consider the interaction between the sub-systems, which may impact the performance of a system. The permanent matrix determined using graph theory integrates all the sub-systems and their interactions which can be used to evaluate and analyse the complex problems with all possible alternative solutions.

Identification of flooding zones of a river basin becomes a challenging task when data availability is very limited. Also, it is observed that the policymakers have less attention towards the flood management or flood preparedness of middle to the small size river basin. The present study aims to generate the flood risk map of the Ghaggar river basin, a middle-sized basin, considering all possible static and dynamic variables. Ghaggar River is a seasonal flow river situated in the northern region of India. Although the middle and lower part of the basin lies in the semi-arid and arid regions, respectively, disaster due to flash floods has been frequently reported by state disaster management plan Punjab during 1960–2010 (Talwar 2011). The flood occurred in the year 1962, 1964, 1983, 1985, 1988, 1993, 2004, 2009 and 2010 damaged agricultural land and most of the villages of Punjab and Haryana state. Since most of the required data of the Ghaggar river basin were available for identification of flood risk zone using graph theory and very limited studies have been conducted so far on this basin, this basin is adopted as a case study. The system approach using graph theory has been applied in the present study to obtain the flood risk for this basin. The results obtained using the graph theory approach were validated using the multi-criteria decision analysis of AHP. Very few studies have been implemented the GIS based multi-criteria methodology in the flood risk assessment, which is a relatively new approach (Rincón et al. 2018). The Analytical Hierarchy Process (AHP) is a multi-criteria decision-making (MCDM) method that provides different alternative possible solutions so that the decision-makers can identify the suitable solution.

Similarly, the graph theory is also a multi-criteria decision-making approach and provides possible alternate solutions for decision-makers. Therefore, AHP was adopted as a benchmark for comparison. As per the author's knowledge, the application of the graph theory approach in determining the flood risk of a river basin is not available in the literature.

2. Study area

Ghaggar river basin is located in the Northern Region of India and covers an area of approximately 32,132 km^2. This basin is the sub-basin of the Indus basin and originates from the Shivalik hills of Himachal Pradesh, flows through Punjab, Haryana, and Rajasthan. Most of the time, a flash flood of different extent usually occurs in this basin due to instantaneous heavy rainfall along with the non-maintenance of canal embankment (CWC 2014). The Revenue Department of Punjab (Talwar 2011) has reported several flood histories during 1960–2010, and all of them are in the middle of the basin. Therefore, the present study considers the basin area from origin to the middle of the basin for flood risk analysis. The study area covers 13,978 km^2 of the basin, which is shown in Figure 2. The rain gauge stations, along with their effective area, are also shown in Figure 2. The climate of the middle and lower part of the basin is arid/semi-arid, whereas the upper part of the basin is a moist sub-humid. Therefore, the average annual rainfall received in the lower part of the basin is less but a substantial amount of rainfall during monsoon season occurs at the upper and some of the middle part of the basin. The annual rainfall depends on the rainfall received during the southwest monsoon season (June–September). The flood risk is higher during the southwest monsoon season, but extreme events may also cause floods in non-monsoon seasons. The altitude of the basin varies in the range of 143–1790 m. The elevation varies in the range of 143–250 m above sea level in a significant portion of the basin except for the upper part.

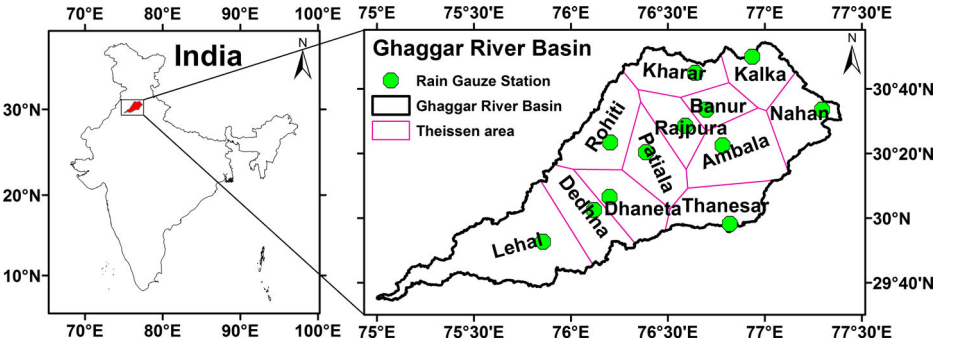

Figure 2. Location of the Ghaggar river basin in India and selected rain gauge stations of the basin.

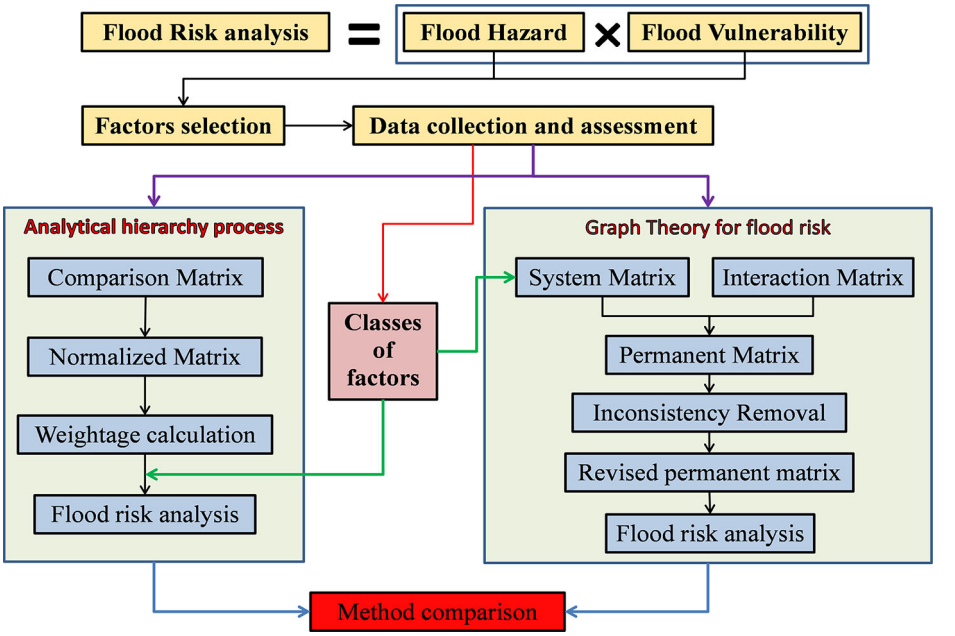

Figure 3. Methodologies applied for the study.

3. Methodology

The present study used two different methodologies for flood risk analysis. They are Graph theory application and Analytical Hierarchy Process (AHP). Graph theory was applied to determine the flood risk of the Ghaggar basin, and AHP was used to validate the results obtained through graph theory application. AHP is the most widely used classical approach for flood risk mapping, whereas graph theory is a system integrated approach that was introduced in the present study for flood risk mapping. The detailed algorithm of methodology is shown in Figure 3.

3.1. Flood risk analysis using graph theory

Identifying structural constituents of flood risk system for any river basin and understanding their impact on the system is the first step to developing a mathematical model using

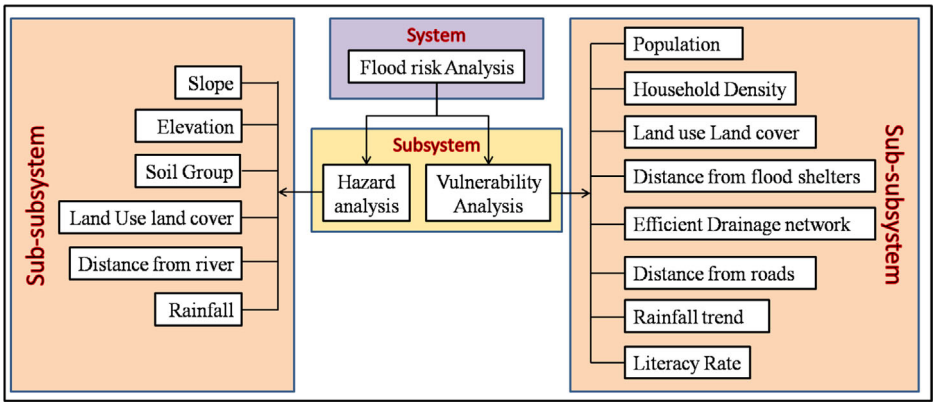

Figure 4. Tree diagram of flood risk analysis.

graph theory. Two major sub-systems are identified for flood risk system, whereas several sub-subsystems are identified which can affect the sub-systems. The effective management of flood hazard and flood vulnerability, which are the two sub-systems of a flood risk system, can reduce the flood risk of a basin.

Figure 4 shows the tree diagram of the flood risk system, which represents two lower levels of sub-systems. The first lower-level sub-systems are flood hazard and flood vulnerability. The conditioning factors for the two sub-systems, flood hazard and flood vulnerability, have been identified and represented in Figure 4 as sub-subsystems. The factors of flood hazard are the internal driving factors that induce the flood risk, whereas the factors of flood vulnerability are the resistance of the flood risk. Suppose any factor is left in the present study but affects the flood risk of a zone. In that case, that can be considered in the future study provided sufficient data of that factor for a study area should be available to incorporate into the final results.

A system or a sub-system can be evaluated using graph theory by identifying the parameters affecting the system/sub-system and preparing a system/sub-system permanent matrix. The magnitude of the diagonal elements of this matrix will be the weightage of each parameter based on its actual performance in the sub-system, and the magnitude of the off-diagonal elements of this matrix are based on the interaction between one sub-system with the other, which may be described as strong, moderate, mild or no interaction. These interactions between two sub-systems are either one-directional or both directions. The present study will follow the bottom-up approach in which initially sub-subsystems will be considered to evaluate the sub-systems of flood risk system. Figure 4 shows that six sub-subsystems are affecting the flood hazard sub-system. The runoff generated due to rainfall sub-subsystem will be affected by slope, elevation, LULC, soil group, and distance from a river. The higher runoff volume and the quick peak occur for a steep slope terrain, leading to an increase in the flood hazard.

The change in slope may also occur during runoff due to erosion of soil. Similarly, the higher runoff volume along with quick peak occurs due to urbanisation, whereas the presence of forest and vegetation decreases the magnitude of runoff peak, which indicates the effect of LULC and Normalised Difference Vegetation Index (NDVI) on runoff. Urbanisation occurs in the area where water is available, revealing the interdependency of urbanisation and distance from the river. If the place where rainfall occurs is close to the river course, then the quick runoff to the river will cause an immediate increase in river discharge, leading to flood hazards. The soil group is also a factor that affects the volume

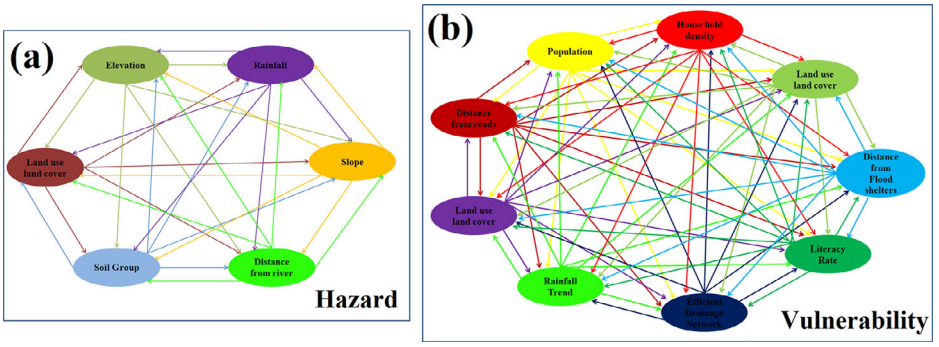

Figure 5. Digraph of flood hazard and flood vulnerability sub-system.

of runoff. The rainfall usually occurs at a higher elevation of a basin quickly collects the water to the river's main course and may create flood hazards in the basin at lower elevation. The runoff generated due to rainfall will be affected by higher NDVI, which leads to a decrease in the possibility of flood hazards. This phenomenon shows that slope has strong interaction with rainfall, whereas rainfall has mild interaction with the slope. Similarly, there is a strong interaction exists between LULC and rainfall and rainfall. The soil group has moderate interaction with rainfall, whereas the rainfall has mild or no interaction with the soil group.

Similarly, Figure 4 shows that eight sub-subsystems are affecting the flood vulnerability sub-system. Population sub-subsystem directly impacts household density, LULC, distance from flood shelters, distance from roads, and literacy rate. Urbanisation and agricultural land cause an increase in population as well as household density. The flood shelters are usually constructed in flood plain areas having good communication facilities. The drainage network should be efficient in urbanized floodplain areas. The literature shows that the rainfall trend is affected due to urbanization (Miao et al. 2011). It is observed that there is a strong interaction existing between population and LULC, population and household density, population and literacy, population and distance from flood shelter, population and efficient drainage network, population and distance from roads, population, and rainfall trend. There is mild or no interaction between rainfall trend and literacy rate, literacy rate and distance from roads, literacy rate, efficient drainage network, literacy rate, and distance from flood shelter.

The performance of a system/sub-system depends on the performance of sub-systems/sub-subsystems. The system and its sub-systems are represented as nodes, whereas their interdependencies are represented in terms of edges. The interactions between these sub-subsystems are represented in Figure 5(a,b) through nodes and edges with direction, known as a digraph. Figure 4 shows the tree diagram, a non-mathematical model, whereas Figure 5(a,b) shows the digraph, a mathematical model. The digraph can be processed through a matrix model. The interrelationship values of sub-systems ($P_{i,j}$) are represented in the adjacency matrix. In the system matrix, the diagonal values are taken using the importance level of that element with respect to flood hazard/flood vulnerability, and weightage is assigned based on its importance. Table 1 shows the qualitative measure of a system/sub-system representing diagonal values of system/sub-system permanent matrix, on a scale of 1–8 in which weightage of 1 indicates exceptionally low whereas weightage of 8 indicates exceptionally high to cause flood hazard/flood vulnerability. In the interaction matrix, the off-diagonal elements are taken using the level of interaction/interdependency between two sub-subsystems of the flood hazard/flood vulnerability sub-

Table 1. Qualitative measure of a system or sub-system used for flood risk analysis.

Weightage	Diagonal or system measurement
1	Exceptionally low
2	Extremely low
3	Very low
4	Normal
5	High
6	Very High
7	Extremely High
8	Exceptionally high

Table 2. Level of the interaction and their corresponding weightage for flood risk analysis.

Weightage	Level of interaction between one sub-system with another sub-system
0	No interaction
1	Weak
2	Moderate
3	Strong

system, and weightage is assigned based on their level of interaction. Table 2 shows the weightage of off-diagonal values on a scale of 0–3, in which weightage of 0 indicates there is no interaction between two sub-subsystems whereas weightage of 3 indicates there is a strong interaction between two sub-subsystems. Although as many as divisions can be created for the qualitative measure of the interdependencies between the sub-systems/sub-subsystems, authors feel that experts will be confused/biased while assigning the type of interaction between sub-systems and assigning that interaction into a qualitative measure. Therefore, the present study adopted the weightage ranging from 0 to 3 for the off-diagonal elements.

The summation of the system matrix and interaction matrix is represented as a system permanent matrix. Equation (1) shows the system matrix, interaction matrix, and system permanent matrix for the flood hazard sub-system, whereas Equation (2) shows the system matrix, interaction matrix, and system permanent matrix for the flood vulnerability sub-system. Since there are six constituents for the flood hazard sub-system, the sub-system permanent matrix is shown in Equation (1) consist of a 6×6 matrix, whereas the flood vulnerability sub-system permanent matrix shown in Equation (2) consists of an 8×8 matrix as there are eight constituents considered for flood vulnerability sub-system.

$$\begin{bmatrix} \mathrm{H}_1 & 0 & 0 & 0 & 0 & 0 \\ 0 & \mathrm{H}_2 & 0 & 0 & 0 & 0 \\ 0 & 0 & \mathrm{H}_3 & 0 & 0 & 0 \\ 0 & 0 & 0 & \mathrm{H}_4 & 0 & 0 \\ 0 & 0 & 0 & 0 & \mathrm{H}_5 & 0 \\ 0 & 0 & 0 & 0 & 0 & \mathrm{H}_6 \end{bmatrix} + \begin{bmatrix} 0 & H_{12} & H_{13} & H_{14} & H_{15} & H_{16} \\ H_{21} & 0 & H_{23} & H_{24} & H_{25} & H_{26} \\ H_{31} & H_{32} & 0 & H_{34} & H_{35} & H_{36} \\ H_{41} & H_{42} & H_{43} & 0 & H_{45} & H_{46} \\ H_{51} & H_{52} & H_{53} & H_{54} & 0 & H_{56} \\ H_{61} & H_{62} & H_{63} & H_{64} & H_{65} & 0 \end{bmatrix} = \begin{bmatrix} \mathrm{H}_1 & H_{12} & H_{13} & H_{14} & H_{15} & H_{16} \\ H_{21} & \mathrm{H}_2 & H_{23} & H_{24} & H_{25} & H_{26} \\ H_{31} & H_{32} & \mathrm{H}_3 & H_{34} & H_{35} & H_{36} \\ H_{41} & H_{42} & H_{43} & \mathrm{H}_4 & H_{45} & H_{46} \\ H_{51} & H_{52} & H_{53} & H_{54} & \mathrm{H}_5 & H_{56} \\ H_{61} & H_{62} & H_{63} & H_{64} & H_{65} & \mathrm{H}_6 \end{bmatrix} \quad (1)$$

$$\begin{bmatrix} V_1 & 0 & 0 & 0 & 0 & 0 & 0 & 0 \\ 0 & V_2 & 0 & 0 & 0 & 0 & 0 & 0 \\ 0 & 0 & V_3 & 0 & 0 & 0 & 0 & 0 \\ 0 & 0 & 0 & V_4 & 0 & 0 & 0 & 0 \\ 0 & 0 & 0 & 0 & V_5 & 0 & 0 & 0 \\ 0 & 0 & 0 & 0 & 0 & V_6 & 0 & 0 \\ 0 & 0 & 0 & 0 & 0 & 0 & V_7 & 0 \\ 0 & 0 & 0 & 0 & 0 & 0 & 0 & V_8 \end{bmatrix} + \begin{bmatrix} 0 & V_{12} & V_{13} & V_{14} & V_{15} & V_{16} & V_{17} & V_{18} \\ V_{21} & 0 & V_{23} & V_{24} & V_{25} & V_{26} & V_{27} & V_{28} \\ V_{31} & V_{32} & 0 & V_{34} & V_{35} & V_{36} & V_{37} & V_{38} \\ V_{41} & V_{42} & V_{43} & 0 & V_{45} & V_{46} & V_{47} & V_{48} \\ V_{51} & V_{52} & V_{53} & V_{54} & 0 & V_{56} & V_{57} & V_{58} \\ V_{61} & V_{62} & V_{63} & V_{64} & V_{65} & 0 & V_{67} & V_{68} \\ V_{71} & V_{72} & V_{73} & V_{74} & V_{75} & V_{76} & 0 & V_{78} \\ V_{81} & V_{82} & V_{83} & V_{84} & V_{85} & V_{86} & V_{87} & 0 \end{bmatrix}$$

$$= \begin{bmatrix} V_1 & V_{12} & V_{13} & V_{14} & V_{15} & V_{16} & V_{17} & V_{18} \\ V_{21} & V_2 & V_{23} & V_{24} & V_{25} & V_{26} & V_{27} & V_{28} \\ V_{31} & V_{32} & V_3 & V_{34} & V_{35} & V_{36} & V_{37} & V_{38} \\ V_{41} & V_{42} & V_{43} & V_4 & V_{45} & V_{46} & V_{47} & V_{48} \\ V_{51} & V_{52} & V_{53} & V_{54} & V_5 & V_{56} & V_{57} & V_{58} \\ V_{61} & V_{62} & V_{63} & V_{64} & V_{65} & V_6 & V_{67} & V_{68} \\ V_{71} & V_{72} & V_{73} & V_{74} & V_{75} & V_{76} & V_7 & V_{78} \\ V_{81} & V_{82} & V_{83} & V_{84} & V_{85} & V_{86} & V_{87} & V_8 \end{bmatrix} \tag{2}$$

Equation (1) shows the permanent matrix formed using sub-system matrix and interaction matrix for flood hazard analysis. Six variables have been used for flood hazard. H_i ($i = 1, 2, 3–6$) represents the contribution of six sub-subsystems of flood hazard sub-system and are represented as diagonal members. H_{ij} ($i = 1, 2, 3–6$; $j = 1, 2, 3–6$) represents the interaction of ith sub-subsystem with jth sub-subsystem and are represented as off-diagonal elements. Similarly, Equation (2) shows the permanent matrix formed using sub-system matrix and interaction matrix for flood vulnerability analysis. Eight variables have been used for flood vulnerability analysis. V_i ($i = 1, 2, 3–8$) represents the contribution of eight sub-subsystems of flood vulnerability sub-system and are represented as diagonal members. V_{ij} ($i = 1, 2, 3–8$; $j = 1, 2, 3–8$) represents the interaction of ith sub-subsystem with jth sub-subsystem and are represented as off-diagonal elements.

$$\begin{aligned} per\ (H) = & \prod_{z=1}^{M} H_z + \sum_i \sum_j \sum_k \ldots\ldots\ldots)] \sum_M (H_{ij}H_{ji})\ H_k H_l \ldots\ldots H_M \\ & + \sum_i \sum_j \sum_k \ldots\ldots\ldots \sum_M (H_{ij}H_{jk}H_{ki} + H_{ik}H_{kj}H_{ji}) H_l H_m \ldots\ldots H_M \\ & + [\left(\sum_i \sum_j \sum_k \ldots\ldots\ldots \sum_M (H_{ij}H_{ji} + H_{kl}H_{lk}) H_m \ldots\ldots\ldots H_M \right) \\ & + \left(\sum_i \sum_j \sum_k \ldots\ldots\ldots \sum_M (H_{ij}H_{jk}H_{kl}H_{li} + H_{il}H_{lk}H_{kj}H_{ji}) H_m \ldots\ldots H_M \right)] \\ & + [\left(\sum_i \sum_j \sum_k \ldots\ldots\ldots \sum_M (H_{ij}H_{ji})(H_{kl}H_{lm}H_{mk} + H_{km}H_{ml}H_{lk}) \right) \\ & + \left(\sum_i \sum_j \sum_k \ldots\ldots\ldots \sum_M (H_{ij}H_{ji})(H_{ij}H_{jk}H_{kl}H_{lm}H_{mi} + H_{im}H_{ml}H_{lk}H_{kj}H_{ji}) \right. \\ & \left. + H_n \ldots\ldots\ldots H_M \right. \end{aligned} \tag{3}$$

The permanent matrix is developed and represented in Equation (3) in a general form. There are $M + 1$ numbers of terms in Equation (3), and a quantitative value will be obtained after solving Equation (3). Since there is no negative sign in any of the terms of Equation (3), the numerical index obtained contains each term's information.

3.1.1. Inconsistency removal of the matrix

The weights in Equations (1) and (2) are usually formulated by several experts. Therefore, the weights assigned by different experts will differ. The removal of such inconsistency is necessary to evaluate the flood risk system accurately. When multiple experts provide the weights, the decision-maker has to combine the weights of all experts and convert them into a single coherent weightage. Behavioural aggregation and mathematical aggregations are the two major ways using which the decision of multiple experts can be combined (Wilson 2017). The experts are in a single place, and weights are decided at a consensus is known as behavioural aggregation. Delphi technique can also be used when the experts are under the control of analysts. In mathematical aggregation, opinion pool and Bayesian aggregation are usually used (Wilson 2017). The present study used the behavioural aggregation where the weights have been decided in a consensus of all three experts. The number of experts for this type of study considered in various literatures are varying from 1 to 14 (Luu et al. 2018; Ekmekcioğlu et al. 2021). It is also suggested in literature that the method should focus on the quality of experts rather than the quantity (Luu et al. 2018).

Further, Equation (4) is used to remove the presence of any type of inconsistencies.

$$(P - \lambda I)x^T = 0 \tag{4}$$

Where, I = identity matrix; x^T = Transpose of the weight vector $(x_1,\ x_2,\ x_3 \ldots\ldots x_n)$; $(P - \lambda I) = 0$ Yields Eigen spectrum

λ_{max} is identified from the Eigen spectrum and is used to calculate weight vector such that $\sum P_i = 1$. Equation (5) shows the revised hazard sub-system permanent matrix.

$$\text{Permanent matrix} = \begin{bmatrix} H_1.P_1 & H_{12}.P_2 & H_{13}.P_3 & H_{14}.P_4 & H_{15}.P_5 & H_{16}.P_6 \\ H_{21}.P_1 & H_2.P_2 & H_{23}.P_3 & H_{24}.P_4 & H_{25}.P_5 & H_{26}.P_6 \\ H_{31}.P_1 & H_{32}.P_2 & H_3.P_3 & H_{34}.P_4 & H_{35}.P_5 & H_{36}.P_6 \\ H_{41}.P_1 & H_{42}.P_2 & H_{43}.P_3 & H_4.P_4 & H_{45}.P_5 & H_{46}.P_6 \\ H_{51}.P_1 & H_{52}.P_2 & H_{53}.P_3 & H_{54}.P_4 & H_5.P_5 & H_{56}.P_6 \\ H_{61}.P_1 & H_{62}.P_2 & H_{63}.P_3 & H_{64}.P_4 & H_{65}.P_5 & H_6.P_6 \end{bmatrix} \tag{5}$$

$P_1 \ldots\ldots P_6$ are the weight vector calculated from $\sum P_i = 1$. The system permanent matrix formed in Equation (5) is free from any bias and the composite score evaluated using Equation (3) will inform the level of flood hazard in the basin.

3.2. Analytical hierarchy process for flood risk mapping

Analytical hierarchy process (AHP) is a multi-criteria decision-making approach in which the complex problem is decomposed into a hierarchy structure. The decision-makers can evaluate each element independently and compare it with others to their impact on an element above them in a hierarchy. Saaty (1977) proposed this robust and flexible methodology for decision making where multi-factors are involved in a complex problem. This method prepares a pair-wise comparison between factors using importance level of value 1 to 9 (Lowest to highest importance) as shown in Table 3. For example, if the relative importance of factor A is very strong than factor B for system analysis, then the importance level of factor A to B will reflect as 7, whereas the importance level of factor B to A will reflect as 1/7 in pair-wise comparison matrix.

The AHP model was performed using the following steps:

Table 3. Importance scale of AHP model (Dahri and Abida 2017).

Importance level	Definition
1	Equal Importance
3	Moderate importance
5	Strong importance
7	Very strong or demonstrated importance
9	Extreme importance
2, 4, 6, 8	Intermediate Values

Table 4. RI values for the different order of the matrix (n) (Dahri and Abida 2017).

N	3	4	5	6	7	8	9	10	11	12	13	14
RI	0.58	0.9	1.12	1.24	1.32	1.41	1.45	1.49	1.51	1.54	1.56	1.57

- A list of factors (n) is selected which are responsible for flood hazard and flood vulnerability in the basin.
- Pair-wise comparison matrix (M) is developed using importance value based on the literature review and expert advice (Dahri and Abida 2017; Chakraborty and Mukhopadhyay 2019; Radwan et al. 2019; Souissi et al. 2020) in which diagonal elements are equal to 1. Weights in the range of 1–9 are assigned in each row of the upper triangular matrix based on the relative importance between two factors, and the inverse of the weights are assigned in each row of the lower triangular matrix. Equation (6) shows the pair-wise comparison matrix of n factors.

$$M = \begin{bmatrix} 1 & a12 & . & . & . & a1n \\ 1/a12 & 1 & . & . & . & a2n \\ . & . & . & . & . & . \\ . & . & . & . & . & . \\ . & . & . & . & . & . \\ 1/a1n & 1/a2n & . & . & . & 1 \end{bmatrix} \tag{6}$$

- Calculate the normalized matrix of the pair-wise comparison matrix shown in Equation (6).
- Calculate the mean of each row in the normalized matrix, and the resulting values represent the weight of those factors (W_i).
- The AHP based flood model will be analyzed using the summation of weightage of each factor (W_i) multiplied by the class of the respective factor(R_i).

$$AHP = \sum_{i=1}^{n} W_i \times R_i \tag{7}$$

- The consistency of the AHP model is checked through consistency ratio (CR). Equation (8) can be used to calculate CR (Ghosh and Kar 2018).

$$CR = \frac{CI}{RI} \tag{8}$$

Where CI is the consistency index, and RI is the random index. The random index for different n values is shown in Table 4. The CI can be calculated as

$$CI = \frac{\lambda_{max} - n}{n - 1} \tag{9}$$

Where, λ_{max} is the principal Eigenvalue of the normalized matrix (Radwan et al. 2019), and n is the order of the matrix.

Table 5. Description of Factors used for flood risk mapping.

S. No.	Factors	Source	Resolution	Weblink	Data version/date
1	Elevation	Shuttle Radar Topography Mission (SRTM)	30 m	https://earthexplorer.usgs.gov/	23.09.2014
2	LULC	Moderate Resolution Imaging Spectroradiometer (MODIS) Landcover V6	500 m	https://earthexplorer.usgs.gov/	2019
3	Population	Socioeconomic Data and Applications Center(SEDAC)	1 km	https://sedac.ciesin.columbia.edu/data/set/india-spatial-india-census-2011	15.05.2020
4	Hydrologic Soil Group	Global Hydrologic Soil Groups (HYSOGs250m) for Curve Number-Based Runoff Modeling	250 m	https://daac.ornl.gov/SOILS/guides/Global_Hydrologic_Soil_Group.html	22-04-2020
5	Rainfall	Indian Meteorological Department, Pune	Stations	http://dsp.imdpune.gov.in/	1969–2018
6	Roads	Open Street Map		https://www.openstreetmap.org/#map=5/21.821/92.065	03.09.2014
7	Literacy Rate	Census of India	Tehsil wise	https://censusindia.gov.in/pca/cdb_pca_census/cd_block.html	2011
8	Household density	Census of India	Tehsil wise	https://censusindia.gov.in/pca/cdb_pca_census/cd_block.html	2011

4. Conditioning factor for flood mapping

In the present study, fourteen factors have been used for flood risk mapping over the basin based on data availability. The data set used for eight factors has been downloaded from various sources mentioned in Table 5 and further processed in different GIS software such as ArcGIS and TerrSet. The sources and details of eight factors are described in Table 5. Figure 6 and 7 shows the spatial map of each factor used to determine the composite score of flood hazard and flood vulnerability mapping of the study area, respectively, using graph theory and AHP.

i. Elevation: Digital elevation model (DEM) was obtained from Shuttle Radar Topography Mission (SRTM) of 30 m resolution and found that the elevation of the basin varies between 143 adn 1790 m above sea level (Figure 6(a)). The elevation of most of the area of the basin lies in a range of 143–350 m above sea level. Elevation of a region can visualise the inundation extent due to flood and has an inverse relationship with flood hazard (Das 2018; Chakraborty and Mukhopadhyay 2019). When a flood occurs, the negative consequences of flooding usually happen in a location that is at a lower elevation. The lower elevated with flat regions are more prone to flood hazards (Das 2018)
ii. Slope: The slope of the basin was analyzed using the surface (slope) module of ArcGIS. The slope is one of the significant factors in flooding as it controls the velocity of water and the infiltration process. The basin slope is lying in the range of 0–80.9° (Figure 6(b)). The slope has an inverse relationship with flood hazard (Das 2018; Chakraborty and Mukhopadhyay 2019). Therefore, the flow of water will be less in flat land.
iii. Hydrologic Soil group for Curve Number (CN): Hydrologic Soil group data was obtained from Global Hydrologic Soil Groups (HYSOGs250m). There are four types of soil groups found in this basin. They are C, D, C/D, and D/D type and consist of approximately 59.1%, 0.2%, 40.5% and 0.2% basin area respectively

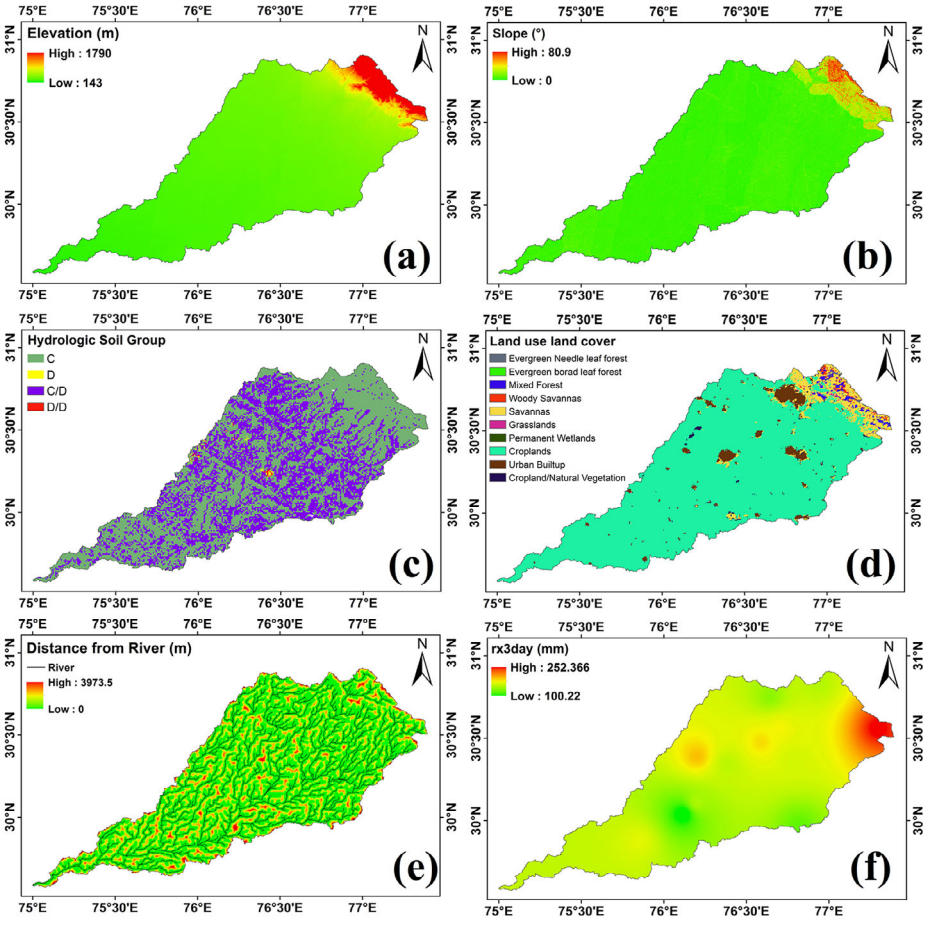

Figure 6. Conditioning factors for flood hazard mapping.

(Figure 6(c)). Soil group C has a moderate runoff potential, where the other three groups have high runoff potential. The high runoff potential zone has a lower infiltration rate which influences the flood risk. Therefore, 59.1% and 40.9% of the basin is lying under moderately and high runoff potential zone.

iv. Land use land cover (LULC): The land use land cover map was obtained from MODIS land cover for 2019 and found that the basin is occupied by different land use land cover categories (Figure 6(d)). The basin is mainly covered by croplands as agriculture which covers 88.3%. Other land types such as Savannas and Urban built-up cover an area of about 6.2% and 3.4%, respectively. The flood risk changes with the land use land cover pattern as there is a high risk of flood in the urban built-up category and low risk in forest areas.

v. Distance from rivers: The river or drainage dataset is extracted using hydrology module (Flow accumulation, flow direction, etc.) in ArcGIS. The river bed or stream network was delineated using a flow accumulation module in ArcGIS with a flow accumulation value greater than 10,000 cell thresholds. The distance from rivers was analyzed using the Euclidean distance module in ArcGIS (Figure 6(e)). Distance from rivers has an inverse relationship to flood hazard of a region, i.e., as

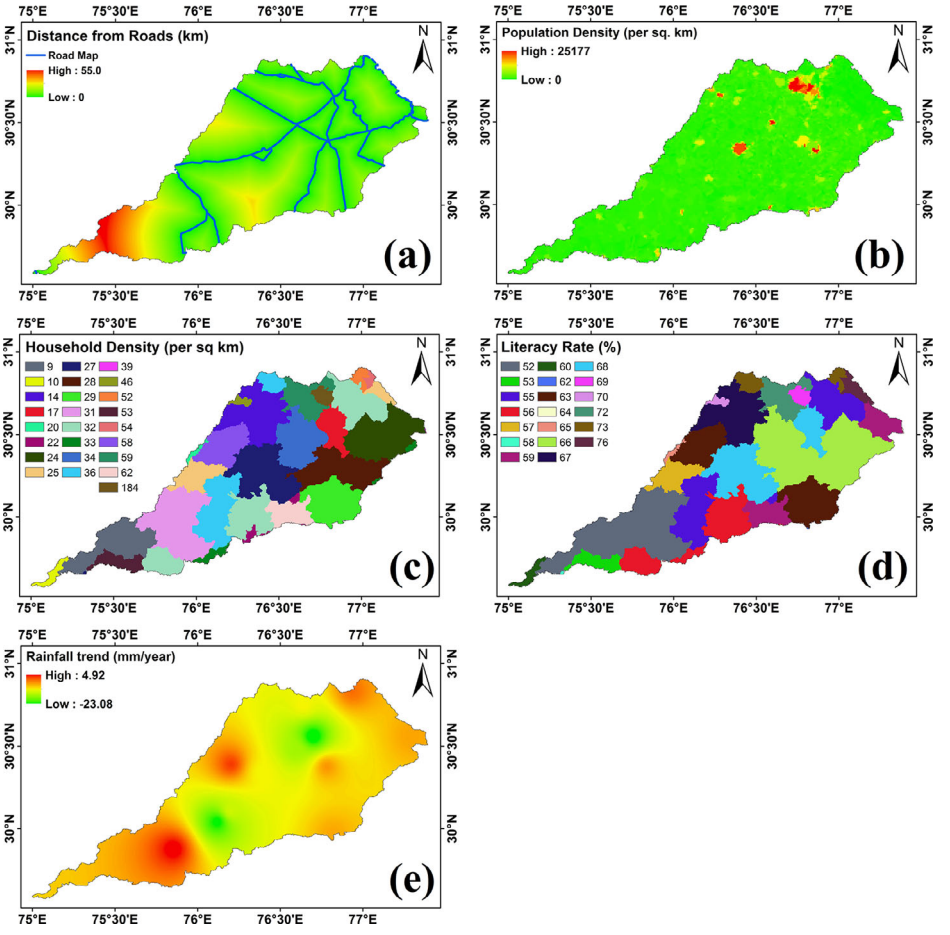

Figure 7. Conditioning factors for flood vulnerability mapping.

flood vulnerability is more at alongside the river (Das 2018; Chakraborty and Mukhopadhyay 2019).

vi. Rainfall: Daily rainfall data from 1969 to 2018 of 12 stations were collected from Indian Meteorological Department (IMD). Figure 2 shows the location of the 12 rain gauge stations in the basin. The rainfall data is sorted as annual by cumulating daily rainfall data for each year. The average annual rainfall over the basin varies between 266 and 1703 mm (Gorai et al. 2021). The extreme event of a three consecutive days rainfall (rx3day) was also analyzed, and found that the average rx3day rainfall of this basin varies between 100 and 252 mm per year (Figure 6(f)). The magnitude of rx3day directly relates to flood hazards in terms of runoff generation (Chakraborty and Mukhopadhyay 2019).

vii. Distance from roads: The road data for the Ghaggar river basin is obtained from an open street map. The distance from the road was analyzed using the Euclidean distance module in ArcGIS (Figure 7(a)). The distance from the road has an inverse relationship to flood vulnerability (Chakraborty and Mukhopadhyay 2019).

viii. Population: The population data based on Census 2011 was obtained from Socio-economic Data and Applications Center (SEDAC) of 1 km resolution, i.e., the population density per km^2. The population density over the basin lies at 0–25,177

per km^2 (Figure 7(b)). The population density has a direct relationship to flood vulnerability (Chakraborty and Mukhopadhyay 2019).

ix. Household Density: The household density data was downloaded from Census data 2011 and found that it varies in 9–184 per km^2 (Figure 7(c)). In Chandigarh Tehsil, the high density of households, i.e., 184/km^2, was found. The household density has a direct relationship to flood vulnerability (Chakraborty and Mukhopadhyay 2019).

x. Literacy rate: Literacy data of the basin was downloaded from Census data 2011 and spatially plotted in Figure 7(d). It is found from Figure 7(d) that the literacy rate of the basin varies between 52% and 76% of the total population over the basin. The literacy rate can measure the level of socioeconomic attainment and prompt decision-making for the safety and rescue of the community. The literacy rate has an inverse relationship to flood vulnerability (Chakraborty and Mukhopadhyay 2019).

xi. Rainfall trend: Innovative trend analysis was proposed by Sen in 2012 has become more popular for the study of trend analysis in the current decades (Caloiero et al. 2018; Praveen et al. 2020; Wang et al. 2020). Gorai et al. (2021) conducted the trend analysis using the Innovative trend analysis method and found that the rainfall trend magnitude of this basin varies −23.0 to 4.9 mm per year (Figure 7(e)). The rainfall trend has a direct relationship to flood vulnerability.

xii. Distance from flood shelters: The distance from flood shelters is a factor that can measure the rescue, safety, and security of the flood victims. There are no special flood shelters exist in the basin. Distance from flood shelters has an inverse relationship to flood vulnerability (Chakraborty and Mukhopadhyay 2019).

xiii. Efficient Drainage network: The drainage network of this basin is not highly efficient. The drainage network has a direct relationship to flood hazards.

5. Flood hazard/flood vulnerability/flood risk mapping

It is observed that both graph theory and AHP calculate the system's performance through the hierarchy process. The weights are usually assigned to all the factors affecting the system and calculate an overall performance in the form of a numeric value in both methods. But the graph theory also considers the interaction between the sub-systems during the evaluation process and therefore acts as an integrated system of performance management. Tables 6 and 7 show the classification, weightage, and area under the respective classification of various sub-subsystems of flood hazard and vulnerability subsystem, respectively. These classifications and their respective weights are used in the present study to prepare flood risk zone using both graph theory and AHP.

The importance level for both flood hazard and flood vulnerability is taken between 1 and 8 for graph theory and AHP methods. Since the weights are converted into percentage form, the numeric value for flood hazard and flood vulnerability in AHP will lie between 100 and 800, and the numeric value for flood risk will lie in the range between 10,000 and 640,000 as per Equation (10).

The permanent value of a system permanent matrix will provide the performance of a system in terms of numeric value. The minimum numeric value will be when the diagonal element of the system permanent matrix is 1, whereas the maximum numeric value will be when the diagonal element of the system permanent matrix is 8. The off-diagonal element of flood hazard and flood vulnerability sub-system permanent matrix is shown in Tables 9 and 10. The minimum numeric value of flood hazard sub-system permanent

Table 6. Classification of various factors and their respective weights considered for flood hazard sub-system.

Sub-subsystems	Classification	Weights(R_i)	Weighted area	Sub-subsystems	Classification	Weights(R_i)	Weighted area
Elevation (m)	0–300	8	0.9065	Slope (°)	0–10	8	0.9541
	300–500	7	0.0458		10–20	7	0.0322
	500–700	6	0.0159		20–30	6	0.0103
	700–900	5	0.0105		30–40	5	0.0028
	900–1100	4	0.0109		40–50	4	0.0004
	1100–1300	3	0.0061		50–60	3	0.0001
	1300–1500	2	0.0034		60–70	2	0.0000
	>1500	1	0.0009		70–80	1	0.0000
Land use Land cover (LULC)	Evergreen Needle leaf Forest	3	0.0102	Rx3day (mm)	<100	4	0.0000
	Evergreen Broad leaf Forest				100–140	5	0.0667
	Mixed Forest				140–170	6	0.6355
	Woody Savannas	4	0.0678		170–200	7	0.2514
	Savannas				>200	8	0.0465
	Grasslands			Distance from rivers (m)	<200	8	0.2981
	Permanent Wetlands	7	0.0001		200–500	7	0.3205
	Croplands	8	0.9219		500–800	6	0.1028
	Urban Built-up				800–1100	5	0.1777
	Cropland/ Natural Vegetation				1100–1400	4	0.0296
Soil Group	C	6	0.5911		1400–1700	3	0.0397
	D	8	0.4089		1700–2000	2	0.0195
	C/D				>2000	1	0.0121
	D/D						

matrix is 1.52, whereas the maximum value is 31.57. Similarly, the minimum numeric value of flood vulnerability sub-system permanent matrix is 0.036, whereas the maximum value is 4.57. The minimum numeric value of the flood risk system permanent matrix is 0.06, whereas the maximum value is 144.26.

The present study made five classifications: very low, low, moderate, high, and very high flood risk/flood hazard/flood vulnerability zone. These classifications have been done in a similar proportion for both graph theory and AHP methods. Table 8 shows the flood zone classification in the form of numeric value for both AHP and Graph theory methods used in the present study.

6. Results and discussion

Flood risk analysis is the composite of flood hazard and flood vulnerability analysis which can be expressed as,

$$\text{Flood Risk} = \text{Flood Hazard} \times \text{Flood Vulnerability} \tag{10}$$

The present study applied graph theory and AHP to identify the flood risk zone of the Ghaggar river basin, and the following points were discussed.

- Identification of flood risk zone of Ghaggar river basin using graph theory
- Identification of flood risk zone of Ghaggar river basin using AHP
- Comparison of the results obtained by these two methods.

Table 7. Classification of various factors and their respective weights considered for flood vulnerability sub-system.

Sub-subsystems	Classification	Weights (R_i)	Weighted area	Sub-subsystems	Classification	Weights (R_i)	Weighted area
Population density (person/km^2)	<100	1	0.0956	Land use Land cover (LULC)	Evergreen Needle leaf Forest	3	0.0102
	100–150	2	0.0867		Evergreen Broad leaf Forest		
	150–250	3	0.3224		Mixed Forest		
	250–500	4	0.3610		Woody Savannas	4	0.0678
	500–1000	5	0.0721		Savannas		
	1000–3000	6	0.0381		Grasslands		
	3000–5000	7	0.0114		Permanent Wetlands	7	0.0001
	>5000	8	0.0128		Croplands	8	0.9219
Household Density (number/km^2)	0–20	1	0.1745		Urban Built-up		
	20–40	2	0.6802		Cropland/ Natural Vegetation		
	40–60	3	0.1103	Distance from roads (m)	<200	8	0.0303
	60–80	4	0.0264		200–500	7	0.0390
	80–100	5	0.0000		500–800	6	0.0468
	100–120	6	0.0000		800–1100	5	0.0189
	120–150	7	0.0000		1100–1400	4	0.0448
	>150	8	0.0085		1400–1700	3	0.0171
Literacy rate (%)	>70	4	0.0662		1700–2000	2	0.0255
	60–70	6	0.4791		>2000	1	0.7775
	50–60	7	0.2963	Distance from flood shelters	No flood shelter in the basin. Therefore the weightage is the same for the whole basin	8	1.0000
	<50	8	0.1584	Rainfall trend	Positive trend	8	0.0496
Efficient drainage system	No efficient drainage system in the basin. Therefore the weightage is the same for the whole basin	8	1.0000		Negative trend	4	0.9504

Table 8. Flood zone classifications concerning its value.

	AHP			Graph theory		
Zone	Hazard	Vulnerability	Risk	Hazard	Vulnerability	Risk
Very low	<200	<200	<40,000	<2.41	<0.12	<0.28
Low	200–400	200–400	40,000–160,000	2.41–5.85	0.12–0.33	0.28–1.93
Moderate	400–500	400–500	160,000–250,000	5.86–9.01	0.34–0.66	1.93–5.94
High	500–700	500–700	250,000–490,000	9.01–20.93	0.66–2.44	5.94–51.19
Very high	>700	>700	>490,000	>20.93	>2.44	>51.19

6.1. Identification of flood risk zone of Ghaggar river basin using graph theory

The combined effects of all sub-subsystems on sub-system and subsequently on flood risk system were assessed using graph theory. The flood risk analysis was analyzed by calculating the permanent matrix of the flood hazard and vulnerability sub-system. Table 9 shows the level of interaction between the sub-subsystems of the flood hazard sub-system, whereas Table 10 shows the level of interaction between the sub-subsystems of the flood vulnerability sub-system. Sr.no of sub-subsystems are mentioned in each column of the level of interaction with which it is interacting. For example, the slope has strong

Table 9. Level of interaction between the sub-subsystems of flood hazard sub-system.

		Level of the interaction of one sub-subsystem with other sub-subsystems for causing flood hazard			
S. No.	Sub-subsystems	Strong (3)	Moderate (2)	Weak (1)	No (0)
1	Slope	2, 4, 6	3	5	
2	Elevation	1, 4, 6	3, 5		
3	Soil group	2, 4	1, 6		5
4	Land use land cover	1, 2, 6	3, 5		
5	Distance from river	4	1, 2, 6	3	
6	Rainfall	1, 2, 4	3, 5		

interaction with elevation (sr. no 2), land use land cover (sr. no 4), and rainfall (sr. no 6), whereas it has moderate interaction with the soil group (sr. no 3) and weak interaction with distance from the river (sr. no 5) for causing the flood hazard. These levels of interactions between the various components of flood hazard or flood vulnerability sub-system were identified through expert advice. Tables 9 and 10 were prepared with the consent of three hydrology experts (Ratha and Agrawal 2014; Ratha and Agrawal 2015).

The weights assigned to the diagonal element of a permanent matrix represent the actual performance of that system. The present study assigned the weights to the diagonal elements in Equation (1) as per the performance of sub-subsystems in the Ghaggar river basin. Since there are twelve rain gauge stations existing in this basin, the whole basin has been divided into twelve numbers of different areas using the Thiessen polygon method. The weights of various flood hazard and flood vulnerability sub-subsystems for all these areas have been assigned according to Tables 6 and 7. These values represent the actual performance of the respective parameters in that area of the basin. It is assumed that there is no spatial variation in the characteristics of conditioning factors within their respective area. Therefore, the weights assigned in that area will remain constant. These weights become the diagonal member of the sub-system matrix. Equations (11)–(16) show the complete sub-system matrix of the effective area covered for the Rohiti rain gauge station. Similarly, sub-system matrices for all other areas for different rain gauge stations were prepared by changing the weightage of the diagonal element according to the performance of that parameter in the respective area.

$$\textit{Permanent matrix of flood hazard} = \begin{matrix} 7.99 & 3 & 2 & 3 & 1 & 3 \\ 3 & 8 & 2 & 3 & 2 & 3 \\ 1 & 3 & 7 & 3 & 0 & 2 \\ 3 & 3 & 2 & 7.97 & 2 & 3 \\ 2 & 2 & 1 & 3 & 5.77 & 2 \\ 3 & 3 & 2 & 3 & 2 & 6.73 \end{matrix} \tag{11}$$

$$\textit{Permanent matrix of flood vulnerability} = \begin{matrix} 3.48 & 3 & 3 & 2 & 3 & 2 & 2 & 2 \\ 3 & 2.23 & 1 & 2 & 1 & 2 & 2 & 2 \\ 3 & 3 & 7.97 & 1 & 2 & 2 & 3 & 1 \\ 2 & 2 & 1 & 8 & 1 & 1 & 2 & 0 \\ 2 & 2 & 2 & 1 & 8 & 1 & 1 & 0 \\ 1 & 1 & 2 & 2 & 1 & 1.54 & 0 & 0 \\ 2 & 2 & 2 & 3 & 2 & 1 & 4.33 & 1 \\ 2 & 2 & 1 & 1 & 1 & 1 & 0 & 6.15 \end{matrix} \tag{12}$$

Table 10. Level of interaction between the sub-subsystems of flood vulnerability sub-system.

S. No.	Sub-subsystem	Level of the interaction of one sub-subsystem with other sub-subsystem for causing flood vulnerability sub-system			
		Strong (3)	Moderate (2)	Weak (1)	Nil (0)
1	Population	2, 3, 5	4, 6, 7, 8		
2	Household Density	1	4, 6, 7, 8	3, 5	
3	Land use land cover	1, 2, 7	5, 6	4, 8	
4	Distance from flood shelters		1, 2, 7	3, 5, 6	8
5	Efficient Drainage Network		1, 2, 3	4, 6, 7	8
6	Distance from roads		3, 4	1, 2, 5	7, 8
7	Rainfall trends	4	1, 2, 3, 5	6	8
8	Literacy rate		1, 2	3, 4, 5	6, 7

The inconsistency of the matrix was removed by finding the weight vector using Equation (4). Equations (13) and (14) show the weight vector used for the removal of inconsistency and the updated subsystem matrix for flood hazard and flood vulnerability are shown in Equations (15) and (16).

$$Hazard\ weight\ factor = (1:0.1726; 2:0.1810; 3:0.1748; 4:0.1806; 5:0.1242; 6:0.1674) \tag{13}$$

$$Vulnerability\ weight\ factor = (1:0.1535; 2:0.0.1071; 3:0.0.1917; 4:0.0.1260; 5:0.0.1319; 6:0.0.0652; 7:0.0.1314; 8:0.0929) \tag{14}$$

The updated flood hazard and flood vulnerability subsystem permanent matrix are represented in Equations (15) and (16).

$$Updated\ permanent\ matrix\ of\ hazard = \begin{matrix} 1.3788 & 0.5430 & 0.3495 & 0.5419 & 0.1241 & 0.5004 \\ 0.5177 & 1.4481 & 0.3495 & 0.5419 & 0.2484 & 0.5004 \\ 0.1726 & 0.5430 & 1.2234 & 0.8450 & 0 & 1.0009 \\ 0.5177 & 0.5430 & 0.3495 & 1.4397 & 0.2484 & 0.5004 \\ 0.3451 & 0.3620 & 0.1748 & 0.5419 & 0.7166 & 0.3336 \\ 0.5177 & 0.5430 & 0.3495 & 0.5419 & 0.2484 & 1.1227 \end{matrix} \tag{15}$$

$$Updated\ permanent\ matrix\ of\ vulnerability = \begin{matrix} 0.5345 & 0.3215 & 0.5751 & 0.2521 & 0.3958 & 0.2638 & 0.2628 & 0.1858 \\ 0.4608 & 0.2390 & 0.1917 & 0.2521 & 0.1319 & 0.2638 & 0.2628 & 0.1858 \\ 0.4608 & 0.3215 & 1.5280 & 0.1261 & 0.2638 & 0.2638 & 0.3942 & 0.0929 \\ 0.3072 & 0.2143 & 0.1917 & 1.0086 & 0.1319 & 0.1319 & 0.2628 & 0 \\ 0.3072 & 0.2143 & 0.3834 & 0.1261 & 1.0553 & 0.1319 & 0.1314 & 0 \\ 0.1536 & 0.1072 & 0.3834 & 0.2521 & 0.1319 & 0.2032 & 0 & 0 \\ 0.3072 & 0.2143 & 0.3834 & 0.3782 & 0.2638 & 0.1319 & 0.5690 & 0.0929 \\ 0.3072 & 0.2143 & 0.1917 & 0.1261 & 0.1319 & 0.1319 & 0 & 0.5714 \end{matrix} \tag{16}$$

The quantitative value using the permanent matrix of flood hazard and flood vulnerability sub-system for the effective area covered under each rain gauge station was calculated and shown in the map (Figure 8(a,b)). Subsequently, the performances of the flood risk system in the form of a numeric value for the effective area covered under each rain gauge station were calculated. It is observed from Figure 8(a,b) that the flood hazard characterization of the Ghaggar river basin is found to vary from high to very high hazard, whereas flood vulnerability characterization is found to vary from moderate to highly vulnerable. Figure 8(c) shows the spatial variation of performance of the flood risk system of the Ghaggar basin in the form of a numeric value. It is observed that the area covered under Rohiti, Ambala, Banur, and Rajpura shows a higher numeric value which indicates the high flood risk zone in comparison to the area covered by other rain gauge stations.

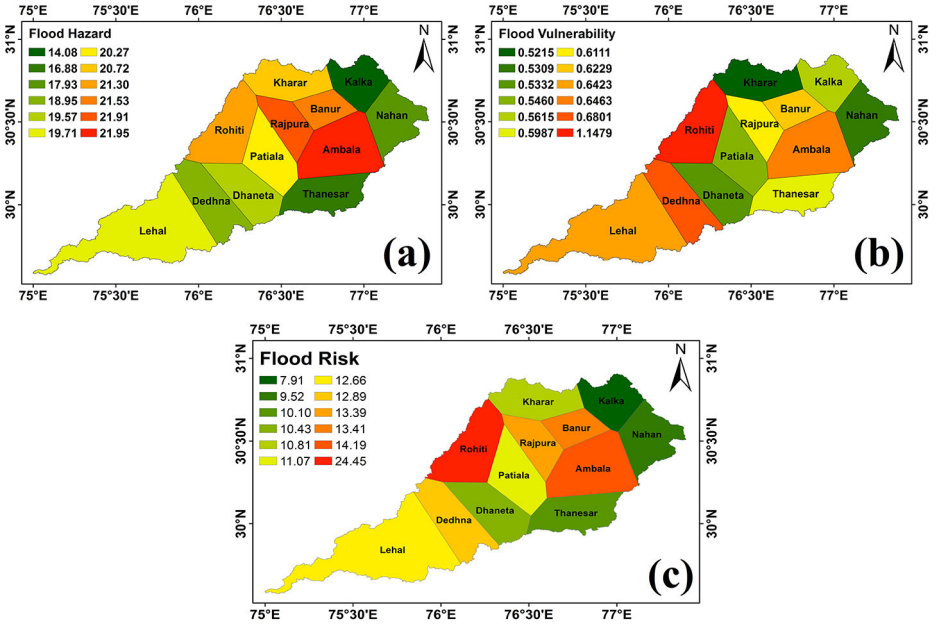

Figure 8. Flood hazard, flood vulnerability and flood risk zoning of Ghaggar river basin using graph theory.

It is observed that around 29.8% of the basin area is prone to very high flood hazard, whereas 70.1% of the basin area is prone to high flood hazard. Similarly, around 17.4% of the basin area is prone to highly vulnerable to flood, whereas 82.5% of the basin area is prone to moderately vulnerable to flood.

6.2. Identification of flood risk zone of Ghaggar river basin using AHP

The combined effect of all factors affecting flood hazard and flood vulnerability of the Ghaggar river basin was determined using AHP. Subsequently, the basin was divided into various zones based on its flood risk. Initially, the pair-wise comparison matrix was prepared based on the importance level of one factor over others (Dahri and Abida 2017; Luu et al. 2018; Ekmekcioğlu et al. 2021). Tables 11 and 12 show the pair-wise comparison matrix for flood hazard and flood vulnerability, respectively. Each row of these tables describes the relative importance of parameters positioned in a row with all six parameters placed in the column. For example, the first row of Table 11 represents the importance level of elevation with elevation, slope, LULC, soil group, rainfall, and distance from rivers. The diagonal elements of Tables 11 and 12 are equal to 1 as the factor in row and column is the same. Table 3 was used to assign the relative importance of each factor over other factors. The pair-wise comparison matrix of hazard and vulnerability was transformed to a normalized matrix. The normalized matrix of flood hazard variables was calculated by dividing each column value of Table 11 by summation of all values positioned in that column which is shown in Table 13.

Similarly, Table 14 shows the normalized matrix of flood vulnerability factors normalised in a similar manner using Table 12. The last column of Tables 13 and 14 shows the weights of each parameter in percentage. The weights of each factor of flood hazard and flood vulnerability were calculated by the average of each row corresponding to that factor and converted into percentage form. Flood hazard and flood vulnerability were calculated

Table 11. Comparison matrix of each parameter of flood hazard.

	Elevation	Slope	LULC	Soil group	Rainfall	Distance from rivers
Elevation	1	0.14	0.14	0.2	0.11	1
Slope	7	1	1	7	1	5
LULC	7	1	1	5	1	5
Soil group	5	0.14	0.20	1	0.20	3
Rx3day	9	1	1	5	1	7
Distance from rivers	1	0.20	0.20	0.33	0.14	1

Table 12. Comparison matrix of each parameter of flood vulnerability.

	Population density	Household density	LULC	Distance from roads	Distance flood shelter	Literacy rate	Rainfall trend	Drainage network
Population density	1	1	1	1	1	3	0.2	0.14
Household density	1	1	0.2	3	0.33	3	0.2	0.14
LULC	1	5	1	5	7	7	1	1
Distance from roads	1	0.33	0.2	1	0.2	3	0.2	0.2
Distance flood shelter	1	3	0.14	5	1	3	0.2	0.2
Literacy rate	0.33	0.33	0.14	0.33	0.33	1	0.14	0.14
Rainfall trend	5	5	1	5	5	7	1	1
Drainage network	7	7	1	5	5	7	1	1

Table 13. Normalized pair-wise comparison matrix of flood hazard.

	Elevation	Slope	LULC	Soil group	Rainfall	Distance from rivers	Weighatge (%)
Elevation	0.0333	0.0410	0.0403	0.0108	0.0322	0.0455	3.38
Slope	0.2333	0.2869	0.2823	0.3778	0.2895	0.2273	28.28
LULC	0.2333	0.2869	0.2823	0.2698	0.2895	0.2273	26.49
Soil group	0.1667	0.0410	0.0565	0.0540	0.0579	0.1364	8.54
Rx3day	0.3000	0.2869	0.2823	0.2698	0.2895	0.3182	29.11
Distance from rivers	0.0333	0.0574	0.0565	0.0178	0.0414	0.0455	4.20

using Equations (17) and (18), in which the weights calculated in Tables 13 and 14 were used.

$$\begin{aligned} Flood\ Hazard = {} & (Elevation \times 3.38) + (Slope \times 28.28) + (LULC \times 26.49) \\ & + (Soil\ Group \times 8.54) + (rx3day \times 29.11) \\ & + (Distance\ from\ rivers \times 4.20) \end{aligned} \tag{17}$$

$$\begin{aligned} Flood\ Vulnerability = {} & (Population\ Density \times 7.48) + (Household\ Density \times 5.68) \\ & + (LULC \times 24.37) + (Distance\ from\ roads \times 4.26) \\ & + (Distance\ from\ flood\ shelters \times 8.59) + (Literacy\ rate \times 2.91) \\ & + (Rainfall\ trend \times 22.93) \\ & + (Efficient\ Drainage\ System \times 24.19) \end{aligned} \tag{18}$$

The principal Eigenvalue (λ_{max}) of pair-wise matrixes for flood hazard and vulnerability were 6.298 and 8.893, respectively. The consistency index (CI) was calculated using Equation (9) and found 0.059 and 0.127 for flood hazard and vulnerability, respectively. The Random Index (RI) values from Table 4 are 1.24 and 1.41 for flood hazard and flood vulnerability, respectively. The consistency ratio (CR) was calculated using Equation (8) and found as 0.048 and 0.091 for flood hazard and flood vulnerability, respectively. If the

Table 14. Normalized pair-wise comparison matrix of flood vulnerability.

	Population density	Household density	LULC	Distance from roads	Distance flood shelter	Literacy rate	Rainfall trend	Drainage network	Weightage (%)
Population density	0.0577	0.0441	0.2137	0.0395	0.0504	0.0882	0.0508	0.0366	7.48
Household density	0.0577	0.0441	0.0427	0.1184	0.0166	0.0882	0.0508	0.0366	5.68
LULC	0.0577	0.2207	0.2137	0.1974	0.3525	0.2059	0.2538	0.2618	24.37
Distance from roads	0.0577	0.0146	0.0427	0.0395	0.0101	0.0882	0.0508	0.0524	4.26
Distance flood shelter	0.0577	0.1324	0.0299	0.1974	0.0504	0.0882	0.0508	0.0524	8.59
Literacy rate	0.0190	0.0146	0.0299	0.0130	0.0166	0.0294	0.0355	0.0366	2.51
Rainfall trend	0.2885	0.2207	0.2137	0.1974	0.2518	0.2059	0.2538	0.2618	22.93
Drainage network	0.4039	0.3089	0.2137	0.1974	0.2518	0.2059	0.2538	0.2618	24.19

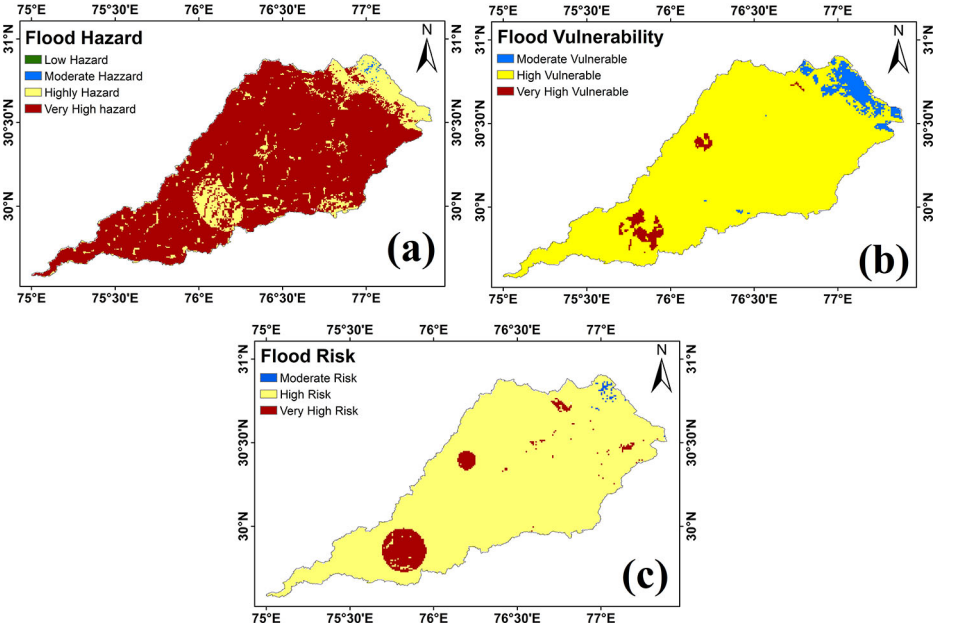

Figure 9. Flood hazard, flood vulnerability, and flood risk zoning of Ghaggar river basin using AHP.

CR value of the comparison matrix is greater than 0.10, then the comparison matrix is inconsistent and should be revised (Rahman et al. 2019). In the present study, since the CR is less than 0.1, the comparison matrixes for flood hazard and flood vulnerability are consistent.

6.2.1. Spatial variation of flood hazard analysis

The flood hazard map of the Ghaggar river basin was prepared in ArcMap 10.5 (Raster Analysis) using Equation (17), and the classified flood zone is shown in Table 8. The spatial map of flood hazard is shown in Figure 9(a) and found that the flood hazard level of the basin varies from high to very high category. It is observed from Figure 9(a) that around 14.54% (2033.5 km^2) and 85.2% (11,922.7 km^2) of the basin area are lying under the high and very high categories of flood hazard, respectively. Around 0.15% of the basin area (21.3 km^2) is observed under the moderate flood hazard category. A moderate level of flood hazard is observed in the upper portion of the basin, where the elevation is greater than 500 m.

Table 15. Comparison table of AHP and graph theory results.

	Hazard		Vulnerability		Risk	
Stations	AHP	Graph theory	AHP	Graph theory	AHP	Graph theory
Ambala	Very high	Very high	High	Moderate	High	High
Banur	Very high	Very high	High	Moderate	High	High
Dedhna	Very high	High	High	High	High	High
Dhaneta	Very high	High	High	Moderate	High	High
Kalka	High	High	High	Moderate	High	High
Kharar	Very high	High	High	Moderate	High	High
Lehal	Very high	High	High	Moderate	High	High
Nahan	Very high	High	High	Moderate	High	High
Patiala	Very high	High	High	Moderate	High	High
Rajpura	Very high	Very high	High	Moderate	High	High
Rohiti	Very high	Very high	High	High	High	High
Thanesar	Very high	High	High	Moderate	High	High

6.2.2. Spatial variation in flood vulnerability analysis

The flood vulnerability map of the Ghaggar river basin was prepared in ArcMap (Raster Analysis) using Equation (18) and the classified flood zone shown in Table 8. The spatial map of flood vulnerability is shown in Figure 9(b). It is observed from Figure 9(b) that around 93.25% (13,035.2 km^2) and 2.3% (322 km^2) of the basin area are lying under the high and very high categories of flood vulnerability, respectively. Around 4.44% of the basin area (620.7 km^2) is observed under the moderate flood vulnerable category.

6.2.3. Spatial variation of flood risk analysis

The spatial variation of the flood risk map was processed in ArcGIS 10.5 using raster analysis. Figure 9(c) shows the flood risk mapping of the Ghaggar river basin, and it is observed from Figure 9(c) that the flood risk of the Ghaggar river basin varies from moderate to very high category. But, most part of the basin, i.e., 94.1% (13,165.2 km^2), is at high risk of flood, whereas only 5.52% (771.6 km^2) is very high risk of flood. The basin areas under moderate risk to flood are observed to be 0.2% (41.09 km^2). The upper part of the basin, which is at a higher elevation, rapidly declined slope, forest cover, lowest population density have been observed as a moderate flood risk area. Although the magnitude of the rx3day is very high at the upper part of the basin, other hazard or vulnerability factors are such that the overall flood risk is moderate. The major part of the basin is at high risk to flood due to lying in plane area, urbanization, high population density, lack of efficient drainage network, and absence of flood shelters.

6.3. Comparison of the results obtained by these two methods

Flood hazard, vulnerability, and risk zone obtained through graph theory were compared with results obtained through AHP and shown in Table 15. It is observed from Table 15 that a high flood risk zone was obtained through both graph theory and AHP, whereas there is a small difference in results obtained in flood hazard and vulnerability characterization. Similar flood hazard characterization was obtained for Ambala, Banur, Rajpura, Rohiti, and Kalka rain gauge stations by both methods. Other basin areas were observed as very high flood hazard zones in AHP, whereas high hazard zones were obtained through graph theory. Similarly, most of the area of the basin was observed as highly vulnerable to flood through AHP, whereas moderate vulnerable to the flood was observed for those areas through graph theory. Since graph theory considers the interaction between sub-systems/sub-subsystems, the results obtained seem to integrate all the

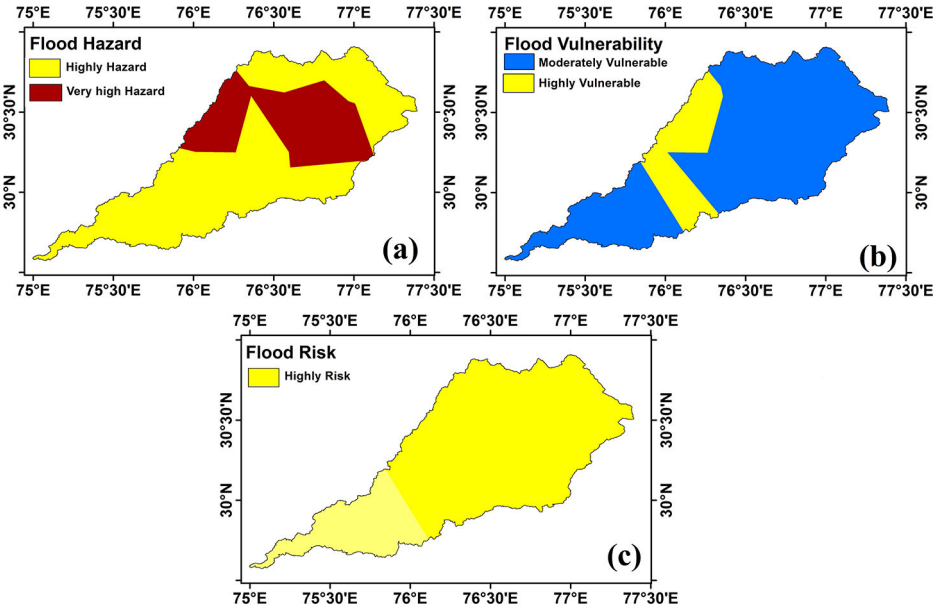

Figure 10. Flood hazard, vulnerability and risk classification of Ghaggar river basin using graph theory.

interactions/effects between all system components and believe to be more accurate in managing a complex problem. It is concluded from Table 15 that the characterization of flood hazard and flood vulnerability using graph theory under predicts than AHP.

The graph theory is a multi-criteria decision-making approach and provides possible alternate solutions for decision-makers. Table 15 and Figure 10 shows that the flood hazard, vulnerability and risk of Ghaggar river basin. It is observed that the basin is at high flood risk which also confirms from AHP. The graph theory analysis will help decision-makers to provide the possible solutions for effective flood management of the basin. The minimum numeric value of the flood risk system permanent matrix is 0.06, whereas the maximum value is 144.26. According to the classification of flood risk mentioned in Table 8, if the numeric value of the flood risk system permanent matrix lies in between 0.06 and 5.94, the basin will be under very low to moderate flood risk. The numeric value of permanent depends on the diagonal value of the system matrix. When the inheritance of system/sub-systems are efficient to reduce the flood risk of a basin, the matrix will contain the diagonal elements equal to 1, and the numeric value of the permanent matrix will be minimum. The sub-subsystems, which directly affect the flood risk of a basin, require improvement. Once the performance of the sub-subsystems improves, the weights of the diagonal element of the permanent matrix will lie in the range of 1–4 i.e., exceptionally low–normal flood risk. It is observed from Equation (11) that the weights of all the diagonal elements of the flood hazard permanent matrix equation are on the higher side.

Similarly, it is observed from Equation (12) that the weights of LULC, distance from flood shelters, efficient drainage network, and literacy rate sub-subsystems represented in the diagonal elements of flood vulnerability permanent matrix equation are on the higher side. These weights will be reduced when their effect on the flood vulnerability is minimum, and decision-makers should provide the solutions to subdue the impact of LULC, distance from flood shelters, efficient drainage network, and literacy rate sub-subsystems by providing efficient drainage in the basin, constructing flood shelters and restricting the

construction in the flood plain. Subsequently, the performance of sub-subsystems will improve, and the qualitative characteristics of respective diagonal elements will change from extreme risk to normal or low risk. The numeric value of the system permanent matrix will also shift from extreme flood vulnerability to moderate or low vulnerability. Similarly, decision-makers should provide the solutions to reduce the worst impact of conditioning factors on flood hazard of the Ghaggar river basin. The improvement of performance of both the flood hazard and vulnerability sub-system will reduce the flood risk of the basin.

7. Conclusion

Flood risk, flood hazard, and flood vulnerability analysis are widely used for better flood management of a river basin. The present study considers six factors for flood hazard and eight factors for flood vulnerability analysis of the Ghaggar river basin. The assessment was integrated with ArcGIS 10.5. The present study proposed a graph theory method for flood risk analysis and compared the obtained results with the AHP method. It is concluded that graph theory is also capable to identify flood risk zone on a catchment scale. Since it is considering the interaction between the sub-systems/sub-subsystems apart from their own performance the results obtained are believed to be more accurate than other similar methods. The flood hazard, vulnerability, and risk are characterised into five zones: very low, low, moderate, high, and very high. It is observed from the AHP method that around 85.2%, 14.54%, and 0.15% area of the basin are under very high, high, and moderate flood hazard zone respectively, whereas graph theory suggests that around 29.8 and 70.2% area of the basin shows very high and high flood hard zone respectively. The area under flood vulnerability using AHP shows that 2.3%, 93.25%, and 4.44% are very high, high, and moderately vulnerable to flood zone respectively, whereas graph theory suggests that around 17.47 and 82.53% of areas are high and moderately vulnerable to flood respectively. The flood risk analysis using the AHP method shows most part of the basin i.e., 94.1% (13,165.2 km^2), is at high risk to flood, whereas only 5.52% (771.6 km^2) under very high risk. The basin areas under moderate risk to flood are observed to be 0.2% (41.09 km^2). Graph theory suggests that all the considered study areas of the basin are under high flood risk zone. It is concluded that both AHP and graph theory methods are suggesting similar results for the Ghaggar river basin, and it is concluded that the Ghaggar river basin is prone to a high risk of flood. Therefore, decision-makers can use these results to establish preventive measures in this basin to protect the flood.

It is concluded that graph theory can also identify the flood risk zone of a river basin precisely and show acceptable accuracy. Although both AHP and graph theory are powerful tools for dividing a basin into different flood zones, graph theory manages the whole process better by considering the interaction between the factors affecting the system. The limitation of this methodology is the availability of the datasets having reasonable accuracy, aggregation of weights assigned by experts and requires good computation facility in order to calculate the numeric value for each pixel. The aggregation of weights assigned by multiple experts can be further improved for more accurate results. This algorithm can be further refined to provide possible alternate management solutions on a catchment scale so that the role of decision-makers can be introduced for better flood risk management.

Acknowledgement

Authors would like to acknowledge Indian meteorological Department (IMD) Pune for providing rainfall data of the study area. We appreciate the editor and anonymous reviewers for their constructive comments which greatly helped to improve our manuscript

ORCID

Dwarikanath Ratha http://orcid.org/0000-0002-3309-2648
Amit Dhir http://orcid.org/0000-0002-6705-5888

References

Anand J, Gosain AK, Khosa R. 2018. Prediction of land use changes based on Land Change Modeler and attribution of changes in the water balance of Ganga basin to land use change using the SWAT model. Sci Total Environ. 644:503–519.

Arabameri A, Rezaei K, Cerdà A, Conoscenti C, Kalantari Z. 2019. A comparison of statistical methods and multi-criteria decision making to map flood hazard susceptibility in Northern Iran. Sci Total Environ. 660:443–458.

Asare-Kyei D, Forkuor G, Venus V. 2015. Modeling flood hazard zones at the sub-district level with the rational model integrated with GIS and remote sensing approaches. Water. 7(12):3531–3564.

Bahremand A, De Smedt F, Corluy J, Liu YB, Poorova J, Velcicka L, Kunikova E. 2007. WetSpa model application for assessing reforestation impacts on floods in Margecany–Hornad Watershed, Slovakia. Water Resour Manage. 21(8):1373–1391..

Caloiero T, Coscarelli R, Ferrari E. 2018. Application of the innovative trend analysis method for the trend analysis of rainfall anomalies in Southern Italy. Water Resour Manage. 32(15):4971–4983.

Cao C, Xu P, Wang Y, Chen J, Zheng L, Niu C. 2016. Flash flood hazard susceptibility mapping using frequency ratio and statistical index methods in Coalmine subsidence areas. Sustain. 8(9):948.

Chakraborty S, Mukhopadhyay S. 2019. Assessing flood risk using analytical hierarchy process (AHP) and geographical information system (GIS): application in Coochbehar district of West Bengal, India. Nat Hazards. 99(1):247–274.

Chen Y-R, Yeh C-H, Yu B. 2011. Integrated application of the analytic hierarchy process and the geographic information system for flood risk assessment and flood plain management in Taiwan. Nat Hazards. 59(3):1261–1276..

Costache R, Tien Bui D. 2020. Identification of areas prone to flash-flood phenomena using multiple-criteria decision-making, bivariate statistics, machine learning and their ensembles. Sci Total Environ. 712:136492.

CWC. 2014. River Development & Ganga Rejuvenation, Annual Report 2013–14 India.

Dahri N, Abida H. 2017. Monte Carlo simulation-aided analytical hierarchy process (AHP) for flood susceptibility mapping in Gabes Basin (southeastern Tunisia). Environ Earth Sci. 76(7):302.

Darabi H, Choubin B, Rahmati O, Torabi Haghighi A, Pradhan B, Kløve B. 2019. Urban flood risk mapping using the GARP and QUEST models: a comparative study of machine learning techniques. J Hydrol. 569:142–154.

Das S. 2018. Geographic information system and AHP-based flood hazard zonation of Vaitarna basin, Maharashtra, India. Arab J Geosci. 11(19):576.

De Brito MM, Evers M. 2016. Multi-criteria decision-making for flood risk management: A survey of the current state of the art. Nat Hazards Earth Syst Sci. 16(4):1019–1033.

Ekmekcioğlu Ö, Koc K, Özger M. 2021. District based flood risk assessment in Istanbul using fuzzy analytical hierarchy process. Stoch Environ Res Risk Assess. 35(3):617–637..

Fortini M, Bragalli C, Artina S. 2014. Identifying the high-level flow model of water distribution networks using graph theory. Procedia Eng. 89:1192–1199.

Fotovatikhah F, Herrera M, Shamshirband S, Chau K, Faizollahzadeh Ardabili S, Piran MJ. 2018. Survey of computational intelligence as basis to big flood management: challenges, research directions and future work. Eng Appl Comput Fluid Mech. 12(1):411–437..

Fu M, Fan T, Ding Z, Salih SQ, Al-Ansari N, Yaseen ZM. 2020. Deep learning data-intelligence model based on adjusted forecasting window scale: application in daily streamflow simulation. IEEE Access. 8: 32632–32651. https://ieeexplore.ieee.org/document/9007531/.

Ghosh A, Kar SK. 2018. Application of analytical hierarchy process (AHP) for flood risk assessment: a case study in Malda district of West Bengal, India. Nat Hazards. 94(1):349–368.
Gorai S, Ratha D, Dhir A. 2021. Adapting rainfall variability to flood risk: a case study of the Ghaggar river basin. J Geol Soc India. 97:1347–1354.
Haghizadeh A, Siahkamari S, Haghiabi AH, Rahmati O. 2017. Forecasting flood-prone areas using Shannon's entropy model. J Earth Syst Sci. 126(3):39. http://link.springer.com/10.1007/s12040-017-0819-x.
Hajebi S, Roshani E, Cardozo N, Barrett S, Clarke A, Clarke S. 2016. Water distribution network sectorisation using graph theory and many-objective optimisation. J Hydroinformatics. 18(1):77–95.
Hammami S, Zouhri L, Souissi D, Souei A, Zghibi A, Marzougui A, Dlala M. 2019. Application of the GIS based multi-criteria decision analysis and analytical hierarchy process (AHP) in the flood susceptibility mapping (Tunisia). Arab J Geosci. 12(21):653.
Heidinger H, Carvalho L, Jones C, Posadas A, Quiroz R. 2018. A new assessment in total and extreme rainfall trends over central and southern Peruvian Andes during 1965–2010. Int J Climatol. 38: e998–e1015.
Hong H, Panahi M, Shirzadi A, Ma T, Liu J, Zhu A-X, Chen W, Kougias I, Kazakis N. 2018. Flood susceptibility assessment in Hengfeng area coupling adaptive neuro-fuzzy inference system with genetic algorithm and differential evolution. Sci Total Environ. 621:1124–1141. https://www.sciencedirect.com/science/article/pii/S0048969717328176.
Kalantari Z, Cavalli M, Cantone C, Crema S, Destouni G. 2017. Flood probability quantification for road infrastructure: Data-driven spatial-statistical approach and case study applications. Sci Total Environ. 581–582:386–398. https://www.sciencedirect.com/science/article/pii/S0048969716328376.
Kaya CM, Tayfur G, Gungor O. 2019. Predicting flood plain inundation for natural channels having no upstream gauged stations. J Water Clim Chang. 10(2):360–372. https://iwaponline.com/jwcc/article/10/2/360/38950/Predicting-flood-plain-inundation-for-natural.
Kittipongvises S, Phetrak A, Rattanapun P, Brundiers K, Buizer JL, Melnick R. 2020. AHP-GIS analysis for flood hazard assessment of the communities nearby the world heritage site on Ayutthaya Island, Thailand. Int J Disaster Risk Reduct. 48:101612.
Kourgialas NN, Karatzas GP. 2017. A national scale flood hazard mapping methodology: The case of Greece—protection and adaptation policy approaches. Sci Total Environ. 601–602:441–452. https://www.sciencedirect.com/science/article/pii/S0048969717313049.
Lee M, Kang J, Jeon S. 2012. Application of frequency ratio model and validation for predictive flooded area susceptibility mapping using GIS. In: 2012 IEEE Int Geosci Remote Sens Symp. p. 895–898.
Levy JK. 2005. Multiple criteria decision making and decision support systems for flood risk management. Stoch Environ Res Ris Assess. 19(6):438–447.
Liu K, Li Z, Yao C, Chen J, Zhang K, Saifullah M. 2016. Coupling the k-nearest neighbor procedure with the Kalman filter for real-time updating of the hydraulic model in flood forecasting. Int J Sediment Res. 31(2):149–158. https://www.sciencedirect.com/science/article/pii/S1001627916300117.
Luu C, Von Meding J, Kanjanabootra S. 2018. Assessing flood hazard using flood marks and analytic hierarchy process approach: a case study for the 2013 flood event in Quang Nam, Vietnam. Nat Hazards. 90(3):1031–1050.
Lyu H-M, Zhou W-H, Shen S-L, Zhou A-N. 2020. Inundation risk assessment of metro system using AHP and TFN-AHP in Shenzhen. Sustain Cities Soc. 56:102103.
Masood M, Takeuchi K. 2012. Assessment of flood hazard, vulnerability and risk of mid-eastern Dhaka using DEM and 1D hydrodynamic model. Nat Hazards. 61(2):757–770.
Miao S, Chen F, Li Q, Fan S. 2011. Impacts of urban processes and urbanization on summer precipitation: a case study of heavy rainfall in Beijing on 1 August 2006. J Appl Meteorol Climatol. 50(4): 806–825.
Mohan KS, Shankar N, Murty BS. 2008. State estimation in water distribution networks using graph-theoretic reduction strategy. J Water Resour Plan Manag. 134(5):395–403.
Mondal A, Khare D, Kundu S. 2015. Spatial and temporal analysis of rainfall and temperature trend of India. Theor Appl Climatol. 122(1–2):143–158.
Mosavi A, Ozturk P, Chau K. 2018. Flood prediction using machine learning models: literature review. Water. 10(11):1536. https://www.mdpi.com/2073-4441/10/11/1536.
Oeurng C, Sauvage S, Sánchez-Pérez J-M. 2011. Assessment of hydrology, sediment and particulate organic carbon yield in a large agricultural catchment using the SWAT model. J Hydrol. 401(3–4): 145–153. https://www.sciencedirect.com/science/article/pii/S0022169411001247.

Pagano A, Sweetapple C, Farmani R, Giordano R, Butler D. 2019. Water distribution networks resilience analysis: a comparison between graph theory-based approaches and global resilience analysis. Water Resour Manage. 33(8):2925–2940.
Pradhan B. 2010. Flood susceptible mapping and risk area delineation using logistic regression, GIS and remote sensing. J Spat Hydrol. 9(2):1–18.
Praveen B, Talukdar S, Shahfahad Mahato S, Mondal J, Sharma P, Islam ARMT, Rahman A. 2020. Analyzing trend and forecasting of rainfall changes in India using non-parametrical and machine learning approaches. Sci Rep. 10(1):10342.
Radwan F, Alazba AA, Mossad A. 2019. Flood risk assessment and mapping using AHP in arid and semi-arid regions. Acta Geophys. 67(1):215–229.
Rahman M, Ningsheng C, Islam MM, Dewan A, Iqbal J, Washakh RMA, Shufeng T. 2019. Flood susceptibility assessment in Bangladesh using machine learning and multi-criteria decision analysis. Earth Syst Environ. 3(3):585–601.
Rahmati O, Pourghasemi HR, Zeinivand H. 2016. Flood susceptibility mapping using frequency ratio and weights-of-evidence models in the Golastan Province, Iran. Geocarto Int. 31(1):42–70..
Ratha D, Agrawal VP. 2014. Structural modeling and analysis of water resources development and management system: a graph theoretic approach. Water Resour Manage. 28(10):2981–2997.
Ratha D, Agrawal VP. 2015. A digraph permanent approach to evaluation and analysis of integrated watershed management system. J Hydrol. 525:188–196.
Rincón D, Khan UT, Armenakis C. 2018. Flood risk mapping using GIS and multi-criteria analysis: a greater Toronto area case study. Geosci. 8(8):275.
Saaty TL. 1977. A scaling method for priorities in hierarchical structures. J Math Psychol. 15(3):234–281.
Shahiri Tabarestani E, Afzalimehr H. 2021. A comparative assessment of multi-criteria decision analysis for flood susceptibility modelling. Geocarto Int. 2021:1–24..
Shamshirband S, Hashemi S, Salimi H, Samadianfard S, Asadi E, Shadkani S, Kargar K, Mosavi A, Nabipour N, Chau K-W. 2020. Predicting standardized streamflow index for hydrological drought using machine learning models. Eng Appl Comput Fluid Mech. 14(1):339–350..
Souissi D, Zouhri L, Hammami S, Msaddek MH, Zghibi A, Dlala M. 2020. GIS-based MCDM—AHP modeling for flood susceptibility mapping of arid areas, southeastern Tunisia. Geocarto Int. 35(9): 991–1017.
Talwar AR. 2011. State Disaster Management Plan Punjab. Punjab, India.
Tang Z, Zhang H, Yi S, Xiao Y. 2018. Assessment of flood susceptible areas using spatially explicit, probabilistic multi-criteria decision analysis. J Hydrol. 558:144–158.
Taormina R, Chau K-W. 2015. ANN-based interval forecasting of streamflow discharges using the LUBE method and MOFIPS. Eng Appl Artif Intell. 45:429–440. https://linkinghub.elsevier.com/retrieve/pii/S0952197615001748.
Tehrany MS, Pradhan B, Jebur MN. 2013. Spatial prediction of flood susceptible areas using rule based decision tree (DT) and a novel ensemble bivariate and multivariate statistical models in GIS. J Hydrol. 504:69–79. https://www.sciencedirect.com/science/article/pii/S0022169413006872.
Tehrany MS, Pradhan B, Mansor S, Ahmad N. 2015. Flood susceptibility assessment using GIS-based support vector machine model with different kernel types. CATENA. 125:91–101. https://www.sciencedirect.com/science/article/pii/S034181621400294X.
Thanh Son N, Thi Thu Trang N, Bui XT, Thi Da C. 2021. Remote sensing and GIS for urbanization and flood risk assessment in Phnom Penh, Cambodia. Geocarto Int. 2021:1–18..
Tien Bui D, Pradhan B, Nampak H, Bui Q-T, Tran Q-A, Nguyen Q-P. 2016. Hybrid artificial intelligence approach based on neural fuzzy inference model and metaheuristic optimization for flood susceptibilitgy modeling in a high-frequency tropical cyclone area using GIS. J Hydrol. 540:317–330. https://www.sciencedirect.com/science/article/pii/S002216941630378X.
Wang Y, Xu Y, Tabari H, Wang J, Wang Q, Song S, Hu Z. 2020. Innovative trend analysis of annual and seasonal rainfall in the Yangtze River Delta, eastern China. Atmos Res. 231:104673.
Wilson KJ. 2017. An investigation of dependence in expert judgement studies with multiple experts. Int J Forecast. 33(1):325–336. http://dx.doi.org/10.1016/j.ijforecast.2015.11.014.
Wisner B, Blaikie P, Cannon T, Davis I. 2004. At risk, natural hazard, people's vulnerability and disasters. Second. Routledge, London.
Zhao G, Pang B, Xu Z, Yue J, Tu T. 2018. Mapping flood susceptibility in mountainous areas on a national scale in China. Sci Total Environ. 615:1133–1142. https://www.sciencedirect.com/science/article/pii/S0048969717327419.
Zou Q, Zhou J, Zhou C, Song L, Guo J. 2013. Comprehensive flood risk assessment based on set pair analysis-variable fuzzy sets model and fuzzy AHP. Stoch Environ Res Risk Assess. 27(2):525–546..

Sustainable Water Resources Management (2023) 9:102
https://doi.org/10.1007/s40899-023-00876-5

ORIGINAL ARTICLE

Prediction of agricultural water deficiency and its management using long-term rainfall trends

Sanjoy Gorai[1] · Dwarikanath Ratha[2] · Amit Dhir[1]

Received: 20 March 2022 / Accepted: 17 May 2023
© The Author(s), under exclusive licence to Springer Nature Switzerland AG 2023

Abstract

The present study is focused on the rainfall trend analysis of Punjab state in India. In this regard, thirty-three rain gauge stations were considered. The rainfall trend was predicted using the innovative trend analysis and compared with the Mann–Kendall test and Sen Slope estimator. The analysis reveals that most of the semi-urban areas of the Punjab state are experiencing a declining trend of rainfall, whereas urban and rural areas are experiencing an increasing annual rainfall trend at 5% level of significance in the last two decades of the twentieth century. The effect of declining trend of rainfall on frequency of occurrence drought was analysed using standardised precipitation index (SPI) and observed that the frequency of occurrence of drought is more in last two decades in the semi-urban areas of Punjab state. The effect of negative rainfall trend and drought condition is causing a significant rise in rain water deficit for agriculture and is expected to lie in a range of 30–48% of current water demand in next 15 years for Patiala district. The deficit rainwater will cause more extraction of groundwater for agriculture and the stress on groundwater may lead to food security issue. The stress on groundwater can be relieved by identifying the potential rainwater harvesting zone and it is observed that around 60% area of the Patiala district have good potential for rainwater harvesting. The spatio-temporal variation of rainfall trend, and drought analysis of the present study is expected to help in better planning and efficient management of agricultural practices.

Keywords Rainfall trend · Mann–Kendall test · Innovative trend analysis · Pettit's change point · Rainwater harvesting

Introduction

Rainfall is a component of the hydrological cycle that facilitates the water supply, agriculture, recharging of groundwater, and socio-economic development of a country (Praveen et al. 2020). Since India is an agricultural country and people depend on rainfall for agriculture, rainfall variability is one of the essential climatological parameters required to study for better understanding of the agricultural efficiency and groundwater management (Kundu and Mondal 2019). The changes in the rainfall pattern lead to an adverse impact on the environment in terms of flooding, droughts, ecosystem, agriculture, fisheries, etc. The spatial and temporal variation of rainfall is the climate change indicator on a regional and local scale. The determinations of spatial and temporal rainfall variation on a local scale are sufficient concerning agriculture production and disaster preparedness. Therefore, significant research on rainfall variability due to climate change is necessary for overall management and the sustainable development of agricultural practices in India.

The assessment of changes in rainfall of the global, regional, or local scale depends on the availability of the hydro-meteorological data and its accuracy. Indian Meteorological Department (IMD) is one of the sources for obtaining the hydro-meteorological data of various locations of India based on rain-gauge stations or gridded satellite data. Considerable research has been conducted by several hydrologists on the monthly, seasonal, annual, or any specified period on the pattern of rainfall trends over the world and obtained different results varied from global to local

✉ Dwarikanath Ratha
dnath.ratha@thapar.edu

Sanjoy Gorai
kumarsanjoy7@gmail.com

Amit Dhir
amit.dhir@thapar.edu

[1] School of Energy and Environment, Thapar Institute of Engineering and Technology, Patiala 147001, India

[2] Department of Civil Engineering, Thapar Institute of Engineering and Technology, Patiala, Punjab 147001, India

Published online: 06 June 2023

scale (Salman et al. 2019; Praveen et al. 2020; Wang et al. 2020b; Alemu and Bawoke 2020; Patel et al. 2021). Several hydrologists found significant trends from the long-term trend analysis of Indian rainfall on a regional scale (Mondal et al. 2015; Sanikhani et al. 2018; Praveen et al. 2020; Gorai et al. 2021). The study on rainfall trend analysis of various meteorological divisions of India detected the decreasing rainfall trend after 1951 (Praveen et al. 2020).

The frequently used method for the trend analysis is the Mann–Kendall (MK) test and Sen Slope estimator (Krishan et al. 2015; Mondal et al. 2015; Gorai et al. 2021). It is observed that if hydro-climatological time series are serially correlated, the negative autocorrelation underestimate the significance of trends while positive autocorrelation overestimate the significance trend (Sanikhani et al. 2018). It is assumed that the autocorrelation is absent in considered time series while applying the MK test. Since most of the hydro-climatological time series are serially correlated and Kumar et al. (2014) observed the presence of serial correlation in time series have significant effect on rainfall trend analysis, it is required to remove the autocorrelation before applying the MK test (Kumar et al. 2014). Several studies reported in literature are suffering from this limitation and their result seems to be inaccurate.

Şen (2012) proposed Innovative Trend Analysis (ITA) methods to find out the trend and its magnitude and Şen (2017) developed a statistical methodology of ITA that can calculate the slope value, trend indicator, and significance test. Recently, several studies analysed the trend using ITA methods validated by the MK test (Cui et al. 2017; Wu and Qian 2017; Wang et al. 2020b; Patel et al. 2021). It is observed that very few studies are available on applying the statistical methodology of ITA for determination of slope value, trend indicator and significance test of ITA (Wang et al. 2020a; Harkat and Kisi 2021). The study on trend analysis and change-point analysis are frequently used to get more information about the future prediction, which is helpful for water resources planners to execute the proper management plan on a regional or local scale (Mondal et al. 2015; Gorai et al. 2021). Several hydrologists have been reported the regional level study in some states of India, such as Kerala, Chhattisgarh, Madhya Pradesh, Orissa, Delhi, etc. (Patra et al. 2012; Pingale et al. 2014; Kothawale and Rajeevan 2017) but the application of their findings is observed to be missing from their study.

The long-term declining trend of rainfall in an area is one of the reasons of occurrence of drought. Several researchers conducted numerous studies on drought analysis using various numerical models but Standardised Precipitation Index (SPI) and Standardized Precipitation Evapotranspiration Index (SPEI) are the commonly used techniques found in literature (He et al. 2011; Gocic and Trajkovic 2013; Vyas et al. 2015; Li et al. 2019, 2020; Poonia et al. 2021; Wolteji et al. 2022). SPI is observed to be widely used for drought analysis for its ease of computation and its ability to detect drought at multiple time scales (He et al. 2011; Gocic and Trajkovic 2013; Farahmand and AghaKouchak 2015; Diffenbaugh et al. 2015; Li et al. 2019).

According to the Central Ground Water Board (CGWB) report (2018), rainwater is insufficient to fulfil the irrigation water demand in Punjab, where wheat, paddy, and mustard are usually sown as primary crops (CGWB 2018). Therefore, a study on trend analysis and exploring rainfall variability of Punjab state considering the local meteorological data are required for analysing the impact of rainfall trend on agriculture, flood, and drought. Several studies on trend analysis using MK test are reported in literature considering the meteorological data having the effect of serial correlation in time series and therefore the results reported seems to be inaccurate. Hence, the present study used the pre-whitening approach in rainfall time series before applying the MK test in order to remove the effect of serial correlation. Also, the present study compared the results obtained through MK test before and after applying pre-whitening which is rarely found in literatures. Although several studies are available on rainfall trend analysis, limited studies on rainfall variability on a regional scale, and its application are reported in literature (Kaur et al. 2011; Krishan et al. 2015; Singh et al. 2022). Therefore, the rainfall variability analysis of the state level was further applied to the district level to predict the water demand for the agricultural activity of Patiala district for the future 15 years using rainfall-runoff model. The present study also extended the findings of the rainfall trend analysis of study area in water contingency plan for agricultural water management. The amount of water for agricultural activity can be fulfilled through a rainwater harvesting structure. Therefore, this study also aims to find out the potential rainwater harvesting zones which will help the farmers and administrative bodies to build up some rainwater harvesting structures to store rainwater for further utilization in agricultural activity. The results will benefit planners and hydrologists for efficient use of available water, prediction of flood and drought, and encouraging farmers on the crop pattern suitable to the present rainfall pattern.

Study area and dataset used

Punjab state is in northern India with geographical coordinates of 29.30°–32.32° N and 73.55°–76.50° E and covers an area of about 50,362 km^2. Most of the people of this state depend on agriculture for their livelihood. This state is primarily growing wheat and harvesting 37.83% of total wheat grown in India. The state also produces other crops such as rice, cotton, sugarcane, pearl millet, maize, barley, and fruits. The agricultural production and the socio-economic

condition are highly dependent on the rainfall during the southwest monsoon season. Daily rainfall data (1950–2018) of 33 stations were collected from IMD (Indian Meteorological Department) based on their completeness. Out of these 33 stations, 55, 24, and 21% stations are from rural, semi-urban and urban regions respectively. Figure 1a shows the location of rain gauge stations in Punjab state, and Fig. 1b shows the geographical coordinates, elevation, and duration of the collected dataset. IMD classified the Indian season into four, and they are winter season (January–February), pre-monsoon season (March–May), southwest monsoon season (July–September), and post-monsoon season (October–December).

Methodology

Statistical analysis in this study was made using the statistical tool of mean, standard deviation, coefficient variance, etc. The trend and trend magnitude were analyzed using the ITA method and validated using the Mann–Kendall (MK) test and Sen Slope estimator. The change point was analyzed using Pettit's change point test. The drought analysis was analyzed using SPI. The agricultural water balance was prepared from the current rainfall scenario and the runoff produces from the surface. The run-off estimation was analysed using SCS-CN method. Potential rainwater harvesting zone analysis to fulfill the deficit agricultural demand was analyzed using Analytical Hierarchy Process (AHP).

Innovative trend analysis (ITA) method

Şen (2012) developed ITA to identify the rainfall trend of a region. The basic theory of the ITA method is the statistical analysis of two halves of the time series data. The first and second halves of the data are plotted on the x and y-axis, respectively. The plot is found as straight-line making angle 45° passing through the origin. Figure 2 describes the increasing trend, decreasing trend, and no trend. Şen (2017) developed the statistical equation for determination of magnitude of trend and its significance. Equation 1 shows the basic calculation for the slope of the trend line.

$$S = \frac{2(\overline{y_2} - \overline{y_1})}{n} \tag{1}$$

where, $\overline{y_1}$ is the arithmetic mean of the first halves of the dataset, $\overline{y_2}$ is the arithmetic mean of the second halves of the dataset and n is the length of dataset. The arithmetic means of the first and second halves are stochastic variables. The mean of two halves plotted as (y_1, y_2) is known as "centroid point," which is pointed on the data line. The significance test of the slope value is calculated using hypothesis testing i.e., null hypothesis and alternative hypothesis. The null

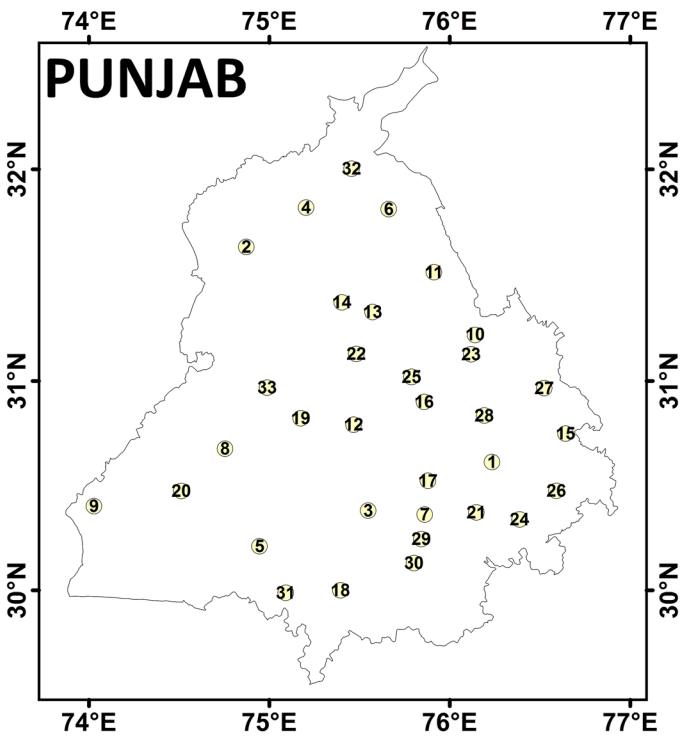

Sr No	STATION NAME	Latitude	Longitude	Altitude (m)	Data Period
1	AMLOH	30.614300	76.233428	257	1954-2018
2	AMRITSAR	31.633951	74.872266	218	1990-2018
3	BARNALA	30.381758	75.547179	227	1953-2018
4	BATALA	31.819525	75.203588	243	1950-2018
5	BHATINDA	30.210994	74.945475	202	1954-2018
6	DASUYA	31.812695	75.661412	238	1950-2018
7	DHURI	30.362986	75.860655	238	1954-2018
8	FARIDKOT	30.677406	74.753927	203	1954-2018
9	FAZILKA	30.403648	74.027962	168	1950-2018
10	GARHSHANKAR	31.217507	76.140693	270	1950-2018
11	HOSHIARPUR	31.514318	75.911483	296	1950-2018
12	JAGRAON	30.792334	75.467019	234	1950-2018
13	JULLUNDAR	31.326015	75.571830	233	1950-2018
14	KAPURTHALA	31.372257	75.401765	225	1950-2018
15	KHARAR	30.749868	76.641109	298	1950-2018
16	LUDHIANA	30.900965	75.857276	243	1950-2018
17	MALERKOTLA	30.524581	75.878344	243	1954-2018
18	MANSA	29.999507	75.393681	212	1950-2018
19	MOGA	30.823011	75.173447	217	1950-2018
20	MUKTESAR	30.476177	74.512160	184	1950-2018
21	NABHA	30.373018	76.146955	245	1954-2018
22	NAKODAR	31.127019	75.481773	222	1950-2018
23	NAWANSHAHR	31.125558	76.118642	283	1950-2018
24	PATIALA	30.339781	76.386880	251	1952-2018
25	PHILLAUR	31.018990	75.787940	234	1950-2018
26	RAJPURA	30.476580	76.590532	259	1954-2018
27	ROOPNAGAR	30.966100	76.523096	253	1950-2018
28	SAMRALA	30.835668	76.191028	249	1950-2018
29	SANGRUR	30.245796	75.842072	232	1954-2018
30	SUNAM	30.130558	75.801397	231	1954-2018
31	TALWANDI (SABO)	29.987507	75.090315	213	1954-2018
32	TIBRI	32.002649	75.455398	262	1950-2018
33	ZIRA	30.968531	74.988089	204	1950-2018

Fig. 1 Geographical position of the rain gauge stations

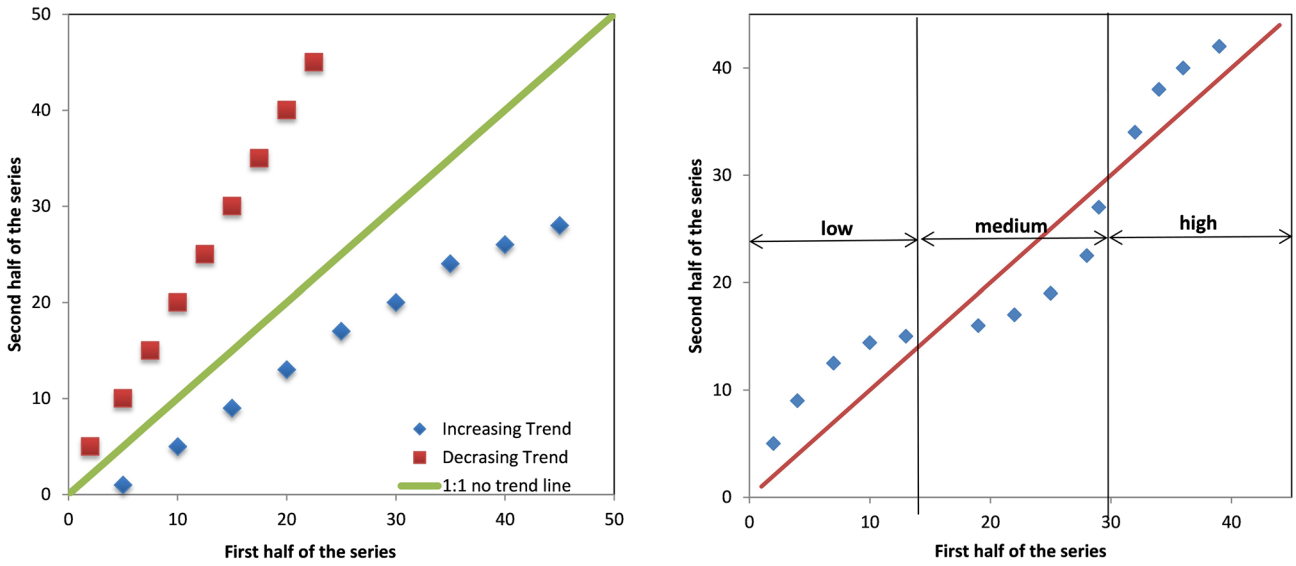

Fig. 2 Innovative trend analysis methodology

hypothesis is accepted where slope value S is below a critical value S_{cr} where the alternative is rejected i.e., $S < S_{cr}$. The first-order moment i.e., expectation of the slope can be calculated by taking expectation on both sides because the arithmetic means of the first and second halves are stochastic variables:

$$E(S) = \frac{2}{n}[E(\overline{y_2}) - E(\overline{y_1})] \tag{2}$$

The value of $E(\overline{y_2})$ will be the same as $E(\overline{y_1})$, if the centroid point falls on a 45° angle straight line i.e., $E(S) = 0$. The variance of the slope can be calculated as using Eq. 3.

$$\sigma_s^2 = E(S^2) - E^2(S) = \frac{4}{n^2}\left[E\left(\overline{y_2}^2\right) - 2E(\overline{y_1 y_2}) + E(\overline{y_1}^2)\right] \tag{3}$$

As $E\left(\overline{y_2}^2\right) = E(\overline{y_1}^2)$, Eq. 3 can be transformed to the following form:

$$\sigma_s^2 = \frac{8}{n^2}\left[E\left(\overline{y_2}^2\right) - E(\overline{y_1 y_2})\right] \tag{4}$$

The correlation coefficient $\left(\rho_{\overline{y_1 y_2}}\right)$ between $\overline{y_2}$ and $-\overline{y_1}$ is explained as:

$$\rho_{\overline{y_1 y_2}} = \frac{E(\overline{y_1 y_2}) - E(\overline{y_2})E(\overline{y_1})}{\sigma_{\overline{y_2}}\sigma_{\overline{y_1}}} \tag{5}$$

The final relation of slope variance is calculated by substitution of numerator correlation coefficient and considering $\sigma_{\overline{y_2}} = \sigma_{\overline{y_1}} = \sigma/\sqrt{n}$ into Eq. 4.

$$\sigma_s^2 = \frac{8}{n^2}\frac{\sigma^2}{n}\left(1 - \rho_{\overline{y_1 y_2}}\right) \tag{6}$$

So, the standard deviation of the slope (σs) can be calculated using Eq. 7 as:

$$\sigma_s = \frac{2\sqrt{2}}{n\sqrt{n}}\sigma\sqrt{\left(1 - \rho_{\overline{y_1 y_2}}\right)} \tag{7}$$

Confidence limit (CL) of the trend slope is shown in Eq. 8 in which standard deviation is S_{cr}. The slope S of the time series is statistically significant if it falls outside the confidence limit.

$$CL_{(1-\alpha)} = 0 \pm S_{cr} \times \sigma_s \tag{8}$$

The trend analysis results obtained from ITA were validated using Mann–Kendall (MK) test and Sen Slope estimator.

Mann–Kendall test

Mann–Kendall test was used in the present study for the validation of the trend analysis results obtained from ITA. Mann–Kendall test is extensively used for the trend analysis in hydro-meteorological data series (Sharma et al. 2016; Wu and Qian 2017; Kundu and Mondal 2019). The presence of serial correlation in the data series was identified and eliminated using pre-whitening approach. The value of standardized test static Z indicates the trends in the rainfall

series data (Jain et al. 2013; Westra et al. 2014; Croitoru et al. 2016).

Equations 9 and 10 were used to determine the test of statistics S and variance of test statistics $Var(S)$ (Jaiswal et al. 2015).

$$S = \sum_{i=1}^{n-1} \sum_{j=i+1}^{n} sgn\left(x_j - x_i\right) \tag{9}$$

$$Var(S) = \frac{1}{18}\left[n(n-1)(2n+5) - \sum_{k=1}^{m} t_k\left(t_k - 1\right)\left(2t_k + 5\right)\right] \tag{10}$$

where, m = number of tied groups and t_k = number of ties of extent k.

Equation 11 shows the computation of standard normal test statistic Z.

$$Z = \begin{cases} \frac{S-1}{\sqrt{Var(S)}} & if\ S > 0 \\ 0 & if\ S = 0 \\ \frac{S+1}{\sqrt{Var(S)}} & ifS < 0 \end{cases} \tag{11}$$

The positive or negative value of Z reflects the positive or negative trend respectively. If the absolute value of Z is greater than $Z_{1-\alpha/2}$, the null hypothesis H_0 should be rejected, and a monotonic trend has been identified at the α significance level otherwise the null hypothesis of no trend should be accepted. The 5% level of significance was used in the present study.

Sen slope estimator

Sen Slope estimator was used to estimate the slope of the trend i.e. the rate of changes per unit time period (Jain et al. 2013; Sharma et al. 2016; Panwar et al. 2018; Alemu and Bawoke 2020). The true slope i.e., change per unit time can be estimated as if there is a linear trend in time series. Equation 12 represents the slope for n numbers of data.

$$\text{Slopeestimator}\left(Q_i\right) = \text{median}\left(\frac{x_j - x_k}{j-k}\right) \quad \text{where} k < j \text{for} j = 1, 2, 3, \ldots\ldots, n \tag{12}$$

The sign of the estimated slope will be either Positive or negative which indicates either increasing or decreasing trend respectively and the magnitude of slope estimator indicates the rate of change per unit time.

Pettit's change point test

Pettit's test is the nonparametric test used for the analysis of the most probable change point in the trend of time series data. For a time-series data of $x_1, x_2, \ldots\ldots x_n$ has a distribution function F(x) as $x_1, x_2, \ldots x_t$ where t is the assuming change point. Equation 13 shows the test statistics U_t (Pandey and Khare 2018).

$$U_t = \sum_{i=1}^{t} \sum_{j=t+1}^{n} \text{sign}(x_t - x_j) \tag{13}$$

where,

$$\text{sign}\left(x_t - x_j\right) = \begin{cases} 1, if\left(x_i - x_j\right) > 0 \\ 0, if\left(x_i - x_j\right) = 0 \\ -1, if\left(x_i - x_j\right) < 0 \end{cases} \tag{14}$$

The change point K is computed as:

$$K = \text{Max}\left|U_t\right| \tag{15}$$

The value of K is between 1 to n. The associated confidence level (ρ) for time series data is computed as:

$$\rho = \exp\left(\frac{-K}{n^2 + n^3}\right) \tag{16}$$

The value of ρ is smaller than the specified confidence level defines the rejection of the null hypothesis.

Standardized Precipitation Index (SPI)

The annual standardized precipitation index (SPI) was analyzed using Eq. 17 (McKee et al. 1993; Li et al. 2020).

$$SPI = \frac{P_i - \mu_t}{\sigma_t} \tag{17}$$

where P(i) is the P at time step i (corresponding to time period); μ(t) and σ(t) are the mean and standard deviation of the annual P time series for time period t (seasonal and annual).

SCS-CN method for run-off calculation

SCS-CN method is mostly used for run-off estimation from rainfall events (Rajasekhar et al. 2020; Karimi and Zeinivand 2021). The CN values are the dependent variable of the method. The CN value usually varies in the range of 30–100 based on the descending order of infiltration rates i.e., 100 means the lowest infiltration rates. The CN value is decided for an area based on its hydrological soil group (HSG), and Land use land cover (LULC). The potential maximum soil moisture retention after run-off begins (S) is calculated as

$$S = \frac{25400}{CN} - 254 \tag{18}$$

The run-off (Q) generated of an area is

$$Q = \frac{(P - 0.2S)^2}{(P + 0.8S)} \tag{19}$$

where, P and Q are the precipitation and run-off in mm respectively.

Spatial analysis

Inverse Distance Weighted (IDW) was used for the spatial analysis. GeoHMS tool in ArcGIS 10.2 was used to analyze CN grid generation over the state using predefined CN values for soil cover and LULC. Map algebra tool was used for the mapping of potential zone for recharge of groundwater.

Analytical hierarchy process (AHP) for RWH potential zones

AHP is a process of prioritizing one factor over others on an importance scale of 1–9. The importance level of each parameter and corresponding pair-wise comparison matrix was developed in which diagonal elements are 1 (Gorai et al. 2022; Rajasekhar et al. 2020). Normalized matrix was developed from pair-wise comparison matrix and subsequently mean of each row of normalized matrix was calculated that represents the weights of each parameter.

The potential zones for RWH using the AHP can be identified using Eq. 20.

$$RWH\ potential\ zone = \sum weighatge \times factor's\ features\ value \tag{20}$$

The numeric value obtained in Eq. 20 will decide the suitability of RWH zones. A higher score will lead to higher suitability and vice versa.

Analysis of results

The methodology described was used for the trend analysis of rainfall. Rainfall data collected from IMD was cumulated as seasonal and annual. Descriptive statistical parameters were calculated using SPSS tools. ITA method was used for finding out the existence of a trend in the dataset and validated through the MK test. The results were further used at the district level to determine the agricultural water budget.

Analysis of rainfall variation

The rainfall variation was analyzed with respect to descriptive statistical analysis, rainfall pattern changes with time i.e. trend analysis, and change point in rainfall pattern.

Descriptive analysis

Statistical analysis for the seasonal and annual rainfall data for all the stations shows that the minimum average annual rainfall is 279.6 mm at Mansa and the maximum average annual rainfall is 885 mm at Nawansahar. The standard deviation of average annual rainfall lies in the range of 148.8–421.8 mm. The minimum and maximum deviations were observed at Faridkot and Nawansahar, respectively. Table 1 shows the probability of occurrence of total rainfall during a season in the percentage of total rainfall. It is observed from Table 1 that there is a 50% probability of occurrence of approximately 83.9, 7.1, 2.7, and 6.7% of total annual rainfall during the southwest monsoon, pre-monsoon, post-monsoon, and winter season, respectively. Similarly, there is an 80% probability of occurrence of approximately 74.2, 3.74, 0.84, and 2.73% of total annual rainfall during the southwest monsoon, pre-monsoon, post-monsoon, and winter season, respectively. Therefore, it can be concluded that around 75% of total annual rainfall received in Punjab state is during the southwest monsoon season only.

Figure 3 shows the seasonal and annual spatial distribution of mean rainfall across the Punjab state. It is observed from Fig. 3 that Tibri, Dasuya, Hoshiarpur, Garhshankar, and Nawansahar regions receive more annual rainfall. In contrast, Mansa, Fazilka, Muktesar, Bhatinda, Faridkot, and Talwandi regions receive less annual rainfall.

Seasonal and annual rainfall trend

Autocorrelation analysis of the dataset was analyzed to check the presence of serial correlation. No serial correlation was found in the winter season dataset. Pre-monsoon season, southwest monsoon season, post-monsoon season, and the

Table 1 Probability of total rainfall during a season in percentage of annual rainfall

Seasons	80% probability of seasonal rainfall in the percentage of annual rainfall	50% probability of seasonal rainfall in the percentage of annual rainfall
Winter	2.73	6.7
Pre-monsoon	3.74	7.1
Southwest monsoon	74.2	83.9
Post-monsoon	0.84	2.7

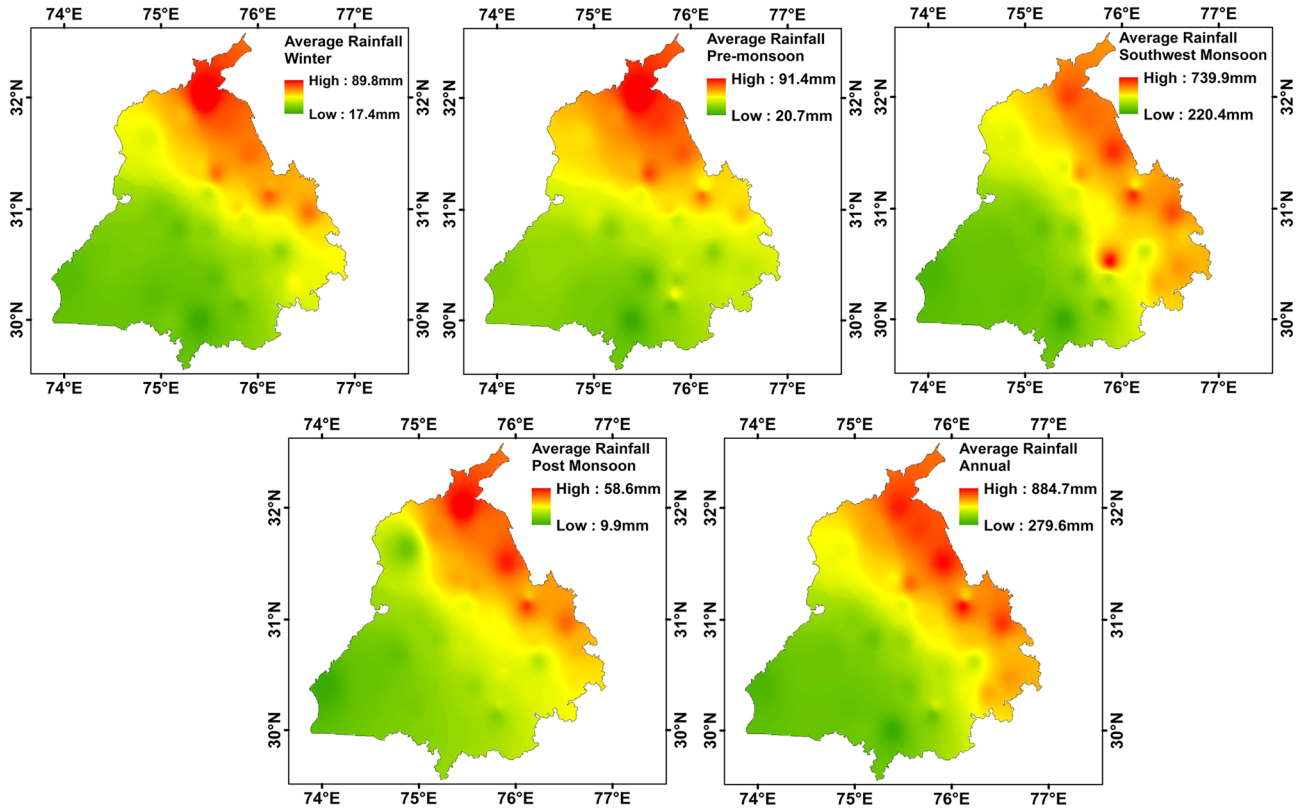

Fig. 3 Seasonal and annual spatial distribution of seasonal and annual average rainfall over Punjab region

annual dataset are found the presence of serial correlation in 17, 13, 20, and 18 stations, respectively. The serial correlation was removed using the pre-whitening approach(Mallick et al. 2021; Ayehu et al. 2021). After removing serial correlation, the trend and slope of rainfall are analyzed using the MK test and Sen Slope estimator.

The results obtained from both ITA and MK test were compared and it is found that the results obtained through both methods are similar in most cases. A significant trend at a significance level of 0.05 for all stations using MK and ITA tests is observed and shown in Table 2. Positive and Negative sign indicates the increasing and decreasing trend respectively. Figure 4 shows the spatial distribution of trend magnitude using the ITA method. It shows that the highest decrease in rainfall trend has been found in Amritsar during the winter season (1.243 mm/year), southwest monsoon seasons (10.6 mm/year), and annually (12.87 mm/year), Phillaur during the pre-monsoon season (1.0 mm/year), and Kapurthala during the post-monsoon season (1.7 mm/year). The highest positive rainfall trend was found in Jalandhar (0.84 mm/year) during the winter season, Tibri (0.704 mm/year) during the pre-monsoon season, Nawansahar (4.14 mm/year) during southwest monsoon seasons, Dasuya (0.8 mm/year) during the post-monsoon season and Nawansahar (4.25 mm/year) annually.

Table 3 shows the comparison of rainfall trend analysis from MK test adopting pre-whitening approach and without pre-whitening approach of the data. Since no serial correlation was found in the data of four rain gauge stations, Table 3 compares the trend summary of 29 rain gauge stations. It is observed in certain cases that the trend became significant after adopting the pre-whitening approach. It is also observed that the trend direction (Positive/Negative) has not changed in most of the rain gauge stations considered in the present study but the percentage of decrease or increase in the magnitude of the slope after pre-whitening is significantly different from that before pre-whitening and lying in a range of − 138 to 100.

Change point in rainfall trend

The change points for seasonal and annual rainfall trends were determined for all the stations using Pettit's test. The change year varies from station to station and from season to annual. Descriptive analysis and trend analysis was made for both before and after the change year.

Descriptive statistics The minimum and maximum average annual rainfall was observed as 272.1 mm at Bhatinda and 1264.1 mm at Rajpura, respectively, before the change point. Similarly, the minimum and maximum average

Table 2 Trend summary of the seasonal and annual significant trend at 5% level of significance over Punjab state using MK test and ITA method

	Winter		Pre-Monsoon		South-west Monsoon		Post-Monsoon		Annual	
	MK test	ITA test	MK test	ITA test	MK test	ITA test	MK test	ITA test	MK test	ITA test
Amritsar				(+)						
Barnala	(−)				(−)		(−)		(−)	
Kharar	(−)		(−)				(−)			
Bhatinda							(−)			
Talwandi (Sabo)							(+)			
Faridkot							(−)		(−)	
Amloh	(−)	(−)			(−)		(+)		(−)	
Zira	(−)				(−)		(−)		(−)	
Fazilka					(−)		(−)		(−)	
Batala		(−)			(−)					
Tibri		(+)								
Hoshiarpur		(+)		(+)			(−)			
Garhshankar	(−)		(−)		(−)		(−)		(−)	
Dasuya					(−)	(+)	(−)		(−)	(+)
Nakodar					(−)		(−)		(−)	
Phillaur		(+)	(−)		(−)		(−)		(−)	
Jullundar						(−)	(−)		(−)	(−)
Kapurthala							(−)			
Ludhiana					(−)				(−)	
Jagraon	(−)		(−)		(−)		(−)		(−)	
Samrala					(−)				(−)	
Mansa			(−)		(−)		(−)		(−)	
Moga					(−)		(−)		(−)	
Muktesar										(−)
Nawanshahr										
Nabha				(−)			(−)		(−)	
Rajpura	(−)				(−)		(−)		(−)	
Patiala										
Roopnagar				(−)						
Dhuri					(−)				(−)	
Sangrur							(−)			(−)
Sunam					(−)		(−)		(−)	
Malerkotla	(−)				(−)		(−)		(−)	

annual rainfall was observed as 124.4 mm at Fazilka and 713.4 mm at Tibri, respectively, after the change point. The average annual rainfalls of most of the stations are decreasing after the change point. It is found that the average annual rainfall in overall Punjab state is decreased by approximately 37% after the change point. The standard deviation of average annual rainfall was observed in the range of 154.8–426.1 mm before the change point, which changes to 77.0–333.3 mm after the change point.

The probability of occurrence of total rainfall during a season in the percentage of total rainfall was determined after the change point. It is observed that there is a 50% probability of occurrence of approximately 83.6, 7.78, 1.30, and 4.81% of total annual rainfall after change point during the southwest monsoon, pre-monsoon, post-monsoon, and winter season, respectively. Similarly, there is an 80% probability of occurrence of approximately 76.6, 4.65, 0.67, and 2.84% of total annual rainfall after change point during the southwest monsoon, pre-monsoon, post-monsoon, and winter season, respectively. Therefore, it is concluded that around 77% of total annual rainfall received in Punjab state is during the southwest monsoon season only. Figure 5 shows the seasonal and annual spatial distribution of mean rainfall before and after the change points across the Punjab state. The decrease in the magnitude of rainfall during all seasons except pre-monsoon is observed in Fig. 5. A

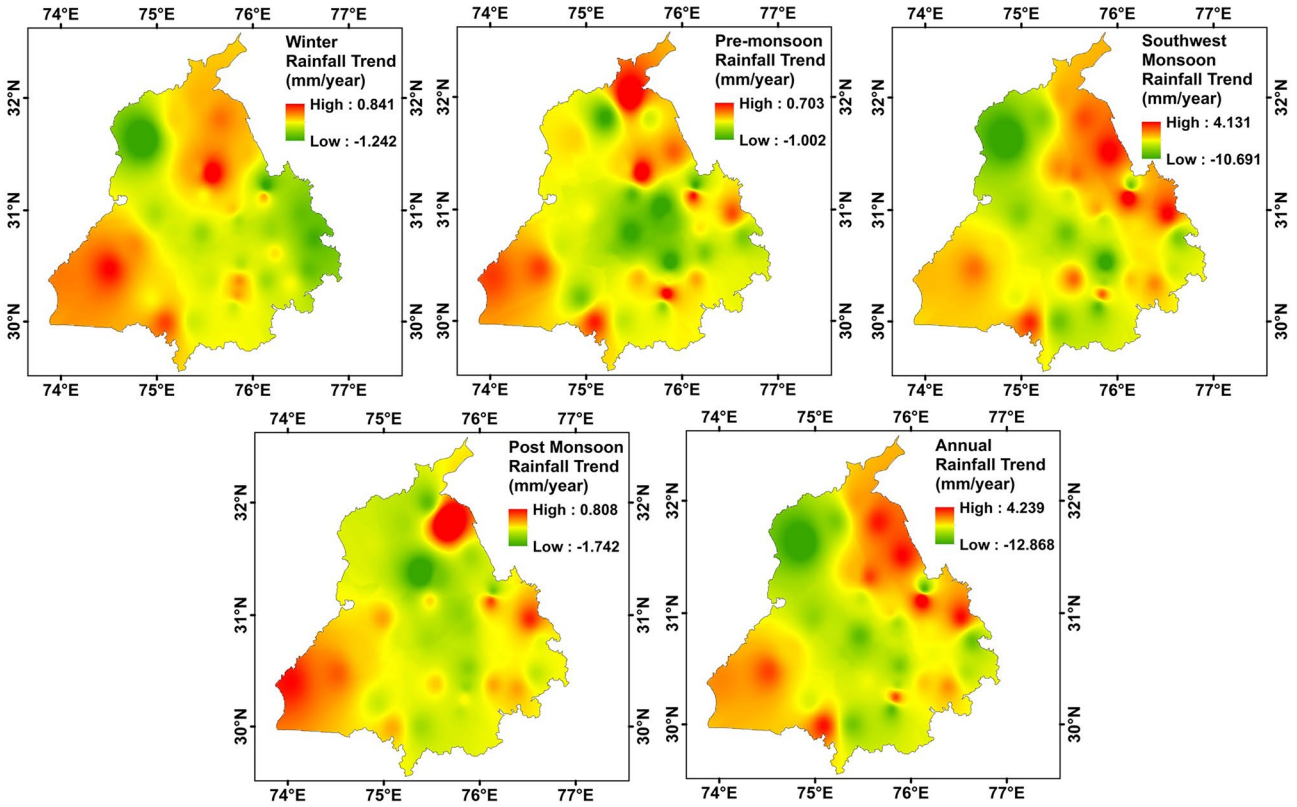

Fig. 4 Seasonal and annual spatial distribution of seasonal and annual average rainfall trend magnitude using ITA method over Punjab region

substantial amount of decreasing annual rainfall after the change point is observed at Tibri.

Trend analysis Figure 6 shows the spatial distribution of trend magnitude before and after the change point. The trend analysis is made using the ITA method, and the results obtained by the ITA method are compared with results obtained from the MK test and Sen Slope estimator. It is observed from trend analysis that 17 stations are decreasing in trend after change point during southwest monsoon season, whereas 16 stations are found increasing in trend. Similarly, 12, 24, and 18 stations are found decreasing trend during pre-monsoon, post-monsoon, and winter season respectively. The number of stations in decreasing rainfall trend during the southwest monsoon, pre-monsoon, post-monsoon, and winter season before change point was 15, 5, 29, and 19, respectively. It is concluded that the decreasing trend of rainfall is increasing in the number of stations after the change point for southwest monsoon and pre-monsoon seasons. Since the percentage of annual rainfall during post-monsoon and winter is significantly less, the increasing trend of rainfall during these seasons does not improve the average annual rainfall.

Similarly, it is observed that 18 stations are decreasing annual rainfall trend after change point whereas 15 stations were decreasing annual rainfall trend before change point. Since more stations are showing the negative trend of rainfall annually and southwest monsoon season, it is concluded that there is a sign of climate change in Punjab state. It is found from the analysis that 61%, 50%, 44%, and 33% of rural stations have increasing rainfall trends during pre-monsoon, winter, southwest monsoon, and post-monsoon season respectively, whereas 50% of rural stations have an increasing rainfall trend during annually after the change point. Similarly, 75%, 25%, 37%, and 12% of semi-urban stations have increasing rainfall trends during pre-monsoon, winter, southwest monsoon, and post-monsoon season respectively, whereas 25% of semi-urban stations have an increasing rainfall trend annually after the change point. 57%, 42%, 71%, and 28% of urban stations have increasing rainfall trends during pre-monsoon, winter, southwest monsoon, and post-monsoon season respectively, whereas 57% of urban stations have increasing rainfall trends annually after the change point.

Annual standardized precipitation index

The drought was analysed using annual SPI. The early warning of meteorological drought can be identified through shorter time scale of SPI values such as one month, three months or six months whereas hydrological

Table 3 Comparison of trend slope summary using MK test adopting pre-whitening approach and without pre-whitening approach of the data

Station name	Pre-monsoon		Southwest monsoon		Post monsoon		Annual	
	Pre-whitened	Without pre-whitened	Pre-whitened	Without pre-whitened	Pre-whitened	Without pre-whitened	Pre-whitened	Without pre-whitened
Kharar	−0.45*	−0.41			−0.26*	−0.22	−9.44*	−6.01*
Bhatinda					−0.14*	−0.19*		
Talwandi (Sabo)								
Faridkot					−0.22*	−0.19*		
Amloh	−0.07	0.00			0.00*	−0.11*		
Fazilka	−0.05	−0.14	−3.02*	−1.82*			−3.55*	−2.07*
Zira	−0.19	−0.20	−5.55*	−3.99*	−0.17*	−0.16	−7.36*	−5.38*
Batala	−0.41	−0.36	−5.12*	−3.78*			−7.19*	−4.76*
Tibri			−3.80	−2.68	−0.42	−0.29	−4.77	−3.66
Hoshiarpur	−0.03	−0.12	−2.76	−2.17	−0.42*	−0.34*	−3.19	−2.52
Garhshankar	−0.53*	−0.35*	−8.91*	−5.53*	−0.39*	−0.29*	−11.89*	−7.38*
Dasuya	−0.47	−0.36			−0.43*	−0.43*	−5.86*	−5.89*
Nakodar	−0.36	−0.25			−0.12*	−0.20*	−4.40*	−4.38*
Phillaur	−0.48*	−0.40			−0.38*	−0.35*	−6.51*	−5.76*
Jullundar	0.17	0.00			−0.31*	−0.38*		
Kapurthala					−0.38*	−0.44*		
Jagraon	−0.38*	−0.24	−5.48*	−3.73*			−7.78*	−5.54*
Samrala					−0.15	−0.22*		
Mansa			−5.39*	−2.99*			−7.02*	−3.64*
Moga			−2.63*	−1.32			−3.68*	−1.82
Muktesar								
Nawanshahr			−0.66	−0.65	−0.15	−0.25	−1.29	−1.33
Nabha	0.01	−0.02	−2.54	−2.10	−0.14*	−0.11	−3.54*	−3.13*
Rajpura	−0.10	−0.15			−0.19*	−0.36*		
Patiala	0.04	−0.01			0.00	−0.10		
Roopnagar							−2.30	−2.43
Dhuri	−0.01	−0.10			−0.07	−0.61	−7.10*	−6.59*
Sangrur								
Sunam	−0.11	−0.13	−4.96*	−3.12*			−6.30*	−3.52*
Malerkotla			−10.58*	−4.44*	−0.26*	0.00		

* Values are significant at a level of significance of 0.05

drought can be well identified through longer time scale of SPI such as twelve months (Kaur et al. 2022). Therefore, the present study analysed the drought using annual SPI values. Figure 7 shows the temporal variation of SPI values of 33 station of Punjab. The linear trend line was added to the temporal plots for analysis of trend direction of SPI values. The extent of drought has been categorized as per SPI values i.e. Mild Drought (0 to − 0.99), Moderate Drought (− 1.00 to − 1.49), Severe Drought (− 1.50 to − 1.99) and Extreme Drought (≤ − 2.00) (He et al. 2011). It is observed from the Fig. 7 that the trend line of SPI for all the stations are declining and most of the semi-urban stations shows the negative annual SPI values during many more years of the last two decades. The similar results were also reported by Kaur et al. (2022). It is observed that the variability of SPI values is lying in the range of (−) 2.42–5.15. It is also observed that 71.5% cases of negative SPI values indicate mild drought, 19.8% cases of negative SPI values indicate moderate drought, 6.6% cases of negative SPI values indicate severe drought and 2.1% cases of negative SPI values indicates extreme drought conditions.

Discussions of the results

The results obtained were analyzed and discussed with respect to descriptive statistical analysis, rainfall pattern

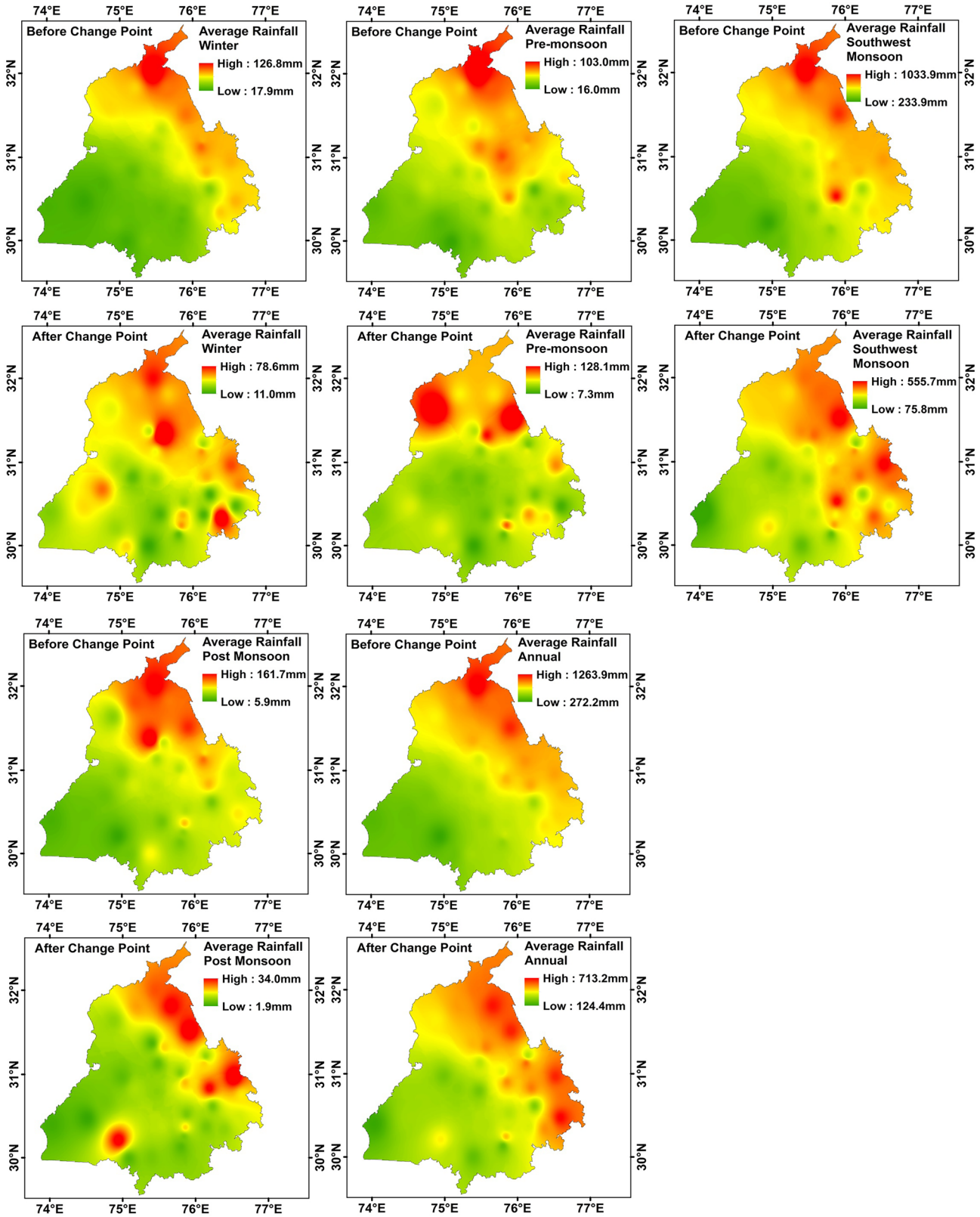

Fig. 5 Seasonal and annual spatial distribution of average annual rainfall before and after change point over Punjab region

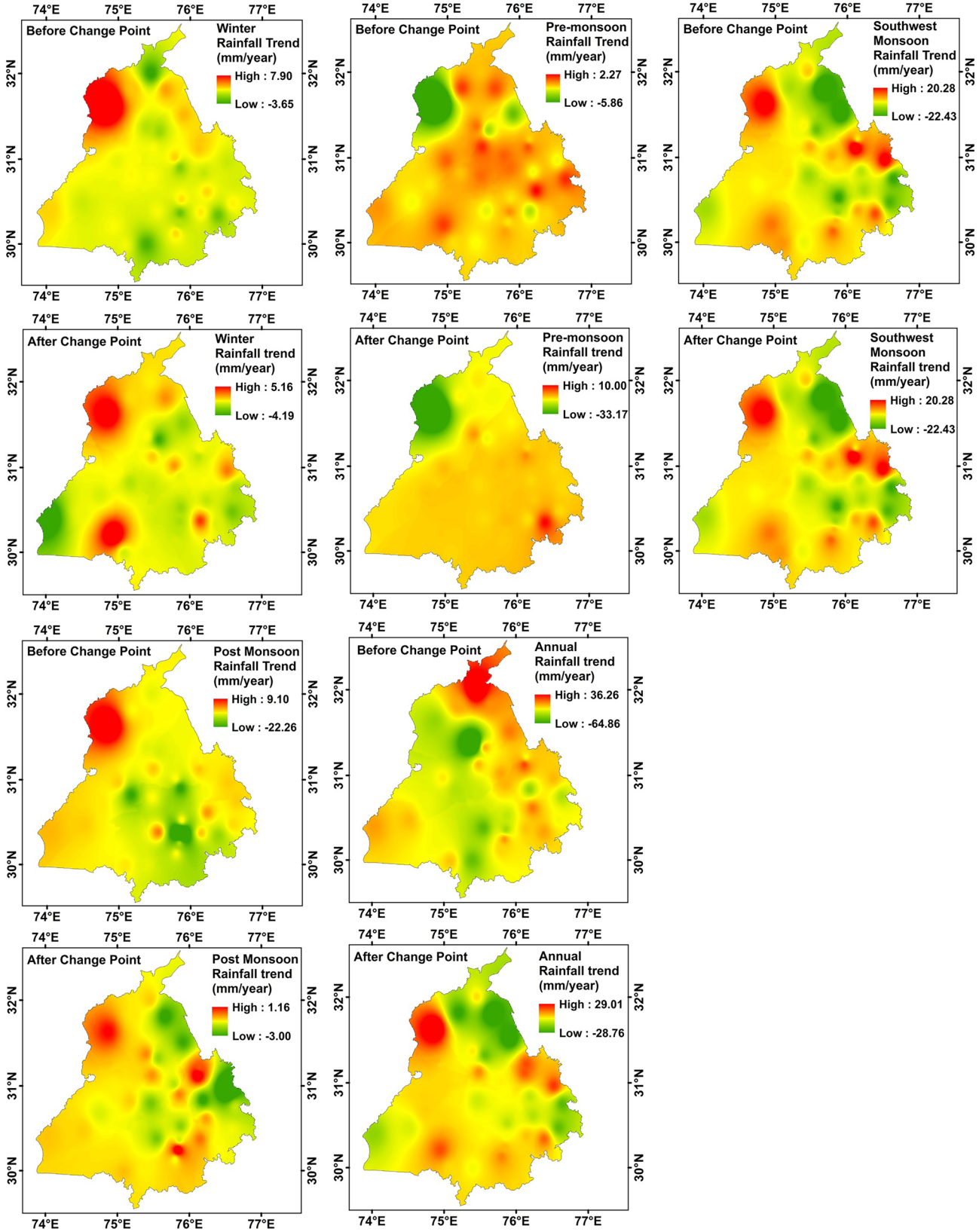

Fig. 6 Seasonal and annual spatial distribution of average annual rainfall trend magnitude before and after change point over Punjab region

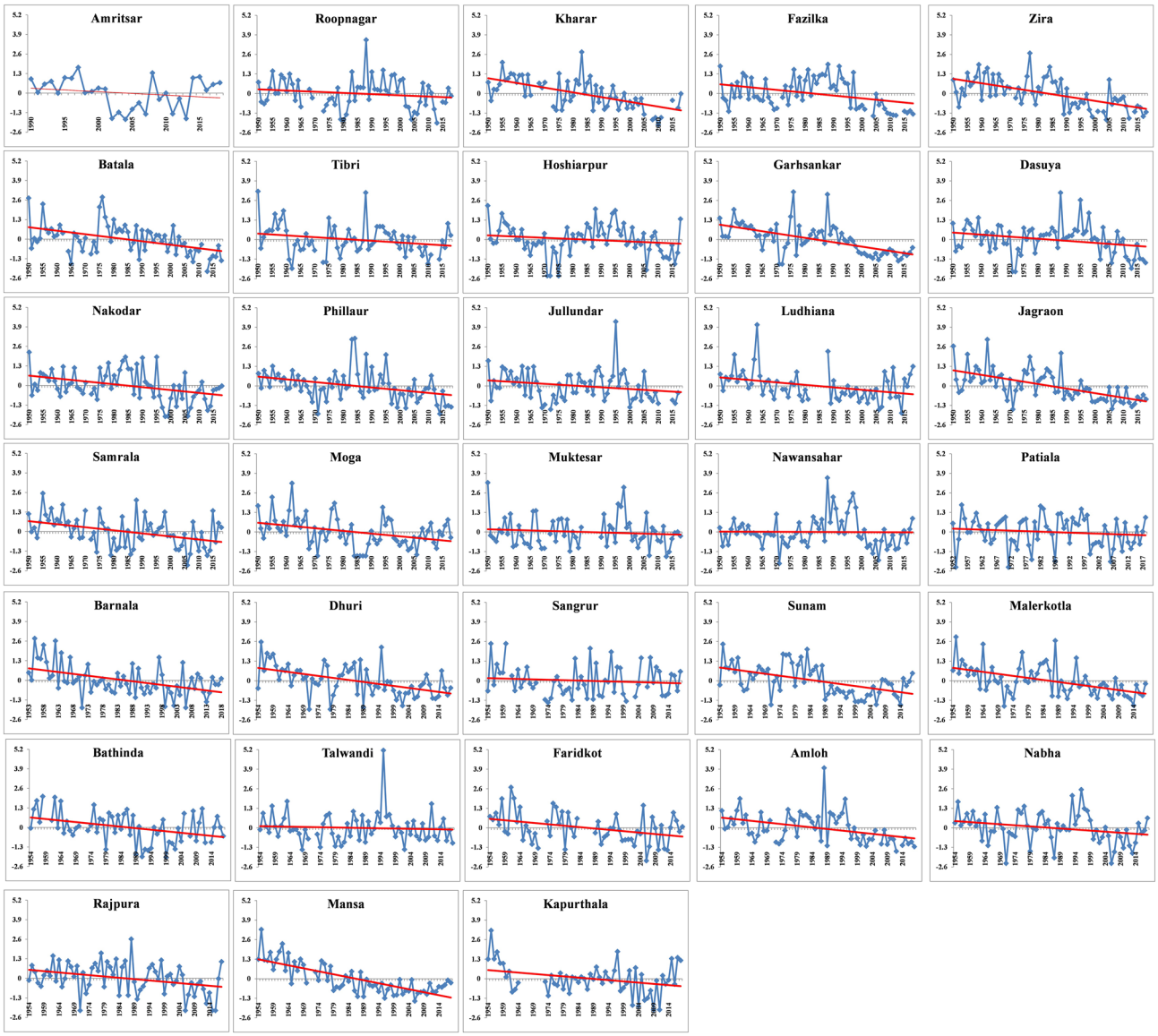

Fig. 7 Temporal variations in annual SPI values of Punjab state

changes with time i.e., trend analysis, and change point in rainfall pattern.

The result of the descriptive analysis reveals that around 48–100% of the total annual rainfall occurs during the southwest monsoon in Punjab, whereas the percentage of total annual rainfall during pre-monsoon, post-monsoon, and winter season lies in the range of 0–33%, 0–39.2%, and 0–21% respectively. The probability of occurring equal to or greater than 80% of total annual rainfall in the southwest monsoon season is 67%. It is also observed that the contribution of rainfall during the post-monsoon season is the least compared to other seasons. However, the post-monsoon rainfall of high magnitudes, such as 39.2% of total rainfall, is observed only once during the last 70 years. The similar results of descriptive statistics have been reported by Kaur et al. (2021). The skewness of the rainfall for the Punjab state over the previous 69 years is 0.27, 0.79, 0.51, 0.79, and 0.29 during southwest, pre-monsoon, post-monsoon, winter, and annual rainfall, respectively. Whereas the skewness of the rainfall of various stations over the last 69 years lies in the range of − 0.32–2.34, 0.75–5.05, 1.89–7.33, and 0.45–3.71 during the southwest, pre-monsoon, post-monsoon, and winter season rainfall, respectively. Similarly, the skewness of the rainfall of various stations over the last 69 years lies in the range of -0.043–2.29 during annual rainfall. The negative skewness has been found during southwest monsoon season rainfall, indicating that the frequency of the higher magnitude rainfall occurrence is more during the southwest

monsoon season. The coefficient of variation of the annual rainfall of various stations lies in the range of 30.3–67.3%. The highest fluctuation of annual rainfall was observed at Mansa, indicating the unstable incidence of rainfall, whereas the lowest rainfall fluctuation is observed at Roopnagar.

The result of the seasonal and annual rainfall trend analysis reveals the decreasing trend of annual rainfall and seasonal rainfall for the overall state of Punjab. The annual rainfall trend for the overall Punjab state has been decreasing at a rate of 3.6 mm/year. In contrast, the seasonal rainfall decreases at a rate of 0.1, 0.3, 2.6, and 0.6 mm/year during winter, pre-monsoon, southwest monsoon, and post-monsoon, respectively. The decreasing trend of southwest monsoon and the post-monsoon has been documented by Praveen et al. (2020), Kaur et al. (2021) and Kashyap and Agarwal (2021). The present study observed the decreasing annual rainfall trend of Punjab state, deviating from the results obtained by Praveen et al. (2020) but the results are in similar line of results obtained by Kaur et al. (2021) and Kashyap and Agarwal (2021). It is concluded from trend analysis that although some of the stations have recorded a positive rainfall trend, overall Punjab state is experiencing a negative rainfall trend. Similar results have also been reported by Kothawale and Rajeevan (2017). It is seen from the annual average rainfall trend analysis that 28% of urban stations, 0% semi-urban stations, and 16% of rural stations are showing a positive rainfall trend. The season-wise rainfall trend analysis concludes that almost all stations of urban, semi-urban, and rural areas have a negative trend during the post-monsoon season. In contrast, most rural stations (50%) show a positive rainfall trend during the winter season. Similarly, 28% of rural stations and 43% of urban stations have a positive trend during the pre-monsoon season. The worst affected area is semi-urban, where all the stations show a negative trend during the southwest monsoon and post-monsoon season. In contrast, the number of semi-urban stations showing a positive trend during the pre-monsoon and winter seasons is non-significant.

The descriptive result of the change point analysis of rainfall trend reveals that around 69–100% of the total annual rainfall of Punjab state occurred due to the southwest monsoon before the change point, whereas the contribution of rainfall during southwest monsoon considerably decreases to 40–100% after the change point. Similarly, the contribution of seasonal rainfall towards the annual rainfall before the change point is 4–10%, 2–18%, and 4–11% during the pre-monsoon, post-monsoon, and winter season, respectively. In contrast, the contribution of seasonal rainfall towards the annual rainfall after change point is 2–28%, 0–7%, and 2–16% during pre-monsoon, post-monsoon, and winter season, respectively. It is inferred that there is a substantial decrease in post-monsoon rainfall, and a considerable increase in pre-monsoon rainfall is observed in the state after the change point. It is also observed that there is a small increase or no change in the contribution of rainfall towards annual rainfall during the winter season.

The skewness of the rainfall for Punjab state before change point was 0.56, 1.03, 1.10, 0.85, and 0.35 during southwest, pre-monsoon, post-monsoon, winter, and annual rainfall respectively, which becomes 0.13, 1.62, 1.04, 1.19, and 0.15 respectively after the change point. The coefficient of variation of the annual rainfall of various stations before and after the change point lies in a range of 22–56.9% and 17.9–83.8%, respectively. The number of stations having a coefficient of variation greater than 50% was only two before the change point. In contrast, the number of stations having a coefficient of variation greater than 50% has risen to sixteen. The rainfall fluctuation has been increased at a significant number of stations indicating the high tendency of the inconsistency of rainfall in the study area (Praveen et al. 2020). The highest fluctuation of annual rainfall was observed at Moga indicates the unstable incidence of rainfall, whereas the lowest fluctuation of rainfall is observed at Kapurthala. It is concluded that the fluctuation of annual rainfall has been increased in most of the stations. It is also observed that the average rainfall during the southwest monsoon, post-monsoon season, and annually is decreasing in all stations except Bhatinda.

The rainfall trend analysis after change point reveals that most urban and rural areas have an increasing annual rainfall trend compared to semi-urban areas. The increase in the percentage of the semi-urban regions in the negative rainfall trend category is due to the addition of two stations, Batala and Muktesar, which had a positive rainfall trend before the change point. Most of the air polluting industries has come up in Batala and Muktesar after 1980. Therefore, it is anticipated that the increasing air pollution due to industrial growth might be one of the reasons for climate change which causes the decreasing rainfall trend at Batala and Muktesar after the change point. Since the rainfall during the southwest monsoon contributes more towards annual average rainfall, the increasing trend in other seasons in the semi-urban area has an insignificant contribution. Kothawale and Rajeevan (2017) published similar results that the overall Punjab state is experiencing a negative rainfall trend for the analysis beyond 1981.

The decreasing trendline of SPI for all the stations is indicating the drought in Punjab state although most of the station is falling under mild drought. Around 9% of total stations are indicating the severe and extreme drought conditions. The erratic rainfall pattern of Punjab state is causing the negative and uncertainty in SPI and increasing the

frequency and intensity of drought conditions over the state and the similar results were also reported by Kaur et al. (2022), Bopche et al. (2022) and Guhathakurta et al. (2017).

Water contingency plan for agricultural water management in the Patiala district

The declining rainfall trends severely impacts the groundwater resources of Punjab (Hira 2009). The paddy and wheat are the major cropping pattern of Punjab state, and such erratic rainfall observed in the present study cannot fulfill the crop water requirements and therefore, the groundwater extraction of this region is very high. Similar observation was also reported by Bopche et al. (2022). The influence of rainfall trend was applied on agriculture water requirement of Patiala district of Punjab state. According to the Central Ground Water Board (CGWB) Punjab, India report, the groundwater of all eight blocks existing in the Patiala district is over-exploited (CGWB 2018). The groundwater level of all the blocks is continuously declining due to the over-exploitation by farmers. Since the rainfall trend is decreasing and the absence of a suitable management plan for rainfall water, farmers are forced to depend on groundwater for irrigation of agriculture fields. Moreover, Fig. 7 also confirms the occurrence of mild to moderate drought in Patiala district in several times during last two decades. Therefore, an effort has been made to prepare a water balance chart based on the rainfall trend and agricultural activities in the Patiala district, considering the current scenario. The data regarding the cropping pattern of this district and their water requirement were collected from the literature (Sharma 2010). Table 4 describes the total area used for different types of crops and their absolute water requirement. It is found from Table 4 that paddy and wheat is the most influential crop in this area and requires the maximum quantity of water. The types of the crops sown in this district, their area, and their water requirements are listed in Table 4. Subsequently, the maximum and minimum quantity of water required was calculated. The maximum, minimum, and average rainfall of the Patiala district was computed using the Thiessen polygon method.

Figure 8 represents the demand for water for agriculture purposes against rainwater for current (2018) and future predictions of 5 years (2023), 10 years (2028), and 15 years (2033). The present study considers the prediction of the water balance chart up to fifteen years because of the rapid change in precipitation trend due to climate change. Total irrigation water requirement for Patiala district varies from 248,816,536–336,553,300 m^3 per year for both Ravi and Kharif crops. The rainfalls for each rain gauge station of the Patiala district are predicted for 5, 10, and 15 years using the rainfall trend result obtained in the current study. The total annual run-off of the district was calculated using SCS-CN method. HSG, DEM, LULC, and rainfall data were used for the estimation of the run-off. The run-off was estimated over the district using the current rainfall, five, ten, and fifteen years. The deficiency of water for agriculture is directly calculated from the requirement for irrigation and actual availability.

Figure 8 shows the value of the negative amount of water describes the deficiency of precipitation required for irrigation provided all precipitated water collected for irrigation. The deficit is observed to be increasing at a rate of 2–3% for every five years, which can be fulfilled from groundwater. The efficient use of rainwater requires a suitable collection and management plan of the rainwater system. The highest deficiency of irrigation water in the coming 15 years is found to be 48% of the current demand. The groundwater will be in stress due to the over exploitation because of negative rainfall trend of Punjab state and similar anticipation has been made by Bopche et al. (2022). Although the deficient water will be fulfilled from groundwater, a sufficient management plan for this district's efficient collection and distribution of rainfall water is required. In the present scenario, farmers of

Table 4 Total annual agricultural water requirement in Patiala district

S. no.	Crop name	Total area sown (Sharma 2010) (hectare)	Water requirement (Critchley and Siegert 1991) (mm)	Type of crop	Minimum water needed (m^3)	Maximum water needed (m^3)	Total Minimum water required (m^3)	Total maximum water required (m^3)
1.	Paddy	243,000	450–700	Kharif	109,350,000	170,100,000	248,816,536	336,553,300
2.	Sugarcane	2000	1500–2500	Kharif	3,000,000	5,000,000		
3.	Maize	1000	500–800	Kharif	500,000	800,000		
4.	Cotton	1000	700–1300	Kharif	700,000	1,300,000		
5.	Wheat	236,000	450–650	Ravi	106,200,000	153,400,000		
6.	Potatoes	4244	500–700	Ravi	18,011,536	2,970,800		
7.	Total Oilseeds	3150	240–400	Ravi	9,922,500	1,260,000		
8.	Onion	1950	350–550	Ravi	682,500	1,072,500		
9.	Barley	1000	450–650	Ravi	450,000	650,000		

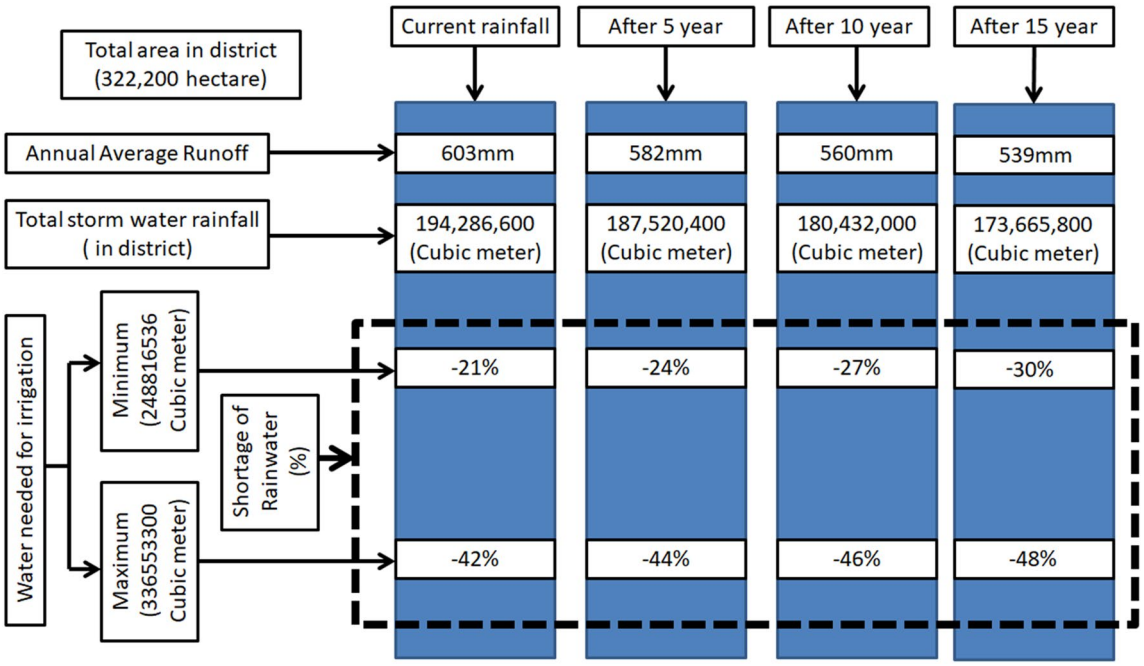

Fig. 8 Water requirements for crops comparison with current and future scenario using average run-off data in Patiala district

the Patiala district are entirely dependent on groundwater for their agricultural work. Also, most of the locations of Patiala city are getting waterlogged during the rainy season. If the rainwater is appropriately used for irrigation, then there will be less stress on groundwater. So, the present model suggests that the rainwater should be collected through the various channels and stored either in a detention pond or passed through a rainwater harvesting structure so that the water will be directly used for irrigation. Also, the wastewater generated from various sources will be treated and can be used for irrigation. The irrigation water requirement of the study area can also be optimized by changing the crop pattern.

Rainwater harvesting potential zones for Patiala district

Because of the declining rainfall trend and increasing water demand, the present study also proposed identifying the potential zones for rainwater harvesting (RWH) in the Patiala district. The RWH potential zone was identified using different thematic layers and an estimated run-off layer using the SCS-CN method. These layers were used in Analytical Hierarchy Process. The executed potential zones show the best suitability of the RWH zone in the district to mitigate the water demand.

Thematic layers used for this study

The thematic layers considered in the present study are LULC, DEM, HSG, drainage density, and run-off model (Torres et al. 2020; Rana and Suryanarayana 2020; Karimi and Zeinivand 2021). Table 5 shows the source of the various dataset used. Table 6 shows the classification of thematic layers with assigned weightage for their features (Karimi and Zeinivand 2021).

Table 5 Primary dataset used for the study and their source details

S. no.	Dataset	Source	Resolution	Data version/date
1.	LULC	Moderate Resolution Imaging Spectroradiometer (MODIS) Land cover V6	500 m	2019
2.	DEM	Shuttle Radar Topography Mission (SRTM)	30 m	23.09.2014
3.	Rainfall (average annual)	Indian Meteorological Department, Pune	Stations	1969–2018
4.	HSG	Global Hydrologic Soil Groups (HYSOGs250m) for CN Based Run-off Modelling	250 m	22-04-2020

Table 6 Classification of thematic layers with assigned rank for their features (Karimi and Zeinivand 2021)

Layers	Features	Rank Code	Layers	Features	Rank code
Run-off	< 527	1	LULC	Savannas	2
	527–578	2		Cropland/natural vegetation	4
	579–624	3		Urban built-up	5
	625–705	4			
	> 705	5	HSG	C, C/D	2
				D, D/D	1
Slope	< 5	1	Drainage density	< 0.5	1
	5–10	2		0.5–1.0	2
	10–15	3		> 1.0	3
	15–30	4			
	> 30	5			

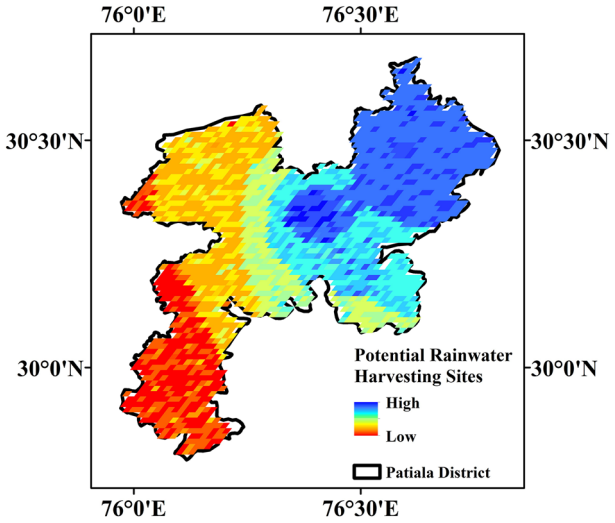

Fig. 9 Potential rainwater harvesting zone of Patiala district

Rainwater potential harvesting zone

The weights for each factor were calculated as described in "Analytical hierarchy process (AHP) for RWH potential zones" and the weights for slope, runoff, LULC, HSG and Drainage density are observed to be 16.6%, 39.6%, 9.6%, 5.7% and 28.4% respectively. Hence, Eq. 20 can be represented as

$$\begin{aligned} &\textit{RWH potential zone in Patiala district} \\ &= (16.6 \times \textit{Slope}) + (39.6 \times \textit{Runoff}) \\ &\quad + (9.6 \times \textit{LULC}) \\ &\quad + (5.7 \times \textit{HSG}) \\ &\quad + (28.4 \times \textit{Drainage Density}) \end{aligned} \tag{21}$$

The score obtained in Eq. 21 will decide the potential RWH zones. A higher score will lead to higher suitability and vice versa. The consistency ratio for the considered comparison matrix is 0.082 and found suitable as it is less than 1.0. A combination of multi-criteria decision-making analysis and GIS techniques was used to identify RWH potential zones. Figure 9 shows the potential RWH zone in the Patiala district. The potential zone classification value range is found 129–352, where the scale is 100–500. The value 129 falls under the low potential zone, and 352 is the high potential zone. The potentiality is divided into three different zones based on Jenk's classification in ArcGIS. It is considered a poor zone when the AHP score is less than 190, whereas it is considered a good zone when the AHP score is greater than 253. It is observed from Fig. 9 that 40.7% of areas of Patiala district are under poor zone whereas 35.8% of areas are under the good zone. The remaining 23.8% of areas are under the medium zone. It is also observed that the northeastern part of the district has a good or higher potentiality of rainwater harvesting, whereas the south-western part of the district has a poor or lower potentiality of rainwater harvesting. The groundwater level of south-western part can be improved by identifying the groundwater flow direction and recharging of rainwater at a suitable area having higher pressure gradient.

Conclusion

The present study was carried out to observe the variability of seasonal and annual rainfall for Punjab state. It is observed that overall Punjab state is experiencing a negative trend. Most urban and rural areas have an increasing trend of annual rainfall compared to the semi-urban area. The drought analysis also reveals that most of the semi-urban areas have negative SPI values during last two decades confirms the increase in frequency of drought in Punjab state. The change point analysis shows that most stations have experienced a change point during 1980–2000. The mean annual rainfall is also found to be decreasing after the change point. The rainfall variability was found to increase significantly after the change point. It is anticipated that the increasing air pollution due to industrial growth might be one of the reasons for climate change which caused

the decreasing rainfall trend after the change point. Also, the present study checked the sufficiency of rainwater for irrigation water requirements for present and future conditions up to 15 years and is observed a significant rise in rain water deficit for agriculture. It is expected that the rain water deficit will lie in a range of 30–48% of current water demand in next 15 years for Patiala district. However, the rainwater of the study area can satisfy the irrigation requirement by changing the crop pattern. Since most of the farmers are using groundwater for agricultural purposes as the climatic condition of the state is arid and semi-arid. Therefore, authors strongly recommend harvesting of rainwater so that it can be used during the lean period. Hence, the rainwater harvesting potential zones have been identified for the Patiala district. It is observed that 40.7% of areas of the district are under the poor zone, 23.8% of areas of the district are under the medium zone, and 35.8%of areas of the district are in the good zone. The negative trend of rainfall and subsequently the increase in frequency of the occurrence of drought will impact on groundwater. The deficiency of groundwater may lead to food security issue and the present study can be further extended to manage these issues for the Punjab state.

Acknowledgements We gratefully acknowledge the Indian Meteorological Department (IMD), Pune, for providing rainfall data used in this study.

Funding All authors certify that they have no affiliations with or involvement in any organization or entity with any financial or non-financial interest in the subject matter or materials discussed in this manuscript. The authors did not receive support from any organization for the submitted work.

Data availability statement The data that support the findings of this study are available from the Indian Meteorological Department, Pune (INDIA), but restrictions apply to the availability of these data, which were used under license for the current study, and so are not publicly available. Data are however available from the authors upon reasonable request and with the permission of Indian Meteorological Department, Pune.

Declarations

Conflict of interest On behalf of the other authors, the corresponding author declares that there is no conflict of interest to declare.

References

Alemu MM, Bawoke GT (2020) Analysis of spatial variability and temporal trends of rainfall in Amhara region, Ethiopia. J Water Clim Chang 11:1505–1520. https://doi.org/10.2166/wcc.2019.084

Ayehu GT, Tadesse T, Gessesse B (2021) Spatial and temporal trends and variability of rainfall using long-term satellite product over the Upper Blue Nile Basin in Ethiopia. Remote Sens Earth Syst Sci. https://doi.org/10.1007/s41976-021-00060-3

Bopche U, Kingra PK, Setia R, Singh SP (2022) Spatio-temporal analysis of meteorological drought in Punjab under past, present and future climate change scenarios. Arab J Geosci 15:756. https://doi.org/10.1007/s12517-022-10025-5

CGWB (2018) Ground water resources of Punjab state. CGWB, Chandigarh

Critchley W, Siegert K (1991) A manual for the design and construction of water harvesting schemes for plant production

Croitoru AE, Piticar A, Burada DC (2016) Changes in precipitation extremes in Romania. Quat Int 415:325–335. https://doi.org/10.1016/j.quaint.2015.07.028

Cui L, Wang L, Lai Z et al (2017) Innovative trend analysis of annual and seasonal air temperature and rainfall in the Yangtze River Basin, China during 1960–2015. J Atmos Solar Terr Phys 164:48–59. https://doi.org/10.1016/j.jastp.2017.08.001

Diffenbaugh NS, Swain DL, Touma D (2015) Anthropogenic warming has increased drought risk in California. Proc Natl Acad Sci 112:3931–3936. https://doi.org/10.1073/pnas.1422385112

Farahmand A, AghaKouchak A (2015) A generalized framework for deriving nonparametric standardized drought indicators. Adv Water Resour 76:140–145. https://doi.org/10.1016/j.advwatres.2014.11.012

Gocic M, Trajkovic S (2013) Analysis of changes in meteorological variables using Mann–Kendall and Sen's slope estimator statistical tests in Serbia. Glob Planet Change 100:172–182. https://doi.org/10.1016/j.gloplacha.2012.10.014

Gorai S, Ratha D, Dhir A (2021) Adapting rainfall variability to flood risk: a case study of the Ghaggar River Basin. J Geol Soc India 97:1347–1354. https://doi.org/10.1007/s12594-021-1873-1

Gorai S, Ratha D, Dhir A (2022) Prediction of flood risk zone of Ghaggar river basin, India using graph theory technique. Geocarto Int 37(25):9425–9452. https://doi.org/10.1080/10106049.2021.2019836

Guhathakurta P, Menon P, Inkane PM et al (2017) Trends and variability of meteorological drought over the districts of India using standardized precipitation index. J Earth Syst Sci 126:120. https://doi.org/10.1007/s12040-017-0896-x

Harkat S, Kisi O (2021) Trend analysis of precipitation records using an innovative trend methodology in a semi-arid Mediterranean environment: Cheliff Watershed Case (Northern Algeria). Theor Appl Climatol 144:1001–1015. https://doi.org/10.1007/s00704-021-03520-4

He B, Lü A, Wu J et al (2011) Drought hazard assessment and spatial characteristics analysis in China. J Geogr Sci 21:235–249. https://doi.org/10.1007/s11442-011-0841-x

Hira GS (2009) Water Management in Northern States and the Food Security of India. J Crop Improv 23:136–157. https://doi.org/10.1080/15427520802645432

Jain SK, Kumar V, Saharia M (2013) Analysis of rainfall and temperature trends in northeast India. Int J Climatol 33:968–978. https://doi.org/10.1002/joc.3483

Jaiswal RK, Lohani AK, Tiwari HL (2015) Statistical analysis for change detection and trend assessment in climatological parameters. Environ Process 2:729–749. https://doi.org/10.1007/s40710-015-0105-3

Karimi H, Zeinivand H (2021) Integrating runoff map of a spatially distributed model and thematic layers for identifying potential rainwater harvesting suitability sites using GIS techniques. Geocarto Int 36:320–339. https://doi.org/10.1080/10106049.2019.1608590

Kashyap D, Agarwal T (2021) Temporal trends of climatic variables and water footprint of rice and wheat production in Punjab, India from 1986 to 2017. J Water Clim Change 12:1203–1219. https://doi.org/10.2166/wcc.2020.093

Kaur P, Singh H, Bal S et al (2011) Quantitative evaluation of weather variability and rice yields in Punjab—a case study. J Res 48:5–15
Kaur L, Rishi MS, Chaudhary BS (2022) Assessment of meteorological and agricultural droughts using remote sensing and their impact on groundwater in an agriculturally productive part of Northwest India. Agric Water Manag 274:107956. https://doi.org/10.1016/j.agwat.2022.107956
Kaur N, Yousuf A, Singh MJ (2021) Long term rainfall variability and trend analysis in lower Shivaliks of Punjab, India. MAUSAM 72:571–582. https://doi.org/10.54302/mausam.v72i3.1307
Kothawale DR, Rajeevan M (2017) Monthly, seasonal and annual rainfall time series for all-India, homogeneous regions and meteorological subdivisions: 1871–2016. Indian Inst Trop Meteorol Earth Syst Sci Organ Minist Earth Sci 02:1–164
Krishan G, Chandniha S, Lohani A (2015) Rainfall trend analysis of Punjab, India using statistical non-parametric test. Curr World Environ 10:792–800. https://doi.org/10.12944/cwe.10.3.09
Kumar R, Singh S, Singh Randhawa S et al (2014) Temperature trend analysis in the glacier region of Naradu Valley, Himachal Himalaya, India. Comptes Rendus Geosci 346:213–222. https://doi.org/10.1016/j.crte.2014.09.001
Kundu S, Mondal D (2019) Analysis of long-term rainfall trends and change point in West Bengal, India. Theor Appl Climatol. https://doi.org/10.1007/s00704-019-02916-7
Li Z, Zhang X, Ma Y et al (2019) A multi-criteria decision making method for urban flood resilience evaluation with hybrid uncertainties. Int J Disaster Risk Reduct 36:101140. https://doi.org/10.1016/j.ijdrr.2019.101140
Li L, She D, Zheng H et al (2020) Elucidating diverse drought characteristics from two meteorological drought indices (SPI and SPEI) in China. J Hydrometeorol 21:1513–1530. https://doi.org/10.1175/JHM-D-19-0290.1
Mallick J, Talukdar S, Alsubih M et al (2021) Analysing the trend of rainfall in Asir region of Saudi Arabia using the family of Mann–Kendall tests, innovative trend analysis, and detrended fluctuation analysis. Theor Appl Climatol 143:823–841. https://doi.org/10.1007/s00704-020-03448-1
McKee TB, Doesken NJ, Kleist J (1993) The relationship of drought frequency and duration to time scales. In: Proceedings of the 8th conference on applied climatology. Boston, pp 179–183
Mondal A, Khare D, Kundu S (2015) Spatial and temporal analysis of rainfall and temperature trend of India. Theor Appl Climatol 122:143–158. https://doi.org/10.1007/s00704-014-1283-z
Pandey BK, Khare D (2018) Identification of trend in long term precipitation and reference evapotranspiration over Narmada river basin (India). Glob Planet Change 161:172–182. https://doi.org/10.1016/j.gloplacha.2017.12.017
Panwar M, Agarwal A, Devadas V (2018) Analyzing land surface temperature trends using non-parametric approach: a case of Delhi, India. Urban Clim 24:19–25. https://doi.org/10.1016/j.uclim.2018.01.003
Patel PS, Rana SC, Joshi GS (2021) Temporal and spatial trend analysis of rainfall on Bhogavo River watersheds in Sabarmati lower basin of Gujarat, India. Acta Geophys 69:353–364. https://doi.org/10.1007/s11600-020-00520-2
Patra JP, Mishra A, Singh R, Raghuwanshi NS (2012) Detecting rainfall trends in twentieth century (1871–2006) over Orissa State, India. Clim Change 111:801–817. https://doi.org/10.1007/s10584-011-0215-5
Pingale SM, Khare D, Jat MK, Adamowski J (2014) Spatial and temporal trends of mean and extreme rainfall and temperature for the 33 urban centers of the arid and semi-arid state of Rajasthan, India. Atmos Res 138:73–90. https://doi.org/10.1016/j.atmosres.2013.10.024
Poonia V, Goyal MK, Gupta BB et al (2021) Drought occurrence in Different River Basins of India and blockchain technology based framework for disaster management. J Clean Prod 312:127737. https://doi.org/10.1016/j.jclepro.2021.127737
Praveen B, Talukdar S, Shahfahad et al (2020) Analyzing trend and forecasting of rainfall changes in India using non-parametrical and machine learning approaches. Sci Rep 10:10342. https://doi.org/10.1038/s41598-020-67228-7
Rajasekhar M, Gadhiraju SR, Kadam A, Bhagat V (2020) Identification of groundwater recharge-based potential rainwater harvesting sites for sustainable development of a semiarid region of southern India using geospatial, AHP, and SCS-CN approach. Arab J Geosci 13:24. https://doi.org/10.1007/s12517-019-4996-6
Rana VK, Suryanarayana TMV (2020) GIS-based multi criteria decision making method to identify potential runoff storage zones within watershed. Ann GIS 26:149–168. https://doi.org/10.1080/19475683.2020.1733083
Salman SA, Shahid S, Ismail T et al (2019) Characteristics of annual and seasonal trends of rainfall and temperature in Iraq. Asia Pac J Atmos Sci 55:429–438. https://doi.org/10.1007/s13143-018-0073-4
Sanikhani H, Kisi O, Mirabbasi R, Meshram SG (2018) Trend analysis of rainfall pattern over the Central India during 1901–2010. Arab J Geosci 11:437. https://doi.org/10.1007/s12517-018-3800-3
Şen Z (2012) Innovative trend analysis methodology. J Hydrol Eng 17:1042–1046. https://doi.org/10.1061/(ASCE)HE.1943-5584.0000556
Şen Z (2017) Innovative trend significance test and applications. Theor Appl Climatol 127:939–947. https://doi.org/10.1007/s00704-015-1681-x
Sharma CS, Panda SN, Pradhan RP et al (2016) Precipitation and temperature changes in eastern India by multiple trend detection methods. Atmos Res 180:211–225. https://doi.org/10.1016/j.atmosres.2016.04.019
Sharma ML (2010) District wise major crops in Punjab. Chandigarh
Singh MC, Satpute S, Prasad V, Sharma KK (2022) Trend analysis of temperature, rainfall, and reference evapotranspiration for Ludhiana district of Indian Punjab using non-parametric statistical methods. Arab J Geosci 15:275. https://doi.org/10.1007/s12517-022-09517-1
Torres MN, Fontecha JE, Zhu Z et al (2020) A participatory approach based on stochastic optimization for the spatial allocation of Sustainable Urban Drainage Systems for rainwater harvesting. Environ Model Softw 123:104532. https://doi.org/10.1016/j.envsoft.2019.104532
Vyas SS, Bhattacharya BK, Nigam R et al (2015) A combined deficit index for regional agricultural drought assessment over semi-arid tract of India using geostationary meteorological satellite data. Int J Appl Earth Obs Geoinf 39:28–39. https://doi.org/10.1016/j.jag.2015.02.009
Wang H, Huang S, Fang W et al (2020a) Multivariable flood risk and its dynamics considering project reasonable service life in a changing environment. J Hydrol 590:125524. https://doi.org/10.1016/j.jhydrol.2020.125524
Wang Y, Xu Y, Tabari H et al (2020b) Innovative trend analysis of annual and seasonal rainfall in the Yangtze River Delta, eastern China. Atmos Res 231:104673. https://doi.org/10.1016/j.atmosres.2019.104673
Westra S, Fowler HJ, Evans JP et al (2014) Future changes to the intensity and frequency of short-duration extreme rainfall. Rev Geophys 52:522–555. https://doi.org/10.1002/2014RG000464
Wolteji BN, Bedhadha ST, Gebre SL et al (2022) Multiple indices based agricultural drought assessment in the Rift Valley Region of

Ethiopia. Environ Challenges 7:100488. https://doi.org/10.1016/j.envc.2022.100488
Wu H, Qian H (2017) Innovative trend analysis of annual and seasonal rainfall and extreme values in Shaanxi, China, since the 1950s. Int J Climatol 37:2582–2592. https://doi.org/10.1002/joc.4866

Publisher's Note Springer Nature remains neutral with regard to jurisdictional claims in published maps and institutional affiliations.

Springer Nature or its licensor (e.g. a society or other partner) holds exclusive rights to this article under a publishing agreement with the author(s) or other rightsholder(s); author self-archiving of the accepted manuscript version of this article is solely governed by the terms of such publishing agreement and applicable law.

24th HYDRO 2019, INTERNATIONAL CONFERENCE, OSMANIA UNIVERSITY, HYDERABAD, INDIA
18-20, December 2019

Seasonal Correlation between Rainfall and Temperature of Patiala City

Sanjoy Gorai[1], Gurnoor Singh[2], Dwarikanath Ratha[3] and Amit Dhir[4]
[1&4]*School of Energy and Environment,* [2&3]*Department of Civil Engineering,*
Thapar Institute of Engineering and Technology, Patiala, India
kumarsanjoy7@gmail.com, gsingh0021@gmail.com, dnath.ratha@thapar.edu, and amit.dhir@thapar.edu

Abstract

Rainfall and temperature are reported the most important climatic variables to study the climate change. Any change in these variables will affect the water demand and stream flow. The present study considers the 18 years data of rainfall and temperature for the seasonal trend analysis of rainfall and temperature of the Patiala city, Punjab. Mann-Kendall (MK) test and Sen Slope estimator (SSE) is used for trend analysis at 0.05 and 0.01 significance level. It is found from the analysis that the average temperature of winter and pre-monsoon season is decreasing trend while the average temperature of southwest monsoon and post monsoon is in increasing trend. Similarly the total rainfall is found in decreasing trend in all season except pre-monsoon season. Pearson correlation, Kendall Tau correlation and Spearman rho correlation is used to find the correlation between total rainfall and minimum, maximum and average temperature at 0.05 and 0.01 significance level. It is found from the analysis that Pearson correlation is fitting the present data suitably in compared to Kendall tau and Spearman rho test.

Keywords: Mann-Kendall test, Rainfall trends, temperature trends, Correlation analysis, Sen Slope's estimator.

1. INTRODUCTION

The temperature and rainfall are the most dominant variable of hydrological and weather studies. Any change in these parameters will directly affect the water demand, stream flow and hydrological cycle (Jain and Kumar, 2012). It is reported in literature that the earth's temperature is increasing continuously in the last few decades. The increase in level of natural green house gases due to human interferences results the climate change which further affect the ecological cycles. This climate change result the changes in the pattern of rainfall and temperature on earth surface. In the present scenario, It is found that number of countries are facing changes in rainfall pattern (Dai et al. 2011). According to NASA's Goddard Organization for Space Studies (GISS), the worldwide mean temperature is getting warmer by0.83 °C from 1951 to 1980. The warmer air of earth surface holds more moisture and it is reported that for increase in temperature of 1°C, water vapour increases by 7%. This increase the chances of occurring extreme events which will leads to increase the flood risk. Other climatic parameters such as wind direction and wind speed are also playing an important role in the changes of rainfall pattern.

Trend analysis of temperature and rainfall is generally conducted to get the knowledge regarding any changes in their pattern due to climate changes. In the literature, the MK test and SSE test has been widely used for the trend identification and quantification of rainfall and temperature.

Jain et al. (2013) carried out the trend analysis of rainfall and temperature of India's north east region covering an area of 255168 km^2 using SSE test, MK test considering the rainfall data from 1871-2008 and temperature data from1901-2003. The outcomes revealed that the mean, maximum minimum temperature and temperature range are in increasing trend and no clear pattern of rainfall was found in both spatially and temporally. Mondal et al. (2012) studied the analysis of north east part of Cuttack district, Orissa. The study was conducted for the daily data of rainfall for the time period of 1971 to 2010 using SSE test and MK test. The outcomes of the analysis were that the significant increasing trend was present for months of January, May, June, September, October and November and negative trend for months of February, March, April, July, August and December. Emmanuel (2019) carried out study on the analysis of trends of rainfall as well as temperature of the Mono river, Togo considering the data ranging from 1981–2010 using MK test and Pettitt's test. The outcomes

show that annual scale of temperature and rainfall all over the watershed showed a rising trend and the second spell of rainfall has been shifted from September to October with a higher magnitude peak in the southern part of study area. Croitoru & Piticar (2013)carried out the analysis of daily extreme temperature trends ranging from 1961-2010 for the region of Carpathians Chain of Romania using Homogeneity test, MK test and SSE test. The outcomes show that the daily minimum and maximum temperatures in the study areas have increased. An increase in the maximum values of minimum and maximum daily temperatures was observed for the tropical nights and summer days.

India is majorly dependent for its water supply on the southwest monsoon which is used for the domestic use, agriculture, energy sectors, and industries. In India, the annual rainfall occurs more than 80 percent during monsoon (Kumar et al., 2010). If any significant change comes in the monsoon period due to climate change, it will severely impact the farming sector in India. Punjab state is also experiencing the variations in rainfall and temperature from past few years. According to the IMD report on the "State level climate change trends in India" (2013), there is significant increase in rainfall trends of Punjab by 0.51mm/year for the month of June and annually decreasing trend by 2.41mm/year. For temperature, significant decreasing monthly trends were found for January and June by 0.03°C/year and 0.05°C/year respectively.

The objective of the present study is to check the trend of rainfall and temperature and the correlation between rainfall and temperature of Patiala city, Punjab. The outcomes will help in agricultural sector of the study area. The present studyis carried out using MK test for trend analysis and SSE for its magnitude of change. Pearson correlation, Kendall Tau correlation and Spearman rho correlation is used to find the correlation between total rainfall and temperature.

2. STUDY AREA AND DATA COLLECTION

2.1. Study area

The study area selected for the present research work is the Patiala city of Punjab state with its climate mainly dry and hot in summer and cold in winter. The seasons in a year are classified according to Indian meteorological department to four seasons which are winter season (January to February), pre-monsoon season (March to May), southwest monsoon season (June to September) and post monsoon season(October to December). The normal monsoon and annual rainfall of Patiala is approximately 535 mm and 632 mm. According to the report of Central ground water board 2013, the mean least and extreme temperature in Patiala ranges from 7.1^0C to 40.4^0C. The Patiala geo-morphology is plain in area and Patiala Nadi flows near to Patiala city as major drainage. Major soil types found in Patiala district are of tropical arid brown and arid brown type soil.

2.2. Data collection

The data of rainfall of Patiala city is downloaded from the Tropical Rainfall Measuring Mission (TRMM) for the duration of 1998-2015 i.e. for 18 years. Similarly the daily temperature data is collected from the National Climatic data Centre-Climate Data Online (NCDC-CDO), Asheville, California for the duration of 1998-2015. The rainfall is used as total rainfall i.e. total rainfall received throughout the season. The temperature data collected is segregated in the form of average temperature (AVT), maximum temperature (MAT) and minimum temperature (MIT) from which average of average temperature, maximum of MAT and minimum of MIT is used for the analysis.

3. METHODOLOGY

3.1. Trend test

Non-parametric Mann Kendall (MK) test is used for analyzing trends of rainfall and temperature. The trend is defined as significant based on the hypothesis test (Croitoru et al., 2016; Westra et al., 2014; Sharma et al., 2016). For n years of data x is analyzed and the test statistics S is computed as

$$S = \sum_{k=1}^{n-1} \sum_{j=k+1}^{n} \mathrm{sgn}(x_j - x_k) \quad \text{.....(1)}$$

Where,

$$\mathrm{sgn}(x_j - x_k) = \begin{cases} 1 \ if(x_j - x_k) > 0 \\ 0 \ if(x_j - x_k) = 0 \\ -1 if(x_j - x_k) < 0 \end{cases} \quad \text{.....(2)}$$

Where x_j and x_k are data values with j greater than k.

The present study considers the significance level of 0.05 which means that there is 5% probability that randomly distributed values are of x_j and H_0 is rejected by mistake giving no trend.

Now for the n greater than 10 in numbers, normal distribution is used. The Eq.3 tells us about the formulation for the calculation of variance of 'S'.

$$\mathrm{VAR(S)} = \frac{n(n-1)(2n+5) - \sum_{p=1}^{q} t_p(t_p-1)(2t_p+5)}{18} \quad \text{.....(3)}$$

Where 'q' signifies number of tied groups and 't_p' signifies number of observations in the p^{th}group. The values obtained from 'S' and VAR(S) are then used in Eq.4 to perform Z-test.

$$Z = \begin{cases} \dfrac{S-1}{\sqrt{\mathrm{VAR(S)}}} for S > 0 \\ 0 \ for S = 0 \\ \dfrac{S+1}{\sqrt{\mathrm{VAR(S)}}} for S < 0 \end{cases} \quad \text{.....(4)}$$

The trend to be significant or non-significant is expressed by the value of 'Z'. Further a positive trend is signified by positive value of 'Z' and a negative value of 'Z' signifies a negative trend. To quantify the trends obtained, SSE test is used.

3.2. Magnitude of trend

The magnitude of the change in trend is determined with Sen slope estimator method(SSE). The test is applicable to linear trend and represents quantified change per unit time (Sen 1968; Gilbert 1987).The slope (Q_i) is calculated by

$$Q_i = \frac{x_j - x_k}{j - k} \quad \text{.....(5)}$$

Where i= 1…N

Here x_j and x_k are data values with j greater than k. For n values in the data, $N = \frac{n(n-1)}{2}$ this is one less than the total number.

Correlation

The correlation analysis of this paper is computed by statistical analysis. The statistical methods used for correlations are Pearson correlation coefficient, Kendall correlation coefficient and Spearman Rho test.

3.2.1. Pearson correlation

The linear dependency among the data set is done through the Pearson Correlation. The values obtained after correlation lies in-between -1 to +1 and negative value tells us about the negative correlation and positive value tells us about the positive correlation. When zero comes as a result, no relation in between the observation is found. The correlation coefficient is generally indicated by " r ". The Eq.12 tells us about the formulation of Pearson correlation.

$$r_{xy} = \frac{\sum_{i=1}^{n}(x_i - \bar{x})(y_i - \bar{y})}{\sqrt{\sum_{i=1}^{n}(x_i - \bar{x})^2}\sqrt{\sum_{i=1}^{n}(y_i - \bar{y})^2}} \quad \text{.....(6)}$$

Where, r_{xy} is Pearson correlation coefficient, 'x' denotes the values of first set of data, 'y' denotes the values of second set of data and n signifies total number of values.

The value of r is defines the positive or negative correlation between the variables. Table 1 shows the how strong the correlation is present between two variables (Akoglu, 2018)

Table 1 Type of correlation

r (both + and – value)	**Correlation**
0.90 to 1.00	Very strong
0.70 to 0.89	Strong
0.40 to 0.69	Moderate
0.20 to 0.39	Weak
0.00 to 0.19	Very weak

3.2.2. Kendall tau rank correlation

This methodology also finds correlation and strength within two variables. Eq. 9 and 10 shows the equation to determine the Kendell

$$\tau_b = \frac{n_c - n_d}{\sqrt{(n_0 - n_1)(n_0 - n_2)}} \quad \text{.....(7)}$$

where,

$$n_0 = {}^{n(n-1)}/_{2}\,, n_1 = \sum_i {}^{t_i(t_i-1)}/_{2}$$

$$n_2 = \sum_j {}^{u_j(u_j-1)}/_{2}$$

n_c=Number of concordant pairs

n_d=Number of discordant pairs

t_i=Number of tied values in the i[th] group of ties for the first quantity

u_j=Number of tied values in the j[th]group of ties for the second quantity

Where t_i is number of tied values of the dataset 'x' and u_i is the number of tied of dataset 'y'.

3.2.3. Spearman rho test

The strength among two variables is evaluated using this test with a monotonic function and helps to find the correlation between them. After finding the difference in between the data pairs, the '+1', '0' and '-1' values are assigned according to the positive, no and negative differences. If we obtain equal ranks, then the values are said to be tied. Researchers (Jaiswal et al., 2015; Ninu Krishnan et al.,2019; Shadmani et al., 2012) also used this methodology for finding the correlation in-between the different parameters. Eq.8 and Eq.9 varies upon having tied value or not.

$$\rho = 1 - \frac{6\sum d_i^2}{n(n^2-1)} \quad \text{.....(8)}$$

$$\rho = \frac{\sum_i (x_i - \bar{x})(y_i - \bar{y})}{\sqrt{\sum_i (x_i - \bar{x})^2 \sum_i (y_i - \bar{y})^2}} \quad \text{.....(9)}$$

Where i = paired score, d = difference between ranks and d^2 = difference squared.

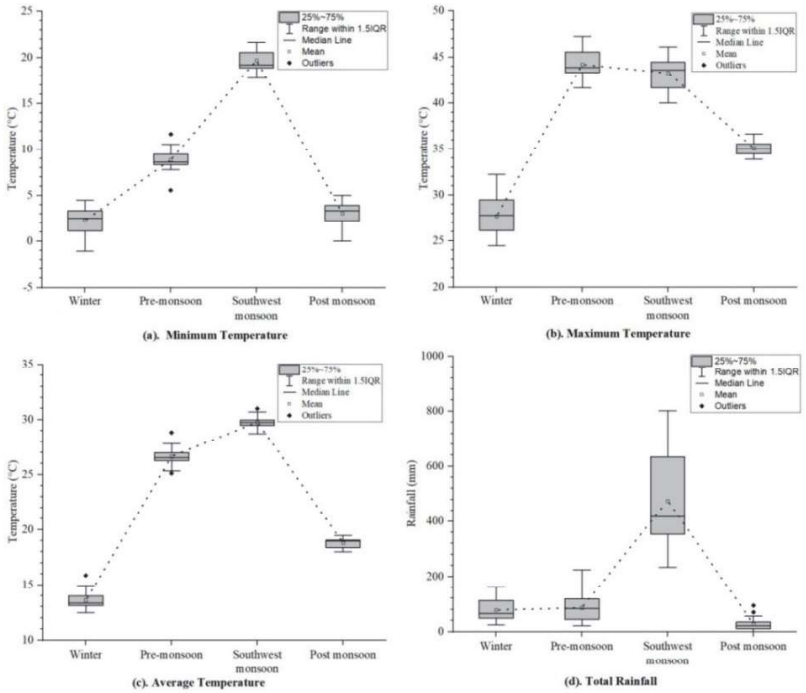

Figure 1 Seasonally statistical distribution of (a) Minimum Temperature (b) Maximum Temperature (c) Average Temperature (d) Total Rainfall

4. RESULTS AND DISCUSSIONS

The rainfall and temperature data downloaded from 1998-2015 are analyzed seasonally. Fig 1 shows the statistical distribution of seasonal rainfall and temperature. The statistical distribution of seasonal temperature comprises of statistical distribution of maximum, minimum and average temperature. It is found from Fig 1a-c that, the minimum temperature in the study area occurs during winter and post monsoon season and maximum temperature occurs during pre-monsoon and southwest monsoon season. But the maximum of average temperature occurs during southwest monsoon season. It is also found from Fig 1a-c that the wide variation of maximum, minimum and average temperature occurs in winter season. The present analysis shows that more than 71% of the rainfall in the study area occurs during south west monsoon season and very little rainfall occurs during the post monsoon season. It is found from Fig 1d that the wide variation of total rainfall occurs during south west monsoon season.

4.1. Analysis of trends and its magnitude

Equations (1-5) are used for the determination of seasonal trend of rainfall as well as the temperature and their magnitude. The trend analysis is made at significance level of 0.05. Various significant and non-significant results were found at 0.05 significance level. In seasonal trend analysis of temperature, significant results were found for both winter and south west monsoon season while analyzing for average and minimum temperature but significant results were found for winter and pre-monsoon season while analyzing for maximum temperature. Table 2 shows the change in magnitude of average, maximum, minimum temperature and total rainfall. It is found from Table 2 that the average temperature of winter and pre-monsoon season is decreasing at the rate of 0.08^{o}C and 0.06^{o}C per year respectively while the minimum temperature of winter season is decreasing at the rate of 0.04^{o}C per year. There is no change found in maximum and minimum temperature of pre-monsoon season. Similarly the minimum, maximum and average temperature of southwest monsoon is increasing at the rate of 0.07^{o}C, 0.17^{o}C and 0.02^{o}C per year respectively while the minimum and average temperature of post monsoon is increasing at the rate of 0.04^{o}C and 0.03^{o}C respectively. There is a decreasing trend of maximum temperature in post monsoon season is found at the rate of 0.04^{o}C per year.

Similarly, in seasonal trend analysis of rainfall it is found that there is a decreasing trend of rainfall in winter, southwest monsoon and post monsoon season at the rate of 1.65, 3.21 and 4.77 mm per year respectively while there is a increasing trend in pre-monsoon season at the rate of 2.81 mm per year.

Table 2 Change in magnitude of average, maximum, minimum temperature and total rainfall

	Average temperature	Maximum temperature	Minimum temperature	Total Rainfall
Winter	-0.08	0.19	-0.04	-1.65
Pre-monsoon	-0.06	0.00	0.00	2.81
Southwest monsoon	0.02	0.17	0.07	-3.21
Post monsoon	0.03	-0.04	0.04	-4.77

4.2. Correlation analysis

Eq 6-9 is used to determine the Pearson correlation, Kendall Taucorrelation and Spearman rho correlation between total rainfall and minimum, maximum and average temperature at 0.05 and 0.01 significance level. Table 3 shows the seasonal correlation between total rainfall and minimum, maximum and average temperature. It is found from Table 3that rainfall and temperature are negatively correlated in seasonal analysis. In the seasonal analysis, south west monsoon season showed negative moderate correlation between rainfall and

average temperature significantly at 0.01 and 0.05 significance level. Non-significant negative correlation found in other season between temperature and total rainfall. Moderately strong non-significant negative relation found between maximum temperature and total rainfall and average temperature and total rainfall in in winter season and pre-monsoon season respectively. Other relation are found non-significant weak and very weak which cannot be used for defining correlation. It is also found from the analysis that Pearson correlation is fitting the present data suitably in compared to Kendall tau and Spearman rho test.

Table 3 Seasonal correlation between total rainfall and minimum, maximum and average temperature

			Minimum temperature	Maximum Temperature	Average Temperature
Pearson Correlation	Winter	Total Rainfall	.088	-.405	-.294
Kendall Tau b			0.000	-.213	-.121
Spearman rho			.012	-.276	-.165
Pearson Correlation	Pre-monsoon	Total Rainfall	-.035	-.236	-.438
Kendall Tau b			-.036	-.213	-.207
Spearman rho			-.079	-.299	-.274
Pearson Correlation	Southwest monsoon	Total Rainfall	-.057	-.165	**-.611****
Kendall Tau b			-.079	-.184	**-.439***
Spearman rho			-.066	-.257	**-.613****
Pearson Correlation	Post monsoon	Total Rainfall	-.121	.112	.109
Kendall Tau b			.230	.089	.132
Spearman rho			.326	.122	.146

*. Correlation is significant at the 0.05 level (2-tailed).
**. Correlation is significant at the 0.01 level (2-tailed).

5. CONCLUSION

The objective of the present study is to check the trend of rainfall and temperature and also to determine the correlation between rainfall and temperature of Patiala city, Punjab. Eighteen year (1998-2015) of rainfall data from TRMM and temperature data from NCDC-CDO is used for the seasonal trend analysis and their correlation. The study concluded that, 71% of total rainfall received during southwest monsoon season. It is found from the analysis that the average temperature of winter and pre-monsoon season is decreasing trend while the average temperature of southwest monsoon and post monsoon is in increasing trend. Similarly maximum temperature of all season is found in increasing trend except post monsoon season. Minimum temperature for of all season is found is increasing trend except for winter season. Similarly the total rainfall is found in decreasing trend in all season except pre-monsoon season. It is also found from the analysis that Pearson correlation is fitting the present data suitably in compared to Kendall tau and Spearman rho test.

ACKNOWLEDGEMENT

The required dataset of rainfall and temperature is downloaded by Manmeet Singh from National Climate Data Centre – Climate Data Online (NCDC- CDO) and Tropical Rainfall Measuring Mission (TRMM) is greatly acknowledged.

REFERENECE

Akoglu H (2018) User's guide to correlation coefficients. Turkish journal of emergency medicine 18(3): 91–93

Benesty J., Chen J., Huang Y., Cohen I. (2009) Pearson Correlation Coefficient. In: Noise Reduction in Speech Processing. Springer Topics in Signal Processing, vol 2. Springer, Berlin, Heidelberg

Bishara, A. J., & Hittner, J. B. (2012). Testing the significance of a correlation with nonnormal data: Comparison of Pearson, Spearman, transformation, and resampling approaches. Psychological Methods 17(3), 399-417

Bonett DG, Wright TA (2000) Sample size requirements for estimating pearson, kendall and spearman correlations. Psychometrika 65(1): 23-28

Croitoru AE, Piticar A, Burada DC (2016) Changes in precipitation extremes in Romania. Quatary International 415: 315-325

Dai SW, Yang XG, Zhao M, Li Y, Wang WF, Liu ZJ (2011) Changes of China Agricultural Climate Resources under the Background of Climate Change. II. Spatiotemporal Change Characteristics of Agricultural Climate Resources in Southwest China. Chinese Journal of Applied Ecology 22(2): 442–452

Eisinga R, Grotenhuis M, Pelzer B (2013) The reliability of a two-item scale: Pearson, Cronbach, or Spearman-Brown?. International Journal of Public Health DOI: https://doi.org/10.1007/s00038-012-0416-3

Emmanuel LA, Hounguè NR, Biaou CA, Badou DF (2019) Statistical Analysis of Recent and Future Rainfall and Temperature Variability in the Mono River Watershed (Benin, Togo). Climate 7(8): 1-17.

Gilbert RO (1987) Statistical methods for environmental pollution monitoring", Van No strand Rienhold Company, Inc., New York.

Jain SK, Kumar V (2012) Trend Analysis of Rainfall and Temperature Data for India. Current Science 102(1): 37-49

Jain SK, Kumar V, Saharia M (2013) Analysis of Rainfall and Temperature Trends in Northeast India. International Journal of Climatology 33(4): 968–978

Jaiswal,RK. Lohani AK, Tiwari HL (2015) Statistical Analysis for Change Detection and Trend Assessment in Climatological Parameters. Environmental Processes 2(4): 729–749.

Kumar N, Tischbein B , Beg MK (2018) Multiple Trend Analysis of Rainfall and Temperature for a Monsoon-Dominated Catchment in India. Meteorology and Atmospheric Physics 131(4): 1019-1033

Mondal A, Kundu S, Mukhopadhyay (2012) Rainfall trend analysis by Mann-Kendall test: a case study of North-Eastern part of Cuttack district, Orissa. An Online International Journal Available at 2(1): 70–78

Ninu Krishnan MV, Prasanna MV, Vijith H (2019) Annual and Seasonal Rainfall Trends in an Equatorial Tropical River Basin in Malaysian Borneo." Environmental Modeling and Assessment. https://doi.org/10.1007/s10666-018-9649-8

Noether GE (1981) Why Kendall Tau?. Teaching Statistics 3: 41-43.

Sen PK (1968) Estimates of the regression coefficient based on Kendall's. Journal of the American Statistical Association 63: 1379- l389

Shadmani M, Marofi S, Roknian M (2012) Trend Analysis in Reference Evapotranspiration Using Mann-Kendall and Spearman's Rho Tests in Arid Regions of Iran. Water Resources Management 26(1): 211–224.

Sharma CS, Panda SN, Pradhan RP, Singh A, Kawamura A (2016) Precipitation and temperature changes in eastern India by multiple trend detection methods. Atmospheric Research 180: 211–225

Shieh GS (1998) A weighted Kendall's tau statistic. Statistics & Probability Letters 39(1): 17-24

Westra S, Fowler HJ, Evans JP, Alexander LV, Berg P, Johnson F (2014) Future changes to the intensity and frequency of short-duration extreme rainfall. Rev Geophysics 52(3): 522–555.

Waterlogging risk assessment of Patiala city, Punjab using Analytical Hierarchy Process and GIS analysis: A case study

Sanjoy Gorai[1], Amit Dhir[1], Dwarikanath Ratha[2]

[1]*PhD Research Scholar, School of Energy and Environment, Thapar Institute of Engineering and Technology, Patiala, 147004, India;* Email : *kumarsanjoy7@gmail.com*

[2]*Associate Professor, School of Energy and Environment, Thapar Institute of Engineering and Technology, Patiala, 147004, India;* Email : *amit.dhir@thapar.edu*

[3] *Associate Professor, Department of Civil Engineering, Thapar Institute of Engineering and Technology, Patiala, 147004, India: dnath.ratha@thapar.edu*

Abstract

Waterlogging is one of the most critical environmental problems of an urban area and requires proper management. Urbanization without proper planning causes waterlogging, resulting in significant built-up damages, economic losses, and negative impacts on health. To manage this issue properly, waterlogging mapping is the preliminary task to identify the probable waterlogging areas. In this study, we carried out a waterlogging risk analysis and prepared a waterlogging risk zone for the Patiala city of Punjab. Analytical Hierarchy Process (AHP) incorporated with GIS techniques has been used to prepare waterlogging risk mapping. Four criteria are selected for AHP based on the best data availability. These criteria are elevation, slope, land use land cover, and hydrologic soil group. These criteria are further classified into different importance levels relating to flood risk. The pair-wise comparison matrix of AHP is prepared using the importance level suggested by experts, and the weights of four different criteria are calculated. The waterlogging map is produced using the weights and representative factors of the respective criteria. The results of the waterlogging risk map are split up into five risk zones: severe, high, moderate, low, and very low. These findings of the water-logging map will demonstrate the areas under flood risk for which decision-makers may take necessary action to prevent such environmental problems.

Keywords: *Waterlogging, Analytical Hierarchy Process, GIS analysis, Patiala city*

1. Introduction

Waterlogging, the accumulation of rainwater in an urban area, became a serious issue to handle. Rapid urbanization is the primary cause behind waterlogging in a metropolitan area. Urbanization replaces natural surfaces with built-up areas such as roads, buildings, etc., preventing rainwater from entering the soil. Therefore, the rainwater accumulated on the surface produces runoff immediately. But other factors such as elevation, slope, soil group, etc., play a crucial role in transporting the water to rivers or water bodies. The disturbances on these factors will directly impact stormwater's transportation, which will be stopped, and the accumulation will start. The proliferation of rainwater will lead to waterlogging in an urban area. For mitigation of waterlogging problem, a waterlogging risk map should be executed.

The analysis of areas prone to waterlogging in an urban area is conducted worldwide, and numerous studies are available on the execution of waterlogging risk map (Quan et al., 2010; Sar et al., 2015; Zeng and Huang, 2018; Roy et al., 2021). Execution of waterlogging risk map is the integration of thematic layers statistical modeling in GIS. Statistical modeling, Analytical Hierarchy Process (AHP), frequency ration, fuzzy logic, machine learning

techniques, etc., are used (Souissi et al., 2020). AHP is one the most popular method to assess waterlogging maps and used by several authors (Quan et al., 2010; Sar et al., 2015; Zeng and Huang, 2018; Roy et al., 2021).

AHP is a statistical model based on multi-criteria decision-making developed by Saaty in 1977 (Saaty, 1977). The criteria of AHP are not limited to any numbers but should be sufficient to execute the risk map. The importance level of selected criteria for waterlogging of an area is given from surveys or works of literature. The importance level will form a pair-wise comparison matrix, and the weight of each criterion will be analyzed by normalizing the pair-wise comparison matrix. The weight of each criterion will be integrated with that criterion's class to evaluate the risk map.

Patiala city is the fourth largest and populated city of Punjab state and is located in the Ghaggar river basin of northern India. Frequent flood events are occurred in the basin, mainly due to extreme rainfall. In the last 22years (1988-2010), five significant floods occurred in the basin (Bhattacharya and Kumar, 2010). The city is located at a distance of 50km from the foothill of the Himalayas, and therefore a higher probability of flash flood exists. In context to frequent floods in the Ghaggar river basin and nearest Himalaya, it is essential to determine the waterlogging risk zone over Patiala city. Therefore, the study's objective is to prepare the waterlogging risk map of Patiala city of Punjab using AHP analysis and GIS analysis. The study's findings will help to take the initiative for waterlogging preventive measures for future flood events.

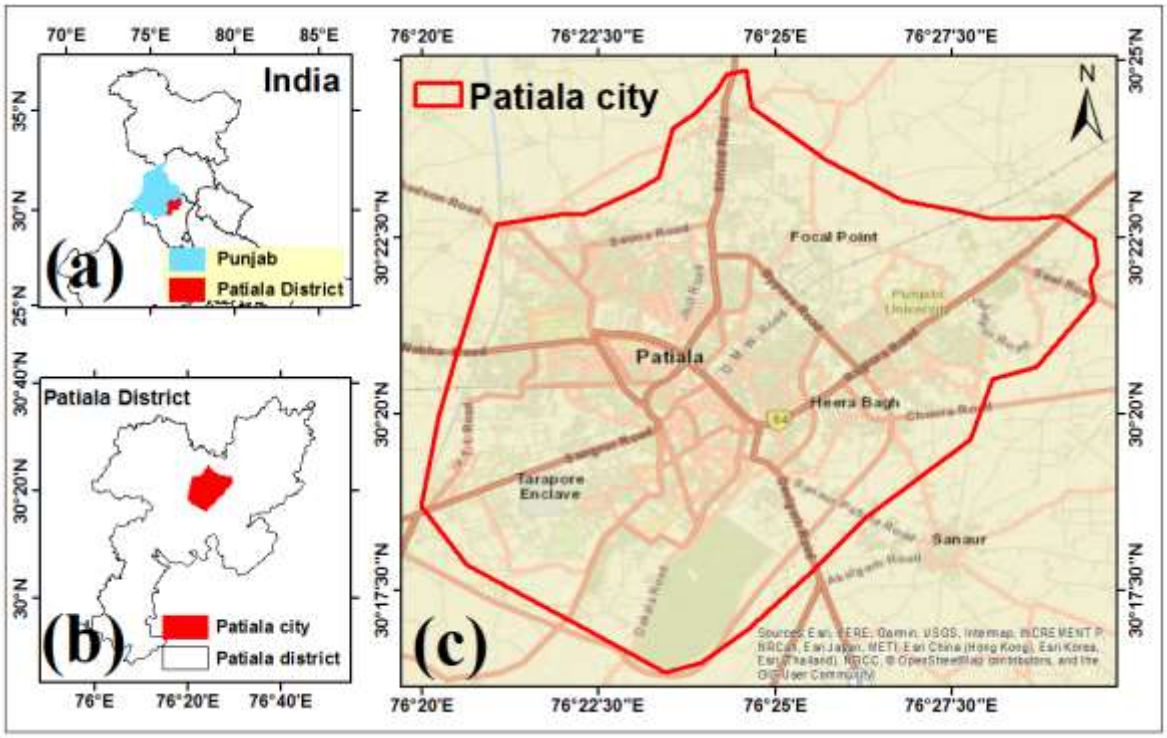

Figure 1 Study area of Patiala city. (a. The northern part of India shows the state of Punjab, Patiala district is showing inside Punjab state; b. Patiala district is showing the Patiala city; c. The study area of Patiala city)

2. Study area and Data source

Patiala is the fourth largest city of Punjab state in India and is located in the latitude of

30°20'24" N and longitude of 76°22'47.98" E. This city lies at an elevation of 255 m above the mean sea level. The annual average temperature of Patiala is 24.5°C, where the highest temperature is observed in June, and the lowest temperature is observed in January. The Patiala city is located under the semi-arid region's climatic condition, and southwest monsoon rainfall is the primary source of rainwater. The average annual rainfall of Patiala is 698mm, where the average southwest monsoon rainfall is 575mm (Gorai et al., 2021). The city's total area is 160 $km^{2,}$ and the city's total population is 763280 (projected to 2020). Therefore the density of Patiala city is 4800/ km^2. Figure 1 shows the study area in the Patiala district of Punjab state of India.

2.1. Criteria used for AHP

The criteria used for AHP analysis are Elevation, Slope, Soil group, and land use land cover (LULC) based on their data availability for Patiala city.

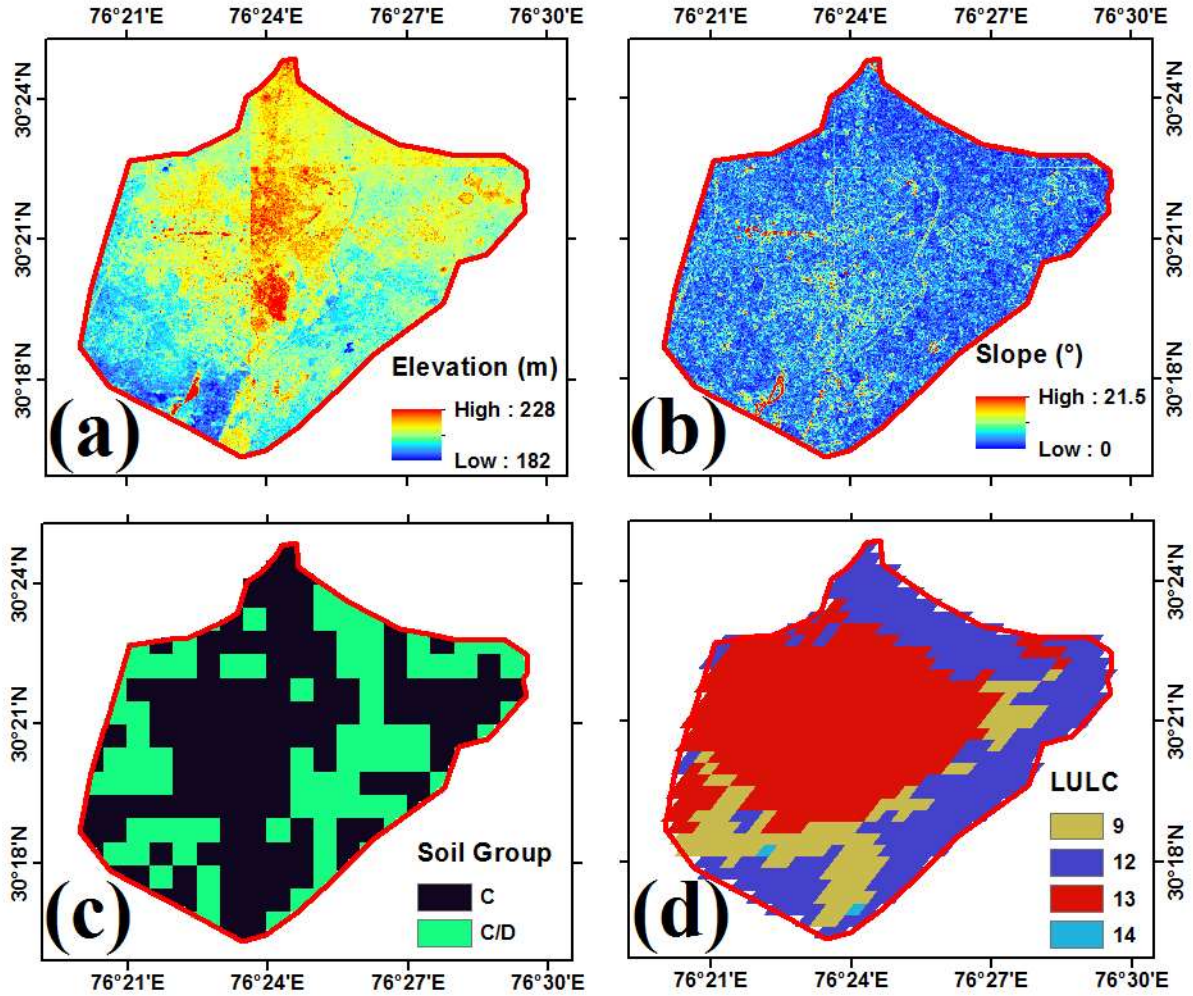

Figure 2 Thematic layers of (a) Elevation, (b) Slope, (c) Hydrologic soil group and (d) Land use land cover (LULC) [9:Savanas ; 12: Cropland; 13: Urban Built-up; 14: Cropland/natural vegetation].

Elevation: The 30m resolution elevation data was collected from Shuttle Radar Topography Mission (SRTM) dated 23.09.2014. Figure 3(a) shows the elevation profile of Patiala city. The elevation of Patiala city ranges between 182-228m. The average elevation of Patiala city is 206m.

Slope: The slope data is calculated from the elevation data. The conversion factor for slope calculation in ArcGIS is 9.26×10^{-06}. Figure 3(b) shows the slop profile of Patiala city. The slope of Patiala city lies in the range of 0-21.5°. The average slope of Patiala city is 1.89°.

Soil group: The soil group data is collected from Global Hydrologic Soil Groups (HYSOGs250m) for Curve Number-Based Runoff modeling dated 22.04.2020. Figure 3(c) shows the soil group of Patiala city. The hydrologic soil group of Patiala city is covered by C (62.13%) and C/D group (37.87%).

Land use land cover: The 500m resolution Land use land cover is collected from MODIS Land cover V6, 2019. Figure 3(f) shows the land use land cover pattern of Patiala city. The land use land cover of Patiala city is covered by Savannas (15.12), Cropland (37.64%), Urban Built-up (46.92%), and Cropland/natural vegetation (0.32%).

3. Materials and Methods

The waterlogging risk map is analyzed using the AHP method, and the waterlogging risk can be stated as follows (Dahri and Abida, 2017)

$$Waterlogging\ Risk\ = \sum_{i=1}^{n} W_i \times R_i \qquad (1)$$

Where, W_i is the weightage of each criterion and R_i is the classified values of each criterion. The weightage of each criterion is calculated using AHP.

The AHP method is selected for waterlogging risk mapping using different criteria. A pair-wise comparison matrix is constructed based on the relative importance (Equation 2). The importance values are shown in Table 1. The values are given based on the importance of each row of the matrix compared with the matrix column. In the pair-wise comparison matrix, the rows follow the inverse value of each criterion and its significance with others. The diagonal value of the matrix will be equally important.

$$\text{Pair} - \text{wise comparison matrix} = \begin{bmatrix} P_{11} & P_{12} & . & P_{1n} \\ P_{21} & P_{22} & . & P_{2n} \\ . & . & . & . \\ P_{n1} & P_{n1} & . & P_{nn} \end{bmatrix}, P_{11} = P_{22} = P_{nn} = 1 \qquad (2)$$

After constructing the pair-wise comparison matrix, the matrix is transformed to a normalized matrix calculating the weightage in each row. After that, the mean of each column is calculated from the normalize matrix and weightage fraction (W_i) of each factor will be derived. This weightage factor can be transformed to a percentage form multiplying by 100. The consistency ratio (CR) of the pair-wise matrix is analyzed using the following equation

$$CR = \frac{CI}{RI} \qquad (3)$$

Where; RI is the random index given in Table 2 and CI can be calculated as

$$CI = \frac{\lambda_{max} - n}{n-1} \qquad (4)$$

Where, λ_{max} is the principal Eigenvalue of the comparison matrix, and n is the total number of criteria.

Table 1 The level of importance for pair-wise comparison matrix (Dahri and Abida, 2017)

Level of importance	*Definition*	*Level of importance*	*Definition*
1	Equally Important	*7*	Very strong Important
3	Moderate Important	*9*	Extreme Important
5	Strong Important	*2,4,6,8*	Intermediate values

Table 2 Random Index (RI) value (Luu et al., 2018)

n	*3*	*4*	*5*	*6*	*7*
RI	0.58	0.90	1.12	1.24	1.32

4. Results and Discussions

4.1. AHP model formulation

Four criteria are selected for waterlogging risk mapping are elevation, slope, soil group, and land use land cover. A pair-wise comparison matrix is constructed upon experts' decisions, as shown in Table 3 for waterlogging risk in the city. The pair-wise comparison matrix is transformed to a normalized matrix calculating weightage by taking each relation value upon its column summation (Table 4). Now, calculating the average of each row value will give the weightage of each criterion (W_i) and later, this weightage is converted in percentage multiplying by 100. The weightage of elevation is 5.04%; the slope is 44.50%; land use land cover is 40.75%, and the soil group is 9.71%. Therefore, Equation 1 can be revised as

$$Waterlogging\ Risk = (5.04 \times Elevation) + (44.50 \times Slope) + (40.75 \times Land\ use\ land\ cover) + (9.71 \times Soil\ group) \quad (5)$$

The maximum Eigenvalue (λ_{max}) is found 4.121, and the total number of criteria is 4. Therefore, CI is calculated using Equation 4 and found 0.040. The RI value is taken from Table 3 and found 0.90. Now the consistency ratio value is found 0.0448 using Equation 3. The normalized matrix is found consistent as its value is less than 0.10.

Table 3: Pair-wise comparison matrix for AHP flood risk mapping

	Elevation	*Slope*	*LULC*	*Soil Group*
Elevation	1	0.14	0.14	0.33
Slope	7	1	1	7
LULC	7	1	1	5
Soil Group	3	0.14	0.2	1

Table 4: Normalized matrix of pair-wise comparison matrix and weightage of criteria for flood risk mapping.

	Elevation	*Slope*	*LULC*	*Soil Group*	W_i	W_i *(%)*
Elevation	0.0556	0.0614	0.0598	0.0248	0.0504	5.04
Slope	0.3889	0.4386	0.4274	0.5251	0.4450	44.50
LULC	0.3889	0.4386	0.4274	0.3751	0.4075	40.75
Soil Group	0.1667	0.0614	0.0855	0.0750	0.0971	9.71

4.2. Criteria Factor Classification

Four criteria decided for waterlogging map is classified into different categories based on its importance level for waterlogging in the city. Table 5 shows the classification based on its

importance level along with the respective weighted area. Figure 3 shows the spatial classification of four criteria's thematic layers of the study area. The elevation and slope of the city are classified into 1-7 using Jenks Natural Break classification in the ArcGIS module. Land use land cover (LULC) is classified into three categories based on its pattern. The soil group is classified based on infiltration capacity. Soil group C and C/D have an ability of low and very low infiltration rates, respectively, and therefore the classification is based on this.

Table 5 Classification table of different criteria for waterlogging risk mapping

Parameter	*Classification*	*Importance Level*	*Weightage*
Elevation	<200m	1	0.038
	200-203	2	0.146
	203.1-206	3	0.338
	206.1-208	4	0.235
	208.1-211	5	0.183
	211.1-215	6	0.052
	>215	7	0.008
Slope	<1.067	1	0.329
	1.067-2.052	2	0.330
	2.053-3.109	3	0.204
	3.110-4.432	4	0.092
	4.433-6.527	5	0.034
	6.528-10.556	6	0.009
	>10.556	7	0.002
LULC	Savannas	3	0.151
	Cropland Cropland/Natural Vegetation	5	0.380
	Urban Built-up	7	0.469
Soil	C	5	0.621
	C/D	7	0.379

4.3. Waterlogging risk analysis

The waterlogging analysis is analyzed using Equation (5) and processed in the ArcGIS 10.5 raster calculator module. The relative weight of the factor is used in Table 5. Figure 4 shows the waterlogging risk map of Patiala city. The highest importance level is used for the analysis is 1 to 7; therefore, the risk analysis value will be lies between 100 to 700. Based upon the range, the five types of risk zone is classified are very low (100-250), low (251-400), moderate (401-500), high (501-600), and very high (601-700). It is found from risk analysis that a significant portion of the city is under moderate risk to waterlogging, i.e., 42.37%, and low risk, i.e., 41.02%. The very low, high, and very high area is 3.90%, 12.03%, and 0.68%.

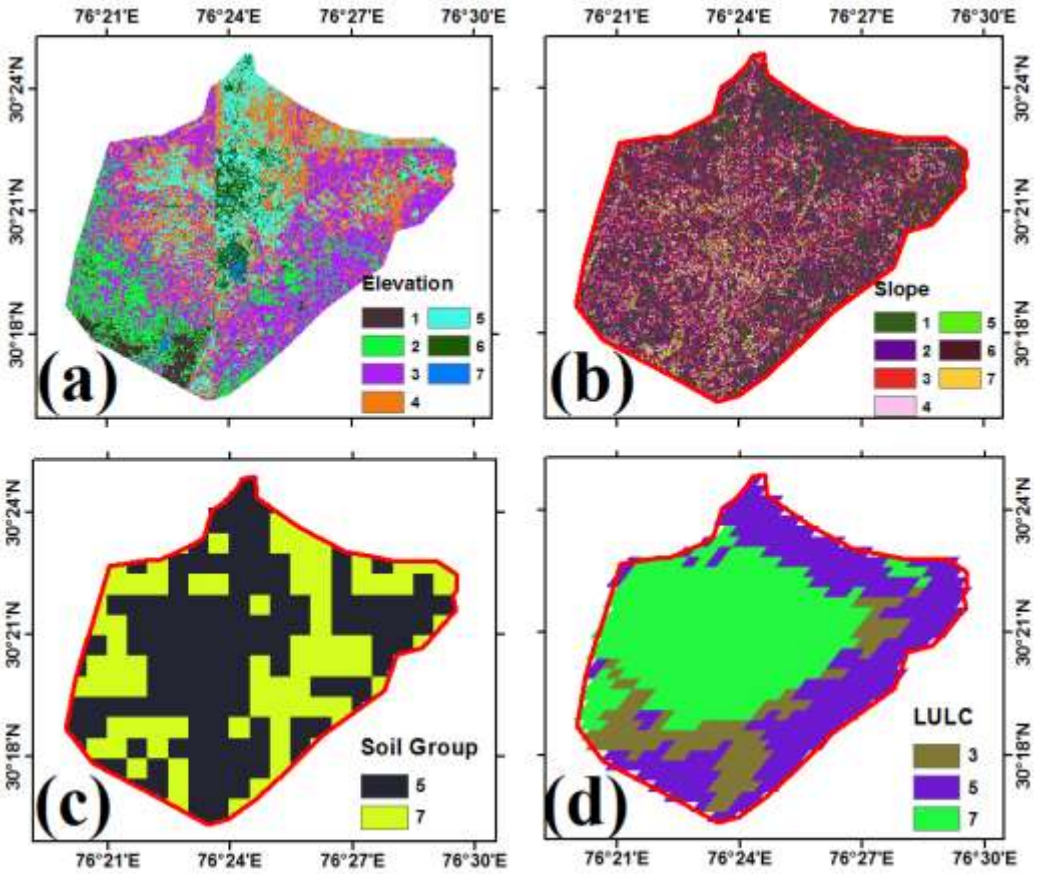

Figure 3 Classification of thematic layers of (a) elevation, (b) slope, (c) soil group, and (d) LULC.

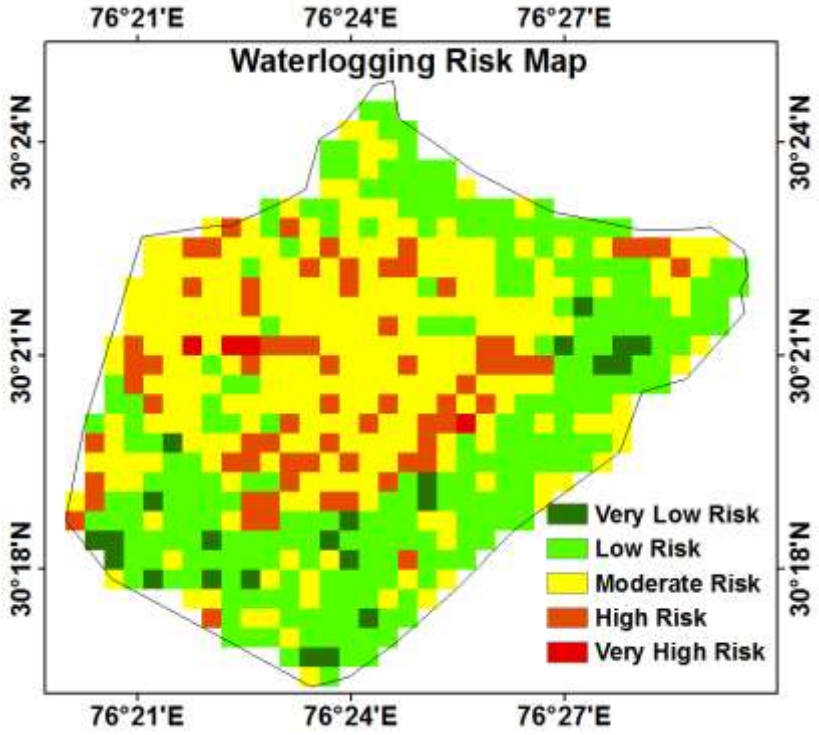

Figure 4 Waterlogging risk map of Patiala city

5. Conclusions

This study analyses the waterlogging risk map of Patiala city of Punjab district. Analytical hierarchy process integrating with ArcGIS is used for the analysis. Four thematic layers or criteria, elevation, slope, land use land cover, and soil group, are used for the analysis. The city's elevation lies in the range of 182-228, and the slope lies in the range of 0-21.5°. The LULC pattern of the city is Savannas (15.12), Cropland (37.64%), Urban Built-up (46.92%) and Cropland/natural vegetation (0.32%). The soil cover of the city is covered by C (62.13%) and C/D (37.87%). The pair-wise comparison matrix is prepared based on expert advice, and the weighted of each criterion is analyzed by normalizing the pair-wise comparison matrix. The weightage of elevation is 5.04%; the slope is 44.50%; land use land cover is 40.75%, and the soil group is 9.71%. These criteria are classified for the relative weight of its category. The waterlogging risk map is analyzed and found that the area under very low, low, moderate, high, and very high risk is 3.90%, 41.02%, 42.37%, 12.03%, and 0.68%, respectively. The major portion of the city is under low to moderate risk, but a part of the city is under high risk. Some preventive measures such as climate-resilient infrastructure, construction and management of sustainable drainage systems, rainwater harvesting, conservation of water bodies, early warning system, etc., might be adopted to reduce waterlogging risk and impacts social, economic, and environmental.

Reference

Bhattacharya, S., and Kumar, V. (2010). Unprecedented floods in Ghaggar Basin. *Dams Rivers and People*, July, 1–9.

Dahri, N., and Abida, H. (2017). Monte Carlo simulation-aided analytical hierarchy process (AHP) for flood susceptibility mapping in Gabes Basin (southeastern Tunisia). *Environmental Earth Sciences*, 76(7),302.

Gorai, S., Ratha, D., and Dhir, A. (2021). Adapting rainfall variability to flood risk: a case study of the Ghaggar river basin. *Journal of Geological Society of India,* Accepted Manuscript.

Luu, C., Von, M. J., and Kanjanabootra, S. (2018). Assessing flood hazard using flood marks and analytic hierarchy process approach: a case study for the 2013 flood event in Quang Nam, Vietnam. *Natural Hazards*, 90(3),1031–1050.

Quan, R. S., et al. (2010). Waterlogging risk assessment based on land use/cover change: A case study in Pudong New Area, Shanghai. *Environmental Earth Sciences*, 61(6), 1113–1121.

Roy, S. et al. (2021). Urban waterlogging risk as an undervalued environmental challenge: An Integrated MCDA-GIS based modeling approach. *Environmental Challenges*, 4(May), 100194.

Saaty, T. L. (1977). A scaling method for priorities in hierarchical structures. Journal of Mathematical Psychology. 15(3),234–281.

Sar, N., Chatterjee, S., and Das, A. M. (2015). Integrated remote sensing and GIS based spatial modelling through analytical hierarchy process (AHP) for water logging hazard, vulnerability and risk assessment in Keleghai river basin, India. *Modeling Earth Systems and Environment*, 1(4), 1–21.

Souissi, D., Zouhri, L., Hammami, S., Msaddek, M. H., Zghibi, A., and Dlala, M. (2020). GIS-based MCDM – AHP modeling for flood susceptibility mapping of arid areas, southeastern Tunisia. *Geocarto International*, 35(9),991–1017.

Zeng, J., and Huang, G. (2018). Set pair analysis for karst waterlogging risk assessment based on AHP and entropy weight. *Hydrology Research*, 49(4), 1143–1155.